Improving thermal ablation of liver tumors

Modeling and parameter identification of laser-induced interstitial thermotherapy

Matthias Andres

Dedication

Dedicated in gratitude to my parents

Acknowledgments

First of all, I would like to express my sincere gratitude to my advisor Prof. Dr. René Pinnau for his continuous support of my study and research. He motivated me to investigate the field of delayed heat transfer and parameter identification in the context of laser-induced interstitial thermotherapy, which is the basis for this work. As my advisor, he offered me a lot of freedom to pursue my own ideas and, at the same time, always had the right hints readily available when I was yet again stuck in one of my proofs.

I would like to thank Prof. Dr. Axel Klar for his support during my PhD program and helpful discussions on moment approximations for radiative transfer.

Special thanks go to Dr. Florian Schneider, who guided me at the beginning of my PhD program entering the academic world. Furthermore, I thank him for introducing me to the field of moment approximations for radiative transfer and investigating the P_N^{2nd} formulation with me, which is the basis for the second part of this thesis. I am very grateful to Prof. Dr. Claudia Totzeck for her support and patience in the second half of my PhD program, when it came to the functional analytical discussion of the proposed Cattaneo–LITT model and the related inverse problem — I always found an open door.

This thesis was conducted as part of the prognostic-MR-thermometry project (proMT), which was funded by the German Federal Ministry of Education and Research (BMBF). I thank my colleagues of the proMT consortium Prof. Dr. Axel Klar, Dr. Christian Leithäuser, Prof. Dr. Nicole Marheineke, Dr. Laura Müller, Prof. Dr. René Pinnau, Dr. Norbert Siedow and Kevin Tolle for the great collaboration.

I am very grateful to my colleagues and friends from the Technomathematics group of the Technische Universität Kaiserslautern for the great past four years and for turning the university into more than just a workplace.

I appreciate Dr. Sebastian Blauth, Dr. Gregor Corbin, Dr. Simon Gottschalk, Dr. Florian Schneider, Dr. Pratik Suchde and Prof. Dr. Claudia Totzeck for proofreading parts of this thesis and their helpful suggestions.

Special thanks go to my longtime friends and roommates Dr. Simon Gottschalk and Dr. Thomas Jung for making Kaiserslautern my home for the past ten years. Furthermore, I would like to thank my colleague and friend Dr. Gregor Corbin for many fruitful discussions on programming and numerical experiments, joint leisure activities and his support during our PhD programs.

Last but not least, I am very grateful to my parents for their infinite love, support and patience — none of this would have been possible without them!

Dissemination

This thesis is based on the joint work with my colleagues from the Technomathematics group of the *Technische Universität Kaiserslautern* and the *Fraunhofer Institute for Industrial Mathematics ITWM*. We published several contents of this thesis in the following articles:

1. Matthias Andres and René Pinnau. *Improving Thermal Ablation of Liver Tumors*. Progress in Industrial Mathematics at ECMI 2018. [10]

2. Matthias Andres and René Pinnau. *The Cattaneo Model in the context of Thermoablation of Liver Tumors*. Proceedings in Applied Mathematics and Mechanics (PAMM), 2019. [12]

3. Sebastian Blauth, Matthias Andres, René Pinnau and Claudia Totzeck. *Optimal Control and Asymptotic Analysis of the Cattaneo Equation*. Proceedings in Applied Mathematics and Mechanics (PAMM), 2019. [18]

4. Matthias Andres, Sebastian Blauth, Christian Leithäuser and Norbert Siedow. *Identification of the blood perfusion rate for laser-induced thermotherapy in the liver*. Journal of Mathematics in Industry, 2020. [9]

Furthermore, we already summarized several results of this thesis in the following manuscripts:

5. Matthias Andres and René Pinnau. *The Cattaneo Model for Laser-Induced Thermotherapy: Identification of the Blood Perfusion Rate*. Modeling, Simulation and Optimization in the Health- and Energy-Sector, 2021 (accepted). [11]

6. Matthias Andres and Florian Schneider. *The second-order formulation of the P_N equations with Marshak boundary conditions*. Manuscript uploaded to ArXiv, 2019. [13]

We provide a detailed overview on the particular contributions in Section 1.3.

All numerical results and related codes of this thesis, including files to reproduce the numerical experiments of this thesis, are publicly available online [8].

This thesis is publicly available online [7].

Abstract

Laser-induced interstitial thermotherapy (LITT) is a minimally invasive procedure to destroy liver tumors through thermal ablation. Mathematical models are the basis for computer simulations of LITT, which support the practitioner in planning and monitoring the therapy.

In this thesis, we propose three potential extensions of an established mathematical model of LITT, which is based on two nonlinearly coupled partial differential equations (PDEs) modeling the distribution of the temperature and the laser radiation in the liver.

First, we introduce the *Cattaneo–LITT model* for delayed heat transfer in this context, prove its well-posedness and study the effect of an inherent delay parameter numerically.

Second, we model the influence of large blood vessels in the heat-transfer model by means of a spatially varying blood-perfusion rate. This parameter is unknown at the beginning of each therapy because it depends on the individual patient and the placement of the LITT applicator relative to the liver. We propose a PDE-constrained optimal-control problem for the identification of the blood-perfusion rate, prove the existence of an optimal control and prove necessary first-order optimality conditions. Furthermore, we introduce a numerical example based on which we demonstrate the algorithmic solution of this problem.

Third, we propose a reformulation of the well-known P_N model hierarchy with Marshak boundary conditions as a coupled system of second-order PDEs to approximate the radiative-transfer equation. The new model hierarchy is derived in a general context and is applicable to a wide range of applications other than LITT. It can be generated in an automated way by means of algebraic transformations and allows the solution with standard finite-element tools. We validate our formulation in a general context by means of various numerical experiments.

Finally, we investigate the coupling of this new model hierarchy with the LITT model numerically.

Zusammenfassung

Laserinduzierte interstitielle Thermotherapie (LITT) ist ein minimalinvasives Verfahren zur Bekämpfung von Lebertumoren durch thermische Ablation. Mathematische Modelle dienen als Grundlage für rechnergestützte Simulationen, die den behandelnden Arzt bei der Planung und Durchführung der Therapie unterstützen.

In dieser Arbeit stellen wir drei mögliche Erweiterungen eines etablierten mathematischen Modells der LITT vor. Dieses besteht aus zwei nichtlinear gekoppelten partiellen Differentialgleichungen (PDE), welche die Verteilung der Temperatur und der Laserstrahlung im Lebergewebe beschreiben.

Zuerst stellen wir das neu entwickelte *Cattaneo–LITT-Modell* zur Beschreibung von verzögertem Wärmetransport in diesem Zusammenhang vor. Wir beweisen, dass dieses wohlgestellt ist, und untersuchen numerisch den Effekt eines zugehörigen Verzögerungsparameters.

Anschließend modellieren wir den Einfluss großer Blutgefäße im Wärmetransportmodell mit Hilfe einer ortsabhängigen Blutperfusionsrate. Dieser Parameter ist zu Beginn einer Therapie unbekannt, da er von dem jeweiligen Patienten und der Platzierung des Applikators relativ zur Leber abhängt. Wir entwickeln ein PDE-restringiertes Optimalsteuerungsproblem zur Identifikation der Blutperfusionsrate, beweisen die Existenz einer optimalen Steuerung und leiten notwendige Optimalitätsbedingungen erster Ordnung her. Wir stellen ein numerisches Modellbeispiel vor, anhand dessen wir die algorithmische Lösung dieses Problems demonstrieren.

Außerdem entwickeln wir eine alternative Formulierung der etablierten P_N Modellhierarchie mit Marshak-Randbedingungen zur Approximation der Strahlungstransportgleichung als gekoppeltes System von PDEs zweiter Ordnung. Die neue Modellhierarchie wird in einem allgemeinen Kontext hergeleitet und findet neben LITT ein breites Anwendungsgebiet. Sie kann auf Basis algebraischer Transformationen automatisch generiert werden und ermöglicht die Lösung mit Hilfe etablierter Finite-Elemente-Bibliotheken. Wir validieren unsere Formulierung in einem allgemeinen Kontext anhand verschiedener numerischer Experimente.

Abschließend untersuchen wir numerisch die Kopplung der neuen Modellhierarchie mit dem LITT Modell.

Contents

II   Second-order formulation of the P$_N$ equations

III   Conclusion and Outlook

IV	**Appendix**	

1 Introduction

How can nonlinear functional analysis and neutron-transport theory help to fight liver cancer?

One-line summary of this thesis

We study a mathematical model of the laser-induced interstitial thermotherapy (LITT), which is a minimally invasive procedure to destroy liver tumors through thermal ablation.

This thesis was compiled as part of the *prognostic-MR-thermometry* project (proMT), which was funded by the German Federal Ministry of Education and Research (BMBF)[1] and which was dedicated to taking the next step from magnetic-resonance (MR) thermometry to *prognostic* MR thermometry (see Figure 1.1).
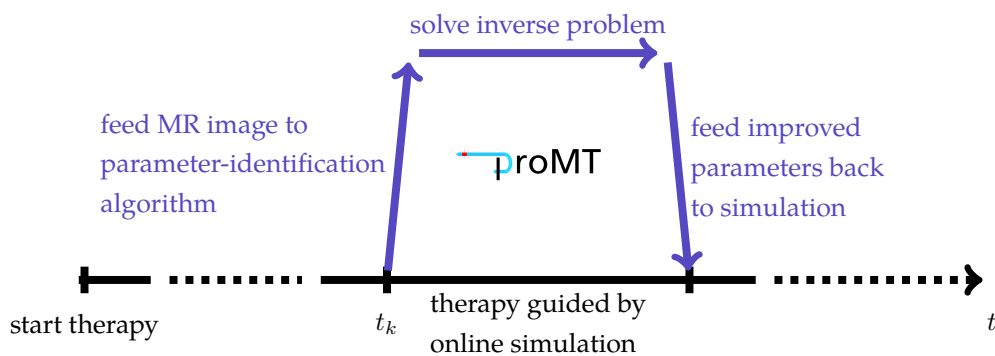
Figure 1.1: Prognostic MR thermometry.

Nowadays, LITT is guided by magnetic-resonance imaging (MRI). In the future, it shall be guided by an online simulation of the temperature distribution and tissue damage. In [65, Sec. 1, p. 3831], the authors stated the need for such an online simulation: *"Unfortunately, MRI is known to have either a good spatial or a good temporal resolution, making it difficult to predict the final size of the coagulated zone. Hence, there is a strong demand for computer simulations of LITT to support therapy planning and finding an optimal dosage."*

For the real application, temperature measurements[2] are provided by MR thermometry about every two minutes and can be used in combination with the simulation to estimate unknown model parameters. The corrected parameters are fed back to the simulation, which increases the prediction accuracy of the temperature distribution and the tissue damage.

---

[1] See the webpage of the German Federal Ministry of Education and Research: `https://www.bmbf.de/` .

[2] We refer to [164] for an overview on different methods for the temperature measurement in irradiated biologic media.

The procedure is based on accurate mathematical models for the underlying multiphysics problem, automated algorithms to identify unknown parameters and fast numerical solvers based on model-order-reduction techniques.

Simulations and therapies which include patient-dependent parameters belong to the field of *individualized medicine* and form the next generation of medical therapies. We note that particular parameters can be measured generally in advance [109, 222], whereas others need to be estimated for each therapy and each patient individually. For instance, the blood-perfusion rate correlates with the location of blood vessels and, thus, has a different spatial distribution for each therapy. Several references given in the next section demonstrate the effect of (large) blood vessels on the temperature distribution and, thus, on the ablation zone. This emphasizes that the knowledge of the vascular structure, i.e., the location of blood vessels, is crucial for an accurate simulation.

In the era of *big data* [172], it is tempting to forward the task of parameter identification or even the prediction of the ablation zone to one of many established *machine learning* algorithms, which are designed to bring some sense into the large amount of unstructured MRI data. So why do we need mathematical models at all, when all information seems to be hidden in the data and is just waiting to be mined?
Two main disadvantages of a purely statistical analysis of data, which is inherent in many black-box models from the field of machine learning, are often missing error bounds and the difficulty to draw valid conclusions in individual cases. Rather than using a purely data-driven approach for LITT, we use the new quality and amount of data to enhance validated physical models and tailor those to the individual patient. This paves the way to reliable simulations with physical laws as basis. Reliability becomes even more important in our application of LITT, where *false positives* and *false negatives* decide over the success or failure of individual cancer treatments.

Before we continue with a detailed introduction, we summarize this thesis in a nutshell and answer the question raised at the very beginning of this section.
We advance an existing mathematical model of LITT as a basis for realistic online simulations in the field. For a thorough understanding of the model, we employ techniques of nonlinear functional analysis and PDE-constrained optimization. Furthermore, based on the established theory of radiative transfer, which goes back to the neutron-transport theory developed in the middle of the last century, we revise a model hierarchy to describe the distribution of laser radiation in the liver.

1.1   Tumor ablation

Tumorous lesions in certain unfavorable positions are impossible to remove by surgical interventions [68, 156]. Furthermore, a surgical intervention is rather invasive and often requires the patient to stay in the hospital.
An extensive overview on alternative, minimally invasive tumor ablation techniques such
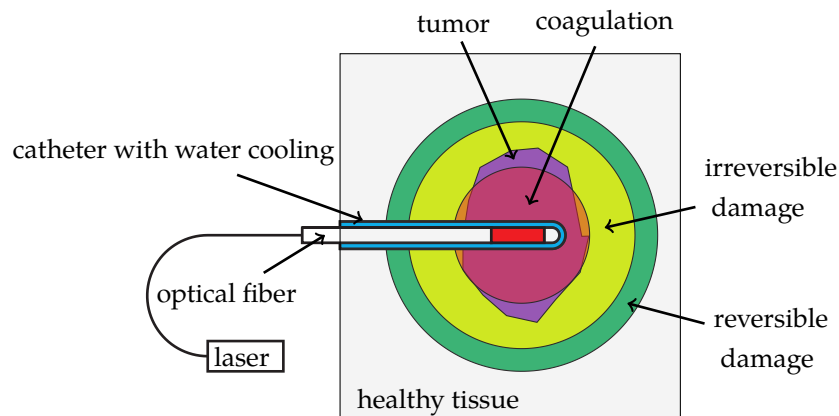
Figure 1.2: Sketch of LITT (cf. [65, Fig. 1, p. 3832]).

as radiofrequency ablation (RFA), cryoablation, microwave ablation, chemical ablation, high-intensity focused ultrasound (HIFU) and laser-induced interstitial thermotherapy (LITT) is given in [187].

One class of techniques (including LITT) uses thermal ablation, which directly alters the local temperature of the tissue. There are several effects relevant to thermal ablation [51, Sec. 1, p. 448]:

> *"The thermal action, precisely, can be either of the following types, namely, hyperthermia, coagulation and volatilisation. Hyperthermia means a moderate rise in temperature of several °C, corresponding to temperatures of 41 °C–44 °C for some tens of minutes and resulting in cell death due to changes in enzymatic processes. Coagulation refers to an irreversible necrosis without immediate tissue destruction. The temperature reached (50 °C–100 °C) for around a second, produces desiccation, blanching, and a shrinking of the tissues by denaturation of proteins and collagen. Volatilisation essentially means a loss of material. The various constituents of tissue disappear in smoke at above 100 °C, in a relatively short time of around one tenth of a second."*

We note that *"after water evaporates, cellular membranes begin their carbonization"* [51, Sec. 1, p. 450]. This limits the maximal zone of ablation because the carbonized tissue is less transparent for laser radiation, which prevents radiative heat transfer into regions more distant to the applicator. Beside carbonization and charring, also a high local blood flow within large blood vessels and an increased distance from the heat source negatively affect heat production in the tissue [179, 187]. We refer to [212] for an extensive overview on thermal damage and rate processes in biologic tissue and, especially, to Table 13.1 therein.

1.1.1 Laser-induced interstitial thermotherapy (LITT)

LITT falls into the category of thermal ablation. Figure 1.2 illustrates the setup of LITT. Guided by computed tomography (CT), a probe is inserted into the tumor. The probe is replaced by a catheter, which is heat resistant and transparent for laser radiation. After placing the catheter, an optical fiber is inserted into it. At its distal end, the fiber has a diffusing tip applicator with a length of about three centimeters, which distributes the laser radiation emitted by the fiber homogeneously in radial direction. The application system (in the following abbreviated by
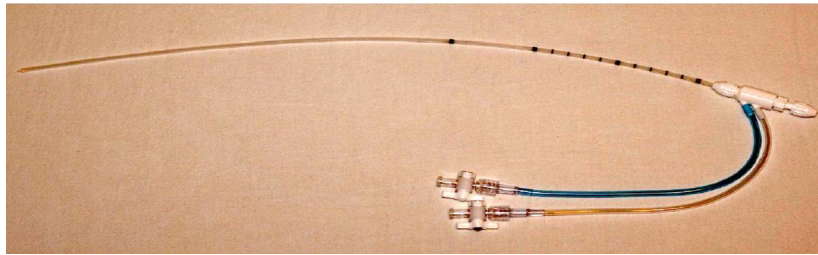
Figure 1.3: LITT applicator.[3]

the applicator), see Figure 1.3, includes an internal circulation system to cool its surface and the surrounding tissue, which shall prevent overheating and consequently tissue carbonization [95, 187, 207, 208].

Like other ablation techniques, LITT is not limited to liver tumors [139], but we restrict ourselves to this particular application.

1.1.2 State of the art: LITT

LITT is a well established method and has been performed in clinical therapies for decades, e.g., [25, 134, 225], and gained attention in the mathematical literature since the 1990s, e.g., [19, 65, 95, 182, 223].

There are studies which investigate the feasibility of online simulations and parameter identification like [72], where the authors align their simulations with in-vivo experiments. They model the blood-perfusion rate as a function which depends on the temperature, but they use a spherically symmetric isotropic solution for the radiative-transfer equation (RTE).

For the choice of a suitable approximation of the RTE, one needs to consider the trade-off between accuracy and computation time. Previous works approximate the solution of the RTE by very simplified models like the Beer–Lambert law [64], the Rosseland approximation [50] or Monte Carlo simulations [120, 182]. In [154], a hierarchy of higher-order P_N approximations of the RTE was investigated, which allows a transition from less accurate but computationally less expensive to more accurate but computationally more expensive models. For a detailed discussion on tissue optics, we refer to [228].

Beside different approximations of the RTE, various details of the LITT model were refined. In [65], the temperature distribution inside the applicator, accounting for the effect of the coolant flow, was investigated. This model was further refined by a simulation of the coolant flow in terms of the Navier–Stokes equations in [154].

In this thesis, we focus on the identification of a heterogeneous parameter modeling the blood-perfusion rate. Extensive studies investigated the influence of blood vessels in the context of LITT and other tumor ablation procedures [32, 33, 66, 82, 113, 199, 200, 218]. In [223], the blood flow in large vessels in the context of LITT was modeled. Our task now is the estimation of this parameter based on temperature measurements.

The starting point for us will be the established and validated LITT model based on the P_1 approximation of the RTE which is discussed in [65, 149, 223].

---

[3] The Image was kindly provided by the *Fraunhofer Institute for Industrial Mathematics ITWM*, Fraunhofer-Platz 1, 67663, Kaiserslautern, Germany. All rights reserved.

1.2 **Starting point of this thesis**

The starting point of this thesis is the classical LITT model presented in [95], which we summarize in the following. It has been used in several other works before [65, 170] and is validated with data from real ex-vivo experiments.

We deal with a multiphysics problem which combines the three modes of heat transfer[4], conduction, convection and thermal radiation, with the coagulation[5] of tissue. Coagulation affects the tissue properties like the optical coefficients and, in case that blood vessels are damaged, also the blood perfusion.

The heat transfer is modeled based on *Pennes' bioheat equation* [165] by

$$
\left\{
\begin{aligned}
\rho c_{\mathrm{p}} \partial_t \vartheta - \operatorname{div}(\kappa \nabla \vartheta) &= \sigma_{\mathrm{a}} \phi + \nu_{\mathrm{b}} \rho \rho_{\mathrm{b}} c_{\mathrm{p,b}} (\vartheta_{\mathrm{b}} - \vartheta) & &\text{in } (0,T) \times \Omega, \\
\kappa \nabla \vartheta \cdot \boldsymbol{n} &= a_{\mathrm{h,cool}}(\vartheta_{\mathrm{cool}} - \vartheta) & &\text{on } (0,T) \times \Gamma_{\mathrm{cool}} \cup \Gamma_{\mathrm{rad}}, \\
\kappa \nabla \vartheta \cdot \boldsymbol{n} &= a_{\mathrm{h,amb}}(\vartheta_{\mathrm{amb}} - \vartheta) & &\text{on } (0,T) \times \Gamma_{\mathrm{amb}}, \\
\vartheta(0,\cdot) &= \vartheta^{(0)} & &\text{in } \Omega
\end{aligned}
\right\}
\tag{1.1}
$$

where $\vartheta = \vartheta(t,x)$ is the temperature (in kelvin) and $T > 0$ is the end time of the simulation (in second). The first equation in (1.1) describes the heat flow inside the liver tissue in terms of the temperature, whereas the boundary conditions describe the exchange of heat with the surrounding tissue along Γ_{amb} and with the applicator along $\Gamma_{\mathrm{cool}} \cup \Gamma_{\mathrm{rad}}$. The term ϕ describes the irradiance (in watt per square meter), i.e., the contribution of the laser radiation to the heat flow, and is detailed in the following. We give details on the occurring parameters in Table 1.1 at the end of this section. The spatial domain $\Omega \subset \mathbb{R}^3$ is illustrated in Figure 4.1.

The distribution of the laser radiation is modeled by the radiative transfer (see Part II), which describes the radiance $\psi(\boldsymbol{x}, \boldsymbol{v})$ of the laser radiation depending on the spatial variable $\boldsymbol{x}$ in the domain Ω and the directional variable $\boldsymbol{v}$ on the unit sphere $\mathcal{S}^2$. Only the irradiance[6] $\phi = \int_{\mathcal{S}^2} \psi(\boldsymbol{x}, \boldsymbol{v}) \, \mathrm{d}\boldsymbol{v}$ appears in the energy-balance equation (1.1) and, thus, is of interest for LITT. This motivates the moment approximation by means of the P_1 method, which yields a much simpler diffusion equation[7] for the irradiance

$$
\left\{
\begin{aligned}
-\operatorname{div}(D \nabla \phi) + \sigma_{\mathrm{a}} \phi &= 0 & &\text{in } (0,T) \times \Omega, \\
D \nabla \phi \cdot \boldsymbol{n} &= |\Gamma_{\mathrm{rad}}|^{-1} q_{\mathrm{rad}} & &\text{on } (0,T) \times \Gamma_{\mathrm{rad}}, \\
D \nabla \phi \cdot \boldsymbol{n} &= 0 & &\text{on } (0,T) \times \Gamma_{\mathrm{cool}}, \\
\frac{1}{2}\phi + D \nabla \phi \cdot \boldsymbol{n} &= 0 & &\text{on } (0,T) \times \Gamma_{\mathrm{amb}}
\end{aligned}
\right\}
\tag{1.2}
$$

---

[4] See [47, Sec. 10.2, p. 279 ff.] for different modes of heat transfer.

[5] Coagulation is defined as *"Optically visible irreversible cell destruction (necrosis) caused by the denaturation of proteins"* [65].

[6] Also known as *radiative energy* [95], although this quantity does not have the units of a physical energy. It must not to be confused with the *radiance* ψ.

[7] We point out that in [95] the Robin boundary conditions are different than in [65]. This is based on the argument that *"radiation leaving through the applicator boundary can [re-]enter the computational domain through the opposite boundary"* [95, p. 1402]. We refer to Section 6.3 for a discussion on the suitable choice of boundary conditions.

with the external energy source introduced by the laser

$$q_{\text{rad}} = \begin{cases} (1 - \beta_q)\hat{q}_{\text{rad}}, & t_{\text{on}} \leq t \leq t_{\text{off}}, \\ 0, & \text{else.} \end{cases}$$

Here, t_{on} and t_{off} denote the times when the laser is switched on and off, respectively. Throughout this thesis, we set $t_{\text{on}} := 0$ and $t_{\text{off}} := T$. The first equation in (1.2) describes the irradiance inside the liver tissue. The laser radiation emitted from the applicator enters the model through the energy flow along Γ_{rad}. For a detailed discussion on the boundary conditions for Γ_{cool} and Γ_{amb}, we refer to Section 6.3.1.

The rise in temperature causes the protein in the tissue to denaturate. The coagulation is modeled by an *Arrhenius law* [231], [212, Sec. 13.3, p. 510 ff.]

$$\gamma(t, x) = \exp\left(-\int_0^t d_{\text{Arr}}(\vartheta)(s, x)\, \mathrm{d}s\right) \tag{1.3}$$

with

$$d_{\text{Arr}}(\vartheta)(t, x) = \begin{cases} A \exp\left(-\frac{E}{R\vartheta(t,x)}\right), & \vartheta \geq 317.15\,\text{K}, \\ 0, & \vartheta < 317.15\,\text{K} \end{cases} \tag{1.4}$$

where the temperature is given in kelvin. The function $\gamma(t, \cdot)\colon \Omega \to [0, 1]$ describes the fraction of coagulated and native tissue at time t, where a point $x \in \Omega$ with $\gamma(t, x) \approx 0$ corresponds to coagulated tissue and a point with $\gamma(t, x) \approx 1$ corresponds to native tissue. The optical coefficients depend on the coagulation [65, Sec. 2, Eq. 2, p. 3832]:

$$\sigma_{\text{a}} = \sigma_{\text{a,c}} + (\sigma_{\text{a,n}} - \sigma_{\text{a,c}})\gamma, \quad \sigma_{\text{s}} = \sigma_{\text{s}} + (\sigma_{\text{s,n}} - \sigma_{\text{s,c}})\gamma, \quad D = (3(\sigma_{\text{a}} + (1 - g)\sigma_{\text{s}}))^{-1}. \tag{1.5}$$

The meaning of the absorption coefficient σ_{a} and the scattering coefficient σ_{s} is explained in detail in Part II.

The dependence of the coagulation on the temperature introduces a nonlinear coupling between the equations (1.1) and (1.2).

Remark 1.1 — Destruction of cells.

As described in [187], the true cell damage is rather complex. It can be divided into two cases. In the first case, the tissue architecture is maintained. Cells are damaged by *direct cell death*, e.g., by destruction of cellular membranes, or by *indirect cell death*, e.g., by cellular dehydration or vessel thrombosis. In the second case, the tissue itself is destroyed by carbonization and charring.

We restrict ourselves to the prediction of the coagulation, which falls into the category of direct cell death. More detailed models could be employed, considering different phases of cell destruction like in [51, 158].

Remark 1.2 — Physical units (cf. [116, Sec. 1.1.5, p. 5]).

The equations in this section describe physical quantities. For the analysis and implementation, we prefer to work with dimensionless expressions (numbers) instead of physical quantities. The variables $\bar{\vartheta} := \frac{\vartheta}{\vartheta_{\text{ref}}}, \bar{x} := \frac{x}{x_{\text{ref}}}$, etc. describe the numerical values of the corre-

sponding physical quantities w.r.t. the reference units. For better readability, we omit the distinction between the physical quantity (including units) and its numerical value w.r.t. the reference unit. For a detailed discussion on physical units in mathematical models and the scaling of differential equations, we refer to [116].

The reference units are given as follows:

$$x_{\mathrm{ref}} = 1\,\mathrm{m}, \quad t_{\mathrm{ref}} = 1\,\mathrm{s}, \quad \vartheta_{\mathrm{ref}} = 1\,\mathrm{K}, \quad \phi_{\mathrm{ref}} = 1\,\mathrm{W\,m^{-2}}, \quad \sigma_{\mathrm{ref}} = 1\,\mathrm{m^{-1}}.$$

The presented classical LITT model is already discussed in a rigorous mathematical way in [219]. Therein, the authors prove the well-posedness of the state system, i.e., they show existence and uniqueness of a state vector (ϑ, ϕ) and the continuous dependence on the given data like boundary and initial conditions. Furthermore, they discuss the identification of the Arrhenius parameters A and E in terms of an optimal-control problem. We take their work as a blueprint for the analytical investigation of our Cattaneo–LITT model in Chapters 2 and 3.

1.3 Contributions of this thesis

There are two ways to increase the accuracy of the already existing LITT model from a mathematical point of view. First, we can investigate more accurate mathematical models for the various physical subproblems. Second, we can improve the accuracy of the existing models by finding suitable values for the occurring parameters based on measurement data. Based on our numerical results, we see the biggest potential for the improvement of LITT in the estimation of the blood-perfusion rate. The blood-perfusion rate depends on the location of large[8] blood vessels and can not be estimated as a general parameter in advance because the relative locations of the vessels to the applicator change in each treatment. The significant influence of this parameter on the accuracy of the predicted coagulation zone is discussed in the literature (see above) and quantified by one of our numerical experiments, see Figure 4.8.

It is essential to estimate the blood-perfusion rate as a heterogeneous coefficient in an automated way during each treatment to pave the way from ex-vivo to in-vivo experiments and for the final application in a clinical context.[9]

We summarize the main contributions of this thesis.

1. Motivated by a detailed literature review in Section 2.1, we introduce the Cattaneo–LITT model. This suggests an alternative heat-transfer model in the LITT context by replacing the bioheat equation with the Cattaneo model for delayed heat transfer. We prove the well-posedness of the Cattaneo–LITT model in Theorem 2.5 and validate the concept of delayed heat transfer by means of Experiment 4.4. The field of delayed heat transfer is well-studied, but, to the best of our knowledge, it has not been studied in the context of LITT. The analytical investigation of a related optimal-control problem in the context of the Cattaneo equation, including the study of the asymptotic behavior for $\tau \to 0$ where τ

---

[8] A blood vessel is considered to be "large" if its diameter is larger than two millimeters [120, p. 801].
[9] The transition from ex-vivo to in-vivo experiments might also affect other parameters like, e.g., the optical coefficients [109, 188], but in this thesis we focus only on the estimation of the blood-perfusion rate.

is a delay parameter inherent in the Cattaneo model, were published in our manuscript [18], which is based on [17]. The numerical investigation of the Cattaneo equation in the context of LITT was discussed in our manuscripts [11, 12].

2. We propose a PDE-constrained optimal-control problem for the formulation of the identification of the heterogeneous blood-perfusion rate in the context of LITT. We prove the existence of a corresponding optimal control in Theorem 3.3 and prove necessary first-order optimality conditions in Corollary 3.14. Based on the choice of an $L^1(\Omega)$-penalty term in the cost functional, we prove in Subsection 3.2.5 that the optimal control has a sparse structure. We introduce a numerical toy example based on which we demonstrate the automated identification of the blood-perfusion rate (Experiments 4.8–4.11). This identification task was already performed in the bioheat context in [96], but, to the best of our knowledge, it has neither been done in the context of the classical LITT model described in Subsection 1.2 nor in the context of the Cattaneo–LITT model. The presented identification of the blood-perfusion rate for the classical LITT model was demonstrated numerically, without a rigorous analytical investigation, in our manuscripts [9, 10], and in the context of the Cattaneo–LITT model in our manuscripts [11, 12].

3. We propose a reformulation[10] of the well-known P_N moment approximation of the radiative-transfer equation with Marshak boundary conditions in terms of second-order derivatives, which we call $\mathrm{P}_N^{\mathrm{2nd}}$ (Theorem 5.1). The procedure itself is well-known [148], whereas the focus of our derivation is an intuitive incorporation of the Marshak boundary conditions in the new formulation on the one hand and, on the other hand, the automated generation of a hierarchy of higher-order models and the possibility of a solution by standard finite-element tools, in view of a later coupling with the LITT simulation and an implementation in the field. This is a great advantage because we can exploit the established expertise in the field of numerical solutions of PDEs at no additional costs on our side of the implementation. Furthermore, our method is applicable not only in the context of LITT but to a very general set of scenarios, including anisotropic scattering, heterogeneous coefficients and general domains. The derivation and the numerical experiments in Chapters 5 and 6 were published in our manuscript [13].

4. We replace the P_1 approximation in the classical LITT model by higher-order $\mathrm{P}_N^{\mathrm{2nd}}$ models and investigate the effect numerically (Experiment 6.6 and Experiment 6.8). On the one hand, different moment models, including the classical P_N approximation, were studied in the context of the classical LITT model in [154], where the authors used customized solvers. On the other hand, the newly derived $\mathrm{P}_N^{\mathrm{2nd}}$ formulation has not been investigated in the context of LITT yet.

As outlined above, we already published several contents presented in this thesis. Here, we build upon those previous results and add a rigorous analytical investigation of the Cattaneo–LITT model. We discuss the proposed numerical example for the identification of the blood-perfusion rate in more detail. Here, different from the procedure in our published manuscripts, we

---

[10] The classical P_N model contains only first-order derivatives, whereas our formulation contains also second-order derivatives.

compute the descent directions by means of algorithmic differentiation (AD). Furthermore, we investigate the coupling of our P_N^{2nd} formulation with the Cattaneo–LITT model numerically. Our codes, written in MATLAB and PYTHON, are open source and publicly available online [8]. The tools for the simulation of the (Cattaneo-) LITT model and the identification of the blood-perfusion rate allow a fast prototyping in the context of LITT. Furthermore, the automated generation and solution of higher-order P_N^{2nd} models is not limited to LITT and can be transferred to various other applications like high-temperature industrial processes [49, 133, 167]. Last, we collect many well-known results regarding the functional analytical treatment of parabolic PDEs and PDE-constrained optimization in our "Hitchhiker's guide" in Appendix B, which might help future scholars to get started in this field.

1.4 Outline

This thesis is organized as follows.

Part I covers the Chapters 2–4 and is dedicated to the Cattaneo–LITT model and the related identification of the blood-perfusion rate. In Chapter 2, we discuss the well-posedness of the Cattaneo–LITT model, starting with a literature review in Section 2.1 to motivate delayed-heat-transfer models. In Chapter 3, we formulate the identification of the blood-perfusion rate in the Cattaneo–LITT model as a PDE-constrained optimal-control problem. We discuss the well-posedness of the related optimization problem and derive a necessary first-order optimality condition. We validate our theoretical results regarding the delayed heat transfer of the Cattaneo–LITT model and the identification of the blood-perfusion rate in Chapter 4 by means of numerical experiments.

Part II covers the Chapters 5 and 6 and focuses on the radiative-transfer equation. In Chapter 5, we formally derive in a general context a second-order formulation of the well-known P_N approximation of the RTE. We demonstrate our approach and its applicability to a broad set of scenarios in several numerical examples in Chapter 6. Furthermore, we replace the P_1 approximation in the classical LITT model by higher-order P_N^{2nd} models and investigate the effect on the predicted temperature and coagulation zone numerically.

In Part III, we draw conclusions and give an outlook for future research.

In the appendices, we provide details on some of the proofs in this thesis and prepare a small "Hitchhiker's guide" collecting selected fundamental results from functional analysis, which were essential to prove the well-posedness of the Cattaneo–LITT model and the related optimal-control problem in Chapters 2 and 3.

A reader who is interested in a rigorous functional analytical treatment of the Cattaneo–LITT model and the related optimal-control problem for the identification of the blood-perfusion rate may read Chapters 2 and 3 and the related appendices A and B. If the reader's interests are mainly numerical methods to solve the RTE, we recommend reading Chapter 5. Someone who is interested in the implications of the studied models for LITT from a quantitative point of view may jump directly to the numerical experiments in Chapters 4 and 6.

Throughout this thesis, we make extensive use of footnotes to provide additional details and references. We recommend, especially to the advanced reader, to skip the footnotes while reading a paragraph for the first time and to come back for reviewing the details in the footnotes later if necessary. Furthermore, some phrases are highlighted in a blue font color, which means that the corresponding definition is given in the glossary.

The symbols in Figure 1.4 may help the reader to keep track of the main ideas. Where possible, we summarize for the advanced reader a proof or a key idea in a special "idea-in-a-nutshell" environment, indicated by the symbol 1.4a. Furthermore, we mark the highlights of this work by the symbol 1.4b.

(a)   **(b)**
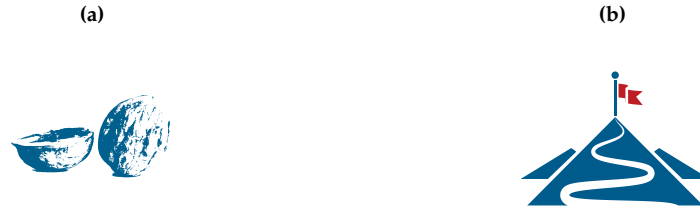
Figure 1.4: Guides through this thesis. (1.4a): "Idea in a nutshell"[11]. Summarizes a proof or an idea in a few words. (1.4b): "A highlight of this thesis". This symbol marks the main contributions listed in Section 1.3.

---

[11] The "nutshell" icon is based on the image in [94], which has been released under the *public domain license* [40].

[12] In [65], also the anisotropy factor g in equation (1.5) changes along with the coagulation. We omit this dependence here to simplify the comparison of higher-order models in Part II.

[13] For simplicity, we assume the blood temperature and the ambient temperature to coincide with the body temperature.

[14] In [95], an ex-vivo situation was considered, i.e., $\nu_b = 0$. In [170], one homogenized value $\nu_{b_n} > 0$ for native (n) tissue was used, where coagulated (c) zones where treated with $\nu_{b_c} = 0$. In [120], the authors explicitly distinguished between capillary vessels and large vessels with a diameter larger than two millimeters. The shrinkage of the capillaries stops the blood flow in those and, like in [65, 170], we set $\nu_{b_{out, c}} = 0$. The four different values for the blood-perfusion rate are combined via

$$\nu_b = \nu_{b_{out}} + (\nu_{b_{in}} - \nu_{b_{out}}) \cdot u(x),$$

with $\nu_{b_{in}}(t, x) = \nu_{b_{in,c}} + (\nu_{b_{in,n}} - \nu_{b_{in,c}})\gamma(t, x)$ and $\nu_{b_{out}}(t, x) = \nu_{b_{out,c}} + (\nu_{b_{out,n}} - \nu_{b_{out,c}})\gamma(t, x)$. The function $u \colon \Omega \to [0, 1]$ indicates the location of large blood vessels. The identification of the parameter u is one of the main tasks of this thesis and is discussed in Chapter 3.

[15] We refer to [109] for an overview on methods used to measure ex-vivo and in-vivo tissue optical properties, and to [222] for methods to measure tissue thermal properties and perfusion.

parameter	value	unit	description	source
ρ	1080	$\mathrm{kg\,m^{-3}}$	tissue density	
c_p	3690	$\mathrm{J\,kg^{-1}\,K^{-1}}$	specific heat capacity at constant pressure (liver tissue)	[80, 95]
κ	0.48	$\mathrm{W\,m^{-1}\,K^{-1}}$	thermal conductivity	
$\sigma_\mathrm{a,n}$	50	$\mathrm{m^{-1}}$	*absorption* coefficient of laser radiation in *native* tissue	
$\sigma_\mathrm{a,c}$	60	$\mathrm{m^{-1}}$	*absorption* coefficient of laser radiation in *coagulated* tissue	[95, 181]
$\sigma_\mathrm{s,n}$	8000	$\mathrm{m^{-1}}$	*scattering* coefficient of laser radiation in *native* tissue	
$\sigma_\mathrm{s,c}$	3×10^4	$\mathrm{m^{-1}}$	*scattering* coefficient of laser radiation in *coagulated* tissue	
g	0.96	1	anisotropy factor	[12]
$a_\mathrm{h,cool}$	250	$\mathrm{W\,m^{-2}\,K^{-1}}$	heat-transfer coefficient on $\Gamma_\mathrm{cool} \cup \Gamma_\mathrm{rad}$	
$a_\mathrm{h,amb}$	0	$\mathrm{W\,m^{-2}\,K^{-1}}$	heat-transfer coefficient on Γ_amb	[9]
β_q	0.14	1	coolant absorption factor	
$\hat{q}_\mathrm{rad}$	22	W	laser power	
A	3.1×10^{98}	$\mathrm{s^{-1}}$	frequency factor	[95, 196, 231]
E	6.28×10^5	$\mathrm{J\,mol^{-1}}$	activation energy	
$c_\mathrm{p,b}$	3640	$\mathrm{J\,kg^{-1}\,K^{-1}}$	specific heat capacity at constant pressure (blood)	[65]
ρ_b	1050	$\mathrm{kg\,m^{-3}}$	blood density	[98]
R	8.314	$\mathrm{J\,mol^{-1}\,K^{-1}}$	universal gas constant	[47]
$\vartheta^{(0)}$	310	K	initial tissue temperature	[180]
ϑ_b	310	K	blood temperature	
ϑ_amb	310	K	ambient temperature	[13]
ϑ_cool	293	K	coolant temperature	[95]
$\nu_\mathrm{bin,n}$	1.67×10^{-4}	$\mathrm{m^3\,kg^{-1}\,s^{-1}}$	blood-perfusion rate inside large vessels, native	
$\nu_\mathrm{bin,c}$	1.67×10^{-4}	$\mathrm{m^3\,kg^{-1}\,s^{-1}}$	blood-perfusion rate inside large vessels, coagulated	
$\nu_\mathrm{bout,n}$	1×10^{-6}	$\mathrm{m^3\,kg^{-1}\,s^{-1}}$	capillary blood-perfusion rate outside large vessels, native	[14]
$\nu_\mathrm{bout,c}$	0	$\mathrm{m^3\,kg^{-1}\,s^{-1}}$	capillary blood-perfusion rate outside large vessels, coagulated	

Table 1.1: Physical parameters.[15]

Part I

The Cattaneo–LITT model

We investigate an alternative heat-transfer model, which goes back to Cattaneo in 1948 [27], in the context of laser-induced interstitial thermotherapy (LITT). We start with a motivation and literature review on delayed heat-transfer models. In Chapter 2, we introduce the Cattaneo–LITT model by replacing the classical heat-transfer model for LITT by the Cattaneo model and prove its well-posedness. In Chapter 3, we propose a PDE-constrained optimal-control problem for the identification of the heterogeneous blood-perfusion rate and the localization of large blood vessels based on measured temperature data in the context of the Cattaneo–LITT model. We prove the existence of an optimal-control and derive necessary first-order optimality conditions. In Section 3.2.5, we further discuss the sparsity of the optimal control induced by an $L^1(\Omega)$-penalty term in the cost functional. In Chapter 4, we investigate the Cattaneo–LITT model and the related optimal-control problem numerically.

The classical LITT model and a related optimal-control problem to estimate the Arrhenius coefficients A and E have been investigated analytically in [219]. We use this work as a blueprint for the analytical investigations in this part. For showing the well-posedness, it is our main task to replace existence results for the solution of the classical heat equation by corresponding results for the Cattaneo equation in the LITT model. As a prerequisite, we need to investigate the Cattaneo equation analytically, for which we follow the procedure in [114].

To the best of our knowledge, neither the Cattaneo model in the context of LITT nor the corresponding identification of a heterogeneous blood-perfusion rate by means of PDE-constrained optimization have been studied yet. We published first numerical results regarding the identification of the blood-perfusion rate for the classical LITT model in [9].

The proposed strategy for the automated estimation of the heterogeneous blood-perfusion rate and, with this, the detection of large blood vessels can be transferred directly to the classical LITT model presented in Chapter 1.

2 Cattaneo–LITT model: analysis

1. *Without loss of generality = I have done an easy special case.*

2. *By a straightforward computation = I lost my notes.*

3. *The details are left to the reader = I can't do it.*

4. *The following alternative proof of X's result may be of interest = I can not understand X.*

5. *Correct to within an order of magnitude = wrong.*

Glossary of Mathematical Writing [92, Sec. 3.9, p. 33]

In this chapter, we investigate the Cattaneo model as an alternative to the classical model for heat transfer in the context of LITT. We introduce the Cattaneo–LITT model and investigate it analytically.

In Section 2.1, we motivate the Cattaneo–LITT model by a detailed literature review on the Cattaneo model for delayed heat transfer. In Section 2.2, we prove the well-posedness of the Cattaneo–LITT model. We move several proofs and technical details to Appendix A.1. Furthermore, in Appendix B, we provide a collection of fundamental theoretical results, which contains the basic tools needed to follow this Chapter.

2.1 Delayed heat transfer: overview

The literature review in this section will be published as part of our manuscript [11].

The *hyperbolic heat equation* (see below) has been studied extensively in the past decades. A very detailed summary of more than 120 related works between 1867 [136] until 1989 is given in [100]. The subsequent literature until 1999 is covered in [30], and a most recent review is given in [130]. An entire book dedicated to *heat waves* is [205]. The following summary is, among others, inspired by their presentations.

As described in [100, Sec. 1, p. 42], heat transfer is a macroscopic phenomenon:

> *"The temperature of a body is the macroscopic consequence of certain kinds of vibratory motions, the motions of molecules of a gas or the vibrations of a lattice in a solid on microscopic scales."*

A widely used basis for the derivation of the classical heat equation is based on *Fourier's law*, which relates the heat flux q at time t and position x linearly to the temperature gradient:

$$q(t, x) = -\kappa \nabla \vartheta(t, x), \tag{2.1}$$

where κ is the thermal conductivity. If we plug this into the energy-balance equation of a rigid conductor, we obtain

$$\frac{\partial \vartheta}{\partial t} = \hat{\kappa} \Delta \vartheta, \tag{2.2}$$

where $\hat{\kappa} = \kappa \rho^{-1} c_{\mathrm{p}}^{-1}$ is the thermal diffusivity, ρ the material density and c_{p} the specific heat capacity. One undesired property of equation (2.2) on a macroscopic level is the *infinite* speed of propagation of ϑ, i.e., a sudden change of $\vartheta(t_0, \cdot)$ at some point in space affects instantly, though, probably with small amplitude, the values of $\vartheta(t, \cdot)$ at all other points in space for all $t > t_0$. The following example is taken from [205] and illustrates this phenomenon by reference to the solution of the classical heat equation in one spatial dimension on the whole line $\mathbb{R}$:

$$\frac{\partial \vartheta}{\partial t} = \hat{\kappa} \frac{\partial^2 \vartheta}{\partial x^2} \quad \text{in } \mathbb{R}_{>0} \times \mathbb{R},$$
$$\vartheta(0, x) = f(x) \quad \text{in } \mathbb{R},$$

where f is a nonnegative, integrable function with compact support. The solution is given by

$$\vartheta(t, x) = \frac{1}{\sqrt{4 \pi \hat{\kappa} t}} \int_{-\infty}^{\infty} f(s) \exp\left(-\frac{(x - s)^2}{4 \hat{\kappa} t}\right) \, \mathrm{d}s.$$

We see that, for every $t > 0$, it holds $\vartheta(t, x) \neq 0$ for all $x \in \mathbb{R}$. *"Thus, we can think of ϑ as having an infinite speed of propagation."* [205, Sec. 1.1, p. 3].

On a microscopic level, there are two modes of heat transfer [100, Sec. 1, p. 41]:

> *"[...] thermal energy is transported by two different mechanisms: by quantized electronic excitations, which are called free electrons, and by the quanta of lattice vibrations, which are called phonons. These quanta undergo collisions of a dissipative nature, giving rise to thermal resistance in the medium."*

As described in [102, Sec. 2.1, p. 1040], already in 1931 the authors in [161] point out that

> *"[...] Fourier's model is in contradiction with the principle of microscopic reversibility. [...] In other words, Fourier's law has the unphysical property that it lacks inertial effects: if a sudden temperature perturbation is applied at one point in the solid, it will be felt instantaneously and everywhere at distant points."*

There have been several attempts to include microstructural effects in the macroscopic formulation, e.g., [220]. In [205], the authors describe eleven different approaches to modify the macroscopic formulation in order to obtain a finite speed of propagation.

A very popular approach goes back to Cattaneo [27]. Even though in the original paper the derivation was slightly different, as pointed out in [205], one can motivate Cattaneo's approach by replacing Fourier's law by a delay equation:

$$q(t + \tau, x) = -\kappa \nabla \vartheta(t, x). \tag{2.3}$$

In the setting of homogeneous, solid materials, the parameter τ is commonly referred to as *thermal relaxation time*, which, as described in [100, Sec. 1, p. 41], can be

> *"[...] associated with the average communication time between the[se] collisions for the commencement of resistive flow."*

If we expand the left-hand side of equation (2.3) and omit terms of order $\mathcal{O}(\tau^2)$, we obtain

$$\tau\frac{\partial^2\vartheta}{\partial t^2} + \frac{\partial\vartheta}{\partial t} = \hat{\kappa}\Delta\vartheta. \tag{2.4}$$

Equation (2.4) is of telegraph type [102] and often referred to as *Cattaneo equation* or *hyperbolic heat equation*.

We reproduce the example from [205, Sec. 1.1.1, p. 6] to illustrate the well-known result that the Cattaneo equation removes the infinite speed of propagation. To this, we look at equation (2.4) in one spatial dimension on the whole line $\mathbb{R}$ with transformed variables $\hat{t} = \frac{t}{2\tau}$ and $\hat{x} = \frac{x}{\sqrt{4\tau\hat{\kappa}}}$, and initial conditions

$$\vartheta(0,\hat{x}) = f(\hat{x}) \quad\text{and}\quad \frac{\partial\vartheta}{\partial\hat{t}}(0,\hat{x}) = g(\hat{x}).$$

Its solution is

$$\vartheta(\hat{t},\hat{x}) = \frac{e^{-\hat{t}}}{2}\left(f(\hat{x}+\hat{t}) + f(\hat{x}-\hat{t}) + \int_{\hat{x}-\hat{t}}^{\hat{x}+\hat{t}} J(s,\hat{x},\hat{t})\,\mathrm{d}s\right), \tag{2.5}$$

where the function J is given by

$$J(s,\hat{x},\hat{t}) = (g(s) + f(s))\,h\left((s-\hat{x})^2 - \hat{t}^2\right) - 2\hat{t}f(s)h'\left((s-\hat{x})^2 - \hat{t}^2\right),$$

with h defined by $h(x) = J_0(\sqrt{x})$, and J_0 being the Bessel function of zeroth order[1]. The solution in equation (2.5) is compactly supported for every $t > 0$, if the initial conditions f and g are compactly supported, which implies a finite speed of propagation.

Other modifications would be, e.g., based on the assumption that the conductivity depends on the temperature, i.e., $\kappa = \kappa(\vartheta)$, or that the heat flux depends on the history of temperature gradients:

$$\boldsymbol{q}(t,x) = -\int_{-\infty}^{t} Q(t-s)\nabla\vartheta(s,x)\,\mathrm{d}s,$$

with Q being a positive, decreasing relaxation function. For $Q(t-s) = \kappa\delta(t-s)$, where δ is the Dirac-delta distribution, we recover Fourier's law. Those modifications might end up in slightly different models, e.g., including mixed derivatives. For our investigation, we choose as the canonical and simplest starting point the Cattaneo equation (2.4). For details, we refer to [205]. A more general approach would be to add *phase lags* on both sides of equation (2.1), which then leads to a dual-phase-lag equation, like discussed in [173, 174, 176]:

$$\boldsymbol{q}(t+\tau,x) = -\kappa\nabla\vartheta(t+\tau_\vartheta,x).$$

As mentioned in [173], the delay τ_ϑ is caused by microstructural interactions such as phonon scattering or phonon-electron interactions, where τ is interpreted again as relaxation time due to fast-transient effects of *thermal inertia*.

The presented modifications have the desired property of a finite speed of propagation. This comes for a price on the analytical end. There are examples, e.g., in the context of thermoelastic

---

[1] See [237, Sec. 0.5, p. 113] for the definition of the Bessel function.

plates, where the solution of the resulting delay equation is instable [173, 176]. Furthermore, as discussed, e.g., in [210], the solution does not respect a physical maximum principle[2] anymore, i.e., the transient temperature distribution might exceed the boundary temperature as well as the initial temperature.

One of the reasons for the success of Fourier's law is the typical scale of τ between 10^{-8} s and 10^{-12} s in homogeneous substances, as reported in [104]. This fact is described also in [100, Sec. 1, p. 42]:

> *"This does not mean that there are big movements afoot to discard Fourier's law. The relaxation time [τ] is thought to be very small in nearly all practical and even exotic applications, so that as a practical matter it is believed that we get Fourier's law even on the shortest time scales of our daily lives."*

The interpretation of τ for homogeneous, solid material as discussed above needs to be altered for nonhomogeneous media, like described in [104, Sec. 3, p. 556]:

> *"[In nonhomogeneous material, the] constant τ characterizes [...] the time needed for accumulating the thermal energy required for propagative transfer to the nearest element of the inner structure.[...] the author suggests that τ represents the interaction of structural elements in inner heat transfer. For homogeneous materials this interaction is at the molecular or crystal lattice level.[...] For nonhomogeneous inner structure materials, the structural heat transfer interaction is at a different level and τ may take a much greater value."*

The authors in [125, Sec. 1, p. 2] go one step further and discuss implications for the heat transfer in living tissue, which is not only a highly heterogeneous medium, but includes also interactions on a cellular level:

> *"However, in non-homogeneous biological materials, τ can have a meaning, which is totally different from the commonly referred thermal relaxation time. Here it is defined as the characteristic time needed for accumulating the thermal energy required for propagative transfer to the nearest element within the non-homogeneous inner structures [...]. This characteristic time can be caused by the non-equilibrium between fluids and solids, as well as the effect of cell membrane as the energy storage and conversion element in biological systems. The mechanisms of τ in non-homogeneous inner structures may reflect energy interaction at the structural level rather than that at the molecular or crystal lattice level in homogeneous materials, and, thus, it may take a much greater value.[...] Obviously, the possible answer lies in the real energy process in the living system. As it may not appear clearly, heating or cooling the living tissues always induces a series of chemical [...], electrical [...] and mechanical [...] activities in addition to the temperature change alone. [...] Nearly every kind of energy conversion occurs at the cell membrane. Therefore biological system is a site with multi-mode energy conversion. And the occurrences of these cellar activities need time."*

In the same work, different references were given which report τ to be in a range of 16 s to 30 s for processed meat. Furthermore, there have been attempts to estimate the range of τ by means of an inverse problem, e.g., in [79].

---

[2] Cf. [63, Sec. 2.3.3, Thm. 4, p. 54] for the maximum principle for the classical heat equation.

Besides the analytical investigation of the hyperbolic nature of heat transfer, several real experiments were conducted to give evidence for wave-like behavior of the temperature evolution, e.g., in liquid helium at low temperatures [221], for sand [104], for processed meat [141], or to investigate the effect of skin burn [99]. Recently, some results of those experimental attempts were revised very critically in [130].

The Cattaneo model was already employed in modeling other thermal ablation methods like the radio-frequency ablation [128, 150, 238].

The effect of blood perfusion, which is of special interest in this thesis, was already discussed in the context of the hyperbolic bioheat equation in [99, 238].

This brief overview suggests that the Cattaneo-like bioheat equation might add value in modeling the laser-induced thermotherapy, especially in in-vivo experiments with the presence of blood vessels. In this thesis, we would like to study the estimation of the blood-perfusion rate in the Cattaneo–LITT model by means of an optimal-control problem. Questions on optimal control in the context of the hyperbolic heat equation were already studied, e.g., in [17, 79, 114].

To conclude this literature review, we note that we look at the Cattaneo equation as a *disturbed heat equation*, caused by modifying Fourier's law. In [100], it is described in great detail that a different stream in research studying *second sound* ended up at this equation as a *damped wave equation*, like summarized in [100, Sec. 1, p. 43]:

> *"[...] we note that whereas Cattaneo proposed to correct diffusion for effects associated with thermal inertia [...] Band and Meyer (1948), the same year as Cattaneo, and Osborne (1950) [...] proposed exactly the same telegraph equation [(2.4)], but with the first time derivative added to the wave equation to account for dissipative effects in liquid helium II."*

2.2 Well-posedness of the Cattaneo–LITT model

2.2.1 Prerequisites

In this section, we give an overview on the notation and general assumptions in this thesis.

Assumption 2.1 — Domain.

Throughout this thesis, let $\Omega \subset \mathbb{R}^d$, $d \in \{2, 3\}$, be a bounded spatial domain, i.e., a *nonempty*, *open*, *connected* and *bounded* set, with $\mathcal{C}^{1,1}$ boundary[a] $\Gamma = \partial\Omega$. Let $I := (0, T) \subset \mathbb{R}$ denote the time domain with the final time $T \in \mathbb{R}_{>0}$.

[a] See, e.g., [63, App. C.1, p. 626], [85, Sec. 1.2.1, Def. 1.2.1.1, p. 5]. This type of regularity is required for using Lemma A.1 and Theorem B.62 as part of the proof that the temperature component of the solution of the Cattaneo–LITT model is continuous.

We write the sets of natural numbers as $\mathbb{N} = \{1, 2, \ldots\}$ and $\mathbb{N}_0 = \mathbb{N} \cup \{0\}$. Vector spaces are always considered over the real numbers. We use a bold font to indicate vectors $\boldsymbol{p} \in \mathbb{R}^d$, $d \in \mathbb{N}$, except for points $x \in \Omega \subset \mathbb{R}^d$ in Part I. The outer unit normal vector of the boundary Γ at $x \in \Gamma$ is denoted by $\boldsymbol{n} = \boldsymbol{n}(x) \in \mathbb{R}^d$. The space-time cylinder is defined as $Q := I \times \Omega$.

Constants which appear in calculations and estimates are positive and can change their values from line to line. With $C(\alpha)$ we emphasize the dependence of a constant C on a particular quantity α, without listing all possible dependencies on other quantities.

For two real Banach spaces X, Y, the set of bounded linear operators is denoted by $\mathcal{L}(X, Y)$. The dual space of a Banach space X is denoted by $X^* := \mathcal{L}(X, \mathbb{R})$, and the corresponding dual pairing is denoted by $\langle \cdot, \cdot \rangle_X := \langle \cdot, \cdot \rangle_{X^*, X}$. We write $(\cdot, \cdot)_H$ for the inner product of a real Hilbert space H.

For two real Banach spaces X, Y with $X \subset Y$, we write $X \hookrightarrow Y$ for a continuous embedding and $X \hookrightarrow\hookrightarrow Y$ for a compact embedding.

For a real Banach space X, we write $\mathcal{C}^0(\overline{I}; X) := \{f : \overline{I} \to X \mid f \text{ is continuous}\}$ for the space of continuous functions. In case of $X = \mathbb{R}$, we write $\mathcal{C}^0(\overline{I})$. This space equipped with the *uniform norm*

$$\|f\|_{\mathcal{C}^0(\overline{I}; X)} := \max_{t \in \overline{I}} \|f(t)\|_X$$

is a Banach space [56, Sec. 7.1, Lem. 7.1.1, p. 151]. The space of Hölder-continuous functions with exponent $\alpha \in (0, 1]$ is denoted by $\mathcal{C}^{0,\alpha}(\overline{\Omega}) := \{f : \overline{\Omega} \to \mathbb{R} \mid \|f\|_{\mathcal{C}^{0,\alpha}(\overline{\Omega})} < \infty\}$, and is equipped with the norm

$$\|f\|_{\mathcal{C}^{0,\alpha}(\overline{\Omega})} := \sup \left\{ \frac{|f(x) - f(y)|}{\|x - y\|^\alpha} \,\middle|\, x, y \in \overline{\Omega}, \ x \neq y \right\}.$$

We recall the *Gelfand triple*[3]

$$H^1(\Omega) \overset{\text{dense}}{\hookrightarrow} L^2(\Omega) \hookrightarrow H^1(\Omega)^*, \tag{2.6}$$

where $H^1(\Omega)^* = \left(H^1(\Omega)\right)^*$ is the *dual space*[4] of the Sobolev space $H^1(\Omega) = W^{1,2}(\Omega)$. We note that $H^1(\Omega)$ is a separable and reflexive Banach space (in fact, it is even a Hilbert space)[5] and dense[6] in $L^2(\Omega)$. The last embedding in (2.6) is given by

$$L^2(\Omega) \ni \vartheta \mapsto (\vartheta, \cdot)_{L^2(\Omega)} \in L^2(\Omega)^* \subset H^1(\Omega)^*.$$

It is common to investigate evolution problems like the heat transfer equation analytically in the context of Bochner spaces, which is a generalization of Lebesgue spaces (L^p spaces) to functions with values in Banach spaces. We refer to [43, XVIII, p. 467 ff.], [235, Ch. 23, p. 402 ff.], [93, Sec. 1.3.2, p. 36 ff.], [186, Ch. 2, p. 33 ff.], [56, Ch. 7–8, p. 150 ff.] for an introduction to Bochner spaces and the notion of weak time derivatives. For real Banach spaces X, Y with $X \hookrightarrow Y$ and $\vartheta \in L^1(I; X)$, the nth weak time derivative[7] $\vartheta^{(n)} \in L^1(I; Y)$ is defined, in analogy to weak spatial derivatives, as the function which fulfills

$$\int_0^T \varphi^{(n)}(t)\vartheta(t)\,\mathrm{d}t = (-1)^n \int_0^T \varphi(t)\vartheta^{(n)}(t)\,\mathrm{d}t \quad \text{for all } \varphi \in \mathcal{C}_c^\infty(I),$$

---

[3] See [235, §23.4, Def. 23.11, p. 416] for the definition of Gelfand triples. Often we find $H_0^1(\Omega) \hookrightarrow L^2(\Omega) \hookrightarrow H^{-1}(\Omega) = H_0^1(\Omega)^*$ (cf. [235, 23.4, Ex. 23.12, p. 416]).

[4] This should not be confused with $H^{-1}(\Omega)$, which is the dual space of $H_0^1(\Omega)$.

[5] See Lemma B.24 on properties of Sobolev spaces.

[6] See Lemma B.51 on density results: follows from $\mathcal{C}^\infty(\overline{\Omega}) \subset H^1(\Omega) \subset L^2(\Omega)$ and the density of $\mathcal{C}^\infty(\overline{\Omega})$ in $L^2(\Omega)$.

[7] See [235, §23.5, Def. 23.15, p. 417], [43, XVIII §1 1, Def. 3, p. 471].

where $\mathcal{C}_c^\infty(I)$ is the space of infinitely-often differentiable functions from I to $\mathbb{R}$ with compact support in I. We use the short notation $(\cdot)' := (\cdot)^{(1)}$ and $(\cdot)'' := (\cdot)^{(2)}$. For a real Banach space X, we define the Banach-space-valued Sobolev space[8]

$$W^{k,p}(I;X) := \{\vartheta \in L^p(I;X) \,|\, \vartheta \text{ has weak time derivatives } \vartheta^{(n)} \in L^p(I;X) \text{ for all } 0 \le n \le k\}.$$

Throughout this thesis, we use without further notice the embeddings in (2.6), the isometric isomorphism[9]

$$L^p(I;L^p(\Omega)) \cong L^p(Q) \quad \text{for } 1 \le p < \infty,$$

and the following embeddings[10]

$$\left.\begin{aligned} L^p(\Omega) &\hookrightarrow L^q(\Omega), \\ L^p(I;X) &\hookrightarrow L^q(I;Y) \end{aligned}\right\} \quad \text{for } 1 \le q \le p \le \infty$$

where X, Y are real Banach spaces with $X \hookrightarrow Y$. Note that this especially implies the embeddings $L^2(I;H^1(\Omega)) \hookrightarrow L^2(I;L^2(\Omega)) \hookrightarrow L^2(I;H^1(\Omega)^*)$.

We define the spaces

$$\begin{aligned} W_\vartheta &:= L^2(I;H^1(\Omega)) \cap H^1(I;L^2(\Omega)) \cap H^2(I;H^1(\Omega)^*) \\ &:= \{\vartheta \in L^2(I;H^1(\Omega)) \,|\, \vartheta' \in L^2(I;L^2(\Omega)), \vartheta'' \in L^2(I;H^1(\Omega)^*)\}, \qquad (2.7) \\ \mathcal{Y}_p &:= L^p(I;W^{1,p}(\Omega)) \times \left[W_\vartheta \cap \mathcal{C}^0(\overline{Q})\right], \quad p \ge 2, \end{aligned}$$

equipped with the norms

$$\|\vartheta\|_{W_\vartheta} := \|\vartheta\|_{L^2(I;H^1(\Omega))} + \|\vartheta'\|_{L^2(I;L^2(\Omega))} + \|\vartheta''\|_{L^2(I;H^1(\Omega)^*)},$$

$$\begin{aligned} \|(\phi,\vartheta)\|_{\mathcal{Y}_p} &:= \|\phi\|_{L^p(I;W^{1,p}(\Omega))} + \|\vartheta\|_{W_\vartheta \cap \mathcal{C}^0(\overline{Q})} \\ &:= \|\phi\|_{L^p(I;W^{1,p}(\Omega))} + \|\vartheta\|_{W_\vartheta} + \|\vartheta\|_{\mathcal{C}^0(\overline{Q})}. \end{aligned}$$

Note that W_ϑ equipped with the inner product

$$(\vartheta,\varphi)_{W_\vartheta} := \int_0^T (\vartheta(t),\varphi(t))_{H^1(\Omega)} \, \mathrm{d}t + \int_0^T (\vartheta'(t),\varphi'(t))_{L^2(\Omega)} \, \mathrm{d}t + \int_0^T (\vartheta''(t),\varphi''(t))_{H^1(\Omega)^*} \, \mathrm{d}t,$$

where the inner product in $H^1(\Omega)^*$ is defined[11] by means of the Riesz-representation theorem[12], is a Hilbert space.[13] Furthermore, the space $\mathcal{Y}_p$ is a Banach space.[14]

---

[8] Cf. [114], [235, 23.6, Prop. 23.23, p. 422]).

[9] See Lemma B.49 on the relation between Lebesgue and Bochner spaces.

[10] See Lemma B.54, Lemma B.55 on embeddings in Bochner and Lebesgue spaces.

[11] Cf. the definition of the Hilbert space $W(0,T) = \{\vartheta \in L^2(I;H) \,|\, \vartheta' \in L^2(I;H^*)\}$, for some Hilbert space H, and its scalar product in [217, Sec. 3.4.3, p. 118].

[12] See [4, Sec. 4.1, p. 171] for the Riesz-representation theorem.

[13] This can be shown analogously to [43, XVIII §1 2 , Prop. 6, p. 473], which states that $L^2(I;H^1(\Omega)) \cap L^2(I;H^1(\Omega)^*)$ is a Hilbert space; see also [17, Sec. 3.1, Rem. 3.2, p. 19]; cf. [43, XVIII §5 1.3 , Rem. 1, p. 555].

[14] See Lemma B.4 on Cartesian products of Banach spaces. See [4, Sec. 1.7, p. 46] for a reference that $\mathcal{C}^0(\overline{Q})$ is a Banach space. To show that $W_\vartheta \cap \mathcal{C}^0(\overline{Q})$ is a Banach space, consider a Cauchy sequence $(\vartheta_n)_{n \in \mathbb{N}} \subset W_\vartheta \cap \mathcal{C}^0(\overline{Q})$ with $\vartheta_n \to \vartheta$ in $W_\vartheta \hookrightarrow L^1(Q)$ and $\vartheta_n \to \hat{\vartheta}$ in $\mathcal{C}^0(\overline{Q}) \hookrightarrow L^1(Q)$. From $\left\|\vartheta - \hat{\vartheta}\right\|_{L^1(Q)} \le \|\vartheta - \vartheta_n\|_{L^1(Q)} + \left\|\hat{\vartheta} - \vartheta_n\right\|_{L^1(Q)}$, it follows that ϑ and $\hat{\vartheta}$ coincide a.e. in Q, thus, we can identify the limits and get a converging sequence in $W_\vartheta \cap \mathcal{C}^0(\overline{Q})$.

Problem statement

We recall the strong formulation of the classical LITT model in equations (1.1)–(1.5), and define
the coefficients

$$
\sigma_{\mathrm{a}}(\vartheta) = \sigma_{\mathrm{a,c}} + (\sigma_{\mathrm{a,n}} - \sigma_{\mathrm{a,c}})\gamma(\vartheta),
$$
$$
\sigma_{\mathrm{s}}(\vartheta) = \sigma_{\mathrm{s,c}} + (\sigma_{\mathrm{s,n}} - \sigma_{\mathrm{s,c}})\gamma(\vartheta), \tag{2.8}
$$
$$
D(\vartheta) = \frac{\varepsilon_{\mathrm{kn}}^2}{3\hat{\sigma}_{\mathrm{t}}(\vartheta)} := \frac{\varepsilon_{\mathrm{kn}}^2}{3\left(\sigma_{\mathrm{a}}(\vartheta) + (1-g)\sigma_{\mathrm{s}}(\vartheta)\right)},
$$

with the coagulation

$$
\gamma(\vartheta)(t,x) = \exp\left(-\int_0^t d_{\mathrm{Arr}}\left(\vartheta(s,x)\right)\mathrm{d}s\right)
$$

and

$$
d_{\mathrm{Arr}}\colon \mathbb{R} \to \mathbb{R},\ d_{\mathrm{Arr}}(\vartheta) = \begin{cases} A\exp\left(-\frac{E}{\vartheta}\right), & \vartheta > 0, \\ 0, & \vartheta \le 0. \end{cases} \tag{2.9}
$$

We call a vector $(\phi, \vartheta) \in \mathcal{Y}_p$, for some $p \ge 2$, a *weak solution* or a state vector of the Cattaneo–LITT
model if it satisfies the *weak formulation* of the Cattaneo–LITT model

$$
\left\{
\begin{aligned}
&\int_0^T F_{\mathrm{r}}(\phi(t), \varphi_1(t); \vartheta, t)\,\mathrm{d}t = \int_0^T (g_{\mathrm{r}}, \varphi_1(t))_{L^2(\Gamma)}\,\mathrm{d}t, \\
&\int_0^T \tau\left\langle \vartheta''(t), \varphi_2(t)\right\rangle_{H^1(\Omega)} + (\vartheta'(t), \varphi_2(t))_{L^2(\Omega)} + F_{\mathrm{h}}(\vartheta(t), \varphi_2(t))\,\mathrm{d}t \\
&\qquad\qquad\qquad\qquad = \int_0^T \left\langle f_{\mathrm{h}}(\vartheta, t, \phi(t)), \varphi_2(t)\right\rangle_{H^1(\Omega)}\,\mathrm{d}t, \\
&\vartheta(0) = \vartheta^{(0)}, \\
&\vartheta'(0) = \vartheta^{(1)}
\end{aligned}
\right\} \tag{2.10}
$$

for all $\varphi = (\varphi_1, \varphi_2) \in L^2(I; H^1(\Omega)) \times L^2(I; H^1(\Omega))$, with

$$
\begin{aligned}
F_{\mathrm{r}}(\phi(t), \varphi_1(t); \vartheta, t) &:= (D(\vartheta)(t)\nabla\phi(t), \nabla\varphi_1(t))_{L^2(\Omega)} \\
&\quad + (\sigma_{\mathrm{a}}(\vartheta)(t)\phi(t), \varphi_1(t))_{L^2(\Omega)} + (a_{\mathrm{r}}\phi(t), \varphi_1(t))_{L^2(\Gamma)}, \\
F_{\mathrm{h}}(\vartheta(t), \varphi_2(t)) &:= \kappa\left(\nabla\vartheta(t), \nabla\varphi_2(t)\right)_{L^2(\Omega)} \\
&\quad + (\xi\vartheta(t), \varphi_2(t))_{L^2(\Omega)} + (a_{\mathrm{h}}\vartheta(t), \varphi_2(t))_{L^2(\Gamma)}, \\
\left\langle f_{\mathrm{h}}(\vartheta, t, \phi(t)), \varphi_2(t)\right\rangle_{H^1(\Omega)} &:= (\hat{\sigma}\sigma_{\mathrm{a}}(\vartheta)(t)\phi(t), \varphi_2(t))_{L^2(\Omega)} \\
&\quad + \vartheta_{\mathrm{b}}\left(\xi, \varphi_2(t)\right)_{L^2(\Omega)} + (g_{\mathrm{h}}, \varphi_2(t))_{L^2(\Gamma)},
\end{aligned} \tag{2.11}
$$

and data as given in Assumption 2.2. Note that we do not prescribe initial conditions for the
irradiance ϕ because the model (2.10) does not contain time derivatives of the irradiance.

For the remainder of the analytical investigation in Chapters 2 and 3, we make the following
assumptions.

> **Assumption 2.2 — Regularity of the data.**
>
> (A1) We assume for the boundary coefficients[a] $a_{\mathrm{h}}, a_{\mathrm{r}} \in L^\infty(\Gamma)$, $g_{\mathrm{r}} \in L^\infty(\Gamma) \cap W^{-1/4,4}(\Gamma)$,
> $g_{\mathrm{h}} \in L^\infty(\Gamma) \cap H^{1/2}(\Gamma)$, and that a_{h} can be written as $a_{\mathrm{h}} = \hat{a}_{\mathrm{h}}|_\Gamma$ for some Lipschitz-
> continuous function[b] $\hat{a}_{\mathrm{h}} \in \mathcal{C}^{0,1}(\overline{\Omega})$. Furthermore, we assume that, for $f \in \{a_{\mathrm{h}}, a_{\mathrm{r}}, g_{\mathrm{h}}, g_{\mathrm{r}}\}$,

there are lower and upper bounds $\underline{f}, \overline{f} \in \mathbb{R}_{>0}$ such that

$$0 < \underline{f} \leq f \leq \overline{f} < \infty \quad \text{a.e. on } \Gamma.$$

(A2) For simplicity, we omit the dependence of the blood-perfusion rate ξ on the coagulation γ for the analytical investigation.

Furthermore, we assume that the blood-perfusion rate fulfills $\xi \in L^\infty(\Omega)$, and that there exist lower and upper bounds $\underline{\xi}, \overline{\xi} \in \mathbb{R}_{>0}$ such that $0 < \underline{\xi} \leq \xi \leq \overline{\xi} < \infty$ a.e. in Ω.

(A3) For the initial conditions, we assume $\vartheta^{(0)} \in H^2(\Omega)$ such that $a_{\text{h}} \vartheta^{(0)} + \kappa \nabla \vartheta^{(0)} \cdot \boldsymbol{n} = g_{\text{h}}$ a.e. on Γ, and $\vartheta^{(1)} \in H^1(\Omega)$.

(A4) For the sake of completeness, we assume the following parameters to be strictly positive:

$$\tau, \kappa, \vartheta_{\text{b}}, \sigma_{\text{a,n}}, \sigma_{\text{a,c}}, \sigma_{\text{s,n}}, \sigma_{\text{s,c}}, \hat{\sigma}, A, E, \varepsilon_{\text{kn}} \in \mathbb{R}_{>0}.$$

---

[a] This rather technical assumption on the boundary coefficient g_{r} enables us to use [6, Sec. 2, Thm. 2.1, p. 4] in Remark 2.18.

[b] The regularity assumptions for a_{h} and g_{h} are needed to apply Lemma A.1 in the proof of Lemma 2.13.

Remark 2.3 — Initial conditions.

1. With the embeddings in (2.6) and (B.54), we get for $\vartheta \in W_\vartheta$ the embeddings

$$\vartheta \in L^2(I; H^1(\Omega)) \hookrightarrow L^2(I; L^2(\Omega)), \quad \vartheta' \in L^2(I; L^2(\Omega)) \hookrightarrow L^2(I; H^1(\Omega)^*),$$

and $\vartheta'' \in L^2(I; H^1(\Omega)^*)$. Theorem B.33 yields $\vartheta \in \mathcal{C}^0(\overline{I}; L^2(\Omega))$ and $\vartheta' \in \mathcal{C}^0(\overline{I}; H^1(\Omega)^*)$. Together with the embeddings $\vartheta^{(0)} \in H^2(\Omega) \hookrightarrow L^2(\Omega)$ and $\vartheta^{(1)} \in H^1(\Omega) \hookrightarrow H^1(\Omega)^*$, this gives sense to the initial conditions in (2.10), cf. [17, Sec. 3.1, Rem. 3.4, p. 20], [93, Sec. 1.3.2.3, Rem. 1.15, p. 42].

2. The initial conditions $\vartheta^{(0)}$ and $\vartheta^{(1)}$ given in Assumption 2.2 can be approximated by the sequences $(\vartheta_m^{(0)})_{m \in \mathbb{N}}, (\vartheta_m^{(1)})_{m \in \mathbb{N}} \subset H^1(\Omega)$ of the form

$$\vartheta_m^{(0)} = \sum_{k=1}^m \left(\vartheta^{(0)}, \omega_k \right)_{L^2(\Omega)} \omega_k \quad \text{and} \quad \vartheta_m^{(1)} = \sum_{k=1}^m \left(\vartheta^{(1)}, \omega_k \right)_{L^2(\Omega)} \omega_k$$

where $(\omega_k)_{k \in \mathbb{N}} \subset H^2(\Omega) \hookrightarrow L^2(\Omega)$ is the set of $L^2(\Omega)$-orthonormal eigenfunctions of the Laplacian defined in Lemma A.1. It holds both $\vartheta_m^{(0)} \to \vartheta^{(0)}$ in $H^1(\Omega)$ and $\vartheta_m^{(1)} \to \vartheta^{(1)}$ in $H^1(\Omega)$. Furthermore, for $g_{\text{h}} = 0$, it holds[a]

$$\left. \begin{aligned} \left\| \vartheta_m^{(0)} \right\|_{H^1(\Omega)} &\leq C \left\| \vartheta^{(0)} \right\|_{H^1(\Omega)}, \\ \left\| \Delta \vartheta_m^{(0)} \right\|_{L^2(\Omega)} &\leq C \left\| \Delta \vartheta^{(0)} \right\|_{L^2(\Omega)}, \\ \left\| \vartheta_m^{(1)} \right\|_{H^1(\Omega)} &\leq C \left\| \vartheta^{(1)} \right\|_{H^1(\Omega)}, \end{aligned} \right\} \quad \text{for all } m \in \mathbb{N}$$

for some constant $C \in \mathbb{R}_{>0}$.

---

[a] See Appendix A.1.2 for a detailed proof.

Remark 2.4 — Relation to the LITT model including physical units.

1. The classical LITT model in (1.1)–(1.5) is stated including physical units. For the analysis, we would like to get rid of the physical units. Furthermore, we would like to remove the constant in front of the time derivative in equation (1.1), so we rescale the equations. The superscript "(o)" denotes the parameter occurring in the original equations including physical units, see Table 1.1. The rescaled parameters used in (2.8)–(2.11) are given as follows:[a]

$$\hat{\sigma} := \frac{\sigma_{\text{ref}}\phi_{\text{ref}}t_{\text{ref}}}{\rho c_{\text{p}}\vartheta_{\text{ref}}}, \qquad \varepsilon_{\text{kn}} := \frac{1}{x_{\text{ref}}\sigma_{\text{ref}}}, \qquad \kappa := \frac{\kappa^{(\text{o})}t_{\text{ref}}}{\rho c_{\text{p}}x_{\text{ref}}^2},$$

$$\xi := \frac{\nu_{\text{b}}\rho_{\text{b}}c_{\text{p,b}}t_{\text{ref}}}{c_{\text{p}}}, \qquad A := A^{(\text{o})}t_{\text{ref}}, \qquad E := \frac{E^{(\text{o})}}{R\vartheta_{\text{ref}}},$$

$$\vartheta_{\text{b}} := \frac{\vartheta_{\text{b}}^{(\text{o})}}{\vartheta_{\text{ref}}}, \qquad \vartheta^{(0)} := \frac{\vartheta^{(0)\,(\text{o})}}{\vartheta_{\text{ref}}}, \qquad a_{\text{h}} := \frac{a_{\text{h}}^{(\text{o})}t_{\text{ref}}}{\rho c_{\text{p}}x_{\text{ref}}},$$

$$g_{\text{h}} := \frac{g_{\text{h}}^{(\text{o})}t_{\text{ref}}}{\rho c_{\text{p}}x_{\text{ref}}\vartheta_{\text{ref}}}, \qquad a_{\text{r}} := a_{\text{r}}^{(\text{o})}\varepsilon_{\text{kn}}, \qquad g_{\text{r}} := \frac{g_{\text{r}}^{(\text{o})}\varepsilon_{\text{kn}}}{\phi_{\text{ref}}},$$

$$f_{\sigma} := \frac{f_{\sigma}^{(\text{o})}}{\sigma_{\text{ref}}}$$

with $f_{\sigma} \in \{\sigma_{\text{a,n}}, \sigma_{\text{a,c}}, \sigma_{\text{s,n}}, \sigma_{\text{s,c}}\}$ and boundary coefficients (constant over time)

$$a_{\text{h}}^{(\text{o})} = \begin{cases} a_{\text{h,amb}}^{(\text{o})}, & \text{on } \Gamma_{\text{amb}}, \\ a_{\text{h,cool}}^{(\text{o})}, & \text{on } \Gamma_{\text{cool}} \cup \Gamma_{\text{rad}}, \end{cases} \qquad g_{\text{h}}^{(\text{o})} = \begin{cases} a_{\text{h,amb}}^{(\text{o})}\vartheta_{\text{amb}}^{(\text{o})}, & \text{on } \Gamma_{\text{amb}}, \\ a_{\text{h,cool}}^{(\text{o})}\vartheta_{\text{cool}}^{(\text{o})}, & \text{on } \Gamma_{\text{cool}} \cup \Gamma_{\text{rad}}, \end{cases}$$

$$a_{\text{r}}^{(\text{o})} = \begin{cases} 0, & \text{on } \Gamma_{\text{rad}}, \\ 0, & \text{on } \Gamma_{\text{cool}}, \\ \frac{1}{2}, & \text{on } \Gamma_{\text{amb}}, \end{cases} \qquad g_{\text{r}}^{(\text{o})} = \begin{cases} \left|\Gamma_{\text{rad}}^{(\text{o})}\right|^{-1}q_{\text{rad}}^{(\text{o})}, & \text{on } \Gamma_{\text{rad}}, \\ 0, & \text{on } \Gamma_{\text{cool}}, \\ 0, & \text{on } \Gamma_{\text{amb}}. \end{cases}$$

Throughout this thesis, we refer to ξ as the blood-perfusion rate.

The Cattaneo–LITT model stated with physical units has two additional parameters $\tau^{(\text{o})}$ and $\vartheta^{(1)\,(\text{o})}$. We obtain the rescaled quantities by $\tau := \tau^{(\text{o})}t_{\text{ref}}^{-1}$ and $\vartheta^{(1)} := \vartheta^{(1)\,(\text{o})}\vartheta_{\text{ref}}^{-1}t_{\text{ref}}$.

2. We omit the case distinction in the original damage function (1.4) for $\vartheta < 317.15\,\text{K}$ and obtain (2.9). For the given parameters, we get the value $d_{\text{Arr}}(317.15) \approx 1.1375 \times 10^{-5}$. On the time scale of our simulations ($T \sim 20\,\text{min}$), this modification does not have a relevant effect on the computed coagulation.

---

[a] See Remark 1.2 for the understanding of the physical reference values denoted by the subscript "ref".

We state the main result of this Chapter about the well-posedness of the Cattaneo–LITT model before going into the details of its proof. This is similar to [219, Sec. 2, Thm. 2.1, p. 6], which states the well-posedness of the classical LITT model.

Theorem 2.5 — Well-posedness of the Cattaneo–LITT model.

Let Assumptions 2.1 and 2.2 hold. Then, for a certain $p \in (2, 6)$, there *exists* a *unique state vector of the Cattaneo–LITT model* $(\phi, \vartheta) \in \mathcal{Y}_p$ with

$$\|\phi\|_{L^p(I;W^{1,p}(\Omega))} \leq C,$$

$$\|\vartheta\|_{W_\vartheta} + \|\vartheta\|_{\mathcal{C}^0(\overline{Q})} \leq C_1(\tau^{-1}, \underline{\xi}, \overline{\xi})$$

for some constants $C, C_1 \in \mathbb{R}_{>0}$.

It holds $\phi \in L^r(I; W^{1,p}(\Omega))$ for all $r \in [1, \infty)$, and[a]

$$\vartheta \in L^\infty(I; H^1(\Omega)) \cap W^{1,\infty}(I; L^2(\Omega)) \cap W^{1,p_1}(I; H^1(\Omega)) \cap L^{p_2}(I; H^2(\Omega)) =: B_{p_1, p_2}$$

with[b]

$$\|\vartheta\|_{B_{p_1, p_2}} \leq C(\tau^{-1}, p_1, p_2, \underline{\xi}, \overline{\xi})$$

for all $p_1, p_2 \in [1, \infty)$. Furthermore, it holds $\vartheta \in \mathcal{C}^{0,\alpha}(\overline{Q})$ with

$$\|\vartheta\|_{\mathcal{C}^{0,\alpha}(\overline{Q})} \leq C(\tau^{-1}, \alpha, \underline{\xi}, \overline{\xi})$$

for all $\alpha \in [0, \frac{1}{4})$.

The state vector depends continuously on the blood-perfusion rate ξ, in the sense that the map

$$\Xi_{\mathrm{ad}} \to L^2(I; H^1(\Omega)) \times L^2(I; H^1(\Omega)), \; \xi \to (\phi, \vartheta)$$

is *Lipschitz continuous*, where $\Xi_{\mathrm{ad}} := \{\xi \in L^2(\Omega) \,|\, \underline{\xi} \leq \xi \leq \overline{\xi} \quad \text{a.e. in } \Omega\} \subset L^2(\Omega)$ is the set of admissible perfusion rates.

---

[a] This means that ϑ is an element of $L^\infty(I; H^1(\Omega))$, which coincides with an element of $W^{1,\infty}(I; L^2(\Omega))$ a.e. in Q, etc.

[b] The norm of B_{p_1, p_2} is given as the sum of the particular norms of the intersecting spaces.

For the sake of readability, we avoid stating explicitly the dependence of the constants C, C_1 in Theorem 2.5 on the given data, i.e., all physical parameters and the domain. Nevertheless, we explicitly state the dependence of C_1 on the parameter τ^{-1}, which is motivated by the following remark.

Remark 2.6 — Limit $\tau \to 0$.

After proving the well-posedness of the Cattaneo–LITT model, the question about the behavior of the state vector (ϕ, ϑ) in the limit case $\tau \to 0$ arises. Does it converge to the solution of the classical LITT model? This question was answered for the Cattaneo-heat-transfer model (without any coupling) in [17]. Note that the transition to the limit is not straight forward because the given state bounds in Theorem 2.5 depend on τ^{-1}. We do not attempt to answer this question in this thesis and leave this task for future research.

2.2.2 Existence of a solution

Auxiliary problem

We observe that the state system (2.10) of the Cattaneo–LITT model is nonlinear because the coefficients σ_a and D depend on the coagulation and, thus, nonlinearly on the temperature. A standard procedure is to define an auxiliary state system which is coupled only in one way, and handle the subproblems consecutively. Finally, we obtain the overall solution by means of the Leray–Schauder fixed-point theorem[15]. This was already done for the classical LITT model in [219] and we follow the procedure therein.

For the auxiliary problem, we multiply the right-hand sides in (2.10) by a factor ρ, motivated by the Leray–Schauder fixed-point theorem, and replace the temperature ϑ occurring in the coefficients by an auxiliary variable ω. The auxiliary problem then reads as follows: For a given $\omega \in L^2(Q)$ and $\rho \in [0,1]$, find $(\phi, \vartheta) \in \mathcal{Y}_p$ such that

$$
\left\{
\begin{aligned}
& \int_0^T F_r(\phi(t), \varphi_1(t); [\omega]_M, t)\, dt = \rho \int_0^T (g_r, \varphi_1(t))_{L^2(\Gamma)}\, dt\,, \\
& \int_0^T \tau \langle \vartheta''(t), \varphi_2(t) \rangle_{H^1(\Omega)} + (\vartheta'(t), \varphi_2(t))_{L^2(\Omega)} + F_h(\vartheta(t), \varphi_2(t))\, dt \\
& \qquad\qquad\qquad = \rho \int_0^T \langle f_h([\omega]_M, t, \phi(t)), \varphi_2(t) \rangle_{H^1(\Omega)}\, dt\,, \\
& \vartheta(0) = \rho \vartheta^{(0)}, \\
& \vartheta'(0) = \rho \vartheta^{(1)}
\end{aligned}
\right\}
\tag{2.12}
$$

for all $\varphi \in L^2(I; H^1(\Omega)) \times L^2(I; H^1(\Omega))$, where

$$
[\,\cdot\,]_M \colon L^2(Q) \to L^\infty(Q),\ \varphi \mapsto \min\left(\max\left(\varphi, -M\right), M\right)
$$

is the *cutoff function*[16], for some $M \in \mathbb{R}_{>0}$. Note that the first equation in (2.12) (in the following, we refer to this as *(auxiliary) radiation equation*) depends no longer on ϑ and can be solved for $\phi = \phi(\omega)$ independently of ϑ. The resulting ϕ can be plugged into the second equation in (2.12) (in the following, we refer to this as *(auxiliary) heat-transfer equation*), which can be solved for $\vartheta = \vartheta(\omega)$. With this procedure, we eliminated the two-way coupling and are left to solve consecutively two one-way-coupled subproblems, one for the irradiance ϕ and one for the temperature ϑ.

We define the operator

$$
S \colon L^2(Q) \times [0,1] \to L^2(Q),\ (\omega, \rho) \mapsto \vartheta
\tag{2.13}
$$

such that (ϕ, ϑ) fulfills the auxiliary system (2.12) for all $\varphi \in L^2(I; H^1(\Omega)) \times L^2(I; H^1(\Omega))$. One prerequisite for the Leray–Schauder fixed-point theorem is that the operator S is well defined, continuous and compact. Second, we need to prove the existence of a uniform bound for all fixed points. Note that this bound needs to allow us to get rid of the cutoff function at the end of the proof. The application of the Leray–Schauder fixed-point theorem then provides us with a fixed point $\vartheta^* = S(\vartheta^*, 1)$, which yields a solution of the original problem (2.10). We move the proofs of some auxiliary results to the appendix, so that we do not get lost in details here.

---

[15] See the Leray–Schauder fixed-point theorem B.64.

[16] The max and min of a measurable function is again measurable ([55, §4.2, Cor. 4.4, p. 119]), thus, the cutoff function is well defined.

Nonlinearity

We show that the coefficients (2.8) are well-defined and continuous maps from $L^\infty(Q)$ to $L^\infty(Q)$ by reformulating them as concatenation of known operators.

Remark B.67 implies[17] that the Nemytskii operators

$$
\begin{aligned}
\phi_1 &\colon L^\infty(Q) \to L^\infty(Q), \ \omega \mapsto d(\omega(\cdot)), \\
\phi_3 &\colon L^\infty(Q) \to L^\infty(Q), \ \omega \mapsto \exp(-\omega(\cdot)), \\
\phi_4^{f_n, f_c} &\colon L^\infty(Q) \to L^\infty(Q), \ \omega \mapsto f_c + (f_n - f_c)\omega, \quad (f_n, f_c \in \mathbb{R}),
\end{aligned}
\tag{2.14}
$$

are well defined. Furthermore, for $M \in \mathbb{R}_{>0}$, there exists a constant $L(M)$ such that for all $\omega, \hat{\omega} \in L^\infty(Q)$ with $\|\omega\|_{L^\infty(Q)} \leq M$, $\|\hat{\omega}\|_{L^\infty(Q)} \leq M$ it holds

$$
\|\phi_i(\omega) - \phi_i(\hat{\omega})\|_{L^p(Q)} \leq L(M) \|\omega - \hat{\omega}\|_{L^p(Q)}
\tag{2.15}
$$

for all $p \in [1, \infty]$, for $i \in \{1, 3, 4\}$.

Next, we look at the map

$$
\phi_2 \colon L^\infty(Q) \to L^\infty(Q), \ \phi_2(\omega)(t, x) = \int_0^t w(s, x)\, \mathrm{d}s.
\tag{2.16}
$$

Lemma 2.7 — Properties of the map ϕ_2.

1. The map ϕ_2 in (2.16) is well defined.

2. For $p \in [1, \infty)$, there is a $C \in \mathbb{R}_{>0}$ such that for all $\omega, \hat{\omega} \in L^\infty(Q)$ it holds[a]

$$
\|\phi_2(\omega) - \phi_2(\hat{\omega})\|_{L^p(Q)} \leq C \|\omega - \hat{\omega}\|_{L^p(Q)}.
\tag{2.17}
$$

3. For $\omega \in L^\infty(Q) \cap L^2(I; H^1(\Omega))$, it holds $\phi_2(\omega) \in \mathcal{C}^0(\overline{I}; H^1(\Omega))$ with

$$
\nabla \phi_2(\omega)(t) = \int_0^t \nabla \omega(s)\, \mathrm{d}s \quad \text{for all } t \in I.
\tag{2.18}
$$

---

[a] This especially implies that $\phi_2 : L^\infty(Q) \to L^p(Q)$ is continuous by means of the embedding $L^\infty(Q) \hookrightarrow L^p(Q)$.

The main ingredients of the proof of Lemma 2.7 are Fubini's theorem and some rules of calculus in Bochner spaces. We provide it in detail in Appendix A.1.3.

Remark 2.8 — Integral operator.
The integral operator ϕ_2 in (2.16) is not continuous as map from $L^\infty(Q)$ to $L^\infty(Q)$, like already observed in [219, Sec. 2.1, Rem. 2.2, p. 7]. The reason is that the spaces $L^\infty(Q)$ and $L^\infty(I; L^\infty(\Omega))$ are not isometric isomorph, see Lemma B.49.

---

[17] The function d_{Arr} (2.9) is an element of $\mathcal{C}^2(\mathbb{R})$ with the first and second derivatives

$$
d'_{\mathrm{Arr}}(\omega) = \begin{cases} EA \exp(-\frac{E}{\omega}) \frac{1}{\omega^2}, & \omega > 0, \\ 0, & \omega \leq 0 \end{cases} \quad \text{and} \quad d''_{\mathrm{Arr}}(\omega) = \begin{cases} EA \exp(-\frac{E}{\omega}) \frac{E - 2\omega}{\omega^4}, & \omega > 0, \\ 0, & \omega \leq 0. \end{cases}
$$

The continuity in $\omega = 0$ can be checked using L'Hôpital's rule [69, §16, Thm. 10, p. 190].

We obtain the following result for the nonlinear coefficients, which was given analogously for $\omega \in \mathcal{C}^0(\overline{Q})$ in [219, Sec. 2.1, Lem. 2.1, p. 7] in the context of the classical LITT model.

Lemma 2.9 — Coagulation depending coefficients.

1. For fixed $\omega \in L^\infty(Q)$, the coefficients $\sigma_\mathrm{a}(\omega), D(\omega)$ in equation (2.8) are elements in $L^\infty(Q)$ with positive lower and upper bounds, i.e.,

$$0 < \underline{f} \le f(\omega) \le \overline{f} \quad \text{a.e. in } Q \tag{2.19}$$

for $f \in \{\sigma_\mathrm{a}, D\}$ and $\underline{f}, \overline{f} \in \mathbb{R}_{>0}$. The bounds $\underline{f}, \overline{f}$ are independent of ω. Furthermore, for a.a. $t \in I$, it holds[a] that $f(\omega)(t) \in L^\infty(\Omega)$ and

$$0 < \underline{f} \le f(\omega)(t) \le \overline{f} \quad \text{a.e. in } \Omega \tag{2.20}$$

with the same bounds as in estimate (2.19).

2. For each $M \in \mathbb{R}_{>0}$, there is a $C(M) \in \mathbb{R}_{>0}$ such that for all $\omega, \hat{\omega} \in L^\infty(Q)$ with $\|\omega\|_{L^\infty(Q)} \le M$, $\|\hat{\omega}\|_{L^\infty(Q)} \le M$ it holds

$$\|f(\omega) - f(\hat{\omega})\|_{L^p(Q)} \le C(M)\,\|\omega - \hat{\omega}\|_{L^p(Q)} \tag{2.21}$$

for $f \in \{\sigma_\mathrm{a}, D\}$ and all $p \in [1, \infty)$.

---
[a] We note that this does not imply $f \in L^\infty(I; L^\infty(\Omega))$ because f is not necessarily Bochner measurable.

For the proof of Lemma 2.9, we write the coefficients σ_a, D as concatenation of the maps ϕ_i, $i \in \{1, \dots, 4\}$ and the function $(\cdot)^{-1}$, and use the properties of those auxiliary maps. A detailed proof is given in Appendix A.1.4.

Remark 2.10

Analogously to [219, Sec. 2.1, Rem. 2.2, p. 7], we would like to stress that the estimate (2.21) holds only for $p < \infty$.

The chain rule yields that higher regularity assumptions on ω translate to the absorption coefficient $\sigma_\mathrm{a}(\omega)$. We need this result later in Lemma 2.14 to show a certain regularity of the fixed point.

Lemma 2.11 — $H^1(\Omega)$ regularity of the absorption coefficient.

For $\omega \in L^\infty(Q) \cap L^2(I; H^1(\Omega))$, we get $\sigma_\mathrm{a}(\omega) \in L^2(I; H^1(\Omega))$ with

$$|\nabla \sigma_\mathrm{a}(\omega)(t)| \le C \int_0^t |\nabla \omega(s, \cdot)|\, \mathrm{d}s \quad \text{for a.a. } t \in I,$$

where C depends neither on ω nor on t.

The proof of Lemma 2.11 is rather short and is given in Appendix A.1.5.

Radiation equation

We look at the radiation equation in the auxiliary problem (2.12), which can be solved independently of ϑ: For $\omega \in L^2(Q)$, find $\phi \in L^p(I; W^{1,p}(\Omega))$, for a suitable $p > 2$, such that

$$\int_0^T F_{\mathrm{r}}(\phi(t), \varphi(t); [\omega]_M, t)\,\mathrm{d}t = \int_0^T (g_{\mathrm{r}}, \varphi(t))_{L^2(\Gamma)}\,\mathrm{d}t \tag{2.22}$$

for all $\varphi \in L^2(I; H^1(\Omega))$.

The existence and uniqueness of such a solution was answered similarly to our next Lemma in [219, Sec. 2.2, Lem. 2.3, p. 8] in the context of the classical LITT model.

Lemma 2.12 — Solution of the radiation equation.

Let Assumptions 2.1 and 2.2 hold, and let $\omega \in L^2(Q)$. Then, for a certain $p \in (2, 6)$, which is independent of ω, there *exists* a *unique* solution $\phi \in L^r(I; W^{1,p}(\Omega))$ which fulfills equation (2.22) for all $\varphi \in L^2(I; H^1(\Omega))$, for all $r \in [1, \infty)$, with the following properties.

1. There is a constant $C(T, r) \in \mathbb{R}_{>0}$ such that

$$\|\phi\|_{L^r(I; W^{1,p}(\Omega))} \leq C(T, r)\,\|g_{\mathrm{r}}\|_{L^\infty(\Gamma)}\,.$$

   The constant $C(T, r)$ depends on the final time T, the parameter r, the domain Ω and the upper and lower bounds of the coefficients σ_{a}, D. Especially, it does not depend on ω.

2. There is a constant $C \in \mathbb{R}_{>0}$, which is independent of ω, such that, for a.a. $t \in I$, it holds[a] $\phi(t) \in W^{1,p}(\Omega) \cap \mathcal{C}^0(\overline{\Omega})$ with

$$\|\phi(t)\|_{W^{1,p}(\Omega)} + \|\phi(t)\|_{\mathcal{C}^0(\overline{\Omega})} \leq C\,\|g_{\mathrm{r}}\|_{L^\infty(\Gamma)}\,. \tag{2.23}$$

   The constant C depends on the domain Ω and the upper and lower bounds of the coefficients σ_{a}, D. Especially, it does not depend on ω.

3. The map $L^2(Q) \to L^2(I; H^1(\Omega))$, $\omega \mapsto \phi(\omega)$, where $\phi(\omega)$ is the solution of (2.22), is continuous.

---
[a] We point out that this does *not* imply $\phi \in L^\infty(I; W^{1,p}(\Omega) \cap \mathcal{C}^0(\overline{\Omega}))$.

The results are stated in parts in [219, Sec. 2.2, Lem. 2.3, p. 8] and we refer to Appendix A.1.6 for details.

Note that the laser power entering the physical system via the boundary Γ_{rad} is included in the model through the parameter g_{r}.

Heat-transfer equation

Next, we look at the heat-transfer equation in the auxiliary problem (2.12), which depends on the already computed solution $\phi = \phi(\omega)$ of equation (2.22): For $\omega \in L^2(Q)$, find $\vartheta \in W_\vartheta \cap \mathcal{C}^0(\overline{Q})$ such that

$$
\left\{
\begin{array}{c}
\displaystyle\int_0^T \tau \langle \vartheta''(t), \varphi(t) \rangle_{H^1(\Omega)} + (\vartheta'(t), \varphi(t))_{L^2(\Omega)} + F_\mathrm{h}(\vartheta(t), \varphi(t)) \, \mathrm{d}t \\[2mm]
= \displaystyle\int_0^T \left\langle f_\mathrm{h}\left([\omega]_M, t, \phi(t)\right), \varphi(t) \right\rangle_{H^1(\Omega)} \mathrm{d}t, \\[2mm]
\vartheta(0) = \vartheta^{(0)}, \\[1mm]
\vartheta'(0) = \vartheta^{(1)}
\end{array}
\right\}
\tag{2.24}
$$

for all $\varphi \in L^2(I; H^1(\Omega))$.

Lemma 2.13 — Solution of the auxiliary heat-transfer equation.

Let Assumptions 2.1 and 2.2 hold, and let $\omega \in L^2(Q)$, $\phi \in L^2(I; L^2(\Omega))$. Then there *exists* a *unique* solution

$$
\vartheta \in L^\infty(I; H^1(\Omega)) \cap W^{1,\infty}(I; L^2(\Omega)) \cap H^1(I; H^1(\Omega)) \cap H^2(I; H^1(\Omega)^*) \hookrightarrow W_\vartheta
$$

which fulfills equation (2.24) for all $\varphi \in L^2(I; H^1(\Omega))$, with the following properties.

1. There is a constant $C(\tau^{-1}, \underline{\xi}, \overline{\xi}) \in \mathbb{R}_{>0}$, which is independent of ω, such that

$$
\begin{aligned}
&\|\vartheta\|_{W_\vartheta} \\
&\leq C \left(\|\vartheta\|_{L^\infty(I; H^1(\Omega))} + \|\vartheta'\|_{L^\infty(I; L^2(\Omega))} + \|\vartheta'\|_{L^2(I; H^1(\Omega))} + \|\vartheta''\|_{L^2(I; H^1(\Omega)^*)} \right) \\
&\leq C(\tau^{-1}, \underline{\xi}, \overline{\xi}).
\end{aligned}
\tag{2.25}
$$

2. The map $L^2(Q) \to W_\vartheta$, $\omega \mapsto \vartheta(\phi(\omega), \omega)$ is continuous, where $\phi(\omega) \in L^p(I; W^{1,p}(\Omega))$ is the solution of equation (2.22) according to Lemma 2.12.

Proof.   1. The heat-transfer equation in the auxiliary problem (2.24) (with fixed right-hand side for given ω) corresponds to a standard second-order evolution problem in t. In the appendix, we provide Lemma A.4 for a general discussion on this type of equation. We need to show here only that we can write the right-hand side as

$$
\int_0^T \left\langle f_\mathrm{h}\left([\omega]_M, t, \phi(t)\right), \varphi(t) \right\rangle_{H^1(\Omega)} \mathrm{d}t = \int_0^T (r(t), \varphi(t))_{L^2(\Omega)} + (g(t), \varphi(t))_{L^2(\Gamma)} \, \mathrm{d}t
$$

for all $\varphi \in L^2(I; H^1(\Omega))$, for some $r \in L^2(I; L^2(\Omega))$ and $g \in L^2(I; L^2(\Gamma))$.

With $\hat{\sigma}\sigma_\mathrm{a}\left([\omega]_M\right) \in L^\infty(Q)$ and $\phi \in L^2(Q)$, we get with Hölder's inequality[18]

$$
\hat{\sigma}\sigma_\mathrm{a}\left([\omega]_M\right) \phi \in L^2(Q) \cong L^2(I; L^2(\Omega)),
\tag{2.26}
$$

where we refer to Lemma B.49 for the relation between Bochner and Lebesgue spaces.

---

[18] See Hölder's inequality B.27.

Assumption 2.2 yields $\vartheta_b \xi \in L^\infty(\Omega)$, so, overall, we get

$$r := \hat{\sigma}\sigma_a \left(\left[\omega \right]_M \right) \phi + \vartheta_b \xi \in L^2(I; L^2(\Omega)).$$

Furthermore, Assumption 2.2 yields $g_h \in L^\infty(\Gamma)$ and, with this, $g := g_h \in L^2(I; L^2(\Gamma))$.

The statement now follows directly from Lemma A.4.

2. The next statement follows from a standard procedure.

> Repeat the argument above for the difference of two solutions.

Let $\omega, \hat{\omega} \in L^2(Q)$ and let $\vartheta = \vartheta(\phi(\omega), \omega), \hat{\vartheta} = \vartheta(\phi(\hat{\omega}), \hat{\omega})$ be the corresponding solutions. Then the difference $\delta\vartheta := \vartheta - \hat{\vartheta}$ fulfills

$$\left\{ \begin{aligned} \int_0^T \tau \left\langle \delta\vartheta''(t), \varphi(t) \right\rangle_{H^1(\Omega)} + (\delta\vartheta'(t), \varphi(t))_{L^2(\Omega)} + F_h(\delta\vartheta(t), \varphi(t)) \, \mathrm{d}t \\ = \int_0^T (r(t), \varphi(t))_{L^2(\Omega)} + (g(t), \varphi(t))_{L^2(\Gamma)} \, \mathrm{d}t, \\ \delta\vartheta(0) = 0, \\ \delta\vartheta'(0) = 0 \end{aligned} \right.$$

for all $\varphi \in L^2(I; H^1(\Omega))$, with[19]

$$\begin{aligned} r &= \hat{\sigma}(\sigma_a - \hat{\sigma}_a)(t)\phi(t) + \hat{\sigma}\hat{\sigma}_a(t)(\phi - \hat{\phi})(t), \\ g &= 0 \end{aligned} \tag{2.27}$$

and the short-hand notation $\sigma_a := \sigma_a([\omega]_M), \hat{\sigma}_a := \sigma_a([\hat{\omega}]_M), \phi := \phi(\omega), \hat{\phi} := \phi(\hat{\omega})$. Analogously to (2.26), we get $r \in L^2(I; L^2(\Omega))$. Furthermore, with the pointwise bounds for $\sigma_a(t)$ and $\phi(t)$ in Lemmas 2.9 and 2.12, we get

$$\begin{aligned} \|r(t)\|_{L^2(\Omega)} &\leq \|\hat{\sigma}(\sigma_a - \hat{\sigma}_a)(t)\phi(t)\|_{L^2(\Omega)} + \left\| \hat{\sigma}\hat{\sigma}_a(t)(\phi - \hat{\phi})(t) \right\|_{L^2(\Omega)} \\ &\leq C \left(\|(\sigma_a - \hat{\sigma}_a)(t)\|_{L^2(\Omega)} + \left\| (\phi - \hat{\phi})(t) \right\|_{L^2(\Omega)} \right) \end{aligned}$$

for a.a. $t \in I$ and, thus, with Young's inequality[20] that

$$\|r\|^2_{L^2(I;L^2(\Omega))} \leq C \left(\|\sigma_a - \hat{\sigma}_a\|^2_{L^2(Q)} + \left\| \phi - \hat{\phi} \right\|^2_{L^2(Q)} \right). \tag{2.28}$$

Like in the first part of the proof, Lemma A.4 implies

$$\delta\vartheta \in L^\infty(I; H^1(\Omega)) \cap W^{1,\infty}(I; L^2(\Omega)) \cap H^1(I; H^1(\Omega))$$

with

$$\|\delta\vartheta\|_{L^\infty(I;H^1(\Omega))} + \|\delta\vartheta'\|_{L^\infty(I;L^2(\Omega))} + \|\delta\vartheta'\|_{L^2(I;H^1(\Omega))} \leq C \|r\|_{L^2(I;L^2(\Omega))} \tag{2.29}$$

---

[19] Note that $\phi, \hat{\phi} \in L^p(I; W^{1,p}(\Omega))$ for some $p > 2$ and $\sigma_a, \hat{\sigma}_a \in L^q(I; L^q(\Omega))$ for all $q \in [1, \infty)$. Hölder's inequality yields that the integrals in equation (2.27) are well defined.

[20] See Young's inequality B.25.

and, thus, with Hölder's inequality that

$$
\begin{aligned}
&\left| \langle \delta\vartheta'', \varphi \rangle_{L^2(I;H^1(\Omega))} \right| \\
&= \frac{1}{\tau} \left| \int_0^T -(\delta\vartheta'(t), \varphi(t))_{L^2(\Omega)} - F_{\mathrm{h}}(\delta\vartheta(t), \varphi(t)) + (r(t), \varphi(t))_{L^2(\Omega)} \, \mathrm{d}t \right| \\
&\leq C \left(\|\delta\vartheta'\|_{L^2(I;L^2(\Omega))} + \|\delta\vartheta\|_{L^2(I;H^1(\Omega))} + \|r\|_{L^2(I;L^2(\Omega))} \right) \|\varphi\|_{L^2(I;H^1(\Omega))} \\
&\leq C \|r\|_{L^2(I;L^2(\Omega))} \|\varphi\|_{L^2(I;H^1(\Omega))} .
\end{aligned}
\tag{2.30}
$$

We combine the estimates (2.28)–(2.30) and get

$$
\|\delta\vartheta\|_{W_\vartheta}^2 \leq C \left(\|\sigma_{\mathrm{a}} - \hat{\sigma}_{\mathrm{a}}\|_{L^2(Q)}^2 + \left\| \phi - \hat{\phi} \right\|_{L^2(Q)}^2 \right).
\tag{2.31}
$$

Together with the continuity of the cutoff operator $[\,\cdot\,]_M : L^2(Q) \to L^2(Q)$, the Lipschitz continuity of the optical coefficients in (2.21) and the continuity of the map $\omega \mapsto \phi(\omega)$ in Lemma 2.12, estimate (2.31) yield that ϑ is continuous w.r.t. ω, i.e., $\hat{\omega} \to \omega$ in $L^2(Q)$ implies $\hat{\vartheta} \to \vartheta$ in W_ϑ.

∎

As a prerequisite for two main results of this thesis, Theorems 2.15 and 3.3, we need the following regularity result for fixed points of the operator S defined in (2.13).

Lemma 2.14 — Regularity of fixed points.

Let Assumptions 2.1 and 2.2 hold. Then every fixed point $\vartheta \in L^2(Q)$ of the operator S defined in (2.13) fulfills

$$
\vartheta \in L^\infty(I; H^1(\Omega)) \cap W^{1,\infty}(I; L^2(\Omega)) \cap H^2(I; H^1(\Omega)^*) \cap \mathcal{C}^{0,\alpha}(\overline{Q}) =: B_\alpha
$$

for all $\alpha \in [0, \frac{1}{4})$, and there is a constant $C(\tau^{-1}, \alpha, \underline{\xi}, \overline{\xi}) \in \mathbb{R}_{>0}$ such that[a]

$$
\|\vartheta\|_{W_\vartheta} + \|\vartheta\|_{\mathcal{C}^{0,\alpha}(\overline{Q})} \leq C \|\vartheta\|_{B_\alpha} \leq C(\tau^{-1}, \alpha, \underline{\xi}, \overline{\xi}).
$$

Furthermore, the fixed point ϑ is an element of $W^{1,p_1}(I; H^1(\Omega)) \cap L^{p_2}(I; H^2(\Omega))$ with

$$
\|\vartheta\|_{W^{1,p_1}(I;H^1(\Omega))} + \|\vartheta\|_{L^{p_2}(I;H^2(\Omega))} \leq C(\tau^{-1}, p_1, p_2, \underline{\xi}, \overline{\xi})
$$

for all $p_1, p_2 \in (1, \infty)$.

Especially, the constants $C(\tau^{-1}, \alpha, \underline{\xi}, \overline{\xi}), C(\tau^{-1}, p_1, p_2, \underline{\xi}, \overline{\xi})$ do not depend on the particular fixed point ϑ and, thus, bound all fixed points of S.

---
[a] The norm of B_α is given as the sum of the particular norms of the intersecting spaces.

Proof. Let $\vartheta \in L^2(Q)$ be a fixed point. Then it fulfills the auxiliary heat-transfer equation (2.24) for $\omega = \vartheta$, and we can apply a bootstrap argument to show that ϑ has in fact a higher regularity. This means, if we consider the right-hand side in (2.24) for the given ϑ as fixed, then ϑ still fulfills the heat-transfer equation (2.24) and we can apply regularity results for this type of equation, as discussed in Lemma A.4.

To this, we need to find $r_2 \in H^1(I; L^2(\Omega))$, $g \in H^{1/2}(\Gamma)$, and $r_1 \in L^2(I; L^2(\Omega))$ with $r_1(t) \in H^1(\Omega)$ and $\|r_1(t)\|_{H^1(\Omega)} \leq \tilde{r}(t)$ for a.a. $t \in I$, for some $\tilde{r} \in L^2(I)$, such that for all $\varphi \in L^2(I; H^1(\Omega))$ it holds

$$\int_0^T \left\langle f_{\mathrm{h}} \left(\left[\omega \right]_M, t, \phi(t) \right), \varphi(t) \right\rangle_{H^1(\Omega)} \mathrm{d}t$$
$$= \int_0^T (r_1(t), \varphi(t))_{L^2(\Omega)} + (r_2(t), \varphi(t))_{L^2(\Omega)} + (g, \varphi(t))_{L^2(\Gamma)} \, \mathrm{d}t \,.$$

We define

$$r_1 := \hat{\sigma}\sigma_{\mathrm{a}} \left(\left[\vartheta \right]_M \right) \phi \left(\left[\vartheta \right]_M \right), \qquad r_2 := \vartheta_{\mathrm{b}}\xi, \quad g := g_{\mathrm{h}}.$$

First, we note that Lemma 2.13 implies $\vartheta \in L^2(I; H^1(\Omega))$ for the fixed point. Furthermore, Equation (2.26) implies $r_1 \in L^2(I; L^2(\Omega))$.

The cutoff function $\left[\cdot \right]_M \colon \mathbb{R} \to \mathbb{R}$, $x \mapsto \min(\max(x, -M), M)$, for a given $M \in \mathbb{R}_{>0}$, is Lipschitz continuous[21], which yields together with the chain rule given in Lemma B.41 that $\left[\vartheta \right]_M \in L^\infty(Q) \cap L^2(I; H^1(\Omega))$.

From Lemmas 2.9 and 2.11 we get that $\hat{\sigma}\sigma_{\mathrm{a}} \left(\left[\vartheta \right]_M \right)(t) \in L^\infty(\Omega) \cap H^1(\Omega)$ for a.a. $t \in I$, and from Lemma 2.12 that $\phi(t) \in L^\infty(\Omega) \cap H^1(\Omega)$ for a.a. $t \in I$. The product rule[22] now implies $r_1(t) \in H^1(\Omega)$. Furthermore, it holds with $\sigma_{\mathrm{a}} := \sigma_{\mathrm{a}} \left(\left[\vartheta \right]_M \right)$ and the bounds in Lemmas 2.9, 2.11 and 2.12 that

$$\left| \nabla \left(\sigma_{\mathrm{a}}(t)\phi(t) \right) \right| \leq \left| \phi(t)\nabla\sigma_{\mathrm{a}}(t) \right| + \left| \sigma_{\mathrm{a}}(t)\nabla\phi(t) \right| \leq C \left(\|\vartheta\|_{L^2(I;H^1(\Omega))} + \|g_{\mathrm{r}}\|_{L^\infty(\Gamma)} \right) =: \tilde{r}(t).$$

With Bochner's theorem[23], we get that $\tilde{r} \in L^2(I)$ and that $\|r_1(t)\|_{H^1(\Omega)} \leq \tilde{r}(t)$ holds for a.a. $t \in I$ as desired.

Assumption 2.2 implies $g \in H^{1/2}(\Gamma)$ and $r_2 \in L^\infty(\Omega)$, which yields $r_2 \in H^1(I; L^2(\Omega))$.

This allows us to apply Lemma A.4 to the auxiliary heat-transfer equation (2.24) for $\omega = \vartheta$, which yields the desired regularity and estimates. ∎

---

[21] The functions

$$f \colon \mathbb{R} \to \mathbb{R}, \ x \mapsto \min(x, M) \quad \text{and} \quad \hat{f} \colon \mathbb{R} \to \mathbb{R}, \ x \mapsto \max(x, -M)$$

are Lipschitz continuous, for all $M \in \mathbb{R}_{>0}$. In fact, for $x, y \in \mathbb{R}$, it holds

$$|f(x) - f(y)| = |\min(x, M) - \min(y, M)| = \begin{cases} |x - y|, & x \leq M, y \leq M, \\ |x - M|, & x \leq M, y > M, \\ |M - y|, & x > M, y \leq M, \\ 0, & \text{else} \end{cases} \leq |x - y| \,.$$

The estimate for $\hat{f}$ can be shown analogously. Thus, the cutoff function is Lipschitz continuous as concatenation of Lipschitz continuous functions.

[22] See the product rule for weak derivatives in Theorem B.43.

[23] See Bochner's theorem B.47.

Coupled system

We are now ready to prove the main result of this section on the existence of a state vector, cf.
[219, Sec. 2.4, Thm. 2.2, p. 10].

Theorem 2.15 — Existence of state vectors.

Let Assumptions 2.1 and 2.2 hold. Then, for a certain $p \in (2,6)$, there exists a state vector of
the Cattaneo–LITT model $(\phi, \vartheta) \in \mathcal{Y}_p$ with

$$\|\phi\|_{L^p(I;W^{1,p}(\Omega))} \leq C,$$

$$\|\vartheta\|_{W_\vartheta} + \|\vartheta\|_{\mathcal{C}^0(\overline{Q})} \leq C_1(\tau^{-1}, \underline{\xi}, \overline{\xi})$$

for some constants C, C_1.
It holds $\phi \in L^r(I; W^{1,p}(\Omega))$, for all $r \in [1, \infty)$, and[a]

$$\vartheta \in L^\infty(I; H^1(\Omega)) \cap W^{1,\infty}(I; L^2(\Omega)) \cap W^{1,p_1}(I; H^1(\Omega)) \cap L^{p_2}(I; H^2(\Omega)) =: B_{p_1, p_2}$$

with[b]

$$\|\vartheta\|_{B_{p_1, p_2}} \leq C(\tau^{-1}, p_1, p_2, \underline{\xi}, \overline{\xi})$$

for all $p_1, p_2 \in (1, \infty)$. Furthermore, it holds $\vartheta \in \mathcal{C}^{0,\alpha}(Q)$ with

$$\|\vartheta\|_{\mathcal{C}^{0,\alpha}(\overline{Q})} \leq C(\tau^{-1}, \alpha, \underline{\xi}, \overline{\xi})$$

for all $\alpha \in [0, \frac{1}{4})$.

---
[a] This means that ϑ is an element of $L^\infty(I; H^1(\Omega))$, which coincides with an element of $W^{1,\infty}(I; L^2(\Omega))$ a.e. in Q,
     etc.
[b] The norm of B_{p_1, p_2} is given as the sum of the particular norms of the intersecting spaces.

Remark 2.16 — State bounds in Theorem 2.15 are independent of the blood-perfusion rate.
We point out that the constants which appear in the state bounds in Theorem 2.15 depend
on the upper and lower bounds of the blood-perfusion rate ξ but not on ξ itself. This
will be important in Chapter 3, where we formulate the identification of the unknown
blood-perfusion rate in terms of an optimal-control problem.

Proof of Theorem 2.15.

Apply the Leray–Schauder fixed-point theorem to the operator S defined in (2.13).

The proof is basically identical to the proof of [219, Sec. 2.4, Thm. 2.2, p. 10] and we follow it step
by step. We need only to exchange the classical heat-transfer model therein by our Cattaneo heat
equation and adapt the corresponding spaces.

With the help of the Leray–Schauder fixed-point theorem[24] we show the existence of a fixed
point of the operator S, which is defined as

$$S \colon L^2(Q) \times [0,1] \to L^2(Q), \ (\omega, \rho) \mapsto \vartheta \tag{2.13}$$

---
[24] See the Leray–Schauder fixed-point theorem B.64.

such that ϑ fulfills the heat-transfer equation in (2.12) for all $\varphi \in L^2(I; H^1(\Omega))$.

Let $\omega \in L^2(Q)$. For the sake of completeness, we mention that $L^2(\Omega)$ is Banach space.[25] Lemmas 2.12 and 2.13 yield unique solutions $\phi(\omega) \in L^p(I; W^{1,p}(\Omega))$, for a certain $p > 2$, and $\vartheta(\phi(\omega), \omega) \in W_\vartheta \hookrightarrow L^2(Q)$ of the subproblems (2.22) and (2.24), thus, the operator S is well defined.

Furthermore, with the same lemmas, the map $L^2(Q) \to W_\vartheta$, $\omega \mapsto \vartheta(\phi(\omega), \omega)$ is continuous. The continuity of S w.r.t. ρ follows directly from estimate (A.20) combined with estimate (2.23). Overall, this yields the continuity of S.

With the theorem of Aubin–Lions[26], we get the compact embedding

$$W_\vartheta \hookrightarrow L^2(I; H^1(\Omega)) \cap H^1(I; L^2(\Omega)) \hookrightarrow\hookrightarrow L^2(I; L^2(\Omega)) \cong L^2(Q),$$

where the last isometric isomorphism follows from Lemma B.49. The operator S is compact as a chain of compact and continuous operators.[27]

Note that for $\rho = 0$, we get the unique solution $\vartheta = 0$, thus,

$$S(\omega, 0) = 0 \quad \text{for all } \omega \in L^2(Q).$$

For a fixed point $\vartheta^* = S(\vartheta^*, 1)$, it follows from Lemma 2.14 that $\vartheta^* \in W_\vartheta \cap \mathcal{C}^{0,\alpha}(\overline{Q})$ for $\alpha \in [0, \frac{1}{4})$ with

$$\|\vartheta^*\|_{\mathcal{C}^{0,\alpha}(\overline{Q})} + \|\vartheta^*\|_{W_\vartheta} \le C(\tau^{-1}).$$

Especially, this implies $\vartheta^* \in \mathcal{C}^0(\overline{Q})$ and

$$\|\vartheta^*\|_{L^2(Q)} \le C \|\vartheta^*\|_{\mathcal{C}^0(\overline{Q})} \le C(\tau^{-1}). \tag{2.32}$$

We point out that the constant $C(\tau^{-1})$ in estimate (2.32) does not depend on the bound M of the cutoff function, and it depends neither on ω nor on the fixed point itself. This allows us to increase M for each fixed point ϑ^* until $\left[\vartheta^*\right]_M = \vartheta^*$, without affecting estimate (2.32).

By means of the Leray–Schauder fixed-point theorem B.64, we get the existence of a fixed point $\vartheta^* \in L^2(Q)$ of $S(\cdot, 1)$, which is in fact an element of $W_\vartheta \cap \mathcal{C}^{0,\alpha}(\overline{Q})$ as seen before. Lemma 2.12 now yields the corresponding solution of the radiation equation $\phi = \phi(\vartheta^*) \in L^p(I; W^{1,p}(\Omega))$, for a certain $p \in (2, 6)$. With the consideration above, it holds $\left[\vartheta^*\right]_M = \vartheta^*$, thus, we can omit the cutoff function in the auxiliary problem for the fixed point ϑ^*. Together with the embedding in Theorem B.59, this implies that $(\phi, \vartheta^*) \in \mathcal{Y}_p$ is in fact a state vector of the Cattaneo–LITT model (2.10). The state bounds now follow from Lemmas 2.12 and 2.14. $\blacksquare$

---

[25] See Lemma B.12 on reflexive Banach spaces.
[26] See the Aubin–Lions theorem B.61 regarding $X_0 = H^1(\Omega)$, $X = L^2(\Omega)$, $X_1 = H^1(\Omega)^*(\Omega)$. Note that $H^1(\Omega)$ is reflexive (Lemma B.24) and, thus, $H^1(\Omega)^*(\Omega)$ is reflexive as its dual (Lemma B.12).
[27] See Lemma B.19 on the concatenation of continuous and compact operators.

2.2.3 Uniqueness

The proof of Theorem 2.15 is based on the Leray–Schauder fixed-point theorem, which does not give us any information on the uniqueness of the state vector of the Cattaneo–LITT model. We prove its uniqueness in the following Theorem (cf. [219, Sec. 2.5, Thm. 2.3, p. 11]).

> **Theorem 2.17 — Uniqueness of the state vector.**
> Let Assumptions 2.1 and 2.2 hold. The state vector of the Cattaneo–LITT model $(\phi, \vartheta) \in \mathcal{Y}_p$, $p \geq 2$, is unique.

Proof.

> Take the difference of the state equations (2.10) for two state vectors and apply Gronwall's inequality.

Let $(\phi_1, \vartheta_1), (\phi_2, \vartheta_2) \in \mathcal{Y}_p$, $p > 2$, be two state vectors of the Cattaneo–LITT model (2.10). We write $\sigma_{\mathrm{a}i} := \sigma_{\mathrm{a}}(\vartheta_i), D_i := D(\vartheta_i), i \in \{1, 2\}$.

Furthermore, for this proof, we assume that there is a $\hat{p} > 3$ and a $C \in \mathbb{R}_{>0}$ such that

$$\phi_i(t) \in W^{1,\hat{p}}(\Omega) \quad \text{and} \quad \|\phi_i(t)\|_{W^{1,\hat{p}}(\Omega)} \leq C \quad \text{for a.a. } t \in I, i \in \{1, 2\}. \tag{2.33}$$

In Remark 2.18, we justify this assumption.

The difference $(\delta\phi, \delta\vartheta) := (\phi_1 - \phi_2, \vartheta_1 - \vartheta_2)$ fulfills

$$\begin{cases} \displaystyle\int_0^T F_{\mathrm{r}}(\delta\phi(t), \varphi_1(t); \vartheta_1, t) + ((D_1(t) - D_2(t))\nabla\phi_2(t), \nabla\varphi_1(t))_{L^2(\Omega)} \\ \qquad\qquad + ((\sigma_{\mathrm{a}1}(t) - \sigma_{\mathrm{a}2}(t))\phi_2(t), \varphi_1(t))_{L^2(\Omega)} \, \mathrm{d}t = 0, \\ \displaystyle\int_0^T \tau \langle \delta\vartheta''(t), \varphi_2(t) \rangle_{H^1(\Omega)} + (\delta\vartheta'(t), \varphi_2(t))_{L^2(\Omega)} + F_{\mathrm{h}}(\delta\vartheta(t), \varphi_2(t)) \, \mathrm{d}t \\ \qquad = \hat{\sigma} \displaystyle\int_0^T (\sigma_{\mathrm{a}1}\delta\phi(t), \varphi_2(t))_{L^2(\Omega)} + ((\sigma_{\mathrm{a}1}(t) - \sigma_{\mathrm{a}2}(t))\phi_2(t), \varphi_2(t))_{L^2(\Omega)} \, \mathrm{d}t, \\ \delta\vartheta(0) = 0, \\ \delta\vartheta'(0) = 0 \end{cases} \tag{2.34}$$

for all $\varphi = (\varphi_1, \varphi_2) \in L^2(I; H^1(\Omega)) \times L^2(I; H^1(\Omega))$. Similarly to [93, Sec. 1.3.2.3, Thm. 1.33, p. 42], we can look at the first equation of (2.34) for single points in time, and it holds for a.a. $t \in I$ that

$$\begin{aligned} F_{\mathrm{r}}(\delta\phi(t), \varphi_1; \vartheta_1, t) = -&((D_1(t) - D_2(t))\nabla\phi_2(t), \nabla\varphi_1)_{L^2(\Omega)} \\ -&((\sigma_{\mathrm{a}1}(t) - \sigma_{\mathrm{a}2}(t))\phi_2(t), \varphi_1)_{L^2(\Omega)} \end{aligned} \tag{2.35}$$

for all $\varphi_1 \in H^1(\Omega)$. We test equation (2.35) with $\varphi_1 = \delta\phi(t) \in H^1(\Omega)$, and obtain with the coercivity of the bilinear form $F_{\mathrm{r}}(\cdot, \cdot; \vartheta_1, t) \colon H^1(\Omega) \times H^1(\Omega) \to \mathbb{R}$, the bounds on $\phi_2(t)$ in (2.23), and Hölder's and Young's inequalities[28] that

$$\begin{aligned} \|\delta\phi(t)\|_{H^1(\Omega)}^2 &\leq C \|\phi_2(t)\|_{W^{1,\hat{p}}(\Omega)}^2 \left(\|D_1(t) - D_2(t)\|_{L^q(\Omega)}^2 + \|\sigma_{\mathrm{a}1}(t) - \sigma_{\mathrm{a}2}(t)\|_{L^q(\Omega)}^2 \right) \\ &\leq C \left(\|D_1(t) - D_2(t)\|_{L^q(\Omega)}^2 + \|\sigma_{\mathrm{a}1}(t) - \sigma_{\mathrm{a}2}(t)\|_{L^q(\Omega)}^2 \right) \end{aligned} \tag{2.36}$$

---

[28] See Hölder's B.27 and Young's B.25 inequalities.

for a.a. $t \in I$, and $q = 2\hat{p}(\hat{p} - 2)^{-1}$.

Next, we look at the second equation in (2.34) for a single point in time $t \in I$, and test with $\varphi_2 = \delta\vartheta'(t) \in H^1(\Omega)$.

We get with the derivative of the norm in Lemma B.38, Hölder's and Young's inequalities, the coercivity of the bilinear form $F_{\mathrm{h}} \colon H^1(\Omega) \times H^1(\Omega) \to \mathbb{R}$, the bounds for $\phi_2(t)$ in (2.23) and the bounds for $\sigma_{\mathrm{a}1}(t)$ in (2.20) that

$$
\left(\|\delta\vartheta'(t)\|^2_{L^2(\Omega)} \right)' + \left(\|\delta\vartheta(t)\|^2_{H^1(\Omega)} \right)' + \|\delta\vartheta'(t)\|^2_{L^2(\Omega)}
$$
$$
\leq C(\varepsilon^{-1}) \left(\|(\sigma_{\mathrm{a}1}(t) - \sigma_{\mathrm{a}2}(t))\phi_2(t)\|^2_{L^2(\Omega)} + \|\sigma_{\mathrm{a}1}(t)\delta\phi(t)\|^2_{L^2(\Omega)} \right) + \varepsilon \|\delta\vartheta'(t)\|^2_{L^2(\Omega)}
$$
$$
\leq C(\varepsilon^{-1}) \left(\|(\sigma_{\mathrm{a}1}(t) - \sigma_{\mathrm{a}2}(t))\|^2_{L^2(\Omega)} + \|\delta\phi(t)\|^2_{L^2(\Omega)} \right) + \varepsilon \|\delta\vartheta'(t)\|^2_{L^2(\Omega)}
$$

for all $\varepsilon > 0$.

We integrate both sides from 0 to t and get with the fundamental theorem of calculus[29], vanishing initial conditions and estimate (2.36) that

$$
\|\delta\vartheta(t)\|^2_{H^1(\Omega)} \leq C\Big(\int_0^t \|(\sigma_{\mathrm{a}1}(s) - \sigma_{\mathrm{a}2}(s))\|^2_{L^2(\Omega)} \,\mathrm{d}s + \int_0^t \|(\sigma_{\mathrm{a}1}(s) - \sigma_{\mathrm{a}2}(s))\|^2_{L^q(\Omega)} \,\mathrm{d}s
$$
$$
+ \int_0^t \|(D_1(s) - D_2(s))\|^2_{L^q(\Omega)} \,\mathrm{d}s \Big). \tag{2.37}
$$

With $\hat{p} > 3$, we get $q = 2\hat{p}(\hat{p} - 2)^{-1} < 6$ and, thus[30], $L^6(\Omega) \hookrightarrow L^q(\Omega)$. We use this together with the Lipschitz continuity of the coefficients[31] in (2.21) and Hölder's inequality to get

$$
\int_0^t \|f_1(s) - f_2(s)\|^2_{L^q(\Omega)} \,\mathrm{d}s \leq C \int_0^t \|f_1(s) - f_2(s)\|^2_{L^6(\Omega)} \,\mathrm{d}s
$$
$$
\leq C \left(\int_0^t \|f_1(s) - f_2(s)\|^6_{L^6(\Omega)} \,\mathrm{d}s \right)^{1/3} \tag{2.38}
$$
$$
\leq C \left(\int_0^t \|\vartheta_1(s) - \vartheta_2(s)\|^6_{L^6(\Omega)} \,\mathrm{d}s \right)^{1/3}
$$

for $f_i \in \{\sigma_{\mathrm{a}i}, D_i\}$, $i \in \{1, 2\}$.

Similarly, we get with the embedding $L^6(\Omega) \hookrightarrow L^2(\Omega)$ that

$$
\int_0^t \|(\sigma_{\mathrm{a}1}(s) - \sigma_{\mathrm{a}2}(s))\|^2_{L^2(\Omega)} \,\mathrm{d}s \leq C \left(\int_0^t \|\vartheta_1(s) - \vartheta_2(s)\|^6_{L^6(\Omega)} \,\mathrm{d}s \right)^{1/3}.
$$

---

[29] See the fundamental theorem of calculus in Bochner spaces B.33.

[30] See the standard embedding result B.55.

[31] Estimate (2.21) and the constant $C(M)$ therein are stated for the space-time cylinder Q, i.e., at first, we have only the estimate $\int_0^T \|f_1(s) - f_2(s)\|^6_{L^6(\Omega)} \,\mathrm{d}s \leq C \int_0^T \|\vartheta_1(s) - \vartheta_2(s)\|^6_{L^6(\Omega)} \,\mathrm{d}s$, where C potentially depends on T, for $f_i \in \{\sigma_{\mathrm{a}i}, D_i\}$, $i \in \{1, 2\}$. Still, we can use (2.21) to derive estimate (2.38) by the following consideration. Let $\tilde{\vartheta}_i := 1_{(0,t)}\vartheta_i$, where $1_{(0,t)} \colon I \to \{0, 1\}$ is the indicator function of the interval $(0, t)$, and let $\tilde{f}_i \in \{\tilde{\sigma}_{\mathrm{a}i}, \tilde{D}_i\}$ be the corresponding coefficient for $i \in \{1, 2\}$. Then it holds

$$
\int_0^t \|f_1(s) - f_2(s)\|^6_{L^6(\Omega)} \,\mathrm{d}s = \int_0^t \left\|\tilde{f}_1(s) - \tilde{f}_2(s)\right\|^6_{L^6(\Omega)} \,\mathrm{d}s \leq \int_0^T \left\|\tilde{f}_1(s) - \tilde{f}_2(s)\right\|^6_{L^6(\Omega)} \,\mathrm{d}s
$$
$$
\leq C \int_0^T \left\|\tilde{\vartheta}_1(s) - \tilde{\vartheta}_2(s)\right\|^6_{L^6(\Omega)} \,\mathrm{d}s = C \int_0^t \|\vartheta_1(s) - \vartheta_2(s)\|^6_{L^6(\Omega)} \,\mathrm{d}s.
$$

We combine the last two estimates with (2.37) and get[32] with the embedding[33] $H^1(\Omega) \hookrightarrow L^6(\Omega)$ that

$$\|\delta\vartheta(t)\|_{L^6(\Omega)}^6 \leq C \, \|\delta\vartheta(t)\|_{H^1(\Omega)}^6 \leq C \int_0^t \|\delta\vartheta(s)\|_{L^6(\Omega)}^6 \, \mathrm{d}s \,.$$

Gronwall's inequality[34] now yields $\|\delta\vartheta(t)\|_{L^6(\Omega)} = 0$ for a.a. $t \in I$, which implies $\delta\vartheta = 0$ in $L^1(I; L^1(\Omega)) \cong L^1(Q)$ and, thus, $\vartheta_1 = \vartheta_2$ a.e. in Q. The uniqueness of the solution of the radiation equation (2.22), see Lemma 2.12, now implies $\phi_1 = \phi_2$. ∎

Remark 2.18 — Regularity of the irradiance.

In the proof of Theorem 2.17, we made the assumption (2.33) that there is a $\hat{p} > 3$ and a $C \in \mathbb{R}_{>0}$ such that

$$\phi_i(t) \in W^{1,\hat{p}}(\Omega) \quad \text{and} \quad \|\phi_i(t)\|_{W^{1,\hat{p}}(\Omega)} \leq C \quad \text{for a.a. } t \in I, i \in \{1,2\}. \tag{2.33}$$

Here, we would like to justify this assumption.

We already know from Theorem 2.15 that, for a certain $p \in (2,6)$, it holds $\phi(t) \in W^{1,p}(\Omega)$ for a.a. $t \in I$. We could proceed like in [219, Sec. 2.5, Rem. 2.5, p. 13], where the authors proposed that $p > 3$ could be obtained by providing sufficiently smooth data and a sufficiently smooth boundary Γ. This would imply further assumptions beyond the ones described in Assumptions 2.1 and 2.2.

Similarly to the proof of Lemma 2.14, we employ the fact that the solution of the radiation equation is more regular if ϑ is more regular. Let $(\phi, \vartheta) \in \mathcal{Y}_p$, $p > 2$, be a state vector of the Cattaneo–LITT model. Similarly to equation (A.39), it holds for a.a. $t \in I$ that

$$(D(\vartheta)(t)\nabla\phi(t), \nabla\varphi(t))_{L^2(\Omega)} + (\sigma_\mathrm{a}(\vartheta)(t)\phi(t), \varphi(t))_{L^2(\Omega)} = (g_\mathrm{r}, \varphi(t))_{L^2(\Omega)} \tag{2.39}$$

for all $\varphi \in H^1(\Omega)$. Note that for finding a fixed-point in the proof of Theorem 2.15, we used only $\vartheta \in L^\infty(Q)$ to prove the regularity for ϕ, whereas now we can employ Hölder continuity of the temperature $\vartheta \in \mathcal{C}^{0,\frac{1}{8}}(\overline{Q})$.

Now we can apply a bootstrap argument to obtain higher regularity of $\phi(t)$. We follow the notation in [6] and define $F := -\sigma_\mathrm{a}(\vartheta)(t)\phi(t)$. With the regularity $\sigma_\mathrm{a}(\vartheta)(t) \in L^\infty(\Omega)$ from Lemma 2.9 and[a] $\phi(t) \in H^1(\Omega) \hookrightarrow\hookrightarrow L^6(\Omega)$, it holds $F \in L^4(\Omega)$.

Furthermore, with $\vartheta(t) \in \mathcal{C}^0(\overline{\Omega})$, we get that $D(\vartheta)(t)$ is uniformly continuous on $\overline{\Omega}$ and, thus, $D(\vartheta)(t)$ is a function of *vanishing mean oscillation* (VMO)[b]. We now obtain $\phi(t) \in W^{1,4}(\Omega)$ for a.a. $t \in I$ directly from [6, Sec. 2, Thm. 2.1, p. 4].

Thus, our assumption (2.33) was justified, which ultimately completes the proof of Theorem 2.17.

---

[32] Use that for $a, b \geq 0$, it holds $(a+b)^3 \leq 7(a^3 + b^3)$.

[33] See standard Sobolev embeddings B.56.

[34] See Gronwall's inequality B.39.

Note that above we employed only the fact that the temperature $\vartheta(t)$ and, thus, the coefficient $D(\vartheta)(t)$ are uniformly continuous on $\overline{\Omega}$. But the coefficient $D(\vartheta)(t)$ is even Hölder continuous. In fact, the coefficient D can be written as the concatenation of a Lipschitz-continuous, thus, Hölder-continuous function (see Lemma 2.9) and ϑ, where ϑ is Hölder continuous as well. A concatenation of Hölder-continuous functions is again Hölder continuous[c].

We do not further investigate the properties of the solution of the radiation equation here, but one might be able to prove even higher regularity for $\phi(t)$. E.g., in [81, Sec. 8.11, Thm. 8.34, p. 211] and [89, Sec. 3.4, Thm. 3.13, p. 60], it is shown that the solution for a similar elliptic problem, also with Hölder-continuous coefficients but instead with Dirichlet boundary conditions, is an element of $\mathcal{C}^{1,\alpha}(\overline{\Omega})$. Also note that we can not directly apply standard results from [85, Ch. 2, p. 81 ff.] because we have only Hölder-continuous coefficients, which are not necessarily Lipschitz continuous.

---

[a] See standard Sobolev embeddings B.56.
[b] See [189] for the definition of *functions of mean vanishing oscillation*. Especially, see [189, Sec. 1, Thm. 1, p. 392] for the implication that uniformly continuous functions are also functions of mean vanishing oscillation.
[c] See [101, Sec. 13.1, Lem. 13.1.1, p. 330] for the fact that the concatenation of Hölder-continuous functions is again Hölder continuous.

2.2.4 Continuous dependence on the data

With Theorems 2.15 and 2.17, we obtain a unique state vector of the Cattaneo–LITT model. For the well-posedness[35], we need to show that this state vector *depends continuously on the data*.

In a real application, basically every physical parameter can be considered as part of the data. In this thesis, the blood-perfusion rate is of special interest. In Chapter 3, we freeze all parameters except for the blood-perfusion rate and demonstrate a strategy to identify this unknown parameter by means of an optimal-control problem. In the next lemma, we restrict ourselves to showing the continuous dependence of the state vector on the blood-perfusion rate.

Lemma 2.19 — Continuous dependence on the blood-perfusion rate.

Let Assumptions 2.1 and 2.2 hold. The state vector of the Cattaneo–LITT model $(\phi, \vartheta) \in \mathcal{Y}_p$, $p > 2$, depends continuously on the blood-perfusion rate ξ, in the sense that the map

$$\Xi_{\mathrm{ad}} \to L^2(I; H^1(\Omega)) \times L^2(I; H^1(\Omega)), \ \xi \to (\phi, \vartheta)$$

is *Lipschitz continuous*, where $\Xi_{\mathrm{ad}} := \{\xi \in L^2(\Omega) \,|\, \underline{\xi} \le \xi \le \overline{\xi} \quad \text{a.e. in } \Omega\} \subset L^2(\Omega)$ is the set of admissible perfusion rates.

Proof.

Take the difference of the state equations (2.10) for two state vectors and apply Gronwall's inequality.

We can repeat the proof of Theorem 2.17 with the only difference that the blood-perfusion rates differ this time.

---

[35] See, e.g., [63, Sec. 1.3.1, p. 7].

Let $\xi_1, \xi_2 \in \Xi_{\mathrm{ad}}$ and $(\phi_1, \vartheta_1), (\phi_2, \vartheta_2) \in \mathcal{Y}_p$, $p > 2$ be the corresponding solutions of the Cattaneo–LITT model (2.10). Like in the proof of Theorem 2.17, we assume that there is a $\hat{p} > 3$ and a $C \in \mathbb{R}_{>0}$ such that

$$\phi_i(t) \in W^{1,\hat{p}}(\Omega) \quad \text{and} \quad \|\phi_i(t)\|_{W^{1,\hat{p}}(\Omega)} \le C \quad \text{for a.a. } t \in I, i \in \{1, 2\}.$$

Again, we refer to Remark 2.18 for its justification.

Like in the proof of Theorem 2.17, we infer for $\delta\phi := (\phi_1 - \phi_2)$ that

$$\begin{aligned}
\|\delta\phi(t)\|_{H^1(\Omega)}^2 &\le C \|\phi_2(t)\|_{W^{1,\hat{p}}(\Omega)}^2 \left(\|D_1(t) - D_2(t)\|_{L^q(\Omega)}^2 + \|\sigma_{\mathrm{a}1}(t) - \sigma_{\mathrm{a}2}(t)\|_{L^q(\Omega)}^2 \right) \\
&\le C \left(\|D_1(t) - D_2(t)\|_{L^q(\Omega)}^2 + \|\sigma_{\mathrm{a}1}(t) - \sigma_{\mathrm{a}2}(t)\|_{L^q(\Omega)}^2 \right)
\end{aligned} \tag{2.40}$$

for a.a. $t \in I$, with $q = 2\hat{p}(\hat{p} - 2)^{-1} < 6$ and $\sigma_{\mathrm{a}i} := \sigma_{\mathrm{a}}(\vartheta_i), D_i := D(\vartheta_i), i \in \{1, 2\}$. Furthermore, it holds with the $\mathcal{C}^0(\overline{Q})$ bound for ϑ_2 and with estimates (2.19), (2.23) that

$$\begin{aligned}
&\left(\|\delta\vartheta'(t)\|_{L^2(\Omega)}^2 \right)' + \left(\|\delta\vartheta(t)\|_{H^1(\Omega)}^2 \right)' + \|\delta\vartheta'(t)\|_{L^2(\Omega)}^2 \\
&\le C(\varepsilon^{-1}) \Big(\|(\sigma_{\mathrm{a}1}(t) - \sigma_{\mathrm{a}2}(t))\|_{L^2(\Omega)}^2 + \|\delta\phi(t)\|_{L^2(\Omega)}^2 + \|\delta\vartheta(t)\|_{L^2(\Omega)}^2 \\
&\qquad + \|\xi_1 - \xi_2\|_{L^2(\Omega)}^2 \Big) + \varepsilon \|\delta\vartheta'(t)\|_{L^2(\Omega)}^2
\end{aligned}$$

for all $\varepsilon > 0$. Integration from 0 to t, the embedding $H^1(\Omega) \hookrightarrow L^2(\Omega)$ and estimate (2.40) yield

$$\begin{aligned}
\|\delta\vartheta(t)\|_{H^1(\Omega)}^2 \le C \Big(&\int_0^t \|\delta\vartheta(s)\|_{H^1(\Omega)}^2 \, \mathrm{d}s + \int_0^t \|(\sigma_{\mathrm{a}1}(s) - \sigma_{\mathrm{a}2}(s))\|_{L^2(\Omega)}^2 \, \mathrm{d}s \\
&+ \int_0^t \|(\sigma_{\mathrm{a}1}(s) - \sigma_{\mathrm{a}2}(s))\|_{L^q(\Omega)}^2 \, \mathrm{d}s + \int_0^t \|(D_1(s) - D_2(s))\|_{L^q(\Omega)}^2 \, \mathrm{d}s \\
&+ \|\xi_1 - \xi_2\|_{L^2(\Omega)}^2 \Big).
\end{aligned}$$

Like in the proof of Theorem 2.17, we get[36]

$$\|\delta\vartheta(t)\|_{H^1(\Omega)}^6 \le C \left(\int_0^t \|\delta\vartheta(s)\|_{H^1(\Omega)}^6 \, \mathrm{d}s + \|\xi_1 - \xi_2\|_{L^2(\Omega)}^6 \right).$$

Gronwall's inequality yields $\|\delta\vartheta(t)\|_{H^1(\Omega)}^6 \le C \|\xi_1 - \xi_2\|_{L^2(\Omega)}^6$ for a.a. $t \in I$. Integration from 0 to T and the standard embedding in Bochner spaces[37] yield

$$\|\delta\vartheta\|_{L^2(I;H^1(\Omega))}^6 \le C \|\delta\vartheta\|_{L^6(I;H^1(\Omega))}^6 \le C \|\xi_1 - \xi_2\|_{L^2(\Omega)}^6. \tag{2.41}$$

For $\xi_1 \to \xi_2$ in $L^2(\Omega)$, we get with (2.41) that $\vartheta_1 \to \vartheta_2$ in $L^2(I; H^1(\Omega))$. Estimate (2.40) together with the Lipschitz continuity of the optical coefficients in Lemma 2.9 implies $\phi_1 \to \phi_2$ in $L^2(I; H^1(\Omega))$.

Overall, estimate (2.41) implies that ϑ depends Lipschitz continuously on ξ. Analogously to (2.38), estimates (2.40) and (2.41) imply

$$\begin{aligned}
\|\delta\phi\|_{L^2(I;H^1(\Omega))}^2 &\le C \left(\int_0^T \|D_1(t) - D_2(t)\|_{L^q(\Omega)}^2 + \|\sigma_{\mathrm{a}1}(t) - \sigma_{\mathrm{a}2}(t)\|_{L^q(\Omega)}^2 \, \mathrm{d}t \right) \\
&\le C \|\delta\vartheta\|_{L^6(I;H^1(\Omega))}^2 \le C \|\xi_1 - \xi_2\|_{L^2(\Omega)}^2.
\end{aligned}$$

Thus, also ϕ depends Lipschitz continuously on ξ.   ∎

---

[36] Hölder's inequality implies $\left(\int_0^t \|\delta\vartheta(s)\|_{H^1(\Omega)}^2 \, \mathrm{d}s \right)^3 \le C \int_0^t \|\delta\vartheta(s)\|_{H^1(\Omega)}^6 \, \mathrm{d}s$.

[37] See Lemma B.54 for standard embeddings in Bochner spaces.

3 Identification of the blood-perfusion rate

True optimization is the revolutionary contribution of modern research to decision processes.

George Bernhard Dantzig [234, Sec. 1, p. 1]

The blood perfusion in the liver acts as a heat sink in the heat-transfer model and influences the temperature and, with this, the coagulation zone induced by LITT. It depends on the underlying vascular structure, which motivates modeling the blood-perfusion rate by a spatially varying parameter. The location of large vessels relative to the LITT applicator changes with each patient and therapy and is unknown at the beginning of a simulation. The estimation of the blood-perfusion rate in the Cattaneo–LITT model based on temperature measurements defines an inverse problem, which we formulate in terms of a PDE-constrained optimal-control problem. We prove the existence of a corresponding optimal control, derive necessary first-order optimality conditions and discuss an optimization strategy to solve the optimal-control problem, i.e., find points which fulfill those first-order optimality conditions. In Chapter 4, we introduce a numerical example to validate this approach. Furthermore, we prove that the optimal control has a sparse structure in case we include an $L^1(\Omega)$-penalty term for the control in the cost functional.

3.1 Optimal-control problem

3.1.1 Motivation

Extensive studies investigated the influence of vessels in the context of LITT as well as in the context of other tumor ablation procedures [32, 33, 66, 113, 199, 200, 218]. The occurrence of large vessels ($>2\,\mathrm{mm}$ [120, p. 801]) motivates a spatially varying blood-perfusion rate.
We model the blood-perfusion rate as[1]

$$\xi = \xi_{\mathrm{out}} + (\xi_{\mathrm{in}} - \xi_{\mathrm{out}})u \tag{3.1}$$

with the *control* $u\colon \Omega \to [0,1]$, and $\xi_{\mathrm{out}}, \xi_{\mathrm{in}} \in \mathbb{R}_{>0}$, $\xi_{\mathrm{out}} < \xi_{\mathrm{in}}$. This formulation suggests the interpretation of the control u as an indicator function for large blood vessels.
It is essential to estimate the blood-perfusion rate in an automated way during each treatment to pave the way from ex-vivo to in-vivo experiments and to the final application in a clinical context. The significant effect of this parameter on the accuracy of the predicted coagulation zone is quantified later by Experiment 4.5 and illustrated in Figure 4.8.

---

[1] Other models with spatially varying blood-perfusion rate can be found, e.g., in [113].

We note that it might be more realistic to model the blood-perfusion rate as a function depending on time because the vascular structure can change during the treatment due to thrombosis and occlusions [32, 34], and the shrinkage of the capillaries [170].

In our numerical experiments, we include the effect of shrinkage of capillary vessels, like in [170], but let the blood-perfusion in large vessels be unaffected. In [9], we presented numerical experiments, where on the one hand the blood-perfusion rate depends on the coagulation, and on the other hand also the location of blood vessels, in our case the control u, might change over time. This additional degree of freedom might be used at a later stage to include the occlusion of large vessels or a secondary stop of blood flow due to thrombosis over time.

Note that there are alternative ways to formulate the identification of the blood-perfusion rate. For instance, it is a common approach to homogenize the effect of capillary blood flow, while treating the large vessels separately [31]. In this approach, large vessels are excluded from the computational domain and the cooling effect is described via suitable boundary conditions. The control, i.e., the location of large vessels, enters the formulation in this approach as geometrical property, which would require remeshing and techniques from the field of shape optimization. We do not follow this approach here because it would complicate the solution of the optimal-control problem.

> We formulate the estimation of the heterogeneous blood-perfusion rate ξ, and, with this, the localization of large vessels, by means of the identification of the unknown control u.

3.1.2 Analysis

We reformulate the weak formulation of the Cattaneo–LITT model (2.10) using the operator

$$
\left\{
\begin{aligned}
&e \colon \mathcal{Y}_p \times U \to Z^*, \\
&\left\langle e((\underbrace{(\phi, \vartheta)}_{y:=}, u), \varphi \right\rangle_{Z^*, Z} := \int_0^T F_r(\phi(t), \varphi_1(t); \vartheta, t)\, \mathrm{d}t - \int_0^T (a_r, \varphi_1(t))_{L^2(\Gamma)}\, \mathrm{d}t \\
&\qquad\qquad + \int_0^T \tau\, \langle \vartheta''(t), \varphi_2(t) \rangle_{H^1(\Omega)} + (\vartheta'(t), \varphi_2(t))_{L^2(\Omega)}\, \mathrm{d}t \\
&\qquad\qquad + \int_0^T F_h(\vartheta(t), \varphi_2(t); u) - \langle f_h(\vartheta, t, \phi(t); u), \varphi_2(t) \rangle_{H^1(\Omega)}\, \mathrm{d}t \\
&\qquad\qquad + \left(\vartheta(0) - \vartheta^{(0)}, \varphi_3 \right)_{L^2(\Omega)} + \left(\vartheta'(0) - \vartheta^{(1)}, \varphi_4 \right)_{L^2(\Omega)}
\end{aligned}
\right\}
\tag{3.2}
$$

with the spaces

$$
\begin{aligned}
Z &:= L^2(I; H^1(\Omega)) \times L^2(I; H^1(\Omega)) \times L^2(\Omega) \times L^2(\Omega), \\
U &:= L^2(\Omega).
\end{aligned}
\tag{3.3}
$$

The space $\mathcal{Y}_p$ was defined earlier in (2.7), and we summarize the state vector of the Cattaneo–LITT model by $y := (\phi, \vartheta) \in \mathcal{Y}_p$. The control u enters the formulation (3.2) via the blood-perfusion rate $\xi = \xi(u)$ in F_h and f_h, according to equation (3.1). A control u and the corresponding unique state vector $y = y(u)$ of the Cattaneo–LITT model (2.10) fulfill

$$
\langle e(y, u), \varphi \rangle_{Z^*, Z} = 0 \quad \text{for all } \varphi \in Z,
$$

which is equivalent[2] to $e(y,u) = 0$ in Z^*.[3]

Like described above, we interpret the control u as indicator function of large vessels, so we introduce the set of *admissible controls*

$$U_{\mathrm{ad}} := \{u \in U \,|\, 0 \leq u \leq 1 \quad \text{a.e. in } \Omega\}. \tag{3.4}$$

In the real application, we obtain temperature measurements by means of magnetic-resonance (MR) thermometry in certain time intervals about every two minutes. One way to incorporate the data would be to include several snap shots of the temperature over a large time horizon in a cost functional at once. Another way would be to perform the simulation and optimization only between two snap shots on a smaller time horizon and treat previous simulation results as initial data for the simulation on the next time interval.

Here, we do not have to decide between the two ways for incorporating several temperature measurements because we consider the optimization only on the first time interval $I = (0, t^*)$, where $t^* > 0$ is the time of the first temperature measurement during the therapy.

We define the spaces

$$W^{(0)} := L^2(I; H^1(\Omega)) \cap H^1(I; L^2(\Omega)) = \{\vartheta \in L^2(I; H^1(\Omega)) \,|\, \vartheta' \in L^2(I; L^2(\Omega))\},$$
$$Y^{(0)} := L^2(I; H^1(\Omega)) \times W^{(0)}$$

with

$$\|\vartheta\|_{W^{(0)}} = \|\vartheta\|_{L^2(I;H^1(\Omega))} + \|\vartheta'\|_{L^2(I;L^2(\Omega))},$$
$$\|(\phi, \vartheta)\|_{Y^{(0)}} = \|\phi\|_{L^2(I;H^1(\Omega))} + \|\vartheta\|_{W^{(0)}},$$

and consider the cost functional

$$J^{(0)} \colon Y^{(0)} \times U \to \mathbb{R}, \; (y, u) \mapsto \frac{1}{2} \|\vartheta(t^*; u) - \vartheta_{\mathrm{d}}\|_{L^2(\Omega)}^2 + \lambda_1 \|u\|_{L^1(\Omega)} + \frac{\lambda_2}{2} \|u\|_{L^2(\Omega)}^2, \tag{3.5}$$

where $\vartheta_{\mathrm{d}} \in L^2(\Omega)$ corresponds to the measured temperature at time t^* and $\lambda_1, \lambda_2 \in \mathbb{R}_{\geq 0}$ weight the control penalty terms. The irradiance ϕ as part of the state vector $y = (\phi, \vartheta)$ does not appear in the cost functional because in the real application we do not have any measurements available for this quantity.

> **Remark 3.1 — Evaluation at time t^*.**
> With $y \in Y^{(0)}$, we especially have $\vartheta \in W^{(0)}$. Thus, the evaluation of ϑ at time t^* in the cost functional is well defined by means of the embedding[a] $W^{(0)} \hookrightarrow \mathcal{C}^0(\bar{I}; L^2(\Omega))$ and yields an element in $L^2(\Omega)$.
>
> ---
> [a] See a classical embedding theorem B.36.

For the remainder of this section, we consider t^* as the final time of our simulation and, thus, set $T = t^*$.

---

[2] Cf. [219, Sec. 2.4, Eq. 2.6, p. 10].

[3] The state system $e(y, u) = 0$ in Z^* is formulated in an operator sense. For a detailed explanation, we refer to [43, XVIII, p. 467 ff.], especially [43, XVIII §5 2.1, Rem. 2, p. 559].

Note that the $L^1(\Omega)$ term in the cost functional (3.5) is a tool to promote a *sparse* control, see Section 3.2.5. The $L^1(\Omega)$ term, in general, causes the cost functional to be nondifferentiable and we would need to consider *subgradients* (generalized derivatives [37, Ch. 2, p. 24 ff.]) for the investigation of necessary optimality conditions. However, we are interested only in admissible controls in the set U_{ad}. For $u \in U_{\mathrm{ad}}$, it holds $u \geq 0$ a.e. in Ω and, thus, the cost functional $J^{(0)}$ in (3.5) coincides on U_{ad} with the cost functional

$$J \colon Y^{(0)} \times U \to \mathbb{R}, \; (y, u) \mapsto \frac{1}{2} \left\| \vartheta(t^*; u) - \vartheta_{\mathrm{d}} \right\|_{L^2(\Omega)}^2 + \lambda_1 \int_\Omega u \, \mathrm{d}x + \frac{\lambda_2}{2} \left\| u \right\|_{L^2(\Omega)}^2 . \tag{3.6}$$

Here, we replaced the nondifferentiable $L^1(\Omega)$ norm by the linear and, thus, differentiable operator $L^1(\Omega) \to \mathbb{R}$, $u \mapsto \int_\Omega u \, \mathrm{d}x$, which will turn out to be useful in the remainder of this discussion. This is a classical trick to avoid subgradients in this special case and was already suggested in [26, Sec. 2, Rem. 2.1, p. 797].

We formulate the identification of u as the following optimal-control problem:

$$\min_{(y,u) \in Y^{(0)} \times U} J(y, u) \quad \text{s.t.} \; (y, u) \in \mathcal{Y}_p \times U_{\mathrm{ad}} \quad \text{and} \quad e(y, u) = 0 \text{ in } Z^*, \tag{3.7}$$

where we define $(\bar{y}, \bar{u}) \in Y^{(0)} \times U$ to be *optimal* if it fulfills the constraints, i.e., $(\bar{y}, \bar{u}) \in \mathcal{Y}_p \times U_{\mathrm{ad}}$ and $e(\bar{y}, \bar{u}) = 0$ in Z^*, and

$$J(\bar{y}, \bar{u}) \leq J(y, u) \quad \text{for all } (y, u) \in \mathcal{Y}_p \times U_{\mathrm{ad}} \quad \text{with} \quad e(y, u) = 0 \text{ in } Z^*.$$

Note that the parameter $p \in (2, 6)$ is determined by means of the well-posedness of the Cattaneo–LITT model and depends on the domain and the upper and lower bounds of the optical coefficients, see Theorem 2.5.

In the following lemma, we list some useful properties of the cost functional J, which allow us to treat the minimization problem (3.7) in the framework of well-studied optimal-control problems.

Lemma 3.2 — Properties of the cost functional.

1. The cost functional J defined in (3.6) is sequentially weakly lower semicontinuous, i.e., for $(y_k, u_k)_{k \in \mathbb{N}} \subset Y^{(0)} \times U$ and $(y, u) \in Y^{(0)} \times U$, the weak convergence $(y_k, u_k) \rightharpoonup (y, u)$ in $Y^{(0)} \times U$ implies $J(y, u) \leq \liminf\limits_{k \to \infty} J(y_k, u_k)$.

2. The cost functional J defined in (3.6) is continuously Fréchet differentiable at every $(y, u) \in Y^{(0)} \times U$ with

$$\begin{aligned} \mathrm{D}_y J(y, u) \colon Y^{(0)} \to \mathbb{R}, \quad & h_y \mapsto (\vartheta(t^*; u) - \vartheta_{\mathrm{d}}, h_y)_{L^2(\Omega)} , \\ \mathrm{D}_u J(y, u) \colon U \to \mathbb{R}, \quad & h_u \mapsto \lambda_1 \int_\Omega h_u \, \mathrm{d}x + \lambda_2 \, (u, h_u)_{L^2(\Omega)} \end{aligned} \tag{3.8}$$

for all $(h_y, h_u) \in Y^{(0)} \times U$.

This is a classical result and we refer to Appendix A.2.1 for details.

The properties of the cost functional help us to investigate whether there exist solutions of the stated minimization problem (3.7). The answer is given in the next theorem, which is proven analogously in [219, Sec. 3, Thm. 3.1, p. 13] for the classical LITT model.

> **Theorem 3.3 — Existence of a minimizer.**
>
> Let Assumptions 2.1 and 2.2 hold, and let $\vartheta_\mathrm{d} \in L^2(\Omega)$. Then, for a certain[a] $p \in (2,6)$, *there exists at least* one minimizer $(\bar{y}, \bar{u}) \in \mathcal{Y}_p \times U_\mathrm{ad}$ which solves the constrained minimization problem (3.7).
>
> ---
> [a] Note that the parameter p is determined by means of the well-posedness of the Cattaneo–LITT model, see Theorem 2.5.

> **Remark 3.4 — A minimizer might not be unique.**
>
> We do not obtain necessarily a unique minimizer of problem (3.7) because the set of minimizers might not be convex due to the nonlinear state constraints given by $e(y, u) = 0$ in Z^*, cf. [219, Sec. 3, p. 13].

Proof of Theorem 3.3.

> Construct a minimizing sequence with a weak limit fulfilling the constraints.

The proof follows a standard procedure (cf. [93, Sec. 1.5.1, Thm. 1.43, p. 53], [93, Sec. 1.5.2, Thm. 1.45, p. 55]), like demonstrated in the proof of [219, Sec. 3, Thm. 3.1, p. 13].

(**I**) First, we construct a minimizing sequence.

The feasible set $F_\mathrm{ad} = \{(y, u) \in \mathcal{Y}_p \times U_\mathrm{ad} \,|\, e(y, u) = 0 \text{ in } Z^*\}$ is nonempty (e.g., for $u \equiv 0$, there is a solution given by Theorem 2.5). By definition of U_ad, the cost functional $J \geq 0$ is bounded from below on F_ad. Thus, we can define the infimum $J^* := \inf_{(y,u)\in F_\mathrm{ad}} J(y, u) \geq 0$, and there is a minimizing sequence $((y_k, u_k))_{k\in\mathbb{N}} \subset F_\mathrm{ad}$ such that

$$\lim_{k\to\infty} J(y_k, u_k) = J^*.$$

By definition of U_ad, it holds $0 \leq u_k \leq 1$ a.e. in Ω for all $k \in \mathbb{N}$, thus, the sequence $(u_k)_{k\in\mathbb{N}}$ is bounded in $L^2(\Omega)$. Furthermore, we can bound the blood-perfusion rate in (3.1) uniformly for all occurring controls $u \in U_\mathrm{ad}$, i.e.,

$$0 \leq \underline{\xi} \leq \|\xi(u)\|_{L^\infty(\Omega)} \leq \overline{\xi} \quad \text{a.e. in } \Omega,$$

and, thus, we can bound all state vectors $y = y(u)$ uniformly in the $\mathcal{Y}_p$ norm for a certain $p > 2$ according to Theorem 2.5.

Since W_ϑ, $L^2(\Omega)$ and $L^p(I; W^{1,p}(\Omega))$, for $p \in (2, 6)$, are reflexive[4], we can consecutively extract weakly convergent subsequences such that $u_{k_l} \rightharpoonup \bar{u}$ in $L^2(\Omega)$, $\phi_{k_l} \rightharpoonup \bar{\phi}$ in $L^p(I; W^{1,p}(\Omega))$ and $\vartheta_{k_l} \rightharpoonup \bar{\vartheta}$ in W_ϑ, where we reuse the same index k_l for a better readability. With Lemma B.4 on the Cartesian product of normed spaces, we get $y_{k_l} \rightharpoonup \bar{y}$

---
[4] In fact, W_ϑ is a Hilbert space, see Section 2.2.1. See further Lemma B.12 on reflexive Banach spaces and Lemma B.24 on Sobolev spaces.

in $L^p(I; W^{1,p}(\Omega)) \times W_\vartheta$, which implies[5] also weak convergence in $Y^{(0)}$.

Lemma 3.2 implies that the cost functional J is weakly lower semicontinuous, so we have

$$J(\bar{y}, \bar{u}) \leq \liminf_{l \to \infty} J(y_{k_l}, u_{k_l}) = J^*,$$

which directly implies $J(\bar{y}, \bar{u}) = J^*$.

(II) Next, we need to show $(\bar{y}, \bar{u}) \in \mathcal{Y}_p \times U_{\text{ad}}$.

Note that the set U_{ad} is a nonempty, convex and closed subset[6] of the Banach space U. A classical result on convex and closed subsets of Banach spaces now implies[7] that U_{ad} is weakly sequentially closed and, thus, $\bar{u} \in U_{\text{ad}}$.

By means of Theorem 2.5, we have that the sequence $(\vartheta_k)_{k \in \mathbb{N}} \subset \mathcal{C}^{0, \frac{1}{8}}(\overline{Q})$ is uniformly bounded, i.e., $\|\vartheta_k\|_{\mathcal{C}^{0, \frac{1}{8}}(\overline{Q})} \leq C$ for all $k \in \mathbb{N}$, where C does not depend on k.

The compact and, thus, continuous embedding[8] $\mathcal{C}^{0, \frac{1}{8}}(\overline{Q}) \hookrightarrow\hookrightarrow \mathcal{C}^0(\overline{Q})$ implies that the sequence $(\vartheta_k)_{k \in \mathbb{N}}$ is bounded in $\mathcal{C}^0(\overline{Q})$. Furthermore, we get that the sequence is uniformly equicontinuous.[9] The theorem of Arzelà–Ascoli[10] now implies that the set $\{\vartheta_k \mid k \in \mathbb{N}\} \subset \mathcal{C}^0(\overline{Q})$ is relatively compact, which yields an element $\hat{\vartheta} \in \mathcal{C}^0(\overline{Q})$ and yet another subsequence (reusing the same index as above) such that $\vartheta_{k_l} \to \hat{\vartheta}$ in $\mathcal{C}^0(\overline{Q})$. The strong convergence in $\mathcal{C}^0(\overline{Q}) \hookrightarrow L^1(Q)$ implies the weak convergence[11] in $L^1(Q)^*$. Furthermore, with $W_\vartheta \subset L^1(Q)$, we get $L^1(Q)^* \subset W_\vartheta^*$. Overall, we get

$$\vartheta_{k_l} \rightharpoonup \bar{\vartheta} \text{ in } L^1(Q) \quad \text{and} \quad \vartheta_{k_l} \rightharpoonup \hat{\vartheta} \text{ in } L^1(Q).$$

The uniqueness of the weak limit[12] implies $\bar{\vartheta} = \hat{\vartheta}$ in $L^1(Q)$, i.e., $\bar{\vartheta} = \hat{\vartheta}$ a.e. in Q. As shown above, we already have $\bar{y} \in L^p(I; W^{1,p}(\Omega)) \times W_\vartheta$, so, ultimately, we get $\bar{y} \in \mathcal{Y}_p$.

(III) Last, we need to show that $(\bar{y}, \bar{u})$ fulfills the constraint $e(\bar{y}, \bar{u}) = 0$ in Z^*.

Note that, for $\varphi \in L^2(I; H^1(\Omega))$, the maps

$$g_l : L^2(\Omega) \to \mathbb{R}, \quad u \mapsto \int_0^T \int_\Omega (\xi_{\text{in}} - \xi_{\text{out}}) u(x) \vartheta_{k_l}(t, x) \varphi(t, x) \, dx \, dt,$$

$$g : L^2(\Omega) \to \mathbb{R}, \quad u \mapsto \int_0^T \int_\Omega (\xi_{\text{in}} - \xi_{\text{out}}) u(x) \bar{\vartheta}(t, x) \varphi(t, x) \, dx \, dt$$

---

5   See Lemma B.17 on dual spaces of subsets. Note that $L^p(I; W^{1,p}(\Omega)) \hookrightarrow L^2(I; H^1(\Omega))$ and $W_\vartheta \hookrightarrow W^{(0)}$.
6   Cf. [217, Sec. 2.5.1, p. 39]. Let $u_k \to u$ in $L^2(\Omega)$ with $(u_k)_{k \in \mathbb{N}} \subset U_{\text{ad}}$. Then there is a subsequence $(u_{k_l})_{l \in \mathbb{N}} \subset U_{\text{ad}}$ which converges to u a.e. in Ω [236, App. (36a), p. 1023]. Thus, for all $\varepsilon > 0$ and a.a. $x \in \Omega$, we can find an $L \in \mathbb{N}$ such that for all $l \geq L$ it holds $|u_{k_l}(x) - u(x)| < \varepsilon$. This implies $u(x) \in [0, 1]$ for a.a. $x \in \Omega$ and, thus, $u \in U_{\text{ad}}$, i.e., U_{ad} is closed in U.
7   Classical result on convex and closed subsets of Banach spaces, see Lemma B.15.
8   See Theorem B.59 on embeddings in Hölder spaces.
9   In fact, for $\varepsilon > 0$, choose $\delta := \left(\frac{\varepsilon}{2C}\right)^{1/\alpha}$ with $\alpha = \frac{1}{8}$. Then, for $k \in \mathbb{N}$ and $x, y \in \overline{Q}$ with $\|x - y\| < \delta$, it holds $|\vartheta_k(x) - \vartheta_k(y)| \leq C \|x - y\|^\alpha < \varepsilon$. See further Theorem B.68 for the definition of equicontinuous functions.
10 See the theorem of Arzelà–Ascoli B.68.
11 See [4, Sec. 6, Bem. 6.3, p. 238].
12 See Remark B.8 on the uniqueness of weak limits.

define elements in $L^2(\Omega)^*$. It holds[13] $g_l \to g$ in $L^2(\Omega)^*$ and[14]

$$\langle g_l, u_{k_l}\rangle_{L^2(\Omega)} \to \langle g, \bar{u}\rangle_{L^2(\Omega)} \qquad \text{for } l \to \infty. \tag{3.9}$$

Furthermore, the map

$$\hat{g}\colon W_\vartheta \to \mathbb{R}, \quad \vartheta \mapsto \int_0^T \tau \left\langle \vartheta''(t), \varphi(t)\right\rangle_{H^1(\Omega)}$$

$$+ \left(\vartheta'(t), \varphi(t)\right)_{L^2(\Omega)} + \kappa \left(\nabla\vartheta(t), \nabla\varphi(t)\right)_{L^2(\Omega)}$$

$$+ \xi_{\text{out}} \left(\vartheta(t), \varphi(t)\right)_{L^2(\Omega)} + \left(a_{\text{h}}\vartheta(t), \varphi(t)\right)_{L^2(\Gamma)} \mathrm{d}t$$

defines an element in W_ϑ^*, and the weak convergence $\vartheta_{k_l} \rightharpoonup \bar{\vartheta}$ implies

$$\langle \hat{g}, \vartheta_{k_l}\rangle_{W_\vartheta} \to \langle \hat{g}, \bar{\vartheta}\rangle_{W_\vartheta} \qquad \text{for } l \to \infty. \tag{3.10}$$

The strong convergence $\vartheta_{k_l} \to \bar{\vartheta}$ in $\mathcal{C}^0(\overline{Q})$ together with $\|\vartheta_{k_l}\|_{\mathcal{C}^0(\overline{Q})} \le M$ for all $l \in \mathbb{N}$, for a certain $M \in \mathbb{R}_{>0}$, implies that also the limit $\bar{\vartheta} \in \mathcal{C}^0(\overline{Q}) \hookrightarrow L^\infty(Q)$ is bounded by M.

Lemma 2.9 yields that there is a constant $C(M)$ such that

$$\left\|f(\vartheta_{k_l}) - f(\bar{\vartheta})\right\|_{L^q(Q)} \le C(M) \left\|\vartheta_{k_l} - \bar{\vartheta}\right\|_{L^q(Q)}$$

for $f \in \{\sigma_{\text{a}}, D\}$ and all $q \in (1, \infty)$, thus, the optical coefficients $\sigma_{\text{a}}(\vartheta_{k_l}), D(\vartheta_{k_l})$ converge strongly in $L^q(Q)$.

Like in the proof of Lemma 2.12, the strong convergence of the coefficients $\sigma_{\text{a}}(\vartheta_{k_l}), D(\vartheta_{k_l})$ combined with the weak convergence $\phi_{k_l} \rightharpoonup \bar{\phi}$ in $L^p(I; W^{1,p}(\Omega))$, together with the limits in (3.9) and (3.10), allows passing to the limit in the weak formulation, and we get

$$0 = \langle e(y_{k_l}, u_{k_l}), \varphi\rangle_{Z^*, Z} \to \langle e(\bar{y}, \bar{u}), \varphi\rangle_{Z^*, Z} \qquad \text{for all } \varphi \in Z.$$

This implies $\langle e(\bar{y}, \bar{u}), \varphi\rangle_{Z^*, Z}$ for all $\varphi \in Z$. Thus, $\bar{y} = (\bar{\phi}, \bar{\vartheta})$ is indeed a solution of the Cattaneo–LITT model.

∎

---

[13] In fact, g_l is linear by construction, and, with Hölder's inequality B.27, it holds

$$|g_l(u)| \le \|\vartheta_{k_l}\|_{\mathcal{C}^0(\overline{Q})} \int_0^T \int_\Omega |(\xi_{\text{in}} - \xi_{\text{out}})u(x)\varphi(t,x)| \,\mathrm{d}x \,\mathrm{d}t \le C \,|\xi_{\text{in}} - \xi_{\text{out}}| \,\|\vartheta_{k_l}\|_{\mathcal{C}^0(\overline{Q})} \,\|\varphi\|_{L^2(Q)} \,\|u\|_{L^2(\Omega)}.$$

This holds analogously for g. The convergence $g_l \to g$ follows form the strong convergence $\vartheta_{k_l} \to \bar{\vartheta}$ in $\mathcal{C}^0(\overline{Q})$.
[14] See Lemma B.9 on limits of sequences in dual pairings.

3.2 First-order optimality conditions

We derive necessary first-order optimality conditions for the optimal-control problem (3.7).
These consist of three ingredients: the *state system*, the *adjoint state system* and a *variational inequality*.

The unique solvability of the Cattaneo–LITT model for $u \in U_{\text{ad}}$ (see Theorem 2.5) allows us to
define the *control-to-state map*

$$S \colon U_{\text{ad}} \to \mathcal{Y}_p,\ u \mapsto y \tag{3.11}$$

where y is the unique state vector of the Cattaneo–LITT model for a given control u according to
Theorem 2.5, and the *reduced cost functional*

$$\hat{J} \colon U_{\text{ad}} \to \mathbb{R},\ u \mapsto J(S(u), u). \tag{3.12}$$

The standard approach, e.g., [93, Sec. 1.7, p. 65 ff.], [217, Sec. 2.8, p. 49 ff.], would be to show
that the reduced cost functional is Gâteaux differentiable and to proceed from there. In our
situation, we face the following problem with this standard procedure. On the one hand, we
choose the control space $U = L^2(\Omega)$ because it allows us to describe descent directions by means
of the Riesz-representation theorem. This is especially useful for the numerical treatment of this
optimization problem with gradient-descent algorithms. On the other hand, the control-to-state
map is defined only for controls in the admissible set U_{ad}. Unfortunately, the set U_{ad} does not
contain any inner points w.r.t. the standard topology induced by the $L^2(\Omega)$ norm. Furthermore,
there is no open[15] set V with $U_{\text{ad}} \subset V \subset U$ such that the control-to-state map would be well
defined for controls in $u \in V$.[16]

Thus, the reduced cost functional can not be Gâteaux differentiable according to the standard
definition.[17] The authors in [38] faced a similar problem. We follow their lead and adapt the
structure of [38, Sec. 3, p. 443 ff.] to our situation.

> **Definition 3.5 — Admissible direction [38, Sec. 3.1, p. 446].**
> We call $h \in U$ an *admissible direction* w.r.t. $\bar{u} \in U_{\text{ad}}$ if there exists a $\bar{\lambda} \in \mathbb{R}_{>0}$ such that
> $u^\lambda := \bar{u} + \lambda h \in U_{\text{ad}}$ for all $\lambda \in \mathbb{R}_{>0}$ with $0 < \lambda \leq \bar{\lambda}$.

> **Remark 3.6 — Admissible direction.**
> Definition 3.5 together with the definition of U_{ad} in (3.4) implies that admissible directions
> are elements of $L^\infty(\Omega)$.

---

[15] Open w.r.t. the standard topology induced by the $L^2(\Omega)$ norm.

[16] In fact, this can be shown by the following example. For readability, we consider the special case $\Omega = (0, 1) \subset \mathbb{R}$.
Let $u \in U_{\text{ad}}$ and define $v_\delta := \frac{1}{\sqrt{\delta}} 1_{[0,\delta]}$, for $\delta \in (0, 1)$, where $1_{[0,\delta]} \colon \Omega \to \{0, 1\}$ is the indicator function of the
interval $[0, \delta]$. It holds $v_\delta \in L^2(\Omega)$ and $\|v_\delta\|_{L^2(\Omega)} = 1$. For the control-to-state map to be well defined (see
equation (3.1) and Assumption 2.2) for an input $\bar{u}$ in the neighborhood of u, we need $-\varepsilon_0 \leq \bar{u} \leq C$ a.e. in Ω for
$\varepsilon_0 = \frac{\xi_{\text{out}} - \xi}{\xi_{\text{in}} - \xi_{\text{out}}}$ and $C = \frac{\xi - \xi_{\text{out}}}{\xi_{\text{in}} - \xi_{\text{out}}}$. For $\varepsilon > 0$, we define $\delta := \frac{\varepsilon^2}{4(\varepsilon_0 + 1)^2 + 1}$ and the function $\bar{u} := u - \frac{\varepsilon}{2} v_\delta$. It holds
$\|\bar{u} - u\|_{L^2(\Omega)} = \frac{\varepsilon}{2} \|v_\delta\|_{L^2(\Omega)} < \varepsilon$, but for a.a. $x \in (0, \delta)$ it holds $\bar{u}(x) \leq 1 - \frac{\varepsilon}{2\sqrt{\delta}} < -\varepsilon_0$. This proves the existence
of an element in the ε-neighborhood of u for which the control-to-state map is a-priori not well defined (based only on
Theorem 2.5).

[17] See [93, Sec. 1.4.1, Def. 1.29, p. 50], [217, Sec. 2.6, p. 44], [236, §25.5, p. 509].

> **Definition 3.7 — Directionally differentiable[a].**
>
> Let X, Y be real Banach spaces, $V \subset X$ be a convex subset and $f \colon V \to Y$ a function. We call f *directionally differentiable* at $\bar{x} \in V$ in direction $h \in X$, if there is a $\bar{\lambda} \in \mathbb{R}_{>0}$ such that the function
>
> $$\bar{f} \colon [0, \bar{\lambda}) \to Y, \lambda \mapsto f(\bar{x} + \lambda h)$$
>
> is well defined and differentiable in zero, i.e., there exists an element $\mathrm{D}\bar{f} \in Y$ such that
>
> $$\left\| \bar{f}(\lambda) - \bar{f}(0) - \lambda \mathrm{D}\bar{f} \right\|_Y \in o(\lambda),$$
>
> i.e.,
>
> $$\frac{\bar{f}(\lambda) - \bar{f}(0) - \lambda \mathrm{D}\bar{f}}{\lambda} \to 0 \quad \text{in } Y \quad \text{for } \lambda \to 0, \lambda \geq 0.$$
>
> We call $\mathrm{D}_x f(\bar{x})[h] \coloneqq \mathrm{D}\bar{f}$ the directional derivative at $\bar{x}$ in direction h.
>
> ---
> [a] This definition differs from the standard formulation, e.g., [93, Sec. 1.4.1, Def. 1.29, p. 50], because the subset V is not assumed to be open.

Let $\bar{u} \in U_{\mathrm{ad}}$ and let h be an admissible direction w.r.t. $\bar{u}$. Like in [38], our goal is to determine the directional derivative of the reduced cost functional (3.12) at $\bar{u} \in U_{\mathrm{ad}}$ in direction h, which is denoted by $\mathrm{D}_u \hat{J}(\bar{u})[h]$. This requires the directional derivative $\mathrm{D}_u S(\bar{u})[h]$ of the control-to-state map at $\bar{u}$ in direction h. We investigate this directional derivative in two steps. First, we derive the linearized state system. Second, we show by means of the definition that the solution of the linearized state system is in fact the directional derivative of the control-to-state map.

3.2.1 Linearized state system

First, we need to discuss the differentiability of the optical coefficients, which introduce nonlinearities in the Cattaneo–LITT model.

> **Lemma 3.8 — Differentiability of the optical coefficients (cf. [219, Sec. 2.1, Lem. 2.1, p. 7], [219, Sec. 2.1, Lem. 2.2, p. 7]).**
>
> The coefficients σ_{a}, D in (2.8) viewed as maps from $\mathcal{C}^0(\overline{Q})$ to $\mathcal{C}^0(\overline{Q})$ are well defined and continuously Fréchet differentiable. The derivatives at $\vartheta \in \mathcal{C}^0(\overline{Q})$ in an arbitrary direction $h \in \mathcal{C}^0(\overline{Q})$ are given by
>
> $$\mathrm{D}_\vartheta \sigma_{\mathrm{a}}(\vartheta)[h] = (\sigma_{\mathrm{a,n}} - \sigma_{\mathrm{a,c}}) \mathrm{D}_\vartheta \gamma(\vartheta)[h],$$
>
> $$\mathrm{D}_\vartheta D(\vartheta)[h] = -\frac{\varepsilon_{\mathrm{kn}}^2}{3 \left(\hat{\sigma}_{\mathrm{t}}(\vartheta)\right)^2} (\hat{\sigma}_{\mathrm{t, n}} - \hat{\sigma}_{\mathrm{t, c}}) \mathrm{D}_\vartheta \gamma(\vartheta)[h],$$
>
> with[a]
>
> $$\mathrm{D}_\vartheta \gamma(\vartheta)[h](t, x) = -\gamma(\vartheta)(t, x) \int_0^t d'_{\mathrm{Arr}}(\vartheta(s, x)) h(s, x) \, \mathrm{d}s \quad \text{for } (t, x) \in Q.$$
>
> ---
> [a] The function d_{Arr} is defined in equation (2.9).

Lemma 3.8 is proven in a more general case in [219, Sec. 2.1, Lem. 2.2, p. 7]. We especially refer to [219, Sec. 2.2, Rem. 2.1, p. 7]. The proof uses a formulation of the coefficients as a chain of Nemytskii operators.

Note that, for a fixed $\vartheta \in \mathcal{C}^0(\overline{Q})$, it holds

$$\|\mathrm{D}_\vartheta \gamma(\vartheta)[h]\|_{\mathcal{C}^0(\overline{Q})} \leq C(\vartheta) \int_0^t \|h(s)\|_{\mathcal{C}^0(\overline{\Omega})} \, \mathrm{d}s \quad \text{for all } h \in \mathcal{C}^0(\overline{Q}), \tag{3.13}$$

which will be a useful estimate to prove Lemma 3.9 below.

The differentiability of the optical coefficients allows us to define the following *weak formulation* of the *linearized state system* at $(y, u) = ((\phi, \vartheta), u) := (S(u), u) \in \mathcal{Y}_p \times U_{\mathrm{ad}}$ in the admissible direction $h \in L^\infty(\Omega)$ w.r.t. u: find $(\rho, \eta) \in L^2(I; H^1(\Omega)) \times (W_\vartheta \cap \mathcal{C}^0(\overline{Q}))$ such that

$$\left\{ \begin{aligned}
&\int_0^T F_{\mathrm{r}}(\rho(t), \varphi_1(t); \vartheta, t) \, \mathrm{d}t \\
&\qquad = -\int_0^T (\mathrm{D}_\vartheta D(\vartheta)[\eta](t) \nabla \phi(t), \nabla \varphi_1(t))_{L^2(\Omega)} \, \mathrm{d}t \\
&\qquad\quad - \int_0^T (\mathrm{D}_\vartheta \sigma_{\mathrm{a}}(\vartheta)[\eta](t) \phi(t), \varphi_1(t))_{L^2(\Omega)} \, \mathrm{d}t \,, \\
&\int_0^T \tau \langle \eta''(t), \varphi_2(t) \rangle_{H^1(\Omega)} + (\eta'(t), \varphi_2(t))_{L^2(\Omega)} + F_{\mathrm{h}}(\eta(t), \varphi_2(t); u) \, \mathrm{d}t \\
&\qquad = \int_0^T (\hat{\sigma} \sigma_{\mathrm{a}}(\vartheta)(t) \rho(t), \varphi_2(t))_{L^2(\Omega)} + (\hat{\sigma} \mathrm{D}_\vartheta \sigma_{\mathrm{a}}(\vartheta)[\eta](t) \phi(t), \varphi_2(t))_{L^2(\Omega)} \, \mathrm{d}t \\
&\qquad\quad + \int_0^T ((\xi_{\mathrm{in}} - \xi_{\mathrm{out}})(\vartheta_{\mathrm{b}} - \vartheta(t))h, \varphi_2(t))_{L^2(\Omega)} \, \mathrm{d}t \,, \\
&\eta(0) = 0, \\
&\eta'(0) = 0
\end{aligned} \right. \tag{3.14}$$

for all $\varphi = (\varphi_1, \varphi_2) = L^2(I; H^1(\Omega)) \times L^2(I; H^1(\Omega))$. We call the vector (ρ, η) the linearized state vector corresponding to the control u. Note that the control u enters the linearized state system (3.14) implicitly via the state vector $(\phi, \vartheta) = S(u)$, and explicitly via the blood-perfusion rate in the bilinear form F_{h}.

Lemma 3.9 — Existence of a unique linearized state.
Let Assumptions 2.1 and 2.2 hold, and let $(\phi, \vartheta) = S(u) \in \mathcal{Y}_p$ with $p > 3$ be the state vector of the Cattaneo–LITT model for a given control $u \in U_{\mathrm{ad}}$.[a]
For every admissible direction $h \in L^\infty(\Omega)$ w.r.t. u, the linearized state system (3.14) has a unique solution in $L^2(I; H^1(\Omega)) \times (W_\vartheta \cap \mathcal{C}^0(\overline{Q}))$, i.e., there *exists* a *unique* linearized state vector $(\rho, \eta) \in L^2(I; H^1(\Omega)) \times (W_\vartheta \cap \mathcal{C}^0(\overline{Q}))$ which fulfills the weak formulation (3.14) for all $\varphi \in L^2(I; H^1(\Omega)) \times L^2(I; H^1(\Omega))$.

---
[a] The assumption $p > 3$ is justified by Lemma 2.12 and Remark 2.18.

The proof of Lemma 3.9 follows a standard procedure, but it is rather technical. The idea is to freeze the linear state in the memory term $\int_0^t \eta(s) \, \mathrm{d}s$ on the right-hand side, solve the two equations for the two components of the linearized state vector consecutively using standard results and, finally, apply Banach's fixed point theorem in a specially weighted space. We provide the details in Appendix A.2.2.

3.2.2 Directional derivatives

Let $\bar{u} \in U_{\text{ad}}$, $h \in L^{\infty}(\Omega)$ be an admissible direction w.r.t. $\bar{u}$, and let $\lambda \in \mathbb{R}_{>0}$ such that $u := \bar{u} + \lambda h \in U_{\text{ad}}$. With the state vectors of the Cattaneo–LITT model $y = (\phi, \vartheta) := S(u)$ and $\bar{y} = (\bar{\phi}, \bar{\vartheta}) := S(\bar{u})$ and the linearized state vector $(\bar{\rho}, \bar{\eta})$ corresponding to the control $\bar{u}$, we define

$$\mathrm{d}\vartheta^{\lambda} := \vartheta - \bar{\vartheta} - \lambda\bar{\eta} \quad \text{and} \quad \mathrm{d}\phi^{\lambda} := \phi - \bar{\phi} - \lambda\bar{\rho}. \tag{3.15}$$

For a better readability, we omit the superscript λ of $\mathrm{d}\vartheta^{\lambda}$ and $\mathrm{d}\phi^{\lambda}$.

Analogously to (3.15), we subtract the equations of the state system (2.10) for $\bar{y}$ and λ-times the equations of the linearized system (3.14) for $(\bar{\rho}, \bar{\eta})$ from the equations of the state system (2.10) for y, and get that the differences $(\mathrm{d}\phi, \mathrm{d}\vartheta)$ fulfill

$$\left\{ \begin{aligned} & \int_0^T F_{\text{r}}(\mathrm{d}\phi(t), \varphi_1(t); \bar{\vartheta}, t) \, \mathrm{d}t \\ & \quad = -\int_0^T \left((D(\vartheta)(t) - D(\bar{\vartheta})(t) - \lambda \mathrm{D}_{\vartheta} D(\bar{\vartheta})[\bar{\eta}](t)) \nabla\phi(t), \nabla\varphi_1(t) \right)_{L^2(\Omega)} \mathrm{d}t \\ & \qquad - \int_0^T \lambda \left(\mathrm{D}_{\vartheta} D(\bar{\vartheta})[\bar{\eta}](t) (\nabla\phi(t) - \nabla\bar{\phi}(t)), \nabla\varphi_1(t) \right)_{L^2(\Omega)} \mathrm{d}t \\ & \qquad - \int_0^T \left((\sigma_{\text{a}}(\vartheta)(t) - \sigma_{\text{a}}(\bar{\vartheta})(t) - \lambda \mathrm{D}_{\vartheta} \sigma_{\text{a}}(\bar{\vartheta})[\bar{\eta}](t)) \phi(t), \varphi_1(t) \right)_{L^2(\Omega)} \mathrm{d}t \\ & \qquad - \int_0^T \lambda \left(\mathrm{D}_{\vartheta} \sigma_{\text{a}}(\bar{\vartheta})[\bar{\eta}](t) (\phi(t) - \bar{\phi}(t)), \varphi_1(t) \right)_{L^2(\Omega)} \mathrm{d}t \,, \\ & \int_0^T \tau \langle (\mathrm{d}\vartheta)''(t), \varphi_2(t) \rangle_{H^1(\Omega)} + ((\mathrm{d}\vartheta)'(t), \varphi_2(t))_{L^2(\Omega)} + F_{\text{h}}(\mathrm{d}\vartheta(t), \varphi_2(t); \bar{u}) \, \mathrm{d}t \\ & \quad = \int_0^T \left(\hat{\sigma}(\sigma_{\text{a}}(\vartheta)(t) - \sigma_{\text{a}}(\bar{\vartheta})(t) - \lambda \mathrm{D}_{\vartheta} \sigma_{\text{a}}(\bar{\vartheta})[\bar{\eta}](t)) \phi(t), \varphi_2(t) \right)_{L^2(\Omega)} \mathrm{d}t \\ & \qquad + \int_0^T \left(\hat{\sigma} \sigma_{\text{a}}(\bar{\vartheta})(t) (\phi(t) - \bar{\phi}(t) - \lambda\bar{\rho}(t)), \varphi_2(t) \right)_{L^2(\Omega)} \mathrm{d}t \\ & \qquad + \int_0^T \lambda \left(\hat{\sigma} \mathrm{D}_{\vartheta} \sigma_{\text{a}}(\bar{\vartheta})[\bar{\eta}](t) (\phi(t) - \bar{\phi}(t)), \varphi_2(t) \right)_{L^2(\Omega)} \mathrm{d}t \\ & \qquad + \int_0^T \lambda \left((\xi_{\text{in}} - \xi_{\text{out}})(\bar{\vartheta}(t) - \vartheta(t)) h, \varphi_2(t) \right)_{L^2(\Omega)} \mathrm{d}t \,, \\ & \mathrm{d}\vartheta(0) = 0, \\ & (\mathrm{d}\vartheta)'(0) = 0 \end{aligned} \right. \tag{3.16}$$

for all $\varphi = (\varphi_1, \varphi_2) \in L^2(I; H^1(\Omega)) \times L^2(I; H^1(\Omega))$.

Lemma 3.10 — Directional derivatives of the control-to-state map.

Let Assumptions 2.1 and 2.2 hold. We consider the control-to-state map in (3.11) as function[a]

$$S \colon U_{\text{ad}} \to Y^{(0)}, \; u \mapsto (\phi, \vartheta),$$

which is well defined because of the embedding $\mathcal{Y}_p \hookrightarrow Y^{(0)}$. Let $\bar{u} \in U_{\text{ad}}$ be an admissible control and let $h \in L^{\infty}(\Omega)$ be an admissible direction w.r.t. $\bar{u}$. Then the corresponding linearized state vector $(\bar{\rho}, \bar{\eta}) \in L^2(I; H^1(\Omega)) \times (W_{\vartheta} \cap \mathcal{C}^0(\overline{Q}))$ is the directional derivative of

the control-to-state map at $\bar{u}$ in direction h, i.e.,

$$\lambda^{-1}\left(\left\|\mathrm{d}\phi^\lambda\right\|_{L^2(I;H^1(\Omega))} + \left\|\mathrm{d}\vartheta^\lambda\right\|_{L^2(I;H^1(\Omega))} + \left\|(\mathrm{d}\vartheta^\lambda)'\right\|_{L^2L^2(\Omega)}\right) \to 0 \quad \text{for } \lambda \to 0.$$

---

[a] Note that the evaluation of $\vartheta(T)$ in the reduced cost functional is well defined by means of the embedding $W^{(0)} = L^2(I;H^1(\Omega)) \cap H^1(I;L^2(\Omega)) \hookrightarrow \mathcal{C}^0(\bar{I};L^2(\Omega))$, see Remark 2.3.

Proof. We look at the first equation in (3.16). We choose $\varphi_1 = \mathrm{d}\phi$ and get with the coercivity of the bilinear form $F_\mathrm{r}(\cdot,\cdot;\bar{\vartheta},t)$ and Hölder's inequality[18]

$$\lambda^{-1}\|\mathrm{d}\phi\|_{L^2(I;H^1(\Omega))} \leq C\Bigg[\underbrace{\lambda^{-1}\left\|D(\vartheta) - D(\bar{\vartheta}) - \lambda \mathrm{D}_\vartheta D(\bar{\vartheta})[\bar{\eta}]\right\|_{\mathcal{C}^0(\overline{Q})}}_{\to 0}\|\phi\|_{L^2(I;H^1(\Omega))}$$

$$+ \underbrace{\lambda^{-1}\left\|\sigma_\mathrm{a}(\vartheta) - \sigma_\mathrm{a}(\bar{\vartheta}) - \lambda \mathrm{D}_\vartheta \sigma_\mathrm{a}(\bar{\vartheta})[\bar{\eta}]\right\|_{\mathcal{C}^0(\overline{Q})}}_{\to 0}\|\phi\|_{L^2(I;H^1(\Omega))}$$

$$+ \left(\left\|\mathrm{D}_\vartheta D(\bar{\vartheta})[\bar{\eta}]\right\|_{\mathcal{C}^0(\overline{Q})} + \left\|\mathrm{D}_\vartheta\sigma_\mathrm{a}(\bar{\vartheta})[\bar{\eta}]\right\|_{\mathcal{C}^0(\overline{Q})}\right)\underbrace{\left\|\phi - \bar{\phi}\right\|_{L^2(I;H^1(\Omega))}}_{\to 0}\Bigg].$$

The right-hand side tends to zero for $\lambda \to 0$ because of the differentiability of the optical coefficients[19] and the continuity of the state vector w.r.t. the control[20]. This implies that $\bar{\rho}$ is in fact the directional derivative of $\phi(u)$ at $u = \bar{u}$ in direction h.

Next, we look at the equation for $\mathrm{d}\vartheta$. We choose $\varphi_2 = (\mathrm{d}\vartheta)'$ and get with the coercivity of the bilinear form F_h, Hölder's inequality and the derivative of the norm[21] (analogously to the proof of Theorem 2.17)

$$\lambda^{-1}\left(\|\mathrm{d}\vartheta\|_{L^2(I;H^1(\Omega))} + \|(\mathrm{d}\vartheta)'\|_{L^2(I;L^2(\Omega))}\right)$$

$$\leq C\Bigg[\underbrace{\lambda^{-1}\left\|\sigma_\mathrm{a}(\vartheta) - \sigma_\mathrm{a}(\bar{\vartheta}) - \lambda \mathrm{D}_\vartheta \sigma_\mathrm{a}(\bar{\vartheta})[\bar{\eta}]\right\|_{\mathcal{C}^0(\overline{Q})}}_{\to 0}\|\phi\|_{L^2(Q)}$$

$$+ \underbrace{\lambda^{-1}\|\mathrm{d}\phi\|_{L^2(Q)}}_{\to 0}\left\|\sigma_\mathrm{a}(\bar{\vartheta})\right\|_{\mathcal{C}^0(\overline{Q})} + \|h\|_{L^\infty(\Omega)}\underbrace{\left\|\bar{\vartheta} - \vartheta\right\|_{L^2(Q)}}_{\to 0}$$

$$+ \left\|\mathrm{D}_\vartheta\sigma_\mathrm{a}(\bar{\vartheta})[\bar{\eta}]\right\|_{\mathcal{C}^0(\overline{Q})}\underbrace{\left\|\phi - \bar{\phi}\right\|_{L^2(Q)}}_{\to 0}\Bigg].$$

This implies that $\bar{\eta}$ is in fact the directional derivative of $\vartheta(u)$ at $u = \bar{u}$ in direction h.

∎

3.2.3 Variational inequality

In this section, we derive a variational inequality in terms of the linearized state vector, which yields a necessary first-order condition for an optimal control. In the subsequent section, we reformulate the variational inequality in terms of adjoint state vectors, which has several advantages from a practical point of view as described therein.

---

[18] See Hölder's inequality B.27.
[19] See Lemma 3.8.
[20] See Lemma 2.19. In fact, with $\lambda \to 0$, we also have $u \to \bar{u}$ in $L^2(\Omega)$ and, thus, $\phi \to \bar{\phi}$ in $L^2(I;H^1(\Omega))$.
[21] See Lemma B.38 on the derivative of the norm.

The next lemma is analog to [38, Sec. 3.2, Cor. 3.4, p. 454].

Lemma 3.11 — Variational inequality.

Let $\bar{u} \in U_{\mathrm{ad}}$ be a (not necessarily optimal) control of the problem (3.7) with associated state vector of the Cattaneo–LITT model $\bar{y} = (\bar{\phi}, \bar{\vartheta}) = S(\bar{u}) \in \mathcal{Y}_p$ and let $h \in L^\infty(\Omega)$ be an admissible direction w.r.t. $\bar{u}$. Then the reduced cost functional is directionally differentiable at $\bar{u}$ in direction h and it holds

$$\mathrm{D}_u \hat{J}(\bar{u})[h] = \int_\Omega (\vartheta(T; \bar{u}) - \vartheta_{\mathrm{d}}) \, \bar{\eta}(T) + \lambda_1 h + \lambda_2 \bar{u} h \, \mathrm{d}x \tag{3.17}$$

where $(\bar{\rho}, \bar{\eta})$ is the linearized state vector corresponding to $\bar{u}$.
If $\bar{u}$ is an optimal control for the problem (3.7), it further holds

$$\mathrm{D}_u \hat{J}(\bar{u})[u - \bar{u}] \geq 0 \quad \text{for all } u \in U_{\mathrm{ad}}.$$

Proof. We follow the proof of [38, Sec. 3.2, Cor. 3.4, p. 454]. Let $h \in L^\infty(\Omega)$ be an admissible direction w.r.t. $\bar{u}$.
It holds

$$\frac{J(S(\bar{u} + \lambda h), \bar{u} + \lambda h) - J(S(\bar{u}), \bar{u})}{\lambda} = \frac{J(S(\bar{u} + \lambda h), \bar{u} + \lambda h) - J(S(\bar{u} + \lambda h), \bar{u})}{\lambda} \tag{3.18}$$
$$+ \frac{J(S(\bar{u} + \lambda h), \bar{u}) - J(S(\bar{u}), \bar{u})}{\lambda}.$$

The left-hand side of (3.18) converges for $\lambda \to 0$ to the directional derivative $\mathrm{D}_u \hat{J}(\bar{u})[h]$. The derivative of the cost functional (3.8) implies that the first term on the right-hand side converges for $\lambda \to 0$ to $\lambda_1 \int_\Omega h \, \mathrm{d}x + \lambda_2 \int_\Omega \bar{u} h \, \mathrm{d}x$.
The chain rule[22] implies that the second term on the right-hand side converges for $\lambda \to 0$ to $\int_\Omega (\vartheta(T; \bar{u}) - \vartheta_{\mathrm{d}}) \bar{\eta}(T) \, \mathrm{d}x$ (with $t^* = T$), where we used that we can identify the directional derivative of the control-to-state map $\bar{\eta} = \mathrm{D}_u S(\bar{u})[h]$ by means of Lemma 3.10.

Next, we assume $\bar{u}$ to be an optimal control and define $h = u - \bar{u}$, for an arbitrary $u \in U_{\mathrm{ad}}$. Note that the direction h is admissible w.r.t. $\bar{u}$ because the admissible set U_{ad} is convex. From the optimality of $\bar{u}$ it follows

$$J(S(\bar{u}), \bar{u}) \leq J(S(\bar{u} + \lambda h), \bar{u} + \lambda h)$$

and, thus,

$$0 \leq \frac{J(S(\bar{u} + \lambda h), \bar{u} + \lambda h) - J(S(\bar{u}), \bar{u})}{\lambda} \to \mathrm{D}_u \hat{J}(\bar{u})[u - \bar{u}] \quad \text{for } \lambda \to 0,$$

which yields the variational inequality.

∎

Lemma 3.11 yields an abstract necessary condition for an optimal control, which is of limited use from a practical point of view for two reasons though. First, for each admissible direction h, we would need to solve the linearized state system (3.14) to obtain the corresponding linearized state vector (ρ, η) before we could evaluate the variational inequality (3.17). Second, if we aim to solve

---

[22] Analog to the chain rule B.42 for Fréchet-differentiable functions.

this optimization problem numerically by means of a gradient-descent strategy, this formulation of the variational inequality does not give us any hint for a potential descent direction.

To this, in the next step, we eliminate the linearized state η from the variational inequality (3.17) by means of the adjoint states.

3.2.4 Adjoint state system

The *adjoint state system* of the Cattaneo–LITT model corresponding to the cost functional (3.5) at $((\phi, \vartheta), u) = (S(u), u) \in \mathcal{Y}_p \times U_{\mathrm{ad}}$ is, for a better readability, stated in the strong formulation given as follows:

$$
\begin{cases}
-\mathrm{div}(D(\vartheta)\nabla z_1) + \sigma_{\mathrm{a}}(\vartheta)(z_1 - \hat{\sigma} z_2) = 0 & \text{in } (0,T) \times \Omega, \\
\tau z_2'' - z_2' - \mathrm{div}(\kappa \nabla z_2) + \xi(u)z_2 + f_D + f_{\sigma_{\mathrm{a}}} = 0 & \text{in } (0,T) \times \Omega, \\
a_{\mathrm{h}} z_2 + \kappa \nabla z_2 \cdot \boldsymbol{n} = 0 & \text{on } (0,T) \times \Gamma, \\
a_{\mathrm{r}} z_1 + D(\vartheta)\nabla z_1 \cdot \boldsymbol{n} = 0 & \text{on } (0,T) \times \Gamma, \\
z_2(T) - \tau z_2'(T) = \vartheta(T) - \vartheta_{\mathrm{d}} & \text{in } \Omega, \\
\tau z_2(T) = 0 & \text{in } \Omega,
\end{cases}
$$

with[23]

$$
f_{\sigma_{\mathrm{a}}} = -(\sigma_{\mathrm{a,n}} - \sigma_{\mathrm{a,c}})d'(\vartheta) \int_t^T \gamma(\vartheta)(s)\phi(s)(z_1(s) - \hat{\sigma} z_2(s))\,\mathrm{d}s\,,
$$

$$
f_D = (\hat{\sigma}_{\mathrm{t,n}} - \hat{\sigma}_{\mathrm{t,c}})d'(\vartheta) \int_t^T \frac{1}{3\left(\hat{\sigma}_{\mathrm{t}}(\vartheta)(s)\right)^2} \gamma(\vartheta)(s)\left((\nabla\phi(s))^{\mathrm{T}} \cdot \nabla z_1(s)\right)\mathrm{d}s
$$

and

$$
d'(\vartheta)(t,x) = A \exp\left(-\frac{E}{\vartheta(t,x)}\right)\frac{E}{\vartheta(t,x)^2}.
$$

The *weak formulation* of the adjoint state system at $((\phi, \vartheta), u)$ is given as follows: find $(z_1, z_2) \in L^2(I; H^1(\Omega)) \times W_\vartheta$ such that

$$
\begin{cases}
\displaystyle\int_0^T F_{\mathrm{r}}(z_1(t), \varphi_1(t); \vartheta, t)\,\mathrm{d}t \\
\qquad\qquad = \displaystyle\int_0^T \hat{\sigma}\left(\sigma_{\mathrm{a}}(\vartheta)(t)z_2(t), \varphi_1(t)\right)_{L^2(\Omega)}\mathrm{d}t\,, \\
\displaystyle\int_0^T \tau \langle z_2''(t), \varphi_2(t)\rangle_{H^1(\Omega)} - (z_2'(t), \varphi_2(t))_{L^2(\Omega)} + F_{\mathrm{h}}(z_2(t), \varphi_2(t); u)\,\mathrm{d}t \\
\qquad\qquad = -\displaystyle\int_0^T \left(f_D(z_1)(t) + f_{\sigma_{\mathrm{a}}}(z_1, z_2)(t), \varphi_2(t)\right)_{L^2(\Omega)}\mathrm{d}t\,, \\
z_2(T) - \tau z_2'(T) = \vartheta(T) - \vartheta_{\mathrm{d}}, \\
\tau z_2(T) = 0
\end{cases}
\tag{3.19}
$$

for all $\varphi \in L^2(I; H^1(\Omega)) \times L^2(I; H^1(\Omega))$. We call the vector (z_1, z_2) the adjoint state vector corresponding to the control u.

---

[23] Remember $D = (3\hat{\sigma}_{\mathrm{t}})^{-1}$.

Lemma 3.12 — Existence of a unique adjoint state.

Let $(\phi, \vartheta) = S(u) \in \mathcal{Y}_p$ be a sufficiently regular state vector of the Cattaneo–LITT model for a given control $u \in U_{\mathrm{ad}}$, e.g., with[a] $\phi \in L^\infty(I; W^{1,\infty}(\Omega))$. Then, for every admissible direction $h \in L^\infty(\Omega)$ w.r.t. u, the adjoint state system (3.19) has a unique weak solution, i.e., there *exists* a *unique* adjoint state vector $(z_1, z_2) \in L^2(I; H^1(\Omega)) \times W_\vartheta$ which fulfills (3.19) for all $\varphi \in L^2(I; H^1(\Omega)) \times L^2(I; H^1(\Omega))$.

---

[a] Note that this in fact an assumption because, in general, we can prove only $\phi \in L^p(I; W^{1,p}(\Omega))$ for a certain $p \in (2, 6)$, see Theorem 2.5. See also Remark 2.18.

The adjoint system (3.19) has a similar structure as the linearized state system (3.14), and Lemma 3.12 can be shown similarly to the proof of Lemma 3.9. We provide details in Appendix A.2.3.

Lemma 3.13 — Adjoint representation of the directional derivative.

Let Assumptions 2.1 and 2.2 hold. Let $u \in U_{\mathrm{ad}}$ be a (not necessarily optimal) control of the problem (3.7) with associated state vector of the Cattaneo–LITT model $y = (\phi, \vartheta) = S(u) \in \mathcal{Y}_p$ and let $(z_1, z_2) \in L^2(I; H^1(\Omega)) \times W_\vartheta$ be the corresponding adjoint state vector. Furthermore, let $h \in L^\infty(\Omega)$ be an admissible direction w.r.t. u. Then the reduced cost functional is directionally differentiable at u in direction h and it holds

$$\mathrm{D}_u \hat{J}(u)[h] = \left(\lambda_1 + \lambda_2 u + \int_0^T (\xi_{\mathrm{in}} - \xi_{\mathrm{out}})(\vartheta_\mathrm{b} - \vartheta(t))z_2(t)\,\mathrm{d}t\,, h \right)_{L^2(\Omega)}.$$

The exchange of the linearized state vector by the adjoint state vector in the variational inequality is a standard technique in optimal-control theory. The proof is based on a repeated integration by parts and is given in the Appendix A.2.4. The advantage of this procedure is that we separate the direction $u - \bar{u}$ from all other terms in the variational inequality. We can interpret the term $\lambda_1 + \lambda_2 u + \int_0^T (\xi_{\mathrm{in}} - \xi_{\mathrm{out}})(\vartheta_\mathrm{b} - \vartheta(t))z_2(t)\,\mathrm{d}t$ as Riesz representative of the directional-derivatives operator $\mathrm{D}_u \hat{J}(u)$ w.r.t. the space $L^2(\Omega)$. In Section 3.3, we employ this representation to formulate a descent algorithm for the numerical solution of the optimization problem.

Corollary 3.14 — Variational inequality (adjoint formulation) (cf. [38, Sec. 3.3, Lem. 3.5, p. 455]).

Let Assumptions 2.1 and 2.2 hold. Let $\bar{u} \in U_{\mathrm{ad}}$ be an optimal control for the problem (3.7) with associated state vector of the Cattaneo–LITT model $\bar{y} = (\bar{\phi}, \bar{\vartheta}) = S(\bar{u}) \in \mathcal{Y}_p$. Then it holds

$$\left(\lambda_1 + \lambda_2 \bar{u} + \int_0^T (\xi_{\mathrm{in}} - \xi_{\mathrm{out}})(\vartheta_\mathrm{b} - \bar{\vartheta}(t))\tilde{z}_2(t)\,\mathrm{d}t\,, u - \bar{u} \right)_{L^2(\Omega)} \geq 0 \quad \text{for all } u \in U_{\mathrm{ad}}$$

where $(\tilde{z}_1, \tilde{z}_2)$ is the adjoint state vector corresponding to $\bar{u}$.

Corollary 3.14 follows directly from the variational inequality (3.17) and the adjoint representation of the directional derivative in Lemma 3.13.

3.2.5 Sparse control

We are now able to motivate the $L^1(\Omega)$ term in the cost functional in the view of sparsity.

Note that the $L^1(\Omega)$ term in the cost functional (3.5) is a tool to promote a *sparse* control. A sparse spatial structure of the control might be desirable for the interpretation of the function u as indicator function for large vessels.

In Remark 3.4, we discussed that the optimal control does not necessarily need to be unique. In fact, if we compare the computed optimal controls of Experiments 4.8 and 4.11, we observe that different initial guesses for the descent algorithm might lead to different optimal controls, or more precisely, to different stationary points. Heuristically speaking, we have several candidates for an optimal control, and the $L^1(\Omega)$ regularization helps us to "pick" one with a sparse structure.

This becomes even more important later in the real application in the presence of measurement noise (cf. Experiment 4.10), where we want to avoid overfitting to the disturbed data.

For details, we refer to [26, 203], where the effect of such an $L^1(\Omega)$ regularization was studied in the context of elliptic optimal-control problems.

Let $\bar{u} \in U_{\text{ad}}$ be an optimal control for the problem (3.7), and $(\bar{\phi}, \bar{\vartheta}) = S(\bar{u})$ the associated state vector of the Cattaneo–LITT model, $(\tilde{z}_1, \tilde{z}_2)$ the associated adjoint state vector and $\lambda_1, \lambda_2 \in \mathbb{R}_{>0}$. Lemma 3.13 implies that the directional-derivative operator $\mathrm{D}_u \hat{J}(\bar{u})$ is a linear functional on the set of admissible directions with $L^2(\Omega)$ Riesz representative

$$g(u) := \lambda_1 + \lambda_2 u + \int_0^T (\xi_{\text{in}} - \xi_{\text{out}})(\vartheta_{\text{b}} - \bar{\vartheta}(t))\tilde{z}_2(u)(t)\,\mathrm{d}t\,. \tag{3.20}$$

A classical result of control theory[24] now implies[25]

$$\bar{u} = P(\bar{u} - \alpha g) \quad \text{for all } \alpha > 0,$$

where

$$P\colon L^2(\Omega) \to U_{\text{ad}},\ P(u)(x) = \min(\max(u(x), 0), 1) \tag{3.21}$$

is the projection operator onto U_{ad}. This implies for $\alpha = \lambda_2^{-1}$ that

$$\bar{u} = P\left(-\frac{1}{\lambda_2}\left(\lambda_1 + \int_0^T (\xi_{\text{in}} - \xi_{\text{out}})(\vartheta_{\text{b}} - \bar{\vartheta}(t))\tilde{z}_2(t)\,\mathrm{d}t\right)\right). \tag{3.22}$$

Analogously to the proof of [26, Sec. 3, Cor. 3.2, p. 800], it follows from (3.22) that

$$\bar{u}(x) = 0 \quad \text{if and only if} \quad \int_0^T (\xi_{\text{in}} - \xi_{\text{out}})(\vartheta_{\text{b}} - \bar{\vartheta}(t))\tilde{z}_2(t)\,\mathrm{d}t\ \geq -\lambda_1,$$

which implies *sparsity* of the optimal control $\bar{u}$ according to [26, Sec. 3, Rem. 3.3, p. 801].

3.3 Optimization algorithm

For a general overview on optimization methods in Banach spaces with focus on PDE-constrained optimization, we refer to [93, Ch. 2, p. 97 ff.] and [217].

---

[24] See Lemma B.69 on the projection operator. Note that U_{ad} is a convex and closed subset of the Hilbert space U (see the proof of Theorem 3.3), which is a prerequisite for the given lemma.

[25] Cf. [38, Sec. 3.3, Rem. 5, p. 458], [26, Sec. 3, Cor. 3.2, p. 800].

It is nontrivial to find a solution to the optimization problem (3.7): *"Usually, we are already satisfied if the method can be proved to converge to stationary points. These are points that satisfy the first-order necessary optimality conditions."* [93, Sec. 2.1, p. 97]

The analytical representation of directional derivatives allows us to follow the *first-optimize-then-discretize* approach. One advantage of this is that we can develop an optimization strategy independent of the underlying discretization. For details on mesh dependence in PDE-constrained optimization, we refer to [197].

There are several ways to deal with the control constraint $u \in U_{\mathrm{ad}}$. For simplicity, we follow the suggestion in [217, Sec. 2.12.2, p. 76 ff.] and use a *projected gradient method*, which is described in the following.

Let $u \in U_{\mathrm{ad}}$ be an admissible control, $(\phi, \vartheta) = S(u)$ the corresponding state vector of the Cattaneo–LITT model and (z_1, z_2) the corresponding adjoint state vector.

First, we need to find a search direction. Usually, one would define the negative gradient as search direction. Unfortunately, our reduced cost functional is not Gâteaux differentiable, so formally we can not speak of gradients. Nevertheless, the adjoint formulation of the variational inequality in Corollary 3.14 gives us a hint for potential descent directions. In case that the adjoint representation $g(u)$ of the directional derivative $\mathrm{D}_u \hat{J}(u)[h]$ in (3.20) is an admissible direction, we obtain a descent direction by $d := -g(u)$. In fact, there is an $s > 0$ such that $u(s) := u + sd \in U_{\mathrm{ad}}$ and

$$\hat{J}(u(s)) = \hat{J}(u) + s\mathrm{D}_u \hat{J}(u)[d] + o(s) = \hat{J}(u) - \underbrace{s(g(u), g(u))_{L^2(\Omega)}}_{>0} + o(s) < \hat{J}(u).$$

Second, we need to solve the line search problem

$$s^* := \underset{s>0}{\mathrm{argmin}}\, \hat{J}(P(u + sd)), \tag{3.23}$$

with the projection operator (3.21). Note that the projection operator ensures that the updated controls $P(u + sd) \in U_{\mathrm{ad}}$ are admissible.

The solution of the line search problem (3.23) is nontrivial due to the projection, and one often needs to settle for an "acceptable" step size determined by means of an *inexact line search problem*. For simplicity, we choose the *projected Armijo rule* (see [93, Sec. 2.2.2.1, p. 107]): for a given initial step size $s_0 \in \mathbb{R}_{>0}$, choose the maximum $s \in \{s_0 \beta^j \mid j \in \mathbb{N}_0\}$ for which

$$\hat{J}(P(u + sd)) - \hat{J}(u) \le -\frac{\gamma_{\mathrm{arm}}}{s} \|P(u + sd) - u\|_{L^2(\Omega)}^2, \tag{3.24}$$

with constants $\gamma_{\mathrm{arm}}, \beta \in (0, 1)$. This technique is also called *backtracking*.[26]

Similar to [93, Sec. 2.2.2.1, p. 107], we define with $g(u)$ in (3.20) the *stationary measure* as

$$\Sigma \colon U_{\mathrm{ad}} \to \mathbb{R},\ u \mapsto \|u - P(u - g(u))\|_{L^2(\Omega)}, \tag{3.25}$$

which is used to terminate the descent method.

We summarize the solution strategy in the following algorithm.

---

[26] See [106, Sec. 3.1, p. 39].

■ **Algorithm 3.15 — (Gradient) descent strategy with Armijo line search.**

Input:

- Admissible initial control $u_0 \in U_{\mathrm{ad}}$,

- initial step size $s_0 \in \mathbb{R}_{>0}$,

- Armijo parameters $\gamma_{\mathrm{arm}}, \beta \in (0,1)$,

- tolerances for the stationary measure $\textsc{tol\_abs} \in \mathbb{R}_{>0}$, $\textsc{tol\_rel} \in (0,1)$,

- iteration limits $\textsc{max\_iter\_descent}$, $\textsc{max\_iter\_armijo} \in \mathbb{N}$.

Output: Improved control $u \in U_{\mathrm{ad}}$ with $\hat{J}(u) \ll \hat{J}(u_0)$.

1: Compute $r_0 := \Sigma(u_0)$.
2: **for** $k = 0, \dots, \textsc{max\_iter\_descent} - 1$ **do**
3:     Set search direction $d := -g(u_0)$ (see (3.20)).
4:     Normalize direction[a] $d := \|d\|_{L^\infty(\Omega)}^{-1} \, d$.
5:     Set $\textsc{flag} := \text{``dec''}$; $\hat{\beta} := \beta$ (decrease)
6:     **if** Armijo condition (3.24) (with $u = u_k$, $s = s_0$) is $\textsc{true}$ **then**
7:         Set $\textsc{flag} := \text{``inc''}$; $\hat{\beta} := 1/\beta$ (increase)
8:     **for** $j = 1, \dots, \textsc{max\_iter\_armijo} - 1$ **do**[b]
9:         Set step size $s := s_0 \hat{\beta}^j$.
10:         **if** Armijo condition (3.24) (with $u = u_k$) is $\textsc{true}$ **and** $\textsc{flag} = \text{``dec''}$ **then**
11:             Set starting point for next iteration: $u_{k+1} := P(u_k + sd)$.
12:             Exit inner loop (over j).
13:         **else if** Armijo condition (3.24) (with $u = u_k$) is $\textsc{false}$ **and** $\textsc{flag} = \text{``inc''}$ **then**
14:             Revert step size $s := s_0 \hat{\beta}^{j-1}$.
15:             Set starting point for next iteration: $u_{k+1} := P(u_k + sd)$.
16:             Exit inner loop (over j).
17:         **else if** $j = \textsc{max\_iter\_armijo} - 1$ **and** $\textsc{flag} = \text{``dec''}$ **then**
18:             Stop with warning: *Line search failed: max. number of iterations reached.*
19:         **else if** $j = \textsc{max\_iter\_armijo} - 1$ **and** $\textsc{flag} = \text{``inc''}$ **then**
20:             Set starting point for next iteration: $u_{k+1} := P(u_k + sd)$.
21:             Continue with warning: *Line search stopped: max. number of iterations reached.*
22:     **if** $\Sigma(u_{k+1}) \leq \textsc{tol\_abs} + \textsc{tol\_rel} \times r_0$ **then**
23:         Stop with $\bar{u} := u_{k+1}$ (method converged successfully).
24: Stop with warning: *Descent method failed: max. number of iterations reached.*

---

[a] We did not assume $g \in L^\infty(\Omega)$ so far. Later in the implementation, this is well-defined because we approximate the related functions in terms of finite elements.

[b] This loop starts from $j = 1$ because we checked the case for $j = 0$ in line 6. Nevertheless, in the implementation this would require a check for the (uncommon) case of $\textsc{max\_iter\_armijo} = 1$ (otherwise u_{k+1} would be undefined in line 22), which we omit here for readability.

Unlike suggested in the classical Armijo rule (3.24), we allow in Algorithm 3.15 the step sizes also to increase if the first step size of each descent iteration is already admissible. We use a constant initial step size, but we normalize the direction by means of its $L^\infty(\Omega)$ norm. Note that so far we did not assume that the descent directions are elements of $L^\infty(\Omega)$, but this will be the case in the implementation due to the finite-element approximation of the corresponding functions. We consider the descent strategy to be converged once the stationary measure meets the absolute or relative tolerance, as suggested in [106, Sec. 5.4.1, Eq. 5.18, p. 93].

We do not discuss the convergence of Algorithm 3.15, but we validate it by means of numerical experiments in Section 4.3.

4 Cattaneo–LITT model: numerical experiments

Code is like humor: If you have to explain it, it's bad.

Common opinion on source code and its documentation [14]

In this chapter, we perform several numerical experiments to gain a better understanding of the Cattaneo–LITT model. We look at the effect of the delay parameter τ (see Section 2.1) on the evolution of the solution over time. Furthermore, we quantify the effect of the blood-perfusion rate on the estimated region of coagulation. Last, we introduce a numerical example to demonstrate the automated identification of the parameter u in equation (3.1) based on measured temperature data using derivative information and a descent algorithm.

The presented experiments should be understood as toy examples and the implementation as a proof of concept rather than a highly-optimized code ready for deployment. The implementation is aligned with the presentation within this thesis and is designed in a modularized way, which makes it easy to couple different models for the subproblems and to exchange the used schemes for discretization or optimization. Similarly to [121, 198], we follow the FAIR guiding principles for scientific research [229] and make all codes, including files to reproduce the numerical results of this thesis, publicly available online [8].

4.1 Discretization and details on the implementation

In Table 4.1 we list the versions of the software we used for the numerical experiments in this thesis.

Discretization

We refer to [86], for a general discussion of the numerical treatment of partial differential equations.
For the implementation, we divide the heat-transfer equation (1.1) by ρc_{p}, which removes the factor in front of the time derivative[1]. Next, we add the Cattaneo delay term $\tau \partial_{tt} \vartheta$.
We follow *Rothe's method* [86, Sec. 5.1.5, p. 343 ff.] for the discretization and first discretize the time derivatives in the heat-transfer equation with a standard backward-finite-difference scheme

$$\partial_t \, \vartheta(t) \approx \frac{\vartheta(t) - \vartheta(t - \Delta t)}{\Delta t}, \quad \partial_{tt} \, \vartheta(t) \approx \frac{\vartheta(t) - 2\vartheta(t - \Delta t) + \vartheta(t - 2\Delta t)}{\Delta t^2} \tag{4.1}$$

---
[1] See also Remark 2.4.

Software	Version
Operating System: Ubuntu	18.04.5 LTS
Matlab [135]	9.4.0.813654 (R2018a)
Matlab's Symbolic Math Toolbox	Version 8.1 (R2018a)
Python [171]	3.8.1
NumPy [157]	1.18.1
SciPy [224]	1.4.1
FEniCS [3]	2019.1.0
dolfin-adjoint [144]	2019.1.0
Pint [83]	0.10.1
Gmsh [78]	3.0.6
ParaView [162]	5.6.0

Table 4.1: Software used in the numerical experiments.

on an *equidistant time grid* $I_h = (0, \Delta t, 2\Delta t, \dots, T)$ with *time step* Δt. Note that for $\tau = 0$ the discretization (4.1) of the Cattaneo–LITT model reproduces a backward-finite-difference scheme for the classical LITT model. For each point t_k in the discrete time grid I_h, we get a weak formulation of a PDE for $\vartheta(t_k)$, which depends only on the spatial variable.

Different from Chapter 2, we allow the blood-perfusion rate $\xi = \xi_c + (\xi_n - \xi_c)\gamma$ to depend on the coagulation γ [32, 65, 199]. Thus, the bilinear forms F_h and F_r as well as the right hand side f_h in equation (2.11) depend on the coagulation γ here.

In each time step, we face a system of nonlinearly coupled PDEs because the coagulation γ depends nonlinearly on the temperature ϑ. There are several ways for the numerical solution of such systems, like fixed-point iterations (Gauss–Seidel multiphysics coupling), Newton's method or multiphysics operator splittings [108, Sec. 1.2, Alg. 1–3, p. 7–8].

For instance, in [154], the classical LITT model as discussed in Section 1.2 is solved, after spatial discretization, in each time step with Newton's method.

For simplicity, we use the numerical scheme presented in Algorithm 4.1, which corresponds to a standard multiphysics operator splitting. We choose a semi-implicit discretization in time which allows us to solve for each discrete point in time consecutively two separate *elliptic boundary-value problems* instead of a system of two nonlinearly coupled elliptic boundary-value problems. The error which is introduced by the operator splitting is negligible in our simulations for $\Delta t \to 0$. This is validated in Experiment 4.4, where several solutions computed with a time step of $1\,\mathrm{s}$ show no significant deviation compared to the corresponding solutions computed with a time step of $0.1\,\mathrm{s}$.

■ **Algorithm 4.1 — Numerical scheme for the Cattaneo–LITT model.**

Required:

- A finite-dimensional subspace $V_n \subset H^1(\Omega)$ according to a finite-element method,

- an equidistant time grid $I_h = (0, \Delta t, 2\Delta t, \dots, T)$ with time step Δt.

1: Initialize[a] : $\gamma(t_0) \equiv 1$, $\phi(t_0) \equiv 0$, $\vartheta(t_0) = \vartheta^{(0)}$, $\vartheta(t_{-1}) = \vartheta^{(0)}$ in V_n.

2: **for** $k \geq 1$ **do**

3:     Solve for $\phi(t_k) \in V_n$:

$$F_{\mathrm{r}}(\phi(t_k), \varphi; \gamma(t_{k-1})) = (g_{\mathrm{r}}, \varphi)_{L^2(\Gamma)} \quad \text{for all } \varphi \in V_n. \tag{4.2}$$

4:     Solve for $\vartheta(t_k) \in V_n$:

$$\left(\frac{\tau}{\Delta t^2} + \frac{1}{\Delta t} \right) (\vartheta(t_k), \varphi)_{L^2(\Omega)} + F_{\mathrm{h}}(\vartheta(t_k), \varphi; \gamma(t_{k-1}))$$

$$= \langle f_{\mathrm{h}}(\phi(t_k), \gamma(t_{k-1})), \varphi \rangle_{H^1(\Omega)} + \left(\left(\frac{2\tau}{\Delta t^2} + \frac{1}{\Delta t} \right) \vartheta(t_{k-1}) - \frac{\tau}{\Delta t^2} \vartheta(t_{k-2}), \varphi \right)_{L^2(\Omega)} \tag{4.3}$$

   for all $\varphi \in V_n$.

5:     Compute[b]

$$\gamma(t_k) = \frac{1}{1 + \Delta t \cdot d(\vartheta(t_k))} \gamma(t_{k-1}).$$

---

[a] The choice of $\vartheta(t_{-1}) = \vartheta^{(0)}$ corresponds to the choice of $\vartheta'(0) = \vartheta^{(1)} = 0$. The numerical value of the initial temperature $\vartheta^{(0)}$ is given w.r.t. kelvin because the computation of the coagulation in step 5 expects numerical values w.r.t. kelvin.

[b] We write the Arrhenius law (1.3) as ODE: $\partial_t \gamma = -d_{\mathrm{Arr}}(\vartheta) \cdot \gamma$, with $\gamma(0, x) = 1$ for all $x \in \Omega$, and apply one step of the implicit Euler method [87, Sec. 6.5, p. 89].

The problems (4.2) and (4.3) are elliptic boundary-value problems which can be solved numerically, e.g., by means of the *finite-element method*.[2] We use *triangular linear Lagrange finite elements* and employ FENICS to assemble and solve the corresponding linear systems. The resulting linear systems are solved with the default solver of FENICS, which uses a *sparse LU decomposition (Gaussian elimination)* [115, Ch. 5.2, p. 115]. For the later application in three-dimensional spatial domains, one might switch to *iterative solvers* to speed up the computation and reduce the memory requirement. The occurring integrals are computed via quadrature rules. The quadrature degree is automatically determined by FENICS such that the quadrature rule is exact for the highest order polynomial in the form being assembled. We project all occurring functions (nonlinear coefficients, initial data, etc.) onto our finite-element space, i.e., we work with globally continuous functions which are piecewise linear on each triangle of the mesh.

---

[2] Two reasons why we decided for the finite-element method. *"The finite element method combines geometric flexibility, the availability of a wide range of discrete function spaces, [..], and a particular elegant mathematical representation which facilitates rigorous analysis."* [197, Ch. 1, p. 2] Furthermore, it allows us to use well-established tools like FENICS and DOLFIN-ADJOINT. For further reading on the numerical treatment of PDEs including the finite-element method, we refer to [86].

Reduction of the spatial dimension

For our proof of concept, we would like to reduce the spatial dimension from 3D to 2D in order to reduce the computational costs. We note that our code provided in [8] allows computations in 3D, like demonstrated in Experiment 4.2.

We assume that the domain Ω as well as all coefficients and boundary conditions are rotationally symmetric w.r.t. rotations around the y-axis, where the y-axis is aligned with the applicator, like illustrated in Figure 4.1.

We note that the boundary

$$\Gamma_{\text{sym}} = \{(0, y, 0)^{\text{T}} \mid y \in [0\,\text{cm}, 0.75\,\text{cm}]\} \tag{4.4}$$

does not represent a boundary of the original 3D model. This boundary is aligned with the symmetry axis. Consequently, we impose homogeneous Neumann boundary conditions

$$\left.\begin{aligned} \kappa\nabla\vartheta \cdot \boldsymbol{n} = 0 \\ D\nabla\phi \cdot \boldsymbol{n} = 0 \end{aligned}\right\} \text{ on } I \times \Gamma_{\text{sym}} \tag{4.5}$$

with the outward pointing normal vector $\boldsymbol{n} = [-1, 0]^{\text{T}}$. The area of the radiating surface is

$$|\Gamma_{\text{rad}}| = 2\pi \times 0.25\,\text{cm} \times 2\,\text{cm} = \pi \times 10^{-4}\,\text{m}^2. \tag{4.6}$$

For the transformation of the integrals of the weak formulation, we need to include the functional determinant of the transformation from cylindrical to Cartesian coordinates. We provide details in Appendix A.3.

We validate our reduction of the three-dimensional, rotationally symmetric problem to the corresponding two-dimensional problem with the following experiment.

■ **Experiment 4.2 — Validation of reduction 3D → 2D.**

We compute the temperature of the Cattaneo–LITT model for three different meshes. The mesh $\Omega_{\text{2D},h}^{(0)}$ is locally refined around the applicator, which is illustrated in the cross section in Figure 4.1. We refine $\Omega_{\text{2D},h}^{(0,0)}$ by splitting (see Figure 4.2) and obtain $\Omega_{\text{2D},h}^{(0,1)}$ as a reference mesh in 2D. Furthermore, we extrude $\Omega_{\text{2D},h}^{(0,0)}$ rotationally around the y-axis and obtain the 3D mesh $\Omega_{\text{3D},h}^{(0,0)}$. We summarize the mesh details in the following table:

mesh	number of nodes	number of elements
$\Omega_{\text{2D},h}^{(0,0)} \subset \mathbb{R}^2$	1557	3007 (triangles)
$\Omega_{\text{2D},h}^{(0,1)} \subset \mathbb{R}^2$	6120	12028 (triangles)
$\Omega_{\text{3D},h}^{(0,0)} \subset \mathbb{R}^3$	62883	379328 (tetrahedra)

We evaluate the numerical solution for the temperatures for each mesh at the final time T on the reference line $\Omega_{\text{1D, ref}}$ and on the "artificial" 2D boundary Γ_{sym} (see Figure 4.1 and equation (4.4)). Furthermore, we evaluate the 3D solution on the circle C with radius $0.34\,\text{cm}$ in the x–z-plane at $y = 2.5\,\text{cm}$ around the y-axis, i.e.,

$$C = \{0.34\,\text{cm} \times (\cos\theta, 0, \sin\theta)^{\text{T}} + (0, 2.5\,\text{cm}, 0)^{\text{T}} \mid \theta \in [0, 2\pi)\}.$$

We use the physical parameters given in Table 1.1 and the following simulation details:

τ	$= 0\,\mathrm{s}$	(parameter in the Cattaneo model)
Δt	$= 1\,\mathrm{s}$	(discrete time step)
T	$= 120\,\mathrm{s}$	(final time of the simulation)
$\vartheta^{(1)}(x)$	$= 0\,\mathrm{K\,s^{-1}}$	(second initial condition for the temperature)
$u(x)$	$= 0.15$	(constant control)[a]

[a] See Remark 4.6.

(a) **(b)**

Figure 4.1: Rotational symmetric spatial domain Ω. (4.1a): Segment of the rotational symmetric domain in $\mathbb{R}^3$. (4.1b): Corresponding slice in the x–y-plane[3]. The green line defines the reference line $\Omega_{1\mathrm{D,\,ref}} = \{(x, 2.5\,\mathrm{cm}, 0)^{\mathrm{T}} \,|\, x \in [0.25\,\mathrm{cm}, 3\,\mathrm{cm}]\}$. It holds $|\Gamma_{\mathrm{rad}}| = \pi \times 10^{-4}\,\mathrm{m}^2$.

Figure 4.2: Refinement by splitting (implemented in GMSH [78]).

---

[3] The unit of length in 4.1b is *centimeter*.

Figures 4.3 and 4.4 illustrate and compare three numerical solutions for the temperature in Experiment 4.2 (one for each mesh $\Omega_{2D,h}^{(0,0)}$, $\Omega_{2D,h}^{(0,1)}$, $\Omega_{3D,h}^{(0,0)}$). We note that the colors in the 3D visualization may deviate from the colors of the 2D visualization due to artificial lighting.

Figure 4.3c shows that the approximation of the 2D solution is converged w.r.t. the spatial discretization, in the order of the scale of this visualization, and accounting for interpolation errors.

The deviation between the 2D and 3D solutions is in the range of the deviation of the 3D solution on the circle C. Ideally, the 3D solution would be rotational symmetric and, thus, constant on the circle C. Its deviation is due to discretization errors of our numerical method for solving the LITT system on the one hand, on the other hand due to interpolation errors induced by the evaluation of the numerical solution (piecewise constant) on the circle C.

Figure 4.4 shows that the 2D and 3D solutions coincide along the artificial 2D boundary Γ_{sym} up to discretization and interpolation errors, which validates the choice of the homogeneous Neumann boundary conditions (4.5) for the 2D model.

Experiment 4.2 validates the two-dimensional implementation of the solver for the Cattaneo–LITT model and the reduction of the corresponding three-dimensional, rotationally symmetric problem to a two-dimensional problem.

In the following experiments of this chapter, we restrict ourselves to the two-dimensional domain. This reduces the computational costs and allows us to use a further refined mesh, shown in Figure 4.5. The increased spatial resolution of the mesh is especially useful in Section 4.3, where we want to reconstruct the heterogeneous blood-perfusion rate. We point out that, for the assembly of the corresponding linear systems, we need to incorporate the functional determinant of the transformation from cylindrical to Cartesian coordinates, as stated above.

Remark 4.3 — Colormap.

The colormap in Figure 4.3 is based on the *bent-cool-warm* colormap in [152, 153]. We fitted it in such a way that there is a sharp bend at $60\,°C$, which indicates roughly the region of coagulation. This is based on rather simplistic coagulation models, e.g., [166, 170], where the coagulation is defined as

$$\gamma(t, x) = \begin{cases} 1, & \text{there is an } s \in [0, t] \text{ with } \vartheta(s, x) > 60\,°C, \\ 0, & \text{else,} \end{cases}$$

which means, that the tissue at a position x is assumed to be coagulated once the temperature reached the threshold of $60\,°C$. In [187, p. 248] and the references therein, it is reported that at temperatures between $60\,°C$ and $100\,°C$ necrosis occurs immediately.

In cases where the temperature is monotonically increasing in every point over the duration of the simulation, e.g., later in the real application, this technique yields a simple and fast way to estimate the coagulation zone purely based on current temperature data. Nevertheless, in this thesis we compute the coagulation always by means of the Arrhenius law.
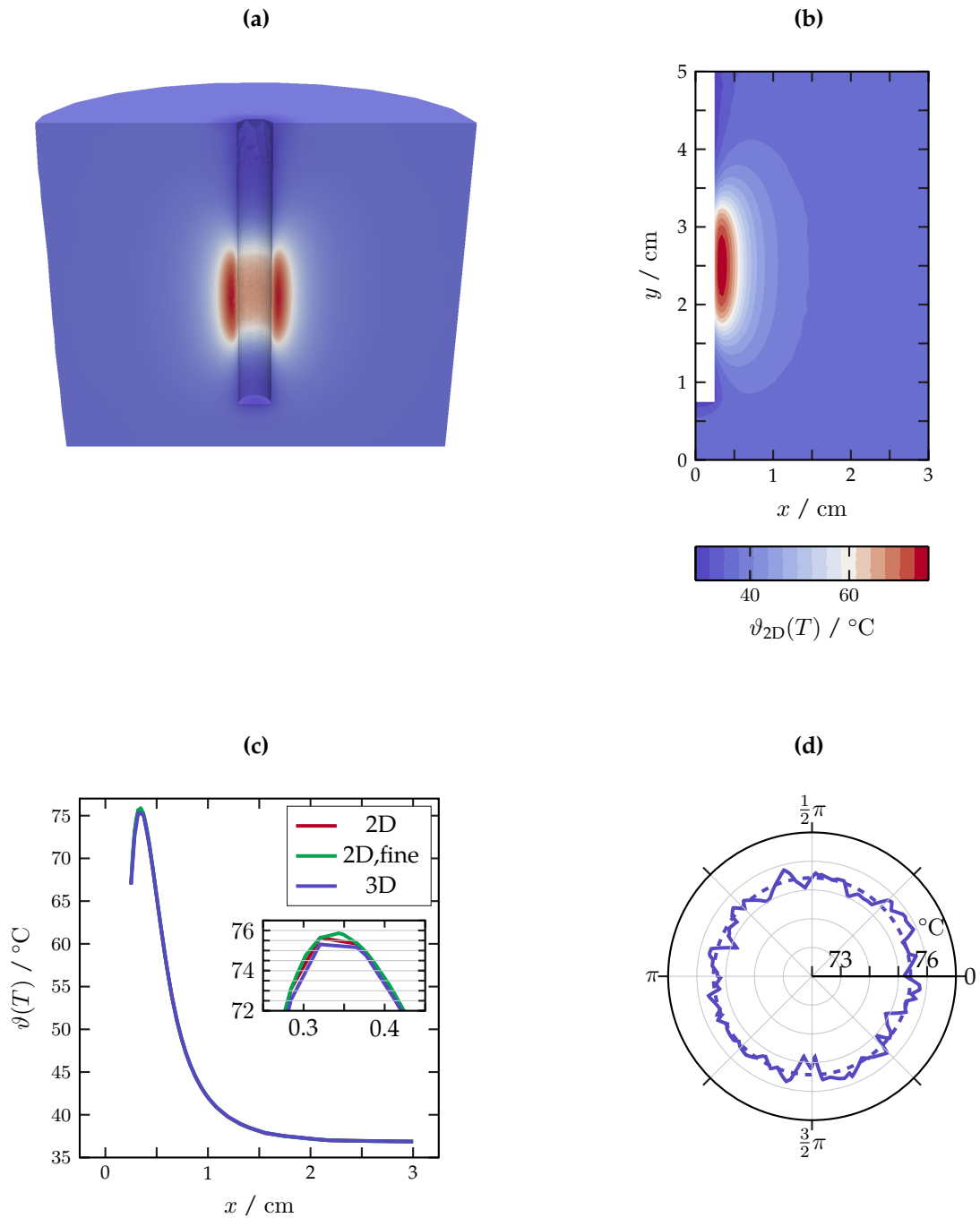
(a)
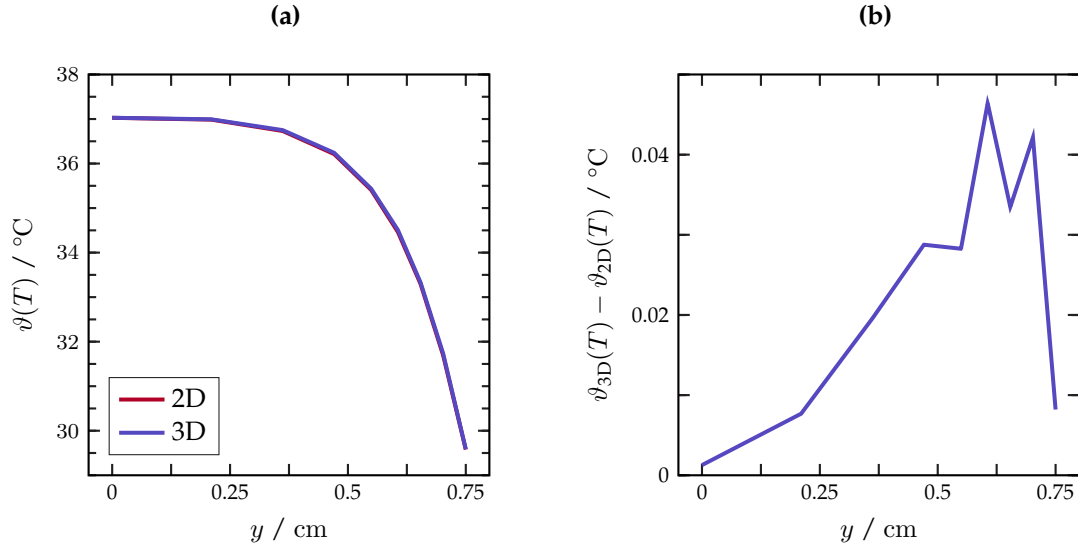
(b)

$\vartheta_{2D}(T)$ / °C

(c)

(d)

Figure 4.3: Results of Experiment 4.2. Numerical solutions for the temperature of the rotational symmetric model in 3D ($\vartheta_{3D}(T)$) and the corresponding 2D model ($\vartheta_{2D}(T)$, on coarse and fine mesh) at time $T = 120$ s. (4.3a): Slice through the x–y-plane of $\vartheta_{3D}(T)$ visualized with ParaView. (4.3b): 2D solution $\vartheta_{2D}(T)$. (4.3c): Solutions evaluated on the reference line $\Omega_{1D,\,ref}$. (4.3d): Deviation of $\vartheta_{3D}(T)$ on the circle C. The dashed line indicates the mean value on this circle.

(a) **(b)**

Figure 4.4: Results of Experiment 4.2. Numerical solutions for the temperature of the rotational symmetric model in 3D ($\vartheta_{3\mathrm{D}}(T)$) and the corresponding 2D model (on coarse mesh $\Omega_{2\mathrm{D},h}^{(0,0)}$) at time $T = 120\,\mathrm{s}$. (4.4a): Evaluation of $\vartheta_{3\mathrm{D}}(T)$ and $\vartheta_{2\mathrm{D}}(T)$ on the "artificial" 2D boundary Γ_{sym}. (4.4b): Difference $\vartheta_{3\mathrm{D}}(T) - \vartheta_{2\mathrm{D}}(T)$ on the "artificial" 2D boundary Γ_{sym}.

(a) **(b)** **(c)**
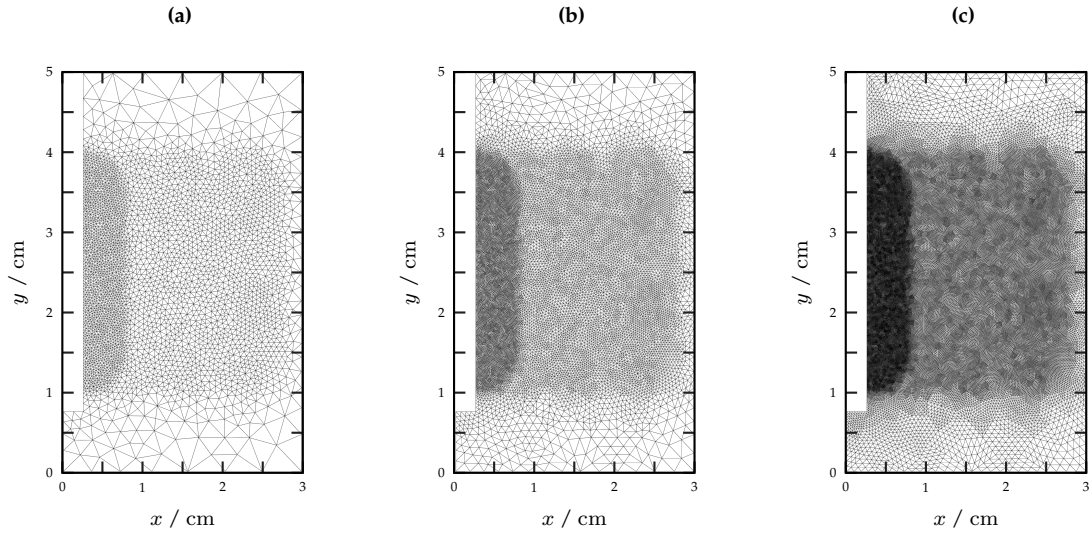
Figure 4.5: Hierarchy of discretizations of the spatial domain Ω for Experiments 4.4–4.11, 6.6 and 6.8, refined by splitting. The mesh is locally refined along the applicator boundary Γ_{rad} to improve the accuracy of the solution for the irradiance ϕ. Furthermore, the mesh is locally refined in a certain subdomain where we place artificial blood vessels in Section 4.3. (4.5a): $\Omega_{2\mathrm{D},h}^{(1,0)}$ with 3607 nodes and 7074 triangles. (4.5b): $\Omega_{2\mathrm{D},h}^{(1,1)}$ with 14287 nodes and 28296 triangles. (4.5c): $\Omega_{2\mathrm{D},h}^{(1,2)}$ with 56869 nodes and 113184 triangles.

4.2 Delayed heat transfer

The following numerical experiment demonstrates the effect of the delay parameter τ in the Cattaneo–LITT model.

■ **Experiment 4.4 — Delayed heat transfer.**

We compute the temperature and coagulation of the Cattaneo–LITT model for different values of τ, each with the two time steps Δt and Δt_{fine} in the finite-difference scheme (4.1). We evaluate the solutions for different points in time on the reference line $\Omega_{\text{1D, ref}}$.

We use the physical parameters given in Table 1.1 and the following simulation details:

τ	$\in \{0\,\text{s}, 15\,\text{s}, 30\,\text{s}, 60\,\text{s}\}$	(delay parameter in the Cattaneo model)
Δt	$= 1\,\text{s}$	(discrete time step)
Δt_{fine}	$= 0.1\,\text{s}$	(refined discrete time step)
T	$= 300\,\text{s}$	(final time of the simulation)
$\vartheta^{(1)}(x)$	$= 0\,\text{K}\,\text{s}^{-1}$	(second initial condition for the temperature)
$u(x)$	$= 0.15$	(constant control)[a]

For the spatial discretization, we use the mesh $\Omega_{\text{2D},h}^{(1,0)}$ shown in Figure 4.5 with 3607 nodes and 7074 elements (triangles).

---
[a] See Remark 4.6.

In Figure 4.6, we visualize the results of Experiment 4.4. We observe the delaying effect of the parameter τ at the beginning of the simulation, here at the times $t \in \{30\,\text{s}, 60\,\text{s}\}$. At some point, the temperatures for $\tau > 0$ overshoot the temperature for $\tau = 0$, as can be seen at $t = 150\,\text{s}$. This behavior is expected from a mathematical point of view[4], and a further investigation would need to discuss the implications of those overshoots from a physical point of view. Towards the end of the simulation, the solutions for $\tau > 0$ converge to the one for $\tau = 0$. We do not show the solutions for times larger than $t = 300\,\text{s}$ because the deviations between the solutions for different values of τ decrease even further.

In view of the optimal-control problem discussed in Chapter 3 and Section 4.3, the first 1–2 minutes of the simulation are crucial. There, we attempt to identify the blood-perfusion rate based on the difference between the measured temperature and the simulation output at the time of the first measurement, which is available in the real application around two minutes after the start of the therapy. In the targeted application of prognostic LITT, the blood-perfusion rate is estimated during the first part of the therapy and is fed back to the simulation for the remaining part of the therapy in real time. Deviations of the models in the first part of the simulation might have a relevant effect on the estimation of the blood-perfusion rate and, thus, on the remaining simulation based on the updated parameter. This feed-back effect can not be observed in our experiment because we run the simulation with a fixed control u, but should be discussed and quantified in future work by further numerical experiments.

---
[4] Cf. [100, VIII, paragraph on *"1972, Y. Taitel, Int. J. Heat Mass Transfer 15, 369"*, p. 62].

In Section 2.1, we discussed a possible range for values of τ based on a literature review, but it is unclear to this point which value for τ is suitable for our application. The answer to this question requires the validation with real experimental data. Nevertheless, a value of $\tau = 60\,\text{s}$ seems rather large in this context, whereas for smaller values the differences between the solutions of the classical ($\tau = 0$) and the Cattaneo–LITT model ($\tau > 0$) becomes relatively small, considering that the time scale of a real therapy is around $1200\,\text{s}$. It depends on the quality of the measured temperature data whether the correction given by the Cattaneo heat-transfer model (with appropriate values for τ, probably much smaller than $30\,\text{s}$) increases the accuracy of the final prediction compared to the classical LITT model, respecting the fact that the measured temperature data as well as the used physical parameters are disturbed, e.g., by measurement errors.

In summary, the numerical experiment validates the suggested delaying effect of the parameter τ in the Cattaneo–LITT model.[5]

---

[5] The Cattaneo model is also known as "delayed heat-transfer model".
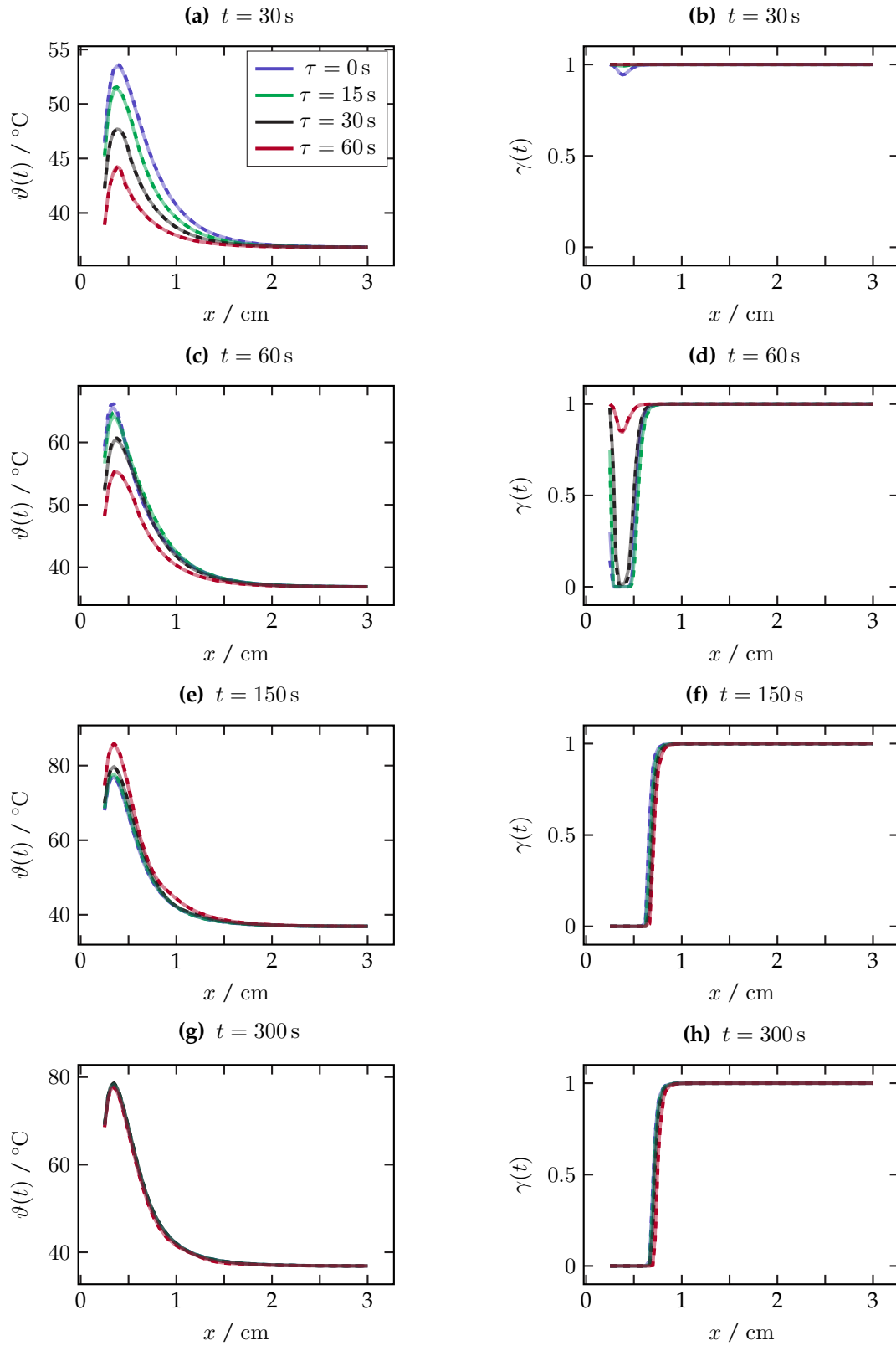
Figure 4.6: Results of Experiment 4.4. Temperature ϑ and coagulation γ (1: native, 0: coagulated) for different delay parameters τ, evaluated on the reference line $\Omega_{1D,\,ref}$ at different points in time. The solid and dashed lines correspond to the solutions computed with a time step Δt and Δt_{fine}, respectively. The legend of Figure 4.6a holds for all subfigures.

4.3   Identification of the blood-perfusion rate

We give a proof of concept for the automated identification of the unknown control u that models the spatial distribution of the blood-perfusion rate in equation (3.1). The spatial distribution is influenced by the location of large vessels, which suggests the interpretation of the control u as an indicator function for large blood vessels.

In Figure (4.7), we define the ground-truth data u_{true} for the identification. We use u_{true} to produce synthetic measurement data by running the Cattaneo–LITT simulation with $u = u_{\mathrm{true}}$ and defining the corresponding simulated temperature at a given point in time T as the desired temperature $\vartheta_{\mathrm{d}} := \vartheta(T; u_{\mathrm{true}})$ (see equation (3.5)). We proposed a similar numerical example to demonstrate the identification of the blood-perfusion rate in our manuscripts [9–12].
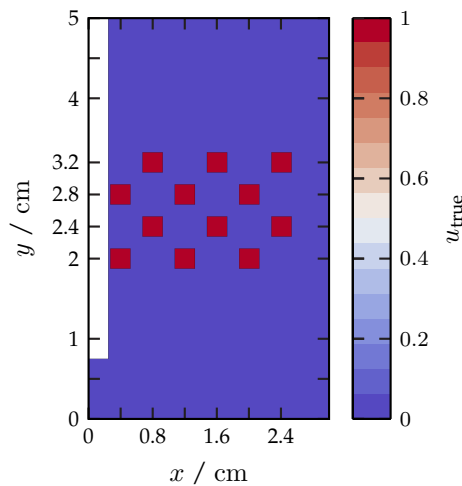
Figure 4.7: Synthetic control u_{true}. The red square patches mark the interior of large blood vessels. The side length of each red square patch is $0.25\,\mathrm{cm}$. The ticks on the x-axis and y-axis mark the centers of each patch. The blue area contains only capillary vessels.

4.3.1   Influence of the blood-perfusion rate

With the following experiment, we want to quantify the influence of the control u and, with this, of the location of large vessels on the predicted coagulation zone, for our specific set of parameters.

■ **Experiment 4.5 — Influence of the blood-perfusion rate.**

We compute the coagulation γ for the three different choices of the control $u = u_i, i \in \{1, 2, 3\}$. We use the physical parameters given in Table 1.1 and the following simulation details:

τ	$= 0\,\mathrm{s}$	(parameter in the Cattaneo model)
Δt	$= 1\,\mathrm{s}$	(discrete time step)
T	$= 1200\,\mathrm{s}$	(final time of the simulation)
$\vartheta^{(1)}(x)$	$= 0\,\mathrm{K\,s^{-1}}$	(second initial condition for the temperature)
$u_1(x)$	$= 0.0$	(constant control)
$u_2(x)$	$= 0.15$	(constant control, see Remark 4.6)
u_3	$= u_{\mathrm{true}}$	(true control, see Figure 4.7)

For the spatial discretization, we use the mesh $\Omega_{2D,h}^{(1,0)}$ given in Figure 4.5 with 3607 nodes and 7074 elements (triangles). We refine the mesh by splitting and obtain the mesh $\Omega_{2D,h}^{(1,1)}$ with 14287 nodes and 28296 elements, which we use to compute reference solutions.

(a) **(b)**
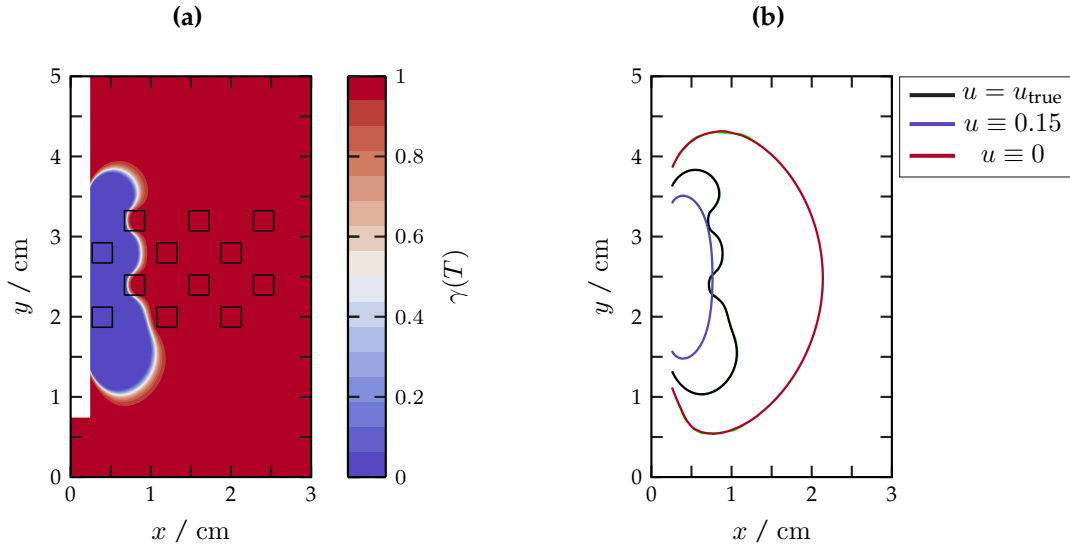
Figure 4.8: Results of Experiment 4.5. Influence of the blood-perfusion rate on the estimated tissue damage. (4.8a): Coagulation $\gamma(T)$ at the final time T for $u = u_{\mathrm{true}}$. The black lines indicate the contours of the underlying vessel structure, i.e., the contours of u_{true}. (4.8b): Contour lines of the coagulation at the final time T at level $\gamma(T) = 0.5$ for the different choices of the control u. The green lines (almost not visible) indicate the corresponding solutions on the refined mesh.

In Figure 4.8, we observe that the shape of the boundary of the coagulated zone is influenced by the presence of large blood vessels, i.e., regions where the control u is close to one. As expected, the coagulation zone spreads slower near the blood vessels due to the cooling effect of the blood flow.

Figure 4.8b compares the contour lines at level $\gamma(T) = 0.5$ of the coagulated zone for different choices of the control u. The predicted coagulation zone in the case where we neglect all large vessels ($u \equiv 0$) deviates more than $1\,\mathrm{cm}$ in x-direction from the other two scenarios. Furthermore, we observe a difference between the coagulated zones for $u \equiv 0.15$ and $u = u_{\mathrm{true}}$. According to Remark 4.6, the choice $u \equiv 0.15$ represents an averaged version of u_{true}. We see from the difference between the contour lines that averaging does not capture the local influence of large
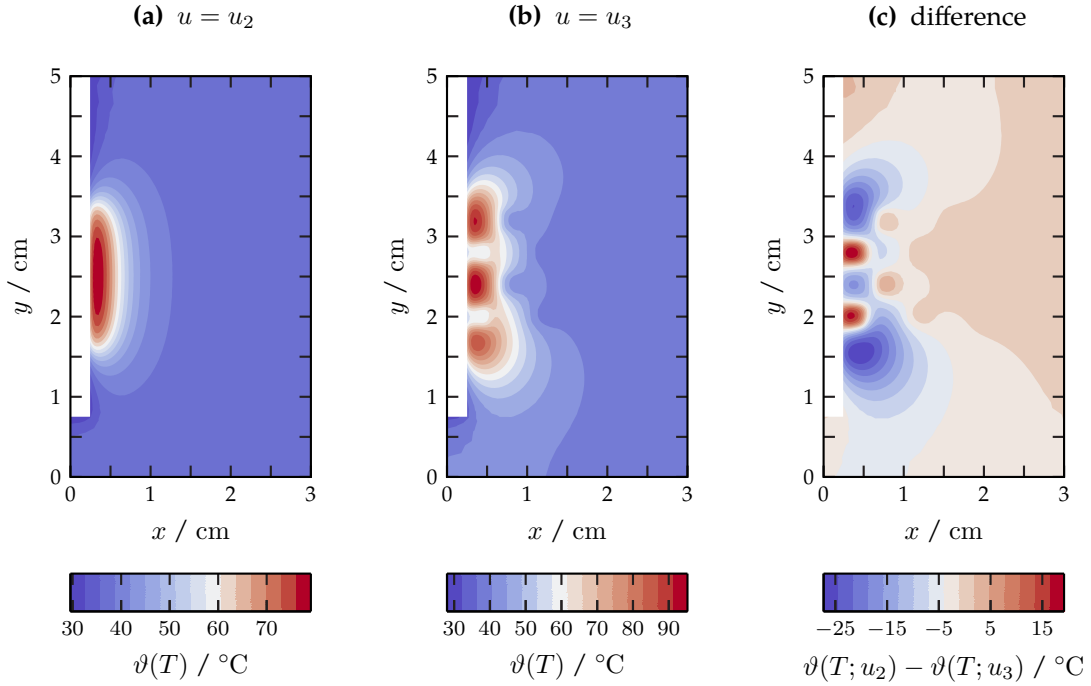
Figure 4.9: Results of Experiment 4.5. Influence of the blood-perfusion rate on the simulated temperature. (4.9a): Temperature for $u = u_2$ at the final time T. (4.9b): Temperature for $u = u_3$ at the final time T. This coincides with the synthetic temperature measurement data ϑ_d. (4.9c): Difference between simulated temperatures for $u = u_2$ and for $u = u_3$ at the final time T.

blood vessels, especially at the boundary of the coagulated zone.

A deviation of the predicted coagulation zone of this range would lead to a wrong therapy planning in the real application and might have fatal consequences for the success of the cancer treatment.

The choice of the control u also influences the temperature distribution. Figure 4.9 shows that the simulated temperature correlates with the given control. In Figure 4.9c, even the spatial distribution of the true control becomes visible.

This motivates us to use the measured temperature data ϑ_d to identify the parameter u and, with this, the spatial distribution of the blood-perfusion rate. In fact, the temperature difference in Figure 4.9c (for another final time T) enters the cost functional described in Chapter 3. The numerical investigation of the parameter identification problem follows in the next section.

Remark 4.6 — Homogeneous blood-perfusion rate.

We choose $u_2 \equiv \bar{u}_2 = 0.15$ in several experiments. This numerical value is motivated by the homogenized value of u_true over the rectangular subregion

$$\Omega_\mathrm{rad} := [0.0025, 0.0275] \times [0.015, 0.035]$$

(left boundary coincides with Γ_{rad}, see Figure 4.1b). More precisely, we want the following equation to be satisfied:

$$\bar{u}_2 \, |\Omega_{\text{rad}}| = \int_{\Omega_{\text{rad}}} u_2(x) \, \mathrm{d}x \overset{!}{\approx} \int_{\Omega_{\text{rad}}} u_{\text{true}}(x) \, \mathrm{d}x = 12A$$

with $A = l^2$ the area of the 2D vessel-boxes in Figure 4.7 with side length $l = 0.0025 \, \text{m}$ and $|\Omega_{\text{rad}}| = 5.0 \times 10^{-4} \, \text{m}^2$. This yields $\bar{u}_2 = 12A \, |\Omega_{\text{rad}}|^{-1} = 0.15$.

4.3.2 Algorithmic details

In Chapter 3, we formulated the identification of the control u in the context of PDE-constrained optimization. For a general overview on optimization with PDE constraints and corresponding numerical methods, we refer to [93] and [217].

We implement the descent algorithm 3.15 presented in Section 3.3, where we compute the search direction in line 3 by means of algorithmic differentiation (AD), as described in the next subsection.

Computation of descent directions

In Section 3.3, we presented a descent strategy based on the directional derivatives of the reduced cost functional. Note that the reduced cost functional $\hat{J} \colon U_{\text{ad}} \to \mathbb{R}$ is not Gâteaux differentiable, so, formally, we can not speak of gradients. On the other hand, Lemma 3.13 yields that the directional-derivative operator $h \mapsto \mathrm{D}_u \hat{J}(u)[h]$ can be expressed via a linear functional on the set of admissible directions. The corresponding Riesz representative w.r.t. the $L^2(\Omega)$ scalar product (in the following: L^2 Riesz representative) g is our candidate for a descent direction:

$$g(u) = \lambda_1 + \lambda_2 u + \int_0^T (\xi_{\text{in}} - \xi_{\text{out}})(\vartheta_{\text{b}} - \vartheta(u)(t)) z_2(u)(t) \, \mathrm{d}t \tag{3.20}$$

where ϑ is part of the state vector of the Cattaneo–LITT model and z_2 part of the corresponding adjoint state vector for a given control u.

There are two ways to compute this suggested search direction $d \coloneqq -g(u)$ in Algorithm 3.15. First, we could solve the Cattaneo–LITT system and the corresponding adjoint system (see Section 3.2) for a given control u, e.g., by means of a finite-element discretization, and compute the right-hand side in (3.20).

This would correspond to the classical *first-optimize-then-discretize* principle. We validated this approach in numerical experiments presented in [9–12].

The second approach follows the *first-discretize-then-optimize* principle, where we first discretize the problem and then develop algorithms for the optimization. In the latter case, one approximates the control $u : \Omega \to \mathbb{R}$ In terms of a finite-element discretization as follows:

$$u \approx u_{\text{d}} = \sum_{i=1}^n u_i \varphi_i, \quad u_i \in \mathbb{R}, \quad \boldsymbol{u} \coloneqq \left[u_1, \ldots, u_n\right]^{\mathrm{T}},$$

where $(\varphi_i)_{i=1}^n$ is a globally continuous, piecewise linear nodal basis according to a given mesh, where n denotes the number of nodes. This allows us to consider the discretized reduced cost

functional

$$\hat{J}_{\mathrm{d}} : \mathbb{R}^n \to \mathbb{R}, \; \boldsymbol{u} \mapsto \hat{J}(u_{\mathrm{d}}). \tag{4.7}$$

One disadvantage of this approach is that this formulation explicitly includes information of the underlying spatial discretization, i.e., the subsequent optimization might be *mesh dependent*[6]. We refer to [197] for details on mesh dependence in PDE-constrained optimization.

Nevertheless, this approach allows us to use algorithmic differentiation to compute the gradient of the discretized reduced cost functional $\hat{J}_{\mathrm{d}}$, which comes with three great advantages.

First, we need to implement only a solver for the Cattaneo–LITT model. It helps to produce an elegant implementation by means of *operator overloading*, which enhances readability of our code[7] and, thus, reusability for future research.

Second, we implement the simulation of the Cattaneo–LITT model in FEniCS, which allows us to incorporate the tested and established algorithmic differentiation (AD) framework realized in the DOLFIN-ADJOINT package. This means that we obtain gradient information without any major effort from an implementation point of view on our side.

Last, the AD framework provides the gradient of the discretized reduced cost functional with an accuracy in the order of machine precision. This allows us to verify the computed derivative by means of a *Taylor-remainder convergence test* . We quote the DOLFIN-ADJOINT documentation [143]:

> "This test is based on the observation that
>
> $$r^{(1st)}(\lambda) := \left| \hat{J}_d(\boldsymbol{u} + \lambda\boldsymbol{h}) - \hat{J}_d(\boldsymbol{u}) \right| \to 0 \quad at \; \mathcal{O}(\lambda),$$
>
> but that
>
> $$r^{(2nd)}(\lambda) := \left| \hat{J}_d(\boldsymbol{u} + \lambda\boldsymbol{h}) - \hat{J}_d(\boldsymbol{u}) - \lambda\nabla^{AD}\hat{J}_d(\boldsymbol{u})^{\mathrm{T}} \cdot \boldsymbol{h} \right| \to 0 \quad at \; \mathcal{O}(\lambda^2),$$
>
> by Taylor's theorem. We can verify the correctness of $\nabla^{AD}\hat{J}_d$ by computing the second-order Taylor remainder $r^{(2nd)}(\lambda)$ for some choice of λ and $\boldsymbol{h}$, then repeatedly halving λ and checking that the result decreases by a factor 4."

This procedure is already implemented in the DOLFIN-ADJOINT package.

For readers who are not familiar with algorithmic differentiation, we refer to [155] for a great introduction. For a detailed discussion on AD, we refer to [84].

For the following experiments, we follow [197] and combine the advantages of both principles. First, we compute the gradient of the discretized reduced cost functional by means of AD.[8] Next, we use this gradient information for our original descent strategy presented in Algorithm 3.15. We note that the variation of the reduced cost functional in the direction of the ith nodal basis corresponds to variation of the discretized reduced cost functional in the ith component (see Remark 4.7 below):

$$\mathrm{D}_u \hat{J}(u)[\varphi_i] = (g(u), \varphi_i)_{L^2(\Omega)} \overset{!}{\approx} \left(\nabla^{\mathrm{AD}} \hat{J}_{\mathrm{d}}(\boldsymbol{u}) \right)_i. \tag{4.8}$$

---

[6] "In this context, mesh-independent convergence of the optimisation algorithm means that, for a discretisation given on a sufficiently fine mesh, the number of iterations required to solve the optimisation problem to a given tolerance is bounded." [197, Ch. 2, p. 53]

[7] Available under [8].

[8] If one wants to proceed from here in the classical first-discretize-then-optimize sense and employ standard techniques of finite-dimensional optimization, we refer to the PYTHON package MOOLA [73]. It is recommended by the official DOLFIN-ADJOINT documentation, e.g., [142].
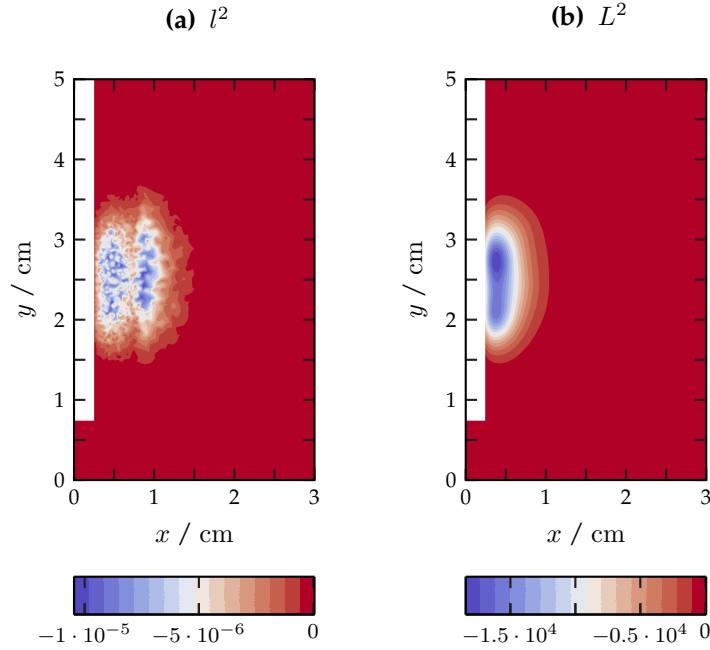
(a) l^2 **(b)** L^2

Figure 4.10: Riesz representatives of the discretized reduced cost functional (4.7) (cf. [197, Sec. 2.3.2.1, Fig. 2.5, p. 73]) w.r.t. different scalar products. The simulation details are the same as in Experiment 4.8. (4.10a): $\nabla^{\mathrm{AD}} \hat{J}_{\mathrm{d}}(\boldsymbol{u}_0)$: Gradient of the discretized reduced cost functional, i.e., l^2 Riesz representative of the derivative. (4.10b): g_{d}: L^2 Riesz representative of the derivative $\mathrm{D}_{\boldsymbol{u}} \hat{J}_{\mathrm{d}}(\boldsymbol{u})$ of the discretized reduced cost functional.

We approximate the function $g(u)$ by means of an expansion w.r.t. the given nodal basis

$$g(u) \approx g_{\mathrm{d}}(u) = \sum_{i=1}^{N} g_i \varphi_i \tag{4.9}$$

and plug this into equation (4.8), which yields the following linear system[9]:

$$M \cdot \boldsymbol{g} = \nabla^{\mathrm{AD}} \hat{J}_{\mathrm{d}}(\boldsymbol{u}) \tag{4.10}$$

with the mass matrix $M = \left((\varphi_i, \varphi_j)_{L^2(\Omega)} \right)_{i=1, j=1}^{n,n} \in \mathbb{R}^{n \times n}$ and the vector $\boldsymbol{g}$ containing the components g_i of the expansion (4.9). Note that the mass matrix *"reflects the structure of the underlying mesh, that is, the spatial distribution of elements and their sizes"* [197, Sec. 2.2.4, p. 60]. The solution $\boldsymbol{g}$ of the linear system (4.10) defines the function $g_{\mathrm{d}}(u)$ by means of the expansion (4.9) and, thus, the search direction $d = -g(u)$ in our descent algorithm.

Note that, in Section 3.2, we interpret the function $g(u)$ as L^2 Riesz representative of the directional-derivative operator $\mathrm{D}_u \hat{J}(u)$. Analogously, we can interpret $g_{\mathrm{d}}(u)$ as the L^2 Riesz representative of the derivative $\mathrm{D}_{\boldsymbol{u}} \hat{J}_{\mathrm{d}}(\boldsymbol{u})$ of the discretized reduced cost functional, whereas the gradient $\nabla^{\mathrm{AD}} \hat{J}_{\mathrm{d}}(\boldsymbol{u}) \in \mathbb{R}^n$ is the corresponding l^2 Riesz representative, i.e., w.r.t. the Euclidean

---

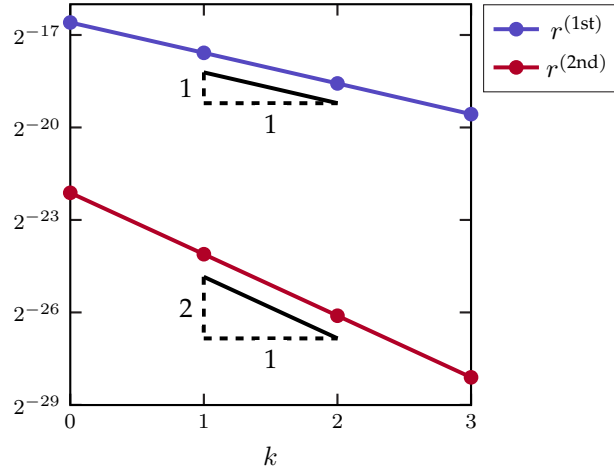[9] Cf. [197, Sec. 2.2.3, Eq. 2.19, p. 59].

Figure 4.11: Taylor-remainder convergence test. Visualization of Table 4.2.

scalar product. In fact, it holds

$$(g_{\mathrm{d}}(u), h)_{L^2(\Omega)} = \mathrm{D}_{\boldsymbol{u}} \hat{J}_{\mathrm{d}}(\boldsymbol{u})[\boldsymbol{h}] = \sum_{i=1}^{n} h_i \left(\nabla^{\mathrm{AD}} \hat{J}_{\mathrm{d}}(\boldsymbol{u}) \right)_i$$

for all $h = \sum_{i=1}^{n} h_i \varphi_i$, $\boldsymbol{h} = \left[h_1, \ldots, h_n \right]^{\mathrm{T}}$.

This approach can be seen as a preconditioning[10] to eliminate the dependence of the mesh. We demonstrate the effect of the preconditioning by visualizing the gradient of the discretized reduced cost functional $\nabla^{\mathrm{AD}} \hat{J}_{\mathrm{d}}(\boldsymbol{u_0})$ next to the corresponding $L^2(\Omega)$ representative $g_{\mathrm{d}}(u_0)$ in Figure 4.10, based on the simulation details given in the next Experiment 4.8. The underlying mesh structure becomes visible in the visualization of $\nabla^{\mathrm{AD}} \hat{J}_{\mathrm{d}}(\boldsymbol{u})$, in contrary to the visualization of $g_{\mathrm{d}}(u)$.

Before we look into the numerical experiments regarding the identification of the control u, we use the Taylor-remainder convergence test (see above) to validate the derivative of the discretized reduced cost functional $\nabla^{\mathrm{AD}} \hat{J}_{\mathrm{d}}$ in the next Experiment 4.8. We compute the derivative $\mathrm{D}_{\boldsymbol{u}} \hat{J}_{\mathrm{d}}(\boldsymbol{u_0})[\boldsymbol{h}]$ at $\boldsymbol{u_0} \equiv 0$ in direction $\boldsymbol{h} \equiv 0.2$ by means of algorithmic differentiation and present the results of the convergence test with initial step size $\lambda_0 = 0.01$ (default value in DOLFIN-ADJOINT) in Table 4.2. Each value in the second column is approximately half of its preceding value in the same column, and each value in the fourth column is approximately a quarter of its preceding value in the same column. We compute the convergence rate of the first Taylor remainder (analogously for the second Taylor remainder) for a given λ_0 as

$$\text{convergence rate} = \log \left(\frac{r^{(1\mathrm{st})}(\lambda_0 2^{-(k-1)})}{r^{(1\mathrm{st})}(\lambda_0 2^{-k})} \right) / \log(2).$$

The values in the third columns should be close to one and the values in the fifth column should be close to two. We visualize the convergence of the Taylor remainders $r^{(1\mathrm{st})}, r^{(2\mathrm{nd})}$ in Figure 4.11. The Taylor-remainder convergence test here validates the correctness of the computed gradient of the discrete reduced cost functional.

---

[10] This interpretation is suggested in [197].

k	$r^{(\text{1st})}(\lambda_0 2^{-k})$	convergence rate	$r^{(\text{2nd})}(\lambda_0 2^{-k})$	convergence rate
0	1.012×10^{-5}		2.199×10^{-7}	
1	5.115×10^{-6}	0.9845	5.530×10^{-8}	1.9912
2	2.571×10^{-6}	0.9922	1.387×10^{-8}	1.9956
3	1.289×10^{-6}	0.9961	3.472×10^{-9}	1.9978

Table 4.2: Taylor-remainder convergence test for $\nabla^{\text{AD}} \hat{J}_{\text{d}}(\boldsymbol{u}_0)^{\text{T}}$ at $\boldsymbol{u}_0 \equiv 0$ in direction $\boldsymbol{h} \equiv 0.2$ with initial step size $\lambda_0 = 0.01$. Ideally, the values of the first column "convergence rate" should be close to 1.0, the values of the second column "convergence rate" should be close to 2.0.

Note that, in our previously published manuscripts [9–11], we did not use the AD framework to compute the descent directions as discussed here, but we implemented a solver for the adjoint state system (3.19) and we computed the descent direction by means of the adjoint gradient representation according to Lemma 3.13.

> **Remark 4.7 — Technical detail on admissible directions.**
>
> The first equality in (4.8) follows from Lemma 3.13, provided that φ_i is an admissible direction at u, where $(\varphi_i)_{i=1}^n$ again is a globally continuous and piecewise linear nodal basis according to a given mesh, where n denotes the number of nodes.
>
> We consider a control $u = \sum_{i=1}^n u_i \varphi_i$ with $u_i = 1$ for some $i \in \{1, \ldots, n\}$.
>
> Technically, we did not show the existence of directional derivatives of the original reduced cost functional at u in the direction φ_i because $u^\lambda := u + \lambda \varphi_i$ is not an element of U_{ad} for all sufficiently small $\lambda \in \mathbb{R}_{>0}$, see Section 3.2 for details.
>
> In this situation, we could define the admissible direction
>
> $$ h_i = \begin{cases} \varphi_i, & \text{if } u(x_i) < 1, \\ -\varphi_i, & \text{if } u(x_i) = 1 \end{cases} $$
>
> for $i \in \{1, \ldots, n\}$, where $(x_i)_{i=1}^n$ are the nodes of the mesh.
>
> If we choose the directions h_i instead of φ_i in equation (4.8), the potential negative signs on both sides cancel, and we again obtain the linear system (4.10).
>
> Note that we could define a control-to-state map and, thus, the reduced cost functional on a set $\{u \in L^2(\Omega) \mid -\varepsilon \leq u \leq 1 + \varepsilon \quad \text{a.e. in } \Omega\}$ for some $\varepsilon > 0$ because for the existence of a state vector we just require the blood-perfusion rate to be strictly positive[a]. This translates to the discretized reduced cost functional, which is even differentiable[b] at the corresponding vector $\boldsymbol{u}$. Thus, the ith component of $\nabla^{\text{AD}} \hat{J}_{\text{d}}(\boldsymbol{u})$ in fact describes the (classical) partial derivative of $\hat{J}_{\text{d}}$ w.r.t. the ith component of $\boldsymbol{u}$.
>
> ---
>
> [a] E.g., choose $\varepsilon = \frac{1}{2} \xi_{\text{out}} (\xi_{\text{in}} - \xi_{\text{out}})^{-1}$.
>
> [b] The evaluation of the discretized reduced cost functional employs only differentiable operations, like assembling and solving the linear system. Especially the nonlinear optical coefficients are composed of differentiable functions.

4.3.3 Experiments

In the following experiments, we demonstrate the automated identification of the control u. We try different initial guesses and parameters for the cost functional.

■ **Experiment 4.8 — Identification of blood vessels: no control penalty.**

We reconstruct the control $u = u_{\text{true}}$ based on the synthetic temperature measurement ϑ_{d}. We use the physical parameters given in Table 1.1 and the following simulation details:

τ	$= 15\,\text{s}$	(parameter in the Cattaneo model)
Δt	$= 4\,\text{s}$	(discrete time step)
T	$= 120\,\text{s}$	(final time of the simulation)
$\vartheta^{(1)}(x)$	$= 0\,\text{K}\,\text{s}^{-1}$	(second initial condition for the temperature)
u_{true}	see Figure 4.7	(true control)
ϑ_{d}	$= \vartheta(T; u_{\text{true}})$	(desired temp. from synthetic measurement[a].)
MAX_ITER_DESCENT	$= 150$	(maximum number of descent iterations)
MAX_ITER_ARMIJO	$= 15$	(maximum number of line-search iterations)
γ_{arm}	$= 10^{-4}$	(relaxation parameter in the Armijo rule[b])
β	$= \frac{1}{2}$	(reduction parameter in the Armijo rule)
s_0	$= 1.0$	(initial step size in the Armijo rule)
TOL_ABS	$= 0$	(absolute tolerance in the descent algorithm)
TOL_REL	$= 10^{-2}$	(absolute tolerance in the descent algorithm)
λ_1	$= 0$	(L^1 control-penalty factor, see (3.5))
λ_2	$= 0$	(L^2 control-penalty factor, see (3.5))
$u_0(x)$	$= 0.15$	(constant initial guess for the control)

For the spatial discretization, we use the hierarchy of successively refined meshes given in Figure 4.5, with the following details:

mesh	number of nodes	number of triangles
$\Omega_{\text{2D},h}^{(1,0)}$	3607	7074
$\Omega_{\text{2D},h}^{(1,1)}$	14287	28296
$\Omega_{\text{2D},h}^{(1,2)}$	56869	113184

The synthetic measurement $\vartheta_{\text{d}} := \vartheta(u_{\text{true}})$ is given by running the Cattaneo–LITT simulation with the control $u = u_{\text{true}}$.

We run the descent algorithm 3.15 with the details for the following combinations of discrete time steps and meshes:

$$(\Delta t, \Omega_h) \in \left\{ \left(1\,\text{s}, \Omega_{\text{2D},h}^{(1,0)}\right), \left(2\,\text{s}, \Omega_{\text{2D},h}^{(1,0)}\right), \left(4\,\text{s}, \Omega_{\text{2D},h}^{(1,0)}\right), \left(4\,\text{s}, \Omega_{\text{2D},h}^{(1,1)}\right), \left(4\,\text{s}, \Omega_{\text{2D},h}^{(1,2)}\right) \right\}.$$

We compare the values of the cost functional, the stationary measure and the number of Armijo steps during the descent iteration (k-loop in Algorithm 3.15) for the different combinations of space and time discretizations listed here.

Furthermore, for the discretization $(\Delta t, \Omega_h) = \left(4\,\mathrm{s}, \Omega_{2\mathrm{D},h}^{(1,2)}\right)$, we evaluate the temperature along the reference line $\Omega_{1\mathrm{D,\,ref}}$ (see Figure 4.1) and compute the contour lines of the coagulation at the final time $\gamma(T)$ at level $\gamma(T) = 0.5$, for the controls at different iterations of the descent algorithm.

_____

[a]   Run the Cattaneo–LITT simulation with $u = u_{\mathrm{true}}$.
[b]   Classical choice for the finite-dimensional case in [106, Sec. 5.4, Eq. 5.13, p. 91].

In Figures 4.12 and 4.13, we present the results of Experiment 4.8.

In Figure 4.12, we show the cost functional, the stationary measure and the number of Armijo steps over the descent iteration k in Algorithm 3.15 (outer loop) for different discretizations. We observe that, independent of the temporal or spatial discretization, the cost functional is monotonically decreasing, which validates our considerations on the choice of the descent direction. Even though the cost functional becomes almost stationary for iterations $k \geq 100$, the stationary measure does not show a significant decrease. In fact, we can observe the effect of the projection operator in the stationary measure (3.25), which causes the frequent jumps. We note that the descent algorithm stopped after reaching the maximum number of MAX_ITER_DESCENT iterations and not because the stopping criterion regarding the stationary measure was fulfilled. Nevertheless, if we have a look at the results, we observe that we are still able to improve the accuracy of the predicted temperature and coagulation.

The three subfigures 4.13a–4.13c show the intermediate controls at iterations $k \in \{0, 10, 50, 150\}$. From the temperatures in 4.13d we see that the temperature based on the chosen initial guess for the control underestimates the true temperature.

We see that intermediate controls 4.13a–4.13c are similar to the true control and the spatial resolution of the heterogeneities becomes more accurate for an increasing number of iterations. In regions distant from the applicator, the descent strategy does not significantly change the control. The blood-perfusion rate in those regions does not have a relevant influence on the temperature. The deviation from the true control has only a minor influence on the corresponding gradient of the cost functional and, thus, has no effect in the descent algorithm.

In Figure 4.13e, we see the contours $\gamma(T, u_k)$ of the coagulations at the final time T for the intermediate controls at different iterations. Already after ten iterations, the contour lines of the approximate coagulation match the contour lines of the approximation after 150 iterations and of the true coagulation well.

Even though the descent algorithm did not converge in terms of the stationary measure, we could decrease the cost functional and observe an improvement of the prediction, even after fewer steps than the maximum number of iterations. This raises the question for future work whether we should seek for a different stopping criterion for the real application.

Last, we mention the large amount of positive numbers of the Armijo rule, shown in Subfigure 4.12c, in which cases the step size in the corresponding descent iteration k was increased.
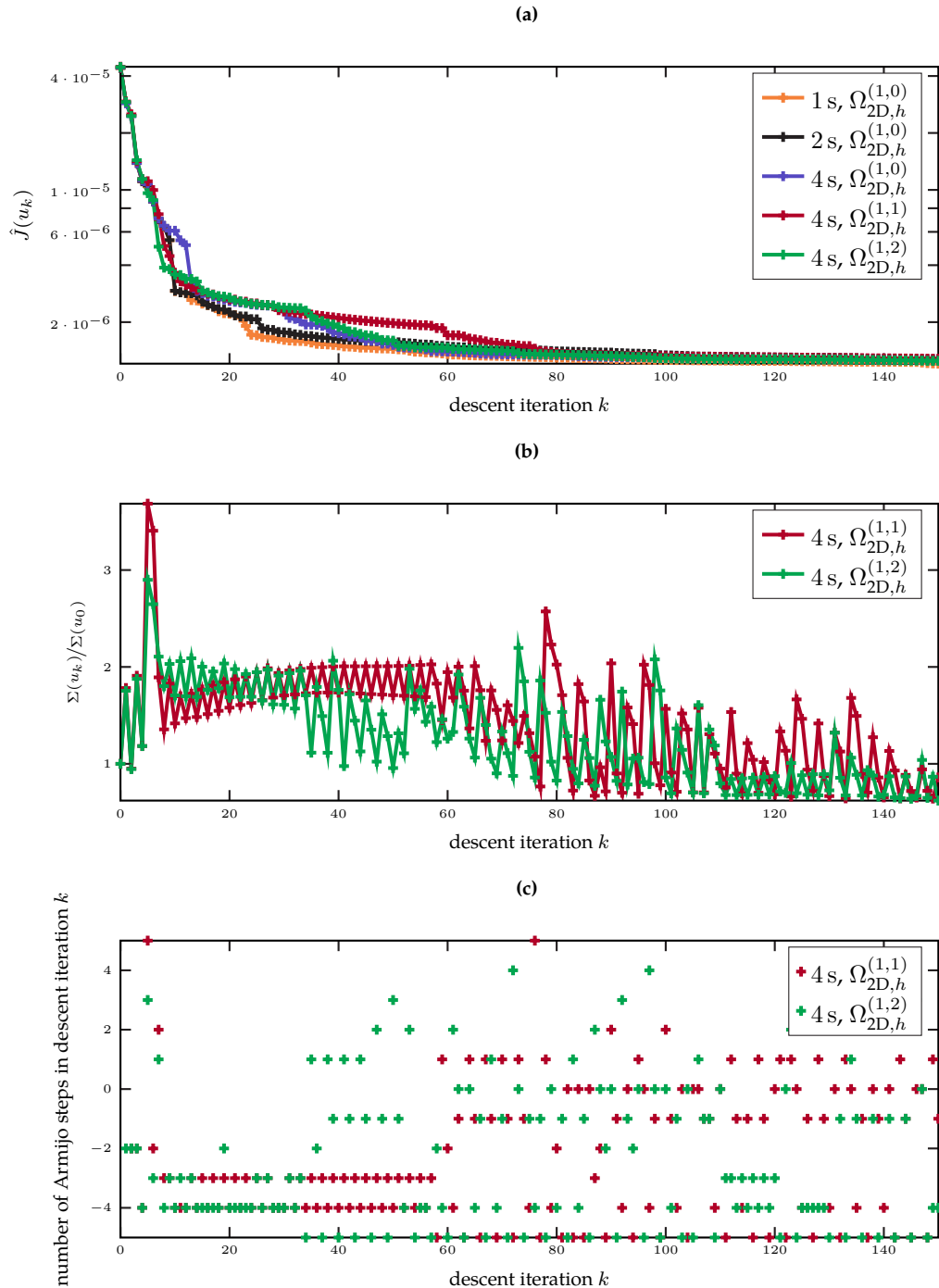
(a)

(b)

(c)

Figure 4.12: Results of Experiment 4.8. (4.12a): Reduced cost functional evaluated for controls u_k over the descent iterations k (outer loop of Alg. 3.15), for different discrete time steps and spatial meshes. (4.12b): Relative stationary measure evaluated for controls u_k over the descent iterations k (outer loop of Alg. 3.15), for different discrete time steps and spatial meshes. (4.12c): Number of Armijo steps j (inner loop of Alg. 3.15) over the descent iterations k (outer loop of Alg. 3.15). Positive: increase step size; negative: decrease stepsize.

(a) $k = 10$ **(b)** $k = 50$ **(c)** $k = 150$

(d)   **(e)**
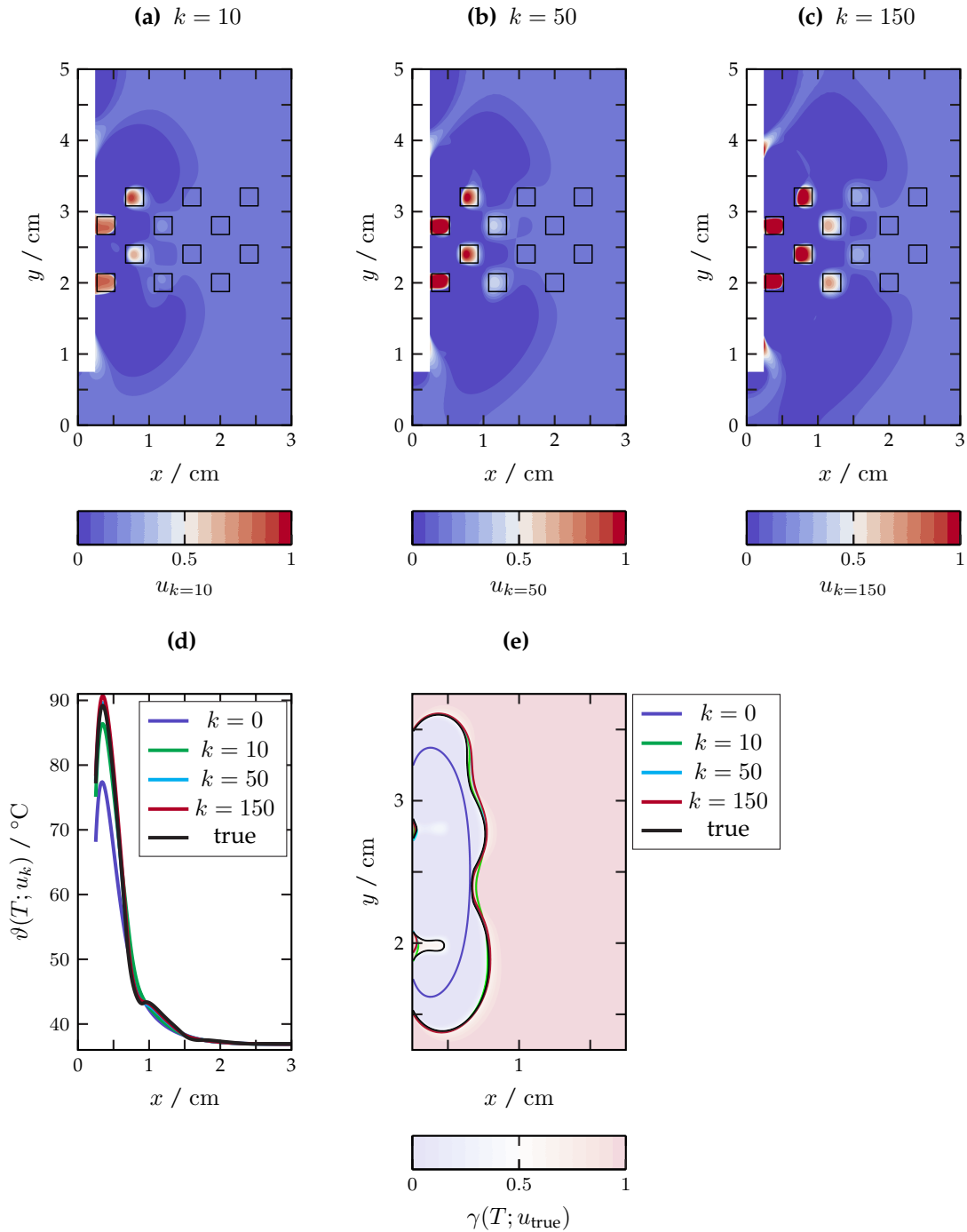
Figure 4.13: Results of Experiment 4.8, for the discretization $(\Delta t, \Omega_h) = \left(4\,\mathrm{s}, \Omega_{2\mathrm{D},h}^{(1,2)}\right)$. (4.13a–4.13c): Intermediate controls of the descent method at iterations $k \in \{10, 50, 150\}$. The black lines indicate the contours of the true control in Figure 4.7. (4.13d): Temperatures at the final time T for the intermediate controls at iterations $k \in \{0, 10, 50, 200\}$, evaluated on the reference line $\Omega_{1\mathrm{D},\,\mathrm{ref}}$, where $u_{k=0}$ corresponds to the initial guess. (4.13e): Contour lines of the coagulation at the final time T for the intermediate controls at iterations $k \in \{0, 10, 50, 200\}$ at level $\gamma(T) = 0.5$, where $u_{k=0}$ corresponds to the initial guess. The coagulation for the true control is visualized by the transparent background color and the corresponding contour line at level $\gamma(T; u_{\mathrm{true}}) = 0.5$ in red. We modified the axis scale for a better readability.

The only disadvantage is that the suggested optimal control keeps the value of the initial guess in regions more distant to the applicator. We counter this in the next experiment by activating the control-penalty terms in the cost functional.

■ **Experiment 4.9 — Identification of blood vessels: control penalty.**

We reconstruct the control $u = u_{\text{true}}$ based on the synthetic temperature measurement ϑ_{d} with Algorithm 3.15. We use the same setup as in Experiment 4.8, except for the following details (where we restrict ourselves to one discretization):

Δt	$= 4\,\text{s}$	(discrete time step)
Ω_h	$= \Omega_{\text{2D},h}^{(1,1)}$	(spatial mesh)
λ_1	$= 10$	(L^1 control-penalty factor, see (3.5))
λ_2	$= 1$	(L^2 control-penalty factor, see (3.5))

In Figure 4.14, we present the results of Experiment 4.9 analogously to Figure 4.13.

Again, the algorithm stopped after reaching the maximum number of $k = 150$ descent iterations. We observe that the true control in 4.14c is reconstructed well in regions close to the applicator. Also, the contour line of the coagulation at the final time and the temperature along the reference line are approximated well. Nevertheless, compared to Figure 4.13, we see that the quality of the approximation of the temperature and the coagulation for intermediate controls at iterations $k \in \{10, 50\}$ decreased.

This shows that the use of penalty terms might improve the reconstruction of the blood-perfusion rate, but at the same time might decrease the quality of the approximation of the quantities which are relevant to the real application, namely the coagulation.

From this example it might not be apparent why one should consider penalty terms at all. Note that those will play an important role in the real application later to account for measurement noise, where we want to avoid overfitting to disturbed data. The influence of measurement noise requires its own discussion, and we forward a detailed investigation to future work. Though, a first attempt to quantify the influence of measurement noise in context of the classical LITT model is presented in [9].

In the following experiment, we want to get a first impression on the influence of noisy temperature measurements for this specific experimental setup.
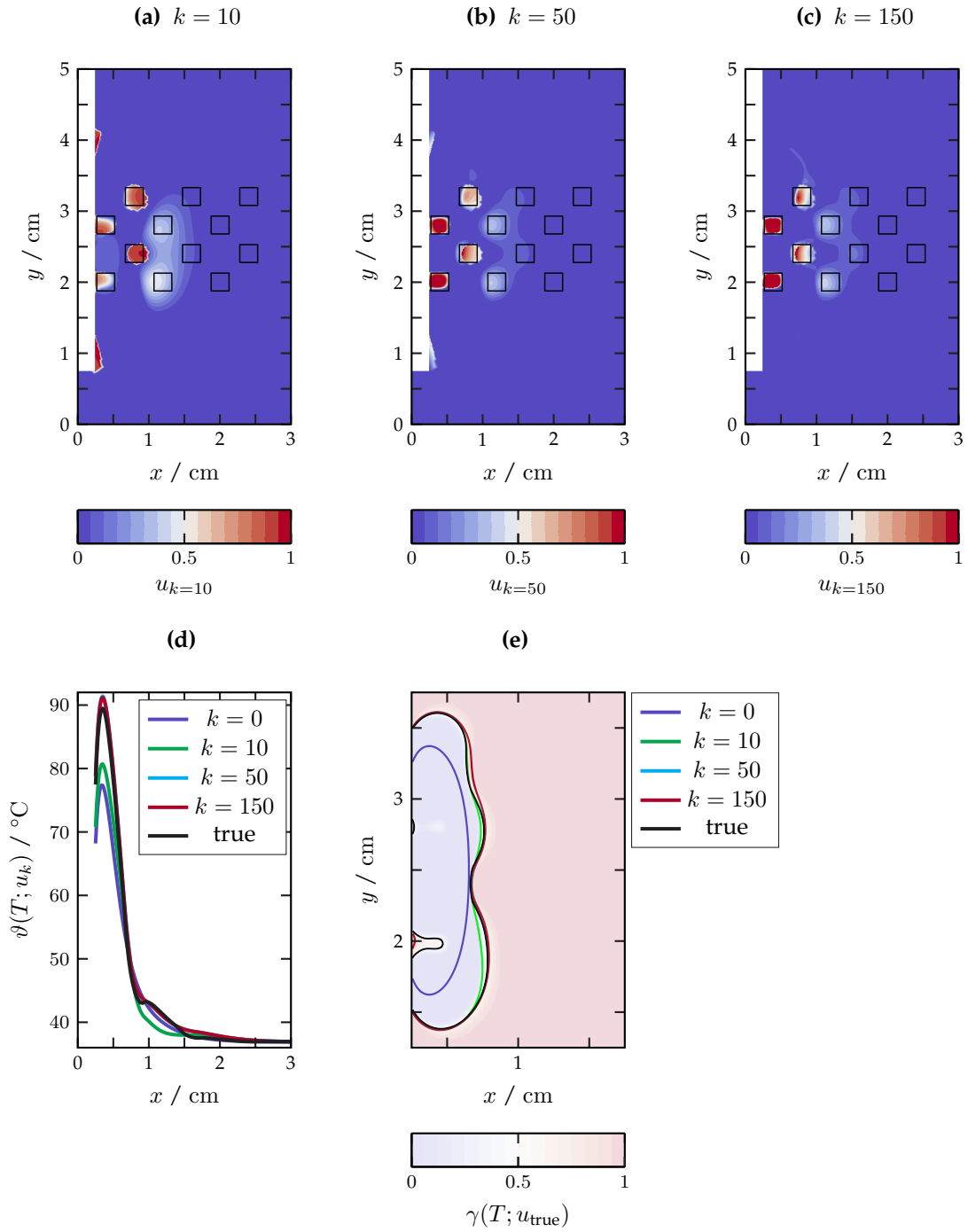
(a) $k = 10$ **(b)** $k = 50$ **(c)** $k = 150$

(d)   **(e)**

Figure 4.14: Results of Experiment 4.9. (4.14a–4.14c): Intermediate controls of the descent method at iterations $k \in \{10, 50, 150\}$. The black lines indicate the contours of the true control in Figure 4.7. (4.14d): Temperatures at the final time T for the intermediate controls at iterations $k \in \{0, 10, 50, 150\}$, evaluated on the reference line $\Omega_{1\mathrm{D,\,ref}}$, where $u_{k=0}$ corresponds to the initial guess. (4.14e): Contour lines of the coagulation at the final time T for the intermediate controls at iterations $k \in \{0, 10, 50, 150\}$ at level $\gamma(T) = 0.5$, where $u_{k=0}$ corresponds to the initial guess. The coagulation for the true control is visualized by the transparent background color and the corresponding contour line at level $\gamma(T; u_{\mathrm{true}}) = 0.5$ in red. We modified the axis scale for a better readability.

■ **Experiment 4.10 — Identification of blood vessels: noisy temperature measurements.**

We reconstruct the control $u = u_{\text{true}}$ based on the synthetic temperature measurement ϑ_{d} with Algorithm 3.15. We use the same setup as in Experiment 4.9, but we disturb the artificial measurements by $1\%, 2\%$ and 5%. More precisely, we compute the finite-element approximation of $\vartheta_{\text{d}} := \vartheta(T; u_{\text{true}})$, and disturb each nodal value (indexed with i) as follows:

$$(\vartheta_{\text{d}})_i^p := (\vartheta_{\text{d}})_i + \varepsilon_i$$

where $\varepsilon_i \sim \mathcal{N}(\mu_i, \sigma_i^2)$ is a random number generated from the normal distribution with mean value $\mu_i = \vartheta(T; u_{\text{true}})_i$ and standard deviation $\sigma_i = (\vartheta_{\text{d}})_i \cdot p$, where the standard deviation is computed in the Celsius scale, for $p \in \{0.01, 0.02, 0.05\}$.

We run the identification algorithm three times, once with each ϑ_{d}^p as artificial temperature measurement at time $t = T$, and obtain corresponding optimal controls u_{opt}^p. We compare the optimal controls u_{opt}^p as well as the predicted coagulations $\gamma(T; u_{\text{opt}}^p)$ to the undisturbed case, i.e., to u_{opt}^0 and $\gamma(T; u_{\text{opt}}^0)$.

In Figure 4.15, we visualize the disturbed artificial temperatures and the corresponding optimal controls. Also in this experiment, the algorithm did not converge, but stopped after reaching the maximum number of iterations, i.e., $u_{\text{opt}}^p = u_{k=150}^p$. In Figures 4.15a–4.15c, we increased the resolution of the color space to make also the small disturbances visible.

At this point, we would like to highlight the importance of an underlying physical model to make use of the measured temperature data for the prediction of the coagulation zone. The color space in Figures 4.15a–4.15c is chosen in such a way that the white transition marks the temperature of $60\,°\text{C}$, which can be used in a simplistic model for the estimation of the coagulation zone, see Remark 4.3. If we take only this information to estimate the coagulation zone, we see the potential prediction error induced by measurement noise in Figure 4.15c. Also regions far distant from the applicator show temperatures around $60\,°\text{C}$ here, although we know that the true coagulation zone is located near the applicator, like shown in Figure 4.14e. The prediction based on the physical model can be seen as a filter to enhance the measured data.

We recognize a small influence of the disturbed measurements, but, overall, we observe a good agreement with the optimal control for the undisturbed case, visualized in Figure 4.16 (which visualizes the same control as Figure 4.14c). Again, the ultimate measure relevant to the therapy is the coagulation zone, which is visualized by its contour line at level $\gamma(T; u_{\text{opt}}^p) = 0.5$ in Figure 4.16b. Also here, on a visual scale, the influence is very small. We quantify the errors in Table 4.3.
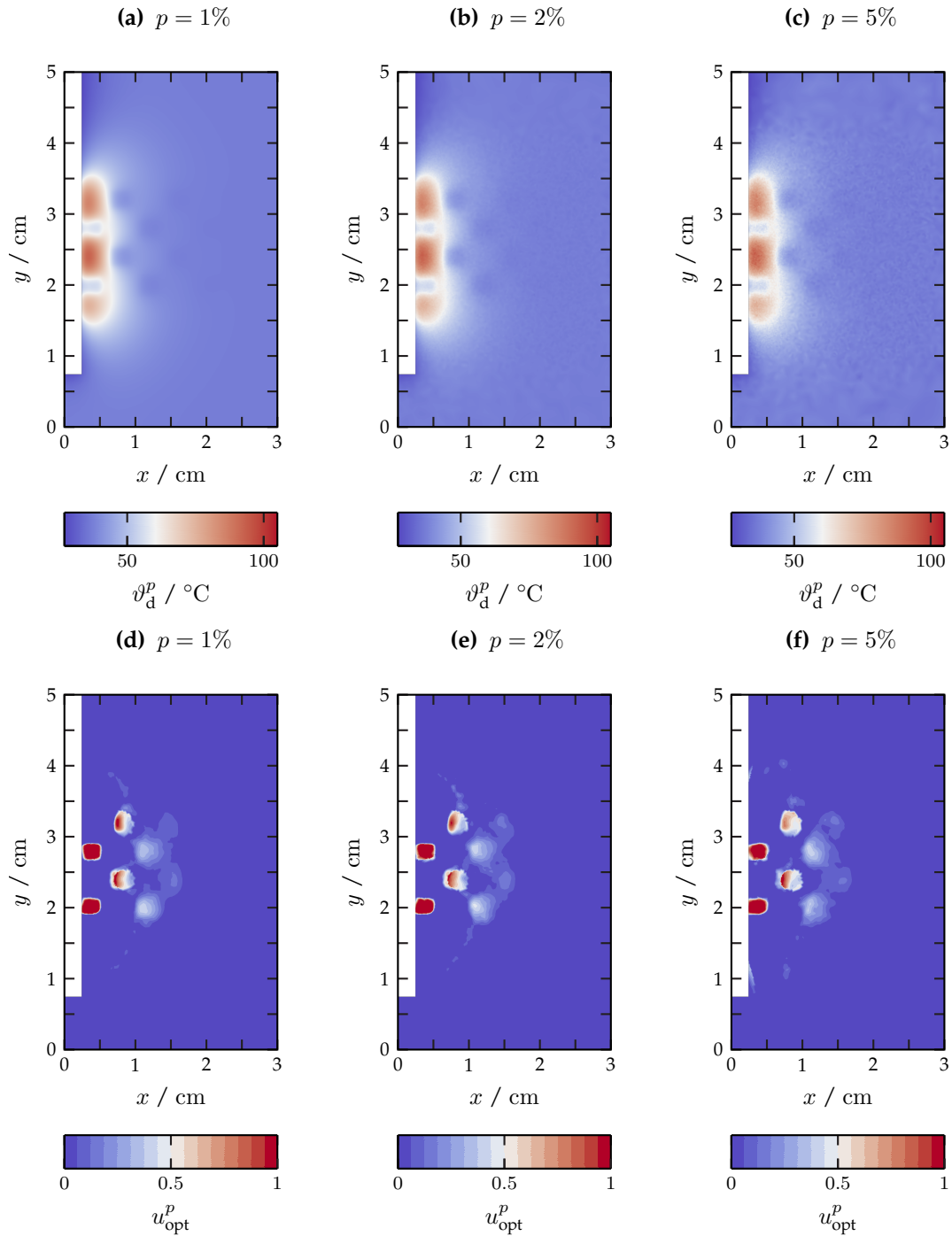
(a) $p = 1\%$ **(b)** $p = 2\%$ **(c)** $p = 5\%$

(d) $p = 1\%$ **(e)** $p = 2\%$ **(f)** $p = 5\%$

Figure 4.15: Results of Experiment 4.10. (4.15a–4.15c): Disturbed artificial temperature measurements $\vartheta_{\mathrm{d}}^{p}$ for different values of $p \in \{1\%, 2\%, 5\%\}$. The white transition in the color space marks $60\,°\mathrm{C}$ and yields a (rough) approximation of the boundary of the coagulation zone. (4.15d–4.15f): Computed optimal controls u_{opt}^{p} for the corresponding disturbed artificial temperature measurements.

p	$\left\|\vartheta_{\mathrm{d}}^p - \vartheta_{\mathrm{d}}^0\right\|_{L^\infty(\Omega)}$ / °C	$\dfrac{\left\|\vartheta_{\mathrm{d}}^p - \vartheta_{\mathrm{d}}^0\right\|_{L^2(\Omega)}}{\left\|\vartheta_{\mathrm{d}}^0\right\|_{L^2(\Omega)}}$	$\dfrac{\left\|u_{\mathrm{opt}}^p - u_{\mathrm{opt}}^0\right\|_{L^2(\Omega)}}{\left\|u_{\mathrm{opt}}^0\right\|_{L^2(\Omega)}}$	$\dfrac{\left\|\gamma(T;u_{\mathrm{opt}}^p) - \gamma(T;u_{\mathrm{opt}}^0)\right\|_{L^2(\Omega)}}{\left\|\gamma(T;u_{\mathrm{opt}}^0)\right\|_{L^2(\Omega)}}$
1%	3.189	6.973×10^{-3}	7.506×10^{-2}	8.253×10^{-4}
2%	5.514	1.434×10^{-2}	1.122×10^{-1}	1.252×10^{-3}
5%	15.101	3.469×10^{-2}	2.269×10^{-1}	3.616×10^{-3}

Table 4.3: Results of Experiment 4.10. (Col. 1): Relative disturbance p, see experiment description. (Col. 2): Absolute $L^\infty(\Omega)$ difference between the disturbed and undisturbed artificial temperature measurements ϑ_{d}^p and ϑ_{d}^0 in Celsius. (Col. 3): Relative $L^2(\Omega)$ difference between the disturbed and undisturbed artificial temperature measurements ϑ_{d}^p and ϑ_{d}^0, where the temperatures are given in Celsius. (Col. 4): Relative $L^2(\Omega)$ differences between the corresponding optimal controls for the undisturbed and disturbed case u_{opt}^p and u_{opt}^0. (Col. 5): Relative $L^2(\Omega)$ differences between the corresponding coagulations at the final time for the undisturbed and disturbed case $\gamma(T; u_{\mathrm{opt}}^p)$ and $\gamma(T; u_{\mathrm{opt}}^0)$.
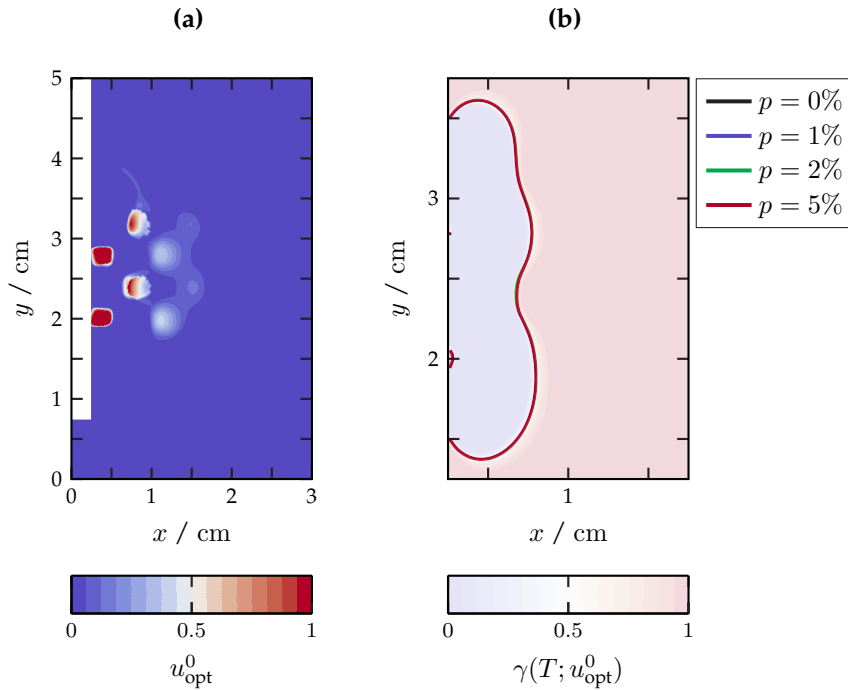
Figure 4.16: Results of Experiment 4.10. (4.16a): Computed optimal control u_{opt}^0 (for $p = 0$). (4.16b): Contour lines of the coagulation at the final time T for the different optimal controls u_{opt}^p for the values of $p \in \{0\%, 1\%, 2\%, 5\%\}$ at level $\gamma(T; u_{\mathrm{opt}}^p) = 0.5$. Furthermore, the coagulation for $p = 0\%$ is visualized by the transparent background color. We modified the axis scale for a better readability.

We conclude this chapter with a final experiment. Here, we choose a naive initial guess for the optimization, and observe that the reconstruction of the blood-perfusion rate is sensitive to the choice of the initial guess and especially that the optimal-control problem has several stationary points. Like mentioned before, we are restricted to solve the optimal-control problem

by searching for stationary points. In these terms, the solution to our optimal-control problem, i.e., a stationary point, is not unique.

■ **Experiment 4.11 — Identification of blood vessels: naive initial guess.**

We reconstruct the control $u = u_{\text{true}}$ based on the synthetic temperature measurement ϑ_{d} with Algorithm 3.15. We use the same setup as in Experiment 4.8, except for the following details (where we restrict ourselves to one discretization):

Δt	$= 4\,\text{s}$	(discrete time step)
Ω_h	$= \Omega_{\text{2D},h}^{(1,1)}$	(spatial mesh)
λ_1	$= 0$	(L^1 control-penalty factor, see (3.5))
λ_2	$= 0$	(L^2 control-penalty factor, see (3.5))
$u_0(x)$	$= 0.0$	(constant initial guess for the control)

In Figure 4.17, we present the results of Experiment 4.11 analogously to Figure 4.13.

As outlined in Remark 4.6, the initial guess $u_0 \equiv 0.0$ implies a wrong energy balance in the heat equation because of the absence of any heat sink in the domain. The first intermediate control $u_{k=1}$, without any initial tuned step-size restriction on $s^{(0)}$, overshoots in correcting for this balance and suggests a large area as heat sink. In the following steps, the intermediate controls approximate step by step the fine structure of the blood vessels near the applicator, but the gradient in regions far from the applicator are too small to correct for this first overshoot, which can be seen by the large connected red area in the center of the domains in 4.17a–4.17c.

This first overshoot can also be observed from the temperatures in subfigure 4.17d. Whereas the temperature for the initial guess ($k = 0$) is much larger than the true temperature, the following iterates are approaching the real temperature.

In Figure 4.17e, we see the contours of the coagulations at the final time T for the intermediate controls at different iterations. Again, we see that the initial guess ($k = 0$) predicts a coagulation zone which deviates from the true coagulation about $1\,\text{cm}$. This is in fact the most dangerous prediction error because in the real application this would suggest stopping the therapy although the coagulation zone does not fully cover the tumorous regions. The subsequent iterations approximate the contour lines from inside, again caused by the first overshoot in the optimization.

On the one hand, the controls in 4.17a–4.17c do not look much alike the true control in 4.7. On the other hand, we see that we could improve the prediction of the temperature as well as the coagulated zone.

Overall, we see that different initial guesses might yield to different optimal controls computed by our algorithm. This suggests that there are more than one stationary point of the optimal-control problem. This motivates the further investigation of additional regularization terms in the cost functional, e.g., an $L^1(\Omega)$ regularization to promote stationary points with a sparse structure.
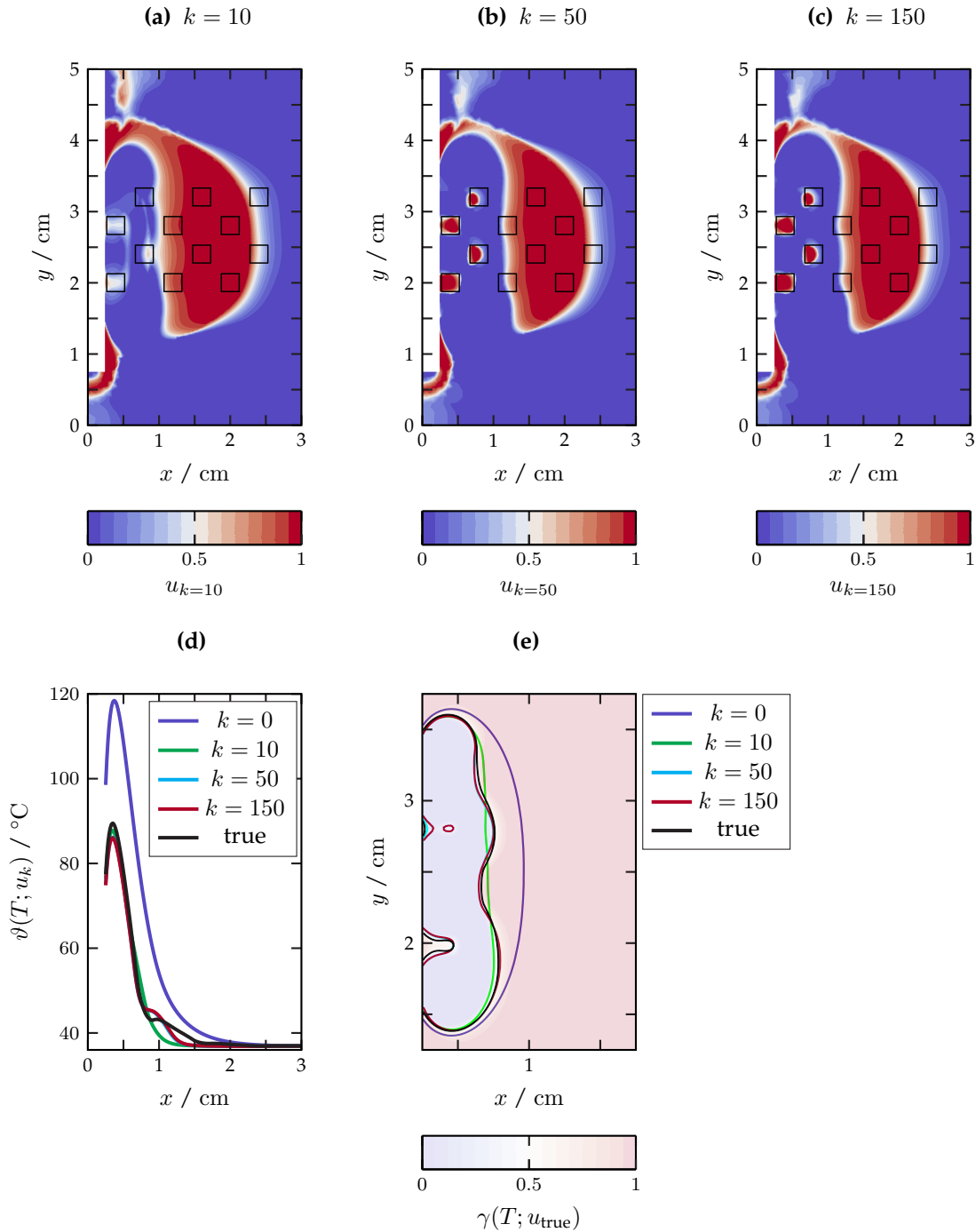
(a) $k = 10$　　　　　　**(b)** $k = 50$　　　　　　**(c)** $k = 150$

(d)　　　　　　　　　　　**(e)**

Figure 4.17: Results of Experiment 4.11. (4.17a–4.17c): Intermediate controls of the descent method at iterations $k \in \{10, 50, 150\}$. The black lines indicate the contours of the true control in Figure 4.7. (4.17d): Temperatures at the final time T for the intermediate controls at iterations $k \in \{0, 10, 50, 150\}$, evaluated on the reference line $\Omega_{1D,\,ref}$, where $u_{k=0}$ corresponds to the initial guess. (4.17e): Contour lines of the coagulation at the final time T for the intermediate controls at iterations $k \in \{0, 10, 50, 150\}$ at level $\gamma(T) = 0.5$, where $u_{k=0}$ corresponds to the initial guess. The coagulation for the true control is visualized by the transparent background color and the corresponding contour line at level $\gamma(T; u_{\text{true}}) = 0.5$ in red. We modified the axis scale for a better readability.

4.3.4 Conclusion: Identification of the blood-perfusion rate

In general, the quality of the reconstruction decreases in regions far from the applicator. This is due to the fact that the difference between the tissue temperature and the blood temperature in those regions is smaller, which directly affects the descent direction (cf. (3.20)). In those regions, large vessels have less influence on the temperature. This is a curse and blessing at the same time. On the one hand, this prevents the reconstruction of the desired control. On the other hand, errors in the reconstruction far away from the applicator might, for the same reason, not have a relevant influence on the predicted temperature and coagulation.

The ultimate measure of performance relevant to the later application is the boundary of the coagulation zone. The numerical experiments have shown that the presented estimation of the blood-perfusion rate can improve the accuracy of the Cattaneo–LITT simulation significantly, at least for our chosen parameter setup.

We have seen both from the decrease in the cost functional and from the approximation of the true control, temperature and coagulation, that our identification strategy improves the accuracy of the LITT simulation, even if it does not converge in terms of the stationary measure before reaching the maximum number of iterations. For the later application, we suggest investigating alternative stopping criteria, which guarantee an acceptable accuracy of the reconstruction but maybe do not rely on the stationary measure. The cost functionals in all experiments decrease fast at the beginning and rather slowly for later iterations, so the choice of a stopping criterion which stops the iteration earlier seems reasonable. Alternatively, one might investigate variants of the stationary measure tailored to this optimal-control problem.

Furthermore, the steepest descent strategy was chosen only as a starting point and for a proof of concept. Newton-based methods might speed up the convergence of our method, which would be promising for future investigations. Especially in view of real-time capability of the identification, it will be necessary to choose a trade-off between accuracy in the reconstruction of the blood-perfusion rate, or better, of the coagulation zone, and the computational burden which comes with numerous descent iterations.

We have seen that the choice of different initial guesses influences the quality of the approximation of the true control, temperature and coagulation. A suitable choice of an initial guess for the control might help to decrease the number of iterations needed to reach a certain accuracy. The fact that there are several stationary points motivates the further investigation of additional regularization terms in the cost functional, e.g., an $L^1(\Omega)$ regularization to promote stationary points with a sparse structure.

The presented experiments are understood as a proof of concept for the identification of the blood-perfusion rate. The fine-tuning of the optimization strategy needs to be performed and validated on data from the real therapy.

Part II

Second-order formulation of the P_N equations

In Part I, we discussed an alternative model for the heat transfer in the LITT model. Next, we look at an alternative model to compute the irradiance. We let Willem Star introduce this for us [204, Sec. 6.3.2, p. 153]:

> "*Light is principally described as particles with energy $h\nu$ and velocity c[1]. These particles are scattered or absorbed by structures in turbid media such as biological tissues and are reflected at boundaries between media with different refractive index, according to the laws of Fresnel. [...] The radiative-transfer equation (RTE)[2] is an integro-differential equation for the radiance[3] ψ. [...] Its general stationary form, neglecting polarization, is*
>
> $$\boldsymbol{v} \cdot \nabla_{\boldsymbol{x}}\psi(\boldsymbol{x},\boldsymbol{v}) + \sigma_t(\boldsymbol{x})\psi(\boldsymbol{x},\boldsymbol{v}) = \sigma_s(\boldsymbol{x}) \int_{\mathcal{S}^2} \mathcal{K}\left(\boldsymbol{v},\boldsymbol{v}'\right)\psi(\boldsymbol{x},\boldsymbol{v}')\ \mathrm{d}\boldsymbol{v}' + Q(\boldsymbol{x},\boldsymbol{v}).\text{"}\quad (5.1)$$

The occurring variables are explained in detail in the next section.

This equation appears as a model for radiative transfer also in the context of LITT [65, 95, 170] and other physical applications, e.g., in high-temperature processes in industry [167]. Note that we consider the mono-energetic case in this thesis.

The dependence of the radiance on five independent variables (three spatial coordinates and two directional coordinates) makes it hard to solve the RTE in the real applications, so we look for suitable approximations. The established models in the LITT context use a P_1 approximation, which we review in a more general context in the following. In Chapter 5.2 we propose a second-order formulation of the P_N equations, which we call $P_N^{2\mathrm{nd}}$. Our formulation allows a straight-forward incorporation of the Marshak boundary conditions. It is derived in a general context and is applicable to various scenarios, including heterogeneous coefficients, anisotropic scattering and irregular meshes.

The P_N moment approximation (with spherical harmonics) and also derivations of second-order formulations are well-studied subjects in literature. Nevertheless, our formulation is designed in such a way that the necessary algebraic transformations can be handed to a computer algebra system and the resulting weak formulation can be solved using standard finite-element tools. This allows a direct integration in our existing LITT simulations. We make our code available online and the presented method can easily be transferred to other applications.

We validate our approach in several numerical examples in a general context in Chapter 6. Finally, we investigate the effect of higher-order moment approximations in the LITT context. For an overview on the RTE, we refer to [145] and, especially for tissue optics, to [228].

To the best of our knowledge, our derivation and final form of the $P_N^{2\mathrm{nd}}$ formulation has not been presented yet. Furthermore, such a second-order formulation has not been studied in combination with the classical LITT model or the Cattaneo–LITT model yet.

Before we start, I would like to acknowledge the joint work with Dr. Florian Schneider, which is the basis for this Part II. We published the derivation of the $P_N^{2\mathrm{nd}}$ formulation in Chapter 5 and

---

[1] Planck's constant $h \approx 6.6261 \times 10^{34}\,\mathrm{J\,s}$, photon's energy ν, speed of light $c = 299\,792\,458\,\mathrm{m\,s^{-1}}$, [48, App., p. 448]

[2] Corresponds to the *mono-energetic stationary linear transport equation*.

[3] This quantity has physical units $\mathrm{W\,m^{-2}\,sr^{-1}}$. Sometimes authors refer to this as *radiative intensity* [21, 145]. This is confusing because the SI-standard [97] defines the radiant intensity as a quantity with physical units $\mathrm{W\,sr^{-1}}$. We align our nomenclature with the one suggested in [227, Sec. 1.2, Tab. 1.1, p. 7 ff.].

the general numerical experiments in Section 6.2, with slight modifications, in our manuscript [13]. Furthermore, I would like to thank my colleagues Dr. Christian Leithäuser and Dr. Norbert Siedow from the Fraunhofer Institute for Industrial Mathematics ITWM for helpful discussions on the coupling of the P_N^{2nd} formulation with the LITT model in Section 6.3.

5 Second-order formulation of the P_N equations: derivation

Clean code does one thing well.

<div align="right">

Robert C. Martin [132]

</div>

5.1 Overview

We provide a straight-forward derivation of a hierarchy of approximate models for the RTE (5.1) based on the P_N equations with Marshak boundary conditions. This is done in a general context and later applied to the LITT model. The method is designed to be applicable in a general set of situations, e.g., irregular meshes with up to three spatial coordinates, heterogeneous coefficients, anisotropic scattering or anisotropic boundary sources. We provide a demo implementation in Matlab and Python which allows a fast prototyping.

The dependence on up to three spatial coordinates and two directional coordinates makes it hard to solve the RTE directly. One common way to discretize the solution is the P_N moment approximation (with spherical harmonics), e.g., [21, 46, 145], a type of spectral approximation in the directional variables, which results in a system of first-order PDEs in the spatial variable. We refer to [198] for a good start into the numerical treatment of the resulting system of equations, therein described for the time-dependent case on a staggered grid.

Another way of approximation are *Simplified P_N (SP_N) methods*, which can be derived from the P_N equations in various ways. All of them have the common goal to derive a smaller system of second-order (elliptic) PDEs in the spatial variable, which then can be solved with the help of standard finite-element tools, e.g., [77]. Like mentioned in [211], the second-order formulation has less unknowns and does not require additional stabilization for the price of the generated matrix being less sparse. A review on different ways to derive SP_N equations is given in [137]. The described SP_N models are under restrictive assumptions (e.g., slab geometry) equivalent to the corresponding P_N models and numerical results suggested that the SP_N models give higher-order corrections to the diffusion approximation of the RTE [137].

We follow the approach of "successive elimination" [46] similar to [76, 146, 148] and call it P_N^{2nd} method. We take a subset of the P_N equations to express the odd moments in terms of even moments by algebraic transformations. We plug the resulting expressions into the remaining equations and, with this, transform the system of first-order PDEs into a system of second-order PDEs. The choice of a suitable formulation of the P_N system allows us to delegate the transformation to a computer algebra system (e.g., Matlab's Symbolic Toolbox [135]) and,

thus, automatize the tedious algebraic calculations. The result can be forwarded to a standard finite-element tool, e.g., the Python Toolbox FEniCS [3, 127].

We perform all algebraic transformations on the full 3D system, which makes this approach different from the classical ad-hoc SP$_N$ derivation in 1D slab geometry, e.g., [88, 111, 126, 147, 239]. Even though our approach looks similar to the above mentioned ad-hoc derivation, it does not yield a "simplified" version of the P$_N$ equations, but an equivalent "second-order" formulation, provided that the P$_N$ solution is smooth enough to allow all steps during the transformations. This advantage comes with a price: Instead of obtaining a system of N equations like in the SP$_N$ method, we obtain a system with $\sim \frac{1}{2} N^2$ equations. Nevertheless, this is still an advantage over the classical P$_N$ formulation, which consists of $\sim N^2$ equations, probably at the cost that the coupled system of the P$_N^{2nd}$ formulation is less sparse than the P$_N$ system[1].

We note that there is an ambiguity in the choice of the set of Marshak boundary conditions for the P$_N$ method, discussed in detail later in this chapter. Our formulation suggests a certain selection of boundary half-moments which enables us to derive the weak formulation of the second-order system.

Note that other second-order formulations of the P$_N$ equations have been presented yet [146, 148]. The proposed formulation in this work allows an intuitive selection and incorporation of Marshak boundary conditions and allows us to forward the necessary algebraic transformations to established computer-algebra systems. This is demonstrated in Chapter 6 and our open-source codes in [8].

For a general overview on the radiative-transfer equation, we refer to [21, 145].

In Section 5.2, we review the standard P$_N$ approach, which is then reformulated as a system of second-order PDEs in space in Section 5.3. In Section 6.2, we look at different examples to demonstrate the wide applicability of our approach. In Section 6.3, we couple the P$_N^{2nd}$ models to the Cattaneo–LITT model and investigate the effect on the approximated irradiance.

Before we start, let us have a look at the main result of this chapter.

---

[1] Cf. [211, Ch. 3, p. 12], where the authors point out that, in general, second-order formulations in this context are less sparse.

> **Theorem 5.1 — Weak formulation at a glance.**
>
> Based on the assumptions made in this chapter, we propose an approximate model of the RTE of the form
>
> $$\sum_{i,j=1}^{3} \int_{\Omega} \partial_{x_i} \boldsymbol{\varphi}^{\mathrm{T}} \cdot K_{x_i x_j} \cdot \partial_{x_j} \mathbf{u}_{\mathrm{e}} \, \mathrm{d}\boldsymbol{x} + \int_{\Omega} \boldsymbol{\varphi}^{\mathrm{T}} \cdot C_{\mathrm{ee}} \cdot \mathbf{u}_{\mathrm{e}} \, \mathrm{d}\boldsymbol{x} + \int_{\Gamma} \boldsymbol{\varphi}^{\mathrm{T}} \cdot B_{\mathrm{l}}(\boldsymbol{n}) \cdot \mathbf{u}_{\mathrm{e}} \, \mathrm{d}\boldsymbol{s}$$
>
> $$= \int_{\Gamma} \boldsymbol{\varphi}^{\mathrm{T}} \cdot B_{\mathrm{r}}(\boldsymbol{n}) \cdot \mathbf{u}_{\Gamma} \, \mathrm{d}\boldsymbol{s} - \int_{\Omega} \boldsymbol{\varphi}^{\mathrm{T}} \boldsymbol{q}_{\mathrm{e}} \, \mathrm{d}\boldsymbol{x} + \sum_{i=1}^{3} \int_{\Omega} (\partial_{x_i} \boldsymbol{\varphi})^{\mathrm{T}} \boldsymbol{f}_i \, \mathrm{d}\boldsymbol{x}$$
>
> with the unknown $\mathbf{u}_{\mathrm{e}} \colon \Omega \to \mathbb{R}^{n_{\mathrm{e}}}$, the known matrices $K_{x_i x_j}, C_{\mathrm{ee}}, B_{\mathrm{l}}(\boldsymbol{n}) \in \mathbb{R}^{n_{\mathrm{e}} \times n_{\mathrm{e}}}$ and $B_{\mathrm{r}}(\boldsymbol{n}) \in \mathbb{R}^{n_{\mathrm{e}} \times n_{\mathrm{o}}}$, known right-hand sides $\boldsymbol{q}_{\mathrm{e}}, \boldsymbol{f}_i \colon \Omega \to \mathbb{R}^{n_{\mathrm{e}}}$ depending on the external source inside the domain, known odd moments of the external source at the boundary $\mathbf{u}_{\Gamma} \colon \Gamma \to \mathbb{R}^{n_{\mathrm{o}}}$, the outward-pointing unit normal vector at the boundary $\boldsymbol{n} \colon \Gamma \to \mathbb{R}^3$, and suitable test functions $\boldsymbol{\varphi} \colon \Omega \to \mathbb{R}^{n_{\mathrm{e}}}$, with $n_{\mathrm{e}} = \frac{1}{2}(N^2 + N), n_{\mathrm{o}} = \frac{1}{2}N^2 + \frac{3}{2}N + 1$ (for the full three-dimensional setting).
>
> The coefficients stored in the vector $\mathbf{u}_{\mathrm{e}}$ correspond to an expansion of the radiance ψ in terms of real spherical harmonics. Especially the first entry of $\mathbf{u}_{\mathrm{e}}$ is a multiple of the irradiance ϕ. Like demonstrated in Chapter 6 and our demo codes in [8], a system of this structure can be handed to standard finite-element tools like FENICS [3, 127].

Even though the derivation is straightforward, we would like to point out that our approach addresses the needs of other researchers in this field. We cite a part of the conclusion of [169]:

> *"In fact, the study of the SP$_N$ equations is far from over because the strongest theoretical results exist for homogeneous, infinite media. The boundary and interface conditions [which] give SP$_N$-P$_N$ equivalence in heterogeneous problems are a major, open problem. A less ambitious, but useful result, would be the development [of] an algorithm that efficiently generates SP$_N$ moments for anisotropic external source[s]."*

5.2 Classical P$_N$ equations

The RTE is considered as the mono-energetic stationary linear transport equation[2]

$$\boldsymbol{v} \cdot \nabla_{\boldsymbol{x}} \psi + \sigma_{\mathrm{a}} \psi = \sigma_{\mathrm{s}} \mathcal{C}(\psi) + Q, \tag{5.1}$$

which describes the time-stationary density of particles at *position* $\boldsymbol{x} = (x, y, z)^{\mathrm{T}}$ in a domain $\Omega \subseteq \mathbb{R}^3$ with speed $\boldsymbol{v} \in \mathcal{S}^2$ on the unit sphere $\mathcal{S}^2 = \{\boldsymbol{v} \in \mathbb{R}^3 \mid \|\boldsymbol{v}\|_2 = 1\}$. The scattering coefficient and absorption coefficient are denoted by $\sigma_{\mathrm{s}}(\boldsymbol{x})$ and $\sigma_{\mathrm{a}}(\boldsymbol{x})$. The quantity $\sigma_{\mathrm{t}} \coloneqq \sigma_{\mathrm{a}} + \sigma_{\mathrm{s}}$ is called the attenuation coefficient and $Q = Q(\boldsymbol{x}, \boldsymbol{v})$ models a radiative source term in the interior of the domain[3].

---

[2] See, e.g., [28].

[3] In our LITT model, the laser applicator itself is not a part of the domain (other than, e.g., [154]). It is modeled as an external source of radiation which enters our LITT model via a boundary condition. Another source of radiation is given by the total thermal radiation according to Boltzmann's law $S = \sigma_{\mathrm{a}} \sigma \pi^{-1} \vartheta^4$ (in units $\mathrm{W\,m^{-3}\,sr^{-1}}$) [47, Ch. 10.2.5.4, p. 291], with the Stefan-Boltzmann constant $\sigma \approx 5.670\,51 \times 10^{-8}\,\mathrm{W\,m^{-2}\,K^{-4}}$ and the temperature ϑ [167,

Collisions of the particles are modeled using the BGK-type *collision operator* [122, 163]

$$C\left(\psi\right) = \int_{\mathcal{S}^2} \mathcal{K}(\boldsymbol{v}, \boldsymbol{v}')\psi(\boldsymbol{x}, \boldsymbol{v}')\,\mathrm{d}\boldsymbol{v}' - \int_{\mathcal{S}^2} \mathcal{K}(\boldsymbol{v}', \boldsymbol{v})\psi(\boldsymbol{x}, \boldsymbol{v})\,\mathrm{d}\boldsymbol{v}'$$

with *scattering kernel* $\mathcal{K} \colon \mathcal{S}^2 \times \mathcal{S}^2 \to \mathbb{R}$.

> **Assumption 5.2 — Kernel.**
>
> We assume the scattering kernel $\mathcal{K}$ to be:
>
> (A1) *strictly positive*: there exists a $\mathcal{K}_0 \in \mathbb{R}_{>0}$ such that $\mathcal{K}(\boldsymbol{v}, \boldsymbol{v}') \geq \mathcal{K}_0$ for all $\boldsymbol{v}, \boldsymbol{v}' \in \mathcal{S}^2$;
>
> (A2) *symmetric*: it holds $\mathcal{K}(\boldsymbol{v}, \boldsymbol{v}') = \mathcal{K}(\boldsymbol{v}', \boldsymbol{v})$ for all $\boldsymbol{v}, \boldsymbol{v}' \in \mathcal{S}^2$;
>
> (A3) *normalized*: it holds $\int_{\mathcal{S}^2} \mathcal{K}(\boldsymbol{v}', \boldsymbol{v})\,\mathrm{d}\boldsymbol{v}' = 1$ for all $\boldsymbol{v} \in \mathcal{S}^2$.

Note that with Assumption (A3) we retrieve the RTE in its formulation (5.1) given in the introduction of Part II.

> ■ **Example 5.3 — Isotropic scattering.**
> A constant scattering kernel, i.e., $\mathcal{K}(\boldsymbol{v}, \boldsymbol{v}') \equiv \frac{1}{|\mathcal{S}^2|} = \frac{1}{4\pi}$ for all $\boldsymbol{v}, \boldsymbol{v}' \in \mathcal{S}^2$, models isotropic scattering.

> ■ **Example 5.4 — Henyey–Greenstein.**
> A typical example for anisotropic scattering is the *Henyey–Greenstein* kernel [91]:
>
> $$\mathcal{K}\left(\boldsymbol{v}, \boldsymbol{v}'\right) = \frac{1}{4\pi} \frac{1 - g^2}{\left(1 + g^2 - 2g\cos\left(\boldsymbol{v}^{\mathrm{T}}\boldsymbol{v}'\right)\right)^{3/2}}.$$
>
> The parameter $g \in [-1, 1]$ can be used to blend from backscattering ($g = -1$) over isotropic scattering ($g = 0$) to forward scattering ($g = 1$).

The RTE (5.1) is equipped with *semi-transparent boundary conditions*[4] of the form

$$\psi(\boldsymbol{x}, \boldsymbol{v}) = \rho(\boldsymbol{x}, \boldsymbol{v})\psi(\boldsymbol{x}, r\left(\boldsymbol{v}\right)) + (1 - \rho(\boldsymbol{x}, \boldsymbol{v}))\psi_\Gamma(\boldsymbol{x}, \boldsymbol{v}), \quad \text{for } \boldsymbol{x} \in \Gamma, \quad \boldsymbol{n}(\boldsymbol{x}) \cdot \boldsymbol{v} < 0, \qquad (5.2)$$

where $\Gamma := \partial\Omega$ again denotes the boundary of the domain with outward-pointing unit normal vector $\boldsymbol{n}(\boldsymbol{x}) \in \mathbb{R}^3$, $\psi_\Gamma(\boldsymbol{x}, \boldsymbol{v})$ is a given boundary distribution, $\rho(\boldsymbol{x}, \boldsymbol{v}) \in [0, 1)$ is the reflectivity coefficient of the boundary and $r\left(\boldsymbol{v}\right) = \boldsymbol{v} - 2(\boldsymbol{n} \cdot \boldsymbol{v})\boldsymbol{n}$ is the direction reflected at the plane $\{\boldsymbol{v} \in \mathcal{S}^2 \,|\, \boldsymbol{n} \cdot \boldsymbol{v} = 0\}$. Note that it is possible to prescribe boundary data only for ingoing particles ($\boldsymbol{n}(\boldsymbol{x}) \cdot \boldsymbol{v} < 0$) since particles moving in the opposite direction do not enter but leave the domain.

Sec. 1, p. 1262], [21, Sec. 1.1, p. 9 ff.]. We can neglect the source term S because of the range of the temperature in our LITT application ($\vartheta \lesssim 100\,^\circ\mathrm{C}$).

[4] See [119].

> **Remark 5.5 — Reflectivity at the boundary.**
>
> The reflectivity coefficient $\rho(\boldsymbol{x}, \boldsymbol{v})$ describes the ratio between reflected and transmitted radiation at a point $\boldsymbol{x} \in \Gamma$ at the boundary. It can be calculated according to *Fresnel's equation* and *Snell's law*[a] and depends on the *refractive indices* of the adjacent materials inside and outside the domain. Furthermore, the reflectivity coefficient depends on the inner product $\boldsymbol{n}(\boldsymbol{x}) \cdot \boldsymbol{v}$, i.e., on the angle of the direction relative to the normal vector. In order to simplify the derivation of the second-order formulation and reduce complex boundary effects in the numerical test cases, we drop the directional dependency, i.e., we set $\rho(\boldsymbol{x}, \boldsymbol{v}) = \rho(\boldsymbol{x})$. The derivation and implementation can be extended to the direction-depending case.
>
> ---
> [a] See [119].

For a rigorous analytical treatment of the RTE, we refer to [44, XXI, p. 209 ff.]. Especially [44, XXI App. of §2 2, Thm. 5, p. 260] gives the existence of the unique solution of the RTE with reflection boundary conditions under certain assumptions on the domain and the data. Here, we are interested only in formal derivations to obtain a scheme for a further numerical treatment, so we settle with the following assumption.

> **Assumption 5.6 — Well-posedness of the RTE.**
>
> For the remainder of this chapter, we assume that the parameters are chosen in such a way that there is a unique solution of the RTE (5.1).

In our situation of LITT as well as in many other applications, e.g., [52, 159, 167], we are not interested in the directional dependence but only in the irradiance

$$\phi(\boldsymbol{x}) := \int_{\mathcal{S}^2} \psi(\boldsymbol{x}, \boldsymbol{v}) \, \mathrm{d}\boldsymbol{v} \tag{5.3}$$

where the distribution function (radiance) ψ solves the RTE (5.1). Throughout this paper we parameterize the direction $\boldsymbol{v}$ in spherical coordinates by

$$\boldsymbol{v} = \left(\sqrt{1 - \mu^2} \cos(\varphi), \sqrt{1 - \mu^2} \sin(\varphi), \mu \right)^{\mathrm{T}} =: (v_x, v_y, v_z)^{\mathrm{T}} \tag{5.4}$$

where $\varphi \in [0, 2\pi)$ is the azimuthal angle and $\mu \in [-1, 1]$ the cosine of the polar angle. This allows us to evaluate the integral over the full unit sphere $\mathcal{S}^2$ as follows:

$$\langle \cdot \rangle := \int_{\mathcal{S}^2} \cdot \, \mathrm{d}\boldsymbol{v} = \int_{-1}^{1} \int_{0}^{2\pi} \cdot \, \mathrm{d}\varphi \, \mathrm{d}\mu \,.$$

This notation must not to be confused with the dual pairing $\langle \cdot, \cdot \rangle_B$ for some Banach space B in Part I.

5.2.1 Moment approximations

The following brief overview on moment approximations is based on and adopted in part from [192].

In general, it is computationally expensive to solve equation (5.1) numerically since with three spatial coordinates the domain $\Omega \times \mathcal{S}^2$ of ψ is a subset of $\mathbb{R}^5$.

For this reason, it is convenient to use some type of spectral or Galerkin method to transform the high-dimensional equation into a system of lower-dimensional equations. Typically, one chooses to reduce the dimensionality by representing the directional dependency of ψ in terms of some angular basis, where in this thesis we choose the so-called real spherical harmonics with *maximum degree N*.

Definition 5.7 — Real spherical harmonics.

The real spherical harmonics [16, 23, 198] are given by [a]

$$S_l^m(\mu, \varphi) = \begin{cases} \Theta_{lm}(\mu)\sqrt{2}\cos(m\varphi), & m > 0, \\ \Theta_{l0}(\mu), & m = 0, \\ \Theta_{l|m|}(\mu)\sqrt{2}\sin(|m|\,\varphi), & m < 0 \end{cases} \tag{5.5}$$

for $0 \leq l \leq N$, $-l \leq m \leq l$, and

$$\Theta_{lm}(\mu) = \sqrt{\frac{2l+1}{4\pi}\frac{(l-m)!}{(l+m)!}}P_l^m(\mu), \quad m \geq 0.$$

Analogously to [16], the associated Legendre polynomials P_l^m are chosen in such a way that they satisfy the Rodrigues' formula[b]

$$P_l^m(\mu) = \frac{1}{2^l l!}(1-\mu^2)^{\frac{m}{2}}\frac{\mathrm{d}^{\,l+m}}{\mathrm{d}\,\mu^{l+m}}\left(\mu^2-1\right)^l, \quad 0 \leq m \leq l. \tag{5.6}$$

Here, l denotes the *degree* of the corresponding function.

---

[a] This formulation coincides with the one in [16], according to the parameterization of the unit sphere (5.4).
[b] Note that sometimes the definition of the *associated Legendre polynomials* includes a prefactor of $(-1)^m$.
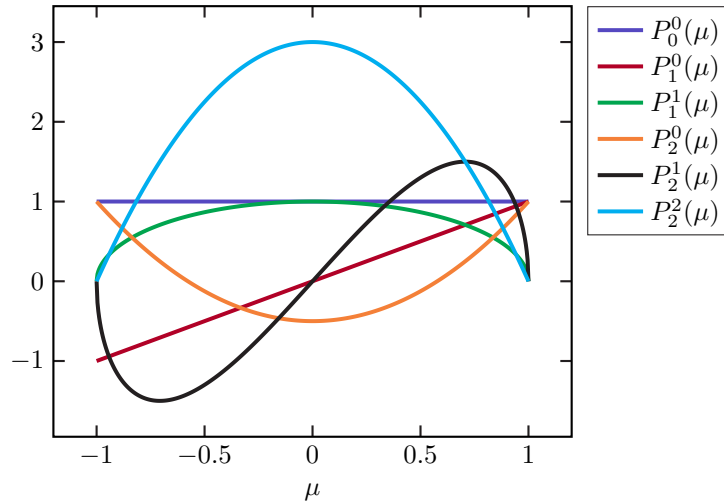
Figure 5.1: First associated Legendre polynomials up to degree $l = 3$ (see equation (5.6)).

■ **Example 5.8 — Associated Legendre polynomials.**

The first associated Legendre polynomials defined in (5.6) read as follows:

$$P_0^0(\mu) = 1, \qquad\qquad P_1^0(\mu) = \mu,$$

$$P_1^1(\mu) = (1 - \mu^2)^{1/2}, \qquad P_2^0(\mu) = \frac{1}{2}(3\mu^2 - 1),$$

$$P_2^1(\mu) = 3\mu(1 - \mu^2)^{1/2}, \quad P_2^2(\mu) = 3(1 - \mu^2)$$

$$P_3^0(\mu) = \frac{1}{2}(5\mu^3 - 3\mu), \quad P_3^1(\mu) = \frac{3}{2}(5\mu^2 - 1)(1 - \mu^2)^{1/2},$$

$$P_3^2(\mu) = 15\mu(1 - \mu^2), \quad P_3^3(\mu) = 15(1 - \mu^2)^{3/2}.$$

We visualize the first associated Legendre polynomials on the interval $[-1, 1]$ in Figure 5.1.

Definition 5.9 — Angular basis and moments.

We call the set of real spherical harmonics with maximum degree N an (angular) basis of order N and write it as a vector-valued function $\mathbf{b} := \mathbf{b}_N \colon \mathcal{S}^2 \to \mathbb{R}^n$.

In some situations, depending on certain symmetry assumptions as discussed in Subsection 5.2.2, we restrict ourselves to a subset of the angular basis.

The so-called *moments* $\mathbf{u}$ of a given distribution function ψ are then defined by

$$\mathbf{u} \colon \Omega \to \mathbb{R}^n, \ \mathbf{u}(\boldsymbol{x}) := \mathbf{u_b}(\boldsymbol{x}) := (u_0(\boldsymbol{x}), \dots, u_{n-1}(\boldsymbol{x}))^{\mathrm{T}} := \langle \mathbf{b}(\boldsymbol{v})\psi(\boldsymbol{x}, \boldsymbol{v})\rangle,$$

where the integration is performed componentwise.

The set of all real spherical harmonics forms an orthonormal basis[5] of $L^2(\mathcal{S}^2, \mathbb{R})$, what especially implies $\langle \mathbf{b}_i \mathbf{b}_j \rangle = \delta_{i,j}$. This allows us to express the distribution ψ in terms of a Fourier series

$$\psi(\boldsymbol{x}, \boldsymbol{v}) = \sum_{i=0}^{\infty} \langle b_i(\boldsymbol{v})\psi(\boldsymbol{x}, \boldsymbol{v})\rangle \, b_i(\boldsymbol{v}) = \sum_{i=0}^{\infty} u_i(\boldsymbol{x})b_i(\boldsymbol{v}). \tag{5.7}$$

Note that by the choice of our basis the first moment

$$u_0 \approx \left\langle \frac{1}{\sqrt{4\pi}}\psi \right\rangle = \frac{1}{\sqrt{4\pi}}\phi \tag{5.8}$$

is an approximation of a multiple of the irradiance defined in equation (5.3).

In order to obtain a set of equations for $\mathbf{u}$, we perform a Galerkin approximation of equation (5.1) by projecting it onto the space spanned by $\mathbf{b}$. Thus, omitting to write the dependencies on $\boldsymbol{x}$ and $\boldsymbol{v}$ in the integrals, we obtain

$$\langle \mathbf{b}(\nabla_{\boldsymbol{x}} \cdot \boldsymbol{v})\psi \rangle + \langle \mathbf{b}\sigma_{\mathrm{a}}\psi \rangle = \langle \mathbf{b}\sigma_{\mathrm{s}}\mathcal{C}(\psi) \rangle + \langle \mathbf{b}Q \rangle. \tag{5.9}$$

Since it is impractical to work with an infinite-dimensional system, the Fourier series has to be truncated, such that a finite number of $n < \infty$ basis functions $\mathbf{b}_N$ of order N remains. Because the real spherical harmonics are orthonormal w.r.t. $\langle \cdot \rangle$, we can choose the ansatz

$$\psi(\boldsymbol{x}, \boldsymbol{v}) \approx \hat{\psi}(\boldsymbol{x}, \boldsymbol{v}) := \sum_{i=0}^{n-1} u_i(\boldsymbol{x})b_i(\boldsymbol{v}) = \mathbf{b}(\boldsymbol{v})^{\mathrm{T}}\mathbf{u}(\boldsymbol{x}). \tag{5.10}$$

---

[5] See [67, II.11, p. 99 ff.].
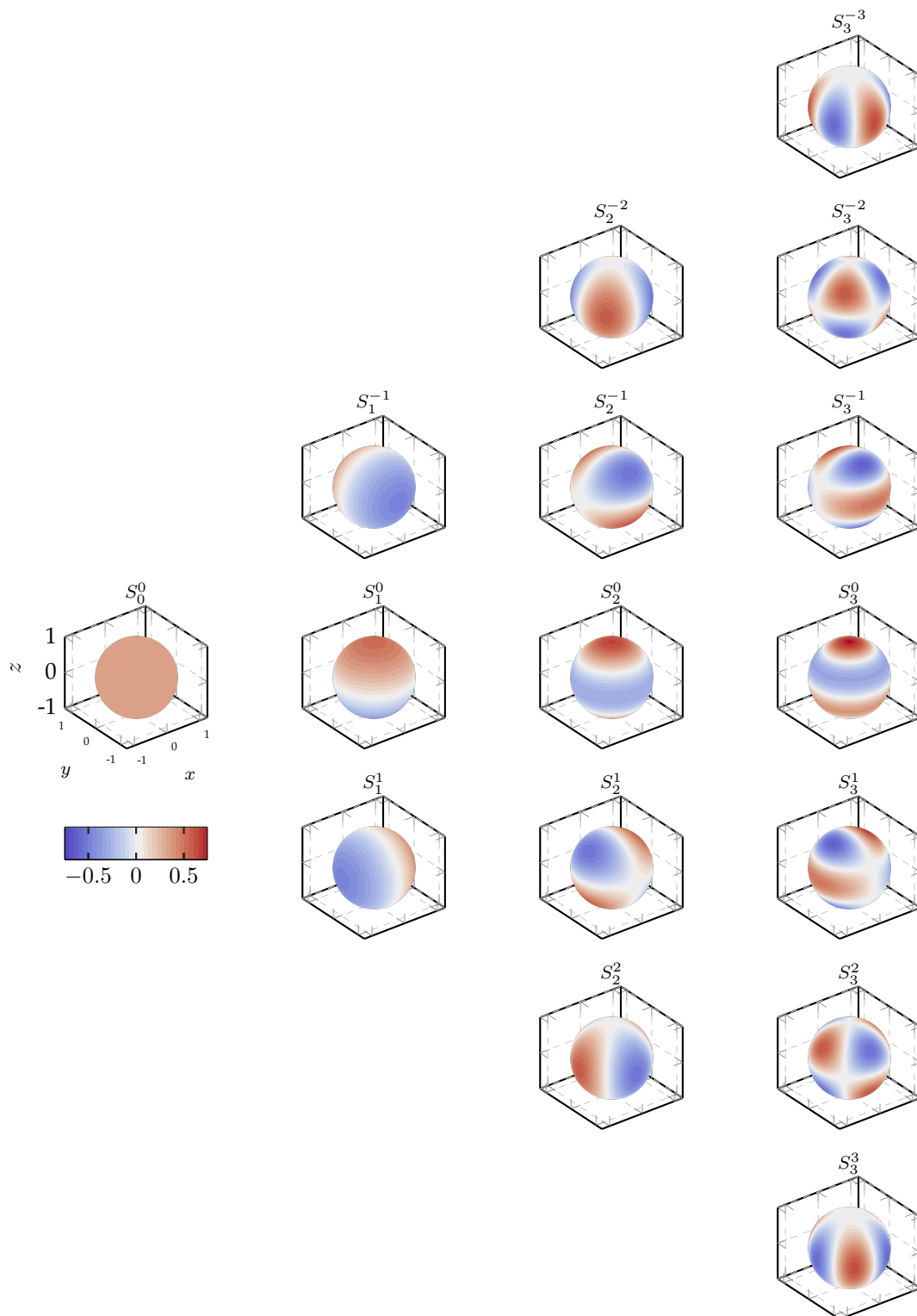
Figure 5.2: Real spherical harmonics up to degree $l = 3$ (see equation (5.5)).

We plug our ansatz (5.10) into equation (5.9), collect known terms and interchange integrals and differentiation where possible, and obtain the moment system

$$\underbrace{\left\langle v_x \mathbf{b}\mathbf{b}^{\mathrm{T}}\right\rangle}_{T_x :=} \cdot \partial_x \mathbf{u} + \underbrace{\left\langle v_y \mathbf{b}\mathbf{b}^{\mathrm{T}}\right\rangle}_{T_y :=} \cdot \partial_y \mathbf{u} + \underbrace{\left\langle v_z \mathbf{b}\mathbf{b}^{\mathrm{T}}\right\rangle}_{T_z :=} \cdot \partial_z \mathbf{u} + \sigma_{\mathrm{a}} \mathbf{u} = \sigma_{\mathrm{s}} \left\langle \mathbf{b}\mathcal{C}\left(\hat{\psi}\right)\right\rangle + \langle \mathbf{b} Q \rangle. \quad (5.11)$$

Our choice of the scattering operator and the Assumption 5.2 on the scattering kernel allow us to write

$$\left\langle \mathbf{b}\mathcal{C}\left(\hat{\psi}\right)\right\rangle = (\Sigma - E_n)\mathbf{u} \quad \text{where} \quad \Sigma = \int_{\mathcal{S}^2} \int_{\mathcal{S}^2} \mathbf{b}(\boldsymbol{v})\mathbf{b}(\boldsymbol{v}')^{\mathrm{T}} \mathcal{K}\left(\boldsymbol{v}, \boldsymbol{v}'\right) \, \mathrm{d}\boldsymbol{v}' \, \mathrm{d}\boldsymbol{v}$$

and E_n denotes the $n \times n$ identity matrix. Furthermore, we define

$$\boldsymbol{q} := \boldsymbol{q}(\boldsymbol{x}) := \langle \mathbf{b}(\boldsymbol{v})Q(\boldsymbol{x}, \boldsymbol{v})\rangle .$$

Odd-order or even-order approximations

"It is known from neutron transport theory that approximations of odd order are more accurate then even ones of next highest order [...]" [145, Sec. 15.2, p. 467] (see also [46, Sec. 10.3.2, p. 127]).

We would like to point out that not all authors agree with this convention. As discussed in the next section, the choice of boundary conditions is ambiguous. Davis tackles this ambiguity by a variational approach and draws the following conclusion [45, V, p. 197]:

> *"Conventionally, odd Marshak conditions have been used for even-order P$_N$ calculations and have given poor results relative to the odd P$_N$ calculations. In fact, it has been generally assumed, for this reason and others [46], that the odd-order P$_N$ approximations hold an advantage over the even-order approximations. Our theoretical results suggest, however, that with the use of even Marshak conditions for even P$_N$ calculations such an advantage may be illusory."*

We need to pick sides and decide for the classical convention:

Assumption 5.10 — Only odd orders.

In the following, we consider only odd values for the order N in the P$_N$ approximation.

Closure problem

Unfortunately, there always exists an index $i \in \{0, \dots, n-1\}$ in equation (5.9) such that the components of $b_i \boldsymbol{v}$ are not in the linear span of $\{b_i \mid i \in \{0, \dots, n-1\}\} \cong \mathbf{b}_N$. Therefore, considering the expansion (5.10), the flux term $\boldsymbol{v} \cdot \nabla_{\boldsymbol{x}} \hat{\psi}$ cannot be expressed in terms of $\mathbf{u}_{\mathbf{b}_N}$ without additional information. Furthermore, the same might be true for the projection of the scattering operator onto the moment space given by $\left\langle \mathbf{b}_N \mathcal{C}\left(\hat{\psi}\right)\right\rangle$. This is the so-called *closure problem*. There exist many different closure strategies related to different types of bases and ansatz functions. Our ansatz (5.10) deals with this closure problem by defining higher-order moments to be zero, i.e., $\mathbf{u}_i := 0, i > n$, where these moments correspond to basis functions b_i with degree larger than N. This corresponds to the well-known *spherical harmonics* P$_N$ *model* [54, 124], which can be understood as a Galerkin semi-approximation in $\boldsymbol{v}$ for equation (5.1).

Disadvantage of the model and possible alternatives

A big disadvantage of the P$_N$ model with the classical closure is the missing positivity of the ansatz function $\hat{\psi}$ for some moments $\mathbf{u}$, whereas the kinetic distribution to be approximated fulfills this property. Another undesired issue, which is a general problem of unlimited high-order approximations, are nonphysical oscillations where the kinetic solution is nonsmooth (the so-called *Gibbs phenomenon* [201, 209]). Additionally, since the resulting system is linear, it might be necessary to use a high number of moments to ensure a reasonable approximation of the desired kinetic solution. A problem coming along with the linearity of the ansatz is the fact that the resulting wave-speeds of this system are fixed and discrete in contrast to those of the kinetic solution. However, the structure of this system is well-understood and allows efficient numerical implementations [75, 198].

In recent years many modifications to this closure have been suggested, including the positive P$_N$ (PP$_N$), filtered P$_N$ (FP$_N$) and diffusive-corrected P$_N$ (D$_N$) [75], curing some of the disadvantages of the original P$_N$ moment approximation (with spherical harmonics) while increasing the complexity of the system at the price of higher computational costs. We also would like to note that the choices of other closures and angular bases are possible, e.g., minimum entropy [2, 21–23, 29, 35, 90, 103, 123, 138, 140, 160], partial and mixed moments [53, 71, 178, 193–195] or Kershaw closures [107, 151, 190, 191].

5.2.2 Reduction of dimensionality

The computational complexity of equation (5.1) motivates the common approach to investigate lower-dimensional models. We achieve this by assuming certain symmetries of the solution which imply that it is sufficient to perform the calculations on lower-dimensional spatial slices and a reduced set of basis functions.

1. We follow [198, Sec. 2, p. 3 ff.] and obtain "*the* slab geometry *radiative transfer equation by considering a slab between two infinite parallel plates. Assume for instance that the z-axis is perpendicular to the plates. If the setting is invariant under translations perpendicular to, and rotations around, the z-axis, then the unknown ψ depends only on the z-component of the spatial variable, and one angular variable μ (cosine of the angle between direction and z-axis)*", i.e., $\partial_x \psi = \partial_y \psi = 0$ and $\psi(\boldsymbol{x}, \boldsymbol{v}) = \psi(z, \mu)$. The functions S_l^m with $m \neq 0$ depend on the azimuthal variable φ and, thus, do not appear in the series expansion of a distribution ψ with the assumed symmetry. This allows us to consider the one-dimensional approximation of the spatial variable, i.e.[6], $\Omega \subset \mathbb{R}$, and define the reduced angular basis

$$\mathbf{b}_N = \left(S_0^0, S_1^0, \ldots, S_N^0 \right).$$

We note that the real spherical harmonics S_l^m with $m = 0$ correspond to the normalized Legendre polynomials[7]. The P$_N$ equations then read

$$T_z \partial_z \mathbf{u} = \left(\sigma_{\mathrm{s}} \Sigma - \sigma_{\mathrm{t}} E_n \right) \mathbf{u} + \boldsymbol{q}. \tag{5.12}$$

---

[6] Note that the same symbol Ω is used for the full space and for the one-dimensional projection.
[7] We use the normalized Legendre polynomials, whereas in the literature typically the unnormalized Legendre polynomials are used in slab geometry.

Due to the recursive structure of the Legendre polynomials [198], the flux matrix has the tridiagonal form

$$\left.\begin{aligned}(T_z)_{l,l+1} &= \sqrt{\frac{1}{4l^2 + 8\,l + 3}}\,(l+1) = (T_z)_{l+1,l}\,,\\(T_z)_{l,l} &= 0\end{aligned}\right\} \quad \text{for} \quad l = 0, \dots, N.$$

2. If the domain is instead assumed to be infinitely elongated in the z-direction and all data are z-independent, the solution ψ of the RTE (5.1) is also z-independent and even w.r.t. μ [198], i.e., $\partial_z\psi = 0$ and $\psi(\boldsymbol{x}, \mu, \varphi) = \psi(\boldsymbol{x}, -\mu, \varphi)$. The functions S_l^m for which $(l + |m|)$ is odd are odd in μ and, thus, do not appear in the series expansion of the solution. This allows us to consider the two-dimensional approximation of the spatial variable, i.e., $\Omega \subset \mathbb{R}^2$, and define the reduced angular basis

$$\mathbf{b}_N = \left(S_0^0, S_1^{-1}, S_1^1, \dots, S_N^{-N}, S_N^{-N+2}, \dots, S_N^{N-2}, S_N^N\right)^{\mathrm{T}},$$

i.e., we use only the subset of the real spherical harmonics where $(l + |m|)$ is even. The corresponding system then has the form

$$T_x \partial_x \mathbf{u} + T_y \partial_y \mathbf{u} = (\sigma_{\mathrm{s}}\Sigma - \sigma_{\mathrm{t}}E_n)\,\mathbf{u} + \boldsymbol{q}.$$

The matrices T_x, T_y, T_z can be found in [198] and are given for $N = 1$ in Example 5.12 below.

3. If we do not assume any symmetry properties of the data and the solution, we include all real spherical harmonics up to degree N in our angular basis:

$$\mathbf{b}_N = \left(S_0^0, S_1^{-1}, S_1^0, S_1^1, \dots, S_N^{-N}, S_N^{-N+1}, \dots, S_N^{N-1}, S_N^N\right)^{\mathrm{T}}.$$

Remark 5.11 — Reduced angular basis.

Based on the symmetry assumption described above, some of the basis functions which are necessary in the full three-dimensional setting can be neglected because the corresponding moments would be zero. The spatial dimension of the reduced model and the size of the angular basis, depending on the odd moment order N, can be found in the table below. We also give the number of even basis elements, which equals the number of coupled second-order PDEs in the final formulation, i.e., the number of components of the solution vector.

symmetry assumption	spatial dimension	number of basis elements	number of even basis elements
rot. symmetry around z-axis	1	$N + 1$	$\frac{1}{2}(N + 1)$
symmetry along z-axis	2	$\frac{1}{2}N^2 + \frac{3}{2}N + 1$	$\frac{1}{4}N^2 + \frac{1}{2}N + \frac{1}{4}$
no symmetry: full problem	3	$N^2 + 2N + 1$	$\frac{1}{2}N^2 + \frac{1}{2}N$

■ **Example 5.12 — Flux and scattering matrices.**

For isotropic scattering and moment order $N = 1$, we get for the full three-dimensional setup, i.e., $\mathbf{b}_1 = \left(S_0^0, S_1^{-1}, S_1^0, S_1^1\right)$, the following matrices defining the P$_N$ equations:

$$T_x = \begin{bmatrix} 0 & 0 & 0 & \frac{1}{\sqrt{3}} \\ 0 & 0 & 0 & 0 \\ 0 & 0 & 0 & 0 \\ \frac{1}{\sqrt{3}} & 0 & 0 & 0 \end{bmatrix}, \quad T_y = \begin{bmatrix} 0 & \frac{1}{\sqrt{3}} & 0 & 0 \\ \frac{1}{\sqrt{3}} & 0 & 0 & 0 \\ 0 & 0 & 0 & 0 \\ 0 & 0 & 0 & 0 \end{bmatrix},$$

$$T_z = \begin{bmatrix} 0 & 0 & \frac{1}{\sqrt{3}} & 0 \\ 0 & 0 & 0 & 0 \\ \frac{1}{\sqrt{3}} & 0 & 0 & 0 \\ 0 & 0 & 0 & 0 \end{bmatrix}, \quad \Sigma = \begin{bmatrix} 1 & 0 & 0 & 0 \\ 0 & 0 & 0 & 0 \\ 0 & 0 & 0 & 0 \\ 0 & 0 & 0 & 0 \end{bmatrix}.$$

5.3 Second-order formulation of the P$_N$ equations

In this section we propose a reformulation of the classical P$_N$ equations, described above, as system of second-order PDEs in the spatial variable. The idea to reformulate the P$_N$ equations in terms of second-order derivatives is not new [146, 148], but, to the best of our knowledge, our derivation and resulting formulation has not been presented yet. Our formulation has a simple structure, can be generated automatically with the help of computer-algebra systems, and can easily be handed to a standard finite-element tool for its numerical solution, like demonstrated in our implementation [8].

Express the odd moments in terms of the even moments by means of algebraic transformations and symmetry properties of the real spherical harmonics.

Remark 5.13 — Smoothness.

We would like to point out that the formal derivation requires additional smoothness of the solution, i.e., equivalence of the two formulations is given only for P$_N$ solutions with a sufficient regularity. Furthermore, we do not discuss the well-posedness of the resulting second-order system here.

5.3.1 Algebraic transformations

The reformulation of the P$_N$ equations in second-order form is based on the parity property w.r.t. the directional variable $\boldsymbol{v}$ of the real spherical harmonics:

$$S_l^m(-\boldsymbol{v}) = (-1)^l S_l^m(\boldsymbol{v}) \quad \text{for all } \boldsymbol{v} \in \mathcal{S}^2.$$

The real spherical harmonics are called even or odd if the corresponding degree $l \in \mathbb{N}_0$ is even or odd, respectively.

We organize the basis functions for the full problem[8] into even and odd functions

$$\mathbf{b}_\mathrm{e} := \left(S_0^0, S_2^{-2}, S_2^{-1}, \ldots, S_2^2, S_4^{-4}, \ldots, S_4^4, \ldots, S_{N-1}^{-N+1}, \ldots, S_{N-1}^{N-1} \right), \quad \text{(even)}$$

$$\mathbf{b}_\mathrm{o} := \left(S_1^{-1}, S_1^0, S_1^1, S_3^{-3}, S_3^{-2}, \ldots, S_3^3, \ldots, S_N^{-N}, \ldots, S_N^N \right) \qquad \text{(odd)}$$

and rearrange the moments $\mathbf{u}_\mathrm{e} = \left\langle \mathbf{b}_\mathrm{e} \hat{\psi} \right\rangle$ and $\mathbf{u}_\mathrm{o} = \left\langle \mathbf{b}_\mathrm{o} \hat{\psi} \right\rangle$, respectively. We write for the number of even and odd basis functions $n_\mathrm{e} = \frac{1}{2} N^2 + \frac{1}{2} N$ and $n_\mathrm{o} = \frac{1}{2} N^2 + \frac{3}{2} N + 1$, respectively. Now we can rewrite the P$_N$ ansatz (5.10) as

$$\hat{\psi}(\boldsymbol{x}, \boldsymbol{v}) = \mathbf{b}_\mathrm{e}^\mathrm{T}(\boldsymbol{v}) \mathbf{u}_\mathrm{e}(\boldsymbol{x}) + \mathbf{b}_\mathrm{o}^\mathrm{T}(\boldsymbol{v}) \mathbf{u}_\mathrm{o}(\boldsymbol{x}). \tag{5.13}$$

In particular, with v_x, v_y, v_z being odd and the entries of $\mathbf{b}_\mathrm{e} \mathbf{b}_\mathrm{e}^\mathrm{T}, \mathbf{b}_\mathrm{o} \mathbf{b}_\mathrm{o}^\mathrm{T}$ being even functions w.r.t. $\boldsymbol{v}$, we can find that the flux matrices in equation (5.11) decouple, based on the following observation:

$$\begin{pmatrix} \left\langle (\nabla_{\boldsymbol{x}} \cdot \boldsymbol{v}) \mathbf{b}_\mathrm{e} \hat{\psi} \right\rangle \\ \left\langle (\nabla_{\boldsymbol{x}} \cdot \boldsymbol{v}) \mathbf{b}_\mathrm{o} \hat{\psi} \right\rangle \end{pmatrix} \overset{(5.13)}{=} \begin{pmatrix} \left\langle (\nabla_{\boldsymbol{x}} \cdot \boldsymbol{v}) \mathbf{b}_\mathrm{e} \mathbf{b}_\mathrm{e}^\mathrm{T} \right\rangle \mathbf{u}_\mathrm{e} + \left\langle (\nabla_{\boldsymbol{x}} \cdot \boldsymbol{v}) \mathbf{b}_\mathrm{e} \mathbf{b}_\mathrm{o}^\mathrm{T} \right\rangle \mathbf{u}_\mathrm{o} \\ \left\langle (\nabla_{\boldsymbol{x}} \cdot \boldsymbol{v}) \mathbf{b}_\mathrm{o} \mathbf{b}_\mathrm{e}^\mathrm{T} \right\rangle \mathbf{u}_\mathrm{e} + \left\langle (\nabla_{\boldsymbol{x}} \cdot \boldsymbol{v}) \mathbf{b}_\mathrm{o} \mathbf{b}_\mathrm{o}^\mathrm{T} \right\rangle \mathbf{u}_\mathrm{o} \end{pmatrix} \overset{\text{parity}}{=} \begin{pmatrix} \left\langle (\nabla_{\boldsymbol{x}} \cdot \boldsymbol{v}) \mathbf{b}_\mathrm{e} \mathbf{b}_\mathrm{o}^\mathrm{T} \right\rangle \mathbf{u}_\mathrm{o} \\ \left\langle (\nabla_{\boldsymbol{x}} \cdot \boldsymbol{v}) \mathbf{b}_\mathrm{o} \mathbf{b}_\mathrm{e}^\mathrm{T} \right\rangle \mathbf{u}_\mathrm{e} \end{pmatrix}.$$

The P$_N$ equations can now be rewritten as

$$\overbrace{T_\mathrm{eo}^x \partial_x \mathbf{u}_\mathrm{o} + T_\mathrm{eo}^y \partial_y \mathbf{u}_\mathrm{o} + T_\mathrm{eo}^z \partial_z \mathbf{u}_\mathrm{o}}^{T_\mathrm{e}(\mathbf{u}_\mathrm{o}) :=} = \overbrace{(\sigma_\mathrm{s} \Sigma_\mathrm{ee} - \sigma_\mathrm{t} E_{n_\mathrm{e}})}^{C_\mathrm{ee} :=} \mathbf{u}_\mathrm{e} + \overbrace{\sigma_\mathrm{s} \Sigma_\mathrm{eo}}^{C_\mathrm{eo} :=} \mathbf{u}_\mathrm{o} + \boldsymbol{q}_\mathrm{e}, \tag{5.14a}$$

$$\underbrace{T_\mathrm{oe}^x \partial_x \mathbf{u}_\mathrm{e} + T_\mathrm{oe}^y \partial_y \mathbf{u}_\mathrm{e} + T_\mathrm{oe}^z \partial_z \mathbf{u}_\mathrm{e}}_{T_\mathrm{o}(\mathbf{u}_\mathrm{e}) :=} = \underbrace{\sigma_\mathrm{s} \Sigma_\mathrm{oe}}_{C_\mathrm{oe} :=} \mathbf{u}_\mathrm{e} + \underbrace{(\sigma_\mathrm{s} \Sigma_\mathrm{oo} - \sigma_\mathrm{t} E_{n_\mathrm{o}})}_{C_\mathrm{oo} :=} \mathbf{u}_\mathrm{o} + \boldsymbol{q}_\mathrm{o} \tag{5.14b}$$

where $T_\mathrm{eo}^i := \left\langle v_i \mathbf{b}_\mathrm{e} \mathbf{b}_\mathrm{o}^\mathrm{T} \right\rangle$ and $T_\mathrm{oe}^i := \left\langle v_i \mathbf{b}_\mathrm{o} \mathbf{b}_\mathrm{e}^\mathrm{T} \right\rangle$, for $i \in \{x, y, z\}$, and $\Sigma_\mathrm{ee}, \Sigma_\mathrm{eo}, \Sigma_\mathrm{oe}, \Sigma_\mathrm{oo}, \boldsymbol{q}_\mathrm{e}, \boldsymbol{q}_\mathrm{o}$ are the rows and columns of Σ and $\boldsymbol{q}$ according to the reordering of $\mathbf{u} = (\mathbf{u}_\mathrm{e}, \mathbf{u}_\mathrm{o})^\mathrm{T}$. Here, T_e and T_o define formal linear differential operators. In Lemma 5.15, we show that $C_\mathrm{oo} \in \mathbb{R}^{n_\mathrm{o} \times n_\mathrm{o}}$ is invertible.[9] We can then formally solve equation (5.14b) for $\mathbf{u}_\mathrm{o}$, i.e.,

$$\mathbf{u}_\mathrm{o} = C_\mathrm{oo}^{-1} \left(T_\mathrm{o} \left(\mathbf{u}_\mathrm{e} \right) - C_\mathrm{oe} \mathbf{u}_\mathrm{e} - \boldsymbol{q}_\mathrm{o} \right), \tag{5.15}$$

and plug it into equation (5.14a) to obtain a second-order system of linear, stationary drift-diffusion equations:

$$\begin{aligned} T_\mathrm{e} \left(\mathbf{u}_\mathrm{o} \right) &= T_\mathrm{e} \left(C_\mathrm{oo}^{-1} \left(T_\mathrm{o} \left(\mathbf{u}_\mathrm{e} \right) - C_\mathrm{oe} \mathbf{u}_\mathrm{e} - \boldsymbol{q}_\mathrm{o} \right) \right) \\ &= C_\mathrm{ee} \mathbf{u}_\mathrm{e} + C_\mathrm{eo} C_\mathrm{oo}^{-1} \left(T_\mathrm{o} \left(\mathbf{u}_\mathrm{e} \right) - C_\mathrm{oe} \mathbf{u}_\mathrm{e} - \boldsymbol{q}_\mathrm{o} \right) + \boldsymbol{q}_\mathrm{e}. \end{aligned} \tag{5.16}$$

> **Assumption 5.14 — No-drift property.**
> We assume that the kernel $\mathcal{K}$ is chosen such that $C_\mathrm{oe} = 0 \in \mathbb{R}^{n_\mathrm{o} \times n_\mathrm{e}}$ and $C_\mathrm{eo} = 0 \in \mathbb{R}^{n_\mathrm{e} \times n_\mathrm{o}}$. See Remark 5.17 and Lemma 5.15 for a detailed discussion on this assumption.

Based on Assumption 5.14, the second-order formulation (5.16) reduces to

$$T_\mathrm{e} \left(\mathbf{u}_\mathrm{o} \right) = C_\mathrm{ee} \mathbf{u}_\mathrm{e} + \boldsymbol{q}_\mathrm{e} \tag{5.17}$$

or, equivalently,

$$T_\mathrm{e} \left(C_\mathrm{oo}^{-1} T_\mathrm{o} \left(\mathbf{u}_\mathrm{e} \right) \right) = C_\mathrm{ee} \mathbf{u}_\mathrm{e} + \boldsymbol{q}_\mathrm{e} + T_\mathrm{e} \left(C_\mathrm{oo}^{-1} \boldsymbol{q}_\mathrm{o} \right).$$

---

[8] For the slab geometry or a two-dimensional geometry, the reduction has to be performed accordingly.

[9] We show this under the assumption of $\sigma_\mathrm{t} > 0$.

Note that C_{oo} depends on the quantities σ_{s} and σ_{a}. Thus, it can not be pulled out of the differential operator if the physical coefficients are not space-homogeneous.

The reduction operator (5.15) is well defined. In fact, the next Lemma tells us that we can solve for $\mathbf{u}_{\text{o}}$ in equation (5.14b).

> **Lemma 5.15 — Reduction operator in equation** (5.15) **is well defined.**
> Let the kernel $\mathcal{K}$ satisfy Assumption 5.2. The matrix $C_{\text{oo}} = (\sigma_{\text{s}}\Sigma_{\text{oo}} - \sigma_{\text{t}}E_{n_{\text{o}}})$ is invertible whenever $\sigma_{\text{a}} + \sigma_{\text{s}} = \sigma_{\text{t}} > 0$.

The proof of Lemma 5.15 is given in Appendix C.1.2, where we show that the matrix C_{oo} is negative definite.

> **Remark 5.16 — Decoupled structure.**
> The fact that the P$_N$ equations decouple is a well-known result. E.g., in [198], this was used to derive an efficient implementation for the time-dependent P$_N$ equations, where the decoupled structure was employed on a staggered grid.

We conclude this subsection with a discussion on the no-drift property in Assumption 5.14.

> **Remark 5.17 — There are kernels causing drift terms.**
> We would like to point out that the previous Assumption 5.14 is necessary to get rid of the drift terms in equation (5.16). An example for a kernel which satisfies Assumption 5.2 but does not satisfy Assumption 5.14 is given by
>
> $$\mathcal{K}(\boldsymbol{v}, \boldsymbol{v}') = \frac{3\left(25\mu^2 + 25(\mu')^2 - 75\mu^2(\mu')^2 + 45\mu^2\mu' + 45\mu(\mu')^2 - 27\mu\mu' - 15\mu - 15\mu' + 150\right)}{1900\pi}.$$
>
> For $N = 3$, it yields the matrix
>
> $$\Sigma_{\text{eo}} = \begin{pmatrix} 0 & 0 & 0 & 0 & 0 & 0 & 0 & 0 & 0 & 0 \\ 0 & 0 & 0 & 0 & 0 & 0 & 0 & 0 & 0 & 0 \\ 0 & 0 & 0 & 0 & 0 & 0 & 0 & 0 & 0 & 0 \\ 0 & \frac{6\sqrt{15}}{475} & 0 & 0 & 0 & 0 & 0 & 0 & 0 & 0 \\ 0 & 0 & 0 & 0 & 0 & 0 & 0 & 0 & 0 & 0 \\ 0 & 0 & 0 & 0 & 0 & 0 & 0 & 0 & 0 & 0 \end{pmatrix}$$
>
> and, with this, especially $C_{\text{eo}} \neq 0 \in \mathbb{R}^{n_{\text{e}} \times n_{\text{o}}}$. We visualize this kernel, projected onto the z-component of $\boldsymbol{v}$, in Figure 5.3.

In the next Lemma we show that for a certain class of kernels the desired no-drift property is fulfilled.
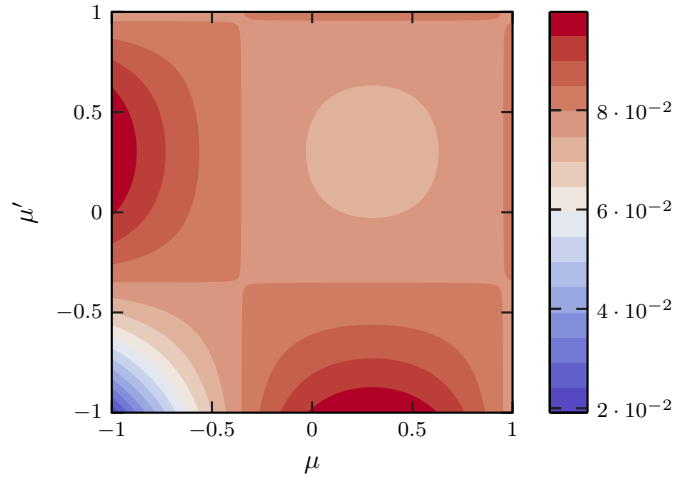
Figure 5.3: Surface plot of the kernel in Remark 5.17, which violates the no-drift assumption (Assumption 5.14). The value of $\mathcal{K}(\boldsymbol{v}, \boldsymbol{v}') = \mathcal{K}(\mu, \mu')$ is encoded in the color scale.

Lemma 5.18 — No drift.

Let the kernel $\mathcal{K}$ satisfy Assumption 5.2 and fulfill $\mathcal{K}(\boldsymbol{v}, \boldsymbol{v}') = \hat{\mathcal{K}}(\boldsymbol{v}^{\mathrm{T}} \boldsymbol{v}')$ for all $\boldsymbol{v}, \boldsymbol{v}' \in \mathcal{S}^2$, for some continuous[a] function $\hat{\mathcal{K}} \colon [-1, 1] \to \mathbb{R}_{>0}$. Then the kernel satisfies Assumption 5.14, i.e., no drift terms occur in the resulting P_N^{2nd} formulation. In particular, this holds true for the kernels in Examples 5.3 and 5.4 (for $g \in (-1, 1)$).

---
[a] The continuity of $\hat{\mathcal{K}}$ guarantees that the occurring integrals in the proof are well defined.

The proof of Lemma 5.18 is given in Appendix C.1.1 and is based on symmetry properties of the spherical harmonics and the scattering kernel.

5.3.2 Weak formulation and boundary conditions

One major problem of the P_N equations is that the semi-transparent boundary conditions (5.2) of the transfer equation have to be prescribed only for inward-pointing angles ($\boldsymbol{n} \cdot \boldsymbol{v} < 0$), whereas the hyperbolic P_N system requires information for the characteristic variables related to ingoing characteristics [216]. Although these quantities are somehow related, a consistent approximation of boundary conditions for moment models is nontrivial [118, 168, 185, 206].

Without thinking too much about these implications for the P_N equations, we want to use the Marshak ([145, Sec. 15.3, p. 470]) approach to derive consistent boundary conditions for equation (5.16).[10] The basic idea is to replace ψ in the boundary conditions (5.2) with the P_N ansatz $\hat{\psi}$ and take half moments over $\{\boldsymbol{v} \in \mathcal{S}^2 \mid \boldsymbol{n} \cdot \boldsymbol{v} < 0\}$ of the equation w.r.t. to a suitable subset of basis functions, that is

$$\int_{\boldsymbol{n} \cdot \boldsymbol{v} < 0} \hat{\psi}(\boldsymbol{v}) S_l^m(\boldsymbol{v}) \, \mathrm{d}\boldsymbol{v} = \int_{\boldsymbol{n} \cdot \boldsymbol{v} < 0} \rho \hat{\psi}(r(\boldsymbol{v})) S_l^m(\boldsymbol{v}) \, \mathrm{d}\boldsymbol{v} + \int_{\boldsymbol{n} \cdot \boldsymbol{v} < 0} (1 - \rho) \psi_\Gamma(\boldsymbol{v}) S_l^m(\boldsymbol{v}) \, \mathrm{d}\boldsymbol{v}, \quad l \text{ odd.} \quad (5.18)$$

---
[10] Another famous set of boundary conditions would be Mark's boundary conditions [145, Sec. 15.3, p. 469].

> **Remark 5.19 — A suitable subset of boundary conditions.**
>
> If we test equation (5.2) with all basis functions, we usually obtain more boundary conditions than needed. This ambiguity is well known and there are different conventions. The authors of [146] suggest to choose "all relevant" basis functions. Modest phrases this as follows: *"Thus, on intuitive grounds it is accepted practice to satisfy equation (5.18) for all relevant [i.e., nonzero] m for $l = 1, 2, ..., \frac{1}{2}(N-1)$, and for as many relevant m as possible for $l = \frac{1}{2}(N+1)$."* [145, Sec. 15.3, p. 471]
>
> Marshak recommends the choice of odd basis functions in equation (5.2) (in a one-dimensional setup), based on the following remark: *"Dr. Mark has pointed out that the apparent ambiguity in the choice of the boundary conditions is removed if one recalls that in the Milne problem for the-half-plane the exact even "half-moments" have an infinite derivative at the boundary, whereas the exact odd "half-moments" have a finite derivative, just as they do in any odd P approximation."* [131, Sec. 2, footnote 2, p. 444]
>
> In a classical SP$_N$ context, it is also common to choose all odd half moments [88].

We choose all odd basis functions in $\mathbf{b}_\text{o}$ for the half moments at the boundary because those are the ones which appear naturally in the weak formulation as discussed below. This choice also leads to more equations than unknowns but guarantees that the second-order formulation is well defined, as shown in Lemma 5.20.

We start to derive the weak form for $\mathbf{u}_\text{e}$. Let $\varphi \colon \Omega \to \mathbb{R}$ denote a suitable spatial test function and let $i \in \{1, \ldots, n_\text{e}\}$. The weak formulation of (5.17) then reads

$$
\begin{aligned}
\int_\Omega (C_\text{ee}\mathbf{u}_\text{e})_i \varphi \,\mathrm{d}\boldsymbol{x} &+ \int_\Omega \boldsymbol{q}_{\text{e},i} \varphi \,\mathrm{d}\boldsymbol{x} \stackrel{(5.17)}{=} \int_\Omega \left(T_\text{e}\left(\mathbf{u}_\text{o}\right)\right)_i \varphi \,\mathrm{d}\boldsymbol{x} \\
&= \int_\Omega \left[\left\langle v_x\left(\mathbf{b}_\text{e}\right)_i \mathbf{b}_\text{o}^\text{T} \right\rangle \partial_x \mathbf{u}_\text{o} + \left\langle v_y\left(\mathbf{b}_\text{e}\right)_i \mathbf{b}_\text{o}^\text{T} \right\rangle \partial_y \mathbf{u}_\text{o} + \left\langle v_z\left(\mathbf{b}_\text{e}\right)_i \mathbf{b}_\text{o}^\text{T} \right\rangle \partial_z \mathbf{u}_\text{o} \right] \varphi \,\mathrm{d}\boldsymbol{x} \\
&= \int_\Omega \left[\partial_x \left\langle v_x\left(\mathbf{b}_\text{e}\right)_i \left(\mathbf{b}_\text{o}^\text{T}\mathbf{u}_\text{o}\right) \right\rangle + \partial_y \left\langle v_y\left(\mathbf{b}_\text{e}\right)_i \left(\mathbf{b}_\text{o}^\text{T}\mathbf{u}_\text{o}\right) \right\rangle + \partial_z \left\langle v_z\left(\mathbf{b}_\text{e}\right)_i \left(\mathbf{b}_\text{o}^\text{T}\mathbf{u}_\text{o}\right) \right\rangle \right] \varphi \,\mathrm{d}\boldsymbol{x} \quad (5.19) \\
&= \int_\Omega \mathrm{div}\left(\left\langle \boldsymbol{v}\left(\mathbf{b}_\text{e}\right)_i \left(\mathbf{b}_\text{o}^\text{T}\mathbf{u}_\text{o}\right) \right\rangle \right) \varphi \,\mathrm{d}\boldsymbol{x} \\
&\stackrel{\text{Gauss}}{=} - \int_\Omega \left\langle \boldsymbol{v}\left(\mathbf{b}_\text{e}\right)_i \left(\mathbf{b}_\text{o}^\text{T}\mathbf{u}_\text{o}\right) \right\rangle \cdot \nabla\varphi \,\mathrm{d}\boldsymbol{x} + \int_\Gamma \left\langle \left(\boldsymbol{n}\cdot\boldsymbol{v}\right)\left(\mathbf{b}_\text{e}\right)_i \left(\mathbf{b}_\text{o}^\text{T}\mathbf{u}_\text{o}\right) \right\rangle \varphi \,\mathrm{d}\boldsymbol{s}
\end{aligned}
$$

where we used Gauss's theorem[11] in the last step. We now want to eliminate $\mathbf{u}_\text{o}$ in equation (5.19) using the boundary conditions. Therefore, we plug the ansatz $\hat{\psi} = \mathbf{b}_\text{e} \cdot \mathbf{u}_\text{e} + \mathbf{b}_\text{o} \cdot \mathbf{u}_\text{o}$ into equation (5.18) and test with all odd basis elements in $\mathbf{b}_\text{o}$, which yields

$$
\left[\int_{\boldsymbol{n}\cdot\boldsymbol{v}<0} \mathbf{b}_\text{o}(\boldsymbol{v})\left(\mathbf{b}_\text{o}^\text{T}(\boldsymbol{v}) - \rho\mathbf{b}_\text{o}^\text{T}(r\left(\boldsymbol{v}\right))\right) \mathrm{d}\boldsymbol{v} \right] \mathbf{u}_\text{o} + \left[\int_{\boldsymbol{n}\cdot\boldsymbol{v}<0} \mathbf{b}_\text{o}(\boldsymbol{v})\left(\mathbf{b}_\text{e}^\text{T}(\boldsymbol{v}) - \rho\mathbf{b}_\text{e}^\text{T}(r\left(\boldsymbol{v}\right))\right) \mathrm{d}\boldsymbol{v} \right] \mathbf{u}_\text{e} = \mathbf{u}_\Gamma
$$

$$(5.20)$$

with

$$
\mathbf{u}_\Gamma := \mathbf{u}_\Gamma(\boldsymbol{x}, \boldsymbol{n}) := \int_{\boldsymbol{n}\cdot\boldsymbol{v}<0} (1-\rho)\mathbf{b}_\text{o}(\boldsymbol{v})\psi_\Gamma(\boldsymbol{x}, \boldsymbol{v}) \,\mathrm{d}\boldsymbol{v} \,.
$$

---

[11] See [63, App. C.2, Thm. 2, p. 628] for Gauss's theorem.

We define the matrices

$$
\begin{aligned}
H_\mathrm{o}(\boldsymbol{n}) &:= \int\limits_{\boldsymbol{n}\cdot\boldsymbol{v}<0} \mathbf{b}_\mathrm{o}(\boldsymbol{v})\left(\mathbf{b}_\mathrm{o}^\mathrm{T}(\boldsymbol{v}) - \rho\mathbf{b}_\mathrm{o}^\mathrm{T}(r\left(\boldsymbol{v}\right)))\right) \mathrm{d}\boldsymbol{v}\,, \\
H_\mathrm{e}(\boldsymbol{n}) &:= \int\limits_{\boldsymbol{n}\cdot\boldsymbol{v}<0} \mathbf{b}_\mathrm{o}(\boldsymbol{v})\left(\mathbf{b}_\mathrm{e}^\mathrm{T}(\boldsymbol{v}) - \rho\mathbf{b}_\mathrm{e}^\mathrm{T}(r\left(\boldsymbol{v}\right)))\right) \mathrm{d}\boldsymbol{v}
\end{aligned}
\tag{5.21}
$$

and rewrite equation (5.20) as

$$
\mathbf{u}_\mathrm{o} = H_\mathrm{o}(\boldsymbol{n})^{-1}\left(\mathbf{u}_\Gamma - H_\mathrm{e}(\boldsymbol{n})\,\mathbf{u}_\mathrm{e}\right). \tag{5.22}
$$

The following Lemma ensures that the last step (5.22) in the reduction is well defined.

> **Lemma 5.20 — Reduction step** (5.22) **is well defined.**
> The matrix $H_\mathrm{o}(\boldsymbol{n})$ in (5.21) is invertible for all $\rho \in (-1, 1)$.

The proof of Lemma 5.20 is based on symmetry properties of the real spherical harmonics and is given in Appendix C.1.3.

> **Remark 5.21 — Boundary conditions are well defined.**
> Lemma 5.20 proves the invertibility of the matrix $H_\mathrm{o}(\boldsymbol{n})$ for $\rho \in (-1, 1)$, which especially includes our case $\rho \in [0, 1)$.

> **Remark 5.22 — Properties of auxiliary matrices.**
> Because of the parity of the real spherical harmonics and the fact that $r\left(-\boldsymbol{v}\right) = -r\left(\boldsymbol{v}\right)$, for all $\boldsymbol{v} \in \mathcal{S}^2$, we get that $H_\mathrm{o}(\boldsymbol{n}) = H_\mathrm{o}(-\boldsymbol{n})$ and $H_\mathrm{e}(\boldsymbol{n}) = -H_\mathrm{e}(-\boldsymbol{n})$.

With equations (5.15), (5.19) and (5.22), we are now able to precisely define the matrices occurring in the final weak formulation[12] of the $\mathrm{P}_N^{\mathrm{2nd}}$ model as announced in Theorem 5.1:

$$
\begin{aligned}
\sum_{i,j=1}^{3} \int_\Omega \partial_{x_i}\boldsymbol{\varphi}^\mathrm{T} \cdot K_{x_i x_j} \cdot \partial_{x_j}\mathbf{u}_\mathrm{e}\,\mathrm{d}\boldsymbol{x} + \int_\Omega \boldsymbol{\varphi}^\mathrm{T} \cdot C_\mathrm{ee} \cdot \mathbf{u}_\mathrm{e}\,\mathrm{d}\boldsymbol{x} + \int_\Gamma \boldsymbol{\varphi}^\mathrm{T} \cdot B_\mathrm{l}(\boldsymbol{n}) \cdot \mathbf{u}_\mathrm{e}\,\mathrm{d}\boldsymbol{s} \\
= \int_\Gamma \boldsymbol{\varphi}^\mathrm{T} \cdot B_\mathrm{r}(\boldsymbol{n}) \cdot \mathbf{u}_\Gamma\,\mathrm{d}\boldsymbol{s} - \int_\Omega \boldsymbol{\varphi}^\mathrm{T} \cdot \boldsymbol{q}_\mathrm{e}\,\mathrm{d}\boldsymbol{x} + \sum_{i=1}^{3} \int_\Omega \left(\partial_{x_i}\boldsymbol{\varphi}\right)^\mathrm{T} \cdot \boldsymbol{f}_i\,\mathrm{d}\boldsymbol{x}
\end{aligned}
\tag{5.23}
$$

with

$$
\begin{aligned}
K_{x_i x_j} &= T_\mathrm{eo}^{x_i} C_\mathrm{oo}^{-1} T_\mathrm{oe}^{x_j} && \text{for } i, j \in \{1, 2, 3\}, \\
B_\mathrm{l}(\boldsymbol{n}) &= \left\langle (\boldsymbol{n}\cdot\boldsymbol{v})\mathbf{b}_\mathrm{e}\mathbf{b}_\mathrm{o}^\mathrm{T}\right\rangle H_\mathrm{o}(\boldsymbol{n})^{-1} H_\mathrm{e}(\boldsymbol{n}), \\
B_\mathrm{r}(\boldsymbol{n}) &= \left\langle (\boldsymbol{n}\cdot\boldsymbol{v})\mathbf{b}_\mathrm{e}\mathbf{b}_\mathrm{o}^\mathrm{T}\right\rangle H_\mathrm{o}(\boldsymbol{n})^{-1}, \\
\boldsymbol{f}_i &= T_\mathrm{eo}^{x_i} C_\mathrm{oo}^{-1} \boldsymbol{q}_\mathrm{o} && \text{for } i \in \{1, 2, 3\}
\end{aligned}
\tag{5.24}
$$

and a suitable vector of test functions $\boldsymbol{\varphi}\colon \Omega \to \mathbb{R}^{n_\mathrm{e}}$.

In the next chapter, we demonstrate that a system with the structure like (5.23) can be handed to standard finite-element tools like FENICS [3, 127].

---

[12] For readability, we use the notation $\boldsymbol{x} = \begin{bmatrix} x & y & z \end{bmatrix}^\mathrm{T} = \begin{bmatrix} x_1 & x_2 & x_3 \end{bmatrix}^\mathrm{T} \in \mathbb{R}^3$.

6 Second-order formulation of the P_N equations: numerical experiments

Any fool can write code that a computer can understand. Good programmers write code that humans can understand.

Yet another opinion on source code and its documentation [14]

In this chapter, we apply our P_N^{2nd} formulation derived in Chapter 5 to several test cases and solve the resulting equations numerically. We do this in a general context first and, finally, couple the P_N^{2nd} formulation with the Cattaneo–LITT model and investigate the effect of higher-order models in this context.

The different test cases demonstrate the broad applicability to different scenarios, including heterogeneous coefficients, anisotropic scattering, anisotropic boundary sources and different spatial dimensions. We reduced the computational complexity by focusing on problems with reduced spatial dimension like described in Section 5.2.2. Nevertheless, the code to compute the P_N^{2nd} system matrices also covers the 3D case. Like in Chapter 4, we make all codes, including files to reproduce the numerical results of this thesis, publicly available online [8].

6.1 Implementation details

Table 4.1 shows a list of the used software. Our Matlab code for the evaluation of the real spherical harmonics is based on [16]. We would like to note here that our implementation of the associated Legendre polynomials (5.6) does not include the *Condon–Shortley phase* ($(-1)^m$ prefactor), in contrary to, e.g., Matlab's legendre function[1]. The (permuted version of the) P_N flux matrices are given explicitly in [198].

In cases for which we do not know the kinetic reference solution of the RTE or the solution of the original P_N equations, we compare our result to the approximate solution of the discrete-ordinates method (DOM), described in Section 6.1.2.

For the DOM as well as for the derivation of the P_N^{2nd} equations, we need to approximate integrals over (subdomains of) the unit sphere $\mathcal{S}^2$ by means of spherical quadrature rules.

For the P_N^{2nd} equations, we use the quadrature rule described in Section 6.1.1 which is exact for polynomials up to degree $\deg\mathcal{K} + 2N$, where $\deg\mathcal{K}$ denotes the degree of the kernel function

---

[1] See https://de.mathworks.com/help/matlab/ref/legendre.html, accessed: Apr, 10th 2020.

written as trigonometric polynomial.

The nodes of the chosen spherical quadrature rule are further used as set of discrete ordinates for the DOM.

We consider the rescaled RTE, where we eliminated all physical units from the equation (see Remark 1.2). For the discretization of the weak formulation of the P$_N^{2\text{nd}}$ systems, we use triangular linear Lagrange finite elements (FEM) with the help of FEniCS, like described in Chapter 4. The resulting linear systems are solved with the default solver of FEniCS, which uses a *sparse LU decomposition (Gaussian elimination)* [115, Sec. 5.2, p. 115].

We interpolate all occurring coefficients linearly in space w.r.t. our finite-element space, i.e., as piecewise linear functions on each triangle of the mesh. In the following, we write n for the number of nodes in the mesh. The integrals occurring in the weak formulation are computed via quadrature rules. The quadrature degree is automatically determined by FEniCS such that the quadrature is exact for the highest-order polynomial in the form being assembled. Furthermore, in the following experiments the evaluation of the $L^\infty(\Omega)$ norm needs to be understood on the discrete level and returns the maximum nodal value due to linear interpolation.

In all experiments, we neglect the external source and set $Q \equiv 0$. Furthermore, we focus on the approximation of the irradiance because this is the only quantity of interest in our LITT context.

6.1.1 Spherical quadrature rule

We approximate integrals over the unit sphere by

$$\int_{\mathcal{S}^2} \psi(\boldsymbol{x}, \boldsymbol{v}) \, \mathrm{d}\boldsymbol{v} \approx \sum_{k=1}^{S} w_k \psi(\boldsymbol{x}, \boldsymbol{v}_k)$$

where $\{w_k\}_{k=1}^S \subset \mathbb{R}_{>0}$ are the weights and $\{\boldsymbol{v}_k\}_{k=1}^S \subset \mathcal{S}^2$ the ordinates of a spherical quadrature rule.

One way to construct a spherical quadrature rule is based on a one-dimensional *trigonometric Gaussian quadrature rule* [42] with weights $\{w_k^{(1)}\}_{k=0}^\delta \subset \mathbb{R}_{>0}$ and nodes $\{\varphi_k\}_{k=0}^\delta \subset (a,b) \subset (0, 2\pi)$, which is exact for every trigonometric polynomial[2] p up to degree δ on in the interval (a,b). Trigonometric polynomials are functions of the following form:

$$p \colon \mathbb{R} \to \mathbb{R}, \ \varphi \mapsto \frac{a_0}{2} + \sum_{k=1}^{\delta} a_k \cos(k\varphi) + b_k \sin(k\varphi)$$

with real coefficients $a_0, a_k, b_k \in \mathbb{R}$, $k \in \{1, \ldots, \delta\}$.

We obtain a quadrature rule for polynomials on the sphere[3] which is exact up to degree δ by combining two trigonometric Gaussian quadrature rules with weights $\{w_k^{(1)}\}_{k=0}^\delta, \{\hat{w}_k^{(1)}\}_{k=0}^{\delta+1} \subset \mathbb{R}_{>0}$

---

[2] The nomenclature of trigonometric polynomials is motivated as follows. We can write p in a complex formulation $p(\varphi) = \sum_{k=-\delta}^{\delta} c_k e^{ik\varphi}$ with $c_0 = \frac{a_0}{2}$, $c_k = \frac{a_k - ib_k}{2}$, $c_{-k} = \frac{a_k + ib_k}{2}$, $k \in \{1, \ldots, \delta\}$, which corresponds to the Laurent polynomial ("complex polynomial with positive and negative powers") restricted to the unit circle.

[3] The real spherical harmonics of degree $\delta = l$: $S_{l=1}^{-1} \sim y, S_{l=2}^{-2} \sim xy, S_{l=2}^2 \sim x^2 - y^2$, etc., are given in Cartesian coordinates. The connection to trigonometric polynomials after parameterization becomes clear with $x = \cos(\varphi)$,

and corresponding nodes[4] $\{\varphi_k\}_{k=0}^{\delta} \subset (0, 2\pi)$, $\{\hat{\varphi}_k\}_{k=0}^{\delta+1} \subset (0, \pi)$ as

$$\int_{\mathcal{S}^2} \psi(\boldsymbol{x}, \boldsymbol{v}) \, \mathrm{d}\boldsymbol{v} = \int_0^{2\pi} \int_0^{\pi} \psi(\boldsymbol{x}, \varphi, \hat{\varphi}) \sin(\hat{\varphi}) \, \mathrm{d}\hat{\varphi} \, \mathrm{d}\varphi \approx \sum_{k=0}^{\delta} \sum_{j=0}^{\delta+1} \psi(\boldsymbol{x}, \varphi_k, \hat{\varphi}_j) \sin(\hat{\varphi}_j) \hat{w}_j^{(1)} w_k^{(1)}.$$

The final quadrature rule on the sphere exact up to degree δ, before relabeling, is given by the $S = \delta^2 + 3\delta + 2$ nodes and weights

$$\left. \begin{aligned} \boldsymbol{v}_{k,j} &= \begin{bmatrix} \cos(\varphi_k) & \sin(\varphi_k) & \cos(\hat{\varphi}_j) \end{bmatrix}^{\mathrm{T}} \in \mathcal{S}^2, \\ w_{k,j} &= \sin(\hat{\varphi}_j) \hat{w}_j^{(1)} w_k^{(1)} \in \mathbb{R}_{>0}, \end{aligned} \right\} \quad k = 0, \ldots \delta, \; j = 0, \ldots, \delta+1,$$

illustrated in Figure 6.1.

We employ the implementation of this quadrature rule in MATLAB provided in [41]. For a detailed investigation in the reduced two-dimensional case, see [192].

(a)   **(b)**
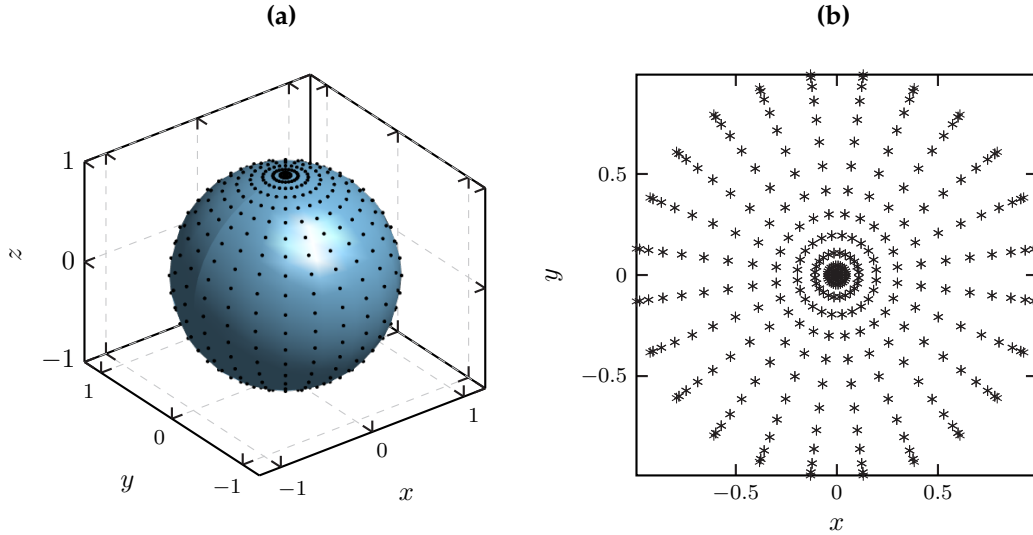
Figure 6.1: Quadrature nodes for the spherical quadrature rule exact up to degree $\delta = 23$, with $S = 600$ nodes. (6.1a): 3D view. (6.1b): Top view in direction $-e_z$ on the x–y-plane.

$y = \sin(\varphi)$, $z = \cos(\hat{\varphi})$ and the following formulae [237, Sec. 0.2.8, Eq. 0.37, p. 57]:

$$\sin(\varphi)\cos(\varphi) = \frac{1}{2}\sin(2\varphi),$$

$$\cos^{2m}(\varphi) = \frac{1}{2^{2m}}\binom{2m}{m} + \frac{1}{2^{2m-1}}\sum_{k=0}^{m-1}\binom{2m}{k}\cos(2(m-k)\varphi),$$

$$\cos^{2m+1}(\varphi) = \frac{1}{4^m}\sum_{k=0}^{m}\binom{2m+1}{k}\cos((2m+1-2k)\varphi).$$

The last two formulae follow by induction and [237, Sec. 0.2.8, Eq. 0.42, p. 60], see [112, p. 576], [226].

[4] If $\psi(\varphi, \hat{\varphi})$ is a polynomial on the sphere with degree δ, then $\psi(\varphi, \hat{\varphi})\sin(\hat{\varphi})$ has degree $\delta + 1$.

6.1.2 Discrete-ordinates method (DOM)

The discrete-ordinates method (DOM) is a brute-force ansatz to approximate the solution of the RTE. For an introduction on the application to radiative heat transfer, we refer to [145, Ch. 16, p. 498 ff.].

We discretize the unit sphere by a finite set of discrete ordinates $\{v_k\}_{k=1}^S \subset \mathcal{S}^2$, which are defined by a spherical quadrature rule. Here, the number of quadrature nodes S coincides with the number of discrete ordinates. For each discrete ordinate v_k, we approximate the radiance $\psi(\cdot, v_k) \colon \Omega \to \mathbb{R}$ by piecewise constant functions w.r.t. the given mesh, which yields

$$\psi(\boldsymbol{x}, \boldsymbol{v}) \approx \sum_{k=1}^S 1_{\boldsymbol{v}_k}(\boldsymbol{v})\psi^k(\boldsymbol{x}) \approx \sum_{k=1}^S 1_{\boldsymbol{v}_k}(\boldsymbol{v}) \sum_{i=1}^{n_{\text{e}}} 1_{\mathcal{T}_i}(\boldsymbol{x})\psi_i^k \tag{6.1}$$

where $\mathcal{T}_i$ denotes an element (e.g. triangle in 2D) of the mesh, n_{e} the number of elements, $1_{\mathcal{T}_i} \colon \Omega \to \{0, 1\}$ the indicator function of the ith element, and $1_{\boldsymbol{v}_k} \colon \mathcal{S}^2 \to \{0, 1\}$ the indicator function for kth ordinate, i.e., the set $\{\boldsymbol{v} \in \mathcal{S}^2 \mid \boldsymbol{v} = \boldsymbol{v}_k\}$.

We use the approximation (6.1) in equation (5.1) (for external source $Q \equiv 0$) and take the average over each element $\mathcal{T}_i \colon \Omega \to \{0, 1\}$, which gives us

$$\frac{1}{|\mathcal{T}_i|} \int_{\mathcal{T}_i} \boldsymbol{v}_k \cdot \nabla \psi_i^k \, \mathrm{d}\boldsymbol{x} = -\frac{1}{|\mathcal{T}_i|} \int_{\mathcal{T}_i} \sigma_{\text{t}} \psi_i^k \, \mathrm{d}\boldsymbol{x} + \frac{1}{|\mathcal{T}_i|} \int_{\mathcal{T}_i} \sigma_{\text{s}} \int_{\mathcal{S}^2} \mathcal{K}(\boldsymbol{v}_k, \boldsymbol{v}) \, \psi_i(\boldsymbol{v}) \, \mathrm{d}\boldsymbol{v}$$

$$\approx -\sigma_{\text{t}}^i \psi_i^k + \sigma_{\text{s}}^i \sum_{j=1}^S w_j \mathcal{K}(\boldsymbol{v}_k, \boldsymbol{v}_j) \, \psi_i^j \, \mathrm{d}\boldsymbol{x} \tag{6.2}$$

for $k \in \{1, \ldots, S\}$, $i \in \{1, \ldots, n_{\text{e}}\}$, where $\{w_j\}_{j=1}^S$ are the weights of the spherical quadrature rule corresponding to the nodes $\{v_j\}_{j=1}^S$.

We reformulate the left-hand side of equation (6.2) by means of Gauss's theorem[5] and an upwind scheme[6], which yields

$$\frac{1}{|\mathcal{T}_i|} \int_{\mathcal{T}_i} \boldsymbol{v}_k \cdot \nabla \psi_i^k \, \mathrm{d}\boldsymbol{x} = \frac{1}{|\mathcal{T}_i|} \int_{\mathcal{T}_i} \operatorname{div}(\boldsymbol{v}_k \psi_i^k) \, \mathrm{d}\boldsymbol{x} = \frac{1}{|\mathcal{T}_i|} \int_{\partial \mathcal{T}_i} \psi_i^k \boldsymbol{v}_k \cdot \boldsymbol{n} \, \mathrm{d}s$$

$$= \frac{1}{|\mathcal{T}_i|} \sum_{e \in \mathcal{E}_i} \int_e \psi_i^k \boldsymbol{v}_k \cdot \boldsymbol{n}_e \, \mathrm{d}s$$

$$\approx \frac{1}{|\mathcal{T}_i|} \sum_{e \in \mathcal{E}_i} |e| \left[\underbrace{\max(\boldsymbol{v}_k \cdot \boldsymbol{n}_e, 0)\psi_i^k}_{\text{outflow}} + \underbrace{\min(\boldsymbol{v}_k \cdot \boldsymbol{n}_e, 0)\psi_{\text{adj}(i,e)}^k}_{\text{inflow}} \right]$$

where $\mathcal{E}_i$ denotes the set of boundary elements of the element $\mathcal{T}_i$. Here, $\boldsymbol{n}_e$ denotes the unit normal vector at boundary element e pointing outward w.r.t. $\mathcal{T}_i$. The expression $\operatorname{adj}(i, e) \in \{1, \ldots, n_{\text{e}}\}$ denotes the index of the element which is adjacent to $\mathcal{T}_i$ and shares the boundary e. At the boundary of the domain, the term $\psi_{\text{adj}(i,e)}^k$ is replaced according to the boundary condition.

We approximate the boundary conditions (5.2) in the same way:

$$\psi_i^k = \rho \psi_i(\boldsymbol{v}_k') + (1 - \rho) \frac{1}{|e|} \int_e \psi_\Gamma(s, \boldsymbol{v}_k) \, \mathrm{d}s$$

with $\boldsymbol{v}_k' = \boldsymbol{v}_k - 2(\boldsymbol{v}_k \cdot \boldsymbol{n}_e)\boldsymbol{n}_e$. In nonrectangular spatial domains, the ordinates $\boldsymbol{v}_k'$ are not necessarily contained in the set of discrete ordinates. We approximate the radiance in the

---

[5] See [63, App. C.2, Thm. 2, p. 628] for Gauss's theorem.
[6] See [86, Sec. 6.3, p. 406 ff.] for details on the upwind scheme.

direction of those ordinates by means of a *distance-based interpolation on the sphere*[7] as described in [24, Sec. 3.2, p. 101 ff.]:

$$\psi_i(\boldsymbol{v}'_k) \approx \sum_{k=1}^{S} \lambda_k \psi_i^k$$

for certain weights $\lambda_k \in \mathbb{R}_{\geq 0}$ with $\sum_{k=1}^{S} \lambda_k = 1$, $k \in \{1, \ldots, S\}$.

Finally, we obtain an approximation of the irradiance (5.3) by

$$\phi_{\mathrm{DOM}}(\boldsymbol{x}) := \sum_{k=1}^{S} w_k \cdot \left[\sum_{i=1}^{n_{\mathrm{e}}} \psi_i^k \cdot 1_{\mathcal{T}_i}(\boldsymbol{x}) \right]. \tag{6.3}$$

We obtain a (huge) linear system for the variables $(\psi_i^k)_{i=1,\ldots,n_{\mathrm{e}}, k=1\ldots,S}$ with $n_{\mathrm{e}} \cdot S$ unknowns, with n_{e} the number of elements of the spatial mesh and S the number of discrete ordinates. The resulting linear system has a sparse structure. In our one-dimensional test cases, we solve the resulting linear systems with MATLAB's function MLDIVIDE, which uses a variant of the Gaussian elimination. In our two-dimensional test case, we use MATLAB's implementation of the iterative solver BICGSTAB.

The advantage of the DOM is its straight-forward derivation and implementation. The disadvantage is the size of the resulting linear system. The computational effort forbids its application in our real-time context of LITT. Here, we use it to generate only reference solutions for our test cases.

For a recent survey of the discrete ordinates method and relevant references, we refer to [117].

---

[7] Consider a triangulation of the unit sphere with geodesic triangular elements and let $\boldsymbol{v} \in \mathcal{S}^2$ be inside such an element with nodes $\{\boldsymbol{v}_{i_1}, \boldsymbol{v}_{i_2}, \boldsymbol{v}_{i_3}\} \subset \{\boldsymbol{v}_k\}_{k=1}^{S}$. The weights are computed via the geodesic distances h_k between the query ordinate $\boldsymbol{v}$ and the corresponding reference ordinate $\boldsymbol{v}_k$, and are given by

$$w_k = \begin{cases} h_k \, (h_{i_1} + h_{i_2} + h_{i_3})^{-1}, & k \in \{i_1, i_2, i_3\}, \\ 0, & \text{else.} \end{cases}$$

6.2 Proof-of-concept experiments

We published the numerical experiments presented in this section, regarding the approximation of the RTE in a general context, earlier in our manuscript [13].

6.2.1 Test case "Simple 1D"

The first test case is rather simple and we are able to compute analytic reference solutions for the radiative-transfer equation (RTE) and the original P$_N$ equations, which allow us to validate our code for the P$_N^{2\text{nd}}$ model and the discrete-ordinates method (DOM) in this setup.

> ■ **Experiment 6.1 — Test case "Simple 1D".**
>
> We consider the RTE (5.1) with the following details:
>
> | | | |
> |---|---|---|
> | Ω | $= [0,1]$ | (spatial domain) |
> | $\sigma_{\text{a}}(z)$ | $= 1$ | (absorption coefficient) |
> | $\sigma_{\text{s}}(z)$ | $= 0$ | (scattering coefficient) |
> | $\mathcal{K}(\boldsymbol{v}, \boldsymbol{v}')$ | $= \frac{1}{4\pi}$ | (scattering kernel) |
> | $\psi_{\Gamma}(z = 0, \mu \geq 0)$ | $= \frac{1}{4\pi}$ | (radiance at the left boundary) |
> | $\psi_{\Gamma}(z = 1, \mu < 0)$ | $= 0$ | (radiance at the right boundary) |
> | $\rho(z = 0)$ | $= 0$ | (reflectivity at the left boundary) |
> | $\rho(z = 1)$ | $= 0$ | (reflectivity at the right boundary) |
> | $Q(z)$ | $= 0$ | (external source) |
>
> We compute:
>
> 1. the analytical solution of the RTE (6.4), where we approximate the first integral in (6.5) by the spherical quadrature in Section 6.1.1 which is exact up to degree $\delta = 50$ (with $S = 2652$ nodes),
>
> 2. the analytical solution of the original P$_N$ equations (6.9) for moment orders $N \in \{1, 3, \ldots, 21\}$,
>
> 3. the FEM solutions of the P$_N^{2\text{nd}}$ equations for all combinations of numbers of equidistant grid points $n \in \{11, 21, 41, 81, 161, 321, 641\}$ and moment orders $N \in \{1, 3, \ldots, 21\}$,
>
> 4. the DOM solution, on a spatial grid with $n = 641$ equidistant nodes. We consider the spherical quadrature rule in Section 6.1.1 which is exact up to degree $\delta = 50$. The resulting $S = 2652$ nodes define the set of discrete ordinates. The solution does not depend on the φ component of the ordinates, which allows us to reduce the number of discrete ordinates in the implementation to 52. We compute the irradiance of the DOM solution according to equation (6.3).
>
> The irradiances for the P$_N$ and P$_N^{2\text{nd}}$ solutions are given as a multiple of the corresponding first moments according to (5.8).

Analytical solution of the RTE

It is easy to check that the analytical solution of the RTE (5.1) for this test case is given by

$$\psi(\boldsymbol{x}, \boldsymbol{v}) = \psi(z, \mu) = \begin{cases} \frac{1}{4\pi} e^{-\frac{\sigma_a}{\mu} z}, & \mu > 0, \\ 0, & \mu \leq 0, \end{cases} \tag{6.4}$$

with irradiance

$$\phi_{\text{ref}}(z) = \int_{\mathcal{S}^2} \psi(\boldsymbol{x}, \boldsymbol{v}) \, \mathrm{d}\boldsymbol{v} = 2\pi \int_{-1}^{1} \psi(z, \mu) \, \mathrm{d}\mu. \tag{6.5}$$

Analytical solution of the original P_N equations

In this simple case, we can reformulate the corresponding original P_N equations as an initial-value problem, which can be solved analytically. The analytical solution serves as reference for the finite-element approximation of the P_N^{2nd} solution and allows us to investigate the convergence for the grid size $\frac{1}{n-1}$ tending to zero.

We consider the original P_N equations (5.12) after reducing the spatial dimension to 1D for this test case

$$T_z \mathbf{u}_z = C\mathbf{u}$$

with boundary conditions (5.20)

$$\begin{aligned} B\mathbf{u}_{\text{L}} &= \mathbf{u}_{\Gamma \text{L}}, \\ B\mathbf{u}_{\text{R}} &= \mathbf{u}_{\Gamma \text{R}} \end{aligned} \tag{6.6}$$

where the subscripts L, R denote the quantities at the left ($z = 0$) and right ($z = 1$) boundary, respectively. We diagonalize the symmetric, positive definite moment matrix T_z via $T_z = VDV^{-1}$, where D is a diagonal matrix, and obtain by multiplication of (6.6) from left with V^{-1}

$$\boldsymbol{w}_z = H\boldsymbol{w} \tag{6.7}$$

with $\boldsymbol{w} := V^{-1}\mathbf{u}$ and $H := D^{-1}V^{-1}CV$. For isotropic scattering and homogeneous coefficients, the matrix C and, thus, the matrix H do not depend on z, so we obtain a solution $\boldsymbol{w}(z) = \exp(Hz)\boldsymbol{w}_{\text{L}}$ by means of the matrix exponential. With $\boldsymbol{w}_{\text{R}} = \boldsymbol{w}(z = 1) = \exp(H)\boldsymbol{w}_{\text{L}}$, we reformulate the boundary conditions (6.6) as

$$\begin{bmatrix} BV \\ BV\exp(H) \end{bmatrix} \boldsymbol{w}_{\text{L}} = \begin{bmatrix} \mathbf{u}_{\Gamma \text{L}} \\ \mathbf{u}_{\Gamma \text{R}} \end{bmatrix}. \tag{6.8}$$

Note that for a one-dimensional spatial domain and for odd moment order N, we have $B \in \mathbb{R}^{n_o \times 2n_o}$ and, by the choice of boundary moments, $\mathbf{u}_{\Gamma \text{L}} \in \mathbb{R}^{n_o}$ (with $n_o = \frac{N+1}{2}$). We solve the linear system (6.8) for $\boldsymbol{w}_{\text{L}}$ using an LU decomposition and obtain the solution of the P_N equations

$$\mathbf{u}(z) = V\exp(Hz)\boldsymbol{w}_{\text{L}}. \tag{6.9}$$

Results

We visualize the results in Figure 6.2. The analytical solution of the RTE (6.4) yields a reference solution for the irradiance. The analytical solutions of the original P_N equations yield reference solutions for the P_N^{2nd} formulation. We note that the irradiance of the DOM solution in Figure 6.2a is in fact piecewise constant, which can not be observed due to the fine resolution of the spatial grid.
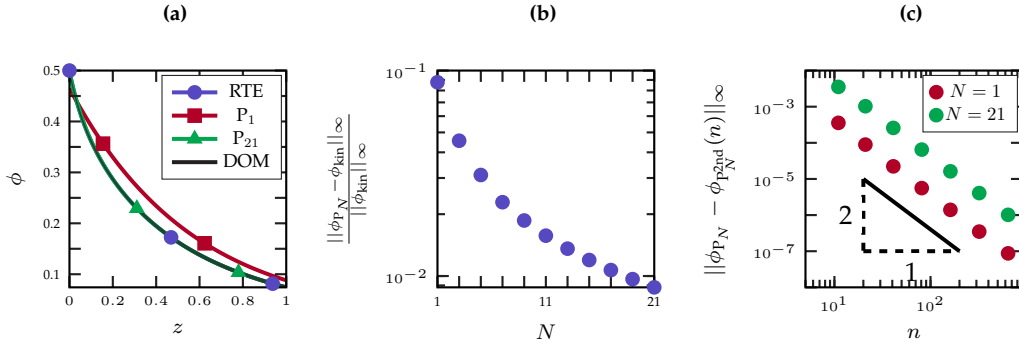
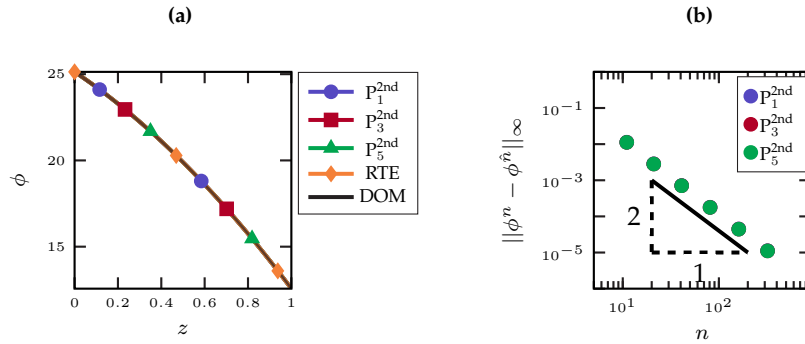Figure 6.2: Results of Experiment 6.1. (6.2a): Irradiances ϕ of the DOM solution, of the analytical solutions of the original P_1 and P_{21} equations and of the analytical solution of the RTE. The latter one defines the reference solution. The solutions are given on a grid with $n = 641$ equidistant nodes. (6.2b): Relative maximum difference between the irradiances of the analytical solutions of the original P_N equations and the RTE, for different moment orders N, on a grid with $n = 641$ equidistant nodes. (6.2c): Maximum differences between the irradiances of the analytical solutions of the original P_N equations and the FEM solutions of the P_N^{2nd} equations, for different numbers of equidistant grid points n.

The irradiances of the P_N solutions converge to the reference solution for increasing model order N. From the analytical solution of the RTE we see that we would need infinitely many real spherical harmonics in the basis expansion (5.7) to describe the reference solution, which might be the reason for the slow convergence in the $L^\infty(\Omega)$ norm.

The irradiances of the FEM solutions of the P_N^{2nd} equations converge to the irradiances of the analytical solutions of the original P_N equations for the grid size tending to zero.

In Figure 6.2c, we see that for a given mesh size the absolute error between the original P_N solution and its finite-element approximation via the P_N^{2nd} formulation for $N = 21$ is larger than for $N = 1$. This implies that the choice of higher moment orders N does not necessarily decrease the overall approximation error

$$\left\|\phi_{\text{true}} - \phi_{P_N^{2nd}}\right\|_\infty \leq \left\|\phi_{\text{true}} - \phi_{P_N}\right\|_\infty + \left\|\phi_{P_N} - \phi_{P_N^{2nd}}\right\|_\infty$$

if we use the same spatial discretization or if we can not bound the finite-element discretization error, e.g., using adaptive grid refinement and a-posteriori error estimates[8].

This test case validates the solution of the P_N equations as approximation of the desired RTE solution, in terms of the irradiance. Furthermore, the irradiances of the original P_N equations and the P_N^{2nd} formulation coincide up to numerical errors, which validates our second-order formulation as equivalent reformulation of the original P_N equations, in cases where the derivation is justified. Last, it validates our implementation of the DOM.

We emphasize the great advantage of our P_N^{2nd} formulation that it can be solved with standard finite-element tools. This allows us to exploit the established expertise in the field of numerical solutions of PDEs at no extra costs on our side of the implementation.

---

[8] See [86, Sec. 4.7, p. 287] for error estimators and adaptive FEM.

6.2.2 Test case "Heterogeneous coefficients 1D"

The second test case demonstrates that the P_N^{2nd} model allows for heterogeneous coefficients, nonvanishing reflectivity at the boundary and anisotropic boundary sources.

> ■ **Experiment 6.2 — Test case "Heterogeneous coefficients 1D".**
> We consider the RTE (5.1) with the following details:
>
> | | | |
> |---|---|---|
> | Ω | $= [0, 1]$ | (spatial domain) |
> | $\sigma_{\text{a}}(z)$ | $= \frac{2+\sin(2\pi z)}{10}$ | (absorption coefficient) |
> | $\sigma_{\text{s}}(z)$ | $= \frac{3-z^2}{10}$ | (scattering coefficient) |
> | $\mathcal{K}(\boldsymbol{v}, \boldsymbol{v}')$ | $= \frac{1}{4\pi}$ | (scattering kernel) |
> | $\psi_\Gamma(z = 0, \mu \geq 0)$ | $= \mu^2$ | (radiance at the left boundary) |
> | $\psi_\Gamma(z = 1, \mu < 0)$ | $= 0$ | (radiance at the right boundary) |
> | $\rho(z = 0)$ | $= \frac{1}{2}$ | (reflectivity at the left boundary) |
> | $\rho(z = 1)$ | $= \frac{1}{2}$ | (reflectivity at the right boundary) |
> | $Q(z)$ | $= 0$ | (external source) |
>
> We compute
>
> 1. the FEM solutions of the P_N^{2nd} equations analog to Experiment 6.1,
>
> 2. the DOM solution analog to Experiment 6.1,
>
> 3. an approximate solution for the original P_N equations for all combinations of moment orders $N \in \{1, 3\}$ and numbers of equidistant grid points $n \in \{11, 21, 41, 81, 161, 321, 641\}$. Note that we can not solve the ODE (6.7) analytically like in Experiment 6.1 because of the heterogeneous coefficients. We solve the ODE numerically with Matlab's ode45 solver (explicit *Runge-Kutta (4,5) solver*) with relative tolerance relTol=1e-10 and absolute tolerance absTol=1e-10.

Results

We visualize the results in Figure 6.3. The DOM solution yields a reference solution for the irradiance. It is piecewise constant, which can not be observed in Figure 6.3 due to the fine resolution of the spatial grid. The numerical solutions of the original P_N equations yield reference solutions for the P_N^{2nd} formulation.

The FEM solutions of the P_N^{2nd} equations converge to the corresponding reference solutions of the original P_N equations for the grid size tending to zero. Furthermore, the P_N^{2nd} solutions converge to the DOM solution for increasing moment order. We observe the largest gain in the accuracy in the lower moment orders $N \leq 7$.

This test case validates the P_N^{2nd} formulation and implementation for heterogeneous coefficients, nonvanishing reflectivity at the boundary and anisotropic boundary sources.

(a)   (b)   (c)
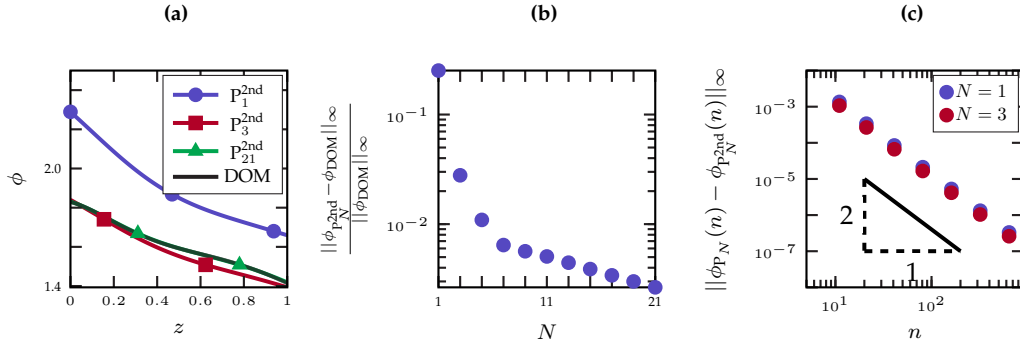
Figure 6.3: Results of Experiment 6.2. (6.3a): Irradiances ϕ of the DOM solution and of the finite-element solutions of the P$_1^{2nd}$, P$_3^{2nd}$ and P$_{21}^{2nd}$ models. The solutions are given on a grid with $n = 641$ equidistant nodes. (6.3b): Relative maximum difference between the irradiances of the finite-element solution of the P$_N^{2nd}$ equations and the DOM, for different moment orders N, on a grid with $n = 641$ equidistant nodes. (6.3c): Maximum differences between the irradiances of the numerical solutions of the original P$_N$ equations and the finite-element solutions of the P$_N^{2nd}$ equations, for different numbers of equidistant grid points n.

6.2.3 Test case "Anisotropic scattering 1D"

The third test case demonstrates that our method is not limited to isotropic scattering.

■ **Experiment 6.3 — Test case "Anisotropic scattering 1D".**

We consider the RTE (5.1) with the following details:

Ω	$= [0, 1]$	(spatial domain)
$\sigma_a(z)$	$= 0$	(absorption coefficient)
$\sigma_s(z)$	$= 1 + z$	(scattering coefficient)
$\mathcal{K}(\boldsymbol{v}, \boldsymbol{v}')$	$= \frac{1}{8\pi}\big[(\mu - 1)(\mu' - 1)$	
	$\quad + (\mu + 1)(\mu' + 1)\big]$	(scattering kernel)
$\psi_\Gamma(z = 0, \mu \geq 0)$	$= \mu + 2$	(radiance at the left boundary)
$\psi_\Gamma(z = 1, \mu < 0)$	$= \mu + 1$	(radiance at the right boundary)
$\rho(z = 0)$	$= 0$	(reflectivity at the left boundary)
$\rho(z = 1)$	$= 0$	(reflectivity at the right boundary)
$Q(z)$	$= 0$	(external source)

We compute

1. the analytical solution of the RTE (6.10) and the corresponding irradiance (6.11),

2. the FEM solutions of the P$_N^{2nd}$ equations for all combinations of numbers of equidistant grid points $n \in \{11, 21, 41, 81, 161, 321, 641\}$ and moment orders $N \in \{1, 3, 5\}$, and the corresponding irradiances according to equation (5.8),

3. the DOM solution, on a spatial grid with $n = 641$ equidistant nodes. We consider

the spherical quadrature rule in Section 6.1.1 which is exact up to degree $\delta = 25$. The resulting $S = 702$ nodes define the set of discrete ordinates.[a] We compute the irradiance of the DOM solution according to equation (6.3).

---

[a] Other than in Experiment 6.1, we can not reduce the number of ordinates here because of the anisotropic scattering kernel.

Analytical reference solution

There is an analytical reference solution of the RTE (5.1) for this test case:

$$\psi(\boldsymbol{x}, \boldsymbol{v}) = \mu - \frac{z(z+2)}{3} + 2, \tag{6.10}$$

with irradiance

$$\phi_{\text{ref}}(z) = \int_{\mathcal{S}^2} \psi(\boldsymbol{x}, \boldsymbol{v})\, \mathrm{d}\boldsymbol{v} = 2\pi \int_{-1}^{1} \psi(z, \mu)\, \mathrm{d}\mu = 2\pi\left(4 - \frac{2}{3}z(z+2)\right). \tag{6.11}$$

We see that the analytical solution (6.10) is a first-order polynomial in $\boldsymbol{v}$. Thus, we expect that the solution of the P_1 equations yields the exact solution of the RTE.

Results

We visualize the results in Figure 6.4. As expected, we recover the analytical solution for $N = 1$, and the solutions of the higher-order models yield the same result.

This test case validates the P_N^{2nd} formulation and implementation for anisotropic scattering.

(a)   **(b)**

Figure 6.4: Results of Experiment 6.3. (6.4a): Irradiances ϕ of the DOM solution, of the analytical solution of the RTE and of the FEM solutions of the P_1^{2nd}, P_3^{2nd} and P_5^{2nd} equations. (6.4b): Maximum difference between the irradiances ϕ for successive grid-refinement levels. Here, ϕ^n denotes the FEM solution of the P_N^{2nd} equations on a grid with n nodes, and $\phi^{\hat{n}}$ the solution according to the next finer grid with $\hat{n} = 2(n-1)+1$ nodes. Each difference is evaluated on the corresponding finer grid.

6.2.4 Test case "Nonstandard domain"

This test case demonstrates that our method is not limited to rectangular domains and especially can be used with irregular grids.

■ **Experiment 6.4 — Test case "Nonstandard domain".**

We consider the RTE (5.1) with the following details:

Ω	see Figure 6.5	(spatial domain)
$\sigma_{\text{a}}(\boldsymbol{x})$	$= 0$	(absorption coefficient)
$\sigma_{\text{s}}(\boldsymbol{x})$	$= \frac{1}{10}$	(scattering coefficient)
$\mathcal{K}(\boldsymbol{v}, \boldsymbol{v}')$	$= \frac{1}{4\pi}$	(scattering kernel)
$\psi_\Gamma(\boldsymbol{x} \in \Gamma_I)$	$= 0$	(radiance at the boundary Γ_I)
$\psi_\Gamma(\boldsymbol{x} \in \Gamma_{II})$	$= 0$	(radiance at the boundary Γ_{II})
$\psi_\Gamma(\boldsymbol{x} \in \Gamma_{III})$	$= 0$	(radiance at the boundary Γ_{III})
$\psi_\Gamma(\boldsymbol{x} \in \Gamma_{IV})$	$= 1$	(radiance at the boundary Γ_{IV})
$\rho(\boldsymbol{x} \in \Gamma_I)$	$= 0.5$	(reflectivity at the boundary Γ_I)
$\rho(\boldsymbol{x} \in \Gamma_{II})$	$= 0$	(reflectivity at the boundary Γ_{II})
$\rho(\boldsymbol{x} \in \Gamma_{III})$	$= 0.5$	(reflectivity at the boundary Γ_{III})
$\rho(\boldsymbol{x} \in \Gamma_{IV})$	$= 0$	(reflectivity at the boundary Γ_{IV})
$Q(\boldsymbol{x})$	$= 0$	(external source)

For the spatial discretization, we use a triangular mesh with $n = 2530$ nodes and 4847 elements (triangles). The mesh and the partition of the boundary $\Gamma = \Gamma_I \cup \Gamma_{II} \cup \Gamma_{III} \cup \Gamma_{IV}$ are illustrated in Figure 6.5. We refine the mesh by splitting (see Figure 4.2) and obtain a mesh with 9906 nodes and 19388 elements for numerical reference solutions.

We compute

1. the FEM solutions of the P$_N^{\text{2nd}}$ equations for moment orders $N \in \{1, 3, 5, 7\}$, each on the coarse and the fine spatial mesh, and the corresponding irradiances according to equation (5.8),

2. two DOM solutions on the coarse spatial mesh (with $n = 2530$ nodes), one for a coarse and one for a fine set of discrete ordinates. We consider the spherical quadrature rules in Section 6.1.1 which are exact up to degree $\delta = 19$ and $\delta = 27$. Symmetry allows us in the implementation to restrict the ordinates to the upper half sphere ($\mu \geq 0$).[a] The resulting $S = 420$ and $S = 812$ nodes define the two sets of discrete ordinates, and the corresponding DOM solutions are denoted by $\phi_{\text{DOM, c}}$ and $\phi_{\text{DOM,f}}$. We solve the resulting linear systems with Matlab's iterative solver bicgstab, with relative residual tolerance tol $=$ 1e-5 and a maximum number of iterations maxit=1000. We compute the irradiances of the DOM solutions according to equation (6.3).

---

[a] To this, choose the second trigonometric Gaussian quadrature rule with nodes $\{\hat{\varphi}_k\}_{k=0}^{\delta+1}, \subset (0, \frac{\pi}{2})$. Note that the number of nodes is the same as for the full sphere.
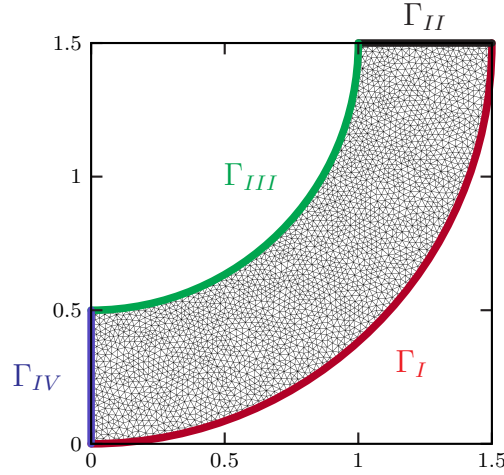
Figure 6.5: Mesh (2530 nodes and 4847 elements) and boundaries for Experiment 6.4.

Results

We visualize the results in Figure 6.6. The BICGSTAB method used to solve the linear system of the DOM stopped after the maximum number of iterations with relative residuals 0.0016 for $\delta = 19$ and 0.0022 for $\delta = 27$.

The relative error between the irradiances of the coarse and the fine DOM solution is about

$$\frac{\|\phi_{\text{DOM, c}} - \phi_{\text{DOM, f}}\|_{L^\infty(\Omega)}}{\|\phi_{\text{DOM, f}}\|_{L^\infty(\Omega)}} \approx 2.984 \times 10^{-2},$$

$$\frac{\|\phi_{\text{DOM, c}} - \phi_{\text{DOM, f}}\|_{L^1(\Omega)}}{\|\phi_{\text{DOM, f}}\|_{L^1(\Omega)}} \approx 1.965 \times 10^{-2}$$

w.r.t. the $L^\infty(\Omega)$ norm and $L^1(\Omega)$ norm, respectively. This difference between the irradiances is illustrated in Figure 6.6f.

In Table 6.1, we show the relative $L^\infty(\Omega)$ and $L^1(\Omega)$ between the irradiances of the P_N^{2nd} and fine DOM solutions (both on the coarse spatial mesh).[9] The $L^\infty(\Omega)$ does not indicate any form of convergence, which does not reflect our observation from Figure 6.6, whereas the relative $L^1(\Omega)$ is (slowly) decreasing for increasing moment order. We point out that the relative errors in the $L^1(\Omega)$ norm are in the same range as the relative error of the coarse and fine DOM solution. This shows that the usability of the DOM solution as reference solution is limited in this case.

The resulting linear system for the fine discretization of the DOM in this experiment has with $n_e = 4847$ elements and $S = 812$ overall $n \times S = 3935764$ degrees of freedom. The corresponding matrix has a sparse structure with more than 3.201×10^9 nonzero entries, which consumes more than 25.5 Gigabyte of memory (in DOUBLE precision, i.e., 8 bytes per entry), not including any overhead to store the sparse structure. For this reason, we do not attempt to further increase the number of ordinates.

Nevertheless, we see that for increasing moment order N the FEM solution of the P_N^{2nd} equations tends towards the DOM solution, on a visual scale.

---

[9] Integral over each triangle approximated by a quadrature rule exact for polynomials up to degree one. Note that, in general, the integrated function is nonlinear after taking the absolute value.

N	$\dfrac{\|\phi_{P_N^{2nd}} - \phi_{P_N^{2nd,f}}\|_{L^\infty(\Omega)}}{\|\phi_{P_N^{2nd,f}}\|_{L^\infty(\Omega)}}$	$\dfrac{\|\phi_{P_N^{2nd}} - \phi_{P_N^{2nd,f}}\|_{L^1(\Omega)}}{\|\phi_{P_N^{2nd,f}}\|_{L^1(\Omega)}}$	$\dfrac{\|\phi_{P_N^{2nd}} - \phi_{DOM,f}\|_{L^\infty(\Omega)}}{\|\phi_{DOM,f}\|_{L^\infty(\Omega)}}$	$\dfrac{\|\phi_{P_N^{2nd}} - \phi_{DOM,f}\|_{L^1(\Omega)}}{\|\phi_{DOM,f}\|_{L^1(\Omega)}}$
1	9.258×10^{-5}	1.424×10^{-5}	4.382×10^{-1}	3.124×10^{-1}
3	2.567×10^{-3}	3.822×10^{-4}	5.108×10^{-1}	1.293×10^{-1}
5	3.693×10^{-3}	1.081×10^{-3}	6.167×10^{-1}	8.381×10^{-2}
7	6.739×10^{-3}	4.014×10^{-3}	6.406×10^{-1}	7.001×10^{-2}

Table 6.1: Results of Experiment 6.4. (Col. 1): Moment order. (Col. 2 - 3): Relative $L^\infty(\Omega)$ and $L^1(\Omega)$ difference between the irradiances of the P$_N^{2nd}$ solutions on the coarse and refined (f) spatial mesh. (Col. 4 - 5): Relative $L^\infty(\Omega)$ and $L^1(\Omega)$ difference between the irradiances of the P$_N^{2nd}$ solution and the fine DOM solution (both on the coarse spatial mesh).

In Table 6.1, we further show the relative $L^\infty(\Omega)$ and $L^1(\Omega)$ difference between the irradiances of the P$_N^{2nd}$ solutions on the coarse and refined mesh. To this, we evaluate the coarse solution on the fine mesh and evaluate the $L^\infty(\Omega)$ norm and $L^1(\Omega)$ norm on the fine mesh.[10] We see that the irradiances of the P$_N^{2nd}$ solutions differ less than one percent in the $L^\infty(\Omega)$ norm.

This test case validates the P$_N^{2nd}$ formulation and implementation for irregular, two-dimensional spatial grids. At the same time, it demonstrates the increasing complexity for test cases with more than one spatial dimension and emphasizes the need for alternative models to compute the irradiance.

6.3 P$_N^{2nd}$ coupled with LITT

Finally, we would like to combine the two parts of this thesis and investigate the P$_N^{2nd}$ formulation in the context of LITT. We compute different P$_N^{2nd}$ approximations for the irradiance in the LITT model, as a proof of concept in a two-dimensional spatial domain. The reduction of the P$_N^{2nd}$ model to a two-dimensional problem in space is based on the assumption that the data and, thus, the solution do not depend on the z-coordinate (outward pointing direction w.r.t. two-dimensional domain, see Figure 4.1), see Section 5.2.2. Hence, different than in Chapter 4, we do not assume rotational symmetry of the LITT model but independence of the z-coordinate. This simplifies the coupling with the P$_N^{2nd}$ models from Chapter 5.
For a better comparison with the numerical results in Chapter 4, we choose for the remainder of this section the term $|\Gamma|$ to have the same value as in the rotational symmetric, full 3D case given in equation (4.6).

Before starting with the experiments, we would like to note that the original model like given in [65] uses the Henyey–Greenstein kernel function for scattering and allows the anisotropy factor to take different values for native and coagulated tissue, whereas our LITT model uses a fixed anisotropy factor of $g = 0.96$. We simplified the situation by assuming the anisotropy factor to be constant because we can generate the P$_N^{2nd}$ formulation only for a fixed scattering kernel. We leave the question on how to handle varying anisotropy factors in this context for future work.

---

[10] See footnote 9.

(a) P_1^{2nd}

(b) P_3^{2nd}

(c) P_5^{2nd}

(d) P_7^{2nd}

(e) DOM, $\delta = 27$

(f) difference DOM
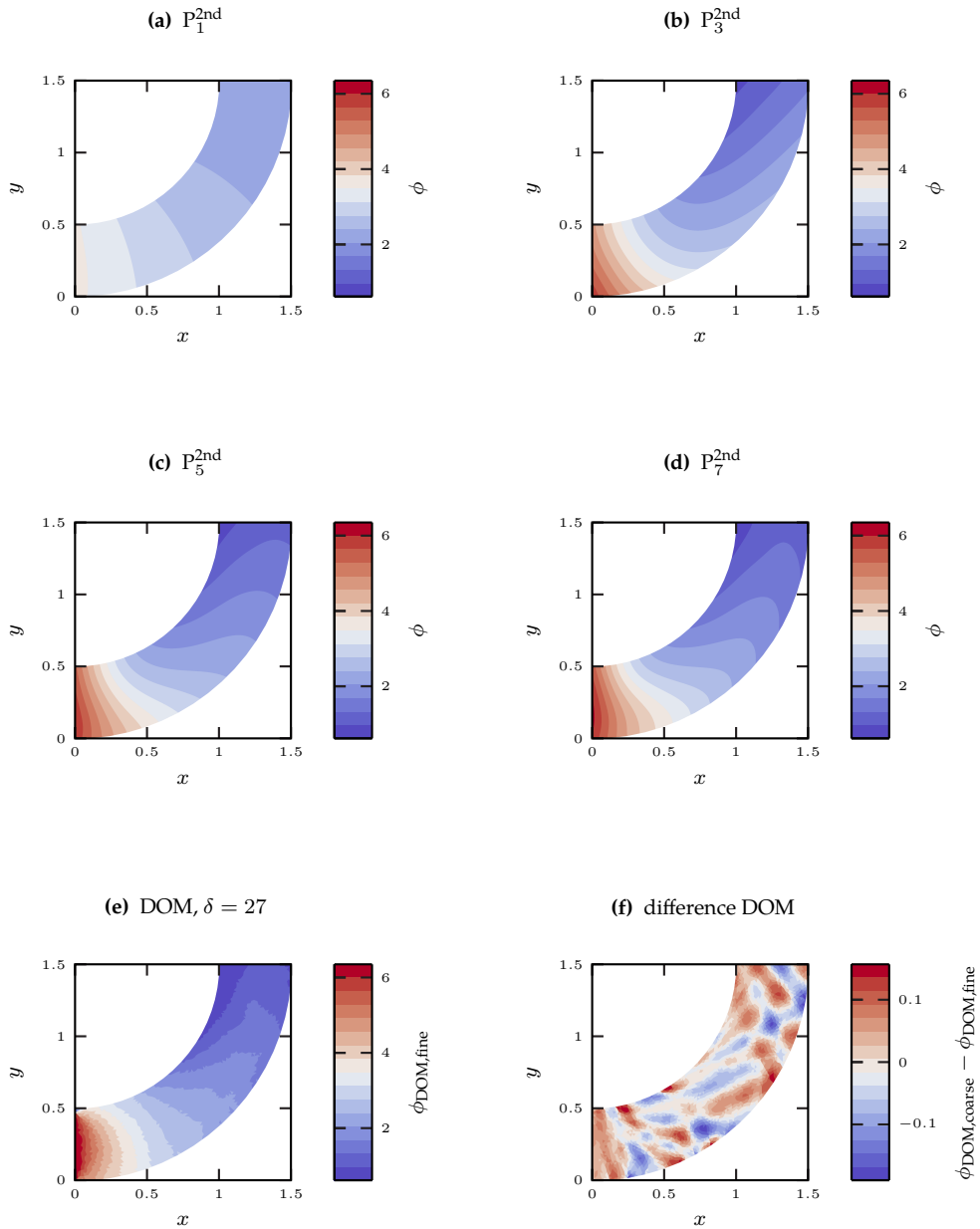
Figure 6.6: Results of Experiment 6.4. (6.6a–6.6d): Irradiances of the FEM solutions of the P_N^{2nd} equations on the coarse mesh, for different moment orders N. (6.6e): Irradiance of the fine DOM solution for the set of ordinates according to the quadrature rule exact up to degree $\delta = 27$. (6.6f): Difference between the irradiances of the two DOM solutions $\phi_{DOM,c}$ and $\phi_{DOM,f}$, for the set of ordinates according to the quadrature rules exact up to degree $\delta = 19$ and $\delta = 27$, respectively.

6.3.1 The established P$_1$ model vs. the P$_1^{\text{2nd}}$ formulation

We recall the established P$_1$ approximation in the LITT context (for $t \geq t_{\text{on}}$) described in Subsection 1.2, reduced to two spatial coordinates based on the assumption $\partial_z = 0$:

$$
(\text{P}_1^{\text{ref}}) \quad
\begin{cases}
-\operatorname{div}(D\nabla\phi) + \sigma_{\text{a}}\phi = 0 & \text{on } I \times \Omega, \\[4pt]
D\nabla\phi \cdot \boldsymbol{n} = \dfrac{1}{|\Gamma_{\text{rad}}|}(1-\beta_q)\hat{q}_{\text{rad}} & \text{on } I \times \Gamma_{\text{rad}}, \\[4pt]
D\nabla\phi \cdot \boldsymbol{n} = 0 & \text{on } I \times \Gamma_{\text{cool}}, \\[4pt]
\dfrac{1}{2}\phi + D\nabla\phi \cdot \boldsymbol{n} = 0 & \text{on } I \times (\Gamma_{\text{amb}} \cup \Gamma_{\text{sym}})
\end{cases}
\tag{1.2}
$$

with $D = (3(\sigma_{\text{a}} + (1-g)\sigma_{\text{s}}))^{-1}$. We refer to this model throughout this section as P_1^{ref} *reference model*. The reduction to a two-dimensional problem is not based on rotational symmetry along the z-axis, so we do not assume a homogeneous Neumann boundary condition on Γ_{sym} as before in Section 1.2, but treat this boundary like the ambient boundary.

The P$_1^{\text{2nd}}$ model has the strong formulation

$$
(\text{P}_1^{\text{2nd}}) \quad
\begin{cases}
-\operatorname{div}(D\nabla\phi) + \sigma_{\text{a}}\phi = 0 & \text{on } I \times \Omega, \\[4pt]
\dfrac{1-\rho}{2(1+\rho)}\phi + D\nabla\phi \cdot \boldsymbol{n} = 2\pi\dfrac{(1-\rho)}{1+\rho}\dfrac{1}{|\Gamma_{\text{rad}}|}(1-\beta_q)\hat{q}_{\text{rad}} & \text{on } I \times \Gamma_{\text{rad}}, \\[4pt]
\dfrac{1-\rho}{2(1+\rho)}\phi + D\nabla\phi \cdot \boldsymbol{n} = 0 & \text{on } I \times \Gamma_{\text{cool}}, \\[4pt]
\dfrac{1-\rho}{2(1+\rho)}\phi + D\nabla\phi \cdot \boldsymbol{n} = 0 & \text{on } I \times (\Gamma_{\text{amb}} \cup \Gamma_{\text{sym}})
\end{cases}
\tag{6.12}
$$

where ρ models the reflectivity at the corresponding boundary by a single number[11]. Note that the prefactor $\frac{1-\rho}{2(1+\rho)}$ in (6.12) collapses for $\rho = 0$ to $\frac{1}{2}$, like on Γ_{amb} in the reference model (1.2) and as suggested in [65].

The P$_1^{\text{2nd}}$ formulation is given in its weak form in (5.23). With the number of even moments $n_{\text{e}} = 1$ the system of PDEs indeed consists of only one equation on the domain for the only even moment u_0. Note that for better comparison we state the strong formulation (6.12) not in terms of the zeroth moment u_0 as suggested by the P$_1^{\text{2nd}}$ formulation, but directly in terms of the irradiance ϕ. This is achieved by multiplying the original P$_1^{\text{2nd}}$ equation (5.23) in terms of u_0 with the factor $2\sqrt{\pi}$. This allows us to substitute the first moment according to equation (5.8)

$$
\phi = 2\sqrt{\pi}u_0.
\tag{5.8}
$$

We can formally derive the strong formulation by looking at the system matrices for the domain in (5.24)

$$
K_{xx} = K_{yy} = \frac{1}{\sigma_{\text{a}} + (1-g)\sigma_{\text{s}}} = D, \quad K_{xy} = K_{yx} = 0, \quad C_{\text{ee}} = -\sigma_{\text{a}}
$$

---

[11] See Remark 5.5 on the reflectivity at the boundary.

and the boundaries

$$B_l(\boldsymbol{n}_1) = B_l(\boldsymbol{n}_2) = B_l(\boldsymbol{n}_3) = B_l(\boldsymbol{n}_4) = \frac{\rho - 1}{2(1 + \rho)},$$

$$B_r(\boldsymbol{n}_1) = -B_r(\boldsymbol{n}_3) = \begin{bmatrix} 0 & \frac{2}{\sqrt{3}(1+\rho)} \end{bmatrix},$$

$$B_r(\boldsymbol{n}_2) = -B_r(\boldsymbol{n}_4) = \begin{bmatrix} \frac{2}{\sqrt{3}(1+\rho)} & 0 \end{bmatrix},$$

$$\mathbf{u}_\Gamma = \int\limits_{\boldsymbol{n}\cdot\boldsymbol{v}<0} (1-\rho)\mathbf{b}_o\psi_\Gamma(\boldsymbol{x},\boldsymbol{v})\,\mathrm{d}\boldsymbol{v} = \begin{cases} \begin{bmatrix} 0 & \frac{\sqrt{3}\pi}{2}(1-\rho)|\Gamma_{\mathrm{rad}}|^{-1}(1-\beta_q)\hat{q}_{\mathrm{rad}} \end{bmatrix}^{\mathrm{T}}, & \text{on } \Gamma_{\mathrm{rad}}, \\ \begin{bmatrix} 0 & 0 \end{bmatrix}^{\mathrm{T}}, & \text{else}, \end{cases}$$

$$\boldsymbol{q}_e = \mathbf{0},$$

$$\boldsymbol{q}_o = \mathbf{0}$$

with normal vectors $\boldsymbol{n}_1 := (1,0,0)^{\mathrm{T}}$, $\boldsymbol{n}_2 := (0,1,0)^{\mathrm{T}}$, $\boldsymbol{n}_3 := (-1,0,0)^{\mathrm{T}}$ and $\boldsymbol{n}_4 := (0,-1,0)^{\mathrm{T}}$. For validation, we also specify the corresponding auxiliary matrices:

$$H_e(\boldsymbol{n}_1) = -H_e(\boldsymbol{n}_3) = \begin{bmatrix} 0 & \frac{\sqrt{3}}{4}(\rho - 1) \end{bmatrix}^{\mathrm{T}},$$

$$H_e(\boldsymbol{n}_2) = -H_e(\boldsymbol{n}_4) = \begin{bmatrix} \frac{\sqrt{3}}{4}(\rho - 1) & 0 \end{bmatrix}^{\mathrm{T}},$$

$$H_o(\boldsymbol{n}_1) = H_o(\boldsymbol{n}_3) = \begin{bmatrix} \frac{1}{2}(1-\rho) & 0 \\ 0 & \frac{1}{2}(1+\rho) \end{bmatrix},$$

$$H_o(\boldsymbol{n}_2) = H_o(\boldsymbol{n}_4) = \begin{bmatrix} \frac{1}{2}(1+\rho) & 0 \\ 0 & \frac{1}{2}(1-\rho) \end{bmatrix},$$

$$\langle (\boldsymbol{n}_1 \cdot \boldsymbol{v})\mathbf{b}_e\mathbf{b}_o^{\mathrm{T}} \rangle = -\langle (\boldsymbol{n}_3 \cdot \boldsymbol{v})\mathbf{b}_e\mathbf{b}_o^{\mathrm{T}} \rangle = \begin{bmatrix} 0 & \frac{1}{\sqrt{3}} \end{bmatrix},$$

$$\langle (\boldsymbol{n}_2 \cdot \boldsymbol{v})\mathbf{b}_e\mathbf{b}_o^{\mathrm{T}} \rangle = -\langle (\boldsymbol{n}_4 \cdot \boldsymbol{v})\mathbf{b}_e\mathbf{b}_o^{\mathrm{T}} \rangle = \begin{bmatrix} \frac{1}{\sqrt{3}} & 0 \end{bmatrix}.$$

Before we investigate the effect of different P_N^{2nd} models in the context of LITT, we would like to compare the irradiances of the P_1^{ref} reference model and our P_1^{2nd} formulation here. We note that there are structural differences in the boundary conditions of the two models in (1.2) and (6.12). The P_1^{ref} reference model suggests Neumann boundary conditions on the radiating and cooling boundaries Γ_{rad} and Γ_{cool}, whereas the P_1^{2nd} formulation (for zero reflectivity $\rho = 0$) prescribes the classical Robin boundary condition with prefactor $\frac{1}{2}$, like suggested in [65].

On the other hand, the P_1^{2nd} formulation has an additional factor 2π in its right-hand side of the radiation boundary Γ_{rad} (again in case of zero reflectivity $\rho = 0$). Because of this, we do not expect the solutions of (1.2) and (6.12) to coincide.

The Neumann boundary conditions in the context of LITT are motivated as follows [95, p. 1402]:

> *"The idea is that radiation flows in and out of the domain at the same time. The radiation flowing out of the half space goes away to infinity and needs not to be considered anymore for the calculation. However, due to the radial symmetry of the applicator boundary, this is not valid anymore. Radiation leaving through the applicator boundary can enter the computational domain through the opposite boundary. Taking this effect into consideration leads to the following boundary condition for the energy flux [in (1.2)]".*

In fact, the RTE with partially reflecting boundary conditions

$$\boldsymbol{v} \cdot \nabla_{\boldsymbol{x}} \psi + \sigma_\mathrm{a} \psi = \sigma_\mathrm{s} \mathcal{C}\left(\psi\right) + Q, \tag{5.1}$$

$$\psi(\boldsymbol{x}, \boldsymbol{v}) = \rho(\boldsymbol{x}, \boldsymbol{v}) \psi(\boldsymbol{x}, r\left(\boldsymbol{v}\right)) + (1 - \rho(\boldsymbol{x}, \boldsymbol{v})) \psi_\Gamma(\boldsymbol{x}, \boldsymbol{v}), \quad \text{for } \boldsymbol{x} \in \Gamma, \quad \boldsymbol{n}(\boldsymbol{x}) \cdot \boldsymbol{v} < 0, \tag{5.2}$$

where the applicator is excluded from the computational domain, appears not to be the correct model in the context of LITT because radiation that leaves the computational domain at the applicator boundary can not reenter the domain here. So, from a modeling perspective, the P$_1^\mathrm{ref}$ reference model is a valid modification of the standard P$_1$ model in the context of LITT, but it comes with one disadvantage: It is not straight forward how to extend this modification to higher-order P$_N$ models, i.e., for $N > 1$.

Our P$_N^{2nd}$ formulation approximates the RTE, so if we want to use the P$_N^{2nd}$ formulation in the context of LITT, we need to modify our model of the applicator. We outline several suggestions, how this could be accomplished.

First, we could modify the model for the reflectivity at the applicator boundary. Following the motivation above, it would be reasonable to prescribe $\rho = 1$ because this would prevent the radiation from leaving the computational domain, which has the same effect as allowing the radiation to reenter. In fact, a value $\rho = 1$ at the applicator boundary $\Gamma_\mathrm{rad} \cup \Gamma_\mathrm{cool}$ yields Neumann boundary conditions in the P$_1^{2nd}$ model as well. The reason why we do not follow this approach here is that, in the standard understanding of the RTE, the boundary source is separated from the computational domain by the reflecting boundary, i.e., $\rho = 1$ would prevent any radiation to enter the domain. This can also be seen in (6.12), where the right-hand side on the radiation boundary Γ_rad becomes zero for $\rho = 1$. Thus, further modeling of the behavior of the boundary source, especially of the interaction of applicator and tissue, is required to align the P$_1^\mathrm{ref}$ reference model and the P$_1^{2nd}$ model, which we forward to future work.

Second, we could model the boundary radiation $\hat{q}_\mathrm{rad} = \hat{q}_\mathrm{rad}(\phi)$ depending on the irradiance because the irradiance entering at a point on the radiation boundary is the sum of the irradiances produced by the laser fiber and the share of the irradiance, which entered the applicator somewhere and reenters the domain at this specific point again. In cases where we can not assume rotational symmetry this would introduce a nonlocal term in the model. We leave the investigation of such a model for future work.

Third, we could include the applicator as part of the domain and model the radiation also inside the applicator. This way, we would not "lose" any radiation through the boundary. Unfortunately, modeling the radiation in the applicator requires knowledge on the interface conditions at the laser-fiber-cooling and cooling-tissue interfaces. This approach was investigated in [154] for the classical P$_N$ equations.

Before looking into the experiment, we would like to share a technical detail. For the derivation of the P$_N^{2nd}$ formulation, we need to compute spherical integrals. In Remark 6.5 we demonstrate that an accurate approximation of spherical integrals incorporating the Henyey–Greenstein kernel with anisotropy factors close to one (forward scattering) is numerically challenging.

Remark 6.5 — Evaluation of the Henyey–Greenstein scattering kernel.

We derive the P_N^{2nd} formulation by means of the quadrature rule described in Subsection 6.1.1. The exact evaluation of the occurring integrals requires a quadrature rule which is exact for polynomials up to degree $\delta = \deg\mathcal{K} + 2N$, where $\deg\mathcal{K}$ denotes the degree of the kernel function written as trigonometric polynomial. Unfortunately, the trigonometric expansion of the Henyey–Greenstein kernel requires infinitely many terms [105].

The evaluation and integration of the Henyey–Greenstein kernel becomes challenging for anisotropy factors g close to one [62]. We illustrate this in the following example.

We use different values for δ in the spherical quadrature rule[a] to derive the P_1^{2nd} formulation. The matrix K_{xx} in equation (5.24) is of the form

$$K_{xx} = \frac{1}{3(\sigma_a + (1 - \hat{g})\sigma_s)}.$$

Exact integration would yield $\hat{g} = g = 0.96$.

The following table illustrates the (slow) convergence of the value $\hat{g}$ to g in the term K_{xx} for increasing order of the quadrature rule.

δ (exact degree)	S (number of ordinates)	$\hat{g}$
22	552	4.4069
42	1892	1.6669
62	4032	1.169
82	6972	1.0314
102	10712	0.98631
122	15252	0.97018
142	20592	0.96406
162	26732	0.96166
182	33672	0.96069
202	41412	0.96029

[a] This means that polynomials up to degree δ are integrated exactly.

In summary, the RTE with partially reflecting boundary conditions does not model the radiation transport in the context of LITT correctly. Our P_1^{2nd} formulation is the "correct" first-order P_N approximation of the RTE with partially reflecting boundary conditions, whereas the P_1^{ref} reference model is a corrected version to account for the model deficiency of the RTE with partially reflecting boundary conditions in the context of LITT.

6.3.2 Influence of different moment orders and disturbed optical coefficients on the irradiance in LITT

Now we are ready to quantify the influence of different moment orders in the P_N^{2nd} formulation on the irradiance in the LITT context. We compare the results to the P_1^{2nd} model with disturbed optical coefficients and to the P_1^{ref} reference model.

At this point, we would like to emphasize that the coolant absorption factor β_q is estimated based on data from the real LITT application and customized to the P$_1^{ref}$ reference model [95]. We expect this parameter to take a different value when it is fitted to the P$_1^{2nd}$ model, which would be interesting to check in future work. It is necessary to estimate this parameter again for the P$_N^{2nd}$ models before those can be applied to the real application. In order to allow a comparison with the P$_1^{ref}$ reference model and previous experiments, we use the following values for the coolant absorption factor for the P$_N^{2nd}$ model in the following Experiments 6.6 and 6.8:

$$\beta_q^{2nd,1} := 1 - (1 - \beta_q^{(0)}) \frac{\left\| \phi_{P_1^{ref}}(\gamma \equiv 1) \right\|_{L^\infty(\Omega)}}{\left\| \phi_{P_1^{2nd}}(\gamma \equiv 1) \right\|_{L^\infty(\Omega)}} = 0.5579 \ (0.5578),$$

$$\beta_q^{2nd,2} := 1 - (1 - \beta_q^{(0)}) \frac{\left\| \phi_{P_1^{ref}}(\gamma \equiv 0.5) \right\|_{L^\infty(\Omega)}}{\left\| \phi_{P_1^{2nd}}(\gamma \equiv 0.5) \right\|_{L^\infty(\Omega)}} = 0.4166 \ (0.4164)$$

(6.13)

where we have $\beta_q^{(0)} = 0.14$ (see Table 1.1) and

$$\left\| \phi_{P_1^{ref}}(\gamma \equiv 1) \right\|_{L^\infty(\Omega)} = 2.7204 \times 10^5 \ (2.7210 \times 10^5),$$

$$\left\| \phi_{P_1^{2nd}}(\gamma \equiv 1) \right\|_{L^\infty(\Omega)} = 5.2920 \times 10^5 \ (5.2919 \times 10^5),$$

$$\left\| \phi_{P_1^{ref}}(\gamma \equiv 0.5) \right\|_{L^\infty(\Omega)} = 3.9764 \times 10^5 \ (3.9773 \times 10^5),$$

$$\left\| \phi_{P_1^{2nd}}(\gamma \equiv 0.5) \right\|_{L^\infty(\Omega)} = 5.8618 \times 10^5 \ (5.8614 \times 10^5).$$

(6.14)

The values are based on the simulation details in Experiment 6.6, corresponding to the coarse (fine) mesh therein.

Note that the coagulation has a different effect on the P$_1^{ref}$ and P$_1^{2nd}$ solutions due to different boundary conditions. Because of this, the choice of $\beta_q^{2nd,1}$ in Experiment 6.8 aligns the models only at the beginning of the simulation as long as $\gamma \equiv 1$ holds. This different behavior can already be observed from the values in (6.14), where the irradiances differ for the two different examples of the coagulation γ.

■ **Experiment 6.6 — Comparison of the radiation models for LITT: irradiance.**
We compute the irradiances of the P$_1^{ref}$ reference model (1.2) and our P$_N^{2nd}$ formulation (6.12) in the context of LITT.
We use the physical parameters given in Table 1.1 and the following simulation details:

Ω	see Figure 4.5	(spatial domain)
$\gamma_1(\boldsymbol{x})$	$= 1$	(homogeneous coagulation)
$\gamma_2(\boldsymbol{x})$	$= 0.5$	(homogeneous coagulation)
$\beta_q^{(0)}$	$= 0.14$	(original coolant absorption factor)
$\beta_q^{2nd,1}$	see (6.13)	(coolant absorption factor for γ_1)
$\beta_q^{2nd,2}$	see (6.13)	(coolant absorption factor for γ_2)

The absorption and scattering coefficients are defined according to (1.5). We compute the irradiances of the P_1^{ref} reference model and the P_N^{2nd} formulation for fixed homogeneous coagulations $\gamma \in \{\gamma_1, \gamma_2\}$.

For the P_1^{ref} reference model, we use the original coolant absorption factor $\beta_q = \beta_q^{(0)}$. For the P_N^{2nd} formulation, we use the modified coolant absorption factors $\beta_q = \beta_q^{(1)}$ and $\beta_q = \beta_q^{(2)}$ in cases $\gamma = \gamma_1$ and $\gamma = \gamma_2$, respectively. This is done for a better comparison of the different models as motivated above in (6.13).

Furthermore, again for each of the two parameter sets $(\beta_q^{(1)}, \gamma_1)$ and $(\beta_q^{(2)}, \gamma_2)$, we disturb the optical coefficients $\sigma_{\text{a,n}}, \sigma_{\text{a,c}}, \sigma_{\text{s,n}}, \sigma_{\text{s,c}}$ by $\pm 5\%$ and compute the irradiance of the P_1^{2nd} model (6.12) for each of the 81 combinations of disturbed parameters in

$$C = \{(\sigma_{\text{a,n}} \cdot p_1, \sigma_{\text{a,c}} \cdot p_2, \sigma_{\text{s,n}} \cdot p_3, \sigma_{\text{s,c}} \cdot p_4) \,|\, p_i \in \{0.95, 1.0, 1.05\}\}.$$

We evaluate the irradiances along the reference line $\Omega_{\text{1D, ref}}$ (see Figure 4.1).

For $\boldsymbol{x} \in \Omega_{\text{1D, ref}}$ and each combination of disturbed parameters in C, we compute the relative difference between the disturbed P_1^{2nd} solution and the undisturbed P_1^{2nd} solution. We compute the pointwise maxima and minima over all differences

$$\begin{aligned}
\text{upb}(\boldsymbol{x}) &:= \max_{c \in C} \frac{\phi_{P_1^{\text{2nd}}}(\boldsymbol{x}; c) - \phi_{P_1^{\text{2nd}}}(\boldsymbol{x}; c_0)}{m}, \\
\text{lob}(\boldsymbol{x}) &:= \min_{c \in C} \frac{\phi_{P_1^{\text{2nd}}}(\boldsymbol{x}; c) - \phi_{P_1^{\text{2nd}}}(\boldsymbol{x}; c_0)}{m}
\end{aligned} \tag{6.15}$$

with $m = \max\limits_{\boldsymbol{x} \in \Omega_{\text{1D, ref}}} |\phi_{P_1^{\text{2nd}}}(\boldsymbol{x}; c_0)|$ and $c_0 = (\sigma_{\text{a,n}}, \sigma_{\text{a,c}}, \sigma_{\text{s,n}}, \sigma_{\text{s,c}})$ the combination of undisturbed parameters.

We derive the corresponding P_N^{2nd} formulation for the Henyey–Greenstein scattering kernel[a] with anisotropy factor $g = 0.96$ and zero reflectivity $\rho = 0$ at the boundary. The required integrals over the unit sphere are computed by means of a spherical quadrature rule which is exact for polynomials up to degree $\delta = 200 + 2N$, which has, e.g., for $N = 7$, $S = 46440$ nodes on the sphere.

For the spatial discretization, we use the mesh $\Omega_{\text{2D, h}}^{(1)}$ given in Figure 4.5 with 3607 nodes and 7074 elements. We refine the mesh by splitting and obtain the mesh $\Omega_{\text{2D, h, fine}}^{(1)}$ with 14287 nodes and 28296 elements. We compute each solution on the coarse and the fine mesh.

---

[a] See Example 5.4.

Remark 6.7 — Reflectivity.

In the real application, the refractive indices of the applicator and the tissue differ, which implies a reflectivity ρ larger than zero according to Snell's and Fresnel's law, see [48, Sec. 8.4.2, Eq. 8.58, p. 222] and [48, Sec. 8.4.3, Eq. 8.61a, p. 223]. Here, we do not focus on modeling the tissue properties of the applicator and choose $\rho = 0$ for simplicity.

(a)

(b)

(c)

(d)
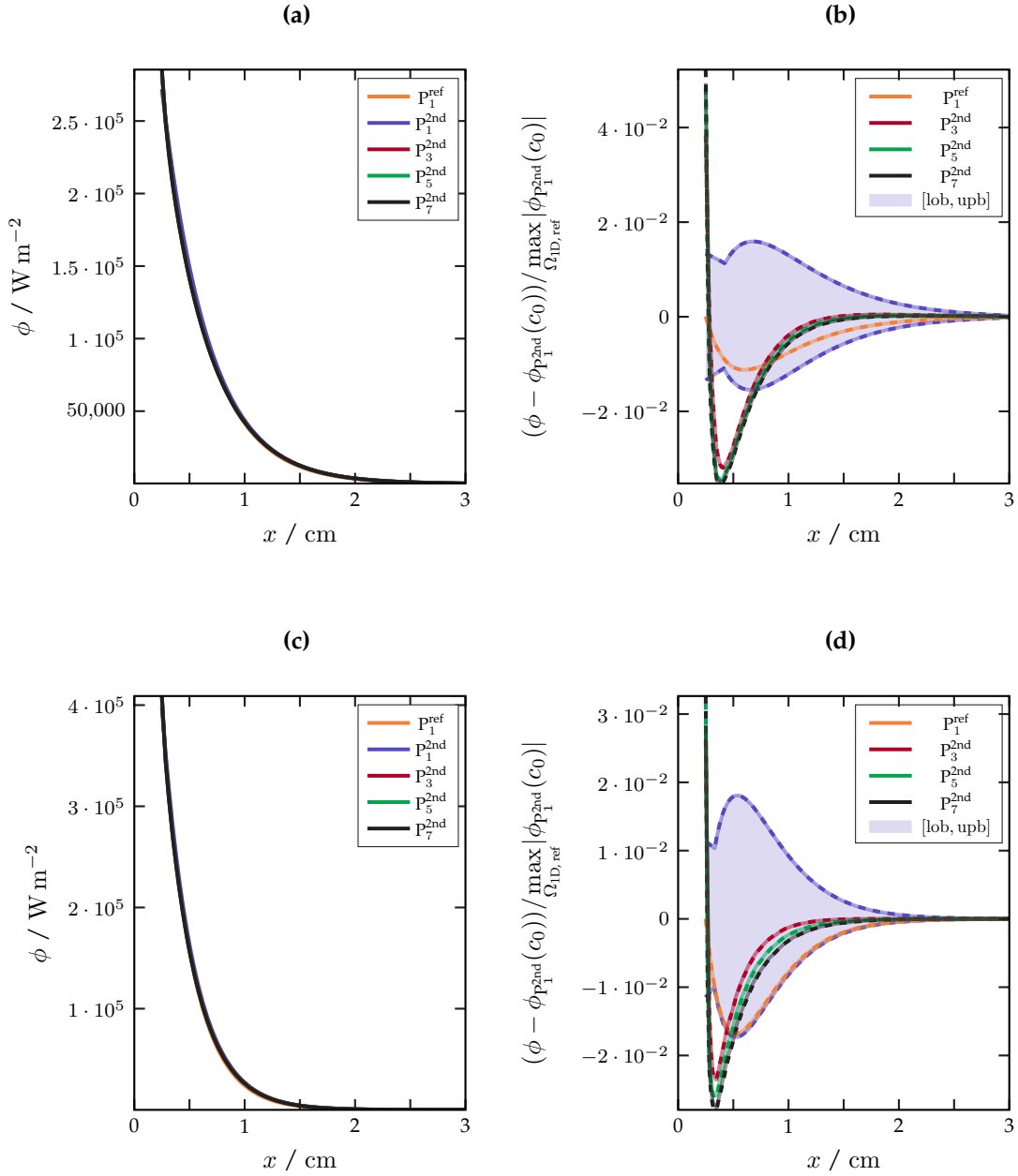
Figure 6.7: Results of Experiment 6.6. (6.7a): Irradiance of P$_1^{ref}$ and P$_N^{2nd}$ solutions on coarse mesh along the reference line $\Omega_{1D,\,ref}$, for $\gamma \equiv 1$. (6.7b): Relative differences between the irradiances of the P$_N^{2nd}$ / P$_1^{ref}$ solutions and P$_1^{2nd}$ solution with undisturbed parameters along the reference line $\Omega_{1D,\,ref}$, for $\gamma \equiv 1$. For each combination of disturbed coefficients, we compute the relative difference between the disturbed P$_1^{2nd}$ solution and the undisturbed (denoted by c_0) P$_1^{2nd}$ solution. The pointwise maxima upb and minima lob over all differences bound the blue-shaded area, see equation (6.15). The solid and dashed lines correspond to the solutions on the coarse and fine mesh, respectively. (6.7c): Like 6.7a for $\gamma \equiv 0.5$. (6.7d): Like 6.7b for $\gamma \equiv 0.5$.

Results

We visualize the results in Figure 6.7. In Figures 6.7a, 6.7c we visualize the irradiances along the reference line $\Omega_{1D,\,ref}$ for the P_1^{ref} reference model and different P_N^{2nd} models, each for the different fixed coagulation values $\gamma \equiv 1$ and $\gamma \equiv 0.5$, respectively. In Figures 6.7b, 6.7d we visualize the relative differences between the irradiances of the different P_N^{2nd} models and the P_1^{2nd} model, and between the irradiance of the P_1^{ref} reference model and the P_1^{2nd} model along the reference line $\Omega_{1D,\,ref}$. The upper and lower bounds for the relative differences between the disturbed P_1^{2nd} solutions and the undisturbed P_1^{2nd} solution in equation (6.15) bound the blue-shaded area in Figures 6.7b and 6.7d, which quantifies the influence of disturbed coefficients on the computed irradiance.

The dashed lines indicate the corresponding solutions computed on the refined mesh and match (on the visual scale) with the solutions on the coarse mesh, which validates that the observed deviations are not caused by spatial discretization errors.

Note that without modifying the coolant absorption factor β_q for the P_N^{2nd} models there would be a significant deviation of the irradiances predicted by the P_N^{2nd} formulation compared to the P_1^{ref} reference model.

We observe that near the radiation boundary Γ_{rad}, i.e., for x close to zero, the differences between the P_N^{2nd} solutions and the undisturbed P_1^{2nd} solution are larger than the maximum difference between the disturbed and undisturbed P_1^{2nd} solutions. If we assume for the moment, that the physical parameters are known up to a relative error of $\pm 5\%$, this experiment suggests that the use of P_N^{2nd} models might add value to the simulation of LITT. Ultimately, this can be quantified only by running the LITT simulation over time and comparing the predicted temperatures and especially the predicted coagulation zones, which is our goal in the next experiment.

6.3.3 Influence of different moment orders and disturbed optical coefficients on the temperature and coagulation in LITT

In this final experiment, we quantify the influence of different moment orders in the P_N^{2nd} formulation on the temperature and coagulation in the LITT context. We compare the results to the P_1^{2nd} model with disturbed optical coefficients and the P_1^{ref} reference model. For a better comparison with previous results and the P_1^{ref} reference model, we again change the absorption cooling factor β_q for the P_N^{2nd} models like in the previous experiment.

■ **Experiment 6.8 — Comparison of the radiation models for LITT: temperature and coagulation.**
We run the LITT simulation (see Section 1.2 and Chapter 4), where we compute the irradiance in each time step by means of the P_N^{2nd} models and the P_1^{ref} reference model. We use the physical parameters given in Table 1.1 and the following simulation details:

$$
\begin{array}{lll}
\tau & = 0\,\mathrm{s} & \text{(parameter in the Cattaneo model)} \\
\Delta t & = 1\,\mathrm{s} & \text{(discrete time step)} \\
T & = 300\,\mathrm{s} & \text{(final time of the simulation)} \\
\vartheta^{(1)}(\boldsymbol{x}) & = 0\,\mathrm{K\,s^{-1}} & \text{(second initial condition for the temperature)} \\
u(\boldsymbol{x}) & = 0.15 & \text{(constant control)}^a \\
\beta_q^{(0)} & = 0.14 & \text{(original coolant absorption factor)} \\
\beta_q^{2\mathrm{nd},1} & \text{see (6.13)} & \text{(coolant absorption factor for P}_N^{2\mathrm{nd}}\text{ models)}
\end{array}
$$

For the P$_1^{\mathrm{ref}}$ reference model, we use the established coolant absorption factor $\beta_q = \beta_q^{(0)}$. For the P$_N^{2\mathrm{nd}}$ models, we use the modified coolant absorption factor $\beta_q = \beta_q^{2\mathrm{nd},1}$, motivated in equation (6.13).

This experiment follows Experiment 6.6, with the only difference that, for a given point in time $t \in [0, T]$, we compute the following upper and lower bounds:

$$
\begin{aligned}
\mathrm{upb}_\vartheta(t, \boldsymbol{x}) &:= \max_{c \in C} \left(\vartheta_{\mathrm{P_1^{2nd}}}(t, \boldsymbol{x}; c) \right), \\
\mathrm{lob}_\vartheta(t, \boldsymbol{x}) &:= \min_{c \in C} \left(\vartheta_{\mathrm{P_1^{2nd}}}(t, \boldsymbol{x}; c) \right), \\
\mathrm{upb}_{\mathrm{d}\vartheta}(t, \boldsymbol{x}) &:= \max_{c \in C} \frac{\vartheta_{\mathrm{P_1^{2nd}}}(t, \boldsymbol{x}; c) - \vartheta_{\mathrm{P_1^{2nd}}}(t, \boldsymbol{x}; c_0)}{m_\vartheta}, \\
\mathrm{lob}_{\mathrm{d}\vartheta}(t, \boldsymbol{x}) &:= \min_{c \in C} \frac{\vartheta_{\mathrm{P_1^{2nd}}}(t, \boldsymbol{x}; c) - \vartheta_{\mathrm{P_1^{2nd}}}(t, \boldsymbol{x}; c_0)}{m_\vartheta}, \\
\mathrm{upb}_\gamma(t, \boldsymbol{x}) &:= \max_{c \in C} \left(\gamma_{\mathrm{P_1^{2nd}}}(t, \boldsymbol{x}; c) \right), \\
\mathrm{lob}_\gamma(t, \boldsymbol{x}) &:= \min_{c \in C} \left(\gamma_{\mathrm{P_1^{2nd}}}(t, \boldsymbol{x}; c) \right)
\end{aligned}
\tag{6.16}
$$

with $m_\vartheta = \max\limits_{\boldsymbol{x} \in \Omega_{\mathrm{1D, ref}}} |\vartheta_{\mathrm{P_1^{2nd}}}(\boldsymbol{x}; c_0)|$ and $c_0 = (\sigma_{\mathrm{a,n}}, \sigma_{\mathrm{a,c}}, \sigma_{\mathrm{s,n}}, \sigma_{\mathrm{s,c}})$ the combination of undisturbed parameters.

---

^{a} See Remark 4.6.

Results

We visualize the results in Figure 6.8 exemplary for two time steps $t \in \{30\,\mathrm{s}, 150\,\mathrm{s}\}$. The main dynamics of this experiment take place within the first $150\,\mathrm{s}$ of the simulation and the temperature becomes almost stationary after that time.

Note that the computed temperatures differ from the results in Chapter 4, e.g., Figure 4.6, because we do not simulate the rotational symmetric case but the classical 2D case with $\partial_z = 0$, which changes the integrals in the 2D weak formulation (see Appendix A.3 for details).

In all subfigures, we visualize the effect of the disturbed optical coefficients for the P$_1^{2\mathrm{nd}}$ model. We compute the P$_1^{2\mathrm{nd}}$ solution for each combination of disturbed coefficients. The pointwise maxima and minima defined in equation (6.16) define the bounds of the corresponding blue-shaded areas.

Furthermore, in all subfigures, the dashed lines indicate the corresponding solutions computed on the refined mesh and match (on the visual scale) with the solutions on the coarse mesh, which validates the accuracy of the spatial discretization.

(a) $t = 30\,\mathrm{s}$

(b) $t = 150\,\mathrm{s}$

(c) $t = 30\,\mathrm{s}$

(d) $t = 150\,\mathrm{s}$

(e) $t = 30\,\mathrm{s}$

(f) $t = 150\,\mathrm{s}$
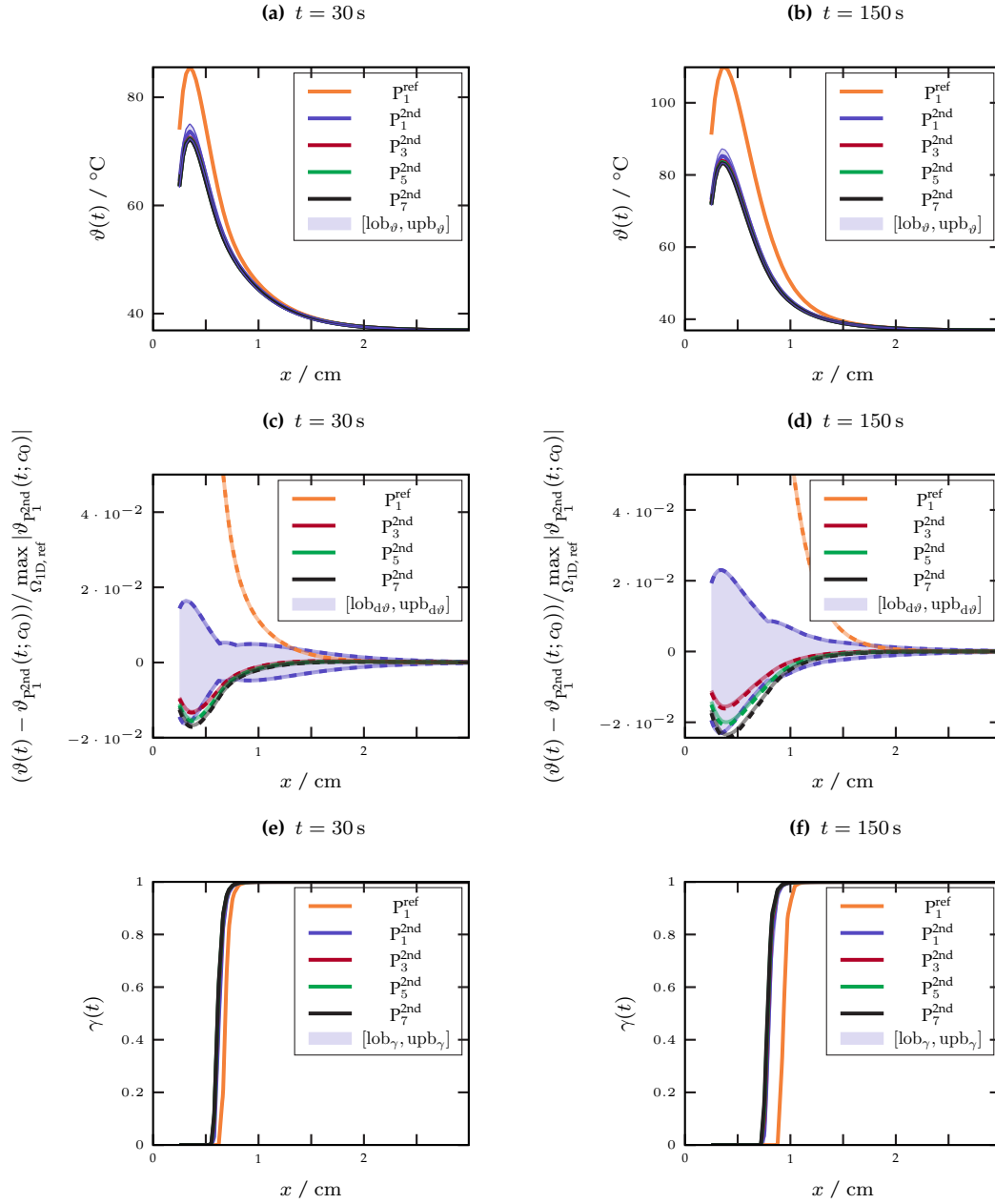
Figure 6.8: Results of Experiment 6.8. All functions are visualized along the reference line $\Omega_{1D,\,ref}$. For the definition of the pointwise maxima and minima bounding the blue-shaded areas, see equation (6.16). In all subfigures, the solid and dashed lines correspond to the solutions on the coarse and fine mesh, respectively. (6.8a, 6.8b): Temperature for different P_N^{2nd} models and the P_1^{ref} reference model at time steps $t \in \{30\,\mathrm{s}, 150\,\mathrm{s}\}$. The pointwise maxima upb_ϑ and minima lob_ϑ over all disturbed P_1^{2nd} solutions bound the blue-shaded area. (6.8c, 6.8d): Relative differences between temperatures of P_N^{2nd} / P_1^{ref} solutions and P_1^{2nd} solution along the reference line. For each combination of disturbed coefficients, we compute the relative difference between the disturbed P_1^{2nd} solution and the undisturbed (denoted by c_0) P_1^{2nd} solution. The pointwise maxima $\mathrm{upb}_{d\vartheta}$ and minima $\mathrm{lob}_{d\vartheta}$ bound the blue-shaded area. (6.8e, 6.8f): Coagulation for different P_N^{2nd} models and P_1^{ref} reference model at time steps $t \in \{30\,\mathrm{s}, 150\,\mathrm{s}\}$. The pointwise maxima upb_γ and minima lob_γ over all disturbed P_1^{2nd} solutions bound the blue-shaded area, which is barely visible here.

In all subfigures, the deviation between the P$_1^{2nd}$ model and the P$_1^{ref}$ reference model is apparent and is discussed at the end of this section.

In Figures 6.8a–6.8d, we observe a relatively small deviation ($\sim 2\%$) between the irradiances of the P$_N^{2nd}$ solutions and the irradiance of the P$_1^{2nd}$ solution. The differences are in the same range as the deviation induced by disturbed optical coefficients for the P$_1^{2nd}$ model, as can be seen from the blue-shaded area. So, at this point, using higher-order P$_N^{2nd}$ solutions does not seem to add value to the accuracy of the simulation if we can not bound the uncertainty of the given optical coefficients by (far) less than 5%.

With view on the later application, the ultimate measure for the relevance of different radiation models is the coagulation because this determines if the therapy is successful or not. In Figures 6.8e–6.8f, we visualize the coagulation for the different P$_N^{2nd}$ models. On a visual scale, we can not detect a significant difference between the coagulation boundary along the reference line. This holds in fact also for later points in time.

This experiment tells us three things.
First, for this specific parameter set, disturbed optical coefficients ($\sim 5\%$) have a limited influence on the prediction of the temperature ($\sim 2\%$) or the coagulation.
Second, at this point, we can not deduce a significant benefit from the use of P$_N^{2nd}$ in the LITT context. Thus, the use of the first-order P$_1^{2nd}$ (or P$_1$) model is justified in the context of LITT. We need to weigh the gain in accuracy for the temperature of about 2% against the increased computational effort. In each time step, the P$_1^{2nd}$ model requires the solution of one elliptic PDE, whereas the P$_7^{2nd}$ requires the solution of 28 coupled second-order PDEs in the three-dimensional case (16 PDEs for the two-dimensional case). This motivates to use the P$_1$ approximation of the RTE in the LITT context, as long as the uncertainty regarding the optical coefficients can not be quantified to be significantly less than 5% (in this specific example).
Last, the P$_1^{2nd}$ model can not be aligned with the P$_1^{ref}$ reference model by simply adjusting the coolant absorption factor. The coagulation has a different influence on the particular boundary conditions. Our modification of the coolant absorption factor $\beta_q = \beta_q^{2nd,1}$ is valid only at the beginning for $\gamma \equiv 1$. Once coagulation takes place, the predicted temperature based on the P$_1^{ref}$ reference model deviates significantly from the temperature predicted by the P$_1^{2nd}$ model.

Like mentioned earlier in this section, the P$_1^{2nd}$ approximates the irradiance of the RTE with partially reflecting boundary conditions in its current form (5.1)–(5.2) more accurately than the P$_1^{ref}$ reference model. Nevertheless, the reference model is validated by real experimental data, and the modifications are motivated in terms of the energy balance looking at the entire LITT model, which does not stop at the boundary of the domain. This mismatch could be solved in future by reconsidering the model of the RTE in the LITT context, like discussed earlier in this section. Such a new model is a prerequisite if one wants to use higher-order P$_N^{2nd}$ models in the LITT context.

Part III

Conclusion and Outlook

7 Conclusion and Outlook

I am not able to learn mathematics unless I can see some problem I am going to solve with mathematics, and I don't understand anyone who can teach mathematics without having a battery of problems that the student is going to be inspired to want to solve and then see that he or she can use the tools for solving them.

Steve Weinberg [235, §21, p. 229]

We discussed different aspects of modeling and parameter identification in the context of laser-induced interstitial thermotherapy. We investigated three possible extensions of an already established and validated model, regarding the heat-transfer model, the automated identification of unknown parameters and the approximation of radiative transfer.

Summary and Outlook

We summarize the highlights of this thesis and present possible directions for future work.

Delayed heat-transfer model

In Part I, we discussed the Cattaneo model as an alternative heat-transfer model in the LITT context. In Chapter 2, we introduced the Cattaneo–LITT model and proved its well-posedness, i.e., the existence of a unique state vector, which depends continuously on the blood-perfusion rate. We validated the effect of delayed heat transfer in the Cattaneo–LITT model in a numerical experiment in Chapter 4. We observed that the delay parameter τ has a significant influence on the solution only for values much larger than reported in the literature. We gave the theoretical foundation for this model but remain skeptical if this new model improves the approximation in the real application. Nevertheless, we have seen that the models for different values of τ differ especially at the beginning of the simulation, which is the part of the therapy where unknown parameters like the blood-perfusion rate have to be identified. This could affect the estimation of those unknown parameters. In the later application, the estimated parameters are fed back to the simulation and, thus, have an influence on future predictions of the desired quantities like the temperature. The answer to the question whether the effect of the delayed heat transfer is relevant to the simulation of LITT, especially in view of uncertainty of the tissue parameters and the measurement data, depends on the actual value of τ and can ultimately only be given by the validation with real experimental data.

We proved the well-posedness of the Cattaneo–LITT model analytically. As discussed, e.g., in [210], the solution does not respect a physical maximum principle. It would be interesting to investigate the maximum principle in this Cattaneo–LITT context. Furthermore, the transition $\tau \to 0$, like discussed in [17] for the standard heat-transfer model, would be interesting from an analytical point of view.

Identification of the blood-perfusion rate

In Part I, we discussed the identification of the blood-perfusion rate based on MRI data in the LITT context. In Chapter 2, we proposed an optimal-control problem for the identification of a parameter u, which models the location of large blood vessels. We proved analytically the existence of an optimal control and derived necessary first-order optimality conditions. Furthermore, we were able to prove that the optimal control has a sparse structure, in case we include an $L^1(\Omega)$-penalty term for the control in the cost functional.

In Chapter 4, we introduced a numerical example to demonstrate the automated identification of this parameter. We observed that in our synthetic environment the presented algorithm is able to reconstruct the parameter u, even for noisy measurement data. The quality of the reconstruction in a certain region is correlated negatively with the distance to the applicator. The question is whether the quality of the reconstruction is sufficiently high to estimate the coagulation zone accurately in the real application. We saw in Experiment 4.5 that the location of large vessels has a significant influence on the diameter and the shape of the coagulation zone. The results in our Experiments 4.8–4.11 were very promising and motivate the implementation in the field.

In the numerical experiments, we saw that the naive stopping criterion for the descent strategy might be too restrictive. For the real application, one might tune the presented descent strategy and investigate alternative optimization methods, e.g., Newton-based algorithms.

Another step is to investigate the effect of noisy measurement data on the reconstruction of the control parameter. This has been started in [9], but requires further investigation. The most important step might be the validation with real experimental data, especially for the in-vivo case.

A prerequisite for a realistic application in the field is the development of efficient solution strategies both for the forward simulation and the parameter identification. Approaches based on model-order-reduction techniques were discussed in [213–215] and require further investigation.

Second-order formulation of the P_N equations

In Part II, we proposed a second-order formulation of the P_N equations with Marshak boundary conditions. Even though the idea to reformulate the classical P_N equations as system of second-order PDEs is well known, our formulation allows an elegant inclusion of the Marshak boundary conditions in the weak formulation. Furthermore, all steps can be handed to a computer-algebra system, which allows us to generate a hierarchy of models in an automated way. The resulting system can be solved by standard finite-element tools. Our formulation allows for heterogeneous coefficients, irregular meshes for up to three-dimensional spatial domains, anisotropic boundary conditions and anisotropic scattering.

This method is derived independently of the LITT context and can be applied in other scenarios.

We make our code available online which allows a fast prototyping. In Chapter 6, we demonstrated the flexibility of our P_N^{2nd} method in several numerical experiments.

P_N^{2nd} models in LITT

In Chapter 6, we investigated numerically the effect of different P_N^{2nd} models for the radiation in the LITT model. We discussed the difference between the P_1^{ref} reference model, which is already validated in the context of LITT, and our P_1^{2nd} model. The models deviate because the P_1^{ref} reference model is a modified version of the classical P_1 model. This modification corrects a mismatch in the energy balance of the model for radiative transfer in the LITT context, but can not be applied in a straight-forward way to higher-order models. Thus, we suggested different modifications of the model for radiative transfer in the LITT context, which are based on different ways to model the interface between the tissue and the applicator. This requires further modeling effort but is a prerequisite to derive a consistent hierarchy of P_N or P_N^{2nd} models for the approximation of the radiative-transfer equation in the LITT context which respects the energy balance from a physical point of view.

We quantified the influence of higher-order P_N^{2nd} models on the LITT simulation by means of a numerical example and compared it to the influence of disturbed optical coefficients in the P_1^{2nd} model. The deviations between the P_1^{2nd} and the P_N^{2nd} models for different moment orders N were in the same range as the deviations within the P_1^{2nd} model caused by the disturbed parameters. This observation motivates the use of the P_1 or the P_1^{2nd} approximation for the radiation in the LITT context in the future, as long as the uncertainty of the given optical coefficients can not be quantified to be significantly less than 5%.

For the experiments, we assumed the anisotropy factor to be independent of the coagulation. Classically, this parameter also varies with the coagulation [65, 95]. We had to make this simplification because a varying anisotropy factor forbids the offline computation of the P_N^{2nd} equations. The fact that the algebraic transformations can be performed in beforehand is one of the advantages of the P_N^{2nd} formulation. It would be interesting to investigate how to include a heterogeneous anisotropy factor in the P_N^{2nd} model.

Conclusion

We showed how advanced mathematical models can help to improve thermal ablation of liver tumors. We investigated alternative mathematical models both for the heat-transfer equation and for the radiative-transfer equation. Furthermore, we discussed the task of parameter identification in this context.

The investigation of the Cattaneo–LITT model was challenging from an analytical point of view because it required techniques from nonlinear functional analysis to prove its well-posedness. Future students might benefit from our "Hitchhiker's guide" in Appendix B, which collects many classical results needed for the functional analytical treatment of parabolic PDEs and PDE-constrained optimal-control problems.

The developed P_N^{2nd} models and, especially, the provided code can be applied also in other scenarios than LITT and might be of use for everyone dealing with the radiative-transfer equation. It allows a smooth transition from less accurate but computationally less expensive to more accurate but computationally more expensive models.

In the current parameter setup, the advantages of the presented "more accurate" models are canceled by the uncertainty inherent in the physical parameters, at least based on the results of our simulations.
Our recommendation in view of the improvement of LITT is to further develop the identification of unknown parameters like the blood-perfusion rate for the already established classical LITT model and to develop fast solution strategies for the forward and inverse problems. Further efforts might take our proof of concept for the automated identification of blood vessels as starting point for the next step from ex-vivo to in-vivo simulations of LITT and their application in the field.

Part IV

Appendix

A   Cattaneo–LITT model

Use several function spaces for the same problem.

The modern strategy for nonlinear partial differential equations
(Eberhard Zeidler) [236, §30, p. 767]

A.1 Details for Chapter 2

A.1.1 Preliminaries

> **Lemma A.1 — Eigenfunctions of the Laplacian.**
> Let $\Omega \subset \mathbb{R}^d$, $d \leq 3$, be a nonempty, open and bounded set with a boundary Γ of class[a] $\mathcal{C}^{1,1}$,
> let $a = \hat{a}|_\Gamma$ for some $\hat{a} \in \mathcal{C}^{0,1}(\overline{\Omega})$ with $\hat{a}(x) \geq 0$ for all $x \in \overline{\Omega}$, and let $\kappa \in \mathbb{R}_{>0}$. Then there is
> a countable set $(w_k)_{k \in \mathbb{N}} \subset H^2(\Omega)$ consisting of eigenfunctions of the Laplacian with *Robin
> boundary conditions*, i.e., there exist real numbers $(\lambda_k)_{k \in \mathbb{N}} \subset \mathbb{R}$ such that
>
> $$\left.\begin{cases} -\kappa \Delta w_k = \lambda_k w_k & \text{a.e. in } \Omega, \\ a w_k + \kappa \nabla w_k \cdot \boldsymbol{n} = 0 & \text{a.e. on } \Gamma \end{cases}\right\} \quad \text{for all } k \in \mathbb{N}.$$
>
> These eigenfunctions form an orthonormal basis of $L^2(\Omega)$, i.e., for all $\vartheta \in L^2(\Omega)$ it holds
>
> $$\vartheta = \sum_{k=1}^{\infty} (\vartheta, w_k)_{L^2(\Omega)}\, w_k \quad \text{in } L^2(\Omega) \tag{A.1}$$
>
> and
>
> $$(w_k, w_j)_{L^2(\Omega)} = \delta_{kj} = \begin{cases} 1, & k = j, \\ 0, & \text{else.} \end{cases}$$
>
> Furthermore, if $\vartheta \in H^1(\Omega)$, the expansion (A.1) converges[b] to ϑ also w.r.t. the $H^1(\Omega)$ norm.
>
> ---
> [a] See, e.g., [63, App. C.1, p. 626], [85, Sec. 1.2.1, Def. 1.2.1.1, p. 5] for a discussion on spatial boundaries.
> [b] In our situation, this is a prerequisite for a Faedo–Galerkin approximation of the solution of the Cattaneo equation,
>   see Lemma A.4 and [43, XVIII §2 1, p. 504].

Proof. This is a standard result. Nevertheless, many references prove this result only for a basis in $L^2(\Omega)$ for Dirichlet boundary conditions [235, §22.13, Prop. 22.35, p. 362], [20, Sec. 9.8, Thm. 9.31, p. 311] or under restrictive assumptions like a $\mathcal{C}^\infty$ boundary [101, Sec. 11.5, Thm. 11.5.2, p. 300], so we decided to give the proof here.

> Apply standard spectral theory to the solution operator of this elliptic PDE.

Without loss of generality, we assume $\kappa = 1$ for this proof. We consider the problem

$$\left\{\begin{array}{ll} -\Delta\omega + \omega = f & \text{a.e. in } \Omega, \\ a\omega + \nabla\omega \cdot \boldsymbol{n} = 0 & \text{a.e. on } \Gamma, \end{array}\right\} \tag{A.2}$$

which has a unique solution $\omega \in H^2(\Omega)$ for $f \in L^2(\Omega)$, see [85, Sec. 2.4.2, Thm. 2.4.2.7, p. 126]. This allows us, together with the compact embedding[1] $H^2(\Omega) \hookrightarrow\hookrightarrow L^2(\Omega)$, to define the compact solution operator

$$S\colon L^2(\Omega) \to L^2(\Omega),\ f \mapsto w$$

such that ω fulfills equation (A.2) in the weak sense for the given $f \in L^2(\Omega)$, i.e., it holds

$$B(\omega, \varphi) = \int_\Omega f\varphi \,\mathrm{d}x \quad \text{for all } \varphi \in H^1(\Omega), \tag{A.3}$$

with the symmetric bilinear form

$$B\colon H^1(\Omega) \times H^1(\Omega),\ B(\omega, \varphi) := \int_\Omega \nabla\omega \cdot \nabla\varphi \,\mathrm{d}x + \int_\Omega \omega\varphi \,\mathrm{d}x + \int_\Gamma a\omega\varphi \,\mathrm{d}s.$$

The operator S is linear and symmetric w.r.t. the $L^2(\Omega)$ scalar product. In fact, for $f, g \in L^2(\Omega)$, it holds

$$\left.\begin{array}{l} B(S(f), \varphi) = (f, \varphi)_{L^2(\Omega)}, \\ B(S(g), \varphi) = (g, \varphi)_{L^2(\Omega)} \end{array}\right\} \quad \text{for all } \varphi \in H^1(\Omega),$$

and we can choose $\varphi = S(g)$ in the first and $\varphi = S(f)$ in the second equation to obtain

$$(f, S(g))_{L^2(\Omega)} = B(S(f), S(g)) = B(S(g), S(f)) = (g, S(f))_{L^2(\Omega)} = (S(f), g)_{L^2(\Omega)}.$$

Furthermore, S is strictly monotone. In fact, for $f \neq 0 \in L^2(\Omega)$, we get by choosing $\varphi = S(f)$ in the weak form (A.3) that

$$(S(f), f)_{L^2(\Omega)} = (f, S(f))_{L^2(\Omega)} = (\nabla S(f), \nabla S(f))_{L^2(\Omega)} + (S(f), S(f))_{L^2(\Omega)} + (aS(f), S(f))_{L^2(\Gamma)}$$
$$\geq \|S(f)\|^2_{H^1(\Omega)} > 0.$$

Note that $f \neq 0$ implies $S(f) \neq 0$, which justifies the last inequality.

Spectral theory for linear, symmetric, compact and strictly monotone operators[2] now yields a countable, complete orthonormal system of eigenvectors $(w_k)_{k\in\mathbb{N}}$ of S in $L^2(\Omega)$, with corresponding positive eigenvalues $(\hat{\lambda}_k)_{k\in\mathbb{N}} \subset \mathbb{R}_{>0}$.

---

[1] See classical Sobolev embeddings B.56.
[2] See a classical result on spectral theory B.65.

The eigenfunctions of the operator S are eigenfunctions of the Laplacian. In fact, if we plug an eigenfunction of S into the weak formulation A.3, we get by means of integration by parts[3] and the variational lemma[4]

$$\Delta w_k = (1 - \hat{\lambda}_k^{-1})w_k \quad \text{a.e. in } \Omega \quad \text{and} \quad a\omega_k + \nabla \omega_k \cdot \boldsymbol{n} = 0 \quad \text{a.e. on } \Gamma.$$

It is left to show that, for $\vartheta \in H^1(\Omega)$, the expansion (A.1) converges to ϑ in $H^1(\Omega)$.

To this, note that the bilinear form B defines a scalar product on $H^1(\Omega)$. The induced norm $\|\omega\|_{H^1(\Omega),B} := B(\omega,\omega)^{1/2}$ is equivalent to the standard $H^1(\Omega)$ norm. In fact, it holds

$$\|\omega\|_{H^1(\Omega)}^2 = \int_\Omega \omega^2 \, \mathrm{d}x + \int_\Omega (\nabla\omega)^2 \, \mathrm{d}x \le \int_\Omega \omega^2 \, \mathrm{d}x + \int_\Omega (\nabla\omega)^2 \, \mathrm{d}x + \int_\Gamma a\omega^2 \, \mathrm{d}s = \|\omega\|_{H^1(\Omega),B}^2$$

and, with Lemma B.23,

$$\|\omega\|_{H^1(\Omega),B}^2 = \int_\Omega \omega^2 \, \mathrm{d}x + \int_\Omega (\nabla\omega)^2 \, \mathrm{d}x + \int_\Gamma a\omega^2 \, \mathrm{d}s \le \int_\Omega \omega^2 \, \mathrm{d}x + C \|\omega\|_{H^1(\Omega)}^2 \le (1+C) \|\omega\|_{H^1(\Omega)}^2.$$

Thus, $H^1(\Omega)$ equipped with the scalar product induced by B is a Hilbert space.

The set $\left(\sqrt{\hat{\lambda}_k}\omega_k \right)_{k \in \mathbb{N}}$ forms a complete B-orthonormal system and, thus[5], a B-orthonormal basis of $H^1(\Omega)$. In fact, for two eigenfunctions ω_k, ω_j of S, it holds

$$B(\omega_k, \omega_j) = \hat{\lambda}_k^{-1} (\omega_k, \omega_j)_{L^2(\Omega)} = \begin{cases} \hat{\lambda}_k^{-1}, & k = j, \\ 0, & \text{else,} \end{cases}$$

where the first equality follows from the weak formulation (A.3) and the second equality from the fact that $(\omega_k)_{k \in \mathbb{N}}$ is an orthonormal basis of the space $L^2(\Omega)$. Furthermore, the set $\left(\sqrt{\hat{\lambda}_k}\omega_k \right)_{k \in \mathbb{N}}$ is complete in $H^1(\Omega)$ because, for $\vartheta \in H^1(\Omega)$ with $B(\vartheta, \omega_k) = 0$ for all $k \in \mathbb{N}$, it follows from (A.3) that $(\vartheta, \omega_k)_{L^2(\Omega)} = 0$ for all $k \in \mathbb{N}$, which implies $\vartheta = 0$ due to the completeness of $(\omega_k)_{k \in \mathbb{N}}$ in $L^2(\Omega)$.

Finally, for $\vartheta \in H^1(\Omega)$, the weak formulation (A.3) yields

$$(\vartheta, \omega_k)_{L^2(\Omega)} \omega_k = (\omega_k, \vartheta)_{L^2(\Omega)} \omega_k = \hat{\lambda}_k B(\omega_k, \vartheta)\omega_k = B\left(\vartheta, \sqrt{\hat{\lambda}_k}\omega_k\right) \sqrt{\hat{\lambda}_k}\omega_k. \tag{A.4}$$

Because $\left(\sqrt{\hat{\lambda}_k}\omega_k \right)_{k \in \mathbb{N}}$ is a B-orthonormal basis of $H^1(\Omega)$, it holds

$$\sum_{k=1}^n B\left(\vartheta, \sqrt{\hat{\lambda}_k}\omega_k\right) \sqrt{\hat{\lambda}_k}\omega_k \to \vartheta \quad \text{in } H^1(\Omega) \text{ w.r.t. the } B \text{ norm, for } n \to \infty. \tag{A.5}$$

Equations (A.4) and (A.5) together imply that the expansion (A.1) converges to ϑ in $H^1(\Omega)$ w.r.t. the B norm and, thus, w.r.t. to the standard $H^1(\Omega)$ norm as seen above.   ∎

---

[3] See integration by parts in Sobolev spaces B.35.
[4] See the variational lemma B.6.
[5] See [235, §19.5, Def. 19.10, p. 117] and [235, §19.5, Thm. 19.A, p. 118] for the completeness criterion.

> **Lemma A.2 — Strong convergence of the auxiliary temperature (cf. [56, Sec. 8.1, Bem. 8.1.13, p. 213]).**
> Let $Q \subset \mathbb{R}^d, d \geq 1$, be a nonempty, open and bounded set, and let $(\omega_k)_{k \in \mathbb{N}} \subset L^2(Q)$ with $\omega_k \to \omega$ in $L^2(Q)$. Then, for all $p \in [1, \infty)$, it holds
>
> $$\left[\omega_k\right]_M \to \left[\omega\right]_M \quad \text{in } L^p(Q), \tag{A.6}$$
>
> where $\left[\omega\right]_M := \min(\max(\omega, -M), M)$ is the cutoff function for some $M \in \mathbb{R}_{>0}$.

Proof. The cutoff function is continuous as map from $L^2(Q)$ to $L^2(Q)$, which implies

$$\left\| \left[\omega_k\right]_M - \left[\omega\right]_M \right\|_{L^2(Q)} \to 0 \quad \text{for } k \to \infty.$$

For $p \in [1, 2]$, the result follows immediately from the embedding $L^2(Q) \hookrightarrow L^p(Q)$:

$$\left\| \left[\omega_k\right]_M - \left[\omega\right]_M \right\|_{L^p(Q)} \leq C \left\| \left[\omega_k\right]_M - \left[\omega\right]_M \right\|_{L^2(Q)}.$$

For $p \in (2, \infty)$, the result follows immediately from $\left\| \left[\omega_k\right]_M - \left[\omega\right]_M \right\|_{L^\infty(Q)} \leq 2M$ together with the following estimate[6]:

$$\left\| \left[\omega_k\right]_M - \left[\omega\right]_M \right\|_{L^p(Q)} \leq \left\| \left[\omega_k\right]_M - \left[\omega\right]_M \right\|_{L^\infty(Q)}^{1-\frac{2}{p}} \left\| \left[\omega_k\right]_M - \left[\omega\right]_M \right\|_{L^2(Q)}^{\frac{2}{p}}.$$

∎

> **Lemma A.3 — A result on regularity.**
> Let $\Omega \subset \mathbb{R}^d, d \in \{2, 3\}$, be a nonempty, open and bounded set with Lipschitz boundary, let $I = (0, T) \subset \mathbb{R}$ be an open interval and define $Q := I \times \Omega$.
> Furthermore, let $(\vartheta_k)_{k \in \mathbb{N}} \subset W^{1,\infty}(I; H^1(\Omega)) \cap L^\infty(I; H^2(\Omega))$ be a bounded sequence[a], i.e.,
>
> $$\|\vartheta_k\|_{W^{1,\infty}(I;H^1(\Omega))} + \|\vartheta_k\|_{L^\infty(I;H^2(\Omega))} \leq M \quad \text{for all } k \in \mathbb{N}.$$
>
> 1. Let $p_1, p_2 \in (1, \infty)$. There is an element $\vartheta \in W^{1,p_1}(I; H^1(\Omega)) \cap L^{p_2}(I; H^2(\Omega))$, independent of the particular choices of p_1, p_2, and a subsequence $(\vartheta_{k_l})_{l \in \mathbb{N}}$ such that
>
> $$\vartheta_{k_l} \rightharpoonup \vartheta \quad \text{in } W^{1,p_1}(I; H^1(\Omega)),$$
> $$\vartheta_{k_l} \rightharpoonup \vartheta \quad \text{in } L^{p_2}(I; H^2(\Omega)),$$
>
>   with
>
> $$\|\vartheta\|_{W^{1,p_1}(I;H^1(\Omega))} + \|\vartheta\|_{L^{p_2}(I;H^2(\Omega))} \leq \left((2T)^{\frac{1}{p_1}} + T^{\frac{1}{p_2}} \right) M.$$

---

[6] For $f \in L^\infty(Q), g \in L^2(Q), p \in (2, \infty)$, it holds

$$\left(\int_Q |f(x)g(x)|^p \, \mathrm{d}x \right)^{\frac{1}{p}} = \left(\int_Q |f(x)g(x)|^{p-2} |f(x)g(x)|^2 \, \mathrm{d}x \right)^{\frac{1}{p}} \leq \|fg\|_{L^\infty(Q)}^{\frac{p-2}{p}} \left(\left(\int_Q |f(x)g(x)|^2 \, \mathrm{d}x \right)^{\frac{1}{2}} \right)^{\frac{2}{p}}.$$

2. It holds $\vartheta \in \mathcal{C}^{0,\alpha}(\overline{Q})$ with

$$\|\vartheta\|_{\mathcal{C}^{0,\alpha}(\overline{Q})} \leq C(T,\alpha)M \tag{A.7}$$

for $\alpha \in [0, \frac{1}{4})$.

The bound (A.7) still holds if the sequence is defined only on a smaller time interval $(0, \tilde{T}) \subset I$, i.e., $(\vartheta_k)_{k \in \mathbb{N}} \subset W^{1,\infty}((0,\tilde{T}); H^1(\Omega)) \cap L^\infty((0,\tilde{T}); H^2(\Omega))$. In this case, get $\|\vartheta\|_{\mathcal{C}^{0,\alpha}([0,\tilde{T}] \times \overline{\Omega})} \leq C(T,\alpha)M.$[b]

---

[a]   We understand the function spaces as subspaces of $L^1(Q)$, which gives sense to the intersection. Two functions in such an intersection are equal if they coincide a.e. in Q. For example, $\vartheta \in W^{1,\infty}(I; H^1(\Omega)) \cap L^\infty(I; H^2(\Omega))$ means that the equivalence class of $\vartheta \in L^1(Q)$ contains a representative $\vartheta_1 \in W^{1,\infty}(I; H^1(\Omega))$ as well as a representative $\vartheta_2 \in L^\infty(I; H^2(\Omega))$ such that $\vartheta_1 = \vartheta_2$ a.e. in Q.

[b]   This technical detail is required for the proof of Lemma A.4, which is used to prove Lemma 3.9.

Proof.

Extract weakly convergent subsequences and identify the limits in $L^1(Q)$.

1. For $p_1, p_2 \in (1, \infty)$, we have the continuous embedding[7]

$$W^{1,\infty}(I; H^1(\Omega)) \cap L^\infty(I; H^2(\Omega)) \hookrightarrow W^{1,p_1}(I; H^1(\Omega)) \cap L^{p_2}(I; H^2(\Omega)).$$

Note that $H^1(\Omega)$ and $H^2(\Omega)$ are reflexive Banach spaces and, thus, also $W^{1,p_1}(I; H^1(\Omega))$ and $L^{p_2}(I; H^2(\Omega))$ are reflexive Banach spaces.[8] Because the sequence is bounded, we can[9] consecutively extract weakly convergent subsequences, where we reuse the same index as in the original sequence for a better readability, with

$$\begin{aligned}
\vartheta_{k_l} &\rightharpoonup \vartheta &&\text{in } L^{p_1}(I; H^1(\Omega)), \\
\vartheta'_{k_l} &\rightharpoonup v &&\text{in } L^{p_1}(I; H^1(\Omega)), \\
\vartheta_{k_l} &\rightharpoonup \hat{\vartheta} &&\text{in } L^{p_2}(I; H^2(\Omega)).
\end{aligned}$$

We can identify $v = \vartheta'$ by means of Lemma B.14.

From $L^{p_1}(I; H^1(\Omega)) \subset L^1(Q)$ and $L^{p_2}(I; H^2(\Omega)) \subset L^1(Q)$, we infer[10] $L^1(Q)^* \subset L^{p_1}(I; H^1(\Omega))^*$ and $L^1(Q)^* \subset L^{p_2}(I; H^2(\Omega))^*$. This yields

$$\vartheta_{k_l} \rightharpoonup \vartheta \quad \text{in } L^1(Q) \quad \text{and} \quad \vartheta_{k_l} \rightharpoonup \hat{\vartheta} \quad \text{in } L^1(Q).$$

The uniqueness of the weak limit[11] implies $\vartheta = \hat{\vartheta}$ in $L^1(Q)$ and, thus, $\vartheta = \hat{\vartheta}$ a.e. in Q.

Furthermore, the uniqueness of the weak limit ensures that the limit ϑ is independent[12] of the particular choices of p_1, p_2.

---

[7]   See embeddings in Bochner spaces B.54.

[8]   See Lemma B.24 on Sobolev spaces and Lemma B.12 on reflexive Banach spaces.

[9]   See the criterion on weak lower semicontinuity B.15.

[10]   See Lemma B.17 on dual spaces of subspaces.

[11]   See Remark B.8 on the uniqueness of weak/weak* limits.

[12]   In fact, let $p, \hat{p} \in (1, \infty)$, and let $\vartheta \in L^p(I; H^1(\Omega))$, $\hat{\vartheta} \in L^{\hat{p}}(I; H^1(\Omega))$ be the corresponding weak limits. From $L^p(I; H^1(\Omega)) \subset L^1(Q)$ and $L^{\hat{p}}(I; H^1(\Omega)) \subset L^1(Q)$, we infer $L^1(Q)^* \subset L^p(I; H^1(\Omega))^*$ and $L^1(Q)^* \subset L^{\hat{p}}(I; H^1(\Omega))^*$ and, thus,

$$\vartheta_{k_l} \rightharpoonup \vartheta \quad \text{in } L^1(Q) \quad \text{and} \quad \vartheta_{k_l} \rightharpoonup \hat{\vartheta} \quad \text{in } L^1(Q).$$

The uniqueness of the weak limit implies $\vartheta = \hat{\vartheta}$ in $L^1(Q)$, which especially yields $\vartheta = \hat{\vartheta}$ a.e. in Q.

The norm is sequentially weakly lower semicontinuous[13], which implies[14]

$$\|\vartheta\|_{W^{1,p_1}(I;H^1(\Omega))} + \|\vartheta\|_{L^{p_2}(I;H^2(\Omega))}$$

$$\leq \liminf_{l\in\mathbb{N}} \left(\|\vartheta_{k_l}\|_{W^{1,p_1}(I;H^1(\Omega))} + \|\vartheta_{k_l}\|_{L^{p_2}(I;H^2(\Omega))} \right)$$

$$\leq((2T)^{\frac{1}{p_1}} + T^{\frac{1}{p_2}})\liminf_{l\in\mathbb{N}} \left(\|\vartheta_{k_l}\|_{W^{1,\infty}(I;H^1(\Omega))} + \|\vartheta_{k_l}\|_{L^{\infty}(I;H^2(\Omega))} \right)$$

$$\leq((2T)^{\frac{1}{p_1}} + T^{\frac{1}{p_2}})M.$$

2. We choose $p := p_1 := p_2 := 2 + \varepsilon$ for some $\varepsilon > 0$, and get with the embeddings in Hölder spaces B.60 and the embeddings $H^1(\Omega) \hookrightarrow L^6(\Omega)$ and $H^2(\Omega) \hookrightarrow W^{1,6}(\Omega)$ (for the spatial dimension $d \leq 3$) that

$$\vartheta \in W^{1,p}(I;L^6(\Omega)) \cap L^p(I;W^{1,6}(\Omega)) \hookrightarrow\hookrightarrow \mathcal{C}^{0,\alpha}(\overline{Q})$$

with $\alpha \in [0, \frac{1+\varepsilon}{2+\varepsilon} - \frac{1}{2})$, i.e.,

$$\|\vartheta\|_{\mathcal{C}^{0,\alpha}(\overline{Q})} \leq C_1(\alpha, T) \|\vartheta\|_{W^{1,p}(I;L^6(\Omega))\cap L^p(I;W^{1,6}(\Omega))} \tag{A.8}$$

for a constant $C_1(\alpha, T)$. The arbitrary choice of ε implies that we can choose $\alpha \in [0, \frac{1}{4})$, where the constant of the embedding might depend on α.

For $\tilde{T} \in I$, we can extend the functions $(\tilde{\vartheta}_k)_{k\in\mathbb{N}} \subset W^{1,\infty}((0,\tilde{T});H^1(\Omega))\cap L^\infty((0,\tilde{T});H^2(\Omega))$ to $(\vartheta_k)_{k\in\mathbb{N}} \subset W^{1,\infty}(I;H^1(\Omega)) \cap L^\infty(I;H^2(\Omega))$ by defining

$$\vartheta_k(t) := \begin{cases} \tilde{\vartheta}_k(t), & t \leq \tilde{T}, \\ \tilde{\vartheta}_k(\tilde{T}), & t > \tilde{T} \end{cases} \quad \text{for all } k \in \mathbb{N}.$$

Note that the evaluation at times $t \in [0, \tilde{T}]$ is well defined because of the embeddings[15]

$$W^{1,\infty}((0,\tilde{T});H^1(\Omega)) \cap L^\infty((0,\tilde{T});H^2(\Omega)) \hookrightarrow \mathcal{C}^{0,\alpha}([0,\tilde{T}]\times\overline{\Omega}) \hookrightarrow \mathcal{C}^0([0,\tilde{T}];\overline{\Omega}).$$

Like above, we get for the weak limit $\vartheta \in \mathcal{C}^{0,\alpha}(\overline{Q}) \hookrightarrow \mathcal{C}^{0,\alpha}([0,\tilde{T}]\times\overline{\Omega})$, where the last embedding follows from restricting ϑ to $[0,\tilde{T}]\times\overline{\Omega}$, and it holds

$$\|\vartheta\|_{\mathcal{C}^{0,\alpha}([0,\tilde{T}]\times\overline{\Omega})} \leq \|\vartheta\|_{\mathcal{C}^{0,\alpha}(\overline{Q})} \leq C_1(\alpha, T) \|\vartheta\|_{W^{1,p_1}(I;H^1(\Omega))\cap L^{p_2}(I;H^2(\Omega))}$$

$$\leq C_1(\alpha, T) \left((2T)^{\frac{1}{p_1}} + T^{\frac{1}{p_2}} \right) M$$

with the same constant as in (A.8).

∎

---

[13] See the criterion on weak lower semicontinuity B.16.

[14] Use the estimate

$$\|\vartheta_{k_l}\|_{W^{1,p_1}(I;H^1(\Omega))} = \left(\int_0^T \|\vartheta_{k_l}(t)\|_{H^1(\Omega)}^{p_1} \, dt + \int_0^T \left\|\vartheta'_{k_l}(t)\right\|_{H^1(\Omega)}^{p_1} \, dt \right)^{\frac{1}{p_1}}$$

$$\leq \left(\left(\|\vartheta_{k_l}\|_{L^\infty(I;H^1(\Omega))}^{p_1} + \left\|\vartheta'_{k_l}\right\|_{L^\infty(I;H^1(\Omega))}^{p_1} \right) \int_0^T 1 \, dt \right)^{\frac{1}{p_1}}$$

$$\leq \left(2 \left(\|\vartheta_{k_l}\|_{L^\infty(I;H^1(\Omega))} + \left\|\vartheta'_{k_l}\right\|_{L^\infty(I;H^1(\Omega))} \right)^{p_1} T \right)^{\frac{1}{p_1}} = (2T)^{\frac{1}{p_1}} \|\vartheta_{k_l}\|_{W^{1,\infty}(I;H^1(\Omega))}.$$

[15] See Lemma B.50 and Theorems B.59 and B.60 for standard embedding results.

Lemma A.4 — Well-posedness of the Cattaneo equation in the context of LITT.

Let Assumptions 2.1 and 2.2 hold and let

$$(r, g) \in L^2(I; L^2(\Omega)) \times L^2(I; L^2(\Gamma)).$$

1. Then there *exists* a *unique* solution

$$\vartheta \in L^\infty(I; H^1(\Omega)) \cap W^{1,\infty}(I; L^2(\Omega)) \cap H^1(I; H^1(\Omega)) \cap H^2(I; H^1(\Omega)^*)$$

   such that

$$\left\{ \begin{aligned} \int_0^T \tau \left\langle \vartheta''(t), \varphi(t) \right\rangle_{H^1(\Omega)} &+ (\vartheta'(t), \varphi(t))_{L^2(\Omega)} + F_{\mathrm{h}}(\vartheta(t), \varphi(t)) \, \mathrm{d}t \\ &= \int_0^T (r(t), \varphi(t))_{L^2(\Omega)} + (g(t), \varphi(t))_{L^2(\Gamma)} \, \mathrm{d}t, \\ \vartheta(0) &= \vartheta^{(0)}, \\ \vartheta'(0) &= \vartheta^{(1)} \end{aligned} \right\} \tag{A.9}$$

   for all $\varphi \in L^2(I; H^1(\Omega))$ with

$$\begin{aligned} \|\vartheta\|_{L^\infty(I;H^1(\Omega))} &+ \|\vartheta'\|_{L^\infty(I;L^2(\Omega))} + \|\vartheta'\|_{L^2(I;H^1(\Omega))} + \|\vartheta''\|_{L^2(I;H^1(\Omega)^*)} \\ &\le C(\tau^{-1}, T) \left(\left\|\vartheta^{(0)}\right\|_{H^1(\Omega)} + \left\|\vartheta^{(1)}\right\|_{L^2(\Omega)} + \|g\|_{L^2(I;L^2(\Gamma))} + \|r\|_{L^2(I;L^2(\Omega))} \right). \end{aligned} \tag{A.10}$$

2. Let $g \in L^2(\Gamma)$, i.e., it is constant in time. Then the solution above fulfills

$$\begin{aligned} \|\vartheta'\|_{L^\infty(I;L^2(\Omega))} &+ \|\vartheta\|_{L^\infty(I;H^1(\Omega))} \\ &\le C \exp(TC_1) \left(\left\|\vartheta^{(0)}\right\|_{H^1(\Omega)} + \left\|\vartheta^{(1)}\right\|_{L^2(\Omega)} + \|g\|_{L^2(\Gamma)} + \|r\|_{L^2(I;L^2(\Omega))} \right), \end{aligned} \tag{A.11}$$

   where C, C_1 depend on τ but not on T.[a]

3. Let $g \in H^{1/2}(\Gamma)$ and $r = r_1 + r_2$ with $r_1 \in L^2(I; H^1(\Omega))$, $r_2 \in H^1(I; L^2(\Omega))$. Then, for all $p_1, p_2 \in (1, \infty)$, the solution ϑ in the previous statement fulfills

$$\vartheta \in W^{1,p_1}(I; H^1(\Omega)) \cap L^{p_2}(I; H^2(\Omega))$$

   with

$$\begin{aligned} \|\vartheta\|_{W^{1,p_1}(I;H^1(\Omega))} &+ \|\vartheta\|_{L^{p_2}(I;H^2(\Omega))} \\ &\le C(\tau^{-1}, p_1, p_2, T) \Big(\left\|\vartheta^{(0)}\right\|_{H^2(\Omega)} + \left\|\vartheta^{(1)}\right\|_{H^1(\Omega)} + \|g\|_{H^{1/2}(\Gamma)} \\ &\qquad + \|r_1\|_{L^2(I;H^1(\Omega))} + \|r_2\|_{H^1(I;L^2(\Omega))} \Big). \end{aligned} \tag{A.12}$$

Especially, we have that the solution is Hölder continuous, i.e., $\vartheta \in \mathcal{C}^{0,\alpha}(\overline{Q})$ for $\alpha \in [0, \frac{1}{4})$, with

$$\|\vartheta\|_{\mathcal{C}^{0,\alpha}(\overline{Q})} \leq C(\tau^{-1}, \alpha, T) \Big(\left\|\vartheta^{(0)}\right\|_{H^2(\Omega)} + \left\|\vartheta^{(1)}\right\|_{H^1(\Omega)} + \|g\|_{H^{1/2}(\Gamma)}$$
$$+ \|r_1\|_{L^2(I;H^1(\Omega))} + \|r_2\|_{H^1(I;L^2(\Omega))} \Big). \tag{A.13}$$

Analogously to Lemma A.3, the bounds (A.12) and (A.13) still hold if we consider a smaller time interval $(0, \tilde{T}) \subset I$ for the problem.[a]

Furthermore, all statements still hold if we exchange the assumptions for r_1 by the following less restrictive but more technical requirements:[b]

(a) $r_1 \in L^2(I; L^2(\Omega))$,

(b) $r_1(t) \in H^1(\Omega)$ for a.a. $t \in I$,

(c) $\|r_1(t)\|_{H^1(\Omega)} \leq \tilde{r}(t)$ for some $\tilde{r} \in L^2(I)$.[c]

In this case, we need to replace the norm $\|r_1\|_{L^2(I;H^1(\Omega))}$ by $\|\tilde{r}\|_{L^2(I)}$ in the estimates above.

---

[a]   This technical detail is required for the proof of Lemma 3.9.
[b]   This does not imply $r_1 \in L^2(I; H^1(\Omega))$ because we do not require $r_1 \colon I \to H^1(\Omega)$ to be Bochner measurable. This technical detail is required for the proof of Theorem 2.15.
[c]   Note that we do not need to show that $t \mapsto \|\nabla r_1(t)\|_{L^2(\Omega)}$ is Lebesgue measurable.

Remark A.5 — Dependence on the final time T.

The reason for us to explicitly state the dependence of the state bounds in estimates (A.10)–(A.13) on the final time T is the proof of Lemma 3.9. There, we need to consider the same evolution problem for smaller time intervals $(0, \tilde{T}) \subset I = (0, T)$, and we need that the corresponding solutions are bounded independently of $\tilde{T}$, for a fixed final time $T \in \mathbb{R}_{>0}$.

Remark A.6 — Approximation of the solution of the Cattaneo equation.

The proof of the first part of Lemma A.4 is based on [43, XVIII §5 1.3, Thm. 1, p. 558], which follows the Faedo–Galerkin procedure[a]. Like described in [43, XVIII §5, p. 552 ff.], we consider a certain sequence of finite-dimensional subspaces, which defines a sequence of auxiliary solutions (see below). One can show that this sequence of auxiliary solutions converges to the solution of equation (A.9) (for homogeneous boundary conditions) for all $\varphi \in L^2(I; H^1(\Omega))$. For the finite-dimensional subspaces, we choose the spaces $V_m = \operatorname{span}\{\omega_k \,|\, k = 1, \dots, m\}$ which are spanned by the eigenfunctions of the Laplacian $(\omega_k)_{k \in \mathbb{N}} \subset H^2(\Omega)$ given in Lemma A.1.

This yields a sequence[b]

$$(\vartheta_m)_{m \in \mathbb{N}} \subset \{\omega \in \mathcal{C}^0(\overline{I}; V_m) \,|\, \omega' \in \mathcal{C}^0(\overline{I}; V_m), \omega'' \in L^2(I; V_m)\} \tag{A.14}$$

of the form

$$\vartheta_m(t) = \sum_{k=1}^{m} g_{km}(t) w_k, \quad g_{km} \in H^2(I)$$

such that each ϑ_m fulfills

$$\left\{ \begin{array}{r} \displaystyle\int_0^T \tau \left(\vartheta_m''(t), \varphi(t)\right)_{L^2(\Omega)} + \left(\vartheta_m'(t), \varphi(t)\right)_{L^2(\Omega)} + F_{\mathrm{h}}(\vartheta_m(t), \varphi(t)) \, \mathrm{d}t \\ \displaystyle = \int_0^T \left(r(t), \varphi(t)\right)_{L^2(\Omega)} + \left(g(t), \varphi(t)\right)_{L^2(\Gamma)} \, \mathrm{d}t \,, \\ \vartheta_m(0) = \vartheta_m^{(0)}, \\ \vartheta_m'(0) = \vartheta_m^{(1)} \end{array} \right\} \quad \text{(A.15)}$$

for all $\varphi \in L^2(I; V_m)$, with initial conditions $\vartheta_m^{(0)}, \vartheta_m^{(1)}$ according to Remark 2.3. The sequence converges to the solution ϑ of (A.9) as follows:[c]

$$\begin{array}{lll} \vartheta_m(t) \to \vartheta(t) & \text{strongly in } H^1(\Omega) & \text{for a.a. } t \in I, \\ \vartheta_m'(t) \to \vartheta'(t) & \text{strongly in } L^2(\Omega) & \text{for a.a. } t \in I, \\ \vartheta_m' \to \vartheta' & \text{strongly in } L^2(I; H^1(\Omega)), \\ \vartheta_m \rightharpoonup \vartheta & \text{weakly in } L^2(I; H^1(\Omega)). \end{array} \quad \text{(A.16)}$$

Furthermore, the following bound for the approximate solutions holds:

$$\begin{aligned} &\|\vartheta_m\|_{L^\infty(H^1(\Omega))} + \|\vartheta_m'\|_{L^\infty(L^2(\Omega))} \\ &\leq C \exp(CT) \left(\left\|\vartheta^{(0)}\right\|_{H^1(\Omega)}^2 + \left\|\vartheta^{(1)}\right\|_{L^2(\Omega)}^2 + \|r\|_{L^2(I;L^2(\Omega))}^2 + \|g\|_{L^2(I;L^2(\Gamma))}^2 \right), \end{aligned} \quad \text{(A.17)}$$

where the constant C depends on τ^{-1}, but does not depend on m and or T.

[a] See [43, XVIII §5 3, p. 561 ff.].
[b] See [43, XVIII §5 3.1, Lem. 2, p. 562].
[c] See [43, XVIII §5 3.3, Lem. 4, p. 564], [43, XVIII §5 4.2, Rem. 5, p. 569] and the subsequence argument in [43, XVIII §5 3.5, p. 566].

Proof of Remark A.6. The existence of the sequence $(\vartheta_m)_{m \in \mathbb{N}}$ follows from [43, XVIII §5 3.1, Lem. 2, p. 562]. The convergence results (A.16) follow from [43, XVIII §5 3.3, Lem. 4, p. 564], [43, XVIII §5 4.2, Rem. 5, p. 569] and the subsequence argument in [43, XVIII §5 3.5, p. 566].

We need to prove only the bound in (A.17).

> Test equation (A.15) with $\varphi = \vartheta_m'$ and apply Gronwall's inequality.

We test equation (A.15) with $\varphi = \vartheta_m'$ and apply Gronwall's inequality[16] to obtain the desired estimates for ϑ_m, which is a standard procedure (cf. [17, Sec. 3.2, Thm. 3.7, p. 22]).

Let ϑ_m be defined like in the statement such that it fulfills equation (A.15) for all $\varphi \in L^2(I; V_m)$, with initial conditions $\vartheta_m^{(0)}, \vartheta_m^{(1)}$ according to Assumption 2.2 and Remark 2.3.

We test equation (A.15) with $\varphi = \vartheta_m'$, which is an element of the test space $L^2(I; V_m)$ by

---

[16] See Gronwall's inequality B.39.

construction. This yields analogously to the proof of Lemma A.4

$$\int_0^t \frac{\tau}{2} \left(\|\vartheta'_m(s)\|^2_{L^2(\Omega)} \right)' + \|\vartheta'_m(s)\|^2_{L^2(\Omega)} + \frac{\kappa}{2} \left(\|\nabla\vartheta_m(s)\|^2_{L^2(\Omega)} \right)' + \left(\left\| \sqrt{\xi}\vartheta_m(s) \right\|_{L^2(\Omega)} \right)' \mathrm{d}s$$
$$+ \int_0^t \left(\|\sqrt{a_\mathrm{h}}\vartheta_m(s)\|^2_{L^2(\Gamma)} \right)' \mathrm{d}s = \int_0^t \int_\Omega r(s)\vartheta'_m(s)\,\mathrm{d}x + \int_\Gamma g(s)\vartheta'_m(s)\,\mathrm{d}\hat{s}\,\mathrm{d}s\,.$$

Thus, with the bounds on the coefficients in Assumption 2.2, Lemma B.23, and Hölder's and Young's inequalities[17], we get

$$\|\vartheta'_m(t)\|^2_{L^2(\Omega)} + \|\vartheta_m(t)\|^2_{H^1(\Omega)} \le C(\tau^{-1}) \left(C_1 + \int_0^t \|\vartheta'_m(s)\|^2_{H^1(\Omega)}\,\mathrm{d}s \right)$$

for a.a. $t \in I$ with

$$C_1 := \left\| \vartheta^{(0)} \right\|^2_{H^1(\Omega)} + \left\| \vartheta^{(1)} \right\|^2_{L^2(\Omega)} + \|r\|^2_{L^2(I;L^2(\Omega))} + \|g\|^2_{L^2(I;L^2(\Gamma))}\,.$$

We note that the constant $C(\tau^{-1})$ does not depend on m or T. Now we apply Gronwall's inequality and get the desired estimate

$$\|\vartheta'_m(t)\|^2_{L^2(\Omega)} + \|\vartheta_m(t)\|^2_{H^1(\Omega)} \le C_1 C(\tau^{-1}) \exp(TC(\tau^{-1}))\,.$$

■

Proof of Lemma A.4. First, we apply a standard result for evolution problems of second order in t in [43, XVIII §5, p. 552 ff.] to show $\vartheta \in W_\vartheta$. Second, we use a bootstrap argument to show $\vartheta \in \mathcal{C}^0(\overline{Q})$, following the idea of [114, Sec. 2.3.2, Lem. 2.3.18, p. 22].

1.

> Apply a standard result for evolution problems of second order in t, based on a Faedo–Galerkin procedure, see [43, XVIII §5, p. 552 ff.].

The existence and uniqueness of a solution $\vartheta \in W_\vartheta$ is given by [43, XVIII §5 1.3, Thm. 1, p. 558][18] [19]. We need to show only that the Cattaneo equation (A.9) fulfills the prerequisites. The cited theorem covers a very general scenario.

We need to show that $F_\mathrm{h}\colon H^1(\Omega) \times H^1(\Omega) \to \mathbb{R}$ is a symmetric, continuous and coercive bilinear form. Furthermore, we need to show that

$$f_Q\colon L^2(I; H^1(\Omega)) \to \mathbb{R}, \varphi \mapsto \int_0^T (r(t), \varphi(t))_{L^2(\Omega)} + (g(t), \varphi(t))_{L^2(\Gamma)}\,\mathrm{d}t$$

is an element of $L^2(I; H^1(\Omega)^*)$, see [43, XVIII §5 4.2, Rem. 4, p. 568].

---

[17] See Hölder's B.27 and Young's B.25 inequalities.

[18] The cited theorem is stated in terms of distributional time derivatives. [43, XVIII §5 2.1, Rem. 2, p. 559] explains the connection to an operator formulation in $L^2(I; H^1(\Omega)^*)$ like considered here, which is based on Lemma B.37.

[19] We note that $\tau > 0$ is explicitly required in order to apply the cited theorem, see [43, XVIII §5 1.2.3, Eq. 5.11, p. 553].

Let $\varphi, \hat{\varphi} \in H^1(\Omega)$. The form F_{h} is a bilinear form as sum of inner products. With the bounds on the coefficients (2.20), Hölder's inequality[20] and the trace theorem[21], we get the continuity of F_{h} from

$$
\begin{aligned}
|F_{\mathrm{h}}(\varphi, \hat{\varphi})| &\leq \left| \int_\Omega \kappa \nabla\varphi \cdot \nabla\hat{\varphi} \, \mathrm{d}x \right| + \left| \int_\Omega \xi \varphi\hat{\varphi} \, \mathrm{d}x \right| + \left| \int_\Gamma a_{\mathrm{h}} \varphi\hat{\varphi} \, \mathrm{d}s \right| \\
&\leq \kappa \int_\Omega |\nabla\varphi \cdot \nabla\hat{\varphi}| \, \mathrm{d}x + \overline{\xi} \int_\Omega |\varphi\hat{\varphi}| \, \mathrm{d}x + \overline{a_{\mathrm{h}}} \int_\Gamma |\varphi\hat{\varphi}| \, \mathrm{d}s \\
&\leq C \left(\|\nabla\varphi\|_{L^2(\Omega)} \|\nabla\hat{\varphi}\|_{L^2(\Omega)} + \|\varphi\|_{L^2(\Omega)} \|\hat{\varphi}\|_{L^2(\Omega)} + \|\varphi\|_{L^2(\Gamma)} \|\hat{\varphi}\|_{L^2(\Gamma)} \right) \\
&\leq C \|\varphi\|_{H^1(\Omega)} \|\hat{\varphi}\|_{H^1(\Omega)},
\end{aligned}
\tag{A.18}
$$

and the coercivity from

$$
F_{\mathrm{h}}(\varphi, \varphi) \geq \kappa \int_\Omega \nabla\varphi \cdot \nabla\varphi \, \mathrm{d}x + \underline{\xi} \int_\Omega \varphi^2 \, \mathrm{d}x + \underline{a_{\mathrm{h}}} \int_\Gamma \varphi^2 \, \mathrm{d}s \geq c \|\varphi\|_{H^1(\Omega)}^2.
$$

We look at the right-hand side and get with Hölder's inequality and the trace theorem that

$$
\begin{aligned}
& \left| \langle f_Q, \varphi \rangle_{L^2(I;H^1(\Omega))} \right| \\
&= \left| \int_0^T (r(t), \varphi(t))_{L^2(\Omega)} + (g(t), \varphi(t))_{L^2(\Gamma)} \, \mathrm{d}t \right| \\
&\leq \int_0^T \|r(t)\|_{L^2(\Omega)} \|\varphi(t)\|_{L^2(\Omega)} + \|g(t)\|_{L^2(\Gamma)} \|\varphi(t)\|_{L^2(\Gamma)} \, \mathrm{d}t \\
&\leq \left(\|r\|_{L^2(I;L^2(\Omega))} + \|g\|_{L^2(I;L^2(\Gamma))} \right) \|\varphi\|_{L^2(I;H^1(\Omega))}
\end{aligned}
$$

for all $\varphi \in L^2(I; H^1(\Omega))$. This implies

$$
\|f_Q\|_{L^2(I;H^1(\Omega))^*} \leq \|r\|_{L^2(I;L^2(\Omega))} + \|g\|_{L^2(I;L^2(\Gamma))},
\tag{A.19}
$$

and with Theorem B.48 we identify $f_Q \in L^2(I; H^1(\Omega))^* = L^2(I; H^1(\Omega)^*)$.

This allows us to apply [43, XVIII §5 1.3, Thm. 1, p. 558] and obtain the existence of a unique solution, with the properties discussed in the following.

Let $\vartheta, \hat{\vartheta}$ be the solutions to given data $\vartheta^{(0)}, \vartheta^{(1)}, f_Q$ and $\hat{\vartheta}^{(0)}, \hat{\vartheta}^{(1)}, \hat{f}_Q$. Then [43, XVIII §5 4.2, Thm. 2, p. 567] yields the estimate

$$
\begin{aligned}
& \left\| \vartheta - \hat{\vartheta} \right\|_{L^\infty(I;H^1(\Omega))} + \left\| \vartheta' - \hat{\vartheta}' \right\|_{L^\infty(I;L^2(\Omega))} + \left\| \vartheta' - \hat{\vartheta}' \right\|_{L^2(I;H^1(\Omega))} \\
& \leq C(T) \left(\left\| \vartheta^{(0)} - \hat{\vartheta}^{(0)} \right\|_{H^1(\Omega)} + \left\| \vartheta^{(1)} - \hat{\vartheta}^{(1)} \right\|_{L^2(\Omega)} + \left\| f_Q - \hat{f}_Q \right\|_{L^2(I;H^1(\Omega)^*)} \right)
\end{aligned}
\tag{A.20}
$$

for some constant $C(T) \in \mathbb{R}_{>0}$. Especially, we get that the solution $\vartheta \in W_\vartheta$ fulfills[22]

$$
\vartheta \in L^\infty(I; H^1(\Omega)) \cap W^{1,\infty}(I; L^2(\Omega)) \cap H^1(I; H^1(\Omega)).
$$

---

[20] See Hölder's inequality B.27.
[21] See the trace theorem B.53.
[22] See also [43, XVIII §5 3.5, Eq. 5.80, p. 566].

If we choose the initial conditions $\hat{\vartheta}^{(0)}$, $\hat{\vartheta}^{(1)}$ and the right-hand side in the Cattaneo equation (A.9) to be zero, i.e., $r = 0$ and $g = 0$, we obtain the unique[23] solution $\hat{\vartheta} = 0$. We use this in estimate (A.20) and obtain similar bounds for the state:

$$
\|\vartheta\|_{L^\infty(I;H^1(\Omega))} + \|\vartheta'\|_{L^\infty(I;L^2(\Omega))} + \|\vartheta'\|_{L^2(I;H^1(\Omega))}
$$
$$
\leq C(T) \left(\left\|\vartheta^{(0)}\right\|_{H^1(\Omega)} + \left\|\vartheta^{(1)}\right\|_{L^2(\Omega)} + \|f_Q\|_{L^2(I;H^1(\Omega)^*)} \right). \tag{A.21}
$$

We use the Cattaneo equation (A.9), Hölder's inequality and the estimates (A.18) and (A.21) to obtain an estimate for ϑ'':

$$
\left| \langle \vartheta'', \varphi \rangle_{L^2(I;H^1(\Omega))} \right|
$$
$$
\leq \frac{1}{\tau} \left(\int_0^T \left| (\vartheta'(t), \varphi(t))_{L^2(\Omega)} \right| + |F_{\mathrm{h}}(\vartheta(t), \varphi(t))| \, \mathrm{d}t + \left| \langle f_Q, \varphi \rangle_{L^2(I;H^1(\Omega))} \right| \right)
$$
$$
\leq \frac{1}{\tau} \left(\|\vartheta'\|_{L^2(I;L^2(\Omega))} + \|\vartheta\|_{L^2(I;H^1(\Omega))} + \|f_Q\|_{L^2(I;H^1(\Omega)^*)} \right) \|\varphi\|_{L^2(I;H^1(\Omega))}
$$
$$
\leq C(\tau^{-1}, T) \left(\left\|\vartheta^{(0)}\right\|_{H^1(\Omega)} + \left\|\vartheta^{(1)}\right\|_{L^2(\Omega)} + \|f_Q\|_{L^2(I;H^1(\Omega)^*)} \right) \|\varphi\|_{L^2(I;H^1(\Omega))} \tag{A.22}
$$

for all $\varphi \in L^2(I; H^1(\Omega))$.

The estimate in (A.10) now follows directly from the estimates (A.19), (A.21) and (A.22).

2. Note that we can specify the dependence of the constant $C(T)$ on the final time T in the case where g is constant in time. We test the Cattaneo equation (A.9) with $\varphi := \vartheta' \in L^2(I; H^1(\Omega))$ and get with integration by parts[24], Lemma B.23 on equivalent norms in $H^1(\Omega)$, the trace theorem and Hölder's and Young's[25] inequalities that[26]

$$
\tau \frac{1}{2} \|\vartheta'(t)\|^2_{L^2(\Omega)} + \frac{1}{2} \|\vartheta(t)\|^2_{H^1(\Omega)}
$$
$$
\leq C \left(\int_0^t (r(s), \vartheta'(s))_{L^2(\Omega)} \, \mathrm{d}s + \int_0^t (g, \vartheta'(s))_{L^2(\Gamma)} \, \mathrm{d}s + \left\|\vartheta^{(0)}\right\|^2_{H^1(\Omega)} + \left\|\vartheta^{(1)}\right\|^2_{L^2(\Omega)} \right)
$$
$$
= C \Big(\int_0^t (r(s), \vartheta'(s))_{L^2(\Omega)} \, \mathrm{d}s + (g, \vartheta(t))_{L^2(\Gamma)} - \left(g, \vartheta^{(0)}\right)_{L^2(\Gamma)}
$$
$$
\qquad + \left\|\vartheta^{(0)}\right\|^2_{H^1(\Omega)} + \left\|\vartheta^{(1)}\right\|^2_{L^2(\Omega)} \Big)
$$
$$
\leq C \Big(\frac{1}{2} \|r\|^2_{L^2(I;L^2(\Omega))} + \frac{1}{2} \int_0^t \|\vartheta'(s)\|^2_{L^2(\Omega)} \, \mathrm{d}s + (\frac{1}{4\varepsilon} + \frac{1}{2}) \|g\|^2_{L^2(\Gamma)} + \frac{1}{2} \left\|\vartheta^{(0)}\right\|^2_{L^2(\Gamma)}
$$
$$
\qquad + \left\|\vartheta^{(0)}\right\|^2_{H^1(\Omega)} + \left\|\vartheta^{(1)}\right\|^2_{L^2(\Omega)} + \varepsilon \|\vartheta(t)\|^2_{H^1(\Omega)} \Big)
$$
$$
=: C_1 + C_2 \int_0^t \|\vartheta'(s)\|^2_{L^2(\Omega)} \, \mathrm{d}s + \tilde{\varepsilon} \|\vartheta(t)\|^2_{H^1(\Omega)}
$$

---

[23] See [43, XVIII §5 1.3, Thm. 1, p. 558].

[24] See Theorem B.36 on the integration by parts in Bochner spaces, which especially implies $\int_0^t \langle \vartheta''(s), \vartheta'(s) \rangle_{H^1(\Omega)} \, \mathrm{d}s = \|\vartheta'(t)\|^2_{L^2(\Omega)} - \|\vartheta'(0)\|^2_{L^2(\Omega)}$.

[25] See Young's inequality B.25.

[26] Since the function ϑ fulfills equation (A.9) for all $\varphi \in L^2(I; H^1(\Omega))$, it especially fulfills the equation for all test functions which are zero on $(t, T] \subset I$, thus, we can consider the integral from 0 to t for all $t \in [0, T]$, cf. [93, Sec. 1.3.2.3, Thm. 1.33, p. 42].

for a.a. $t \in I$ and arbitrary $\varepsilon > 0$, where the constants C_1, C_2 above depend on the domain Ω and on the bounds for the coefficients in F_h but not on the final time T. Gronwall's inequality[27] now implies

$$\|\vartheta'\|_{L^\infty(I;L^2(\Omega))} + \|\vartheta\|_{L^\infty(I;H^1(\Omega))} \leq \tilde{C}_1 \exp(T\tilde{C}_2),$$

where $\tilde{C}_1, \tilde{C}_2$ depend on τ^{-1} but not on T.

3.

> The higher regularity of ϑ follows from a bootstrap argument: Test the Cattaneo equation (A.9) with $-\Delta\vartheta'$ and use integration by parts to shift inconvenient partial derivatives of ϑ to the "data". Finally, apply standard embedding results for Sobolev spaces.

We follow the idea in [114, Ch. 2.3, p. 19 ff.] to prove certain regularity results in the context of Bochner spaces, which then yield the desired regularity results for ϑ by means of suitable embedding theorems. If we apply this lemma to the auxiliary heat-transfer equation (2.24), note that the situation will be slightly different than in the cited reference and needs to be handled with care because the data r_i might depend on the auxiliary temperature ω. In the proof of Theorem 2.15, the regularity of the data r_i depends on the regularity assumptions on ω and is determined by the overall fixed point argument used therein.

(a) First, we show the desired result for homogeneous boundary conditions, i.e., we assume $g = 0$ for the moment.

We consider the spaces $V_m := \mathrm{span}\{\omega_k \mid k = 1, \ldots, m\}$ for $m \in \mathbb{N}$, where $(\omega_k)_{k\in\mathbb{N}}$ are the eigenfunctions of the Laplacian according to Lemma A.1. The solution ϑ can be approximated by a sequence $(\vartheta_m)_{m\in\mathbb{N}} \subset L^2(I; V_m)$ such that $\vartheta_m = \sum_{k=1}^m g_{km}(t) w_k$ for certain $g_{km} \in H^2(I)$, according to Remark A.6. In the following, we prove auxiliary regularity results for the elements ϑ_m and then pass to the limit $m \to \infty$.

Because a_h is constant in time, we get with the boundary conditions $a_\mathrm{h}\omega_k + \kappa\nabla\omega_k \cdot \boldsymbol{n} = 0$ for all $k \in \mathbb{N}$ in Lemma A.1 and with the expansion of ϑ_m that

$$\left.\begin{aligned} \nabla\vartheta_m(t) \cdot \boldsymbol{n} &= -\frac{1}{\kappa}a_\mathrm{h}\vartheta_m(t), \\ \nabla\vartheta'_m(t) \cdot \boldsymbol{n} &= -\frac{1}{\kappa}a_\mathrm{h}\vartheta'_m(t) \end{aligned}\right\} \quad \text{a.e. on } \Gamma \quad \text{for a.a. } t \in I \tag{A.23}$$

for all $m \in \mathbb{N}$. Note that the evaluation of $\nabla\vartheta_m(t) \cdot \boldsymbol{n}$ and $\nabla\vartheta'_m(t) \cdot \boldsymbol{n}$ on the boundary Γ is well defined because, with $\vartheta_m(t), \vartheta'_m(t) \in V_m \subset H^2(\Omega)$, we have $\nabla\vartheta_m(t) \cdot \boldsymbol{n}$ and $\nabla\vartheta'_m(t) \cdot \boldsymbol{n} \in H^1(\Omega) \hookrightarrow W^{\frac{1}{2},2}(\Gamma)$, where the last embedding follows from the trace theorem.

---

[27] See Gronwall's inequality B.39.

As a prerequisite, we reformulate the boundary conditions in the weak formulation. Note that the spatial regularity $\omega_k \in H^2(\Omega)$ allows us to apply integration by parts[28] and to rewrite

$$(\nabla \vartheta_m(t), \nabla \varphi)_{L^2(\Omega)} = - (\Delta \vartheta_m(t), \varphi)_{L^2(\Omega)} + (\nabla \vartheta_m(t) \cdot \boldsymbol{n}, \varphi)_{L^2(\Gamma)} \qquad (A.24)$$

for all $\varphi \in H^1(\Omega)$ and for a.a. $t \in I$.

(b) The key idea now is to test equation (A.15) with $\varphi = -\Delta \vartheta'_m$ like in [114, Sec. 2.3.2, Lem. 2.3.18, p. 22]. Note that the choice of V_m ensures that $\Delta \vartheta'_m = \sum_{k=1}^m g'_{km} \Delta \omega_k$ is indeed an element of the test space $L^2(I; V_m)$.

We reformulate the evolution equation for ϑ_m (A.15), integrated only[29] from 0 to $t \in I$ and tested with $\varphi = -\Delta \vartheta'_m$, by means of the integration-by-parts formula (A.24) and obtain

$$\int_0^t \tau \underbrace{(\vartheta''_m(s), -\Delta \vartheta'_m(s))_{L^2(\Omega)}}_{I} + \underbrace{(\vartheta'_m(s), -\Delta \vartheta'_m(s))_{L^2(\Omega)}}_{II}$$

$$- \kappa \underbrace{(\Delta \vartheta_m(s), -\Delta \vartheta'_m(s))_{L^2(\Omega)}}_{III} \, \mathrm{d}s$$

$$= \int_0^t \underbrace{(r_1(s), -\Delta \vartheta'_m(s))_{L^2(\Omega)}}_{IV} + \underbrace{(r_2(s), -\Delta \vartheta'_m(s))_{L^2(\Omega)}}_{V} - \underbrace{(\xi \vartheta_m(s), -\Delta \vartheta'_m(s))_{L^2(\Omega)}}_{VI} \, \mathrm{d}s$$

$$+ \int_0^t \underbrace{(g(s) - \kappa \nabla \vartheta_m(s) \cdot \boldsymbol{n} - a_{\mathrm{h}} \vartheta_m(s), -\Delta \vartheta'_m(s))_{L^2(\Gamma)}}_{VII} \, \mathrm{d}s \, .$$

In the following, we consider the resulting terms individually.

For the following calculations, we use Hölder's and Young's inequalities along with a few rules of calculus in the context of Bochner spaces, see Appendix B.1.2:

- $\left(\|\vartheta_m(t)\|^2_{L^2(\Omega)} \right)' = 2 \, (\vartheta'_m(t), \vartheta_m(t))_{L^2(\Omega)}$,
- $f(t) = f(0) + \int_0^t f'(s) \, \mathrm{d}s$.
- $\mathrm{D}_{x_i}(\vartheta'_m(t)) = (\mathrm{D}_{x_i} \vartheta_m(t))'$ (short notation, see Lemma B.40 for details).

(I) By definition it holds $\vartheta''_m(t) \in V_m$. With $\vartheta'_m(0) = \vartheta_m^{(1)}$ in (A.15), we get

$$\int_0^t \tau \, (\vartheta''_m(s), -\Delta \vartheta'_m(s))_{L^2(\Omega)} \, \mathrm{d}s$$

$$= \tau \int_0^t (\nabla \vartheta''_m(s), \nabla \vartheta'_m(s))_{L^2(\Omega)} \, \mathrm{d}s - \tau \int_0^t (\vartheta''_m(s), \nabla \vartheta'_m(s) \cdot \boldsymbol{n})_{L^2(\Gamma)} \, \mathrm{d}s$$

$$= \tau \int_0^t \frac{1}{2} \left(\|\nabla \vartheta'_m(s)\|^2_{L^2(\Omega)} \right)' \mathrm{d}s - \tau \int_0^t (\vartheta''_m(s), \nabla \vartheta'_m(s) \cdot \boldsymbol{n})_{L^2(\Gamma)} \, \mathrm{d}s$$

$$= \tau \frac{1}{2} \left(\|\nabla \vartheta'_m(t)\|^2_{L^2(\Omega)} - \left\|\nabla \vartheta_m^{(1)}\right\|^2_{L^2(\Omega)} \right) - \tau \int_0^t (\vartheta''_m(s), \nabla \vartheta'_m(s) \cdot \boldsymbol{n})_{L^2(\Gamma)} \, \mathrm{d}s \, .$$

---

[28] See Theorem B.35 on the integration by parts in Sobolev spaces.

[29] Since the functions ϑ_m fulfill equation (A.15) for all $\varphi \in L^2(I; V_m)$, they especially fulfill the equation for all test functions which are zero on (t, T), thus, we can consider the integral from 0 to t for all $t \in [0, T]$, cf. [93, Sec. 1.3.2.3, Thm. 1.33, p. 42].

With the boundary conditions in (A.23), Hölder's and Young's inequalities and integration by parts[30], we obtain for the boundary term

$$
\begin{aligned}
-\tau \int_0^t \left(\vartheta_m''(s), \nabla\vartheta_m'(s)\cdot\boldsymbol{n}\right)_{L^2(\Gamma)} \mathrm{d}s &= \frac{\tau}{\kappa} \int_0^t \left(\vartheta_m''(s), a_\mathrm{h}\vartheta_m'(s)\right)_{L^2(\Gamma)} \mathrm{d}s \\
&= \frac{\tau}{\kappa} \int_0^t \frac{1}{2}\left(\left\|\sqrt{a_\mathrm{h}}\vartheta_m'(s)\right\|_{L^2(\Gamma)}^2\right)' \mathrm{d}s \\
&= \frac{\tau}{2\kappa}\left(\left\|\sqrt{a_\mathrm{h}}\vartheta_m'(t)\right\|_{L^2(\Gamma)}^2 - \left\|\sqrt{a_\mathrm{h}}\vartheta_m^{(1)}\right\|_{L^2(\Gamma)}^2\right) \\
&\geq \frac{\tau}{2\kappa}\left(\underline{a_\mathrm{h}}\left\|\vartheta_m'(t)\right\|_{L^2(\Gamma)}^2 - \overline{a_\mathrm{h}}\left\|\vartheta_m^{(1)}\right\|_{L^2(\Gamma)}^2\right).
\end{aligned}
$$

(II) With the boundary conditions in (A.23), we get

$$
\begin{aligned}
&\int_0^t \left(\vartheta_m'(s), -\Delta\vartheta_m'(s)\right)_{L^2(\Omega)} \mathrm{d}s \\
&= \int_0^t \left(\nabla\vartheta_m'(s), \nabla\vartheta_m'(s)\right)_{L^2(\Omega)}^2 \mathrm{d}s - \int_0^t \left(\vartheta_m'(s), \nabla\vartheta_m'(s)\cdot\boldsymbol{n}\right)_{L^2(\Gamma)} \mathrm{d}s \\
&= \int_0^t \left\|\nabla\vartheta_m'(s)\right\|_{L^2(\Omega)}^2 \mathrm{d}s + \frac{1}{\kappa}\int_0^t \left(\vartheta_m'(s), a_\mathrm{h}\vartheta_m'(s)\right)_{L^2(\Gamma)} \mathrm{d}s \\
&\geq \int_0^t \left\|\nabla\vartheta_m'(s)\right\|_{L^2(\Omega)}^2 \mathrm{d}s + \frac{\underline{a_\mathrm{h}}}{\kappa}\int_0^t \left\|\vartheta_m'(s)\right\|_{L^2(\Gamma)}^2 \mathrm{d}s \\
&\geq 0.
\end{aligned}
$$

(III) It holds

$$
\begin{aligned}
-\int_0^t \kappa\left(\Delta\vartheta_m(s), -\Delta\vartheta_m'(s)\right)_{L^2(\Omega)} \mathrm{d}s &= \kappa\int_0^t \frac{1}{2}\left(\left\|\Delta\vartheta_m(s)\right\|_{L^2(\Omega)}^2\right)' \mathrm{d}s \\
&= \frac{\kappa}{2}\left(\left\|\Delta\vartheta_m(t)\right\|_{L^2(\Omega)}^2 - \left\|\Delta\vartheta_m^{(0)}\right\|_{L^2(\Omega)}^2\right).
\end{aligned}
$$

(IV) The boundary conditions in (A.23) and the integration by parts in (A.24) imply

$$
\begin{aligned}
&\left(r_1(t), -\Delta\vartheta_m'(t)\right)_{L^2(\Omega)} \\
&= \left(\nabla r_1(t), \nabla\vartheta_m'(t)\right)_{L^2(\Omega)} - \left(r_1(t), \nabla\vartheta_m'\cdot\boldsymbol{n}\right)_{L^2(\Gamma)} \quad\quad (A.25) \\
&= \left(\nabla r_1(t), \nabla\vartheta_m'(t)\right)_{L^2(\Omega)} + \frac{1}{\kappa}\left(r_1(t), a_\mathrm{h}\vartheta_m'(t)\right)_{L^2(\Gamma)}
\end{aligned}
$$

for a.a. $t \in I$.

With r_1 and $\Delta\vartheta_m$ being elements of $L^2(I; L^2(\Omega))$ we get with Hölder's inequality that[31] $r_1\Delta\vartheta_m \in L^1(I; L^1(\Omega)) \stackrel{\cong}{=} L^1(Q)$ and, especially, that $t \mapsto (r_1(t), \Delta\vartheta_m(t))_{L^2(\Omega)}$ is Lebesgue measurable according to Fubini's theorem[32].

With this, also the map

$$
t \mapsto \left(\nabla r_1(t), \nabla\vartheta_m'(t)\right)_{L^2(\Omega)} + \frac{1}{\kappa}\left(r_1(t), a_\mathrm{h}\vartheta_m'(t)\right)_{L^2(\Gamma)}
$$

---

[30] See Theorem B.36 on the integration by parts in Bochner spaces.
[31] See Lemma B.49 on the relation between Bochner and Lebesgue spaces.
[32] See Fubini's theorem B.2.

is Lebesgue measurable. The assumptions on r_1 given in the statement, Hölder's and Young's inequalities, the trace theorem and equation (A.25) imply that

$$
\begin{aligned}
\left|(r_1(t), -\Delta\vartheta_m'(t))_{L^2(\Omega)}\right| &\leq C\left(\|r_1(t)\|_{H^1(\Omega)}^2 + \|\vartheta_m'(t)\|_{H^1(\Omega)}^2\right) \\
&\leq C\left(\tilde{r}(t)^2 + \|\vartheta_m'(t)\|_{H^1(\Omega)}^2\right)
\end{aligned}
\tag{A.26}
$$

for a.a $t \in I$. With $\tilde{r} \in L^2(I)$, we can integrate both sides in (A.26) and obtain the estimate

$$
\int_0^t \left|(r_1(s), -\Delta\vartheta_m'(s))_{L^2(\Omega)}\right| \, ds \leq C\left(\|\tilde{r}\|_{L^2(I)}^2 + \int_0^t \|\vartheta_m'(s)\|_{H^1(\Omega)}^2 \, ds\right).
$$

(V) With integration by parts[33], the initial condition $\vartheta_m(0) = \vartheta_m^{(0)}$ and Hölder's and Young's inequalities, we get

$$
\begin{aligned}
&\left|\int_0^t (r_2(s), -\Delta\vartheta_m'(s))_{L^2(\Omega)} \, ds\right| \\
&= \left|\int_0^t (r_2'(s), \Delta\vartheta_m(s))_{L^2(\Omega)} \, ds - (r_2(t), \Delta\vartheta_m(t))_{L^2(\Omega)} + \left(r_2(0), \Delta\vartheta_m^{(0)}\right)_{L^2(\Omega)}\right| \\
&\leq \left(\frac{1}{4\varepsilon} + \frac{1}{2}\right)\|r_2\|_{L^\infty(I;L^2(\Omega))}^2 + \frac{1}{2}\left\|\Delta\vartheta_m^{(0)}\right\|_{L^2(\Omega)}^2 + \frac{1}{2}\|r_2'\|_{L^2(I;L^2(\Omega))}^2 \\
&\quad + \varepsilon\|\Delta\vartheta_m(t)\|_{L^2(\Omega)}^2 + \frac{1}{2}\int_0^t \|\Delta\vartheta_m(s)\|_{L^2(\Omega)}^2 \, ds
\end{aligned}
$$

for all $\varepsilon > 0$. The evaluation of $r_2(t)$ and $r_2(0)$ in the computation above is well defined because of the continuous embedding[34] $H^1(I;L^2(\Omega)) \hookrightarrow \mathcal{C}^0(\overline{I};L^2(\Omega))$, and it holds[35]

$$
\|r_2\|_{L^\infty(I;L^2(\Omega))} \leq C\|r_2\|_{\mathcal{C}^0(\overline{I};L^2(\Omega))} \leq C\|r_2\|_{H^1(I;L^2(\Omega))} < \infty.
$$

(VI) With ξ being constant in time, $\vartheta_m(0) = \vartheta_m^{(0)}$, integration by parts and Hölder's and Young's inequalities, we get

$$
\begin{aligned}
&\left|\int_0^t (\xi\vartheta_m(s), \Delta\vartheta_m'(s))_{L^2(\Omega)} \, ds\right| \\
&= \left| -\int_0^t ((\xi\vartheta_m(s))', \Delta\vartheta_m(s))_{L^2(\Omega)} \, ds + (\xi\vartheta_m(t), \Delta\vartheta_m(t))_{L^2(\Omega)} \right. \\
&\quad \left. - \left(\xi\vartheta_m^{(0)}, \Delta\vartheta_m^{(0)}\right)_{L^2(\Omega)}\right| \\
&\leq \frac{1}{2}\overline{\xi}^2\|\vartheta_m'\|_{L^2(I;L^2(\Omega))}^2 + \frac{1}{2}\int_0^t \|\Delta\vartheta_m(s)\|_{L^2(\Omega)}^2 \, ds + \frac{1}{4\varepsilon}\overline{\xi}^2\|\vartheta_m(t)\|_{L^2(\Omega)}^2 \\
&\quad + \varepsilon\|\Delta\vartheta_m(t)\|_{L^2(\Omega)}^2 + \frac{1}{2}\overline{\xi}^2\left\|\vartheta_m^{(0)}\right\|_{L^2(\Omega)}^2 + \frac{1}{2}\left\|\Delta\vartheta_m^{(0)}\right\|_{L^2(\Omega)}^2.
\end{aligned}
$$

Note that we can bound $\|\vartheta_m(t)\|_{L^2(\Omega)}$ and $\|\vartheta_m'\|_{L^2(I;L^2(\Omega))}$ by means of the classical state bounds (A.17).

---

[33] See the integration by parts in Bochner spaces B.36.
[34] See the classical embedding theorem B.33.
[35] See classical embedding in Lemma B.52.

(VII) With the boundary conditions in (A.23) and the assumption $g = 0$ it holds

$$\int_0^t \left(\underbrace{g(s)}_{=0} \underbrace{-\kappa \nabla \vartheta_m(s) \cdot \boldsymbol{n} - a_{\mathrm{h}} \vartheta_m(s)}_{=0}, -\Delta \vartheta'_m(s) \right)_{L^2(\Gamma)} \mathrm{d}s = 0.$$

We combine the auxiliary results above and get with the trace theorem, Lemma B.23 on equivalent norms in $H^1(\Omega)$, the following bounds

$$\left\| \vartheta_m^{(0)} \right\|_{H^1(\Omega)} \leq \left\| \vartheta^{(0)} \right\|_{H^1(\Omega)},$$

$$\left\| \Delta \vartheta_m^{(0)} \right\|_{L^2(\Omega)} \leq C \left\| \Delta \vartheta^{(0)} \right\|_{L^2(\Omega)},$$

$$\left\| \vartheta_m^{(1)} \right\|_{H^1(\Omega)} \leq \left\| \vartheta^{(1)} \right\|_{H^1(\Omega)}$$

from Remark 2.3, and $\|r_1\|_{L^2(I;L^2(\Omega))} \leq C \|\tilde{r}\|_{L^2(I)}$ that

$$\|\vartheta'_m(t)\|^2_{H^1(\Omega)} + \|\Delta \vartheta_m(t)\|^2_{L^2(\Omega)}$$

$$\leq \tilde{C}_1 \exp(\tilde{C}_2 T) \Big(\left\| \vartheta^{(0)} \right\|^2_{H^2(\Omega)} + \left\| \vartheta^{(1)} \right\|^2_{H^1(\Omega)}$$

$$+ \|r_2\|^2_{H^1(I;L^2(\Omega))} + \|\tilde{r}\|^2_{L^2(I)}$$

$$+ \int_0^t \|\vartheta'_m(s)\|^2_{H^1(\Omega)} \, \mathrm{d}s + \int_0^t \|\Delta \vartheta_m(s)\|^2_{L^2(\Omega)} \, \mathrm{d}s \Big)$$

$$=: C_1(T) + C_2(T) \int_0^t \|\vartheta'_m(s)\|^2_{H^1(\Omega)} + \|\Delta \vartheta_m(s)\|^2_{L^2(\Omega)} \, \mathrm{d}s$$

for a.a. $t \in I$, where $\tilde{C}_1, \tilde{C}_2$ do not depend on m or the final time T.

We apply Gronwall's inequality[36] to $t \mapsto \|\vartheta'_m(t)\|^2_{H^1(\Omega)} + \|\Delta \vartheta_m(t)\|^2_{L^2(\Omega)}$ and get

$$\|\vartheta'_m(t)\|^2_{H^1(\Omega)} + \|\Delta \vartheta_m(t)\|^2_{L^2(\Omega)} \leq C_1(T) \exp\left(T C_2(T)\right) \tag{A.27}$$

with $C_1(T), C_2(T)$ as given above. Note that the set $\{ C_1(\tilde{T}) \exp\left(C_2(\tilde{T})\tilde{T} \right) \mid \tilde{T} \in I \}$ is bounded by $C_1(T) \exp\left(C_2(T)T \right)$.

The boundary conditions in (A.23) yield together with the Sobolev embeddings B.56, the embedding[37] $H^1(\Omega) \hookrightarrow W^{\frac{1}{2},2}(\Gamma)$ and $a_{\mathrm{h}} \in \mathcal{C}^0(\overline{\Gamma})$ (Assumption 2.2) that

$$\|\nabla \vartheta_m(t) \cdot \boldsymbol{n}\|_{W^{\frac{1}{2},2}(\Gamma)} = \kappa^{-1} \|a_{\mathrm{h}} \vartheta_m(t)\|_{W^{\frac{1}{2},2}(\Gamma)} \leq \kappa^{-1} \overline{a_{\mathrm{h}}} \|\vartheta_m(t)\|_{H^1(\Omega)}.$$

The regularity result in Theorem B.62 now implies

$$\|\vartheta_m(t)\|_{H^2(\Omega)} \leq C \left(\|\Delta \vartheta_m(t)\|_{L^2(\Omega)} + (1 + \kappa^{-1} \overline{a_{\mathrm{h}}}) \|\vartheta_m(t)\|_{H^1(\Omega)} \right) \tag{A.28}$$

for a.a. $t \in I$ and all $m \in \mathbb{N}$, where the constant C is independent of m and T. We can now bound the right-hand side of (A.28) by means of the estimates (A.17) and (A.27).

---

[36] See Gronwall's inequality B.39.
[37] See the trace theorem B.53.

(c) Next, we need to pass to the limit $m \to \infty$ and identify the limit element with the solution.

By construction, ϑ_m and ϑ'_m are simple functions[38], which implies, together with the bounds in (A.27) and (A.28), that

$$\vartheta_m \in L^\infty(I; H^2(\Omega)) \cap W^{1,\infty}(I; H^1(\Omega))$$

for all $m \in \mathbb{N}$.

Lemma A.3 implies that, for $p_1, p_2 \in (1, \infty)$, there is an element

$$\hat{\vartheta} \in L^{p_2}(I; H^2(\Omega)) \cap W^{1,p_1}(I; H^1(\Omega))$$

independent of the particular choices of p_1, p_2, and a subsequence $(\vartheta_{m_l})_{l \in \mathbb{N}}$ such that $\vartheta_{m_l} \rightharpoonup \hat{\vartheta}$ with

$$\left\| \hat{\vartheta} \right\|_{W^{1,p_1}(I;H^1(\Omega))} + \left\| \hat{\vartheta} \right\|_{L^{p_2}(I;H^2(\Omega))}$$
$$\leq C(\tau^{-1}, T) \left((2T)^{\frac{1}{p_1}} + T^{\frac{1}{p_2}} \right) \left(\left\| \vartheta^{(0)} \right\|_{H^2(\Omega)} + \left\| \vartheta^{(1)} \right\|_{H^1(\Omega)} + \|r_2\|_{H^1(I;L^2(\Omega))} + \|\tilde{r}\|_{L^2(I)} \right).$$

Note that this holds analogously for other final times $\tilde{T} \in I$, and the set of corresponding constants $\{C(\tau^{-1}, \tilde{T}) \in \mathbb{R}_{>0} \,|\, \tilde{T} \in I\}$ is bounded. This follows from the estimates (A.27), (A.28) and Lemma A.3.

Furthermore, because of the same Lemma, it holds $\hat{\vartheta} \in \mathcal{C}^{0,\alpha}(\overline{Q})$ for $\alpha \in [0, \frac{1}{4})$ with

$$\left\| \hat{\vartheta} \right\|_{\mathcal{C}^{0,\alpha}(\overline{Q})} \leq C(\tau^{-1}, \alpha, T) \left(\left\| \vartheta^{(0)} \right\|_{H^2(\Omega)} + \left\| \vartheta^{(1)} \right\|_{H^1(\Omega)} + \|r_2\|_{H^1(I;L^2(\Omega))} + \|\tilde{r}\|_{L^2(I)} \right).$$

Like above, this holds analogously for other final times $\tilde{T} \in I$, and the set of corresponding constants $\{C(\tau^{-1}, \alpha, \tilde{T}) \in \mathbb{R}_{>0} \,|\, \tilde{T} \in I\}$ is bounded.

With $L^{p_2}(I; H^2(\Omega)) \hookrightarrow L^1(Q)$, $L^2(I; H^1(\Omega)) \hookrightarrow L^1(Q)$ and with the weak convergence in (A.16), we get[39]

$$\vartheta_{m_l} \rightharpoonup \vartheta \quad \text{in } L^1(Q) \quad \text{and} \quad \vartheta_{m_l} \rightharpoonup \hat{\vartheta} \quad \text{in } L^1(Q).$$

The uniqueness of the weak limit[40] implies $\vartheta = \hat{\vartheta}$ in $L^1(Q)$ and, thus, $\vartheta = \hat{\vartheta}$ a.e. in Q. This means that we can identify the solution $\vartheta \in W_\vartheta$ with the limit $\hat{\vartheta}$ and, thus, as an element in $\mathcal{C}^{0,\alpha}(\overline{Q})$ as well as an element in $W^{1,p_1}(I; H^1(\Omega)) \cap L^{p_2}(I; H^2(\Omega))$.

(d) Last, we consider an arbitrary g like given in Assumption 2.2. A standard result from elliptic theory[41] yields a unique solution $\hat{g} \in H^2(\Omega)$ such that

$$F_{\mathrm{h}}(\hat{g}, \varphi) = (g, \varphi)_{L^2(\Gamma)} \tag{A.29}$$

for all $\varphi \in H^1(\Omega)$ and[42]

$$\|\hat{g}\|_{H^2(\Omega)} \leq C \|g\|_{H^{1/2}(\Gamma)}.$$

---

[38] See [93, Sec. 1.3.2.1, Def. 1.22, p. 37] for the definition of simple functions.

[39] See Lemma B.17 on dual spaces of subspaces.

[40] See Remark B.8 on the uniqueness of weak/weak* limits.

[41] See [85, Sec. 2.4.2, Thm. 2.4.2.7, p. 126].

[42] In fact, looking at (A.29), the coercivity of F_{h} yields $\|\hat{g}\|_{H^1(\Omega)} \leq C \|g\|_{L^2(\Gamma)}$. Integration by parts (A.24) and the variational lemma B.6 yield $\kappa \Delta \hat{g} = \xi \hat{g}$ a.e. in Ω and $\nabla \hat{g} \cdot \boldsymbol{n} = \kappa^{-1}(g - a_{\mathrm{h}}\hat{g})$ a.e. on Γ. The estimate in the $H^2(\Omega)$ norm now follows from Theorem B.62: $\|\hat{g}\|_{H^2(\Omega)} \leq C \left(\|\Delta \hat{g}\|_{L^2(\Omega)} + \|g\|_{H^{1/2}(\Gamma)} + (1 + \kappa^{-1}\overline{a_{\mathrm{h}}}) \|\hat{g}\|_{H^1(\Omega)} \right)$.

Let $\vartheta \in W^{1,p_1}(I; H^1(\Omega)) \cap L^{p_2}(I; H^2(\Omega)) \hookrightarrow \mathcal{C}^{0,\alpha}(\overline{Q})$ be the solution of the Cattaneo equation (A.9) for $g = 0$ from above. The function $\hat{\vartheta} := \vartheta + \hat{g}$ fulfills the Cattaneo equation (A.9) for the chosen g. Finally, we obtain the desired estimate in the corresponding norms by means of the triangle inequality and the estimates for the homogeneous solution ϑ from above.

■

A.1.2 Proof of Remark 2.3

Proof. We need to show only the second statement of Remark 2.3.

According to Lemma A.1, it holds $-\Delta \omega_k = \lambda_k \omega_k$ a.e. in Ω and $\kappa \nabla \omega_k \cdot \boldsymbol{n} = -a_{\mathrm{h}} \omega_k$ a.e. on Γ for certain $\lambda_k \in \mathbb{R}$ for all $k \in \mathbb{N}$.

The approximation in $H^1(\Omega)$ follows from Lemma A.1 and the embedding $\vartheta^{(0)} \in H^2(\Omega) \hookrightarrow H^1(\Omega)$. The convergence in $H^1(\Omega)$ implies (w.l.o.g., for $\left\| \vartheta^{(0)} \right\|_{L^2(\Omega)}, \left\| \vartheta^{(1)} \right\|_{L^2(\Omega)} \neq 0$) that

$$\left. \begin{array}{l} \left\| \vartheta_m^{(0)} \right\|_{H^1(\Omega)} \leq C \left\| \vartheta^{(0)} \right\|_{H^1(\Omega)}, \\[2mm] \left\| \vartheta_m^{(1)} \right\|_{H^1(\Omega)} \leq C \left\| \vartheta^{(1)} \right\|_{H^1(\Omega)} \end{array} \right\} \quad \text{for all } m \in \mathbb{N}.$$

Here, with our assumption $g_{\mathrm{h}} = 0$, we get with Assumption 2.2 on the initial condition that $a_{\mathrm{h}} \vartheta^{(0)} + \kappa \nabla \vartheta^{(0)} \cdot \boldsymbol{n} = 0$. Together with the definition of $\vartheta_m^{(0)}$, we get

$$\Delta \vartheta_m^{(0)} = \sum_{k=1}^m \left(\vartheta^{(0)}, \omega_k \right)_{L^2(\Omega)} \Delta \omega_k = \sum_{k=1}^m \left(\vartheta^{(0)}, \omega_k \right)_{L^2(\Omega)} (-\lambda_k) \omega_k$$

$$= \sum_{k=1}^m \left(\vartheta^{(0)}, (-\lambda_k) \omega_k \right)_{L^2(\Omega)} \omega_k = \sum_{k=1}^m \left(\vartheta^{(0)}, \Delta \omega_k \right)_{L^2(\Omega)} \omega_k$$

$$= \sum_{k=1}^m \left(\left(\Delta \vartheta^{(0)}, \omega_k \right)_{L^2(\Omega)} + \left(\vartheta^{(0)}, \nabla \omega_k \cdot \boldsymbol{n} \right)_{L^2(\Gamma)} - \left(\nabla \vartheta^{(0)} \cdot \boldsymbol{n}, \omega_k \right)_{L^2(\Gamma)} \right) \omega_k$$

$$= \sum_{k=1}^m \left(\left(\Delta \vartheta^{(0)}, \omega_k \right)_{L^2(\Omega)} + \left(\vartheta^{(0)}, -\kappa^{-1} a_{\mathrm{h}} \omega_k \right)_{L^2(\Gamma)} - \left(-\kappa^{-1} a_{\mathrm{h}} \vartheta^{(0)}, \omega_k \right)_{L^2(\Gamma)} \right) \omega_k$$

$$= \sum_{k=1}^m \left(\Delta \vartheta^{(0)}, \omega_k \right)_{L^2(\Omega)} \omega_k.$$

The functions ω_k are orthonormal w.r.t. the $L^2(\Omega)$ scalar product, which yields

$$\left\| \Delta \vartheta_m^{(0)} \right\|_{L^2(\Omega)}^2 = \left(\Delta \vartheta_m^{(0)}, \Delta \vartheta_m^{(0)} \right)_{L^2(\Omega)} = \left(\sum_{k=1}^m \left(\Delta \vartheta^{(0)}, \omega_k \right)_{L^2(\Omega)} \omega_k, \sum_{l=1}^m \left(\Delta \vartheta^{(0)}, \omega_l \right)_{L^2(\Omega)} \omega_l \right)_{L^2(\Omega)}$$

$$= \sum_{k=1}^m \left| \left(\Delta \vartheta^{(0)}, \omega_k \right)_{L^2(\Omega)} \right|^2 \leq \sum_{k=1}^\infty \left| \left(\Delta \vartheta^{(0)}, \omega_k \right)_{L^2(\Omega)} \right|^2$$

$$= \left\| \Delta \vartheta^{(0)} \right\|_{L^2(\Omega)}^2,$$

where the last equality is a standard result for orthonormal bases, see [4, Sec. 7.7, p. 305].

■

A.1.3 Proof of Lemma 2.7

Proof.

> Use Fubini's theorem and some calculus in Bochner spaces.

1. Let $\omega \in L^\infty(Q)$ and $t \in I$. This implies $\omega \in L^p(Q)$ for all $p \in [1, \infty)$, and with Fubini's theorem[43] we get[44] for a.a. $x \in \Omega$ that $\omega(\cdot, x) \in L^p(I)$. Thus, $\int_0^t \omega(s, x) \, ds \in \mathbb{R}$ is well defined for a.a. $x \in \Omega$.

   Again Fubini's theorem yields, for fixed $t \in I$, that $x \mapsto \int_0^t \omega(s, x) \, ds \in L^1(\Omega)$, thus, we can define the function $f \colon I \to L^1(\Omega)$, $t \mapsto \int_0^t w(s, \cdot) \, ds$.

   The function f is continuous. In fact, for $t_1, t_2 \in I$, $t_1 < t_2$, the continuity follows with Hölder's inequality[45] from

   $$\|f(t_2) - f(t_1)\|_{L^1(\Omega)} = \int_\Omega \left| \int_{t_1}^{t_2} \omega(s, x) \, ds \right| dx \leq (|t_2 - t_1| \cdot |\Omega|)^{1/2} \cdot \|\omega\|_{L^2(Q)}.$$

   The embeddings in Lemmas B.55, B.52 and B.49 yield

   $$f \in \mathcal{C}^0(\overline{I}; L^1(\Omega)) \hookrightarrow L^\infty(I; \Omega) \hookrightarrow L^1(I; \Omega) \cong L^1(Q).$$

   From this, we get $\phi_2(\omega) \in L^1(Q)$ and, especially, that $\phi_2(\omega)$ is Lebesgue measurable.

   Now

   $$|\phi_2(\omega)(t, x)| = \left| \int_0^t \omega(s, x) \, ds \right| \leq \int_0^T |\omega(s, x)| \, ds \leq T \|\omega\|_{L^\infty(Q)} \quad \text{a.e. in } Q$$

   implies $\phi_2(\omega) \in L^\infty(Q)$.

2. Let $\omega, \hat{\omega} \in L^\infty(Q)$ and $t \in I$. For fixed $x \in \Omega$, we saw earlier in this proof that $(\omega(\cdot, x) - \hat{\omega}(\cdot, x)) \in L^p(I)$, so we can apply Hölder's inequality to obtain

   $$\left(\int_0^t |1 \cdot (\omega(s, x) - \hat{\omega}(s, x))| \, ds \right)^p \leq C \int_0^t |\omega(s, x) - \hat{\omega}(s, x)|^p \, ds$$
   $$\leq C \int_0^T |\omega(s, x) - \hat{\omega}(s, x)|^p \, ds.$$

   Together with the linearity of ϕ_2, this implies

   $$\|\phi_2(\omega) - \phi_2(\hat{\omega})\|_{L^p(Q)}^p = \int_0^T \int_\Omega \left(\left| \int_0^t \omega(s, x) - \hat{\omega}(s, x) \, ds \right| \right)^p dx \, dt$$
   $$\leq C(T) \|\omega - \hat{\omega}\|_{L^p(Q)}^p,$$

   which directly yields estimate (2.17).

---

[43] See Fubini's theorem B.2, with $\omega^p \in L^1(Q)$.
[44] Cf. proof of [186, Sec. 2.1.1, p. 40], where this is done similarly for a fixed $t \in I$.
[45] See Hölder's inequality B.27.

3. Let $\omega \in L^\infty(Q) \cap L^2(I; H^1(\Omega))$, $\varphi \in \mathcal{C}_0^\infty(\Omega)$ and $t \in I$.

   Like earlier in this proof, we get that the maps $x \mapsto \int_0^t \omega(s, x)\,\mathrm{d}s$ and $x \mapsto \int_0^t \mathrm{D}_{x_i}\omega(s, x)\,\mathrm{d}s$ are elements in $L^2(\Omega)$, which follows again from Fubini's theorem with $\omega^2, (\nabla\omega)^2 \in L^1(Q)$.
   Note that the maps $L^1(\Omega) \ni v \mapsto \int_\Omega v(x)\varphi(x)\,\mathrm{d}x$ and $L^1(\Omega) \ni v \mapsto \int_\Omega v(x)\mathrm{D}_{x_i}\varphi(x)\,\mathrm{d}x$ define elements in $L^1(\Omega)^*$.

   We use this together with Bochner's theorem[46], especially equation (B.3), and the definition of a weak derivative of $\omega(s) \in H^1(\Omega)$ to get

   $$\int_\Omega \left(\int_0^t \omega(s)\,\mathrm{d}s \right)(x)\mathrm{D}_{x_i}\varphi(x)\,\mathrm{d}x = \int_0^t \int_\Omega \omega(s)(x)\mathrm{D}_{x_i}\varphi(x)\,\mathrm{d}x\,\mathrm{d}s$$
   $$= -\int_0^t \int_\Omega \mathrm{D}_{x_i}\omega(s)(x)\varphi(x)\,\mathrm{d}x\,\mathrm{d}s$$
   $$= -\int_\Omega \left(\int_0^t \mathrm{D}_{x_i}\omega(s)\,\mathrm{d}s \right)(x)\varphi(x)\,\mathrm{d}x\,.$$

   The test function φ was chosen arbitrarily, so by definition we can identify the weak derivative

   $$\mathrm{D}_{x_i} \int_0^t \omega(s)\,\mathrm{d}s = \int_0^t \mathrm{D}_{x_i}\omega(s)\,\mathrm{d}s \quad \text{in } L^2(\Omega),$$

   which implies equation (2.18).

   We summarize the results and get $\phi_2(t) \in H^1(\Omega)$. The continuity w.r.t. t now follows from Hölder's inequality:

   $$\|\phi(t_2) - \phi(t_1)\|_{H^1(\Omega)}^2 = \int_\Omega \left(\int_{t_1}^{t_2} \omega(s, x)\,\mathrm{d}s \right)^2 \mathrm{d}x + \int_\Omega \left(\nabla \int_{t_1}^{t_2} \omega(s, x)\,\mathrm{d}s \right)^2 \mathrm{d}x$$
   $$= \int_\Omega \left(\int_{t_1}^{t_2} \omega(s, x)\,\mathrm{d}s \right)^2 \mathrm{d}x + \int_\Omega \left(\int_{t_1}^{t_2} \nabla\omega(s, x)\,\mathrm{d}s \right)^2 \mathrm{d}x$$
   $$\leq |t_2 - t_1| \int_\Omega \int_0^T \omega(s, x)^2\,\mathrm{d}s\,\mathrm{d}x + |t_2 - t_1| \int_\Omega \int_0^T (\nabla\omega(s, x))^2\,\mathrm{d}s\,\mathrm{d}x$$
   $$= |t_2 - t_1| \, \|\omega\|_{L^2(I; H^1(\Omega))}^2\,.$$

   ∎

A.1.4 Proof of Lemma 2.9

Proof.

> Write the coefficients as a concatenation of Nemytskii operators and the integral operator $\int_0^t \cdot \, \mathrm{d}s$.

1. Let $\omega \in L^\infty(Q)$.

   Like discussed in Subsection 2.2.2, the operators ϕ_i, $i \in \{1, \ldots, 4\}$, are well defined and we get $\gamma(\omega) = \phi_3 \circ \phi_2 \circ \phi_1(\omega) \in L^\infty(Q)$. We consider only positive points in time $t > 0$ and, with $d_{\mathrm{Arr}}(\cdot) \geq 0$ in equation (2.9), we infer

   $$0 \leq \gamma(\omega) \leq 1 \quad \text{a.e. in } Q. \tag{A.30}$$

---

[46] See Bochner's theorem B.47.
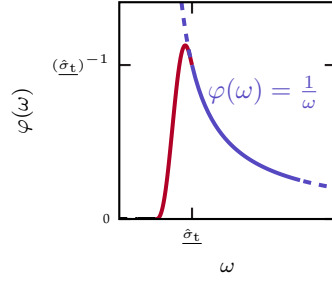
Figure A.1: Extension of $(\cdot)^{-1}$ as $\mathcal{C}^2(\mathbb{R})$ function.

We can write the coefficients as the following concatenation of the auxiliary maps:

$$\sigma_a = \phi_4^{\sigma_{a,n},\sigma_{a,c}} \circ \phi_3 \circ \phi_2 \circ \phi_1 \quad \text{and} \quad \sigma_s = \phi_4^{\sigma_{s,n},\sigma_{s,c}} \circ \phi_3 \circ \phi_2 \circ \phi_1.$$

The definition of ϕ_4 together with estimate (A.30) implies the bounds

$$0 < \underline{f} \leq f(\omega) \leq \overline{f} < \infty \quad \text{a.e. in } Q$$

for $f \in \{\sigma_a, \sigma_s\}$ and certain $\underline{\sigma_a}, \overline{\sigma_a}, \underline{\sigma_s}, \overline{\sigma_s} \in \mathbb{R}_{>0}$.

For simplicity, we write $\hat{\sigma}_t(\omega) = \sigma_a(\omega) + (1-g)\sigma_s(\omega)$, and the upper and lower bounds of σ_a, σ_s together with estimate (A.30) imply that

$$0 < \underline{\hat{\sigma}_t} \leq \hat{\sigma}_t(\omega) \leq \overline{\hat{\sigma}_t} < \infty \quad \text{a.e. in } Q \tag{A.31}$$

for certain $\underline{\hat{\sigma}_t}, \overline{\hat{\sigma}_t} \in \mathbb{R}_{>0}$.

We would like to write D as the concatenation of $(\cdot)^{-1}$ and $\phi_4^{\hat{\sigma}_{t,n},\hat{\sigma}_{t,c}} \circ \phi_3 \circ \phi_2 \circ \phi_1$, with $\hat{\sigma}_{t,n/c} = \sigma_{a,n/c} + (1-g)\sigma_{s,n/c}$, but the function $(\cdot)^{-1}$ is not an element of $\mathcal{C}^2(\mathbb{R})$ and we can not directly apply Remark B.67. However, we can define the map

$$\varphi(\omega)\colon \mathbb{R} \to \mathbb{R}, \omega \mapsto \begin{cases} (\omega)^{-1}, & \omega \geq \underline{\hat{\sigma}_t}, \\ 10\underline{\hat{\sigma}_t}^{-6}\omega^5 - 24\underline{\hat{\sigma}_t}^{-5}\omega^4 + 15\underline{\hat{\sigma}_t}^{-4}\omega^3, & 0 \leq \omega < \underline{\hat{\sigma}_t}, \\ 0, & \omega < 0, \end{cases} \tag{A.32}$$

which is an element of $\mathcal{C}^2(\mathbb{R})$ and coincides with $(\cdot)^{-1}$ on the interval $[\underline{\hat{\sigma}_t}, \infty)$, see Figure A.1. We write

$$\phi_5\colon L^\infty(Q) \to L^\infty(Q), \omega \mapsto \varphi(\cdot, \omega(\cdot))$$

for the associated Nemytskii operator to φ in (A.32) and rewrite the coefficient

$$D = \phi_5 \circ \phi_4^{\hat{\sigma}_{t,n},\hat{\sigma}_{t,c}} \circ \phi_3 \circ \phi_2 \circ \phi_1,$$

which yields the coefficient D as desired because of estimate (A.31). The bounds in (A.31) translate to the bounds in (2.19) for D:

$$(3\overline{\hat{\sigma}_t})^{-1} \leq D \leq (3\underline{\hat{\sigma}_t})^{-1} \quad \text{a.e. in } Q.$$

For the pointwise estimates, we recall the proof of Lemma 2.7, where we saw that the map[47] $f\colon \Omega \to \mathbb{R}_{\geq 0}$, $x \mapsto \int_0^t d_{\mathrm{Arr}}(\omega)(s,x)\,\mathrm{d}s$, for fixed $t \in I$, is well defined and Lebesgue measurable. This implies $f \in L^\infty(\Omega)$. In fact, if we assume

$$|A_M| := \{x \in \Omega \mid |f(x)| > M\} > 0 \quad \text{for all } M > 0,$$

we get for $M = 2T\,\|d_{\mathrm{Arr}}(\omega)\|_{L^\infty(Q)}$ the following contradiction:

$$M\,|A_M| \leq \int_{A_M} |f(x)|\,\mathrm{d}x \leq \int_{A_M} \int_0^t |d_{\mathrm{Arr}}(\omega)(s,x)|\,\mathrm{d}s\,\mathrm{d}x$$
$$\leq T\,\|d_{\mathrm{Arr}}(\omega)\|_{L^\infty(Q)}\,|A_M| < M\,|A_M|.$$

With Theorem B.66 and Remark B.67 on Nemytskii operators, we now get, for a.a. $t \in I$, that $\gamma(\omega)(t) = \exp(-f) \in L^\infty(\Omega)$ with

$$0 \leq \gamma(\omega)(t) \leq 1 \quad \text{a.e. on } \Omega,$$

which implies estimate (2.20) again by means of Theorem B.66.

2. Estimate (2.21) follows from a consecutive application of the estimates (2.15) and (2.17) for the operators $\phi_i, i \in \{1, \ldots, 5\}$.

■

A.1.5 Proof of Lemma 2.11

Proof. The definitions of ϕ_1 and ϕ_2 and Lemma 2.7 imply $0 \leq \phi_2 \circ \phi_1(\omega)(t)$ a.e. in Ω for a.a. $t \in I$. Thus, we can replace the exponential in the definition (2.14) of ϕ_3 by

$$\phi_3(\omega) := \begin{cases} \exp(-\omega), & \omega \geq 0, \\ 1, & \omega < 0, \end{cases}$$

which does not change σ_{a}. The redefined map ϕ_3 and the map $\phi_4^{\sigma_{\mathrm{a,n}},\sigma_{\mathrm{a,c}}}$ are Lipschitz continuous, and the statement now follows from the chain rule[48] and equation (2.18). ■

A.1.6 Proof of Lemma 2.12

Proof.   1. Even though there are no time derivatives in equation (2.22), we are still confronted with a time evolution problem because the coefficients depend on time through their dependence on ω.

The existence of a unique solution $\phi \in L^r(I; W^{1,p}(\Omega))$ of the radiation equation (2.22) for a certain $p \in (2,6)$ and an arbitrary $r \in [2,\infty)$, with

$$\|\phi\|_{L^r(I;W^{1,p}(\Omega))} \leq C\,\|g_{\mathrm{r}}\|_{L^\infty(\Gamma)},$$

where C does not depend on ω, is stated (but not proven) in [219, Sec. 2.2, Lem. 2.3, p. 8] and is based on [74, Sec. 4.1, Thm. 3, p. 482].

---

[47] We used $d_{\mathrm{Arr}}(\omega) \in L^\infty(Q)$ by means of Theorem B.66.
[48] See the chain rule for weak derivatives B.41.

(a) Approximate the coefficients by simple functions and apply standard elliptic theory.

(b) Strong convergence of the coefficients together with the weak convergence of the corresponding solutions allows passing to the limit in the weak formulation.

Let $\omega \in L^\infty(Q)$. For arbitrary $r \in (2, \infty)$, we can approximate the nonlinear coefficients $\sigma_{\mathrm{a}}(\omega), D(\omega) \in L^\infty(Q) \subset L^r(I; L^r(\Omega))$ by simple functions[49]

$$\sigma_{\mathrm{a},k}(t) = \sum_{j=1}^{d_k} \mathbb{1}_{E_{k,j}}(t) \sigma_{\mathrm{a},k,j}, \quad \sigma_{\mathrm{a},k,j} \in L^r(\Omega),$$

$$D_k(t) = \sum_{j=1}^{d_k} \mathbb{1}_{E_{k,j}}(t) D_{k,j}, \quad D_{k,j} \in L^r(\Omega),$$

with pairwise disjoint (for fixed k) and Lebesgue-measurable sets[50] $E_{k,j} \subset I$, such that

$$\sigma_{\mathrm{a},k} \to \sigma_{\mathrm{a}}(\omega) \quad \text{and} \quad D_k \to D(\omega) \quad \text{in } L^r(I; L^r(\Omega)).$$

We recall the bounds on the coefficients

$$0 < \underline{\sigma_{\mathrm{a}}} \le \sigma_{\mathrm{a}}(\omega) \le \overline{\sigma_{\mathrm{a}}} \quad \text{and} \quad 0 < \underline{D} \le D(\omega) \le \overline{D} \quad \text{a.e. in } Q \tag{2.19}$$

and define the sequences

$$\hat{\sigma}_{\mathrm{a},k}(t) := \sum_{j=1}^{d_k} \mathbb{1}_{E_{k,j}}(t) \hat{\sigma}_{\mathrm{a},k,j} := \sum_{j=1}^{d_k} \mathbb{1}_{E_j}(t) \left[\sigma_{\mathrm{a},k,j}\right]_{\underline{\sigma_{\mathrm{a}}}}^{\overline{\sigma_{\mathrm{a}}}},$$

$$\hat{D}_k(t) := \sum_{j=1}^{d_k} \mathbb{1}_{E_{k,j}}(t) \hat{D}_{k,j} := \sum_{j=1}^{d_k} \mathbb{1}_{E_j}(t) \left[D_{k,j}\right]_{\underline{D}}^{\overline{D}},$$

with the cutoff function $[\cdot]_m^M = \min(\max(\cdot, m), M)$. Note that $\hat{\sigma}_{\mathrm{a}}, \hat{D} \in L^r(I; L^\infty(\Omega))$.

With (2.19), we infer

$$|\hat{\sigma}_{\mathrm{a},k} - \sigma_{\mathrm{a}}(\omega)| \le |\sigma_{\mathrm{a}k} - \sigma_{\mathrm{a}}(\omega)| \quad \text{and} \quad \left|\hat{D}_k - D(\omega)\right| \le |D_k - D(\omega)| \quad \text{a.e. in } Q,$$

which implies

$$\hat{\sigma}_{\mathrm{a},k} \to \sigma_{\mathrm{a}}(\omega) \quad \text{and} \quad \hat{D}_k \to D(\omega) \quad \text{in } L^r(Q) \quad \text{for all } r \in [1, \infty). \tag{A.33}$$

From [74, Sec. 4.1, Thm. 3, p. 482][51], we get the existence of a certain $p \in (2, 6)$ and unique solutions $\phi_{k,j} \in W^{1,p}(\Omega)$ such that

$$\left(\hat{D}_{k,j} \nabla \phi_{k,j}, \nabla \varphi\right)_{L^2(\Omega)} + (\hat{\sigma}_{\mathrm{a},k,j} \phi_{k,j}, \varphi)_{L^2(\Omega)} + (a_{\mathrm{r}} \phi_{k,j}, \varphi)_{L^2(\Gamma)} = (g_{\mathrm{r}}, \varphi)_{L^2(\Omega)} \tag{A.34}$$

---

[49] See the classical density results B.51.

[50] Like in [56, Sec. 7.1, Def. 7.1.8, p. 153], we assume the sets $\{E_{k,j} \mid 1 \le j \le d_k\}$ to be pairwise disjoint for fixed k. This is not a restriction because we have $d_k < \infty$ and, thus, $\sigma_{\mathrm{a},k}, D_k$ only attain finitely many values in $L^r(\Omega)$. We can redefine $\sigma_{\mathrm{a},k}, D_k$ as simple functions w.r.t. the inverse images of those finitely many values. Those inverse images are disjoint by definition. They can be written as particular combinations of intersections and unions of the sets $E_{k,j}$ and, thus, are Lebesgue measurable.

[51] Here, we need that the map $W^{1,1}(\Omega) \to \mathbb{R}$, $\varphi \mapsto (f, \varphi)_{L^2(\Gamma)}$ defines an element in $W^{1,1}(\Omega)^* \subset W^{1,q}(\Omega)^*$, with $q = p(p-1)^{-1}$ (see also Lemma B.17 on dual spaces of subspaces).

for all $\varphi \in H^1(\Omega)$, and it holds

$$\|\phi_{k,j}\|_{W^{1,p}(\Omega)} \le C_1 \|g_r\|_{L^\infty(\Gamma)} \quad \text{for all } k, j \in \mathbb{N}.$$

The cited theorem guarantees that the numbers C_1 and p depend only on the domain Ω and on the upper and lower bounds of σ_a and D, due to the cutoff function. Especially, this implies that C_1 and p can be chosen uniformly for all indices k, j and depend neither on ω nor on r.

We define $\phi_k(t) := \sum_{j=1}^{d_k} 1_{E_{k,j}}(t)\phi_{k,j} \in L^r(I; W^{1,p}(\Omega))$, which is uniformly bounded with

$$\|\phi_k\|_{L^r(I;W^{1,p}(\Omega))}^r = \int_0^T \|\phi_k(t)\|_{W^{1,p}(\Omega)}^r \, dt = \int_0^T \sum_{j=1}^{d_k} 1_{E_{k,j}}(t) \|\phi_{k,j}\|_{W^{1,p}(\Omega)}^r \, dt$$

$$\le \sum_{j=1}^{d_k} |E_{k,j}| C \|g_r\|_{L^\infty(\Gamma)}^r \le TC \|g_r\|_{L^\infty(\Gamma)}^r \tag{A.35}$$

for all $k \in \mathbb{N}$, where we used that the sets $E_{k,j}$ are disjoint for a fixed k. Together with the reflexivity[52] of $L^r(I; W^{1,p}(\Omega))$, this allows us to extract a weakly convergent subsequence $\phi_k \rightharpoonup \phi^* \in L^r(I; W^{1,p}(\Omega)))$, where we reuse the same index as in the original sequence.

The weak lower semicontinuity of the norm[53] implies

$$\|\phi^*\|_{L^r(I;W^{1,p}(\Omega))} \le T^{\frac{1}{r}} C \|g_r\|_{L^\infty(\Omega)}. \tag{A.36}$$

Next, we need to show that ϕ^* is in fact a solution of the radiation equation (2.22).

Note that, for fixed $\varphi \in L^2(I; H^1(\Omega))$, the forms

$$\langle F_r^\varphi(\omega), \phi \rangle_{L^r(I;W^{1,p}(\Omega))} := \int_0^T (D(\omega)(t)\nabla\phi(t), \nabla\varphi(t))_{L^2(\Omega)}$$
$$+ (\sigma_a(\omega)(t)\phi(t), \varphi(t))_{L^2(\Omega)} + (a_r\phi(t), \varphi(t))_{L^2(\Gamma)} \, dt,$$

$$\langle F_r^{\varphi,k}, \phi \rangle_{L^r(I;W^{1,p}(\Omega))} := \int_0^T \left(\hat{D}_k(t)\nabla\phi(t), \nabla\varphi(t) \right)_{L^2(\Omega)}$$
$$+ (\hat{\sigma}_{a,k}(t)\phi(t), \varphi(t))_{L^2(\Omega)} + (a_r\phi(t), \varphi(t))_{L^2(\Gamma)} \, dt$$

define elements[54] $F_r^\varphi(\omega), F_r^{\varphi,k} \in L^r(I; W^{1,p}(\Omega))^*$.

The convergence of the coefficients in (A.33) implies $F_r^{\varphi,k} \to F_r^\varphi(\omega)$ in $L^r(I; W^{1,p}(\Omega))^*$ for $k \to \infty$. In fact, for $\phi \in L^r(I; W^{1,p}(\Omega))$ with $\|\phi\|_{L^p(I;W^{1,p}(\Omega))} = 1$, Hölder's inequality[55] yields

$$\left| \langle F_r^{\varphi,k} - F_r^\varphi(\omega), \phi \rangle_{L^p(I;W^{1,p}(\Omega))} \right|$$
$$\le C \left(\|D_k - D(\omega)\|_{L^q(Q)} + \|\hat{\sigma}_{a,k} - \sigma_a(\omega)\|_{L^q(Q)} \right) \|\varphi\|_{L^2(I;H^1(\Omega))},$$

with $q = \max\left(\frac{2p}{p-2}, \frac{2r}{r-2} \right)$.

---

[52] See Lemma B.24 on Sobolev spaces and Lemma B.12 on reflexive Banach spaces.
[53] See [4, Sec. 6.3, p. 239].
[54] Cf. the proof of [235, §23.9, Thm. 23.A, p. 434, part (III-1)].
[55] See Hölder's inequality B.27.

This allows passing to the limit[56]

$$\left\langle F_{\mathrm{r}}^{\varphi,k}, \phi_k \right\rangle_{L^r(I;W^{1,p}(\Omega))} \to \left\langle F_{\mathrm{r}}^{\varphi}(\omega), \phi^* \right\rangle_{L^r(I;W^{1,p}(\Omega))} \quad \text{for } k \to \infty.$$

By construction, the solutions ϕ_k fulfill

$$\left\langle F_{\mathrm{r}}^{\varphi,k}, \phi_k \right\rangle_{L^r(I;W^{1,p}(\Omega))} = \int_0^T (g_{\mathrm{r}}, \varphi(t))_{L^2(\Gamma)} \, \mathrm{d}t \quad \text{for all } \varphi \in L^2(I;H^1(\Omega)), \qquad \text{(A.37)}$$

thus, ϕ^* is a solution of (2.22) because it fulfills

$$\left\langle F_{\mathrm{r}}^{\varphi}(\omega), \phi^* \right\rangle_{L^r(I;W^{1,p}(\Omega))} = \int_0^T (g_{\mathrm{r}}, \varphi(t))_{L^2(\Gamma)} \, \mathrm{d}t \quad \text{for all } \varphi \in L^2(I;H^1(\Omega)). \qquad \text{(A.38)}$$

The uniqueness of the solution $\phi \in L^r(I;W^{1,p}(\Omega))$ follows from the uniqueness of the solution of (A.39) for a.a. $t \in I$, shown in the next step.

The continuous embedding given in Lemma B.54 now yields $\phi \in L^r(I;W^{1,p}(\Omega))$ also for $r \in (1,2]$.

2. Analogously to the proof of [93, Sec. 1.3.2.3, Thm. 1.33, p. 42], we can look at the radiation equation pointwise in t. For a.a. $t \in I$, the solution $\phi \in L^r(I;W^{1,p}(\Omega))$ fulfills

$$(D(\omega)(t)\nabla\phi(t), \nabla\varphi)_{L^2(\Omega)} + (\sigma_{\mathrm{a}}(\omega)\phi(t), \varphi)_{L^2(\Omega)} + (a_{\mathrm{r}}\phi(t), \varphi)_{L^2(\Gamma)} = (g_{\mathrm{r}}, \varphi)_{L^2(\Gamma)} \quad \text{(A.39)}$$

for all $\varphi \in H^1(\Omega)$. We get with [74, Sec. 4.1, Thm. 3, p. 482] and [217, Ch. 4.2.3, Satz 4.7, p. 153] that the solution $\phi(t)$ of equation (A.39) is unique and an element of $W^{1,p}(\Omega) \cap \mathcal{C}^0(\overline{\Omega})$, which fulfills

$$\|\phi(t)\|_{W^{1,p}(\Omega)} + \|\phi(t)\|_{\mathcal{C}^0(\overline{\Omega})} \leq C \|g_{\mathrm{r}}\|_{L^\infty(\Omega)} \quad \text{for a.a. } t \in I,$$

where C neither depends on ω nor on t because of the uniform bounds for $\sigma_{\mathrm{a}}(\omega)(t)$, $D(\omega)(t)$ in (2.20). Note that this does not imply $\phi \in L^\infty(I;W^{1,p}(\Omega) \cap \mathcal{C}^0(\overline{Q}))$ because we do not have any information on ϕ being Bochner measurable w.r.t. the corresponding spaces.

3. Let $(\omega_k)_{k\in\mathbb{N}} \subset L^2(Q)$, $\omega \in L^2(Q)$ with $\omega_k \to \omega$ in $L^2(Q)$.

With Lemma A.2, we get for $M > 0$ and $q \in (1,\infty)$ the strong convergence $[\omega_k]_M \to [\omega]_M$ in $L^q(Q)$ and, thus, with Lemma 2.9, the strong convergence of the coefficients

$$\begin{aligned}
\sigma_{\mathrm{a}}\left([\omega_k]_M\right) &\to \sigma_{\mathrm{a}}\left([\omega]_M\right) \quad \text{in } L^q(Q), \\
D\left([\omega_k]_M\right) &\to D\left([\omega]_M\right) \quad \text{in } L^q(Q).
\end{aligned} \qquad \text{(A.40)}$$

We subtract equation (2.22) evaluated once for ω and once for ω_k and choose the test function $\varphi = \phi(\omega) - \phi(\omega_k)$. With Hölder's inequality and the coercivity of the bilinear form F_{r}, we get

$$\begin{aligned}
\|\phi(\omega) - \phi(\omega_k)\|_{L^2(I;H^1(\Omega))} \leq C\Big[&\left\|D\left([\omega_k]_M\right) - D\left([\omega]_M\right)\right\|_{L^q(Q)} \\
&+ \left\|\sigma_{\mathrm{a}}\left([\omega_k]_M\right) - \sigma_{\mathrm{a}}\left([\omega]_M\right)\right\|_{L^q(Q)} \Big] \|\phi(\omega_k)\|_{L^r(I;W^{1,p}(\Omega))}
\end{aligned}$$

with $q = \max\left(\frac{2p}{p-2}, \frac{2r}{r-2}\right)$, and $p, r > 2$ as discussed above. Now, continuity follows from the convergence of the coefficients in (A.40) and the uniform bound on $\phi(\omega_k)$ in (A.36).

∎

---

[56] See Lemma B.9 on the limit of dual pairings.

A.2 Details for Chapter 3

A.2.1 Proof of Lemma 3.2

Proof. The function J in (3.6) is a standard cost functional, see, e.g., [217, Ch. 3, p. 95 ff.] and [26].

> Write the cost functional as concatenation of continuous, convex and Fréchet-differentiable functions.

First, we consider the functions

$$f_1 \colon L^1(\Omega) \to \mathbb{R}, \qquad u \mapsto \int_\Omega u(x)\,\mathrm{d}x\,,$$

$$f_2 \colon L^2(\Omega) \to \mathbb{R}, \qquad g \mapsto \frac{1}{2}\,\|g\|^2_{L^2(\Omega)}\,,$$

$$E \colon Y^{(0)} \to L^2(\Omega), \quad y \mapsto \vartheta(t^*).$$

The functions f_1 and f_2 are convex and continuous. Especially, f_1 is linear and, thus, Fréchet differentiable.

The "observation operator" E is continuous and linear because of the continuous and linear[57] embedding[58]

$$W^{(0)} \hookrightarrow \left(L^2(I; H^1(\Omega)) \cap H^1(I; H^1(\Omega)^*)\right) \hookrightarrow \mathcal{C}^0(\overline{I}; L^2(\Omega)). \tag{A.41}$$

With the continuous and linear embeddings in (A.41), $U = L^2(\Omega)$ and $E_1 \colon U \hookrightarrow L^1(\Omega)$, we can write the cost functional as

$$J \colon Y^{(0)} \times U,\ (y, u) \mapsto f_2(E(y) - \vartheta_\mathrm{d}) + f_1(E_1(u)) + f_2(u), \tag{A.42}$$

for the given desired temperature $\vartheta_\mathrm{d} \in L^2(\Omega)$.

1. The cost functional $J \colon Y^{(0)} \times U$ is continuous as concatenation of continuous functions in (A.42). Furthermore, each function

$$Y^{(0)} \to \mathbb{R}, \quad y \mapsto f_2(E(y) - \vartheta_\mathrm{d}),$$

$$U \to \mathbb{R}, \qquad u \mapsto f_1(E_1(u)),$$

$$U \to \mathbb{R}, \qquad u \mapsto f_2(u)$$

   is convex[59] as concatenation of an affine linear function and a convex function, thus, the cost functional J is convex as the sum of convex functions.

   Lemma B.16 now implies that the cost functional J is sequentially weakly lower semicontinuous.

---

[57] Embeddings in the context of normed vector spaces are assumed to be linear by definition.

[58] See Theorem B.36 on the integration by parts in Bochner spaces and Lemma B.54 on embeddings of Bochner spaces.

[59] Let X, Y be two Banach spaces, and let $f \colon Y \to \mathbb{R}$ be a convex function, and $g \colon X \to Y$ be an affine linear function, i.e., $g(x) = Ax + b$ for a linear map $A \colon X \to Y$ and some $b \in Y$. Then the concatenation $f \circ g \colon X \to \mathbb{R}$ is convex. In fact, for $\lambda \in [0, 1]$ and $x, \hat{x} \in X$, it holds

$$f(g(\lambda x + (1 - \lambda)\hat{x})) = f(\lambda(Ax + b) + (1 - \lambda)(A\hat{x} + b)) \leq \lambda f(g(x)) + (1 - \lambda)f(g(\hat{x})).$$

2. The function f_2 is continuously Fréchet differentiable[60] with derivative

$$\mathrm{D}f_2(g)\colon L^2(\Omega) \to \mathbb{R},\, h \mapsto \int_\Omega g(x)h(x)\,\mathrm{d}x \quad \text{for } g \in L^2(\Omega).$$

Furthermore, the functions f_1, E_1, E are linear and, thus, Fréchet differentiable with the following derivatives:

$$\mathrm{D}f_1(u)\colon L^1(\Omega) \to \mathbb{R}, \qquad h \mapsto \int_\Omega h(x)\,\mathrm{d}x\,, \qquad \text{for } u \in U,$$

$$\mathrm{D}E_1(u)\colon U \to L^1(\Omega), \qquad h \mapsto h, \qquad\qquad \text{for } u \in U,$$

$$\mathrm{D}E(y)\colon Y^{(0)} \to L^2(\Omega), \quad h \mapsto h, \qquad\qquad \text{for } y \in Y^{(0)}.$$

They are in fact continuously Fréchet differentiable.

By means of the chain rule[61], we get that the cost functional J is continuously Fréchet differentiable as concatenation of continuously Fréchet-differentiable functions in (A.42), with its derivative as stated in (3.8).

∎

A.2.2 Proof of Lemma 3.9

Lemma A.7 — Linearized radiation equation.

Let Assumptions 2.1 and 2.2 hold, and let $(\phi, \vartheta) = S(u) \in \mathcal{Y}_p$, $p \geq 2$, be the state vector of the Cattaneo–LITT model for a given control $u \in U_{\mathrm{ad}}$. Furthermore, let $\tilde{\eta} \in L^\infty(I; H^1(\Omega)) \cap \mathcal{C}^0(\overline{Q})$.

1. Then there exists a unique solution $\rho \in L^p(I; W^{1,p}(\Omega))$ which fulfills the linearized radiation equation

$$\int_0^T F_{\mathrm{r}}(\rho(t), \varphi(t); \vartheta, t)\,\mathrm{d}t = -\int_0^T (\mathrm{D}_\vartheta D(\vartheta)[\tilde{\eta}](t)\nabla\phi(t), \nabla\varphi(t))_{L^2(\Omega)}\,\mathrm{d}t$$
$$\hspace{5cm} -\int_0^T (\mathrm{D}_\vartheta \sigma_{\mathrm{a}}(\vartheta)[\tilde{\eta}](t)\phi(t), \varphi(t))_{L^2(\Omega)}\,\mathrm{d}t \tag{A.43}$$

for all $\varphi \in L^2(I; H^1(\Omega))$, and it holds

$$\|\rho\|_{L^p(I;W^{1,p}(\Omega))} \leq C(\phi, \vartheta, T)\,\|\tilde{\eta}\|_{\mathcal{C}^0(\overline{Q})}\,.$$

2. If we assume[a] $\phi \in L^p(I; W^{1,p}(\Omega))$ with $p > 3$, we get for the solution ρ of the statement above that, for a.a. $t \in I$, it holds $\rho(t) \in L^\infty(\Omega) \cap H^1(\Omega)$ with

$$\|\rho(t)\|_{L^\infty(\Omega)} + \|\rho(t)\|_{H^1(\Omega)} \leq C(\phi, \vartheta, T) \int_0^t \|\tilde{\eta}(s)\|_{\mathcal{C}^0(\overline{\Omega})}\,\mathrm{d}s\,.$$

---

[60] See [217, Sec. 2.6, Rem. (iii), p. 46].
[61] See the chain rule for Fréchet derivatives B.42.

The statement holds analogously for smaller final times $\tilde{T} \in I$. The function which maps the final time $\tilde{T} \in I$ to the corresponding constants $C(\phi, \vartheta, \tilde{T}) \in \mathbb{R}_{>0}$ is essentially bounded, i.e., there is a constant $\tilde{C} \in \mathbb{R}_{>0}$ such that $C(\phi, \vartheta, \tilde{T}) < \tilde{C}$ for a.a. $\tilde{T} \in I$.

[a] The assumption $p > 3$ is justified by Lemma 2.12 and Remark 2.18.

Proof of Lemma A.7.   1. Note that the radiation equation (2.22) and the linearized equation (A.43) have the same left-hand side and differ only in their right-hand sides.

Apply the same procedure as for the radiation equation but with a different right-hand side.

In fact, the proof of the first part of the statement is analog to the proof of Lemma 2.12. Here, we highlight only the necessary modifications regarding the modified right-hand side.

We write for the right-hand side in the linearized equation (A.43) and a fixed $t \in I$

$$f(t)\colon W^{1,q}(\Omega) \to \mathbb{R}, \ \langle f(t), \varphi \rangle_{W^{1,q}(\Omega)} := (\alpha(t), \nabla\varphi)_{L^2(\Omega)} + (\beta(t), \varphi)_{L^2(\Omega)} \tag{A.44}$$

with $q = \frac{p}{p-1}$ and

$$\alpha(t) := \mathrm{D}_\vartheta D(\vartheta)[\tilde{\eta}](t)\nabla\phi(t) \quad \text{and} \quad \beta(t) := \mathrm{D}_\vartheta \sigma_{\mathrm{a}}(\vartheta)[\tilde{\eta}](t)\phi(t).$$

Note that $f(t) \in W^{1,q}(\Omega)^*$ is well defined by means of Hölder's inequality[62].

(a) It holds $f \in L^p(I; W^{1,q}(\Omega)^*)$. In fact, because of $\mathrm{D}_\vartheta D(\vartheta)[\tilde{\eta}], \mathrm{D}_\vartheta \sigma_{\mathrm{a}}(\vartheta)[\tilde{\eta}] \in \mathcal{C}^0(\overline{Q})$ and $\phi \in L^p(I; W^{1,p}(\Omega))$, it holds[63] $\alpha, \beta \in L^p(Q) \cong L^p(I; L^p(\Omega))$, thus, we can approximate α, β by simple functions[64], i.e., there are sequences $(\alpha_k)_{k\in\mathbb{N}}, (\beta_k)_{k\in\mathbb{N}} \subset L^p(I; L^p(\Omega))$ of the form

$$\alpha_k(t) = \sum_{j=1}^{d_k} 1_{E_{k,j}}(t)\alpha_{k,j}, \quad \alpha_{k,j} \in L^p(\Omega),$$

$$\beta_k(t) = \sum_{j=1}^{d_k} 1_{E_{k,j}}(t)\beta_{k,j}, \quad \beta_{k,j} \in L^p(\Omega), \tag{A.45}$$

with Lebesgue measurable sets $E_{k,j} \subset I$, such that

$$\alpha_k \to \alpha \quad \text{and} \quad \beta_k \to \beta \quad \text{in } L^p(I; L^p(\Omega))$$

and

$$\alpha_k(t) \to \alpha(t) \quad \text{and} \quad \beta_k(t) \to \beta(t) \quad \text{in } L^p(\Omega) \quad \text{for a.a. } t \in I. \tag{A.46}$$

We define the simple functions $f_k \in L^p(I; W^{1,q}(\Omega)^*)$ as

$$\langle f_k(t), \varphi \rangle_{W^{1,q}(\Omega)} := (\alpha_k(t), \nabla\varphi)_{L^2(\Omega)} + (\beta_k(t), \varphi(t))_{L^2(\Omega)}$$

$$= \sum_{j=1}^{d_k} 1_{E_{k,j}}(t) \left((\alpha_{k,j}, \nabla\varphi)_{L^2(\Omega)} + (\beta_{k,j}, \varphi)_{L^2(\Omega)} \right).$$

[62] See Hölder's inequality B.27.
[63] Technically, to be precise, α is vector valued and each of its components is an element of $L^p(Q)$.
[64] See Lemma B.51 on the approximation by simple functions.

For fixed $t \in I$ and $\varphi \in W^{1,q}(\Omega)$, it holds with Hölder's inequality that

$$
\begin{aligned}
&\left| \langle f_k(t) - f(t), \varphi \rangle_{W^{1,q}(\Omega)} \right| \\
&= \left| (\alpha_k(t) - \alpha(t), \nabla\varphi)_{L^2(\Omega)} + (\beta_k(t) - \beta(t), \varphi)_{L^2(\Omega)} \right| \\
&\leq \left(\|\alpha_k(t) - \alpha(t)\|_{L^p(\Omega)} + \|\beta_k(t) - \beta(t)\|_{L^p(\Omega)} \right) \|\varphi\|_{W^{1,q}(\Omega)} ,
\end{aligned}
$$

and, with the pointwise convergence in (A.46), we get

$$
f_k(t) \to f(t) \quad \text{in } W^{1,q}(\Omega)^*.
$$

Furthermore, Hölder's inequality and estimate (3.13) imply

$$
\begin{aligned}
&\int_0^T \|f(t)\|_{W^{1,q}(\Omega)^*}^p \, \mathrm{d}t \\
&\leq \left(\|\mathrm{D}_\vartheta D(\vartheta)[\tilde{\eta}]\|_{\mathcal{C}^0(\overline{Q})}^p + \|\mathrm{D}_\vartheta \sigma_\mathrm{a}(\vartheta)[\tilde{\eta}]\|_{\mathcal{C}^0(\overline{Q})}^p \right) \|\phi\|_{L^p(I;W^{1,p}(\Omega))}^p \\
&\leq C(\phi, \vartheta) \|\tilde{\eta}\|_{\mathcal{C}^0(\overline{Q})}^p < \infty,
\end{aligned}
\tag{A.47}
$$

thus, we get $f \in L^p(I; W^{1,q}(\Omega)^*)$.

(b) Because of $f \in L^p(I; W^{1,q}(\Omega)^*)$, we can approximate f by a sequence of simple functions $(f_k)_{k \in \mathbb{N}} \subset L^p(I; W^{1,q}(\Omega)^*)$ of the form

$$
f_k(t) = \sum_{j=1}^{d_k} 1_{E_{k,j}}(t) f_{k,j}, \quad f_{k,j} \in W^{1,q}(\Omega)^*
$$

such that

$$
f_k \to f \quad \text{in } L^p(I; W^{1,q}(\Omega)^*).
\tag{A.48}
$$

Note that it holds $L^p(I; W^{1,q}(\Omega)^*) \subset L^p(I; H^1(\Omega)^*)$ because of $q < 2$.

Analogously to equation (A.34), we get unique solutions $\rho_{k,j} \in W^{1,p}(\Omega)$ (note that the number p depends[65] only on the domain and upper and lower bounds of the coefficients σ_a and D and , thus, can be choosen the same as in Lemma 2.12) such that

$$
\left(\hat{D}_{k,j} \nabla \rho_{k,j}, \nabla\varphi \right)_{L^2(\Omega)} + (\hat{\sigma}_{\mathrm{a},k,j} \rho_{k,j}, \varphi)_{L^2(\Omega)} + (a_\mathrm{r} \rho_{k,j}, \varphi)_{L^2(\Gamma)} = \langle f_{k,j}, \varphi \rangle_{H^1(\Omega)^*}
$$

for all $\varphi \in H^1(\Omega)$, and it holds

$$
\|\rho_{k,j}\|_{W^{1,p}(\Omega)} \leq C \|f_{k,j}\|_{W^{1,q}(\Omega)^*} ,
$$

where the constant C depends only on the domain and the upper and lower bounds of the coefficients σ_a and D.

We define $\rho_k(t) := \sum_{j=1}^{d_k} 1_{E_{k,j}}(t) \rho_{k,j} \in L^p(I; W^{1,p}(\Omega))$, which is, similarly to estimate (A.35), uniformly bounded by[66]

$$
\begin{aligned}
\|\rho_k\|_{L^p(I;W^{1,p}(\Omega))}^p &= \sum_{j=1}^{d_k} |E_{k,j}| \, \|\rho_{k,j}\|_{W^{1,p}(\Omega)}^p \leq C \sum_{j=1}^{d_k} |E_{k,j}| \, \|f_{k,j}\|_{W^{1,q}(\Omega)^*}^p \\
&= C \|f_k\|_{L^p(I;W^{1,q}(\Omega)^*)}^p \leq C \|f\|_{L^p(I;W^{1,q}(\Omega)^*)}^p
\end{aligned}
\tag{A.49}
$$

for all $k \in \mathbb{N}$, where we used Hölder's inequality and the convergence in (A.48).

---

[65] See [74, Sec. 4.1, Thm. 3, p. 482].

[66] Like in estimate (A.35), assume w.l.o.g. that the sets $\{E_{k,j} \mid 1 \leq j \leq d_k\}$ are pairwise disjoint for a fixed k.

(c) Analogously to equation (A.37), it holds $\rho(t) \in H^1(\Omega)$ and

$$\left\langle F_{\mathrm{r}}^{\varphi,k}, \rho_k \right\rangle_{L^p(I;W^{1,p}(\Omega))} = \int_0^T \left\langle f_k(t), \varphi(t) \right\rangle_{H^1(\Omega)} \mathrm{d}t \tag{A.50}$$

for all $\varphi \in L^2(I; H^1(\Omega))$.

The convergence in (A.48) implies

$$\int_0^T \left\langle f_k(t), \varphi \right\rangle_{H^1(\Omega)} \mathrm{d}t \to \int_0^T \left\langle f(t), \varphi \right\rangle_{H^1(\Omega)} \mathrm{d}t$$

for all $\varphi \in L^2(I; H^1(\Omega))$. This allows passing to the limit on both sides of the equation (A.50), which yields, analogously to equation (A.38), that the weak limit ρ^* is a solution of the linearized radiation equation, i.e.,

$$\left\langle F_{\mathrm{r}}^{\varphi}(\omega), \rho^* \right\rangle_{L^p(I;W^{1,p}(\Omega))} = \int_0^T \left\langle f(t), \varphi(t) \right\rangle_{H^1(\Omega)} \mathrm{d}t \quad \text{for all } \varphi \in L^2(I; H^1(\Omega)).$$

(d) Analogously to estimate (A.36), we get with estimates (A.47) and (A.49) that

$$\|\rho\|_{L^p(I;W^{1,p}(\Omega))} \le C \|f\|_{L^p(I;W^{1,q}(\Omega)^*)} \le C(\phi, \vartheta) \|\tilde{\eta}\|_{\mathcal{C}^0(\overline{Q})} .$$

Note that the analog result holds for other final times $\tilde{T} \in I$. We can extend the functions $\tilde{\phi}, \tilde{\vartheta}, \tilde{\rho} \colon (0, \tilde{T}) \to \mathbb{R}$ to the whole time domain I by setting $\tilde{\phi}(t) := \tilde{\vartheta}(t) := \tilde{\rho}(t) := 0$ for $t > \tilde{T}$. With this, $\tilde{\rho}$ still fulfills the resulting linearized radiation equation (A.43) for the extended functions $\tilde{\phi}, \tilde{\vartheta}$ on I, and it holds

$$\|\tilde{\rho}\|_{L^p((0,\tilde{T});W^{1,p}(\Omega))} \le \|\tilde{\rho}\|_{L^p((0,T);W^{1,p}(\Omega))} \le C(\tilde{\phi}, \tilde{\vartheta}) \|\tilde{\eta}\|_{\mathcal{C}^0([0,\tilde{T}];\overline{\Omega})}$$
$$\le C(\phi, \vartheta) \|\tilde{\eta}\|_{\mathcal{C}^0([0,\tilde{T}];\overline{\Omega})} .$$

2. Analogously to the proof of [93, Sec. 1.3.2.3, Thm. 1.33, p. 42], we can look at the linearized radiation equation pointwise in t, i.e., for a.a. $t \in I$ and $f(t)$ given in (A.44), the solution $\rho \in L^p(I; W^{1,p}(\Omega))$ fulfills

$$F_{\mathrm{r}}(\rho(t), \varphi; \vartheta, t) = \left\langle f(t), \varphi \right\rangle_{H^1(\Omega)} \quad \text{for all } \varphi \in H^1(\Omega). \tag{A.51}$$

The assertion $\rho(t) \in L^\infty(\Omega)$ can be shown analogously to the proof of [217, Sec. 4.2.3, Thm. 4.5, p. 151]. In the following, we summarize the proof therein but do not reproduce every single step. We highlight the differences to our situation and derive the required estimates, which need to be replaced in the original proof in order to apply it here.

> Use Stampacchia's method to prove $L^\infty(\Omega)$ bounds.

In [217, Sec. 4.2.3, Thm. 4.5, p. 151], the authors discuss an elliptic equation similar to (A.51), but with a right-hand side given by $f \in L^r(\Omega)$ with $r > \frac{d}{2}$. In fact, for their proof, only the variational form, i.e., the term $(f, \varphi)_{L^2(\Omega)}$ for $\varphi \in H^1(\Omega)$, is required. This allows us to exchange the right-hand side here and reproduce the rest of their proof.

The outline of the proof is as follows. For an arbitrary $k > 0$, we define the function

$$v \colon \Omega \to \mathbb{R}, \ v(x) := \begin{cases} \rho(t)(x) - k, & \rho(t)(x) \geq k, \\ 0, & |\rho(t)(x)| < k, \\ \rho(t)(x) + k, & \rho(t)(x) \leq -k \end{cases}$$

and the set

$$\Omega(k) := \{x \in \Omega \,|\, |\rho(t)(x)| \geq k\}.$$

The idea is to show that, for sufficiently large k, the set $\Omega(k)$ has measure zero, i.e., the function v vanishes a.e. in Ω. This implies that the function $\rho(t)$ is essentially bounded by k.

(a) For $p_0 := 6$, it holds[67] $H^1(\Omega) \hookrightarrow L^{p_0}(\Omega)$ and, thus,[68]

$$\left(\int_{\Omega(k)} |v(x)|^{p_0} \, \mathrm{d}x \right)^{\frac{2}{p_0}} \leq \|v\|^2_{L^{p_0}(\Omega)} \leq C \, \|v\|^2_{H^1(\Omega)}. \tag{A.52}$$

(b) Based on the coercivity of the bilinear form F_{r}, the variational form (A.51) and the properties of v, one can show[69] that

$$c \, \|v\|^2_{H^1(\Omega)} \leq F_{\mathrm{r}}(v, v; \vartheta, t) \leq F_{\mathrm{r}}(\rho(t), v; \vartheta, t) \leq \langle f(t), v \rangle_{H^1(\Omega)}. \tag{A.53}$$

Note that the term $\langle f(t), v \rangle_{H^1(\Omega)}$ in (A.53) replaces the term $(f, v)_{L^2(\Omega)}$ in the original proof.

(c) Next, we need to estimate the term $\langle f(t), v \rangle_{H^1(\Omega)}$.

It holds with Hölder's inequality and the definition of v that

$$\left| (\mathrm{D}_\vartheta \sigma_{\mathrm{a}}(\vartheta)[\tilde{\eta}](t)\phi, v)_{L^2(\Omega)} \right| \leq C(\vartheta) \int_0^t \|\tilde{\eta}(s)\|_{\mathcal{C}^0(\overline{\Omega})} \, \mathrm{d}s \, \|\phi(t)\|_{L^p(\Omega)} \|v\|_{L^q(\Omega(k))},$$

$$\left| (\mathrm{D}_\vartheta D(\vartheta)[\tilde{\eta}](t)\nabla\phi(t), \nabla v)_{L^2(\Omega)} \right| \leq C(\vartheta) \int_0^t \|\tilde{\eta}(s)\|_{\mathcal{C}^0(\overline{\Omega})} \, \mathrm{d}s \, \|\nabla\phi(t)\|_{L^p(\Omega)} \|\nabla v\|_{L^q(\Omega(k))}$$

with $p > 3$ as given in the assumption and $q = \frac{p}{p-1} < \frac{3}{2}$.

With Hölder's inequality and $\hat{p} := \frac{2}{q}$ and $\hat{q} = \frac{\hat{p}}{\hat{p}-1}$ we get

$$\|v\|_{L^q(\Omega(k))} = \left(\int_{\Omega(k)} |v|^q \cdot 1 \, \mathrm{d}x \right)^{\frac{1}{q}} \leq \left(\int_{\Omega(k)} |v|^{q\hat{p}} \, \mathrm{d}x \right)^{\frac{1}{q\hat{p}}} \left(\int_{\Omega(k)} 1 \, \mathrm{d}x \right)^{\frac{1}{q\hat{q}}}$$

$$\leq \|v\|_{L^2(\Omega)} \, |\Omega(k)|^{\frac{1}{q\hat{q}}} \leq C \, \|v\|_{H^1(\Omega)} \, |\Omega(k)|^{\frac{1}{q\hat{q}}}$$

for all $\varepsilon > 0$. The analog results holds for $\|\nabla v\|_{L^q(\Omega(k))}$.

Furthermore, for $\lambda := 3 - \frac{6}{p} > 1$ and $p_0 = 6$ as defined above, it holds

$$\frac{2}{q\hat{q}} = \frac{\hat{p}}{\hat{q}} = \hat{p} - 1 = \frac{2}{q} - 1 = \frac{2(p-1)}{p} - 1 = 1 - \frac{2}{p} = \lambda \frac{2}{p_0}.$$

---

[67] See Sobolev embedding theorem B.56.
[68] See [110, II 5 , Prop. 5.3, p. 36] and [110, II B , Thm. B.2, p. 63] for a reasoning that $v \in H^1(\Omega)$.
[69] Cf. [217, Sec. 7.2.2, Eq. 7.7, p. 281].

Overall, we get with Young's inequality[70]

$$
\left| \langle f(t), v \rangle_{H^1(\Omega)} \right|
$$

$$
\leq C \left(\int_0^t \|\tilde{\eta}(s)\|_{\mathcal{C}^0(\overline{\Omega})} \, \mathrm{d}s \, \|\phi(t)\|_{W^{1,p}(\Omega)} \right)^2 |\Omega(k)|^{\lambda \frac{2}{p_0}} + \varepsilon \|v\|_{H^1(\Omega)}^2 \tag{A.54}
$$

for all $\varepsilon > 0$. Note that, in the original proof, this is estimate replaced by

$$
(f, v)_{L^2(\Omega)} \leq c \|f\|_{L^r(\Omega)}^2 |\Omega(k)|^{\lambda \frac{2}{p_0}} + \varepsilon \|v\|_{H^1(\Omega)}^2 .
$$

(d) Let $h > k$. Then it holds $\Omega(h) \subset \Omega(k)$ and, with this,

$$
\left(\int_{\Omega(k)} (|\rho(t)(x)| - k)^{p_0} \, \mathrm{d}x \right)^{\frac{2}{p_0}} \geq \left(\int_{\Omega(h)} (|\rho(t)(x)| - k)^{p_0} \, \mathrm{d}x \right)^{\frac{2}{p_0}}
$$

$$
\geq \left(\int_{\Omega(h)} (h - k)^{p_0} \, \mathrm{d}x \right)^{\frac{2}{p_0}} = (h - k)^2 \, |\Omega(h)|^{\frac{2}{p_0}} .
$$

Estimates (A.52), (A.53) and (A.54) now yield

$$
(h - k)^2 \left(|\Omega(h)|^{\frac{2}{p_0}} \right) \leq C \left(\int_0^t \|\tilde{\eta}(s)\|_{\mathcal{C}^0(\overline{\Omega})} \, \mathrm{d}s \right)^2 \left(|\Omega(k)|^{\frac{2}{p_0}} \right)^{\lambda} .
$$

(e) Like in the original proof, we are now able to apply the key argument of Stampacchia's method[71] [217, Sec. 7.2.2, Lem. 7.5, p. 297] and obtain a certain h such that $|\Omega(h)| = 0$, which implies the $L^\infty(\Omega)$ bound for $\rho(t)$.

(f) The estimate for $\|\rho(t)\|_{H^1(\Omega)}$ follows from testing equation (A.51) with $\varphi = \rho(t)$ and the estimate

$$
\left| \langle f(t), \rho(t) \rangle_{H^1(\Omega)} \right| \leq C \int_0^t \|\tilde{\eta}(s)\|_{\mathcal{C}^0(\overline{\Omega})} \, \mathrm{d}s \, \|\rho(t)\|_{H^1(\Omega)} .
$$

∎

Proof of Lemma 3.9. Even though the system is linear w.r.t. the state vector (ρ, η), it is not trivial to solve because of the memory term $\int_0^t \eta(s) \, \mathrm{d}s$ included in the derivatives of the coefficients. In [129], the authors considered a similar problem for wave equations with memory terms. We apply their idea for handling the memory term by means of Banach's fixed point theorem[72] to our linearized state system.

> Freeze the linear state in the memory term $\int_0^t \eta(s) \, \mathrm{d}s$ on the right-hand side, solve the two equations for two components of the linearized state vector consecutively and apply Banach's fixed-point theorem in a specially weighted space.

The idea is to freeze the linear state η in the memory term, which allows us to solve the linearized radiation equation separately, and consecutively solve the linearized heat-transfer equation.

---

[70] See Young's inequality B.25.
[71] See also [110].
[72] See [233, Sec. 1.6, Thm. 1.A, p. 19] for Banach's fixed-point theorem.

We consider the space

$$B_\alpha := L^\infty(I; H^1(\Omega)) \cap \mathcal{C}^0(\overline{Q})$$

equipped with the norm

$$\|\eta\|_{B_\alpha} := \left\|e^{-\alpha t}\eta\right\|_{L^\infty(I;H^1(\Omega))} + \left\|e^{-\alpha t}\eta\right\|_{\mathcal{C}^0(\overline{Q})} \tag{A.55}$$

for a certain $\alpha > 0$.

The goal is to apply Banach's fixed-point theorem to the map

$$S\colon B_\alpha \to B_\alpha,\ \tilde{\eta} \mapsto \eta$$

where $\eta \in (L^\infty(I; H^1(\Omega)) \cap H^1(I; H^1(\Omega)) \cap H^2(I; H^1(\Omega)^*) \cap \mathcal{C}^0(\overline{Q})) \hookrightarrow B_\alpha$ fulfills

$$\left\{ \begin{aligned} &\int_0^T \tau \langle \eta''(t), \varphi(t) \rangle_{H^1(\Omega)} + (\eta'(t), \varphi(t))_{L^2(\Omega)} + F_{\mathrm{h}}(\eta(t), \varphi(t); u)\, \mathrm{d}t \\ &\qquad = \int_0^T (\hat{\sigma}\sigma_{\mathrm{a}}(\vartheta)(t)\rho(t), \varphi(t))_{L^2(\Omega)} + (\hat{\sigma}\mathrm{D}_\vartheta\sigma_{\mathrm{a}}(\vartheta)[\tilde{\eta}](t)\phi(t), \varphi(t))_{L^2(\Omega)}\, \mathrm{d}t \\ &\qquad\quad + \int_0^T ((\xi_{\mathrm{in}} - \xi_{\mathrm{out}})(\vartheta_{\mathrm{b}} - \vartheta(t))h, \varphi(t))_{L^2(\Omega)}\, \mathrm{d}t\,, \\ &\eta(0) = 0, \\ &\eta'(0) = 0 \end{aligned} \right\} \tag{A.56}$$

for all $\varphi \in L^2(I; H^1(\Omega))$, and $\rho := \rho(\tilde{\eta}) \in L^2(I; H^1(\Omega))$ fulfills the linearized radiation equation (A.43) for all $\varphi \in L^2(I; H^1(\Omega))$.

A fixed point η of the map S and the corresponding state $\rho = \rho(\eta)$ solve the original linearized state system (3.14) for all $\varphi \in L^2(I; H^1(\Omega)) \times L^2(I; H^1(\Omega))$. On the other hand, a linearized state vector fulfilling (3.14) for all $\varphi \in L^2(I; H^1(\Omega)) \times L^2(I; H^1(\Omega))$ is also a fixed point of S. In the remainder of this proof, we show that the prerequisites of Banach's fixed point theorem are fulfilled, which implies the existence of a unique linearized state vector in B_α.

Before we start, we note that the standard norm ($\alpha = 0$) would induce an upper bound on the final time T when showing that S is a contraction later in this proof, whereas the weighted norm (A.55) with suitable α allows arbitrary final times T.

1. Note that the space B_α equipped with the norm (A.55) is a Banach space, which follows from the fact that $L^\infty(I; H^1(\Omega)) \cap \mathcal{C}^0(\overline{Q})$ equipped with the norm in (A.55) for $\alpha = 0$ is a Banach space[73] and the equivalence of the norms[74]

$$e^{-\alpha T}\|\eta\|_{L^\infty(I;H^1(\Omega))\cap\mathcal{C}^0(\overline{Q})} \leq \|\eta\|_{B_\alpha} \leq \|\eta\|_{L^\infty(I;H^1(\Omega))\cap\mathcal{C}^0(\overline{Q})}\,. \tag{A.57}$$

2. Next, we need to show that the map S is well defined.

   Let $\tilde{\eta} \in B_\alpha$. Lemma A.7 implies the existence of a unique solution $\rho = \rho(\tilde{\eta}) \in L^2(I; H^1(\Omega))$ which fulfills (A.43) for all $\varphi \in L^2(I; H^1(\Omega))$. It holds

$$\|\rho\|_{L^2(I;H^1(\Omega))} \leq C\|\tilde{\eta}\|_{\mathcal{C}^0(\overline{Q})}$$

---

[73] See Theorem B.48.
[74] Cf. [129, Sec. 7.1, p. 20].

and, for a.a. $t \in I$, it holds $\rho(t) \in L^\infty(\Omega) \cap H^1(\Omega)$ with

$$\|\rho(t)\|_{H^1(\Omega)} + \|\rho(t)\|_{L^\infty(\Omega)} \leq C \int_0^t \|\tilde{\eta}(s)\|_{\mathcal{C}^0(\overline{\Omega})} \, \mathrm{d}s. \tag{A.58}$$

Lemma A.4 implies the existence and uniqueness of a solution $\eta \in W_\vartheta \cap \mathcal{C}^0(\overline{Q})$ which fulfills (A.56) for all $\varphi \in L^2(I; H^1(\Omega))$. To this, we need to check the prerequisites and define

$$r_1(t) := \hat{\sigma}\sigma_{\mathrm{a}}(\vartheta)(t)\rho(t) + \hat{\sigma}\mathrm{D}_\vartheta\sigma_{\mathrm{a}}(\vartheta)[\tilde{\eta}](t)\phi(t),$$
$$r_2(t) := (\xi_{\mathrm{in}} - \xi_{\mathrm{out}})(\vartheta_{\mathrm{b}} - \vartheta(t))h,$$
$$g(t) := 0.$$

With estimate (A.58) and Lemmas 2.9, 2.11 2.12, 3.8, we have[75]

$$\sigma_{\mathrm{a}}(\vartheta)(t), \, \mathrm{D}_\vartheta\sigma_{\mathrm{a}}(\vartheta)[\tilde{\eta}](t), \, \phi(t), \, \rho(t) \in H^1(\Omega) \cap L^\infty(\Omega) \quad \text{for a.a. } t \in I,$$

thus, we can apply the product rule[76] and obtain $r_1(t) \in H^1(\Omega)$. Note that it holds

$$\|\mathrm{D}_\vartheta\sigma_{\mathrm{a}}(\vartheta)[\tilde{\eta}](t)\|_{H^1(\Omega)} \leq C(\vartheta) \int_0^t \|\tilde{\eta}(s)\|_{H^1(\Omega)} \, \mathrm{d}s.$$

Furthermore, with the same estimates and lemmas as cited above, we get $r_1 \in L^2(I; L^2(\Omega))$ and

$$\|r_1(t)\|_{H^1(\Omega)} \leq C \int_0^t \|\tilde{\eta}(s)\|_{H^1(\Omega)} + \|\tilde{\eta}(s)\|_{\mathcal{C}^0(\overline{\Omega})} \, \mathrm{d}s =: \tilde{r}(t) \quad \text{for a.a. } t \in I,$$

and it holds $\tilde{r} \in L^2(I)$ according to Bochner's theorem[77].

With $h \in L^\infty(\Omega)$ and $\vartheta \in W_\vartheta$, we get $r_2 \in H^1(I; L^2(\Omega))$ with

$$\|r_2\|_{H^1(I; L^2(\Omega))} \leq C(\vartheta) \|h\|_{L^\infty(\Omega)}.$$

In summary, we are able to apply Lemma A.4, which yields a solution

$$\eta \in L^\infty(I; H^1(\Omega)) \cap H^1(I; H^1(\Omega)) \cap H^2(I; H^1(\Omega)^*) \cap \mathcal{C}^0(\overline{Q}).$$

Furthermore, with Hölder's and Young's inequalities[78], we get

$$\|\eta\|_{L^\infty(I; H^1(\Omega))}^2 + \|\eta\|_{\mathcal{C}^0(\overline{Q})}^2$$
$$\leq C \left(\int_0^T \tilde{r}(t)^2 \, \mathrm{d}t + \|h\|_{L^\infty(\Omega)}^2 \right)$$
$$\leq C \left(\int_0^T \int_0^t \|\tilde{\eta}(s)\|_{H^1(\Omega)}^2 + \|\tilde{\eta}(s)\|_{\mathcal{C}^0(\overline{\Omega})}^2 \, \mathrm{d}s \, \mathrm{d}t + \|h\|_{L^\infty(\Omega)}^2 \right).$$

---

[75] In fact, $\mathrm{D}_\vartheta\gamma(\vartheta)[\tilde{\eta}](t, x) = -\gamma(\vartheta)(t, x) \int_0^t d'_{\mathrm{Arr}}(\vartheta(s, x))\tilde{\eta}(s, x) \, \mathrm{d}s \in H^1(\Omega)$ follows from the product rule B.43 because the individual terms are in $L^\infty(\Omega) \cap H^1(\Omega)$. Note that the weak differentiability (w.r.t. the spatial variable x) of $\gamma(t)$ is shown in the proof of Lemma 2.11, and the $L^\infty(\Omega)$ bound is shown in Lemma 2.9. The differentiability of $d'_{\mathrm{Arr}}(\vartheta(t, x))$ follows from the chain rule B.41. See also the proof of Lemma 2.9 for a more detailed discussion on the function d_{Arr}.

[76] See product rule for weak derivatives B.43.

[77] See Bochner's theorem B.47.

[78] See Hölder's B.27 and Young's B.25 inequalities. Young's inequality implies that for $a, b > 0$ it holds $(a + b)^2 \leq C(a^2 + b^2)$, see Remark B.26.

With the continuous embeddings

$$L^\infty(I; H^1(\Omega)) \cap H^1(I; H^1(\Omega)) \cap H^2(I; H^1(\Omega)^*) \cap \mathcal{C}^0(\overline{Q}) \hookrightarrow L^\infty(I; H^1(\Omega)) \cap \mathcal{C}^0(\overline{Q}) \hookrightarrow B_\alpha,$$

where the last embedding is continuous because of the equivalence of the norms in (A.57), we get that S is well defined as map from B_α to B_α.

3. Last, we need to show that S is a contraction. To this, let $\tilde\eta_1, \tilde\eta_2 \in B_\alpha$ and define $\rho_1 := \rho(\tilde\eta_1)$, $\rho_2 := \rho(\tilde\eta_2)$ and $\eta_1 := \eta(\tilde\eta_1, \rho_1)$, $\eta_2 := \eta(\tilde\eta_2, \rho_2)$ to be the corresponding solutions of (A.43) and (A.56).

The difference $\delta\rho := \rho_1 - \rho_2$ fulfills

$$\int_0^T F_{\mathrm{r}}(\delta\rho(t), \varphi(t); \vartheta, t)\, \mathrm{d}t = -\int_0^T (\mathrm{D}_\vartheta D(\vartheta)[\delta\tilde\eta](t)\nabla\phi(t), \nabla\varphi(t))_{L^2(\Omega)}\, \mathrm{d}t \tag{A.59}$$
$$- \int_0^T (\mathrm{D}_\vartheta \sigma_{\mathrm{a}}(\vartheta)[\delta\tilde\eta](t)\phi(t), \varphi(t))_{L^2(\Omega)}\, \mathrm{d}t$$

for all $\varphi \in L^2(I; H^1(\Omega))$, with $\delta\tilde\eta := \tilde\eta_1 - \tilde\eta_2$.

Because (A.59) has the same structure as the linearized radiation equation (A.43), we get with the same argument that

$$\|\delta\rho\|_{L^2(I; H^1(\Omega))} \leq C(T)\, \|\delta\tilde\eta\|_{\mathcal{C}^0(\overline{Q})}$$

and, similar to estimate (A.58), that

$$\|\delta\rho(t)\|_{L^\infty(\Omega)} + \|\delta\rho(t)\|_{H^1(\Omega)} \leq C(T) \int_0^t \|\delta\tilde\eta(s)\|_{\mathcal{C}^0(\overline{\Omega})}\, \mathrm{d}s\,.$$

The difference $\delta\eta := \eta_1 - \eta_2$ fulfills

$$\left\{ \begin{aligned} & \int_0^T \tau \langle \delta\eta''(t), \varphi(t) \rangle_{H^1(\Omega)} + (\delta\eta'(t), \varphi(t))_{L^2(\Omega)} + F_{\mathrm{h}}(\delta\eta(t), \varphi(t); u)\, \mathrm{d}t \\ & \qquad = \int_0^T (\hat\sigma \sigma_{\mathrm{a}}(\vartheta)(t)\delta\rho(t), \varphi(t))_{L^2(\Omega)}\, \mathrm{d}t \\ & \qquad\quad + \int_0^T (\hat\sigma \mathrm{D}_\vartheta \sigma_{\mathrm{a}}(\vartheta)[\delta\tilde\eta](t)\phi(t), \varphi(t))_{L^2(\Omega)}\, \mathrm{d}t\,, \\ & \delta\eta(0) = 0, \\ & \delta\eta'(0) = 0 \end{aligned} \right. \tag{A.60}$$

for all $\varphi \in L^2(I; H^1(\Omega))$.

We define

$$r_1(t) := \hat\sigma \sigma_{\mathrm{a}}(\vartheta)(t)\delta\rho(t) + \hat\sigma \mathrm{D}_\vartheta \sigma_{\mathrm{a}}(\vartheta)[\delta\tilde\eta](t)\phi(t),$$
$$r_2(t) := 0,$$
$$g(t) := 0.$$

Analogously as above, it holds $r_1 \in L^2(I; L^2(\Omega))$ with

$$\|r_1(t)\|_{H^1(\Omega)} \leq C \int_0^t \|\delta\tilde\eta(s)\|_{H^1(\Omega)} + \|\delta\tilde\eta(s)\|_{\mathcal{C}^0(\overline{\Omega})}\, \mathrm{d}s =: \tilde r(t) \quad \text{for a.a. } t \in I,$$

and it holds $\tilde{r} \in L^2(I)$. With Lemma A.4 we get $\delta\eta \in L^\infty(I; H^1(\Omega)) \cap \mathcal{C}^0(\overline{Q}) \cap H^1(I; H^1(\Omega))$.

This allows us to test equation (A.60), only integrated[79] from 0 to t, with the test function $\varphi = \delta\eta' \in L^2(I; H^1(\Omega))$, and get similarly[80] to the proof of Remark A.6 that

$$
\begin{aligned}
\|\delta\eta'(t)\|^2_{L^2(\Omega)} + \|\delta\eta(t)\|^2_{H^1(\Omega)} &\leq C \int_0^t \tilde{r}(s)^2 \,\mathrm{d}s \\
&\leq C \int_0^t \int_0^s \|\delta\tilde{\eta}(s')\|^2_{H^1(\Omega)} + \|\delta\tilde{\eta}(s')\|^2_{\mathcal{C}^0(\overline{\Omega})} \,\mathrm{d}s' \,\mathrm{d}s
\end{aligned}
\tag{A.61}
$$

for a.a. $t \in I$.

Furthermore, from Lemma A.4, it follows that for arbitrary final times $\tilde{T} < T$ it holds $\delta\eta \in \mathcal{C}^0([0, \tilde{T}] \times \overline{\Omega})$ with the state bound

$$
\begin{aligned}
\sup_{t \in [0,\tilde{T}]} \|\delta\eta(t)\|^2_{\mathcal{C}^0(\overline{\Omega})} &\leq C(\tilde{T}) \int_0^{\tilde{T}} \tilde{r}(t)^2 \,\mathrm{d}t \\
&\leq C(\tilde{T}) \int_0^{\tilde{T}} \int_0^t \|\delta\tilde{\eta}(s)\|^2_{H^1(\Omega)} + \|\delta\tilde{\eta}(s)\|^2_{\mathcal{C}^0(\overline{\Omega})} \,\mathrm{d}s \,\mathrm{d}t,
\end{aligned}
$$

where the second estimate follows with Hölder's and Young's inequalities. As discussed in Lemma A.4, the function which maps the final time $\tilde{T} \in I$ to the corresponding constant $C(\tilde{T}) \in \mathbb{R}_{>0}$ is essentially bounded, thus, we get together with estimate (A.61) that

$$
\|\delta\eta(t)\|^2_{H^1(\Omega)} + \|\delta\eta(t)\|^2_{\mathcal{C}^0(\overline{\Omega})} \leq C \int_0^t \int_0^s \|\delta\tilde{\eta}(s')\|^2_{H^1(\Omega)} + \|\delta\tilde{\eta}(s')\|^2_{\mathcal{C}^0(\overline{\Omega})} \,\mathrm{d}s' \,\mathrm{d}s
\tag{A.62}
$$

for a.a. $t \in I$.

This allows us to proceed like in [129, Sec. 7.1, p. 20]. We multiply both sides of equation (A.62) with $e^{-2\alpha t}$ for $\alpha > 0$ and get, for a.a. $t \in I$, that

$$
\begin{aligned}
&e^{-2\alpha t} \left(\|\delta\eta(t)\|^2_{H^1(\Omega)} + \|\delta\eta(t)\|^2_{\mathcal{C}^0(\overline{\Omega})} \right) \\
&\leq C e^{-2\alpha t} \int_0^t \int_0^s \|\delta\tilde{\eta}(s')\|^2_{H^1(\Omega)} + \|\delta\tilde{\eta}(s')\|^2_{\mathcal{C}^0(\overline{\Omega})} \,\mathrm{d}s' \,\mathrm{d}s \\
&\leq C \int_0^t \int_0^s e^{-2\alpha t} \left(\|\delta\tilde{\eta}(s')\|^2_{H^1(\Omega)} + \|\delta\tilde{\eta}(s')\|^2_{\mathcal{C}^0(\overline{\Omega})} \right) \,\mathrm{d}s' \,\mathrm{d}s \\
&\leq C \int_0^t \int_0^t e^{-2\alpha(t-s')} e^{-2\alpha s'} \left(\|\delta\tilde{\eta}(s')\|^2_{H^1(\Omega)} + \|\delta\tilde{\eta}(s')\|^2_{\mathcal{C}^0(\overline{\Omega})} \right) \,\mathrm{d}s' \,\mathrm{d}s \\
&\leq C T \sup_{s \in I} \left(e^{-2\alpha s} \left(\|\delta\tilde{\eta}(s)\|^2_{H^1(\Omega)} + \|\delta\tilde{\eta}(s)\|^2_{\mathcal{C}^0(\overline{\Omega})} \right) \right) \int_0^t e^{-2\alpha(t-s')} \,\mathrm{d}s' \\
&\leq C T \|\delta\tilde{\eta}\|^2_{B_\alpha} \frac{1 - e^{-2\alpha T}}{2\alpha}.
\end{aligned}
$$

After taking the supremum over $t \in I$, we get

$$
\|\delta\eta\|^2_{B_\alpha} \leq C T \|\delta\tilde{\eta}\|^2_{B_\alpha} \frac{1 - e^{-2\alpha T}}{2\alpha} \leq \frac{CT}{2\alpha} \|\delta\tilde{\eta}\|^2_{B_\alpha}
$$

---

[79] It is feasible to consider the integral in the weak formulation only from 0 to t because it holds for all test functions $\varphi \in L^2(I; H^1(\Omega))$ and , thus, especially for those with $\varphi(s) = 0$ for $s > t$.

[80] Here, we can write

$$
\int_0^t \langle \delta\eta''(s), \delta\eta'(s) \rangle_{H^1(\Omega)} \,\mathrm{d}s = \int_0^t \left(\delta\eta''(s), \delta\eta'(s) \right)_{L^2(\Omega)} \,\mathrm{d}s = \frac{1}{2} \left(\|\delta\eta'(t)\|^2_{L^2(\Omega)} - \|\delta\eta'(0)\|^2_{L^2(\Omega)} \right)
$$

by means of integration by parts in Bochner spaces B.36.

and, thus, for $\alpha = CT$, the desired result

$$\|\delta\eta\|_{B_\alpha}^2 \le \frac{1}{2} \|\delta\tilde{\eta}\|_{B_\alpha}^2 \,.$$

The result now follows from Banach's fixed-point theorem as discussed at the beginning.

■

A.2.3 Proof of Lemma 3.12

Proof.

> Repeat the same procedure as for the linearized state equation in Lemma 3.9.

If we rescaled the time variable by $\hat{t} := T - t$, the adjoint state system (3.19) would have a similar structure as the linearized state system (3.14). The proof follows the same structure, and we highlight only the differences.

We consider the space

$$B_\alpha := L^\infty(I; H^1(\Omega))$$

equipped with the norm

$$\|z_2\|_{B_\alpha} := \left\| e^{\alpha t} z_2 \right\|_{L^\infty(I; H^1(\Omega))}$$

for a certain $\alpha > 0$.

The goal is to apply Banach's fixed-point theorem to the map

$$S \colon B_\alpha \to B_\alpha, \ \tilde{z}_2 \mapsto z_2$$

where $z_2 \in (L^\infty(I; H^1(\Omega)) \cap H^1(I; H^1(\Omega)) \cap H^2(I; H^1(\Omega)^*) \hookrightarrow B_\alpha$ fulfills

$$
\left\{
\begin{aligned}
&\int_0^T \tau \left\langle z_2''(t), \varphi(t) \right\rangle_{H^1(\Omega)} - (z_2'(t), \varphi(t))_{L^2(\Omega)} + F_{\mathrm{h}}(z_2(t), \varphi(t); u) \, \mathrm{d}t \\
&\qquad\qquad = -\int_0^T (f_D(z_1)(t) - f_{\sigma_{\mathrm{a}}}(z_1, \tilde{z}_2)(t), \varphi(t))_{L^2(\Omega)} \, \mathrm{d}t, \\
&z_2(T) - \tau z_2'(T) = \vartheta(T) - \vartheta_{\mathrm{d}}, \\
&\qquad \tau z_2(T) = 0
\end{aligned}
\right\}
\tag{A.63}
$$

for all $\varphi \in L^2(I; H^1(\Omega))$, and $z_1 := z_1(\tilde{z}_2) \in L^2(I; H^1(\Omega))$ fulfills

$$\int_0^T F_{\mathrm{r}}(z_1(t), \varphi(t); \vartheta, t) \, \mathrm{d}t = \int_0^T \hat{\sigma} \left(\sigma_{\mathrm{a}}(\vartheta)(t) \tilde{z}_2(t), \varphi(t)\right)_{L^2(\Omega)} \, \mathrm{d}t \tag{A.64}$$

for all $\varphi \in L^2(I; H^1(\Omega))$.

Like in Lemma 3.9, we need to check the prerequisites for Banach's fixed-point theorem.

1. Analogously to estimate (A.57), it follows that B_α is a Banach space.

2. The map S is well defined.

   To see this, we note that it holds $f(t) = \hat{\sigma} \sigma_{\mathrm{a}}(\vartheta)(t) \tilde{z}_2(t) \in L^2(I; L^2(\Omega))$ for the right-hand side of equation (A.64). Analogously to Lemma A.7, especially equation (A.51), one can show that (A.64) has a unique solution $z_1 \in L^2(I; H^1(\Omega))$ with

   $$\|z_1(t)\|_{H^1(\Omega)}^2 \le C \|\tilde{z}_2(t)\|_{L^2(\Omega)}^2 \quad \text{for a.a. } t \in I.$$

The rather generous assumption $\phi \in L^\infty(I; W^{1,\infty}(\Omega))$ together with $\gamma(\vartheta), d'_{\mathrm{Arr}}(\vartheta), \hat{\sigma}_{\mathrm{t}}(\vartheta)$, $\vartheta \in \mathcal{C}^0(\overline{Q})$ now implies that

$$r := -f_D(z_1) - f_{\sigma_a}(z_1, \tilde{z}_2) \in L^2(I; L^2(\Omega)),$$

thus, with Lemma A.4, we get

$$z_2 \in (L^\infty(I; H^1(\Omega)) \cap H^1(I; H^1(\Omega)) \cap H^2(I; H^1(\Omega)^*) \hookrightarrow B_\alpha.$$

3. Analogously to the proof of Lemma 3.9, we take the difference of the equation (A.63) for two different inputs of S, then we test the resulting equation with $\varphi := \delta z'_2 \in L^2(I; H^1(\Omega))$ and integrate from t to T, where $\delta \tilde{z}_2$ and δz_2 denote the difference of the two inputs and the difference of the two corresponding outputs of S, respectively, and we get with Hölder's and Young's inequalities[81]

$$\|\delta z_2(t)\|^2_{H^1(\Omega)} \leq C(\phi, \vartheta) \int_t^T \int_s^T \|\delta \tilde{z}_2(s')\|^2_{H^1(\Omega)} \, \mathrm{d}s' \, \mathrm{d}s$$

for a.a. $t \in I$. Now we multiply both sides with $e^{2\alpha t}$ and proceed like in the proof of Lemma 3.9.

$\blacksquare$

A.2.4 Proof of Lemma 3.13

> **Lemma A.8**
>
> Let $T \in \mathbb{R}_{>0}$ and $f, g \colon [0, T] \to \mathbb{R}$ be Lebesgue-integrable functions. Then it holds
>
> $$\int_0^T f(t) \left(\int_0^t g(s) \, \mathrm{d}s \right) \mathrm{d}t = \int_0^T g(t) \left(\int_t^T f(s) \, \mathrm{d}s \right) \mathrm{d}t \,.$$

Proof. We define $F(t) = \int_0^t f(s) \, \mathrm{d}s$, $G(t) = \int_0^t g(s) \, \mathrm{d}s$. The fundamental theorem of calculus for Lebesgue integrals[82] yields that F and G are absolutely continuous and differentiable a.e. with $F'(t) = f(t)$ and $G'(t) = g(t)$ for a.a. $t \in [0, T]$. Furthermore, it holds $F(0) = G(0) = 0$.

Integration by parts[83] yields

$$F(T)G(T) - F(0)G(0) = \int_0^T f(t)G(t) \, \mathrm{d}t + \int_0^T F(t)g(t) \, \mathrm{d}t \,.$$

---

[81] See Hölder's B.27 and Young's B.25 inequalities.
[82] See the fundamental theorem of calculus for the Lebesgue integral B.31.
[83] See Theorem B.34 on the integration by parts for absolutely continuous functions.

This implies

$$\int_0^T f(t) \left(\int_0^t g(s)\,\mathrm{d}s \right) \mathrm{d}t = \int_0^T f(t)G(t)\,\mathrm{d}t = F(T)G(T) - F(0)G(0) - \int_0^T F(t)g(t)\,\mathrm{d}t$$

$$= \int_0^T f(t)\,\mathrm{d}t \int_0^T g(t)\,\mathrm{d}t - \int_0^T g(t) \left(\int_0^t f(s)\,\mathrm{d}s \right) \mathrm{d}t$$

$$= \int_0^T g(t) \left(\int_0^T f(s)\,\mathrm{d}s - \int_0^t f(s)\,\mathrm{d}s \right) \mathrm{d}t$$

$$= \int_0^T g(t) \left(\int_t^T f(s)\,\mathrm{d}s \right) \mathrm{d}t\,.$$

∎

Proof of Lemma 3.13.

> Apply integration by parts and Lemma A.8.

Let $u \in U_{\mathrm{ad}}$ be an admissible control and $(\phi, \vartheta) = S(u)$ be the corresponding state vector of the Cattaneo–LITT model. For $h \in L^\infty(\Omega)$ an admissible direction w.r.t. u, we consider the corresponding unique solution of the linearized state system (3.14) $(\rho, \eta) \in L^2(I; H^1(\Omega)) \times (W_\vartheta \cap \mathcal{C}^0(\overline{Q}))$ and the corresponding adjoint state vector $(z_1, z_2) \in L^2(I; H^1(\Omega)) \times L^2(I; H^1(\Omega))$. The regularity of the adjoint state vector allows us to use it as test function for the linearized state system (3.14).

We collect two auxiliary results.

1. The integration by parts formula[84] yields together with the initial conditions for the linearized state (ρ, η) and the adjoint state (z_1, z_2) that

$$\int_0^T \tau \langle \eta''(t), z_2(t) \rangle_{H^1(\Omega)}\,\mathrm{d}t$$

$$= -\int_0^T \tau (\eta'(t), z_2'(t))_{L^2(\Omega)}\,\mathrm{d}t + \tau \left(\eta'(T), \underbrace{z_2(T)}_{=0} \right)_{L^2(\Omega)} - \tau \left(\underbrace{\eta'(0)}_{=0}, z_2(0) \right)_{L^2(\Omega)}$$

$$= \int_0^T \tau \langle z_2''(t), \eta(t) \rangle_{H^1(\Omega)}\,\mathrm{d}t - \tau (z_2'(T), \eta(T))_{L^2(\Omega)} + \tau \left(z_2'(0), \underbrace{\eta(0)}_{=0} \right)_{L^2(\Omega)}$$

$$= \int_0^T \tau \langle z_2''(t), \eta(t) \rangle_{H^1(\Omega)}\,\mathrm{d}t + (\vartheta(T) - \vartheta_{\mathrm{d}}, \eta(T))_{L^2(\Omega)}\,,$$

$$\int_0^T (\eta'(t), z_2(t))_{L^2(\Omega)}\,\mathrm{d}t$$

$$= -\int_0^T (z_2'(t), \eta(t))_{L^2(\Omega)}\,\mathrm{d}t\,.$$

2. We consider the term regarding the derivative of the optical coefficient σ_{a} in the first equation of the linearized state system (the argument goes analogously for the term in

---

[84] See Theorem B.35 on the integration by parts in Sobolev spaces.

the second equation and for the term regarding D) and get with Fubini's theorem[85] and Lemma A.8 that

$$
\int_0^T (\mathrm{D}_\vartheta \sigma_\mathrm{a}(\vartheta)[\eta](t)\phi(t), z_1(t))_{L^2(\Omega)}\,\mathrm{d}t = \int_\Omega \left[\int_0^T f_x(t) \int_0^t g_x(s)\,\mathrm{d}s\,\mathrm{d}t \right]\mathrm{d}x
$$
$$
= \int_\Omega \left[\int_0^T g_x(t) \int_t^T f_x(s)\,\mathrm{d}s\,\mathrm{d}t \right]\mathrm{d}x
$$
$$
= \int_0^T \left(\hat{f}_{\sigma_\mathrm{a}}(t), \eta(t) \right)_{L^2(\Omega)}\,\mathrm{d}t
$$

with[86]

$$
f_x(t) = -(\sigma_{\mathrm{a,n}} - \sigma_{\mathrm{a,c}})\gamma(\vartheta)(t,x)\phi(t,x)z_1(t,x),
$$
$$
g_x(t) = d'(\vartheta(t,x))\eta(t,x),
$$
$$
\hat{f}_{\sigma_\mathrm{a}}(t)(x) = -(\sigma_{\mathrm{a,n}} - \sigma_{\mathrm{a,c}})d'(\vartheta(t,x)) \int_t^T \gamma(\vartheta)(s,x)\phi(s,x)z_1(s,x)\,\mathrm{d}s .
$$

We add the first two equations of the linearized state system tested with the adjoint state and obtain by means of the auxiliary results above:

$$
0 = \int_0^T F_\mathrm{r}(\rho(t), z_1(t); \vartheta, t)\,\mathrm{d}t
$$
$$
+ \int_0^T (\mathrm{D}_\vartheta D(\vartheta)[\eta](t)\nabla\phi(t), \nabla z_1(t))_{L^2(\Omega)} + (\mathrm{D}_\vartheta \sigma_\mathrm{a}(\vartheta)[\eta](t)\phi(t), z_1(t))_{L^2(\Omega)}\,\mathrm{d}t
$$
$$
+ \int_0^T \tau\,\langle \eta''(t), z_2(t) \rangle_{H^1(\Omega)} + (\eta'(t), z_2(t))_{L^2(\Omega)} + F_\mathrm{h}(\eta(t), z_2(t); u)\,\mathrm{d}t
$$
$$
- \int_0^T \hat{\sigma}\,(\sigma_\mathrm{a}(\vartheta)(t)\rho(t), z_2(t))_{L^2(\Omega)}\,\mathrm{d}t - \int_0^T \hat{\sigma}\,(\mathrm{D}_\vartheta \sigma_\mathrm{a}(\vartheta)[\eta](t)\phi(t), z_2(t))_{L^2(\Omega)}\,\mathrm{d}t
$$
$$
- \int_0^T ((\xi_\mathrm{in} - \xi_\mathrm{out})(\vartheta_\mathrm{b} - \vartheta(t))h, z_2(t))_{L^2(\Omega)}\,\mathrm{d}t
$$
$$
= \int_0^T F_\mathrm{r}(z_1(t), \rho(t); \vartheta, t)\,\mathrm{d}t - \int_0^T \hat{\sigma}\,(\sigma_\mathrm{a}(\vartheta)(t)\rho(t), z_2(t))_{L^2(\Omega)}\,\mathrm{d}t
$$
$$
+ \int_0^T \tau\,\langle z_2''(t), \eta(t) \rangle_{H^1(\Omega)} - (z_2'(t), \eta(t))_{L^2(\Omega)} + F_\mathrm{h}(z_2(t), \eta(t); u)\,\mathrm{d}t
$$
$$
+ \int_0^T (f_D(t) + f_{\sigma_\mathrm{a}}(t), \eta(t))_{L^2(\Omega)}\,\mathrm{d}t
$$
$$
+ (\vartheta(T) - \vartheta_\mathrm{d}, \eta(T))_{L^2(\Omega)} - \int_0^T ((\xi_\mathrm{in} - \xi_\mathrm{out})(\vartheta_\mathrm{b} - \vartheta(t))h, z_2(t))_{L^2(\Omega)}\,\mathrm{d}t
$$
$$
= (\vartheta(T) - \vartheta_\mathrm{d}, \eta(T))_{L^2(\Omega)} - \int_0^T ((\xi_\mathrm{in} - \xi_\mathrm{out})(\vartheta_\mathrm{b} - \vartheta(t))h, z_2(t))_{L^2(\Omega)}\,\mathrm{d}t .
$$

Note that the terms vanish in the last equality because they correspond to the adjoint state system (3.19) tested with $\varphi = (\rho, \eta)$, and (z_1, z_2) is just chosen to fulfill (3.19) for all $\varphi \in L^2(I; H^1(\Omega)) \times L^2(I; H^1(\Omega))$.

---

[85] See Fubini's theorem B.2.

[86] Note that, for every $x \in \Omega$, the functions f_x, g_x are Lebesgue measurable by means of Fubini's theorem.

With Lemma 3.11 and Fubini's theorem, we conclude

$$
\mathrm{D}_u \hat{J}(u)[h] = \int_\Omega \left(\vartheta(T;u) - \vartheta_\mathrm{d}\right)\eta(T) + \lambda_1 h + \lambda_2 u h \,\mathrm{d}x
$$

$$
= \left(\lambda_1 + \lambda_2 u + \int_0^T (\xi_\mathrm{in} - \xi_\mathrm{out})(\vartheta_\mathrm{b} - \vartheta(t)) z_2(t) \,\mathrm{d}t \,, h \right)_{L^2(\Omega)}.
$$

∎

A.3 Details for Chapter 4

Reduction of the spatial dimension

We consider the parameterization in cylindrical coordinates[87]

$$
\varphi^\mathrm{cyl} \colon \mathbb{R}_{\geq 0} \times [0, 2\pi) \times \mathbb{R} \to \mathbb{R}^3, \, \boldsymbol{\eta} := \begin{bmatrix} r \\ \theta \\ y \end{bmatrix} \mapsto \boldsymbol{x} := \begin{bmatrix} x \\ y \\ z \end{bmatrix} = \begin{bmatrix} r\cos(\theta) \\ y \\ r\sin(\theta) \end{bmatrix}
$$

with

$$
\mathrm{D}\varphi^\mathrm{cyl}(\boldsymbol{\eta}) = \begin{bmatrix} \cos(\theta) & -r\sin(\theta) & 0 \\ 0 & 0 & 1 \\ \sin(\theta) & r\cos(\theta) & 0 \end{bmatrix} \quad \text{and} \quad \left| \det \mathrm{D}\varphi^\mathrm{cyl}(\boldsymbol{\eta}) \right| = r.
$$

The integrals of the weak formulation are transformed accordingly:

$$
\int_\Omega u(\boldsymbol{x}) v(\boldsymbol{x}) \,\mathrm{d}\boldsymbol{x} = \int_{(\varphi^\mathrm{cyl})^{-1}(\Omega)} \hat{u}(\boldsymbol{\eta})\hat{v}(\boldsymbol{\eta}) \, r \,\mathrm{d}\boldsymbol{\eta},
$$

$$
\int_\Gamma u(s_{\boldsymbol{x}}) v(s_{\boldsymbol{x}}) \,\mathrm{d}s_{\boldsymbol{x}} = \int_{(\varphi^\mathrm{cyl})^{-1}(\Gamma)} \hat{u}(s_{\boldsymbol{\eta}})\hat{v}(s_{\boldsymbol{\eta}}) \, r \,\mathrm{d}s_{\boldsymbol{\eta}},
$$

$$
\int_\Omega (\nabla u(\boldsymbol{x}))^\mathrm{T} \cdot \nabla v(\boldsymbol{x}) \,\mathrm{d}\boldsymbol{x} = \int_{(\varphi^\mathrm{cyl})^{-1}(\Omega)} \left(\frac{\partial \hat{u}}{\partial r}\frac{\partial \hat{v}}{\partial r} + \frac{1}{r^2}\frac{\partial \hat{u}}{\partial \theta}\frac{\partial \hat{v}}{\partial \theta} + \frac{\partial \hat{u}}{\partial y}\frac{\partial \hat{v}}{\partial y} \right) r \,\mathrm{d}\boldsymbol{\eta},
$$

with $\hat{u} = u \circ \varphi^\mathrm{cyl}$, $\hat{v} = v \circ \varphi^\mathrm{cyl}$, where we used the chain rule

$$
\nabla_{\boldsymbol{x}} = (\mathrm{D}\varphi^\mathrm{cyl})^{-T} \cdot \nabla_{\boldsymbol{\eta}} \quad \text{and} \quad (\mathrm{D}\varphi^\mathrm{cyl})^{-1} \cdot (\mathrm{D}\varphi^\mathrm{cyl})^{-T} = \begin{bmatrix} 1 & 0 & 0 \\ 0 & 1/r^2 & 0 \\ 0 & 0 & 1 \end{bmatrix}.
$$

Let $\varphi^{\Gamma_2}(t) = \begin{bmatrix} \varphi_1^{\Gamma_2}(t) & \varphi_2^{\Gamma_2}(t) \end{bmatrix}^\mathrm{T} \left(= \begin{bmatrix} r(t) & y(t) \end{bmatrix}^\mathrm{T} \right) \in \mathbb{R}^2$ be a unit speed parameterization[88] of the two dimensional boundary $\Gamma_2 = \left\{ \begin{bmatrix} r & y \end{bmatrix}^\mathrm{T} \mid \begin{bmatrix} r & 0 & y \end{bmatrix}^\mathrm{T} \in \partial(\varphi^\mathrm{cyl})^{-1}(\Omega) \right\} \subset \mathbb{R}^2$. Then we obtain a parameterization of the boundary in $\Gamma_3 = \partial\Omega \subset \mathbb{R}^3$ with

$$
\varphi^{\Gamma_3}(\theta, t) = \begin{bmatrix} \varphi_1^{\Gamma_2}(t)\cos(\theta) \\ \varphi_2^{\Gamma_2}(t) \\ \varphi_1^{\Gamma_2}(t)\sin(\theta) \end{bmatrix} \quad \text{and} \quad \left\| \frac{\partial \varphi^{\Gamma_3}}{\partial \theta} \times \frac{\partial \varphi^{\Gamma_3}}{\partial t} \right\|_2 = \left| \varphi_1^{\Gamma_2}(t) \right| \left\| (\varphi^{\Gamma_2})'(t) \right\|_2 = r(t).
$$

With the assumption of rotational symmetry, we can neglect the terms $\frac{\partial}{\partial \theta} = 0$ and obtain a problem that depends only on two spatial coordinates $\hat{x} := r$, $\hat{y} := y$.

---

[87] See, e.g., [5, VII.9, Bsp. 9.11.c, p. 260] for more details on cylindrical coordinates.
[88] See [5, VIII.2, Thm. 2.2, p. 303] for the unit speed parameterization of a curve.

B Hitchhiker's guide

The beginner ... should not be discouraged if ... he finds that he does not have the prerequisites for reading the prerequisites.

Paul Halmos [177, I, p. 1]

B.1 Facts

We give a summary of results from functional analysis tailored to our field of application, especially in the context of Bochner spaces.[1]

B.1.1 Basics

> **Definition B.1 — Domain [186, Sec. A.12.1, p. 191].**
> A subset $\Omega \subset \mathbb{R}^d$, $d \in \mathbb{N}$, is called *domain*, if Ω is nonempty, open and connected.

> **Theorem B.2 — Fubini [186, Sec. A.11, Satz 11.16, p. 190].**
> Let (X, S, ν) and (Y, T, λ) be complete measure spaces and let $f \in L^1(X \times Y, S \times T, \nu \times \lambda)$. Then, for ν-almost all $x \in X$, it holds
>
> $$f(x, \cdot) \in L^1(Y, T, \lambda),$$
>
> and the function
>
> $$x \mapsto \int_Y f(x, y) \, \mathrm{d}\lambda(y),$$
>
> which is defined for ν-almost all $x \in X$, is an element of $L^1(X, S, \nu)$.
> Similarly, for λ-almost all $y \in Y$, it holds
>
> $$f(\cdot, y) \in L^1(X, S, \nu),$$
>
> and the function
>
> $$y \mapsto \int_X f(x, y) \, \mathrm{d}\nu(x),$$

---

[1] Of course, this is not the first "hitchhiker's guide" in functional analysis: [1].

which is defined for λ-almost all $y \in Y$, is an element of $L^1(Y, T, \lambda)$. Furthermore, it holds

$$\int_{X \times Y} f(x, y) \, \mathrm{d}(\nu \times \lambda) = \int_Y \left(\int_X f(x, y) \, \mathrm{d}\nu(x) \right) \mathrm{d}\lambda(y)$$

$$= \int_X \left(\int_Y f(x, y) \, \mathrm{d}\lambda(y) \right) \mathrm{d}\nu(x) \, .$$

Lemma B.3 — Characterization of measurable functions in Banach spaces [236, App. (8), p. 1012][a].
Let $M \subseteq \mathbb{R}^d$, $d \in \mathbb{N}$, be a Lebesgue-measurable set and let X be a separable real Banach space. If the function $f \colon M \to X$ is continuous almost everywhere, i.e., there exists a set $Z \subseteq \mathbb{R}^d$ with Lebesgue measure zero such that $f \colon M \backslash Z \to X$ is *continuous*, then f is *measurable[b]*.

---

[a] This Lemma is a consequence of *Pettis' theorem* B.45.
[b] Also referred to as *strongly measurable* [93, Sec. 1.3.2.2, p. 37] or *Bochner measurable* [186, Sec. 2.1, Def. 1.3, p. 34].

Lemma B.4 — Cartesian product of normed spaces[a].
Let $Z = X \times Y$ be the Cartesian product of two normed spaces equipped with the norm

$$\|(x, y)\|_Z = \|x\|_X + \|y\|_Y \, .$$

Then $z^* \in Z^*$ if and only if there exist $x^* \in X^*$ and $y^* \in Y^*$ such that

$$\langle z^*, (x, y) \rangle_{Z^*, Z} = \langle x^*, x \rangle_{X^*, X} + \langle y^*, y \rangle_{Y^*, Y} \quad \text{for all } x \in X, y \in Y.$$

This allows us to identify

$$(X \times Y)^* = X^* \times Y^*.$$

If X and Y are Banach spaces, then also Z is a Banach space.

---

[a] The proof is given in Appendix B.2.1.

Lemma B.5 — Uniform continuity [70, §3, Satz 10, p. 47].
Let X, Y be metric spaces and let X be compact. Then every continuous map $f \colon X \to Y$ is uniformly continuous.

Lemma B.6 — Variational lemma.

1. Let $\Omega \subset \mathbb{R}^d$, $d \in \mathbb{N}$, be a nonempty open set and[a] let $f \in L^1{}_{\mathrm{loc}}(\Omega)$ with

$$\int_\Omega f(x)\varphi(x) \, \mathrm{d}x = 0 \quad \text{for all } \varphi \in \mathcal{C}_{\mathrm{c}}^\infty(\Omega),$$

where $\mathcal{C}_{\mathrm{c}}^\infty(\Omega)$ is the set of infinitely-often differentiable functions on Ω with compact support. Then $f = 0$ a.e. in Ω. [93, Sec. 1.2.2.4, Lem. 1.5, p. 18]

2. Let X be a real Banach space and let $T \in \mathbb{R}_{>0}$. Let $f \in L^1((0,T);X)$ with

$$\int_0^T f(t)\varphi(t)\,\mathrm{d}t = 0 \quad \text{for all } \varphi \in \mathcal{C}_c^\infty((0,T)),$$

where $\mathcal{C}_c^\infty((0,T))$ is the set of infinitely-often differentiable functions on the interval $(0,T)$ with compact support. Then $f = 0$ in $L^1((0,T);X)$, i.e., $f(t) = 0$ for a.a. $t \in (0,T)$. [235, §23.3, Prop. 23.10, p. 415]

---

[a] Especially, it holds $L^p(\Omega) \subset L^1_{\mathrm{loc}}(\Omega)$ for all $p \in [1,\infty]$, see [93, Sec. 1.2.2.3, Rem. 1.2, p. 16].

Definition B.7 — Weak convergence [4, Ch. 6, Def. 6.1, p. 237].

Let X be a real Banach space.

1. A sequence $(x_k)_{k \in \mathbb{N}} \subset X$ is called weakly convergent if there exists an $x \in X$ such that

$$\langle x^*, x_k \rangle \to \langle x^*, x \rangle \quad \text{for } k \to \infty, \quad \text{for all } x^* \in X^*.$$

In this case, we write $x_k \rightharpoonup x$.

2. A sequence $(x_k^*)_{k \in \mathbb{N}} \subset X^*$ is called weakly* convergent if there exists an $x^* \in X^*$ such that

$$\langle x_k^*, x \rangle \to \langle x^*, x \rangle \quad \text{for } k \to \infty, \quad \text{for all } x \in X.$$

In this case, we write $x_k^* \rightharpoonup^* x^*$.

Remark B.8 — Weak/weak* limits are unique [4, Ch. 6, Bem. 6.3 (1), p. 238].

The weak and weak* limits, defined in Definition B.7, are *unique*.

Lemma B.9 — Limit of dual pairings [4, Sec. 6.3 (6), p. 239].

Let X be a real Banach space. Let $(x_k)_{k \in \mathbb{N}} \subset X$, $(x_k^*)_{k \in \mathbb{N}} \subset X^*$ be sequences and let $x \in X$, $x^* \in X^*$ with $x_k^* \to x^*$ (strongly) in X^* and $x_k \rightharpoonup x$ (weakly) in X. Then it holds

$$\langle x_k^*, x_k \rangle_X \to \langle x^*, x \rangle_X.$$

Lemma B.10 — Evaluation map [4, Sec. 6.2, p. 238].

For a real Banach space X, the map

$$J_X \colon X \to X^{**}, \quad \langle J_X x, x^* \rangle_{X^{**},X^*} := \langle x^*, x \rangle_{X^*,X} \quad \text{for } x \in X, x^* \in X^* \tag{B.1}$$

is linear, continuous and isometric.

Definition B.11 — Reflexive Banach space [4, Sec. 6.8, p. 245].

We call a Banach space X reflexive, if J_X in equation (B.1) is surjective.

If X is reflexive, then weak* convergence and weak convergence in X^* coincide [4, Sec. 6.8 (1), p. 245].

Lemma B.12 — Reflexive Banach spaces.

1. Each *bounded* sequence in a *reflexive* real Banach space has a weakly convergent subsequence. [235, §21.7, Thm. 21.D, p. 255]

2. Every Hilbert space is reflexive. [4, Ch. 6, Bsp. 6.11 (1), p. 247]

3. Let $\Omega \subset \mathbb{R}^d$, $d \in \mathbb{N}$, be a nonempty open set. For $p \in (1, \infty)$, the space $L^p(\Omega)$ is a reflexive Banach space and it holds $L^p(\Omega)^* = L^q(\Omega)$ for $q \in (1, \infty)$ with $\frac{1}{p} + \frac{1}{q} = 1$. The dual space of $L^1(\Omega)$ is $L^\infty(\Omega)$, but $L^1(\Omega)$ is *not* reflexive, i.e., $L^1(\Omega)$ is *not* the dual space of $L^\infty(\Omega)$. Similarly, $L^\infty(\Omega)$ is *not* reflexive. [43, XVIII §1 6.2, Ex. 4, p. 500], [4, Ch. 4, Satz 4.12, p. 183]

4. Let X be a reflexive and separable real Banach space, $p \in (1, \infty)$, $T \in \mathbb{R}_{>0}$. Then $L^p((0, T); X)$ is reflexive[a] and it holds $L^p((0, T); X)^* = L^q(0, T; X^*)$ for $q \in (1, \infty)$ with $\frac{1}{p} + \frac{1}{q} = 1$. Furthermore, $L^1((0, T); X)$ has $L^\infty((0, T); X^*)$ as its dual space, but it is *not* reflexive. Similarly, $L^\infty((0, T); X)$ is *not* reflexive. [43, XVIII §1 6.2, Ex. 4, p. 500]

5. A real Banach space X is reflexive if and only if its dual space X^* is reflexive. [4, Sec. 6.8 (4), p. 245]

---
[a] In fact, $L^p((0, T); X)$ is also separable, see Lemma B.22

Lemma B.13 — Subsequence argument [43, XVIII §1 6.3, Prop. 12, p. 502].
Let X be a reflexive real Banach space and let $(x_k)_{k \in \mathbb{N}} \subset X$ be a sequence. We assume that:

1. there is a $C > 0$ such that $\|x_k\|_X \leq C < \infty$ for all $k \in \mathbb{N}$;

2. the set of cluster points of $(x_k)_{k \in \mathbb{N}}$ w.r.t. weak convergence[a] is reduced to $\{x\}$.

Then the sequence $(x_k)_{k \in \mathbb{N}}$ converges to x weakly in X.

---
[a] An element $x \in X$ is called a cluster point of $(x_k)_{k \in \mathbb{N}}$ w.r.t. weak convergence if there is a weakly convergent subsequence with $x_{k_l} \rightharpoonup x$.

Lemma B.14 — Generalized derivatives and weak convergence [235, §23.5, Prop. 23.19, p. 419].
Let X, Y be real Banach spaces with the continuous embedding $X \hookrightarrow Y$, $T \in \mathbb{R}_{>0}$, $n \in \mathbb{N}$, p, $q \in [1, \infty)$, and $f \in L^p((0, T); X)$, $g \in L^q((0, T); X)$. Let $(f_k)_{k \in \mathbb{N}} \subset L^p((0, T); X)$ and $(g_k)_{k \in \mathbb{N}} \subset L^q((0, T); X)$ be two sequences such that

$$f_k^{(n)} = g_k \quad \text{on } (0, T) \quad \text{for all } k \in \mathbb{N}$$

(nth weak time derivative) and

$$f_k \rightharpoonup f \quad \text{in } L^p((0, T); X),$$
$$g_k \rightharpoonup g \quad \text{in } L^q((0, T); Y).$$

Then it holds

$$f^{(n)} = g \quad \text{on } (0, T).$$

Lemma B.15 — Weakly sequentially closed / Relatively weakly sequentially compact.

1. Every convex and closed subset of a real Banach space is *weakly sequentially closed*. [217, Sec. 2.4.2, Satz 2.11, p. 37]

2. Let X be a real Banach space. If X is *reflexive*, then each bounded sequence $(x_k)_{k \in \mathbb{N}} \subset X$ contains a weakly convergent subsequence.[a][b] In other words, every bounded set of a reflexive Banach space is *relatively weakly sequentially compact*. [20, Sec. 3.5, Thm. 3.18, p. 69]

---

[a]   The converse is also true, which means, that this feature characterizes reflexive Banach spaces, see [20, Sec. 3.5, Thm. 3.19, p. 70]. This is a consequence of the Theorem of Eberlein–Šmulian [39, V §13, Thm. 13.1, p. 163].
[b]   The weak limit is an element of X because X is weakly sequentially closed.

Lemma B.16 — Criterion for weak lower semicontinuity [217, Sec. 2.4.2, Satz 2.12, p. 37].

Let X be a real Banach space and let $f \colon X \to (-\infty, \infty]$. If f is continuous and convex, then f is *sequentially weakly lower semicontinuous*, i.e.,

$$x_k \rightharpoonup x \text{ in } X \quad \text{implies} \quad f(x) \leq \liminf_{k \to \infty} f(x_k).$$

Especially, this result is applicable[a] to the corresponding norm $f = \|\cdot\|_X$.

---

[a]   See [4, Sec. 6.3, p. 239].

Lemma B.17 — Dual spaces of subspaces[a].

Let X, Y be real Banach spaces with the continuous embedding $j \colon Y \hookrightarrow X$. Then it holds $X^* \hookrightarrow Y^*$. Especially, for a sequence $(y_k)_{k \in \mathbb{N}} \subset Y \subset X$, the weak convergence $y_k \rightharpoonup y$ in Y implies the weak convergence $j(y_k) \rightharpoonup j(y)$ in X.

---

[a]   The proof is given in Appendix B.2.2.

Definition B.18 — Compact operators [4, Sec. 8.1, p. 331].

Let X, Y be real Banach spaces. A linear map $S \colon X \to Y$ is called compact if it maps bounded sets $M \subset X$ to *relatively compact* sets, i.e., $\overline{S(M)} \subset Y$ is *compact*.

Lemma B.19 — Concatenation of continuous and compact operators [4, Ch. 8, Lem. 8.3, p. 334].

Let X, Y, Z be real Banach spaces and let $S_1 \colon X \to Y$ and $S_2 \colon Y \to Z$ be linear and continuous maps. If S_1 or S_2 is compact[a], then $S_2 \circ S_1 \colon X \to Z$ is compact.

---

[a]   See Definition B.18.

Lemma B.20 — Compact operators and weak convergence [93, Sec. 1.2.3, Lem. 1.6, p. 26].
Let X, Y be real Banach spaces and let $S \colon X \to Y$ a compact operator. Then for all weakly convergent sequences $(x_k)_{k \in \mathbb{N}} \subset X$ with $x_k \rightharpoonup x$ for some $x \in X$, it holds

$$Sx_k \to Sx \quad \text{in } Y.$$

Definition B.21 — Separable spaces [4, Ch. 0, Def. 0.13, p. 21].
Let $(X, \mathcal{T})$ be a topological space.[a] A subset $A \subseteq X$ is called *dense*, if the closure $\overline{A}$ fulfills $\overline{A} = X$. We call X *separable*, if it contains a dense and countable subset.

---
[a] Especially, this includes metric spaces, which are of interest here.

Lemma B.22 — Separable spaces.
Let $\Omega \subset \mathbb{R}^d$, $d \in \mathbb{N}$, be a nonempty open set and let $k \in \mathbb{N}_0$.

1. For $p \in [1, \infty)$, the space $W^{k,p}(\Omega)$ is separable.[a] [4, Ch. 2, Bsp. 2.18, p. 120]

2. If Ω is bounded, then the space $\mathcal{C}^k(\overline{\Omega})$ is separable. [4, Ch. 2, Bsp. 2.18, p. 120]

3. For $p \in [1, \infty)$, $T \in \mathbb{R}_{>0}$, and X a separable real Banach space, the space $L^p((0, T); X)$ is separable. [235, §23.2, Prop. 23.2, p. 407]

4. If X is a separable metric space, then every subset $M \subset X$ is separable. [20, Sec. 3.6, Prop. 3.25, p. 73]

5. If X is an infinite-dimensional real Hilbert space, the following statements are equivalent [4, Ch. 7, Satz 7.8, p. 306]:

   (a) X is separable;

   (b) X has an orthonormal basis, i.e., an orthonormal system $(e_k)_{k \in \mathbb{N}} \subset X$ such that the linear span[b] of the set $\{e_k \mid k \in \mathbb{N}\}$ is dense in X.

6. Let X be a real Banach space. If its dual X^* is separable, then also X is separable. [4, Ch. 6, Lem. 6.9, p. 246]

---
[a] Especially, this includes $L^p(\Omega)$.
[b] The linear span of a set contains all finite linear combinations of elements of this set.

Lemma B.23 — Equivalent norm on $H^1(\Omega)$ [235, §21.3, Thm. 21.A, p. 238].
Let $\Omega \subset \mathbb{R}^d$, $d \in \mathbb{N}$, be a bounded domain[a] with Lipschitz boundary Γ. Then

$$\|f\|^*_{H^1(\Omega)} := \left(\int_\Omega \sum_{i=1}^d (\mathrm{D}_{x_i} f)^2 \, \mathrm{d}x + \int_\Gamma f^2 \, \mathrm{d}s \right)^{1/2}$$

is an equivalent norm on $H^1(\Omega)$, i.e., there are constants $c, C \in \mathbb{R}_{>0}$ such that

$$c \, \|f\|_{H^1(\Omega)} \leq \|f\|_{H^1(\Omega)}^* \leq C \, \|f\|_{H^1(\Omega)} \quad \text{for all } f \in H^1(\Omega).$$

---

[a] For $d = 1$, the domain Ω is a bounded open interval.

Lemma B.24 — Properties of Sobolev spaces.

Let $\Omega \subset \mathbb{R}^d$, $d \in \mathbb{N}$, be a nonempty open set, $k \in \mathbb{N}_0$, $p \in [1, \infty)$, and let $\alpha \in \mathbb{N}_0^d$ denote a multiindex with $|\alpha| := \sum_{k=1}^d \alpha_k$.

1. The space $W^{k,p}(\Omega)$ with the corresponding norm

$$\|\vartheta\|_{W^{k,p}(\Omega)} = \left(\sum_{0 \leq |\alpha| \leq k} \|\mathrm{D}^\alpha \vartheta\|_{L^p(\Omega)}^p \right)^{1/p}$$

   is a real *Banach space*. For $p = 2$, the space $H^k(\Omega) = W^{k,2}(\Omega)$ is a real *Hilbert space* with the scalar product

$$\left(\vartheta, \hat{\vartheta} \right)_{H^k(\Omega)} = \sum_{0 \leq |\alpha| \leq m} \left(\mathrm{D}^\alpha \vartheta, \mathrm{D}^\alpha \hat{\vartheta} \right)_{L^2(\Omega)}.$$

   [235, §21.2, Prop. 21.10, p. 236]

2. The space $W^{k,p}(\Omega)$ (with $W^{0,p}(\Omega) = L^p(\Omega)$) is *separable*.[a] [4, Ch. 2, Bsp. 2.18 (6), p. 120]

3. For $p \in (1, \infty)$, the space $W^{k,p}(\Omega)$ is *reflexive*.[b] [4, Ch. 6, Bsp. 6.11 (3), p. 247]

---

[a] Cf. [236, App. (41), p. 1025] (with stronger assumptions on Ω) or [20, Sec. 9.1, Prop. 9.1, p. 264] (for $k = 1$).
[b] Cf. [236, App. (42), p. 1025] (with stronger assumptions on Ω) or [20, Sec. 9.1, Prop. 9.1, p. 264] (for $k = 1$).

B.1.2 Calculus

Lemma B.25 — Young's inequality (with ε) [63, App. B.2 (7), p. 622].

Let $a, b, \varepsilon \in \mathbb{R}_{>0}$ and let $p, q \in (1, \infty)$ with $\frac{1}{p} + \frac{1}{q} = 1$. Then it holds

$$ab \leq \varepsilon a^p + \frac{1}{(\varepsilon p)^{q/p}} \frac{1}{q} b^q.$$

Remark B.26 — Classical Young's inequality.

For $\varepsilon = \frac{1}{p}$, we obtain from Lemma B.25 Young's inequality in its classical form

$$ab \leq \frac{a^p}{p} + \frac{b^q}{q}.$$

This particular case yields the useful estimate

$$(a + b)^2 \leq 2(a^2 + b^2).$$

Lemma B.27 — Hölder's inequality.

1. Let $\Omega \subset \mathbb{R}^d$, $d \in \mathbb{N}$, be a nonempty Lebesgue-measurable set (e.g., Ω is open or closed) and let $p, q \in [1, \infty]$ with $\frac{1}{p} + \frac{1}{q} = 1$. Then, for $f \in L^p(\Omega)$, $g \in L^q(\Omega)$, it holds $fg \in L^1(\Omega)$ and
$$\|fg\|_{L^1(\Omega)} \le \|f\|_{L^p(\Omega)} \|g\|_{L^q(\Omega)}.$$
[235, §18.6, Prop. 18.13, p. 35]

2. Let X be a real Banach space, $T \in \mathbb{R}_{>0}$ and $p, q \in (1, \infty)$ with $\frac{1}{p} + \frac{1}{q} = 1$. Then, for $f \in L^p((0, T); X)$, $g \in L^q((0, T); X^*)$, it holds $t \mapsto \langle g(t), f(t) \rangle_X \in L^1((0, T); \mathbb{R})$ and
$$\int_0^T |\langle g(t), f(t) \rangle_X| \, \mathrm{d}t \le \|g\|_{L^q((0,T);X^*)} \|f\|_{L^p((0,T);X)}.$$
[235, §23.3, Prop. 23.6, p. 411]

Lemma B.28 — Jensen's inequality [36, Sec. 4.1, Cor. 4.8, p. 63].

1. Let $\phi : \mathbb{R}^d \to \mathbb{R}$, $d \in \mathbb{N}$, be convex and let $f : (0, 1) \to \mathbb{R}^d$ be a function with components $f_i \in L^1((0, 1); \mathbb{R})$, $i \in \{1, \dots, d\}$. Then it holds[a]
$$\phi\left(\int_0^1 f(t) \, \mathrm{d}t\right) \le \int_0^1 \phi(f(t)) \, \mathrm{d}t.$$

2. Let $f \in L^1((0, 1); \mathbb{R})$. For $p \in (0, 1)$, we have[b] $f \in L^p((0, 1); \mathbb{R})$ with
$$\int_0^1 |f(t)|^p \, \mathrm{d}t \le \left(\int_0^1 |f(t)| \, \mathrm{d}t\right)^p.$$

---

[a] The first integral is vector valued.
[b] Apply Jensen's inequality to the function $z \mapsto |z|^{1/p}$, which is convex for $p \in (0, 1)$ (cf. [4, Ch. 2, U2.10, p. 139]).

Definition B.29 — Absolutely continuous functions [55, VII §4 , Def. 4.11, p. 325].

Let $T \in \mathbb{R}_{>0}$. We call a function $f : [0, T] \to \mathbb{R}$ *absolutely continuous*, if for every $\varepsilon > 0$ there is a $\delta > 0$ such that
$$\sum_{k=1}^n |f(\beta_k) - f(\alpha_k)| < \varepsilon$$
for all $0 \le \alpha_1 < \beta_1 \le \alpha_2 < \beta_2 \le \dots \le \alpha_n < \beta_n \le b$ with $\sum_{k=1}^n (\beta_k - \alpha_k) < \delta$.

Remark B.30 — Absolutely continuous [55, VII §4, Cor. 4.12, p. 325].

Every absolutely continuous function is differentiable almost everywhere.

Theorem B.31 — Fundamental theorem of calculus for the Lebesgue integral [55, VII §4, Satz 4.14, p. 326].

Let $T \in \mathbb{R}_{>0}$.

1. Let $f \colon [0, T] \to \mathbb{R}$ be Lebesgue integrable. Then

$$F \colon [0, T] \to \mathbb{R}, \ t \mapsto \int_0^t f(s) \, ds$$

   is absolutely continuous and it holds $F'(t) = f(t)$ for a.a. $t \in [0, T]$.

2. Let $F \colon [0, T] \to \mathbb{R}$ be absolutely continuous, and set $F'(t) \coloneqq 0$ for all $t \in [0, T]$ where F is not differentiable (see Remark B.30). Then F' is Lebesgue integrable on $[0, T]$ and it holds

$$F(t) - F(0) = \int_0^t F'(s) \, ds \quad \text{for all } t \in [0, T].$$

Theorem B.32 — Fundamental theorem of calculus in Bochner spaces.

Let X be a real Banach space, $T \in \mathbb{R}_{>0}$, $p \in [1, \infty]$.

1. Let $f \colon [0, T] \to X$ be Bochner integrable[a] and $F(t) \coloneqq \int_0^t f(s) \, ds$. Then F is *absolutely continuous*. Furthermore, F is differentiable a.e. and $F'(t) = f(t)$ for a.a. $t \in [0, T]$. [15, Sec. 1.2, Prop. 1.2.2, p. 16]

2. Let $F \colon [0, T] \to X$ be absolutely continuous and suppose $f(t) \coloneqq F'(t)$ exists almost everywhere. Then f is Bochner integrable and

$$F(t) = F(0) + \int_0^t f(s) \, ds \quad \text{for all } t \in [0, T].$$

[15, Sec. 1.2, Def. 1.2.3, p. 18]

---

[a] We say that $f \colon [0, T] \to X$ is Bochner integrable if there exists a sequence $(s_k)_{k \in \mathbb{N}}$ of simple functions such that $s_k(t) \to f(t)$ a.e. (i.e, f is Bochner measurable) and

$$\int_0^T \|s_k(t) - f(t)\|_X \, dt \to 0 \quad \text{for } k \to 0,$$

see [93, Sec. 1.3.2.2, Def. 1.23, p. 37].

Theorem B.33 — Fundamental theorem of calculus in Bochner spaces (alternative direction) [63, Sec. 5.9.2, Thm. 2, p. 286].

Let X be a real Banach space, $T \in \mathbb{R}_{>0}$, $p \in [1, \infty]$, and let $f \in W^{1,p}((0, T); X)$.

1. We have the continuous embedding[a]

$$W^{1,p}((0, T); X) \hookrightarrow \mathcal{C}^0([0, T]; X).$$

2. It holds
$$f(t) = f(t_0) + \int_{t_0}^{t} f'(s)\,\mathrm{d}s \quad \text{for all } t_0, t \in [0, T] \text{ with } t_0 \le t.$$

---
[a] Cf. the embedding in Theorem B.36 but with weaker assumptions.

Theorem B.34 — Integration by parts for absolutely continuous functions [55, VII §4, Cor. 4.16, p. 328].
Let $T \in \mathbb{R}_{>0}$ and let $f, g \colon [0, T] \to \mathbb{R}$ be absolutely continuous. Then it holds

$$f(T)g(T) - f(0)g(0) = \int_0^T f'(t)g(t)\,\mathrm{d}t + \int_0^T f(t)g'(t)\,\mathrm{d}t\,.$$

Theorem B.35 — Integration by parts in Sobolev spaces [186, Sec. A.12.3, Satz 12.21, p. 200].
Let $\Omega \subset \mathbb{R}^d$, $d \in \mathbb{N}$, be a bounded domain with Lipschitz boundary Γ, and let $p, q \in [1, \infty)$ with $\frac{1}{p} + \frac{1}{q} = 1$. For $f \in W^{1,p}(\Omega)$ and $g \in W^{1,q}(\Omega)$, it holds[a]

$$\int_\Omega f \mathrm{D}_{x_i} g \,\mathrm{d}x = -\int_\Omega g \mathrm{D}_{x_i} f \,\mathrm{d}x + \int_\Gamma f g n_i \,\mathrm{d}s \quad \text{for } i \in \{1, \ldots, d\}$$

with $\boldsymbol{n} = (n_1, \ldots, n_d)^{\mathrm{T}} \in \mathbb{R}^d$ the outward pointing normal vector on Γ.

---
[a] The boundary integral is defined by means of the trace theorem B.53.

Theorem B.36 — Integration by parts in Bochner spaces [93, Sec. 1.3.2.2, Thm. 1.32, p. 40].
Let $T \in \mathbb{R}_{>0}$ and let $V \overset{\text{dense}}{\hookrightarrow} H \hookrightarrow V^*$ be a Gelfand triple[a] with H, V separable real Hilbert spaces.
Then $W(0, T; H, V) := L^2((0, T); V) \cap H^1((0, T); V^*)$ is a Hilbert space and we have the continuous embedding
$$W(0, T; H, V) \hookrightarrow \mathcal{C}^0([0, T]; H).$$

Moreover, for $f, g \in W(0, T; H, V)$, the integration-by-parts formula holds[b]:

$$(f(t), g(t))_H - (f(t_0), g(t_0))_H = \int_{t_0}^{t} \langle f'(s), g(s) \rangle_{V^*, V} + \langle g'(s), f(s) \rangle_{V^*, V} \,\mathrm{d}s$$

for all $t_0, t \in [0, T]$ with $t_0 \le t$.

---
[a] Continuous and dense embeddings, cf. [93, Sec. 1.3.2.2, Def. 1.26, p. 39], [235, §23.4, Def. 23.11, p. 416].
[b] See also [235, §23.6, Prop. 23.23, p. 422].

Lemma B.37 — Weak time derivative as distribution [43, XVIII §1 2, Prop. 7, p. 477].
Let $T \in \mathbb{R}_{>0}$ and let $V \overset{\text{dense}}{\hookrightarrow} H \hookrightarrow V^*$ be a Gelfand triple[a] with H, V separable real Hilbert spaces. For $f \in L^2((0, T); V) \cap H^1((0, T); V^*)$ and $g \in V$, we have

$$\langle f'(\cdot), g \rangle_{V^*, V} = (f(\cdot), g)_V' \quad \text{in } \mathcal{C}_c^\infty((0, T))^*,$$

where $\mathcal{C}_c^\infty((0,T))^*$ is the dual space of the space of infinitely-often differentiable functions on $(0,T)$ with compact support (distributions).

---
[a] Continuous and dense embeddings, cf. [93, Sec. 1.3.2.2, Def. 1.26, p. 39], [235, §23.4, Def. 23.11, p. 416].

Lemma B.38 — Derivative of the norm [56, Sec. 8.1, Cor. 8.1.10, p. 211][a].

Let $\Omega \subset \mathbb{R}^d$, $d \in \mathbb{N}$, be a bounded domain with Lipschitz boundary and let $T \in \mathbb{R}_{>0}$. For $f \in L^2((0,T); H^1(\Omega)) \cap H^1((0,T); H^1(\Omega)^*)$, it holds

$$\left(\|f(t)\|_{L^2(\Omega)}^2 \right)' = 2 \left\langle f'(t), f(t) \right\rangle_{H^1(\Omega)^*, H^1(\Omega)} \quad \text{for a.a. } t \in (0,T)$$

in the sense of a weak time derivative[b].

Furthermore, it holds

$$\int_0^t \left(\|f(s)\|_{L^2(\Omega)}^2 \right)' \mathrm{d}s = \|f(t)\|_{L^2(\Omega)}^2 - \|f(0)\|_{L^2(\Omega)}^2 \quad \text{for a.a. } t \in (0,T).$$

---
[a] The proof is given in Appendix B.2.3.
[b] I.e., $\int_0^T \varphi'(t) \|f(t)\|_{L^2(\Omega)}^2 \, \mathrm{d}t = - \int_0^T \varphi(t) \left(\|f(t)\|_{L^2(\Omega)}^2 \right)' \mathrm{d}t$ for all $\varphi \in \mathcal{C}_c^\infty((0,T))$.

Theorem B.39 — Gronwall's inequality (cf. [43, XVIII §5 2.2, Lem. 1, p. 559])[a].

Let $T \in \mathbb{R}_{>0}$ and let $f \in L^1((0,T))$ and $\mu \in L^\infty((0,T))$ be nonnegative functions, i.e., $f(t), \mu(t) \geq 0$ for a.a. $t \in [0,T]$, which satisfy

$$f(t) \leq \int_0^t \mu(s) f(s) \, \mathrm{d}s + C \quad \text{for a.a. } t \in [0,T] \tag{B.2}$$

for a constant C. Then

$$f(t) \leq C \exp \left(\int_0^t \mu(s) \, \mathrm{d}s \right) \quad \text{for a.a. } t \in [0,T]$$

with the same constant C as above.

For $C = 0$, we get[b] $f(t) = 0$ for a.a. $t \in [0,T]$.

---
[a] The proof is given in Appendix B.2.4.
[b] See [43, XVIII §5 2.2, Rem. 3, p. 560].

In our proofs we frequently use Theorem B.39 for a function $f: (0,T) \to \mathbb{R}$, $t \mapsto \|\vartheta(t)\|_X$ for some $\vartheta \in L^2((0,T); X)$. With Theorem B.47, we get that f is Lebesgue integrable and fulfills the prerequisites of Theorem B.39.

Lemma B.40 — "Schwarz" - symmetry of second derivatives[a].

Let $\Omega \subset \mathbb{R}^d$, $d \in \mathbb{N}$, be a nonempty open set, $T \in \mathbb{R}_{>0}$, $f \in H^1((0,T); \mathbb{R})$ and $g \in H^k(\Omega)$. Then the function $h: (0,T) \to H^1(\Omega)$, $t \mapsto f(t)g$ is an element of $H^1((0,T); H^k(\Omega))$ and it holds[b]

$$\mathrm{D}^\alpha (h')(t) = (\mathrm{D}^\alpha h)'(t) = f'(t) \mathrm{D}^\alpha g \quad \text{for a.a. } t \in (0,T)$$

for an arbitrary multiindex $\alpha \in \mathbb{N}_0^d$, $0 \leq |\alpha| \leq k$. This means that we can interchange spatial and temporal weak derivatives.[c]

---

[a] The proof is given in Appendix B.2.5.
[b] Here, $D^\alpha h$ is understood to be the map $(0, T) \to H^{k-|\alpha|}(\Omega)$, $t \mapsto D^\alpha(h(t))$, with $h(t) \in H^k(\Omega)$.
[c] Cf. Schwarz's theorem (symmetry of second derivatives) [70, I §5, Thm. 1, p. 66].

Theorem B.41 — Chain rule (weak derivatives) [240, Sec. 2.1, Thm. 2.1.11, p. 48].
Let $\Omega \subset \mathbb{R}^d$, $d \in \mathbb{N}$, be a nonempty open set, $f \colon \mathbb{R} \to \mathbb{R}$ be a Lipschitz continuous function and let $g \in W^{1,p}(\Omega)$ for $p \in [1, \infty)$. If $f \circ g \in L^p(\Omega)$, then $f \circ g \in W^{1,p}(\Omega)$ and it holds[a]

$$D\left(f \circ g\right)(x) = f'(g(x)) \cdot Dg(x) \quad \text{for a.a. } x \in \Omega.$$

---

[a] Note that the Lipschitz continuity of f implies that f is differentiable almost everywhere [63, Sec. 5.8.3, Thm. 6, p. 281].

Theorem B.42 — Chain rule (Fréchet) [234, Sec. 4.7, Thm. 4D, p. 247].
Let X, Y, Z be real Banach spaces, and let the two mappings

$$f \colon U(u) \subset X \to Y \quad \text{and} \quad g \colon V(f(u)) \subset Y \to Z$$

be given, where $U(u)$ and $V(f(u))$ are open neighborhoods of the points $u \in X$ and $f(u) \in Y$, respectively. Let $m \in \mathbb{N}$ be fixed. If the Fréchet derivatives $f^{(m)}(u)$ and $g^{(m)}(f(u))$ exist, then the Fréchet derivative $(g \circ f)^{(m)}(u)$ exists and, for $m = 1$, it holds:

$$(g \circ f)'(u) = g'(f(u)) \circ f'(u).$$

Theorem B.43 — Product rule (weak derivatives) [20, Sec. 9.1, Prop. 9.4, p. 269].
Let $\Omega \subset \mathbb{R}^d$, $d \in \mathbb{N}$, be a nonempty open set and let $f, g \in W^{1,p}(\Omega) \cap L^\infty(\Omega)$ with $p \in [1, \infty]$. Then $fg \in W^{1,p}(\Omega) \cap L^\infty(\Omega)$ and

$$D_{x_i}(fg) = gD_{x_i}f + fD_{x_i}g \quad \text{for } i \in \{1, \ldots, d\}.$$

Theorem B.44 — Product rule (Fréchet) [186, Sec. 2.2, Satz 2.7, p. 45].
Let X, Y, Z, W be real Banach spaces and let $U \subset X$ be an open set. Let $f \colon U \to Y$, $g \colon U \to Z$ be Fréchet differentiable and $B \colon Y \times Z \to W$ be a product[a].
Then the function $F \colon U \to W \colon x \mapsto B(f(x), g(x))$ is Fréchet differentiable and, for the derivative $D_x F \in \mathcal{L}(X, W)$, it holds

$$D_x F(x)[h] = B(D_x f(x)[h], g(x)) + B(f(x), D_x g(x)[h]) \quad \text{for all } h \in X.$$

---

[a] See [186, Sec. 2.2, Def. 2.6, p. 45].

B.1.3 Bochner and Lebesgue spaces

We refer to [43, XVIII, p. 467 ff.], [235, Ch. 23, p. 402 ff.], [93, Sec. 1.3.2, p. 36 ff.], [186, Ch. 2, p. 33 ff.], [56, Ch. 7-8, p. 150 ff.] for an introduction to Bochner spaces and the notion of weak time derivatives.

Theorem B.45 — Pettis [232, Sec. V.4, p. 131].

Let $I \subset \mathbb{R}$ be a real interval and let X be a real Banach space.

A function $f \colon I \to X$ is Bochner measurable[a] if and only if it is weakly measurable[b] and λ-almost separably valued[c].

Especially, if X is a separable Banach space, this implies that $f \colon I \to X$ is Bochner measurable if and only if for all $x^* \in X^*$ the function $I \to \mathbb{R}$, $t \mapsto \langle x^*, f(t) \rangle_{X^*}$ is Lebesgue measurable [56, Sec. 7.1, Thm. 7.1.12, p. 154].

---

[a] A function $f \colon I \to X$ is called *Bochner measurable* if there is a sequence of simple functions $s_k \colon I \to X$, i.e., $s_k = \sum_{i=1}^{m_k} 1_{E_{k,i}}(t) x_i$ with Lebesgue-measurable sets $E_{k,i} \subset I$ and $x_i \in X$, such that $s_k(t) \to f(t)$ for a.a. $t \in I$.

[b] A function $f \colon I \to X$ is called *weakly measurable* if for all $x^* \in X^*$ the function $I \to \mathbb{R}$, $t \mapsto \langle x^*, f(t) \rangle_{X^*}$ is Lebesgue measurable.

[c] A function $f \colon I \to X$ is called *λ-almost separably valued*, if there exists a Lebesgue measurable subset $M \subset I$ with Lebesgue measure zero such that the set $\{ f(t) \mid t \in I \backslash M \} \subset X$ is separable.

Lemma B.46 — Bochner measurable → Lebesgue measurable [186, Sec. 2.1, Lem. 1.7, p. 34].

Let X be a reflexive real Banach space and let $T \in \mathbb{R}_{>0}$. If $f \colon (0, T) \to X$ is Bochner measurable, then $\|f(\cdot)\|_X \colon (0, T) \to \mathbb{R}$, $t \mapsto \|f(t)\|_X$ is Lebesgue measurable.

Theorem B.47 — Bochner [186, Sec. 2.1, Thm. 1.12, p. 36], [186, Sec. 2.1, Cor. 1.14, p. 37].

Let X be a reflexive real Banach space and let $I \subset \mathbb{R}$ be Lebesgue measurable. A Bochner-measurable function $f \colon I \to X$ is Bochner integrable if and only if the function $\|f(\cdot)\|_X \colon I \to \mathbb{R}$ is Lebesgue integrable. Furthermore, let $f \colon I \to X$ be Bochner integrable and let $x^* \in X^*$. Then

$$\left\| \int_0^T f(t) \, \mathrm{d}t \right\|_X \leq \int_0^T \|f(t)\|_X \, \mathrm{d}t$$

and

$$\left\langle x^*, \int_0^T f(t) \, \mathrm{d}t \right\rangle_{X^*, X} = \int_0^T \langle x^*, f(t) \rangle_{X^*, X} \, \mathrm{d}t \,. \tag{B.3}$$

Theorem B.48 — Bochner spaces [93, Sec. 1.3.2.2, Thm. 1.31, p. 39].

Let X be a *separable* real Banach space. Then, for $p \in [1, \infty]$ and $T \in \mathbb{R}_{>0}$, the spaces $L^p((0, T); X)$ are Banach spaces. For $p \in [1, \infty)$, the dual space of $L^p((0, T); X)$ can be isometrically identified with $L^q((0, T); X^*)$ for $q \in [1, \infty)$ with $\frac{1}{p} + \frac{1}{q} = 1$ by means of the

pairing

$$\langle v, y \rangle_{L^q((0,T);X^*),L^p((0,T);X)} = \int_0^T \langle v(t), y(t) \rangle_{X^*,X} \, \mathrm{d}t \,.$$

If H is a separable real Hilbert space, then $L^2((0,T);H)$ is a Hilbert space with inner product

$$(v, y)_{L^2((0,T);H)} := \int_0^T (v(t), y(t))_H \, \mathrm{d}t \,.$$

Lemma B.49 — Relation between Lebesgue and Bochner spaces[a].

Let $\Omega \subset \mathbb{R}^d$, $d \in \mathbb{N}$, be a nonempty Lebesgue-measurable set and let $T \in \mathbb{R}_{>0}$.

1. For $p \in [1, \infty)$, the spaces $L^p((0,T) \times \Omega)$ and $L^p((0,T); L^p(\Omega))$ are *isometrically isomorph*, i.e., we can identify a function $f \in L^p((0,T) \times \Omega)$ as an element $\hat{f} \in L^p((0,T); L^p(\Omega))$ by means of the map

$$\hat{f}(t) := f(t, \cdot) \quad \text{for a.a. } t \in (0,T) \tag{B.4}$$

   and it holds $\left\| \hat{f} \right\|_{L^p((0,T);L^p(\Omega))} = \|f\|_{L^p((0,T) \times \Omega)}$.

2. The spaces $L^\infty((0,T) \times \Omega)$ and $L^\infty((0,T); L^\infty(\Omega))$ are *not* isomorph (by means of (B.4)).

---

[a] The proof is given in the Appendix B.2.6.

Lemma B.50 — Isometric isomorphism between spaces of continuous functions (cf. [56, Sec. 9.1, Ex. 9.2, p. 258])[a].

Let $\Omega \subset \mathbb{R}^d$, $d \in \mathbb{N}$, be a nonempty open set and let $T \in \mathbb{R}_{>0}$. We can identify

$$\mathcal{C}^0([0,T] \times \overline{\Omega}) \cong \mathcal{C}^0([0,T]; \mathcal{C}^0(\overline{\Omega})) \tag{B.5}$$

by means of an isometric isomorphism.

---

[a] The proof is given in Appendix B.2.7.

B.1.4 Embeddings

Lemma B.51 — Density results.

1. Let $\Omega \subset \mathbb{R}^d$, $d \in \mathbb{N}$, be a nonempty open set and let $f \in \mathcal{C}^k(\Omega)$. Then all classical partial derivatives of f up to order k are also generalized derivatives [235, §21.1, Prop. 21.3, p. 232]. Especially, if Ω is bounded, this implies $\mathcal{C}^k(\overline{\Omega}) \hookrightarrow H^k(\Omega)$.

2. Let $\Omega \subset \mathbb{R}^d$, $d \in \mathbb{N}$, be a bounded domain with Lipschitz boundary. Then $\mathcal{C}^\infty(\overline{\Omega})$ is dense in $W^{k,p}(\Omega)$ for all $k \in \mathbb{N}_0$, $p \in [1, \infty)$.[a] [235, §21.2, Cor. 21.15, p. 239][b]

3. Let X be a separable real Banach space and let $p \in [1, \infty)$, $T \in \mathbb{R}_{>0}$. Then $\mathcal{C}_c^\infty((0,T);X)$ as well as $\mathcal{C}^k([0,T];X)$, $k \in \mathbb{N}_0$, are dense in $L^p((0,T);X)$. [93, Sec. 1.3.2.2, Lem. 1.9, p. 39] Furthermore, the continuous kth derivative $\vartheta^k : [0,T] \to X$ is, at the same time, also the generalized kth derivative of ϑ on $(0,T)$. [235, §23.5, Ex. 23.16, p. 418]

4. Let X be a separable real Banach space and let $f \in L^p((0,T);X)$ for $p \in [1,\infty)$, $T \in \mathbb{R}_{>0}$. Then there is a sequence $(s_k)_{k\in\mathbb{N}}$ of simple functions[c] with $s_k \to f$ a.e. in $(0,T)$ and $s_k \to f$ in $L^p((0,T);X)$. [93, Sec. 1.3.2.2, Lem. 1.9, p. 39]

---

[a]   With $\mathcal{C}^\infty(\overline{\Omega}) \subset \mathcal{C}^k(\overline{\Omega}) \subset H^k(\Omega)$, this implies that also $\mathcal{C}^k(\overline{\Omega})$ is dense in $H^k(\Omega)$.

[b]   The given reference states that $\mathcal{C}^\infty(\overline{\Omega})$ is dense only in $H^k(\Omega)$, $k \in \mathbb{N}_0$. We lift this statement to the more general case of $W^{k,p}(\Omega)$ by means of the Sobolev embeddings in Theorem B.56.

[c]   We call $s \colon (0,T) \to X$ a simple function if it has the form $s(t) = \sum_{k=1}^m 1_{E_k}(t)s_k$ with Lebesgue-measurable sets $E_k \subset (0,T)$ and $s_k \in X$ [93, Sec. 1.3.2.2, Def. 1.22, p. 37].

Lemma B.52 — Continuous functions viewed as L^∞ functions[a].

1. Let $\Omega \subset \mathbb{R}^d$, $d \in \mathbb{N}$, be a Lebesgue-measurable set. We have the continuous embedding

$$\mathcal{C}^0(\overline{\Omega}) \hookrightarrow L^\infty(\Omega). \tag{B.6}$$

2. Let X be a real Banach space[b] and let $T \in \mathbb{R}_{>0}$. We have the continuous embedding

$$\mathcal{C}^0([0,T];X) \hookrightarrow L^\infty((0,T);X).$$

---

[a]   The proof is given in Appendix B.2.8.

[b]   For $p \in [1,\infty)$, we get that $\mathcal{C}^0([0,T];X) \hookrightarrow L^p((0,T);X)$ is dense, see [235, §23.2, Prop. 23.2 (c), p. 407].

Theorem B.53 — Trace theorem.

Let $\Omega \subset \mathbb{R}^d$, $d \in \mathbb{N}$, be a bounded domain with Lipschitz boundary Γ.[a]

1. For $p \in [1,\infty]$, there exists a unique linear continuous mapping

$$\mathrm{tr} \colon W^{1,p}(\Omega) \to L^p(\Gamma) \quad \text{(trace operator)}$$

such that

$$\mathrm{tr}(f) = f|_\Gamma \quad \text{for all } f \in W^{1,p} \cap \mathcal{C}^0(\overline{\Omega}).$$

We call $\mathrm{tr}(f)$ the trace of f on Γ. [4, Sec. A6.6, p. 279]

2. For $d \geq 2$, $p \in (1,\infty)$, there exists a unique *surjective* linear continuous mapping

$$\mathrm{tr} \colon W^{1,p}(\Omega) \to W^{1-\frac{1}{p},p}(\Gamma)$$

such that[b c]

$$\mathrm{tr}(f) = f|_\Gamma \quad \text{for all } y \in \mathcal{C}^1(\overline{\Omega}).$$

[236, App. (48) - (49), p. 1029–1030]

---

[a]   For $d = 1$, we consider Ω to be a bounded open interval. In this case, from the Sobolev embeddings in Theorem B.56, we get $W^{1,p}(\Omega) \hookrightarrow \mathcal{C}^0(\overline{\Omega})$, which allows us to evaluate functions in $W^{1,p}(\Omega)$ on the boundary of Ω, cf. [236, App. (48)–(49), p. 1029–1030].

[b]   For details on fractional Sobolev spaces in this context, see [85, Sec. 1.3, p. 14 ff.].

[c]   Note that $\mathcal{C}^1(\overline{\Omega}) \subset W^{1,p}(\Omega)$, see Lemma B.51.

Lemma B.54 — Embedding of Bochner spaces [235, §23.2, Prop. 23.2 (h), p. 407].
Let X, Y be real Banach spaces with the continuous embedding $X \hookrightarrow Y$, $p, q \in [1, \infty]$ with $q \leq p$, and $T \in \mathbb{R}_{>0}$. Then we have the continuous embedding

$$L^p((0, T); X) \hookrightarrow L^q((0, T); Y).$$

Lemma B.55 — Embedding of Lebesgue spaces [235, §18.6, Ex. 18.14, p. 37].
Let $\Omega \subset \mathbb{R}^d$, $d \in \mathbb{N}$, be a nonempty, bounded and Lebesgue-measurable set and let $p, q \in [1, \infty]$ with $q \leq p$. Then we have the continuous embedding

$$L^p(\Omega) \hookrightarrow L^q(\Omega). \tag{B.7}$$

Theorem B.56 — Sobolev embedding (see [93, Sec. 1.2.2.9, Thm. 1.14, p. 22] and references therein).
Let $\Omega \subset \mathbb{R}^d$, $d \in \mathbb{N}$, be a nonempty, open and bounded set with Lipschitz boundary. Let $m \in \mathbb{N}$ and $p \in [1, \infty)$.

1. For all $k \in \mathbb{N}_0$ and $\beta \in (0, 1)$ with

$$m - \frac{d}{p} \geq k + \beta,$$

   we have the *continuous* embedding

$$W^{m,p}(\Omega) \hookrightarrow \mathcal{C}^{k,\beta}(\overline{\Omega}).$$

2. For all $k \in \mathbb{N}_0$ and $\beta \in [0, 1]$ with

$$m - \frac{d}{p} > k + \beta,$$

   we have the *compact* embedding

$$W^{m,p}(\Omega) \hookrightarrow\hookrightarrow \mathcal{C}^{k,\beta}(\overline{\Omega}).$$

3. For $q \in [1, \infty)$ and $l \in \mathbb{N}_0$ with

$$m - \frac{d}{p} \geq l - \frac{d}{q},$$

   we have the *continuous* embedding[a]

$$W^{m,p}(\Omega) \hookrightarrow W^{l,q}(\Omega).$$

   The embedding is *compact*, if

$$m > l \quad \text{and} \quad m - \frac{d}{p} > l - \frac{d}{q}.$$

4. For $m \in \mathbb{N}_0$ and $p, q \in [1, \infty]$ with $q \leq p$, we get the *continuous* embedding

$$W^{m,p}(\Omega) \hookrightarrow W^{m,q}(\Omega).$$

[236, App. (45c), p. 1027]

---

[a] For $l = 0$, we have $W^{0,q}(\Omega) = L^q(\Omega)$.

Theorem B.57 — Compact embedding in Bochner spaces [202, Sec. 8, Cor. 4, p. 85].

Let $T \in \mathbb{R}_{>0}$ and let X, B, Y be real Banach spaces with compact and continuous embeddings

$$X \hookrightarrow\hookrightarrow B \hookrightarrow Y.$$

Let $M \subseteq L^\infty((0,T); X)$ be bounded and let $\{D_t f \mid f \in M\} \subseteq L^p((0,T); Y)$, $p \in (1, \infty)$, be bounded. Then M is *relatively compact*[a] in $\mathcal{C}^0([0,T]; B)$, i.e., its closure $\overline{M}$ is compact.

---

[a] See [202, Sec. 2, p. 70] for the definition of *relatively compact*.

Corollary B.58

Let $\Omega \subset \mathbb{R}^d$, $d \in \{2, 3\}$, be a nonempty, open and bounded set with Lipschitz boundary, $p \in (1, \infty)$ and $T \in \mathbb{R}_{>0}$. Then we have the compact embedding[a]

$$L^\infty((0,T); H^2(\Omega)) \cap W^{1,p}((0,T); L^2(\Omega)) \hookrightarrow\hookrightarrow \mathcal{C}^0([0,T] \times \overline{\Omega}).$$

---

[a] The proof is given in Appendix B.2.9.

Theorem B.59 — Embedding in Hölder spaces I [4, Sec. 8.6, p. 338].

Let $\Omega \subset \mathbb{R}^d$, $d \in \mathbb{N}$, be a nonempty, open and bounded set and let $k_1, k_2 \in \mathbb{N}_0$ and $\alpha_1, \alpha_2 \in [0, 1]$ with

$$k_1 + \alpha_1 > k_2 + \alpha_2.$$

In case $k_1 > 0$, we additionally assume that the domain Ω has a Lipschitz boundary. Then we have the *compact* embedding

$$\mathcal{C}^{k_1, \alpha_1}(\overline{\Omega}) \hookrightarrow\hookrightarrow \mathcal{C}^{k_2, \alpha_2}(\overline{\Omega}). \tag{B.8}$$

Theorem B.60 — Embedding Hölder spaces II [175, Sec. 1, Thm. 1.1, p. 1].

Let $\Omega \subset \mathbb{R}^d$, $d \in \mathbb{N}$, a nonempty, open and bounded set with Lipschitz boundary and let $T \in \mathbb{R}_{>0}$. For $p, q \in (1, \infty)$ with $\frac{1}{p} + \frac{d}{q} < 1$, we have the *compact* embedding

$$L^p((0,T); W^{1,q}(\Omega)) \cap W^{1,p}((0,T); L^q(\Omega)) \hookrightarrow\hookrightarrow \mathcal{C}^{0,\alpha}(\overline{(0,T) \times \Omega})$$

for every $0 \leq \alpha < \frac{p-1}{p} - \frac{d}{q}$.

Theorem B.61 — Aubin–Lions [186, Sec. 3.3.6, Lem. 3.74, p. 121].

Let X, X_0, X_1 be real Banach spaces, with X_0, X_1 being reflexive, and let the following embeddings hold:

$$X_0 \hookrightarrow\hookrightarrow X \hookrightarrow X_1.$$

Let $p_0, p_1 \in (1, \infty)$ and $T \in \mathbb{R}_{>0}$ and define the space

$$W_0 := \{f \in L^{p_0}((0, T); X_0) \,|\, f' \in L^{p_1}((0, T); X_1)\}$$

equipped with the norm

$$\|y\|_{W_0} := \|f\|_{L^{p_0}((0,T);X_0)} + \|f'\|_{L^{p_1}((0,T);X_1)}.$$

Then W_0 is a *reflexive Banach space* with the *compact* embedding

$$W_0 \hookrightarrow\hookrightarrow L^{p_0}((0, T); X).$$

Theorem B.62 — $H^2(\Omega)$ regularity [85, Sec. 2.3.3, Thm. 2.3.3.2, p. 106].

Let $\Omega \subset \mathbb{R}^d$, $d \in \mathbb{N}$, be a nonempty, open and bounded set and Γ its boundary of class $\mathcal{C}^{1,1}$ (see [85, Sec. 1.2.1, Def. 1.2.1.1, p. 5]). Let the operator A be of divergence form

$$Ay := -\sum_{i,j=1}^{d} \mathrm{D}_i(a_{ij}\mathrm{D}_j y)$$

with $a_{ij} = a_{ji} \in \mathcal{C}^{0,1}(\overline{\Omega})$ such that there exists an $\alpha > 0$ with

$$\sum_{i,j=1}^{d} a_{ij}(x)\xi_i\xi_j \geq \alpha |\xi|^2 \quad \text{for all } x \in \overline{\Omega} \text{ and } \xi \in \mathbb{R}^d.$$

The operator B is the co-normal derivative of y w.r.t. A, i.e.,

$$By := -\sum_{i=1}^{d}(\sum_{j=1}^{d} a_{ij}\boldsymbol{n}_j)\mathrm{D}_i y \quad \text{on } \Gamma$$

with $\boldsymbol{n}$ the unit outer normal vector field on Γ.

Then, for $p \in (1, \infty)$, there exists a constant C such that

$$\|y\|_{W^{2,p}(\Omega)} \leq C \left(\|Ay\|_{L^p(\Omega)} + \|By\|_{W^{1-\frac{1}{p},p}(\Gamma)} + \|y\|_{W^{1,p}(\Omega)} \right) \quad \text{for all } y \in W^{2,p}(\Omega).$$

B.1.5 Miscellaneous

> **Theorem B.63 — Lax–Milgram [63, Sec. 6.2.1, Thm. 1, p. 297].**
>
> Let H be a real Hilbert space and let $B\colon H \times H \to \mathbb{R}$ be a bilinear mapping for which there exist constants $c, C > 0$ such that
>
> $$|B(y, \varphi)| \leq C \, \|y\|_H \, \|\varphi\|_H \quad \text{for all } y, \varphi, \in H \quad \text{(continuity)}$$
>
> and
>
> $$c \, \|y\|_H^2 \leq B(y, y) \quad \text{for all } y \in H. \quad \text{(coercivity)}$$
>
> Finally, let $f\colon H \to \mathbb{R}$ be a bounded linear functional.
> Then there exists a unique element $y \in H$ such that
>
> $$B(y, \varphi) = \langle f, \varphi \rangle_H \quad \text{for all } \varphi \in H. \tag{B.9}$$

We note that Theorem B.63 and the coercivity of the bilinear form imply a bound on the solution of the variational problem (B.9):

$$\|y\|_H \leq \frac{1}{c} \, \|f\|_{H^*} \, .$$

> **Theorem B.64 — Leray–Schauder fixed-point theorem [81, Sec. 11.4, Thm. 11.6, p. 286].**
> Let X be a real Banach space and let $S\colon X \times [0, 1] \to X$ be a continuous and compact mapping such that
>
> $$S(x, 0) = 0 \quad \text{for all } x \in X.$$
>
> Suppose there exists a constant $M > 0$ such that
>
> $$\|x\|_X < M$$
>
> for all $(x, \sigma) \in X \times [0, 1]$ satisfying $x = S(x, \sigma)$.
> Then the mapping $T_1\colon X \to X$, $x \mapsto T(x, 1)$ has a fixed point.

> **Lemma B.65 — Some spectral theory [235, §22.11, Thm. 22.E, p. 353].**
> Let $H \neq \{0\}$ be a separable real Hilbert space and $S\colon H \to H$ be a linear, symmetric, compact and strictly monotone operator. Then the operator S has a (countable) complete orthonormal system[a] of eigenvectors in H. The eigenvalues of S are positive and they have finite multiplicity. The eigenvectors related to two different eigenvalues are orthogonal to each other.
>
> ---
> [a] See [235, §19.5, Def. 19.10, p. 117] for details on complete orthonormal systems.

> **Theorem B.66 — Nemytskii [217, Sec. 4.3.1, Lem. 4.11, p. 157], [217, Sec. 4.3.2, Lem. 4.13, p. 161].**
> Let $Q \subseteq \mathbb{R}^d$, $d \in \mathbb{N}$, be a nonempty, open and bounded set and let $\varphi = \varphi(q, \omega)\colon Q \times \mathbb{R} \to \mathbb{R}$ be a function. For each fixed $\omega \in \mathbb{R}$, let $\varphi(\cdot, \omega)\colon Q \to \mathbb{R}$ be Lebesgue measurable, and, for a.a. $q \in Q$,

let $\varphi(q, \cdot)\colon \mathbb{R} \to \mathbb{R}$ be k-times differentiable for[a] $k \in \{0, 1\}$. We assume that there is a constant $K \in \mathbb{R}_{>0}$ such that $\left|\mathrm{D}_\omega^l\, \varphi(q, 0)\right| \leq K$ for a.a. $q \in Q$ and all $l \in \{0, \ldots, k\}$. Furthermore, we assume that, for every constant $M > 0$, there is a constant $L(M) \in \mathbb{R}_{>0}$ such that the estimate $\left|\mathrm{D}_\omega^k\, \varphi(q, \omega) - \mathrm{D}_\omega^k\, \varphi(q, \hat{\omega})\right| \leq L(M)\, |\omega - \hat{\omega}|$ is fulfilled for a.a. $q \in Q$ and all $\omega, \hat{\omega} \in [-M, M]$.[b] Then the following holds:

1. For $k \in \{0, 1\}$, the associated Nemytskii operator

$$\phi\colon L^\infty(Q) \to L^\infty(Q),\ \omega \mapsto \varphi(\cdot, \omega(\cdot)) \tag{B.10}$$

   is well defined and continuous. Furthermore, for $p \in [1, \infty]$ and $\omega, \hat{\omega} \in L^\infty(Q)$ with $\|\omega\|_{L^\infty(Q)} \leq M$, $\|\hat{\omega}\|_{L^\infty(Q)} \leq M$, the estimate

$$\|\phi(\omega) - \phi(\hat{\omega})\|_{L^p(Q)} \leq L(M)\, \|\omega - \hat{\omega}\|_{L^p(Q)}$$

   holds.

2. For $k = 1$, the associated Nemytskii operator (B.10) is continuously Fréchet differentiable on $L^\infty(Q)$ and, for $h \in L^\infty(Q)$, it holds

$$(\mathrm{D}\phi(\omega)[h])\,(q) = \mathrm{D}_\omega\, \varphi(q, \omega(q))\, h(q) \quad \text{for a.a. } q \in Q.$$

---

[a] The zeroth derivative of a function corresponds to the function itself.
[b] For $k = 0$, this means that $\varphi(q, \cdot)$ is locally Lipschitz continuous.

Remark B.67 — Sufficient condition for a Nemytskii operator [217, Sec. 4.3.2, p. 161].
All functions $\varphi = \varphi(\omega)$ in $\mathcal{C}^2(\mathbb{R})$ fulfill the prerequisites of Theorem B.66 and generate continuously Fréchet-differentiable Nemytskii operators in $L^\infty(Q)$.

Theorem B.68 — Arzelà–Ascoli [186, Sec. A.12, Satz 12.4, p. 192].
Let $\Omega \subset \mathbb{R}^d$, $d \in \mathbb{N}$, be a nonempty, open and bounded set. Then a subset $M \subset \mathcal{C}^0(\overline{\Omega})$ is *relatively compact*[a] [b] if and only if M is *bounded* and *uniformly equicontinuous*[c].

---

[a] The space $\mathcal{C}^0(\overline{\Omega})$ is equipped with the uniform norm $\|f\|_{\mathcal{C}^0(\overline{\Omega})} = \sup\limits_{x \in \overline{\Omega}} |f(x)|$.

[b] The set M is relatively compact if $\overline{M}$ is compact.

[c] The set M is uniformly equicontinuous if for all $\varepsilon > 0$ there is a $\delta > 0$ such that for all $f \in M$ and all $x, y \in \overline{\Omega}$ with $\|x - y\| < \delta$ it holds $|f(x) - f(y)| < \varepsilon$.

Lemma B.69 — Projection operator [93, Sec. 1.7.1, Lem. 1.11, p. 69].
Let H be a Hilbert space and let $A \subset H$ be a nonempty, closed and convex subset. Furthermore, let $P\colon H \to A$ denote the projection onto A. Then, for all $x \in H$ and all $\alpha > 0$, the following conditions are equivalent:

$$(1)\quad w \in A, \quad (x, v - w)_X \geq 0 \quad \text{for all } v \in A.$$
$$(2)\quad w - P(w - \alpha x) = 0.$$

B.2 Proofs for the Hitchhiker's guide

B.2.1 Proof of Lemma B.4

Proof. The first result regarding dual pairings is given in [36, Sec. 1.3, Prop. 1.29, p. 16]. It is left to show that Z is complete. Let $(z_k)_{k \in \mathbb{N}} = ((x_k, y_k))_{k \in \mathbb{N}} \subset X \times Y$ be a Cauchy sequence w.r.t. the Z norm, which implies that $(x_k)_{k \in \mathbb{N}}$ and $(y_k)_{k \in \mathbb{N}}$ are Cauchy sequences in X and Y, respectively. Because X and Y are complete, there are elements $x \in X, y \in Y$ such that

$$x_k \to x \text{ in } X \quad \text{and} \quad y_k \to y \text{ in } Y.$$

This implies immediately $z_k \to z = (x, y)$ in Z in the given norm, thus, Z is complete. ∎

B.2.2 Proof of Lemma B.17

Proof. For $x^* \in X^*$, the map $\langle x^*, y \rangle_Y : Y \to \mathbb{R}$, $y \mapsto \langle x^*, j(y) \rangle_X$ defines an element in Y^*. In fact, the map is linear by construction and the continuity follows from

$$|\langle x^*, y \rangle_Y| = |\langle x^*, j(y) \rangle_X| \le \|x^*\|_{X^*} \|j(y)\|_X \le C \|x^*\|_{X^*} \|y\|_Y.$$

Next, we consider a weakly convergent sequence $(y_k)_{k \in \mathbb{N}} \subset Y$ with $y_k \rightharpoonup y$, $y \in Y$, i.e., for all $y^* \in Y^*$ it holds $\langle y^*, y_k \rangle_Y \to \langle y^*, y \rangle_Y$.

For $x^* \in X^*$, we have seen above that $\langle x^*, j(\cdot) \rangle_X$ defines an element in Y^*, which implies $\langle x^*, j(y_k) \rangle_X \to \langle x^*, j(y_k) \rangle_X$ and, thus, weak convergence in X. ∎

B.2.3 Proof of Lemma B.38

Proof. The first result follows from [56, Sec. 8.1, Cor. 8.1.10, p. 211], where we need only that $H^1(\Omega) \stackrel{\text{dense}}{\hookrightarrow} L^2(\Omega) \hookrightarrow H^1(\Omega)^*$ form a Gelfand triple (see Subsection 2.2.1). The required dense embedding follows from $\mathcal{C}^\infty(\overline{\Omega}) \subset H^1(\Omega) \subset L^2(\Omega)$ and the density of $\mathcal{C}^\infty(\overline{\Omega})$ in $L^2(\Omega)$, see Lemma B.51.

The second result is given by means of the fundamental theorem of calculus in Bochner spaces[2] because the map $t \mapsto \|f(t)\|^2_{L^2(\Omega)}$ is an element of $W^{1,1}((0,T);\mathbb{R})$. In fact, the map $t \mapsto \left(\|f(t)\|^2_{L^2(\Omega)} \right)' = 2 \langle f'(t), f(t) \rangle_{H^1(\Omega)}$ is an element of $L^1((0,T);\mathbb{R})$, see Theorem B.36. With the embedding $f \in L^2((0,T);H^1(\Omega)) \hookrightarrow L^2((0,T);L^2(\Omega))$, it follows that also the map $t \mapsto \|f(t)\|^2_{L^2(\Omega)}$ is an element of $L^1((0,T);\mathbb{R})$. ∎

B.2.4 Proof of Theorem B.39

Proof. We reproduce the proof in [43, XVIII §5 2.2, Lem. 1, p. 559], which is given for the case of $f \in L^\infty((0,T))$ and $\mu \in L^1((0,T))$.

Note that $f \in L^\infty((0,T)), \mu \in L^1((0,T))$ imply that $f\mu \in L^1((0,T))$, thus, the map given by $F(t) := \int_0^t \mu(s) f(s) \, ds + C$ is absolutely continuous and it holds $F'(t) = f(t)\mu(t)$ for a.a $t \in [0,T]$, see Theorem B.31.

From (B.2), we deduce

$$\frac{F'(t)}{F(t)} \le \mu(t) \quad \text{for a.a. } t \in [0,T],$$

---

[2] See the fundamental theorem of calculus in Bochner spaces B.33.

which implies

$$\log\left(\frac{F(t)}{C}\right) \le \int_0^t \mu(s)\,\mathrm{d}s$$

with the same constant as before, and consequently

$$f(t) \le F(t) \le C\exp\left(\int_0^t \mu(s)\,\mathrm{d}s\right) \quad \text{for a.a. } t \in [0,T].$$

∎

B.2.5 Proof of Lemma B.40

Proof. The functions $h = fg$ as well as $f'g$ are elements of $L^2(I; H^k(\Omega))$. In fact, because of $f \in L^2(I; \mathbb{R})$, we can approximate f by simple functions $s_k \colon [0,T] \to \mathbb{R}$ such that $s_k(t) \to f(t)$ for a.a. $t \in [0,T]$. This yields a sequence of simple functions $\hat{s}_k \colon [0,T] \to H^1(\Omega)$, $\hat{s}_k(t) := s_k(t)g$ with $\hat{s}_k(t) \to h(t)$ in $H^k(\Omega)$ for a.a. $t \in [0,T]$, thus, h is Bochner measurable. Furthermore, it holds

$$\int_0^T \|h(t)\|_{H^k(\Omega)}^2\,\mathrm{d}t = \int_0^T |f(t)|^2\,\|g\|_{H^k(\Omega)}^2\,\mathrm{d}t = \int_0^T |f(t)|^2\,\mathrm{d}t\,\|g\|_{H^k(\Omega)}^2 < \infty.$$

The proof for $f'g$ goes analogously.

1. First, we show $\mathrm{D}^\alpha(h')(t) = f'(t)\mathrm{D}^\alpha g$.

   Note that $h' = f'g$ holds. In fact, for $\varphi \in \mathcal{C}_c^\infty((0,T))$, it holds by the definition of f' that

   $$\int_0^T \varphi'(t)h(t)\,\mathrm{d}t = \int_0^T \varphi'(t)f(t)g\,\mathrm{d}t = \int_0^T \varphi'(t)f(t)\,\mathrm{d}t\,g$$
   $$= (-1)\int_0^T \varphi(t)f'(t)\,\mathrm{d}t\,g = (-1)\int_0^T \varphi(t)(f'(t)g)\,\mathrm{d}t\,.$$

   For the last step, let $\varphi \in \mathcal{C}_c^\infty(\Omega)$. We get from the definition of $\mathrm{D}^\alpha g$ that

   $$\int_\Omega (\mathrm{D}^\alpha\varphi(x))\,h'(t)(x)\,\mathrm{d}x = \int_\Omega (\mathrm{D}^\alpha\varphi(x))\,f'(t)g(x)\,\mathrm{d}x = \int_\Omega (\mathrm{D}^\alpha\varphi(x))\,g(x)\,\mathrm{d}x\,f'(t)$$
   $$= (-1)^{|\alpha|}\int_\Omega \varphi(x)\mathrm{D}^\alpha g(x)\,\mathrm{d}x\,f'(t)$$
   $$= (-1)^{|\alpha|}\int_\Omega \varphi(x)\,(f'(t)\mathrm{D}^\alpha g(x))\,\mathrm{d}x\,,$$

   which yields the desired result.

2. Next, we show $(\mathrm{D}^\alpha h)'(t) = f'(t)\mathrm{D}^\alpha g$, where $\mathrm{D}^\alpha h$ refers to the map

   $$\mathrm{D}^\alpha h \colon (0,T) \to H^{k-|\alpha|}(\Omega),\ t \mapsto \mathrm{D}^\alpha(h(t))\,,$$

   which is well defined because of $h(t) \in H^k(\Omega)$.

   Similarly as above, we can show that $\mathrm{D}^\alpha(h(t)) = f(t)\mathrm{D}^\alpha g$ for a.a. $t \in (0,T)$.

   The maps $(0,T) \to H^{k-|\alpha|}(\Omega),\ t \mapsto f(t)\mathrm{D}^\alpha g$ and $(0,T) \to H^{k-|\alpha|}(\Omega),\ t \mapsto f'(t)\mathrm{D}^\alpha g$ are both elements of $L^2((0,T); H^{k-|\alpha|}(\Omega))$ as seen earlier in this proof.

For $\varphi \in \mathcal{C}_c^\infty((0,T))$, we now get the desired result from the following computation:

$$\int_0^T \varphi'(t) \mathrm{D}^\alpha \left(h(t) \right) \mathrm{d}t \;=\; \int_0^T \varphi'(t) f(t) \mathrm{D}^\alpha g \, \mathrm{d}t \;=\; \int_0^T \varphi'(t) f(t) \, \mathrm{d}t \, \mathrm{D}^\alpha g$$

$$= (-1) \int_0^T \varphi(t) f'(t) \, \mathrm{d}t \, \mathrm{D}^\alpha g = (-1) \int_0^T \varphi(t) \left(f'(t) \mathrm{D}^\alpha g \right) \mathrm{d}t \,.$$

∎

B.2.6 Proof of Lemma B.49

Proof.   1. This is a well known result, see [186, Sec. 2.1.1, p. 40]. The proof is based on Fubini's theorem[3] and Pettis' theorem[4], and is given for the case of the spatial dimension equal to one, i.e., $d = 1$, in [56, Sec. 7.1, Thm. 7.1.24, p. 165].

2. One can construct the following counter example[5]: The function

$$f \colon (0,1) \times (0,1) \to \mathbb{R}, \; f(t,x) = \begin{cases} 1, & x \le t, \\ 0, & \text{else} \end{cases}$$

is an element of $L^\infty((0,1) \times (0,1))$, but the function

$$\hat{f} \colon (0,1) \to L^\infty((0,1)), \; \tilde{f}(t) := f(t, \cdot)$$

is not Bochner measurable, hence $\hat{f} \notin L^\infty((0,1); L^\infty((0,1)))$. In fact, Pettis' theorem[6] states that a function like $\hat{f}$ is Bochner measurable if and only if it is weakly measurable and separably valued. The function $\hat{f}$ is not separably valued because the range $\hat{f}((0,1)\backslash M) = \{1_{(0,t]} \,|\, t \in (0,1)\backslash M\} \subset L^\infty((0,1))$, where $1_{(0,t]} \colon (0,1) \to \{0,1\}$ denotes the indicator function of the interval $(0,t]$ and $M \subset (0,1)$ denotes an arbitrary subset with Lebesgue measure zero, contains no dense subset w.r.t. the $L^\infty((0,1))$ norm and, thus, is not separable.

A variant of this proof can be found in [56, Sec. 7.1, Ex. 7.1.27, p. 167].

∎

B.2.7 Proof of Lemma B.50

Proof.   1. "$\mathcal{C}^0([0,T] \times \overline{\Omega}) \subseteq \mathcal{C}^0([0,T]; \mathcal{C}^0(\overline{\Omega}))$"

Let $\hat{f} \in \mathcal{C}^0([0,T] \times \overline{\Omega})$ and let $\varepsilon > 0$. We define $f \colon [0,T] \to \mathcal{C}^0(\overline{\Omega})$, $t \mapsto \hat{f}(t, \cdot)$. The function $\hat{f}$ is uniformly continuous[7], i.e., there is a $\delta > 0$ such that, for all $(t,x), (\hat{t}, \hat{x}) \in [0,T] \times \overline{\Omega}$ with $\|(t,x) - (\hat{t}, \hat{x})\|_\infty < \delta$, we get $\left|\hat{f}(t,x) - \hat{f}(\hat{t}, \hat{x})\right| < \frac{\varepsilon}{2}$. For $t, \hat{t} \in [0,T]$ with $|t - \hat{t}| < \delta$, we get

$$\left\| f(t) - f(\hat{t}) \right\|_{\mathcal{C}^0(\overline{\Omega})} = \sup_{x \in \overline{\Omega}} \left| \hat{f}(t,x) - \hat{f}(\hat{t},x) \right| < \varepsilon,$$

which gives us $f \in \mathcal{C}^0([0,T]; \mathcal{C}^0(\overline{\Omega}))$.

---

[3] See Fubini's theorem B.2.
[4] See Pettis' theorem B.45.
[5] See also [15, Sec. 1.1, Ex. 1.1.5, p. 10], [184, Sec. 1.5, Ex. 1.42, p. 24].
[6] See Pettis' theorem B.45.
[7] See Lemma B.5 on uniform continuity.

2. "$\mathcal{C}^0([0,T] \times \overline{\Omega}) \supseteq \mathcal{C}^0([0,T]; \mathcal{C}^0(\overline{\Omega}))$"

   Let $f \in \mathcal{C}^0([0,T]; \mathcal{C}^0(\overline{\Omega}))$, $\varepsilon > 0$ and $(t,x) \in Q$. We define $\hat{f} \colon [0,T] \times \overline{\Omega} \to \mathbb{R}$, $(t,x) \mapsto f(t)(x)$. Because of $f \in \mathcal{C}^0([0,T]; \mathcal{C}^0(\overline{\Omega}))$, there is a $\delta_1 > 0$ such that, for all $\hat{t} \in [0,T]$ with $|\hat{t} - t| < \delta_1$, it holds $\|f(\hat{t}) - f(t)\|_{\mathcal{C}^0(\overline{\Omega})} < \frac{\varepsilon}{2}$. With $f(t) \in \mathcal{C}^0(\overline{\Omega})$, there is another $\delta_2 > 0$ such that, for all $\hat{x} \in \overline{\Omega}$ with $\|\hat{x} - x\|_\infty < \delta_2$, it holds $|f(t)(\hat{x}) - f(t)(x)| < \frac{\varepsilon}{2}$.

   We choose $\delta := \min\{\delta_1, \delta_2\}$ and get for $(\hat{t}, \hat{x}) \in [0,T] \times \overline{\Omega}$ with $\|(\hat{t}, \hat{x}) - (t,x)\|_\infty < \delta$ that

$$
\left|\hat{f}(\hat{t}, \hat{x}) - \hat{f}(t,x)\right| \leq \left|\hat{f}(\hat{t}, \hat{x}) - \hat{f}(t, \hat{x})\right| + \left|\hat{f}(t, \hat{x}) - \hat{f}(t,x)\right|
$$
$$
\leq \left\|f(\hat{t}) - f(t)\right\|_{\mathcal{C}^0(\overline{\Omega})} + |f(t)(\hat{x}) - f(t)(x)| < \varepsilon,
$$

   which implies $\hat{f} \in \mathcal{C}^0([0,T] \times \overline{\Omega})$.

∎

B.2.8 Proof of Lemma B.52

Proof.   1. Lemma B.3 tells us that an element in $\mathcal{C}^0(\overline{\Omega})$ is measurable. With this, we identify an element in $\mathcal{C}^0(\overline{\Omega})$ as an element in $L^\infty(\Omega)$, and the finite value of its uniform norm is translated to the value of its essential-supremum.

2. See [56, Sec. 7.1, Thm. 7.1.23, p. 164].

∎

B.2.9 Proof of Corollary B.58

Proof. It holds

$$
H^2(\Omega) \hookrightarrow\hookrightarrow \mathcal{C}^{0,\frac{1}{4}}(\overline{\Omega}) \overset{(B.8)}{\hookrightarrow} \mathcal{C}^0(\overline{\Omega}),
$$

where the first embedding corresponds to a classical Sobolev embedding[8], and

$$
\mathcal{C}^0(\overline{\Omega}) \overset{(B.6)}{\hookrightarrow} L^\infty(\Omega) \overset{(B.7)}{\hookrightarrow} L^2(\Omega).
$$

Together with Lemma B.19 and the fact, that a chain of continuous functions is again continuous, we get the embeddings

$$
H^2(\Omega) \hookrightarrow\hookrightarrow \mathcal{C}^0(\overline{\Omega}) \hookrightarrow L^2(\Omega).
$$

With Theorem B.57, we infer the compact embedding

$$
L^\infty(I; H^2(\Omega)) \cap W^{1,p}((0,T); L^2(\Omega)) \hookrightarrow\hookrightarrow \mathcal{C}^0(\overline{I}; \mathcal{C}^0(\overline{\Omega})) \overset{(B.5)}{\cong} \mathcal{C}^0(\overline{Q}).
$$

∎

---

[8] See classical Sobolev embeddings in Theorem B.56, with $2 - \frac{d}{2} > \beta$ for $d \in \{2,3\}$, $\beta \in (0, \frac{1}{2})$.

C Second-order formulation of the P_N equations

Documentation is more like "the first time": everybody thinks it's good, everybody thinks all others have done it, but not much has happened so far.

Yet another opinion on source code and its documentation

C.1 Details for Chapter 5

C.1.1 Proof of Lemma 5.18

Proof.

Use symmetry properties of the real spherical harmonics and the scattering kernel.

We show the result only for even $\hat{\mathcal{K}}(\xi)$, i.e., $\hat{\mathcal{K}}(\xi) = \hat{\mathcal{K}}(-\xi)$. The case where $\hat{\mathcal{K}}(\xi)$ is odd works analogously. The final result then follows by considering the even-odd decomposition of the general kernel as $\hat{\mathcal{K}}(\xi) = \hat{\mathcal{K}}_{\mathrm{e}}(\xi) + \hat{\mathcal{K}}_{\mathrm{o}}(\xi)$, where $\hat{\mathcal{K}}_{\mathrm{e}}(\xi) = \frac{1}{2}\left(\hat{\mathcal{K}}(\xi) + \hat{\mathcal{K}}(-\xi)\right)$ and $\hat{\mathcal{K}}_{\mathrm{o}}(\xi) = \frac{1}{2}\left(\hat{\mathcal{K}}(\xi) - \hat{\mathcal{K}}(-\xi)\right)$ denote the even and odd parts of $\hat{\mathcal{K}}(\xi)$, respectively.

Let $\mathcal{R}(v) \in \mathbb{R}^{3\times3}$ be any rotation matrix that rotates v to e_3, i.e., $\mathcal{R}(v)v = e_3$ with $\det(\mathcal{R}) = 1$. We define the new parameterization of v' as

$$\hat{v} = \left[\sqrt{1-\hat{\mu}^2}\cos(\hat{\varphi}) \quad \sqrt{1-\hat{\mu}^2}\sin(\hat{\varphi}) \quad \hat{\mu}\right]^{\mathrm{T}} := \mathcal{R}(v)v'.$$

With the choice of our angular basis, it can be shown [16, 148] that there is a rotation matrix $R(v) \in \mathbb{R}^{n_{\mathrm{o}} \times n_{\mathrm{o}}}$ with

$$\mathbf{b}_{\mathrm{o}}(\mathcal{R}(v)^{\mathrm{T}}\hat{v}) = R^{\mathrm{T}}(v)\mathbf{b}_{\mathrm{o}}(\hat{v}),$$

which holds analogously for the vector of even basis functions. The substitution rule now implies

$$
\begin{aligned}
\Sigma_{\mathrm{eo}} &= \int_{\mathcal{S}^2}\int_{\mathcal{S}^2}\mathbf{b}_{\mathrm{e}}(v)\mathbf{b}_{\mathrm{o}}^{\mathrm{T}}(v')\hat{\mathcal{K}}\left(v^{\mathrm{T}}v'\right)\,\mathrm{d}v'\,\mathrm{d}v \\
&= \int_{\mathcal{S}^2}\int_{-1}^{1}\int_{0}^{2\pi}\mathbf{b}_{\mathrm{e}}(v)\mathbf{b}_{\mathrm{o}}^{\mathrm{T}}(\mathcal{R}(v)^{\mathrm{T}}\hat{v})\hat{\mathcal{K}}(\hat{\mu})\,\mathrm{d}\hat{\varphi}\,\mathrm{d}\hat{\mu}\,\mathrm{d}v \\
&= \int_{\mathcal{S}^2}\mathbf{b}_{\mathrm{e}}(v)\int_{-1}^{1}\int_{0}^{2\pi}\mathbf{b}_{\mathrm{o}}^{\mathrm{T}}(\mathcal{R}(v)^{\mathrm{T}}\hat{v})\hat{\mathcal{K}}(\hat{\mu})\,\mathrm{d}\hat{\varphi}\,\mathrm{d}\hat{\mu}\,\mathrm{d}v \\
&= \int_{\mathcal{S}^2}\mathbf{b}_{\mathrm{e}}(v)\int_{-1}^{1}\int_{0}^{2\pi}\mathbf{b}_{\mathrm{o}}^{\mathrm{T}}(\hat{v})\hat{\mathcal{K}}(\hat{\mu})\,\mathrm{d}\hat{\varphi}\,\mathrm{d}\hat{\mu}\,R(v)\,\mathrm{d}v.
\end{aligned}
$$

We now consider only the inner integral

$$\int_{-1}^{1}\int_{0}^{2\pi} \mathbf{b}_{\mathrm{o}}^{\mathrm{T}}(\hat{\boldsymbol{v}})\hat{\mathcal{K}}\left(\hat{\mu}\right)\,\mathrm{d}\hat{\varphi}\,\mathrm{d}\hat{\mu}$$

$$=\int_{0}^{1}\int_{0}^{2\pi} \mathbf{b}_{\mathrm{o}}^{\mathrm{T}}(\hat{\boldsymbol{v}})\hat{\mathcal{K}}\left(\hat{\mu}\right)\,\mathrm{d}\hat{\varphi}\,\mathrm{d}\hat{\mu}+\int_{-1}^{0}\int_{0}^{2\pi} \mathbf{b}_{\mathrm{o}}^{\mathrm{T}}(\hat{\boldsymbol{v}})\hat{\mathcal{K}}\left(\hat{\mu}\right)\,\mathrm{d}\hat{\varphi}\,\mathrm{d}\hat{\mu}$$

$$=\int_{0}^{1}\int_{0}^{2\pi} \mathbf{b}_{\mathrm{o}}^{\mathrm{T}}(\hat{\boldsymbol{v}})\hat{\mathcal{K}}\left(\hat{\mu}\right)\,\mathrm{d}\hat{\varphi}\,\mathrm{d}\hat{\mu}+\int_{0}^{1}\int_{0}^{2\pi} \mathbf{b}_{\mathrm{o}}^{\mathrm{T}}\left(\begin{pmatrix}\sqrt{1-\hat{\mu}^2}\cos(\hat{\varphi})\\\sqrt{1-\hat{\mu}^2}\sin(\hat{\varphi})\\-\hat{\mu}\end{pmatrix}\right)\hat{\mathcal{K}}\left(-\hat{\mu}\right)\,\mathrm{d}\hat{\varphi}\,\mathrm{d}\hat{\mu}$$

$$=\int_{0}^{1}\int_{0}^{2\pi} \mathbf{b}_{\mathrm{o}}^{\mathrm{T}}(\hat{\boldsymbol{v}})\hat{\mathcal{K}}\left(\hat{\mu}\right)\,\mathrm{d}\hat{\varphi}\,\mathrm{d}\hat{\mu}+\int_{0}^{1}\int_{-\pi}^{\pi} \mathbf{b}_{\mathrm{o}}^{\mathrm{T}}\left(\begin{pmatrix}\sqrt{1-\hat{\mu}^2}\cos(\hat{\varphi}+\pi)\\\sqrt{1-\hat{\mu}^2}\sin(\hat{\varphi}+\pi)\\-\hat{\mu}\end{pmatrix}\right)\hat{\mathcal{K}}\left(-\hat{\mu}\right)\,\mathrm{d}\hat{\varphi}\,\mathrm{d}\hat{\mu}$$

$$=\int_{0}^{1}\int_{0}^{2\pi} \mathbf{b}_{\mathrm{o}}^{\mathrm{T}}(\hat{\boldsymbol{v}})\hat{\mathcal{K}}\left(\hat{\mu}\right)\,\mathrm{d}\hat{\varphi}\,\mathrm{d}\hat{\mu}+\int_{0}^{1}\int_{-\pi}^{\pi} \mathbf{b}_{\mathrm{o}}^{\mathrm{T}}\left(-\hat{\boldsymbol{v}}\right)\hat{\mathcal{K}}\left(-\hat{\mu}\right)\,\mathrm{d}\hat{\varphi}\,\mathrm{d}\hat{\mu}$$

$$\overset{1}{=}\int_{0}^{1}\int_{0}^{2\pi} \mathbf{b}_{\mathrm{o}}^{\mathrm{T}}(\hat{\boldsymbol{v}})\hat{\mathcal{K}}\left(\hat{\mu}\right)\,\mathrm{d}\hat{\varphi}\,\mathrm{d}\hat{\mu}-\int_{0}^{1}\int_{-\pi}^{\pi} \mathbf{b}_{\mathrm{o}}^{\mathrm{T}}\left(\hat{\boldsymbol{v}}\right)\hat{\mathcal{K}}\left(\hat{\mu}\right)\,\mathrm{d}\hat{\varphi}\,\mathrm{d}\hat{\mu}$$

$$=\int_{0}^{1}\int_{0}^{2\pi} \mathbf{b}_{\mathrm{o}}^{\mathrm{T}}(\hat{\boldsymbol{v}})\hat{\mathcal{K}}\left(\hat{\mu}\right)\,\mathrm{d}\hat{\varphi}\,\mathrm{d}\hat{\mu}-\int_{0}^{1}\int_{0}^{2\pi} \mathbf{b}_{\mathrm{o}}^{\mathrm{T}}\left(\hat{\boldsymbol{v}}\right)\hat{\mathcal{K}}\left(\hat{\mu}\right)\,\mathrm{d}\hat{\varphi}\,\mathrm{d}\hat{\mu}$$

$$=0,$$

which implies $\Sigma_{\mathrm{eo}} = 0$ as well. The proof works in the same way for odd kernels, where we define the rotation matrix such that $\mathcal{R}(\boldsymbol{v}')\boldsymbol{v}' = e_3$ and define $\hat{\boldsymbol{v}} = \mathcal{R}(\boldsymbol{v}')\boldsymbol{v}$, and consider only the integral with respect to $\boldsymbol{v}$. ∎

C.1.2 Proof of Lemma 5.15

Proof.

> Show that C_{oo} is negative definite.

It holds by definition

$$\Sigma_{\mathrm{oo}} = \int_{\mathcal{S}^2}\int_{\mathcal{S}^2} \mathbf{b}_{\mathrm{o}}(\boldsymbol{v})\mathbf{b}_{\mathrm{o}}(\boldsymbol{v}')^{\mathrm{T}}\mathcal{K}\left(\boldsymbol{v},\boldsymbol{v}'\right)\,\mathrm{d}\boldsymbol{v}'\,\mathrm{d}\boldsymbol{v}.$$

Especially, Σ_{oo} is symmetric due to the symmetry of $\mathcal{K}$. Let $\mathbf{c} \in \mathbb{R}^{n_{\mathrm{o}}}$ and define $a(\boldsymbol{v}) := \mathbf{c}^{\mathrm{T}}\mathbf{b}_{\mathrm{o}}(\boldsymbol{v})$. Then it holds:

$$\mathbf{c}^{\mathrm{T}}\left(\sigma_{\mathrm{s}}\Sigma_{\mathrm{oo}} - \sigma_{\mathrm{t}}E_{n_{\mathrm{o}}}\right)\mathbf{c} = \sigma_{\mathrm{s}}\int_{\mathcal{S}^2}\int_{\mathcal{S}^2}\mathcal{K}\left(\boldsymbol{v},\boldsymbol{v}'\right)a(\boldsymbol{v})a(\boldsymbol{v}')\,\mathrm{d}\boldsymbol{v}'\,\mathrm{d}\boldsymbol{v} - \sigma_{\mathrm{t}}\left\|\mathbf{c}\right\|_2^2$$

$$= \frac{\sigma_{\mathrm{s}}}{2}\int_{\mathcal{S}^2}\int_{\mathcal{S}^2}\mathcal{K}\left(\boldsymbol{v},\boldsymbol{v}'\right)\left(a^2(\boldsymbol{v})+a^2(\boldsymbol{v}')-(a(\boldsymbol{v})-a(\boldsymbol{v}'))^2\right)\,\mathrm{d}\boldsymbol{v}'\,\mathrm{d}\boldsymbol{v} - \sigma_{\mathrm{t}}\left\|\mathbf{c}\right\|_2^2$$

$$\overset{(A2)}{=} \sigma_{\mathrm{s}}\left\langle a^2\right\rangle - \frac{\sigma_{\mathrm{s}}}{2}\int_{\mathcal{S}^2}\int_{\mathcal{S}^2}\mathcal{K}\left(\boldsymbol{v},\boldsymbol{v}'\right)(a(\boldsymbol{v})-a(\boldsymbol{v}'))^2\,\mathrm{d}\boldsymbol{v}'\,\mathrm{d}\boldsymbol{v} - \sigma_{\mathrm{t}}\left\|\mathbf{c}\right\|_2^2$$

$$\overset{(A1)}{\leq} \sigma_{\mathrm{s}}\left\langle a^2\right\rangle - \frac{\sigma_{\mathrm{s}}}{2}\int_{\mathcal{S}^2}\int_{\mathcal{S}^2}\mathcal{K}_0(a(\boldsymbol{v})-a(\boldsymbol{v}'))^2\,\mathrm{d}\boldsymbol{v}'\,\mathrm{d}\boldsymbol{v} - \sigma_{\mathrm{t}}\left\|\mathbf{c}\right\|_2^2$$

$$= \sigma_{\mathrm{s}}(1-\mathcal{K}_0)\left\langle a^2\right\rangle + \sigma_{\mathrm{s}}\mathcal{K}_0\int_{\mathcal{S}^2}\int_{\mathcal{S}^2}a(\boldsymbol{v})a(\boldsymbol{v}')\,\mathrm{d}\boldsymbol{v}'\,\mathrm{d}\boldsymbol{v} - \sigma_{\mathrm{t}}\left\|\mathbf{c}\right\|_2^2$$

$$\overset{(C.1)}{=} \sigma_{\mathrm{s}}(1-\mathcal{K}_0)\left\langle a^2\right\rangle - \sigma_{\mathrm{t}}\left\|\mathbf{c}\right\|_2^2 \overset{(C.2)}{=} (\sigma_{\mathrm{s}}(1-\mathcal{K}_0)-\sigma_{\mathrm{t}})\left\|\mathbf{c}\right\|_2^2 = -(\sigma_{\mathrm{s}}\mathcal{K}_0+\sigma_{\mathrm{a}})\left\|\mathbf{c}\right\|_2^2,$$

---

[1] Use that $\hat{\mathcal{K}}\left(\xi\right)$ is even.

where we used that

$$\langle a \rangle = \int_{\mathcal{S}^2} a(\boldsymbol{v}) \ \mathrm{d}\boldsymbol{v} = \mathbf{c}^{\mathrm{T}} \int_{\mathcal{S}^2} \mathbf{b}_{\mathrm{o}}(\boldsymbol{v}) \ \mathrm{d}\boldsymbol{v} = 0, \tag{C.1}$$

which holds because every entry in $\mathbf{b}_{\mathrm{o}}$ is orthogonal to $b_0 = \frac{1}{\sqrt{4\pi}}$ and, thus, orthogonal to all constants w.r.t. $\langle \cdot \rangle$, and that

$$\langle a^2 \rangle = \mathbf{c}^{\mathrm{T}} \int_{\mathcal{S}^2} \mathbf{b}_{\mathrm{o}} \mathbf{b}_{\mathrm{o}}^{\mathrm{T}} \ \mathrm{d}\boldsymbol{v} \ \mathbf{c} \stackrel{\mathrm{ONB}}{=} \mathbf{c}^{\mathrm{T}} \mathbf{c} = \|\mathbf{c}\|_2^2 \,. \tag{C.2}$$

In particular, since $\sigma_{\mathrm{t}} = \sigma_{\mathrm{a}} + \sigma_{\mathrm{s}} > 0$ and $\mathcal{K}_0 > 0$, we get that $\sigma_{\mathrm{s}}\mathcal{K}_0 + \sigma_{\mathrm{a}} > 0$, which implies that C_{oo} is negative definite and therefore invertible.   ■

C.1.3 Proof of Lemma 5.20

Proof.

> Use symmetry properties of the real spherical harmonics.

The rotation matrix that rotates a vector around the axis $\boldsymbol{n} = \begin{bmatrix} \boldsymbol{n}_x & \boldsymbol{n}_y & \boldsymbol{n}_z \end{bmatrix}$ by an angle of $180°$ is given by

$$\mathcal{R} = \begin{pmatrix} 2\boldsymbol{n}_x^2 - 1 & 2\boldsymbol{n}_x\boldsymbol{n}_y & 2\boldsymbol{n}_x\boldsymbol{n}_z \\ 2\boldsymbol{n}_y\boldsymbol{n}_x & 2\boldsymbol{n}_y^2 - 1 & 2\boldsymbol{n}_y\boldsymbol{n}_z \\ 2\boldsymbol{n}_z\boldsymbol{n}_x & 2\boldsymbol{n}_z\boldsymbol{n}_y & 2\boldsymbol{n}_z^2 - 1 \end{pmatrix}.$$

The reflection of $\boldsymbol{v}$ at the plane $\{\boldsymbol{v} \in \mathcal{S}^2 \,|\, \boldsymbol{n} \cdot \boldsymbol{v} = 0\}$ can be represented by a rotation around $\boldsymbol{n}$ by an angle of $180°$ and a subsequent negation:

$$r(\boldsymbol{v}) = \boldsymbol{v} - 2(\boldsymbol{n} \cdot \boldsymbol{v})\boldsymbol{n} = \begin{pmatrix} v_x - 2\boldsymbol{n}_x \left(\boldsymbol{v}_x\boldsymbol{n}_x + \boldsymbol{v}_y\boldsymbol{n}_y + \boldsymbol{v}_z\boldsymbol{n}_z\right) \\ v_y - 2\boldsymbol{n}_y \left(\boldsymbol{v}_x\boldsymbol{n}_x + \boldsymbol{v}_y\boldsymbol{n}_y + \boldsymbol{v}_z\boldsymbol{n}_z\right) \\ v_z - 2\boldsymbol{n}_z \left(\boldsymbol{v}_x\boldsymbol{n}_x + \boldsymbol{v}_y\boldsymbol{n}_y + \boldsymbol{v}_z\boldsymbol{n}_z\right) \end{pmatrix} = -\mathcal{R}\boldsymbol{v}.$$

Like in the proof of Lemma 5.18, there is a rotation matrix $R_\pi(\boldsymbol{n}) \in \mathbb{R}^{n_{\mathrm{o}} \times n_{\mathrm{o}}}$, depending only on $\boldsymbol{n}$, with

$$\mathbf{b}_{\mathrm{o}}(\mathcal{R}\boldsymbol{v}) = R_\pi(\boldsymbol{n})\,\mathbf{b}_{\mathrm{o}}(\boldsymbol{v}).$$

We use the parity of the odd real spherical harmonics, i.e., $\mathbf{b}_{\mathrm{o}}(-\mathcal{R}\boldsymbol{v}) = -\mathbf{b}_{\mathrm{o}}(\mathcal{R}\boldsymbol{v})$, and our assumption that the reflectivity ρ does not depend on $\boldsymbol{v}$, and rewrite the matrix as

$$H_{\mathrm{o}}(\boldsymbol{n}) = \int_{\boldsymbol{n} \cdot \boldsymbol{v} < 0} \mathbf{b}_{\mathrm{o}}(\boldsymbol{v}) \left(\mathbf{b}_{\mathrm{o}}^{\mathrm{T}}(\boldsymbol{v}) + \rho\mathbf{b}_{\mathrm{o}}^{\mathrm{T}}(\boldsymbol{v})R_\pi^{\mathrm{T}}(\boldsymbol{n})\right) \mathrm{d}\boldsymbol{v} = \int_{\boldsymbol{n} \cdot \boldsymbol{v} < 0} \mathbf{b}_{\mathrm{o}}(\boldsymbol{v})\mathbf{b}_{\mathrm{o}}^{\mathrm{T}}(\boldsymbol{v}) \, \mathrm{d}\boldsymbol{v} \left(E_{n_{\mathrm{o}}} + \rho R_\pi^{\mathrm{T}}(\boldsymbol{n})\right).$$

Thus, the matrix $H_{\mathrm{o}}(\boldsymbol{n})$ is invertible if $\int_{\boldsymbol{n} \cdot \boldsymbol{v} < 0} \mathbf{b}_{\mathrm{o}}(\boldsymbol{v})\mathbf{b}_{\mathrm{o}}^{\mathrm{T}}(\boldsymbol{v}) \, \mathrm{d}\boldsymbol{v}$ and $E_{n_{\mathrm{o}}} + \rho R_\pi^{\mathrm{T}}(\boldsymbol{n})$ are invertible. For a vector $\mathbf{c} \in \mathbb{R}^{n_{\mathrm{o}}} \setminus \{0\}$, it holds

$$\mathbf{c}^{\mathrm{T}} \int_{\boldsymbol{n} \cdot \boldsymbol{v} < 0} \mathbf{b}_{\mathrm{o}}(\boldsymbol{v})\mathbf{b}_{\mathrm{o}}^{\mathrm{T}}(\boldsymbol{v}) \, \mathrm{d}\boldsymbol{v} \ \mathbf{c} = \int_{\boldsymbol{n} \cdot \boldsymbol{v} < 0} \left(\mathbf{c}^{\mathrm{T}}\mathbf{b}_{\mathrm{o}}(\boldsymbol{v})\right)^2 \mathrm{d}\boldsymbol{v} > 0$$

because of $\mathbf{c} \neq 0$ and the real spherical harmonics being linearly independent and continuous. Thus, the matrix $\int_{\boldsymbol{n} \cdot \boldsymbol{v} < 0} \mathbf{b}_{\mathrm{o}}(\boldsymbol{v})\mathbf{b}_{\mathrm{o}}^{\mathrm{T}}(\boldsymbol{v}) \, \mathrm{d}\boldsymbol{v}$ is symmetric, positive definite and, with this, invertible. The Neumann series[2] implies that $E_{n_{\mathrm{o}}} + \rho R_\pi^{\mathrm{T}}(\boldsymbol{n})$ is invertible if $\left\|\rho R_\pi^{\mathrm{T}}(\boldsymbol{n})\right\| < 1$ for some operator

---

[2] See [4, Sec. 3.7, p. 153] for details on the Neumann series.

norm $\|\cdot\|$. In particular, since $R_\pi^\mathrm{T}(\boldsymbol{n})$ is a rotation matrix, it holds $\left\|R_\pi^\mathrm{T}(\boldsymbol{n})\right\|_2 = 1$ (operator norm induced by the Euclidean norm), and we get $\left\|\rho R_\pi^\mathrm{T}(\boldsymbol{n})\right\| < 1$ if $|\rho| < 1$.

We would like to note that we are note the first ones who use rotation matrices to derive boundary conditions. This has been done in a different way, e.g., in [146, 148]. ∎

Bibliography

[1] C. D. Aliprantis and K. C. Border. *Infinite Dimensional Analysis: A Hitchhiker's Guide*. English. 2nd ed. Springer, 1999. ISBN: 978-3-662-03961-8 DOI: `10.1007/978-3-662-03961-8` (see p. 193)

[2] G. W. Alldredge, C. D. Hauck, and A. L. Tits. *High-Order Entropy-Based Closures for Linear Transport in Slab Geometry II: A Computational Study of the Optimization Problem*. SIAM *Journal on Scientific Computing*, 34: B361–B391, 2012. DOI: `10.1137/11084772X` (see p. 108)

[3] M. Alnæs, J. Blechta, J. Hake, A. Johansson, B. Kehlet, A. Logg, C. Richardson, J. Ring, M. E. Rognes, and G. N. Wells. *The FEniCS Project Version 1.5*. Archive of *Numerical Software*, 3: 9–23, 2015. DOI: `10.11588/ans.2015.100.20553` URL: `https://fenicsproject.org/`(see pp. 64, 100, 101, 115)

[4] H. W. Alt. *Lineare Funktionalanalysis*. German. 6th ed. Springer, 2012. ISBN: 978-3-642-22260-3 DOI: `10.1007/978-3-642-22261-0` (see pp. 23, 48, 169, 175, 195–200, 207, 209, 219, 243, 244)

[5] H. Amann and J. Escher. *Analysis II*. German. 2nd ed. Birkhäuser Verlag, Basel, 2006. xii+400 ISBN: 3-7643-7105-6 DOI: `10.1007/3-7643-7402-0` (see p. 192)

[6] C. Amrouche, C. Conca, A. Ghosh, and T. Ghosh. *Uniform $W^{1,p}$ estimates for an elliptic operator with Robin boundary condition in a C^1 domain*. Calculus of Variations and Partial *Differential Equations*, 59: Paper No. 71, 25, 2020. DOI: `10.1007/s00526-020-1713-y` (see pp. 25, 40)

[7] M. Andres. *Improving thermal ablation of liver tumors: Modeling and parameter identification of laser-induced thermotherapy*. Free online version of this thesis. DOI: `10.26204/KLUEDO/6322` URL: `https://doi.org/10.26204/KLUEDO/6322`(see p. vii)

[8] M. Andres. *Improving thermal ablation of liver tumors: Modeling and parameter identification of laser-induced thermotherapy. Codes and numerical results.* Code repository of this thesis, which contains all Matlab and Python codes used to perform the numerical experiments of this thesis, including the data of the corresponding results ready to be displayed. DOI: `10.26204/data/3` URL: `https://doi.org/10.26204/data/3`(see pp. vii, 9, 63, 66, 78, 100, 101, 110, 117)

[9] M. Andres, S. Blauth, C. Leithäuser, and N. Siedow. *Identification of the blood perfusion rate for laser-induced thermotherapy in the liver*. Journal of Mathematics in Industry, 10: 1–20, 2020. DOI: `10.1186/s13362-020-00085-1` (see pp. vii, 8, 11, 15, 44, 74, 77, 81, 86, 146)

[10]   M. Andres and R. Pinnau. *Improving Thermal Ablation of Liver Tumors*. in: *Progress in Industrial Mathematics at ECMI 2018*. Springer, 2019. isbn: 978-3-030-27550-1 doi: `10.1007/978-3-030-27550-1` (see pp. vii, 8, 15, 74, 77, 81)

[11]   M. Andres and R. Pinnau. *The Cattaneo Model for Laser-Induced Thermotherapy: Identification of the Blood Perfusion Rate*. in: *Modeling, Simulation and Optimization in the Health- and Energy-Sector*. Accepted Springer, 2021. (see pp. vii, 8, 15, 17, 74, 77, 81)

[12]   M. Andres and R. Pinnau. *The Cattaneo Model in the context of Thermoablation of Liver Tumors*. in: *Proceedings in Applied Mathematics and Mechanics (PAMM)*. vol. 19 1 Wiley, 2019. e201900241 doi: `10.1002/pamm.201900241` (see pp. vii, 8, 15, 74, 77)

[13]   M. Andres and F. Schneider. *The second-order formulation of the P_N equations with Marshak boundary conditions*. 2019. url: `https://arxiv.org/abs/1911.00468`(see pp. vii, 8, 98, 122)

[14]   Apiumhub. *Apiumhub Tech Blog*. Accessed: 2020-06-27. url: `https://apiumhub.com/tech-blog-barcelona/programming-jokes-quotes/`(see pp. 63, 117)

[15]   W. Arendt, C. J. K. Batty, M. Hieber, and F. Neubrander. *Vector-valued Laplace Transforms and Cauchy Problems*. English. 2nd ed. vol. 96 Monographs in Mathematics. Birkhäuser / Springer Basel AG, 2011. xii+539 isbn: 978-3-0348-0086-0 doi: `10.1007/978-3-0348-0087-7` (see pp. 201, 215)

[16]   M. A. Blanco, M. Flórez, and M. Bermejo. *Evaluation of the rotation matrices in the basis of real spherical harmonics*. *Journal of Molecular Structure: THEOCHEM*, 419: 19–27, 1997 issn: 0166-1280. doi: `10.1016/S0166-1280(97)00185-1` (see pp. 104, 117, 217)

[17]   S. Blauth. *Optimal Control and Asymptotic Analysis of the Cattaneo Model*. Master thesis, Technische Universität Kaiserslautern, 90, 2018. url: `http://nbn-resolving.de/urn:nbn:de:hbz:386-kluedo-53727`(see pp. 8, 21, 23, 25, 27, 146, 159)

[18]   S. Blauth, M. Andres, R. Pinnau, and C. Totzeck. *Optimal Control and Asymptotic Analysis of the Cattaneo Equation*. in: *Proceedings in Applied Mathematics and Mechanics (PAMM)*. vol. 19 1 Wiley, 2019. e201900184 doi: `10.1002/pamm.201900184` (see pp. vii, 8, 15)

[19]   S. Blauth, F. Hübner, C. Leithäuser, N. Siedow, and T. J. Vogl. *Mathematical modeling of vaporization during laser-induced thermotherapy in liver tissue*. *Journal of Mathematics in Industry*, 10: 2020. doi: `10.1186/s13362-020-00082-4` (see p. 4)

[20]   H. Brezis. *Functional Analysis, Sobolev Spaces and Partial Differential Equations*. English. Universitext. Springer, New York, 2011. xiv+599 isbn: 978-0-387-70913-0 doi: `10.1007/978-0-387-70914-7` (see pp. 152, 197–199, 204)

[21]   T. A. Brunner. *Forms of Approximate Radiation Transport*. *Sandia report*, 2002. doi: `10.2172/800993` (see pp. 97, 99, 100, 102, 108, 247)

[22]   T. A. Brunner and J. P. Holloway. *One-dimensional Riemann solvers and the maximum entropy closure*. *Journal of Quantitative Spectroscopy and Radiative Transfer*, 69: 543–566, 2001 issn: 00224073. doi: `10.1016/S0022-4073(00)00099-6` (see p. 108)

[23]   T. A. Brunner and J. P. Holloway. *Two-dimensional time dependent Riemann solvers for neutron transport*. *Journal of Computational Physics*, 210: 386–399, 2005 issn: 0021-9991. doi: `10.1016/j.jcp.2005.04.011` (see pp. 104, 108)

[24] M. F. Carfora. *Interpolation on spherical geodesic grids: A comparative study*. Journal of Computational and Applied Mathematics, 210: Proceedings of the Numerical Analysis Conference 2005, 99–105, 2007 ISSN: 0377-0427. DOI: 10.1016/j.cam.2006.10.068 (see p. 121)

[25] A. Carpentier, R. J. McNichols, R. J. Stafford, J. Itzcovitz, J.-P. Guichard, D. Reizine, S. Delaloge, E. Vicaut, D. Payen, A. Gowda, and B. George. *Real-time Magnetic Resonance-guided Laser Thermal Therapy for Focal Metastatic Brain Tumors*. Operative Neurosurgery, 63: ONS21–ONS29, 2008 ISSN: 2332-4252. DOI: 10.1227/01.NEU.0000311254.63848.72 (see p. 4)

[26] E. Casas, R. Herzog, and G. Wachsmuth. *Optimality Conditions and Error Analysis of Semilinear Elliptic Control Problems with L^1 Cost Functional*. SIAM Journal on Optimization, 22: 795–820, 2012 ISSN: 1052-6234. DOI: 10.1137/110834366 (see pp. 46, 58, 177)

[27] C. Cattaneo. *Sulla Conduzione del Calore. Atti del Seminario Matematico e Fisico dell'Università di Modena*, 3: 83–101, 1948. (see pp. 15, 18)

[28] C. Cercignani. *The Boltzmann Equation and Its Applications*. English. Applied mathematical sciences ; 67. Springer, Berlin u.a., 1988. ISBN: 3-540-96637-4 DOI: 10.1007/978-1-4612-1039-9 (see p. 101)

[29] J. Cernohorsky and S. Bludman. *Maximum entropy distribution and closure for Bose-Einstein and Fermi-Dirac radiation transport*. The Astrophysical Journal, Part 1, 433: 250–255, 1994. URL: http://adsabs.harvard.edu/full/1994ApJ...433..250C (see p. 108)

[30] D. S. Chandrasekharaiah. *Hyperbolic Thermoelasticity: A Review of Recent Literature*. Applied Mechanics Reviews, 51: 705–729, 1998 ISSN: 0003-6900. DOI: 10.1115/1.3098984 (see p. 17)

[31] M. M. Chen and K. R. Holmes. *Microvascular contributions in tissue heat transfer*. Annals of the New York Academy of Sciences, 335: 137–150, 1980. DOI: 10.1111/j.1749-6632.1980.tb50742.x (see p. 44)

[32] J. Chiang, M. Cristescu, M. H. Lee, A. Moreland, J. L. Hinshaw, F. T. Lee, and C. L. Brace. *Effects of Microwave Ablation on Arterial and Venous Vasculature after Treatment of Hepatocellular Carcinoma*. Radiology, 281: PMID: 27257951, 617–624, 2016. DOI: 10.1148/radiol.2016152508 (see pp. 4, 43, 44, 64)

[33] J. Chiang, K. Hynes, and C. L. Brace. *Flow-dependent vascular heat transfer during microwave thermal ablation*. in: *2012 Annual International Conference of the IEEE Engineering in Medicine and Biology Society*. IEEE 2012. 5582–5585 DOI: 10.1109/EMBC.2012.6347259 (see pp. 4, 43)

[34] J. Chiang, K. Nickel, R. J. Kimple, and C. L. Brace. *Potential Mechanisms of Vascular Thrombosis after Microwave Ablation in an in Vivo Liver*. Journal of Vascular and Interventional Radiology, 28: 1053–1058, 2017. DOI: 10.1016/j.jvir.2017.03.034 (see p. 44)

[35] P. Chidyagwai, M. Frank, F. Schneider, and B. Seibold. *A comparative study of limiting strategies in discontinuous Galerkin schemes for the M_1 model of radiation transport*. Journal of Computational and Applied Mathematics, 342: 399–418, 2018 ISSN: 0377-0427. DOI: 10.1016/j.cam.2018.04.017 (see p. 108)

[36]   F. CLARKE. *Functional Analysis, Calculus of Variations and Optimal Control*. English. vol. 264 Graduate Texts in Mathematics. Springer Science & Business Media, 2013. ISBN: 978-1-4471-4819-7 DOI: 10.1007/978-1-4471-4820-3 (see pp. 200, 213)

[37]   F. H. CLARKE. *Optimization and Nonsmooth Analysis*. English. 2nd ed. Classics in applied mathematics; 5. Reprint, originally published: New York: Wiley, 1983. Society for Industrial and Applied Mathematics, 1990. ISBN: 0-89871-256-4 DOI: 10.1137/1.9781611971309 (see p. 46)

[38]   P. COLLI, G. GILARDI, P. PODIO-GUIDUGLI, and J. SPREKELS. *Distributed optimal control of a nonstandard system of phase field equations*. *Continuum Mechanics and Thermodynamics*, 24: 437–459, 2012. DOI: 10.1007/s00161-011-0215-8 (see pp. 50, 51, 55, 57, 58)

[39]   J. B. CONWAY. *A Course in Functional Analysis*. English. 2nd ed. vol. 96 Graduate Texts in Mathematics. Springer-Verlag, New York, 1990. ISBN: 0-387-97245-5 DOI: 10.1007/978-1-4757-4383-8 (see p. 197)

[40]   CREATIVE COMMONS. *Creative Commons Licensing: Public Domain Dedication (CC0 1.0 Universal)*. Accessed: 2020-06-01. URL: https://creativecommons.org/publicdomain/zero/1.0/(see p. 10)

[41]   G. DA FIES, A. SOMMARIVA, and V. M. *SUBP: MATLAB package for subperiodic trigonometric quadrature and multivariate applications*. Repository which contains codes for product Gaussian quadrature on circular and spherical sections (licensed under GPL 2). Accessed: 2020-01-04. URL: https://www.math.unipd.it/~marcov/mysoft/subp/all.tar(see p. 119)

[42]   G. DA FIES and M. VIANELLO. *Trigonometric Gaussian quadrature on subintervals of the period*. *Electronic Transactions on Numerical Analysis*, 39: 102–112, 2012. URL: http://emis.impa.br/EMIS/journals/ETNA/vol.39.2012/pp102-112.dir/pp102-112.pdf(see p. 118)

[43]   R. DAUTRAY and J.-L. LIONS. *Mathematical Analysis and Numerical Methods for Science and Technology. Vol. 5. Evolution Problems I*. English. With the collaboration of Michel Artola, Michel Cessenat and Hélène Lanchon, Translated from the French by Alan Craig. Springer-Verlag, Berlin, 2000. xiv+709 ISBN: 978-3-540-66101-6 DOI: 10.1007/978-3-642-58090-1 (see pp. 22, 23, 45, 151, 158–162, 196, 202, 203, 205, 213)

[44]   R. DAUTRAY and J.-L. LIONS. *Mathematical Analysis and Numerical Methods for Science and Technology. Vol. 6. Evolution problems II*. English. With the collaboration of Claude Bardos, Michel Cessenat, Alain Kavenoky, Patrick Lascaux, Bertrand Mercier, Olivier Pironneau, Bruno Scheurer, Rémi Sentis. Translated from the French by Alan Craig. Springer-Verlag, Berlin, 2000. ISBN: 978-3-540-66102-3 DOI: 10.1007/978-3-642-58004-8 (see p. 103)

[45]   J. A. DAVIS. *Variational Vacuum Boundary Conditions for a P_N Approximation*. *Nuclear Science and Engineering*, 25: 189–197, 1966. DOI: 10.13182/NSE66-A17736 (see p. 107)

[46]   B. DAVISON and J. B. SYKES. *Neutron transport theory*. English. 2nd ed. Reprint, originally published 1957. Oxford University Press, 1958. DOI: 10.2307/3610992 (see pp. 99, 107)

[47]   W. DEMTRÖDER. *Experimentalphysik 1*. German. 8th ed. Springer, Berlin, Heidelberg, 2018. ISBN: 9783662548462 DOI: 10.1007/978-3-662-54847-9 (see pp. 5, 11, 101)

[48] W. Demtröder. *Experimentalphysik 2*. German. 7th ed. Springer, Berlin, Heidelberg, 2018. isbn: 978-3-662-55789-1 doi: `10.1007/978-3-662-55790-7` (see pp. 97, 137)

[49] N. Dietrich, T. Marx, and R. Pinnau. *Shape Optimization in Phosphate Production*. in: *Proceedings in Applied Mathematics and Mechanics (PAMM)*. vol. 19 1 2019. e201900207 doi: `10.1002/pamm.201900207` (see p. 9)

[50] L. A. Dombrovsky. *Scattering of Radiation and Simple Approaches to Radiative Transfer in Thermal Engineering and Biomedical Applications*. in: *Springer Series in Light Scattering*. Springer, 2019. 71–127 doi: `10.1007/978-3-030-20587-4_2` (see p. 4)

[51] R. Dua and S. Chakraborty. *A novel modeling and simulation technique of photo–thermal interactions between lasers and living biological tissues undergoing multiple changes in phase*. *Computers in biology and medicine*, 35: 447–462, 2005. doi: `10.1016/j.compbiomed.2004.02.005` (see pp. 3, 6)

[52] B. Dubroca, J.-L. Feugeas, and M. Frank. *Angular moment model for the Fokker-Planck equation*. *The European Physical Journal D*, 60: 301–307, 2010 issn: 1434-6060. doi: `10.1140/epjd/e2010-00190-8` (see p. 103)

[53] B. Dubroca and A. Klar. *Half-Moment Closure for Radiative Transfer Equations*. *Journal of Computational Physics*, 180: 584–596, 2002. doi: `10.1006/jcph.2002.7106` (see p. 108)

[54] A. S. Eddington. *The Internal Constitution of the Stars*. English. Dover, 1926. (see p. 107)

[55] J. Elstrodt. *Maß- und Integrationstheorie*. German. 8th ed. Springer, Berlin, Heidelberg, 2018. isbn: 978-3-662-57939-8 doi: `10.1007/978-3-662-57939-8` (see pp. 28, 200–202, 243)

[56] E. Emmrich. *Gewöhnliche und Operator-Differentialgleichungen*. German. 1st ed. Vieweg Verlag, 2004. isbn: 13:978-3-528-03213-5 doi: `10.1007/978-3-322-80240-8` (see pp. 22, 154, 174, 203, 205, 206, 213, 215, 216)

[57] Encyclopaedia Britannica. *Absorption*. Accessed: 2020-09-14, 1998. url: `https://www.britannica.com/science/absorption-physics`(see p. 243)

[58] Encyclopaedia Britannica. *Convection*. Accessed: 2020-09-14, 2019. url: `https://www.britannica.com/science/convection`(see p. 244)

[59] Encyclopaedia Britannica. *Scattering*. Accessed: 2020-09-14, 2008. url: `https://www.britannica.com/science/scattering`(see p. 247)

[60] Encyclopaedia Britannica. *Thermal conduction*. Accessed: 2020-09-14, 2018. url: `https://www.britannica.com/science/thermal-conduction`(see p. 244)

[61] Encyclopaedia Britannica. *Thermal Radiation*. Accessed: 2020-09-14, 2018. url: `https://www.britannica.com/science/thermal-radiation`(see p. 247)

[62] H. Engler. *Computation of scattering kernels in radiative transfer*. 2018. doi: `10.1016/j.jqsrt.2015.06.019` url: `arXiv:1501.02407`(see p. 135)

[63] L. C. Evans. *Partial Differential Equations*. English. 1st ed. vol. 19 Graduate Studies in Mathematics. (Careful: the stated doi refers to the second edition). American Math. Soc., 1998. isbn: 0-8218-0772-2 doi: `10.1090/gsm/019` (see pp. 20, 21, 41, 114, 120, 151, 199, 201, 204, 211)

[64] F. Fanjul-Vélez, O. G. Romanov, and J. L. Arce-Diego. *Efficient 3D numerical approach for temperature prediction in laser irradiated biological tissues. Computers in Biology and Medicine,* 39: 810–817, 2009. DOI: `10.1016/j.compbiomed.2009.06.009` (see p. 4)

[65] A. Fasano, D. Hömberg, and D. Naumov. *On a mathematical model for laser-induced thermotherapy. Applied Mathematical Modelling. Simulation and Computation for Engineering and Environmental Systems,* 34: 3831–3840, 2010 ISSN: 0307-904X. DOI: `10.1016/j.apm.2010.03.023` (see pp. 1, 3–6, 10, 11, 64, 97, 130, 132, 133, 147, 244)

[66] Y. Feng, D. Fuentes, A. Hawkins, J. M. Bass, and M. N. Rylander. *Optimization and real-time control for laser treatment of heterogeneous soft tissues. Computer methods in applied mechanics and engineering,* 198: 1742–1750, 2009. DOI: `10.1016/j.cma.2008.12.027` (see pp. 4, 43)

[67] T. Fliessbach. *Elektrodynamik: Lehrbuch zur Theoretischen Physik II.* German. 6th ed. Springer Spektrum, 2012. ISBN: 978-3-8274-3035-9 DOI: `10.1007/978-3-8274-3036-6` (see p. 105)

[68] Y. Fong, J. Fortner, R. L. Sun, M. F. Brennan, and L. H. Blumgart. *Clinical Score for Predicting Recurrence After Hepatic Resection for Metastatic Colorectal Cancer: Analysis of 1001 Consecutive Cases. Annals of surgery,* 230: 309, 1999. DOI: `10.1097/00000658-199909000-00004` (see p. 2)

[69] O. Forster. *Analysis 1.* German. 12th ed. Springer Fachmedien Wiesbaden, 2016. ISBN: 9783658115449 DOI: `10.1007/978-3-658-11545-6` (see p. 29)

[70] O. Forster. *Analysis 2.* German. 11th ed. Springer Fachmedien Wiesbaden, 2017. ISBN: 978-3-658-19410-9 DOI: `10.1007/978-3-658-19411-6` (see pp. 194, 204)

[71] M. Frank, B. Dubroca, and A. Klar. *Partial moment entropy approximation to radiative heat transfer. Journal of Computational Physics,* 218: 1–18, 2006. DOI: `10.1016/j.jcp.2006.01.038` (see p. 108)

[72] D. Fuentes, Y. Feng, A. Elliott, A. Shetty, R. J. McNichols, J. T. Oden, and R. J. Stafford. *Adaptive Real-Time Bioheat Transfer Models for Computer-Driven MR-Guided Laser Induced Thermal Therapy. IEEE transactions on biomedical engineering,* 57: 1024–1030, 2010. DOI: `10.1109/TBME.2009.2037733` (see p. 4)

[73] S. Funke. *The Moola optimisation package.* URL: `https://github.com/funsim/moola` (see p. 78)

[74] T. Gallouet and A. Monier. *On the regularity of solutions to elliptic equations. Rendiconti di Matematica e delle sue Applicazioni. Serie VII,* 19: 471–488, 1999 ISSN: 1120-7183. URL: `https://www1.mat.uniroma1.it/ricerca/rendiconti/ARCHIVIO/1999(4)/471-488.pdf` (see pp. 173, 174, 176, 180)

[75] C. K. Garrett and C. D. Hauck. *A Comparison of Moment Closures for Linear Kinetic Transport Equations: The Line Source Benchmark. Transport Theory and Statistical Physics,* 42: 203–235, 2013. DOI: `10.1080/00411450.2014.910226` (see p. 108)

[76] W. Ge. *High-Order Spherical Harmonics Methods for Radiative Heat Transfer and Applications in Combustion Simulations.* PhD thesis, UC Merced, 2017. URL: `https://escholarship.org/uc/item/2g85768d` (see p. 99)

[77] W. Ge, R. Marquez, M. F. Modest, and S. P. Roy. *Implementation of High-Order Spherical Harmonics Methods for Radiative Heat Transfer on OpenFOAM*. Journal of Heat Transfer, 137: 052701, 2015. DOI: 10.1115/1.4029546 (see p. 99)

[78] C. Geuzaine and J.-F. Remacle. *Gmsh: a three-dimensional finite element mesh generator with built-in pre- and post-processing facilities*. International Journal for Numerical Methods in Engineering, 79: 1309–1331, 2009. URL: http://www.gmsh.info/ (see pp. 64, 67)

[79] H. R. Ghazizadeh, A. Azimi, and M. Maerefat. *An inverse problem to estimate relaxation parameter and order of fractionality in fractional single-phase-lag heat equation*. International Journal of Heat and Mass Transfer, 55: 2095–2101, 2012 ISSN: 0017-9310. DOI: 10.1016/j.ijheatmasstransfer.2011.12.012 (see pp. 20, 21)

[80] K. Giering, O. Minet, I. Lamprecht, and G. Müller. *Review of thermal properties of biological tissues*. in: *Laser Induced Interstitial Thermotherapy*. SPIE Press Bellingham, WA, USA, 1995. 45–65 ISBN: 0-8194-1859-5 (see p. 11)

[81] D. Gilbarg and N. S. Trudinger. *Elliptic Partial Differential Equations of Second Order*. English. 2nd ed. Reprint of the 1998 edition. Springer, Berlin, Heidelberg, 2001. ISBN: 3-540-41160-7 DOI: 10.1007/978-3-642-61798-0 (see pp. 41, 211)

[82] S. N. Goldberg, P. F. Hahn, K. K. Tanabe, P. R. Mueller, W. Schima, C. A. Athanasoulis, C. C. Compton, L. Solbiati, and G. S. Gazelle. *Percutaneous Radiofrequency Tissue Ablation: Does Perfusion-mediated Tissue Cooling Limit Coagulation Necrosis?* Journal of Vascular and Interventional Radiology, 9: 101–111, 1998 ISSN: 1051-0443. DOI: 10.1016/S1051-0443(98)70491-9 (see p. 4)

[83] H. E. Grecco. *Documentation of Python package Pint*. Accessed: 2020-04-27. URL: https://pint.readthedocs.io/en/0.10.1/ (see p. 64)

[84] A. Griewank and A. Walther. *Evaluating Derivatives: Principles and Techniques of Algorithmic Differentiation*. English. 2nd ed. Society for Industrial and Applied Mathematics (SIAM), Philadelphia, PA, 2008. xxii+438 ISBN: 978-0-898716-59-7 DOI: 10.1137/1.9780898717761 (see p. 78)

[85] P. Grisvard. *Elliptic Problems in Nonsmooth Domains*. English. vol. 69 Classics in Applied Mathematics. Reprint of the 1985 original [MR0775683]. Society for Industrial and Applied Mathematics (SIAM), Philadelphia, PA, 2011. xx+410 ISBN: 978-1-611972-02-3 DOI: 10.1137/1.9781611972030 (see pp. 21, 41, 151, 152, 168, 207, 210)

[86] C. Grossmann and H.-G. Roos. *Numerical Treatment of Partial Differential Equations*. English. 3rd ed. Universitext. Translated and revised from the 3rd (2005) German edition by Martin Stynes. Springer, Berlin, 2007. xii+591 ISBN: 978-3-540-71582-5 DOI: 10.1007/978-3-540-71584-9 (see pp. 63, 65, 120, 124)

[87] L. Grüne and O. Junge. *Gewöhnliche Differentialgleichungen*. German. 2nd ed. Aktualisierte Aufl. 2016. Springer Fachmedien Wiesbaden, 2016. ISBN: 978-3-658-10241-8 DOI: 10.1007/978-3-658-10241-8 (see p. 65)

[88] S. P. Hamilton and T. M. Evans. *Efficient solution of the simplified P_N equations*. Journal of Computational Physics, 284: 155–170, 2015 ISSN: 0021-9991. DOI: 10.1016/j.jcp.2014.12.014 (see pp. 100, 114)

[89]   Q. Han and F. Lin. *Elliptic Partial Differential Equations*. English. 1ˢᵗ ed. vol. 1 Courant Lecture Notes in Mathematics. Courant Institute of Mathematical Sciences, New York; American Mathematical Society, Providence, RI, 2000. ɪsʙɴ: 0-8218-2691-3 ᴅoɪ: `10.1090/cln/001` (see p. 41)

[90]   C. D. Hauck. *High-Order Entropy-Based Closures for Linear Transport in Slab Geometry*. *Communications in Mathematical Sciences*, 9: 2011. ᴅoɪ: `10.4310/CMS.2011.v9.n1.a9` ᴜʀʟ: `https://www.intlpress.com/site/pub/files/_fulltext/journals/cms/2011/0009/0001/CMS-2011-0009-0001-a009.pdf`(see p. 108)

[91]   L. G. Henyey and J. L. Greenstein. *Diffuse radiation in the Galaxy*. *Astrophysical Journal*, 93: 70–83, 1941. ᴅoɪ: `10.1086/144246` (see p. 102)

[92]   N. J. Higham. *Handbook of Writing for the Mathematical Sciences*. English. 2ⁿᵈ ed. Society for Industrial and Applied Mathematics, 1998. ɪsʙɴ: 978-0-898714-20-3 ᴜʀʟ: `https://archive.siam.org/books/ot63/` (see p. 17)

[93]   M. Hinze, R. Pinnau, M. Ulbrich, and S. Ulbrich. *Optimization with PDE Constraints*. English. vol. 23 Mathematical Modelling: Theory and Applications. Springer, New York, 2009. xii+270 ɪsʙɴ: 978-1-4020-8838-4 ᴅoɪ: `10.1007/978-1-4020-8839-1` (see pp. 22, 25, 38, 47, 50, 51, 58, 59, 77, 162, 164, 168, 176, 181, 194, 195, 198, 201–203, 205–208, 212, 242)

[94]   G. Hodan. *Original nutshell image on PublicDomainPictures.net; released under Public Domain license (CC0 1.0)*. Accessed: 2020-06-01. ᴜʀʟ: `https://www.publicdomainpictures.net/en/view-image.php?image=165852&picture=walnuts`(see p. 10)

[95]   F. Hübner, C. Leithäuser, B. Bazrafshan, N. Siedow, and T. J. Vogl. *Validation of a mathematical model for laser-induced thermotherapy in liver tissue*. *Lasers in Medical Science*, 32: 1399–1409, 2017 ɪssɴ: 1435-604X. ᴅoɪ: `10.1007/s10103-017-2260-4` (see pp. 4, 5, 10, 11, 97, 133, 136, 147)

[96]   J. Iljaž and L. Škerget. *Blood perfusion estimation in heterogeneous tissue using BEM based algorithm*. *Engineering Analysis with Boundary Elements*, 39: 75–87, 2014 ɪssɴ: 0955-7997. ᴅoɪ: `10.1016/j.enganabound.2013.11.002` (see p. 8)

[97]   International Organization for Standardization. *ISO 9288:1989, Thermal insulation — Heat transfer by radiation — Physical quantities and definitions*. Accessed: 2020-04-22, 1989. ᴜʀʟ: `https://www.iso.org/obp/ui/#iso:std:iso:9288:ed-1:v1:en`(see pp. 97, 245, 246)

[98]   IT'IS Foundation. *Foundation for Research on Information Technologies in Society (IT'IS)*. Database for tissue properties. Accessed: 2020-02-15. ᴜʀʟ: `https://itis.swiss/virtual-population/tissue-properties/database/density/`(see p. 11)

[99]   Jing Liu, Xu Chen, and L. X. Xu. *New thermal wave aspects on burn evaluation of skin subjected to instantaneous heating*. *IEEE Transactions on Biomedical Engineering*, 46: 420–428, 1999. ᴅoɪ: `10.1109/10.752939` (see p. 21)

[100] D. D. Joseph and L. Preziosi. *Heat waves*. *Review of Modern Physics*, 61: 41–73, 1989. ᴅoɪ: `10.1103/RevModPhys.61.41` (see pp. 17, 18, 20, 21, 71)

[101] J. Jost. *Partial Differential Equations*. English. 3rd ed. vol. 214 Graduate Texts in Mathematics. Springer, 2013. ISBN: 978-1-4614-4808-2 DOI: 10.1007/978-1-4614-4809-9 (see pp. 41, 152)

[102] D. Jou, J. Casas-Vázquez, and G. Lebon. *Extended irreversible thermodynamics revisited (1988-98)*. Reports on Progress in Physics, 62: 1035–1142, 1999. DOI: 10.1088/0034-4885/62/7/201 (see pp. 18, 19)

[103] M. Junk. *Maximum Entropy for Reduced Moment Problems*. Mathematical models and methods in applied sciences, 10: 1001–1025, 2000. DOI: 10.1142/S0218202500000513 (see p. 108)

[104] W. Kaminski. *Hyperbolic Heat Conduction Equation for Materials With a Nonhomogeneous Inner Structure*. Journal of Heat Transfer, 112: 555–560, 1990 ISSN: 0022-1481. DOI: 10.1115/1.2910422 (see pp. 20, 21)

[105] K. Kamiuto. *Study of the Henyey-Greenstein approximation to scattering phase functions*. Journal of Quantitative Spectroscopy and Radiative Transfer, 37: 411–413, 1987 ISSN: 0022-4073. DOI: 10.1016/0022-4073(87)90010-0 (see p. 135)

[106] C. T. Kelley. *Iterative Methods for Optimization*. English. vol. 18 Frontiers in Applied Mathematics. Society for Industrial and Applied Mathematics (SIAM), Philadelphia, PA, 1999. xvi+180 ISBN: 0-89871-433-8 DOI: 10.1137/1.9781611970920 (see pp. 59, 61, 83)

[107] D. S. Kershaw *Flux limiting nature's own way: A new method for numerical solution of the transport equation* English tech. rep. LLNL Report UCRL-78378, July 1976 DOI: 10.2172/104974 (see p. 108)

[108] D. E. Keyes, L. C. McInnes, C. Woodward, W. Gropp, E. Myra, M. Pernice, J. Bell, J. Brown, A. Clo, J. Connors, et al. *Multiphysics simulations: Challenges and opportunities*. The International Journal of High Performance Computing Applications, 27: 4–83, 2013. DOI: 10.1177/1094342012468181 (see p. 64)

[109] A. Kim and B. C. Wilson. *Measurement of Ex Vivo and In Vivo Tissue Optical Properties: Methods and Theories*. in: *Optical-Thermal Response of Laser-Irradiated Tissue* ed. by A. J. Welch and M. J. van Gemert. 2nd ed. Springer Netherlands, Dordrecht, 2011. chap. 8, 267–319 ISBN: 978-90-481-8831-4 DOI: 10.1007/978-90-481-8831-4_8 (see pp. 2, 7, 10)

[110] D. Kinderlehrer and G. Stampacchia. *An Introduction to Variational Inequalities and Their Applications*. English. vol. 31 Classics in Applied Mathematics. Reprint of the 1980 original. Society for Industrial and Applied Mathematics (SIAM), Philadelphia, PA, 2000. xx+313 ISBN: 0-89871-466-4 DOI: 10.1137/1.9780898719451 (see pp. 182, 183)

[111] A. D. Klose and E. W. Larsen. *Light transport in biological tissue based on the simplified spherical harmonics equations*. Journal of Computational Physics, 220: 441–470, 2006 ISSN: 0021-9991. DOI: 10.1016/j.jcp.2006.07.007 (see p. 100)

[112] C. Knight and A. Newbery. *Trigonometric and Gaussian quadrature*. Mathematics of Computation, 24: 575–581, 1970. DOI: 10.2307/2004833 (see p. 119)

[113] T. Kröger, I. Altrogge, T. Preusser, P. L. Pereira, D. Schmidt, A. Weihusen, and H.-O. Peitgen. *Numerical Simulation of Radio Frequency Ablation with State Dependent Material Parameters in Three Space Dimensions*. in: *Medical Image Computing and Computer-Assisted Intervention – MICCAI 2006*. ed. by R. Larsen, M. Nielsen, and J. Sporring Springer, Berlin, Heidelberg, 2006. 380–388 isbn: 978-3-540-44728-3 doi: `10.1007/11866763_47` (see pp. 4, 43)

[114] A. Kröner. *Numerical Methods for Control of Second Order Hyperbolic Equations*. PhD thesis, Technische Universität München, 2011. url: `https://mediatum.ub.tum.de/doc/1084592/1084592.pdf`(see pp. 15, 21, 23, 160, 163, 164, 243)

[115] H. P. Langtangen and A. Logg. *Solving PDEs in Python: The FEniCS Tutorial I*. English. vol. 3 Simula Springer Briefs on Computing. SpringerOpen, 2016. isbn: 978-3-319-52461-0 doi: `10.1007/978-3-319-52462-7` (see pp. 65, 118)

[116] H. P. Langtangen and G. K. Pedersen. *Scaling of Differential Equations*. English. Springer International Publishing Berlin, Germany, 2016. isbn: 978-3-319-32725-9 doi: `10.1007/978-3-319-32726-6` (see pp. 6, 7)

[117] E. W. Larsen and J. E. Morel. *Advances in Discrete-Ordinates Methodology*. English in: *Nuclear Computational Science: A Century in Review* ed. by Y. Azmy and E. Sartori. 1st ed. Springer, 2010. chap. 1 isbn: 978-90-481-3410-6 doi: `10.1007/978-90-481-3411-3_1` (see p. 121)

[118] E. W. Larsen and G. C. Pomraning. *The P_N Theory as an Asymptotic Limit of Transport Theory in Planar Geometry —I: Analysis*. *Nuclear Science and Engineering*, 109: 49–75, 1991. doi: `10.13182/NSE91-A23844` (see p. 113)

[119] E. W. Larsen, G. Thömmes, A. Klar, M. Seaïd, and T. Götz. *Simplified P_N Approximations to the Equations of Radiative Heat Transfer and Applications*. *Journal of Computational Physics*, 183: 652–675, 2002 issn: 0021-9991. doi: `10.1006/jcph.2002.7210` (see pp. 102, 103)

[120] K. S. Lehmann, B. B. Frericks, C. Holmer, A. Schenk, A. Weihusen, V. Knappe, U. Zurbuchen, H. O. Peitgen, H. J. Buhr, and J. P. Ritz. *In vivo validation of a therapy planning system for laser-induced thermotherapy (LITT) of liver malignancies*. *International journal of colorectal disease*, 26: 799, 2011. doi: `10.1007/s00384-011-1175-y` (see pp. 4, 7, 10, 43)

[121] R. J. LeVeque. *Python Tools for Reproducible Research on Hyperbolic Problems*. *Computing in Science Engineering*, 11: 19–27, 2009 issn: 1521-9615. doi: `10.1109/MCSE.2009.13` (see p. 63)

[122] C. D. Levermore. *Moment closure hierarchies for kinetic theories*. *Journal of Statistical Physics*, 83: 1021–1065, 1996 issn: 1572-9613. doi: `10.1007/BF02179552` (see p. 102)

[123] C. D. Levermore. *Relating Eddington factors to flux limiters*. *Journal of Quantitative Spectroscopy and Radiative Transfer*, 31: 149–160, 1984. doi: `10.1016/0022-4073(84)90112-2` (see p. 108)

[124] E. E. Lewis and J. W. F. Miller. *Computational Methods in Neutron Transport*. English. John Wiley and Sons, New York, 1984. url: `https://inis.iaea.org/search/search.aspx?orig_q=RN:17089238` (see p. 107)

[125]   J. Liu. *Preliminary survey on the mechanisms of the wave-like behaviors of heat transfer in living tissues.* Forschung im Ingenieurwesen, 66: 1–10, 2000. DOI: `10.1007/s100100000031` (see p. 20)

[126]   K. Liu, Y. Lu, J. Tian, C. Qin, X. Yang, S. Zhu, X. Yang, Q. Gao, and D. Han. *Evaluation of the simplified spherical harmonics approximation in bioluminescence tomography through heterogeneous mouse models.* Opt. Express, 18: 20988–21002, 2010. DOI: `10.1364/OE.18.020988` (see p. 100)

[127]   A. Logg, K.-A. Mardal, and G. Wells. *Automated Solution of Differential Equations by the Finite Element Method: The FEniCS Book.* English. vol. 84. Springer Science & Business Media, 2012. DOI: `10.1007/978-3-642-23099-8` (see pp. 100, 101, 115)

[128]   J. A. López Molina, M. J. Rivera, M. Trujillo, and E. J. Berjano. *Thermal modeling for pulsed radiofrequency ablation: Analytical study based on hyperbolic heat conduction.* Medical physics, 36: 1112–1119, 2009. DOI: `10.1118/1.3085824` (see p. 21)

[129]   Q. Lü, X. Zhang, and E. Zuazua. *Null controllability for wave equations with memory.* Journal de Mathématiques Pures et Appliquées. Neuvième Série, 108: 500–531, 2017 ISSN: 0021-7824. DOI: `10.1016/j.matpur.2017.05.001` (see pp. 183, 184, 187)

[130]   D. Maillet. *A review of the models using the Cattaneo and Vernotte hyperbolic heat equation and their experimental validation.* International Journal of Thermal Sciences, 139: 424–432, 2019 ISSN: 1290-0729. DOI: `10.1016/j.ijthermalsci.2019.02.021` (see pp. 17, 21)

[131]   R. Marshak. *Note on the spherical harmonic method as applied to the Milne problem for a sphere.* Physical Review, 71: 443, 1947. (see p. 114)

[132]   R. C. Martin. *Clean Code: A Handbook of Agile Software Craftsmanship.* English. Prentice Hall, Upper Saddle River, NJ u.a., 2009. ISBN: 978-0-13-235088-4 (see p. 99)

[133]   T. Marx, N. Dietrich, and R. Pinnau. *Shape Optimization in High Temperature Processes.* in: Proceedings in Applied Mathematics and Mechanics (PAMM). vol. 19 1 2019. e201900208 DOI: `10.1002/pamm.201900208` (see p. 9)

[134]   A. Masters, A. Steger, W. Lees, K. Walmsley, and S. Bown. *Interstitial laser hyperthermia: a new approach for treating liver metastases.* British journal of cancer, 66: 518–522, 1992. DOI: `10.1038/bjc.1992.305` (see p. 4)

[135]   MATLAB. *Matlab and Symbolic Toolbox Release 2018b.* 2018. URL: `https://de.mathworks.com/`(see pp. 64, 99)

[136]   J. C. Maxwell. *On the dynamical theory of gases.* Philosophical transactions of the Royal Society of London, (Careful: doi refers to a reprinted version), 49–88, 1867. DOI: `10.1142/9781848161337_0014` (see p. 17)

[137]   R. G. McClarren. *Theoretical Aspects of the Simplified P_n Equations.* Transport Theory and Statistical Physics, 39: 73–109, 2010. DOI: `10.1080/00411450.2010.535088` (see p. 99)

[138]   L. R. Mead and N. Papanicolaou. *Maximum entropy in the problem of moments.* Journal of Mathematical Physics, 25: 2404, 1984 ISSN: 00222488. DOI: `10.1063/1.526446` (see p. 108)

[139] R. Medvid, A. Ruiz, R. J. Komotar, J. Jagid, M. Ivan, R. Quencer, and M. Desai. *Current Applications of MRI-Guided Laser Interstitial Thermal Therapy in the Treatment of Brain Neoplasms and Epilepsy: A Radiologic and Neurosurgical Overview*. American Journal of Neuroradiology, 36: 1998–2006, 2015. doi: `10.3174/ajnr.A4362` (see p. 4)

[140] G. N. Minerbo. *Maximum entropy Eddington factors*. Journal of Quantitative Spectroscopy and Radiative Transfer, 20: 541–545, 1978. doi: `10.1016/0022-4073(78)90024-9` (see p. 108)

[141] K. Mitra, S. Kumar, A. Vedevarz, and M. K. Moallemi. *Experimental Evidence of Hyperbolic Heat Conduction in Processed Meat*. Journal of Heat Transfer, 117: 568–573, 1995 issn: 0022-1481. doi: `10.1115/1.2822615` (see p. 21)

[142] S. Mitusch. *Documentation on how to handle an example of optimal control of the Poisson equation with the Python package dolfin-adjoint*. Accessed: 2020-08-09. url: `http://www.dolfin-adjoint.org/en/latest/documentation/poisson-mother/poisson-mother.html`(see p. 78)

[143] S. Mitusch. *Documentation on the Taylor-remainder convergence test implemented in the Python package dolfin-adjoint*. Accessed: 2020-08-09. url: `http://www.dolfin-adjoint.org/en/latest/documentation/verification.html`(see p. 78)

[144] S. K. Mitusch, S. W. Funke, and J. S. Dokken. *dolfin-adjoint 2018.1: automated Adjoints for FEniCS and Firedrake*. Journal of Open Source Software, 4: 2019. doi: `10.21105/joss.01292` (see p. 64)

[145] M. F. Modest. *Radiative Heat Transfer*. English. 2nd ed. Academic press, 2003. isbn: 9780125031639 doi: `10.1016/C2010-0-65874-3` (see pp. 97, 99, 100, 107, 113, 114, 120)

[146] M. F. Modest. *Further Development of the Elliptic PDE Formulation of the P_N Approximation and its Marshak Boundary Conditions*. Numerical Heat Transfer, Part B: Fundamentals, 62: 181–202, 2012. doi: `10.1080/10407790.2012.702645` (see pp. 99, 100, 110, 114, 220)

[147] M. F. Modest, J. Cai, W. Ge, and E. Lee. *Elliptic formulation of the Simplified Spherical Harmonics Method in radiative heat transfer*. International Journal of Heat and Mass Transfer, 76: 459–466, 2014 issn: 0017-9310. doi: `10.1016/j.ijheatmasstransfer.2014.04.038` (see p. 100)

[148] M. F. Modest and J. Yang. *Elliptic PDE formulation and boundary conditions of the spherical harmonics method of arbitrary order for general three-dimensional geometries*. Journal of Quantitative Spectroscopy and Radiative Transfer, 109: 1641–1666, 2008 issn: 0022-4073. doi: `10.1016/j.jqsrt.2007.12.018` (see pp. 8, 99, 100, 110, 217, 220)

[149] Y. Mohammed and J. F. Verhey. *A finite element method model to simulate laser interstitial thermo therapy in anatomical inhomogeneous regions*. Biomedical engineering online, 4: 2, 2005. doi: `10.1186/1475-925X-4-2` (see p. 4)

[150] J. A. L. Molina, M. J. Rivera, M. Trujillo, and E. J. Berjano. *Effect of the thermal wave in radiofrequency ablation modeling: an analytical study*. Physics in Medicine and Biology, 53: 1447–1462, 2008. doi: `10.1088/0031-9155/53/5/018` (see p. 21)

[151] P. Monreal. *Moment Realizability and Kershaw Closures in Radiative Transfer*. PhD thesis, RWTH Aachen, 2012. URL: http://publications.rwth-aachen.de/record/210538/files/4482.pdf(see p. 108)

[152] K. Moreland. *Bent-Cool-Warm colormap*. Accessed: 2020-03-08. URL: https://github.com/kennethmoreland-com/kennethmoreland-com.github.io/blob/master/color-advice/bent-cool-warm/bent-cool-warm.ipynb(see p. 68)

[153] K. Moreland. *Why We Use Bad Color Maps and What You Can Do About It*. Electronic Imaging, 2016: 1–6, 2016 ISSN: 2470-1173. DOI: 10.2352/ISSN.2470-1173.2016.16.HVEI-133 (see p. 68)

[154] L. Müller. *Investigation of moment models for population balance equations and radiative transfer equations*. PhD thesis, Technische Universität Kaiserslautern, 2018 ISBN: 978-3-8439-3889-1. (see pp. 4, 8, 64, 101, 134)

[155] R. D. Neidinger. *Introduction to Automatic Differentiation and MATLAB Object-Oriented Programming*. SIAM Review, 52: 545–563, 2010 ISSN: 0036-1445. DOI: 10.1137/080743627 (see p. 78)

[156] B. Nordlinger, M. Guiguet, J.-C. Vaillant, P. Balladur, K. Boudjema, P. Bachellier, and D. Jaeck. *Surgical resection of colorectal carcinoma metastases to the liver: A prognostic scoring system to improve case selection, based on 1568 patients*. Cancer: Interdisciplinary International Journal of the American Cancer Society, 77: 1254–1262, 1996. DOI: 10.1002/(SICI)1097-0142(19960401)77:7<1254::AID-CNCR5>3.0.CO;2-I (see p. 2)

[157] NumPy. NumPy is an open source project aiming to enable numerical computing with Python. URL: https://numpy.org/(see p. 64)

[158] D. P. O'Neill, T. Peng, P. Stiegler, U. Mayrhauser, S. Koestenbauer, K. Tscheliessnigg, and S. J. Payne. *A Three-State Mathematical Model of Hyperthermic Cell Death*. Annals of biomedical engineering, 39: 570–579, 2011. DOI: 10.1007/s10439-010-0177-1 (see p. 6)

[159] E. Olbrant and M. Frank. *Generalized Fokker-Planck Theory for Electron and Photon Transport in Biological Tissues: Application to Radiotherapy*. Computational and mathematical methods in medicine, 11: 313–39, 2010 ISSN: 1748-6718. DOI: 10.1080/1748670X.2010.491828 (see p. 103)

[160] E. Olbrant, C. D. Hauck, and M. Frank. *A realizability-preserving discontinuous Galerkin method for the M1 model of radiative transfer*. Journal of Computational Physics, 231: 5612–5639, 2012 ISSN: 00219991. DOI: 10.1016/j.jcp.2012.03.002 (see p. 108)

[161] L. Onsager. *Reciprocal Relations in Irreversible Processes. I. Physical Review*, 37: 405–426, 1931. DOI: 10.1103/PhysRev.37.405 (see p. 18)

[162] ParaView. ParaView is an open-source, multi-platform data analysis and visualization application. URL: https://www.paraview.org/(see p. 64)

[163] S. J. Park and S.-B. Yun. *Entropy production estimates for the polyatomic ellipsoidal BGK model*. Applied Mathematics Letters, 58: 26–33, 2016 ISSN: 0893-9659. DOI: 10.1016/j.aml.2016.01.021 (see p. 102)

[164] J. A. Pearce, J. W. Valvano, and S. Emelianov. *Temperature Measurements*. in: *Optical-Thermal Response of Laser-Irradiated Tissue* ed. by A. J. Welch and M. J. van Gemert. 2nd ed. Springer Netherlands, Dordrecht, 2011. chap. 11, 399–453 isbn: 978-90-481-8831-4 doi: `10.1007/978-90-481-8831-4_11` (see p. 1)

[165] H. H. Pennes. *Analysis of Tissue and Arterial Blood Temperatures in the Resting Human Forearm*. *Journal of Applied Physiology*, 1: 93–122, 1948. (see p. 5)

[166] R. D. Peters, E. Chan, J. Trachtenberg, S. Jothy, L. Kapusta, W. Kucharczyk, and R. M. Henkelman. *Magnetic resonance thermometry for predicting thermal damage: An application of interstitial laser coagulation in an in vivo canine prostate model*. *Magnetic Resonance in Medicine*, 44: 873–883, 2000. doi: `10.1002/1522-2594(200012)44:6<873::AID-MRM8>3.0.CO;2-X` (see p. 68)

[167] R. Pinnau and G. Thömmes. *Optimal boundary control of glass cooling processes*. *Mathematical Methods in the Applied Sciences*, 27: 1261–1281, 2004. doi: `10.1002/mma.500` (see pp. 9, 97, 101, 103)

[168] G. C. Pomraning. *Variational boundary conditions for the spherical harmonics approximation to the neutron transport equation*. *Annals of Physics*, 27: 193–215, 1964 issn: 0003-4916. doi: `10.1016/0003-4916(64)90105-8` (see p. 113)

[169] C. Pu and R. G. McClarren. *Mathematical and Numerical Validation of the Simplified Spherical Harmonics Approach for Time-Dependent Anisotropic-Scattering Transport Problems in Homogeneous Media*. *Journal of Computational and Theoretical Transport*, 46: 366–378, 2017. doi: `10.1080/23324309.2017.1352516` (see p. 101)

[170] S. Puccini, N.-K. Bär, M. Bublat, T. Kahn, and H. Busse. *Simulations of thermal tissue coagulation and their value for the planning and monitoring of laser-induced interstitial thermotherapy (LITT)*. *Magnetic Resonance in Medicine*, 49: 351–362, 2003. doi: `10.1002/mrm.10357` (see pp. 5, 10, 44, 68, 97)

[171] Python Software Foundation. *Python*. url: `https://www.python.org/` (see p. 64)

[172] S. J. Qin. *Process data analytics in the era of big data*. *AIChE Journal*, 60: 3092–3100, 2014. doi: `10.1002/aic.14523` (see p. 2)

[173] R. Quintanilla and R. Racke. *A note on stability in dual-phase-lag heat conduction*. *International Journal of Heat and Mass Transfer*, 49: 1209–1213, 2006 issn: 0017-9310. doi: `10.1016/j.ijheatmasstransfer.2005.10.016` (see pp. 19, 20)

[174] R. Quintanilla and R. Racke. *Qualitative aspects in dual-phase-lag heat conduction*. *Proceedings of the Royal Society A: Mathematical, Physical and Engineering Sciences*, 463: 659–674, 2006. doi: `10.1098/rspa.2006.1784` (see p. 19)

[175] P. J. Rabier. *Vector-valued Morrey's embedding theorem and Hölder continuity in parabolic problems*. *Electronic Journal of Differential Equations*, 2011: 1–10, 2011 issn: 1072-6691. url: `https://ejde.math.txstate.edu/Volumes/2011/10/rabier.pdf` (see p. 209)

[176] R. Racke. *Heat conduction in elastic systems: Fourier versus Cattaneo*. in: International Conference on Heat Transfer, Fluid Mechanics and Thermodynamics 2015. url: `http://www.math.uni-konstanz.de/~racke/dvidat/m62.pdf` (see pp. 19, 20)

[177] M. Reed and B. Simon. *Functional Analysis*. English. vol. 1 Methods of Modern Mathematical Physics. (Careful: doi refers to originally published version of 1972). Academic Press, Inc., 1980. isbn: 0-12-585050-6 doi: 10.1016/B978-0-12-585001-8.X5001-6 (see p. 193)

[178] J. Ritter, A. Klar, and F. Schneider. *Partial-moment minimum-entropy models for kinetic chemotaxis equations in one and two dimensions*. Journal of Computational and Applied Mathematics, 306: 300–315, 2016 issn: 03770427. doi: 10.1016/j.cam.2016.04.019 url: http://arxiv.org/abs/1601.04482(see p. 108)

[179] J.-P. Ritz, K. Lehmann, C. Isbert, A. Roggan, C. T. Germer, and H. J. Buhr. *Effectivity of laser-induced thermotherapy: In vivo comparison of arterial microembolization and complete hepatic inflow occlusion*. Lasers in Surgery and Medicine: The Official Journal of the American Society for Laser Medicine and Surgery, 36: 238–244, 2005. doi: 10.1002/lsm.20144 (see p. 3)

[180] U. of Rochester: Medical Center. *Health Encyclopedia: Vital Signs*. Accessed: 2020-02-15. url: https://www.urmc.rochester.edu/encyclopedia/content.aspx?ContentType ID=85&ContentID=P00866(see p. 11)

[181] A. Roggan, K. Dorschel, O. Minet, D. Wolff, and G. Müller. *The optical properties of biological tissue in the near infrared wavelength range: review and measurements*. in: *Laser-induced interstitial therapy*. 1995. 10–44 isbn: 0-8194-1859-5 (see p. 11)

[182] A. Roggan and G. J. Mueller. *Two-dimensional computer simulations for real-time irradiation planning of laser-induced interstitial thermotherapy (LITT)*. in: *Medical Applications of Lasers II*. vol. 2327 International Society for Optics and Photonics 1994. 242–252 doi: 10.1117/12.197569 (see p. 4)

[183] D. Rouan. *Radiative Transfer*. in: *Encyclopedia of Astrobiology* ed. by M. Gargaud, R. Amils, J. C. Quintanilla, H. J. Cleaves, W. M. Irvine, D. L. Pinti, and M. Viso. Springer, Berlin, Heidelberg, 2011. 1410–1413 isbn: 978-3-642-11274-4 doi: 10.1007/978-3-642-11274-4_1336 (see p. 246)

[184] T. Roubíček. *Nonlinear Partial Differential Equations with Applications*. English. 1st ed. Birkhäuser Verlag, 2005. isbn: 3-7643-7293-1 doi: 10.1007/3-7643-7397-0 (see p. 215)

[185] R. P. Rulko, E. W. Larsen, and G. C. Pomraning. *The P_N Theory as an Asymptotic Limit of Transport Theory in Planar Geometry —II: Numerical Results*. Nuclear Science and Engineering, 109: 76–85, 1991. doi: 10.13182/NSE91-A23845 (see p. 113)

[186] M. Růžička. *Nichtlineare Funktionalanalysis*. German. 1st ed. Springer, 2004. isbn: 3-540-20066-5 doi: 10.1007/3-540-35022-5 (see pp. 22, 170, 193, 194, 202, 204, 205, 210, 212, 215, 244)

[187] D. F. Saldanha, V. L. Khiatani, T. C. Carrillo, F. Y. Yap, J. T. Bui, M. G. Knuttinen, C. A. Owens, and R. C. Gaba. *Current Tumor Ablation Technologies: Basic Science and Device Review*. in: *Seminars in interventional radiology*. vol. 27 03 © Thieme Medical Publishers 2010. 247–254 doi: 10.1055/s-0030-1261782 (see pp. 3, 4, 6, 68, 244–247)

[188] E. Salomatina and A. Yaroslavsky. *Evaluation of the in vivo and ex vivo optical properties in a mouse ear model*. Physics in Medicine & Biology, 53: 2797, 2008. doi: 10.1088/0031-9155/53/11/003 (see p. 7)

[189] D. Sarason. *Functions of vanishing mean oscillation. Transactions of the American Mathematical Society*, 207: 391–405, 1975. doi: 10.2307/1997184 (see p. 41)

[190] F. Schneider. *Kershaw closures for linear transport equations in slab geometry I: Model derivation. Journal of Computational Physics*, 322: 905–919, 2016 issn: 10902716. doi: 10.1016/j.jcp.2016.02.080 url: http://arxiv.org/abs/1511.02714 (see p. 108)

[191] F. Schneider. *Kershaw closures for linear transport equations in slab geometry II: High-order realizability-preserving discontinuous-Galerkin schemes. Journal of Computational Physics*, 322: 920–935, 2016. doi: 10.1016/j.jcp.2016.07.014 url: http://arxiv.org/abs/1602.02590 (see p. 108)

[192] F. Schneider. *Moment models in radiation transport equations*. PhD thesis, Technische Universität Kaiserslautern, 2016 isbn: 978-3-8439-2437-5. url: https://kplus.ub.uni-kl.de/Record/KLU01-001010407 (see pp. 103, 119)

[193] F. Schneider, G. W. Alldredge, M. Frank, and A. Klar. *Higher Order Mixed-Moment Approximations for the Fokker–Planck Equation in One Space Dimension. SIAM Journal on Applied Mathematics*, 74: 1087–1114, 2014 issn: 0036-1399. doi: 10.1137/130934210 (see p. 108)

[194] F. Schneider, J. Kall, and A. Roth. *First-Order quarter- and mixed-moment realizability theory and Kershaw closures for a Fokker-Planck equation in two space dimensions. Kinetic and Related Models*, 10: 2017 issn: 1937-5093. doi: 10.3934/krm.2017044 (see p. 108)

[195] F. Schneider and T. Leibner. *First-order continuous- and discontinuous-Galerkin moment models for a linear kinetic equation: realizability-preserving splitting scheme and numerical analysis*. 2019. url: https://arxiv.org/abs/1904.03098 (see p. 108)

[196] H.-J. Schwarzmaier, I. V. Yaroslavsky, A. N. Yaroslavsky, V. Fiedler, F. Ulrich, and T. Kahn. *Treatment planning for MRI-guided laser-induced interstitial thermotherapy of brain tumors—The role of blood perfusion. Journal of Magnetic Resonance Imaging*, 8: 121–127, 1998. doi: 10.1002/jmri.1880080124 (see p. 11)

[197] T. Schwedes, D. A. Ham, S. W. Funke, and M. D. Piggott. *Mesh Dependence in PDE-Constrained Optimisation: An Application in Tidal Turbine Array Layouts*. English. Springer-Briefs in Mathematics of Planet Earth. Springer, Cham, 2017. viii + 110 isbn: 978-3-319-59483-5 doi: 10.1007/978-3-319-59483-5 (see pp. 59, 65, 78–80)

[198] B. Seibold and M. Frank. *StaRMAP—A Second Order Staggered Grid Method for Spherical Harmonics Moment Equations of Radiative Transfer. ACM Transactions on Mathematical Software*, 41: 4:1–4:28, 2014 issn: 0098-3500. doi: 10.1145/2590808 (see pp. 63, 99, 104, 108, 109, 112, 117)

[199] Y. Shao, B. Arjun, H. Leo, and K. Chua. *A computational theoretical model for radiofrequency ablation of tumor with complex vascularization. Computers in Biology and Medicine*, 89: 282–292, 2017 issn: 0010-4825. doi: 10.1016/j.compbiomed.2017.08.025 (see pp. 4, 43, 64)

[200] K. S. Shibib, M. A. Munshid, and H. A. Lateef. *The effect of laser power, blood perfusion, thermal and optical properties of human liver tissue on thermal damage in LITT. Lasers in medical science*, 32: 2039–2046, 2017. doi: 10.1007/s10103-017-2321-8 (see pp. 4, 43)

[201] C.-W. Shu. *Essentially non-oscillatory and weighted essentially non-oscillatory schemes for hyperbolic conservation laws*. in: *Advanced Numerical Approximation of Nonlinear Hyperbolic Equations. Lecture Notes in Mathematics.* vol. 1697 Springer, 1998. ISBN: 978-3-540-64977-9 DOI: 10.1007/BFb0096355 (see p. 108)

[202] J. Simon. *Compact sets in the space $L^p(0, T; B)$*. Annali di Matematica Pura ed Applicata. Serie Quarta, 146: 65–96, 1987 ISSN: 0003-4622. DOI: 10.1007/BF01762360 (see p. 209)

[203] G. Stadler. *Elliptic optimal control problems with L_1-control cost and applications for the placement of control devices*. Computational Optimization and Applications, 44: 159–181, 2007. DOI: 10.1007/s10589-007-9150-9 (see p. 58)

[204] W. M. Star. *Diffusion Theory of Light Transport*. in: *Optical-Thermal Response of Laser-Irradiated Tissue* ed. by A. J. Welch and M. J. van Gemert. 2nd ed. Springer Netherlands, Dordrecht, 2011. chap. 6, 145–201 ISBN: 978-90-481-8831-4 DOI: 10.1007/978-90-481-8831-4_6 (see pp. 97, 247)

[205] B. Straughan. *Heat Waves*. English. vol. 177. Springer Science & Business Media, 2011. DOI: 10.1007/978-1-4614-0493-4 (see pp. 17–19)

[206] H. Struchtrup. *Kinetic schemes and boundary conditions for moment equations*. Zeitschrift für angewandte Mathematik und Physik ZAMP, 51: 346, 2000 ISSN: 00442275. DOI: 10.1007/s000330050002 (see p. 113)

[207] C. Sturesson and S. Andersson-Engels. *Tissue temperature control using a water-cooled applicator: Implications for transurethral laser-induced thermotherapy of benign prostatic hyperplasia*. Medical physics, 24: 461–470, 1997. DOI: 10.1118/1.597912 (see p. 4)

[208] C. Sturesson. *Interstitial laser-induced thermotherapy: Influence of carbonization on lesion size*. Lasers in Surgery and Medicine: The Official Journal of the American Society for Laser Medicine and Surgery, 22: 51–57, 1998. DOI: 10.1002/(SICI)1096-9101(1998)22:1<51::AID-LSM12>3.0.CO;2-B (see p. 4)

[209] E. Tadmor. *Approximate solutions of nonlinear conservation laws*. in: *Advanced Numerical Approximation of Nonlinear Hyperbolic Equations. Lecture Notes in Mathematics.* vol. 1697 Springer, 1998. ISBN: 978-3-540-64977-9 DOI: 10.1007/BFb0096352 (see p. 108)

[210] Y. Taitel. *On the parabolic, hyperbolic and discrete formulation of the heat conduction equation*. International Journal of Heat and Mass Transfer, 15: 369–371, 1972. DOI: 10.1016/0017-9310(72)90085-3 (see pp. 20, 146)

[211] J. T. Tencer. *Error analysis for radiation transport*. PhD thesis, The University of Texas at Austin, 2013. URL: https://repositories.lib.utexas.edu/handle/2152/23247 (see pp. 99, 100)

[212] S. Thomsen and J. A. Pearce. *Thermal Damage and Rate Processes in Biologic Tissues*. in: *Optical-Thermal Response of Laser-Irradiated Tissue* ed. by A. J. Welch and M. J. van Gemert. 2nd ed. Springer Netherlands, Dordrecht, 2011. chap. 13, 487–549 ISBN: 978-90-481-8831-4 DOI: 10.1007/978-90-481-8831-4_13 (see pp. 3, 6)

[213] K. Tolle and N. Marheineke. *Efficient Therapy-Planning via Model Reduction for Laser-Induced Thermotherapy*. in: *Progress in Industrial Mathematics at ECMI 2018*. Springer, 2019. 207–213 ISBN: 978-3-030-27550-1 DOI: 10.1007/978-3-030-27550-1_26 (see p. 146)

[214]   K. TOLLE and N. MARHEINEKE. *Multi-Fidelity Optimization using Reduced Order Models.* *PAMM*, 19: e201900168, 2019. DOI: `10.1002/pamm.201900168` (see p. 146)

[215]   K. TOLLE and N. MARHEINEKE. *On Online Parameter Identification in Laser-Induced Thermotherapy.* in: *Modeling, Simulation and Optimization in the Health- and Energy-Sector.* Accepted Springer, 2021. (see p. 146)

[216]   E. F. TORO. *Riemann Solvers and Numerical Methods for Fluid Dynamics.* English. 3rd ed. Springer, Dordrecht u.a., 2009. ISBN: 978-3-540-49834-6 DOI: `10.1007/b79761` (see p. 113)

[217]   F. TRÖLTZSCH. *Optimale Steuerung partieller Differentialgleichungen.* German. 2nd ed. Vieweg + Teubner, Wiesbaden, 2009. ISBN: 978-3-8348-0885-1 DOI: `10.1007/978-3-8348-9357-4` (see pp. 23, 48, 50, 58, 59, 77, 176–178, 181–183, 197, 211, 212)

[218]   N. TSAFNAT, G. TSAFNAT, T. D. LAMBERT, and S. JONES. *Modelling heating of liver tumours with heterogeneous magnetic microsphere deposition.* *Physics in Medicine and Biology*, 50: 2937–2953, 2005. DOI: `10.1088/0031-9155/50/12/014` (see pp. 4, 43)

[219]   O. TSE, R. PINNAU, and N. SIEDOW. *Identification of temperature-dependent parameters in laser-interstitial thermo therapy.* *Mathematical Models and Methods in Applied Sciences*, 22: 1250019, 2012. DOI: `10.1142/S0218202512500194` (see pp. 7, 15, 26, 28–31, 36, 38, 40, 45–47, 51, 173)

[220]   D. Y. TZOU. *A Unified Field Approach for Heat Conduction From Macro- to Micro-Scales.* *Journal of Heat Transfer*, 117: 8–16, 1995 ISSN: 0022-1481. DOI: `10.1115/1.2822329` (see p. 18)

[221]   D. Y. TZOU. *Experimental support for the lagging behavior in heat propagation.* *Journal of Thermophysics and Heat Transfer*, 9: 686–693, 1995. DOI: `10.2514/3.725` (see p. 21)

[222]   J. W. VALVANO. *Tissue Thermal Properties and Perfusion.* in: *Optical-Thermal Response of Laser-Irradiated Tissue* ed. by A. J. WELCH and M. J. VAN GEMERT. 2nd ed. Springer Netherlands, Dordrecht, 2011. chap. 12, 455–485 ISBN: 978-90-481-8831-4 DOI: `10.1007/978-90-481-8831-4_12` (see pp. 2, 10)

[223]   J. VERHEY, Y. MOHAMMED, A. LUDWIG, and K. GIESE. *Implementation of a practical model for light and heat distribution using laser-induced thermotherapy near to a large vessel.* *Physics in Medicine & Biology*, 48: 3595, 2003. DOI: `10.1088/0031-9155/48/21/010` (see p. 4)

[224]   P. VIRTANEN, R. GOMMERS, T. E. OLIPHANT, M. HABERLAND, T. REDDY, D. COURNAPEAU, E. BUROVSKI, P. PETERSON, W. WECKESSER, J. BRIGHT, S. J. VAN DER WALT, M. BRETT, J. WILSON, K. JARROD MILLMAN, N. MAYOROV, A. R. J. NELSON, E. JONES, R. KERN, E. LARSON, C. CAREY, İ. POLAT, Y. FENG, E. W. MOORE, J. VAND ERPLAS, D. LAXALDE, J. PERKTOLD, R. CIMRMAN, I. HENRIKSEN, E. A. QUINTERO, C. R. HARRIS, A. M. ARCHIBALD, A. H. RIBEIRO, F. PEDREGOSA, P. VAN MULBREGT, and S. 1. 0. CONTRIBUTORS. *SciPy 1.0: fundamental algorithms for scientific computing in Python.* *Nature Methods*, 2020. DOI: `10.1038/s41592-019-0686-2` (see p. 64)

[225]   T. J. VOGL, R. STRAUB, S. ZANGOS, M. MACK, and K. EICHLER. *MR-guided laser-induced thermotherapy (LITT) of liver tumours: experimental and clinical data.* *International journal of hyperthermia*, 20: 713–724, 2004. DOI: `10.1080/02656730400007212` (see p. 4)

[226]   E. W. WEISSTEIN. *Trigonometric Power Formulas.* From MathWorld–A Wolfram Web Resource. Accessed: 2020-04-10. URL: `https://mathworld.wolfram.com/TrigonometricPowerFormulas.html` (see p. 119)

[227] A. J. Welch. *Overview of Optical and Thermal Laser-Tissue Interaction and Nomenclature*. in: *Optical-Thermal Response of Laser-Irradiated Tissue* ed. by A. J. Welch and M. J. van Gemert. 2nd ed. Springer Netherlands, Dordrecht, 2011. chap. 1, 3–11 isbn: 978-90-481-8831-4 doi: `10.1007/978-90-481-8831-4_1` (see pp. 97, 243, 246)

[228] A. J. Welch, M. J. van Gemert, and W. M. Star. *Definitions and Overview of Tissue Optics*. in: *Optical-Thermal Response of Laser-Irradiated Tissue* ed. by A. J. Welch and M. J. van Gemert. 2nd ed. Springer Netherlands, Dordrecht, 2011. chap. 3, 3–11 isbn: 978-90-481-8831-4 doi: `10.1007/978-90-481-8831-4_3` (see pp. 4, 97)

[229] M. D. Wilkinson, M. Dumontier, I. J. Aalbersberg, G. Appleton, M. Axton, A. Baak, N. Blomberg, J.-W. Boiten, L. B. da Silva Santos, P. E. Bourne, et al. *The FAIR Guiding Principles for scientific data management and stewardship. Scientific data*, 3: 2016. doi: `10.1038/sdata.2016.18` (see p. 63)

[230] Wolfram Research. *Definition of an inverse problem*. Accessed: 2020-09-02. url: `https://mathworld.wolfram.com/InverseProblem.html` (see p. 245)

[231] N. T. Wright. *On a Relationship Between the Arrhenius Parameters from Thermal Damage Studies. Journal of Biomechanical Engineering*, 125: 300–304, 2003 issn: 0148-0731. doi: `10.1115/1.1553974` (see pp. 6, 11)

[232] K. Yosida. *Functional Analysis*. English. 6th ed. Springer, 1980. isbn: 978-3-540-58654-8 doi: `10.1007/978-3-642-61859-8` (see p. 205)

[233] E. Zeidler. *Applied Functional Analysis: Applications to Mathematical Physics*. English. 1st ed. vol. 108 Applied Mathematical Sciences. Springer Science+Business Media New York, 1995. isbn: 978-1-4612-6910-6 doi: `10.1007/978-1-4612-0815-0` (see p. 183)

[234] E. Zeidler. *Applied Functional Analysis: Main Principles and Their Applications*. English. 1st ed. vol. 109 Applied Mathematical Sciences. Springer Science+Business Media New York, 1995. isbn: 978-1-4612-6913-7 doi: `10.1007/978-1-4612-0821-1` (see pp. 43, 204)

[235] E. Zeidler. *Nonlinear Functional Analysis and its Applications. II/A: Linear Monotone Operators*. English. 1st ed. Springer Science+Business Media New York, 1990. isbn: 978-1-4612-6971-7 doi: `10.1007/978-1-4612-0985-0` (see pp. 22, 23, 145, 152, 153, 175, 195, 196, 198–200, 202, 203, 205–208, 211, 241–243)

[236] E. Zeidler. *Nonlinear Functional Analysis and its Applications. II/B: Nonlinear Monotone Operators*. English. 1st ed. Springer Science+Business Media New York, 1990. isbn: 978-1-4612-6969-4 doi: `10.1007/978-1-4612-0981-2` (see pp. 48, 50, 151, 194, 199, 207, 209)

[237] E. Zeidler. *Springer-Handbuch der Mathematik: Begründet von I.N. Bronstein und K.A. Semendjaew. Weitergeführt von G. Grosche, V. Ziegler und D. Ziegler. Herausgegeben von E. Zeidler*. German. 3rd ed. Springer-Verlag, 2012. isbn: 978-3-8351-0123-4 doi: `10.1007/978-3-8348-2359-5` (see pp. 19, 119)

[238] M. Zhang, Z. Zhou, S. Wu, L. Lin, H. Gao, and Y. Feng. *Simulation of temperature field for temperature-controlled radio frequency ablation using a hyperbolic bioheat equation and temperature-varied voltage calibration: a liver-mimicking phantom study. Physics in Medicine and Biology*, 60: 9455–9471, 2015. doi: `10.1088/0031-9155/60/24/9455` (see p. 21)

[239]   Y. Zhang, J. C. Ragusa, and J. E. Morel. *Iterative performance of various formulations of the SP_N equations*. *Journal of Computational Physics*, 252: 558–572, 2013 issn: 0021-9991. doi: 10.1016/j.jcp.2013.06.009 (see p. 100)

[240]   W. P. Ziemer. *Weakly Differentiable Functions*. English. 1st ed. vol. 120 Graduate Texts in Mathematics. Sobolev spaces and functions of bounded variation. Springer-Verlag, New York, 1989. xvi+308 isbn: 978-1-4612-6985-4 doi: 10.1007/978-1-4612-1015-3 (see p. 204)

Table of notations

Notation	Description	Page List
$\mathbb{N}, \mathbb{N}_0$	$\mathbb{N} = \{1, 2, \ldots\}$, $\mathbb{N}_0 = \mathbb{N} \cup \{0\}$: set of natural numbers (including zero).	21
Ω	$\Omega \subset \mathbb{R}^d$, $d \in \{2, 3\}$: spatial domain.	21
Γ	$\Gamma = \partial\Omega$: boundary of the spatial domain.	21
T	$T \in (0, \infty)$: final time of the model / simulation.	21
I	$I = (0, T) \subset \mathbb{R}$: time domain.	21
Q	$Q = I \times \Omega$: space-time cylinder.	21
$\boldsymbol{n}$	$\boldsymbol{n} \in \mathbb{R}^d$: outer unit normal vector.	21
$(\cdot)'$	Weak time derivative in the context of Bochner spaces: for $\vartheta \in L^1(I; X)$, where X is a real Banach space, we call $\vartheta^{(n)} \in L^1(I; X)$ the nth weak time derivative of ϑ if $\int_0^T \varphi^{(n)}(t)\vartheta(t)\,\mathrm{d}t = (-1)^n \int_0^T \varphi(t)\vartheta^{(n)}(t)\,\mathrm{d}t$ for all $\varphi \in \mathcal{C}_c^\infty(I)$, cf. [235, Ch. 23.5, Def. 23.15, p. 417].	22
$\mathcal{S}^2$	$\mathcal{S}^2 = \{\boldsymbol{v} \in \mathbb{R}^3 \mid \|\boldsymbol{v}\|_2 = 1\}$: unit sphere.	101
$\boldsymbol{v}$	$\boldsymbol{v} \in \mathcal{S}^2$: element on the unit sphere.	101
S_l^m	Real spherical harmonics of degree l: particular functions defined on the surface of the unit sphere, see Definition 5.7.	104
$\mathbf{b}$	Angular basis vector: collection of real spherical harmonics, see Definition 5.9.	105
$(\cdot, \cdot)$	$(\cdot, \cdot) := (\cdot, \cdot)_X$: inner product of a Hilbert space X.	22
$\langle \cdot, \cdot \rangle$	$\langle \cdot, \cdot \rangle = \langle \cdot, \cdot \rangle_X = \langle \cdot, \cdot \rangle_{X^*, X}$: dual pairing between a Banach space X and its dual space X^*. Must not to be confused with the spherical integral $\langle \cdot \rangle = \int_{\mathcal{S}^2} \cdot \, \mathrm{d}\boldsymbol{v}$.	22

Notation	Description	Page List
$\langle \cdot \rangle$	$\langle \cdot \rangle = \int_{\mathcal{S}^2} \cdot \, \mathrm{d}\boldsymbol{v}$: integral over the full unit sphere. Must not to be confused with the dual pairing $\langle \cdot, \cdot \rangle_X$ for a Banach space X.	103
$\hookrightarrow$	Continuous embedding of two Banach spaces $X \subset Y$: the embedding operator $j \colon X \to Y$, $j(u) = u$ is continuous, i.e., $\|u\|_Y \leq C \|u\|_X$ for all $u \in X$. More generally, we speak of an embedding if there are two Banach spaces X, Y and an *injective linear* operator $j \colon X \to Y$. Since j is injective, we can identify u with $j(u)$ and write $X \subset Y$, cf. [235, Ch. 21.3, Def. 21.13, p. 237].	22
$\hookrightarrow\hookrightarrow$	Compact embedding of two Banach spaces $X \subset Y$: the embedding operator $j \colon X \to Y$, $j(u) = u$ is continuous and compact, i.e., each bounded sequence $(u_n)_{n\in\mathbb{N}} \subset X$ has a subsequence $(u_{n_k})_{k\in\mathbb{N}}$ which is convergent in Y, cf. [235, Ch. 21.3, Def. 21.13, p. 237].	22, *see continuous embedding* &
$\rightharpoonup$	Weakly convergent, see Definition B.7.	195
$\rightharpoonup^*$	Weakly* convergent, see Definition B.7.	195
$\mathcal{L}(X, Y)$	$\mathcal{L}(X, Y) = \{f \colon X \to Y \mid f \text{ is linear}, \|f\|_{X,Y} = \sup_{\|x\|_X \leq 1} \|f(x)\|_Y < \infty\}$: the set of bounded linear operators between two Banach spaces X, Y [93, Ch. 1.2.1.2, Def. 1.4, p. 11].	22
X^*	$X^* = \mathcal{L}(X, \mathbb{R})$: dual space of the real Banach space X.	22
$W^{k,p}(\Omega)$	$W^{k,p}(\Omega) = \{f \in L^p(\Omega) \mid f \text{ has weak derivatives } \mathrm{D}^\alpha f \in L^p(\Omega) \text{ for all } |\alpha| \leq k\}$: Sobolev space [93, Ch. 1.2.2.7, Def. 1.14, p. 20].	22
$L^p(I; X)$	$L^p(I; X) = \{f \colon I \to X \mid f \text{ strongly measurable}, \|f\|_{L^p(I;X)} < \infty\}$: Bochner space (generalization of L^p (Lebesgue) spaces to functions with values in a (reflexive) Banach space X) equipped with the norm $\|f\|_{L^p(I;X)} = \left(\int_0^T \|f(t)\|_X^p \, \mathrm{d}t \right)^{1/p}$ for $1 \leq p < \infty$ and $\|f\|_{L^\infty(I;X)} = \operatorname{ess\,sup}_{t\in I} \|f(t)\|_X$.	22, *see Bochner measurable*

Notation	Description	Page List
$W^{k,p}(I; X)$	$W^{k,p}(I;X) =$ $\{f \in L^p(I;X) \,|\, f$ has weak time derivatives $f^{(n)} \in L^p(I;X)$ for all $0 \le n \le k\}$: Banach-space-valued Sobolev space for a real Banach space X, cf. [114], [235, Ch. 23.6, p. 422 ff.].	23, *see* Sobolev space
$\mathcal{C}^{0,\alpha}(\overline{\Omega})$	$\mathcal{C}^{0,\alpha}(\overline{\Omega}) = \{f \colon \overline{\Omega} \to \mathbb{R} \,|\, \|f\|_{\mathcal{C}^{0,\alpha}(\overline{\Omega})} < \infty\}$: space of Hölder-continuous functions equipped with the norm $\|f\|_{\mathcal{C}^{0,\alpha}(\overline{\Omega})} = \sup\left\{ \frac{|f(x)-f(y)|}{|x-y|^\alpha} \,|\, x, y \in \overline{\Omega}, x \ne y \right\}$ [4, Ch. 1, Def. 1.7, p. 46].	22
$\mathcal{C}^0(\overline{I}; X), \mathcal{C}^0(\overline{I})$	$\mathcal{C}^0(\overline{I}; X) = \{f \colon \overline{I} \to X \,|\, f$ is continuous$\}$: space of continuous functions from I to a real Banach space X, equipped with the uniform norm. In case of $X = \mathbb{R}$, we write $\mathcal{C}^0(\overline{I})$.	22, *see* time domain
$\mathcal{C}_c^\infty(I)$	Space of infinitely often differentiable functions from I to $\mathbb{R}$ with compact support in I.	23
σ_a	Absorption coefficient: the probability of absorption per infinitesimal path length Δx is $\sigma_a \Delta x$ [227, Sec. 1.2, Tab. 1.1, p. 7 ff.].	6, 101, *see* absorbed
σ_s	Scattering coefficient: the probability of scattering per infinitesimal path length Δx is $\sigma_s \Delta x$ [227, Sec. 1.2, Tab. 1.1, p. 7 ff.].	6, 101, *see* scattered
σ_t	Attenuation coefficient: the probability of an interaction with the medium per infinitesimal path length Δx is $\sigma_t \Delta x$ [227, Sec. 1.2, Tab. 1.1, p. 7 ff.].	101
a.a.	Almost all: cf. *almost everywhere (a.e.)*.	30, *see* a.e.
absorption	*"In (electromagnetic) wave motion: the transfer of the energy of a wave to matter as the wave passes through it"* [57].	97
adjoint state vector	Two-component vector $(z_1, z_2) \in L^2(I; H^1(\Omega)) \times W_\vartheta$ (see equation (2.7)) which fulfills the adjoint state system (3.19) for all $\varphi \in L^2(I; H^1(\Omega)) \times L^2(I; H^1(\Omega))$.	56–59, 77
AD	Algorithmic differentiation.	9, 77, 78
a.e.	Almost everywhere (in X): all elements of a set X except for those included in a subset of X with (Lebesgue) measure zero, cf. [55, Ch. 4, Def. 4.1, p. 155].	25

Notation	Description	Page List
blood-perfusion rate	The blood-perfusion rate describes the transport of blood through the vascular structure.	2, 15, 26, 43, 63, 74
BMBF	German Federal Ministry of Education and Research (Bundesministerium für Bildung und Forschung).	1
Bochner measurable	Also *strongly measurable*: a function $f \colon I \to X$, where X is a reflexive Banach space, is called strongly measurable if there exist simple functions $s_k \colon I \to X$ with $\lim_{k \to \infty} \|s_k(t) - f(t)\|_X = 0$ for a.a. $t \in I$ [186, Ch. 2, Def. 1.3, p. 34].	30
Cattaneo–LITT model	LITT model with Cattaneo equation as heat-transfer model.	15, 17, 24, 26, 43, 63, 97, 117
chemical ablation	*"A chemical agent is injected into a tumor bed [via a needle]"* [187, p. 251].	3
classical LITT model	Classical LITT model with standard model for heat-transfer, Arrhenius law for coagulation and P$_1$ approximation for the radiation.	5, 15, 97
coagulation	Optically visible irreversible cell destruction (necrosis) caused by the denaturation of proteins [65].	5, 6, 24
compact map	Let X, Y be real Banach spaces. A linear map $T \colon X \to Y$ is called *compact* if it maps bounded sets $M \subset X$ to *relatively compact* sets, i.e., $\overline{T(M)} \subset Y$ is *compact* [4, Ch. 8, Def. 8.1, p. 331].	197
conduction	*"Transfer of energy (heat) arising from temperature differences between adjacent parts of a body"* [60].	5
convection	*"Process by which heat is transferred by movement of a heated fluid such as air or water"* [58].	5
cryoablation	*"Cold temperatures emitted from a probe cause both intra- and extracellular ice crystal formation, which causes both a direct and indirect cell death"* [187, p. 249].	3
delayed heat-trans. mod.	Heat-transfer model which corrects the infinite speed of propagation in the classical heat equation $\partial_t \vartheta = \Delta \vartheta$.	15
DOM	Discrete-ordinates method: technique to transform the transport equation into a system of partial differential equations based on a discrete representation of the directional variation of the radiance.	117, 120, 122, *see* radiative-transfer equation (RTE)

Notation	Description	Page List
ex-vivo	Opposite of in-vivo.	5, 43, *see* in-vivo
FEM	Finite-element method: technique to discretize a partial differential equation and compute an approximate solution.	118
HIFU	High-intensity focused ultrasound: *"In HIFU, an extracorporeal ultrasound probe with a piezoelectric transducer is placed on the patient and a focused beam of sound energy is sent to target lesions. The mechanical vibration of the focus[ed] sound waves is converted into heat within the lesion as well as cavitation from microbubbles that are created"* [187, p. 252].	3
inverse problem	*"To predict the result of a measurement requires a model of the system under investigation, and a physical theory linking the parameters of the model to the parameters being measured. This prediction of observations, given the values of the parameters defining the model constitutes the "normal problem", or, in the jargon of inverse problem theory, the forward problem. The "inverse problem" consists in using the results of actual observations to infer the values of the parameters characterizing the system under investigation"* [230].	43
in-vivo	In-vivo experiments are performed on a living organism.	4, 43
irradiance ϕ	Also *radiation energy density*: radiant power received by a surface per unit area, which is defined as the integral of the radiance over the unit sphere: $\phi(\boldsymbol{x}) = \int_{\mathcal{S}^2} \psi(\boldsymbol{x}, \boldsymbol{v}) \ \mathrm{d}\boldsymbol{v}$. The physical unit is $\mathrm{W\,m^{-2}}$ [97].	5, 103
isotropic	Uniform in all directions.	102
l^2 Riesz repr.	Riesz representative w.r.t. the Euclidean scalar product.	79
L^2 Riesz repr.	Riesz representative w.r.t. the $L^2(\Omega)$ scalar product.	77, 79
lin. state vector	Two-component vector $(\rho, \eta) \in L^2(I; H^1(\Omega)) \times (W_\vartheta \cap \mathcal{C}^0(\overline{Q}))$ (see equation (2.7)) which fulfills the linearized state system (3.14) for all $\varphi \in L^2(I; H^1(\Omega)) \times L^2(I; H^1(\Omega))$.	52, 53, 55

Notation	Description	Page List
LITT	Laser-induced interstitial thermotherapy: a minimally-invasive therapy for the thermal ablation of tumors.	1, 3
Marshak b.c.	Particular set of boundary conditions for the P_N equations.	113
microwave ablation	*"Continuous microwave agitation of surrounding water molecules produces friction and heat, resulting in cell death [, where microwaves are transmitted through a specifically suited antenna inserted into a tumor]"* [187, p. 250].	3
MR thermometry	Technique to extract temperature data from magnetic-resonance imaging (MRI).	1, 45
online	Interactive and real-time capable.	1
optical coefficient	Refers to the absorption and scattering coefficients (and as the case may be to the diffusion coefficient D in the P_1 model).	5–7, 46, 81, 135, 139, *see absorption coefficient* & *scattering coefficient*
P_N method	Moment approximation of the radiative transfer equation, based on the expansion of the solution as linear combination of an angular basis (in this thesis: spherical harmonics).	97, 99, 108
P_N^{2nd}	Second-order formulation of the P_N equations.	97, *see P_N moment approximation (with spherical harmonics)*
radiance ψ	Radiative energy flow per unit solid angle and unit area normal to the rays. ψ is a directional quantity. The physical unit is $\mathrm{W\,m^{-2}\,sr^{-1}}$ [97]. Must not to be confused with the radiant intensity with units $\mathrm{W\,sr^{-1}}$. See also [227, Sec. 1.2, Tab. 1.1, p. 7 ff.].	5, 97
radiative transfer	*"Radiative transfer is the theory describing how electromagnetic radiation is transmitted through a medium [...]. The medium can emit, absorb, and scatter radiation with a behavior that may vary strongly with wavelength according to the different species composing the medium and their physical state"* [183].	5

Notation	Description	Page List
reflexive	A real Banach space X is called *reflexive* if we can identify the dual space of its dual space X^* with X by means of the map in Equation (B.1), i.e., $X^{**} \cong X$ (see Def. B.11).	195
RFA	Radiofrequency ablation: *"For the procedure, an RF needle is directed under imaging guidance into a tumor site. Retractable electrodes within the needle, if present, are then deployed into the lesion. The generator connected to the needle creates [medium frequency alternating] current that is conducted to the electrode tip to produce heat"* [187, p. 248].	3
RTE	Radiative transfer equation: Boltzmann equation when used to treat the propagation of light [204, Sec. 6.3.2, p. 153]. The Boltzmann equation describes how a variety of different types of particles travel through a material [21].	4, 97, 122
scattering	*"Change in the direction of motion of a particle because of a collision with another particle"* [59].	97
spherical quadrature rule	Quadrature rule to approximate integrals of functions $f: \mathcal{S}^2 \to \mathbb{R}$ defined on the unit sphere.	118
SP$_N$ method	Simplified P$_N$ method, usually derived by a reformulation of the P$_N$ equations as system of second-order differential equations by means of asymptotic analysis or algebraic transformations.	99, *see* P$_N$ moment approximation (with spherical harmonics)
state vector of the Cattaneo–LITT model	Two-component vector $(\phi, \vartheta) \in \mathcal{Y}_p$, for some $p \geq 2$ (see equation (2.7)), which fulfills the state system (2.10) for all $\varphi \in L^2(I; H^1(\Omega)) \times L^2(I; H^1(\Omega))$.	24, 27, 36, 38, 41, 44, 50, 52, 53, 55, 57–59, 77, 178, 190, *see* Cattaneo–LITT model
thermal radiation	*"Process by which energy, in the form of electromagnetic radiation, is emitted by a heated surface in all directions and travels directly to its point of absorption at the speed of light; thermal radiation does not require an intervening medium to carry it"* [61].	5, 101

Notation	Description	Page List
trigon. polynomial	Real linear combination of functions $x \mapsto \cos(kx), k \in \mathbb{N}_0$, and $x \mapsto \sin(kx), k \in \mathbb{N}$. It can be interpreted as a polynomial on the unit sphere, e.g., like the real spherical harmonics.	

Index

Akademischer Lebenslauf

2016 Annahme als Doktorand am Fachbereich Mathematik der Technischen Universität Kaiserslautern unter Prof. Dr. René Pinnau.

2016 Masterabschluss (M.Sc.) in Technomathematik am Fachbereich Mathematik der Technischen Universität Kaiserslautern mit dem Schwerpunkt Modellierung und Wissenschaftliches Rechnen und Anwendungsfächern Physik und Informatik.
Thema der Masterarbeit: A Predictive Control Framework to Eliminate Bus Bunching.

2014 Bachelorabschluss (B.Sc.) in Mathematik am Fachbereich Mathematik der Technischen Universität Kaiserslautern mit dem Schwerpunkt Modellierung und Wissenschaftliches Rechnen und Anwendungsfach Physik.
Thema der Bachelorarbeit: Identifikation linearer Systeme.

2011 Immatrikulation an der Technischen Universität Kaiserslautern.

2010 Allgemeine Hochschulreife am Megina-Gymnasium Mayen.

Academic curriculum vitae

2016 Acceptance as a doctoral candidate of Prof. Dr. René Pinnau at the Department of Mathematics of the Technische Universität Kaiserslautern.

2016 Master's degree (M.Sc.) in Industrial Mathematics at the Department of Mathematics of the Technische Universität Kaiserslautern with specialization in Modeling and Scientific Computing and subsidiary subjects Physics and Computer Science.
Title of the Master's thesis: A Predictive Control Framework to Eliminate Bus Bunching.

2014 Bachelor's degree (B.Sc.) in Mathematics at the Department of Mathematics of the Technische Universität Kaiserslautern with specialization in Modeling and Scientific Computing and subsidiary subject Physics.
Title of the Bachelor's thesis: Identifikation linearer Systeme.

2011 Matriculation at the Technische Universität Kaiserslautern.

2010 General higher education entrance qualification at the Megina-Gymnasium Mayen.